UNIVERSITÀ DEGLI STUDI FIRENZE

DOTTORATO DI RICERCA
INTERNATIONAL DOCTORATE IN STRUCTURAL BIOLOGY

CICLO XXX

COORDINATORE Prof. Claudio Luchinat

Applications of metabolomics in biomedicine

Settore Scientifico Disciplinare CHIM/03

Dottorando
Dott. *Alessia Vignoli*

Tutore
Prof. *Claudio Luchinat*

Coordinatore
Prof. *Claudio Luchinat*

Novembre 2014 - 2017

This thesis has been approved by the University of Florence, the University of Frankfurt and the Utrecht University

Universiteit Utrecht

CERM Firenze

FRANKFURT AM MAIN

Abstract

Nuclear magnetic resonance spectroscopy represents an optimal tool in modern chemical and biochemical research; for this reason, numerous applications can be found in both biology, and biomedicine. Despite its lower sensitivity, nuclear magnetic resonance spectroscopy offers many unparalleled advantages over mass spectrometry in order to perform metabolomic analysis. Metabolomics is defined as the analysis of the complete ensemble of low molecular weight molecules, the metabolites, present in a biological specimen. It is an emerging technology that holds promise powerful insights into the mechanisms of human health and disease making personalized medicine even more personalized.

In this methodological thesis, with the aim of demonstrating the potential of NMR-based metabolomics in biomedical research different topics have been addressed and discussed: 1) the use of NMR-metabolomics to provide innovative means to predict response and recurrence of diseases; 2) the characterization of the metabolic signature of pathological states via NMR to uncover their underlying molecular mechanisms; 3) the application of NMR-base metabolomics in the framework of precision medicine by characterizing the human plasma metabolic phenotype and by monitoring the effect of drug treatments or life style interventions on the metabolome; 4) the investigation of potential applications of metabolomics in veterinary research.

In conclusion, the results presented in this thesis, obtained by a combination of biochemistry, analytical chemistry, bioinformatics, and clinical data, showed that fingerprinting analysis by NMR has the potential not only to increase our knowledge on specific diseases, but also to be translated in clinical practice for diagnostic or prognostic purposes.

Candidate contributions

PhD Publications:

PUBLISHED

1. C. Hart, A. Vignoli*, L. Tenori, et al.; *Serum metabolomic profiles identify ER-positive early breast cancer patients at increased risk of disease recurrence in a multicentre population*. Clin. Cancer Res. Off. J. Am. Assoc. Cancer Res. 23, 1422–1431 (2017). I.F. 9.619
2. A. Basoglu, L. Tenori, A. Vignoli, et al.; *Plasma Metabolomics in Calves with Acute Bronchopneumonia*. Metabolomics 12, 128 (2016). I.F. 3.691
3. A. Vignoli*, D.M. Rodio, A. Bellizzi, et al.; *Nuclear magnetic resonance-based metabolomics approach to study urines of chronic inflammatory rheumatic diseases*. Analytical and Bioanalytical Chemistry 409, 1405–1413 (2017). I.F. 3.431
4. A. McCartney, A. Vignoli, C. Hart, et al.; *De-escalating and escalating treatment beyond endocrine therapy in patients with luminal breast cancer*. The Breast doi:10.1016/j.breast.2017.06.021 I.F. 2.801
5. A. Basoglu, L. Tenori, A. Vignoli, et al.; *Effects of Boron Supplementation on Peripartum Dairy Cows' Health*. Biological Trace Element Research. 1–8 (2017). doi:10.1007/s12011-017-0971-9 I.F. 2.339

SUBMITTED

6. A. Vignoli*, L. Tenori, B. Giusti, et al.; *NMR-based Metabolomics identifies high risk of death patients within two years after acute coronary syndrome*.
7. A. Vignoli*, L. Tenori, C. Luchinat, et al. *Age and sex effects on plasma metabolite association networks in healthy subjects*.
8. P. Montuschi, G. Santini, A. Vignoli*, et al.; *Breathomics for assessing the effects of inhaled beclomethasone/formoterol in patients with COPD*.

9. A. Vignoli*, S. Paciotti, P. Eusebi, et al.; *Cerebrospinal fluid metabolic profile correlates with Alzheimer's core biomarkers*.

IN PREPARATION

10. A. Vignoli*, C. Luchinat, A. Calabrò, et al; *The metabolic signature of Primary Biliary Cirrhosis and its comparison with Coeliac Disease*.
11. J. Rittweger, K. Albrach, A. Vignoli, et al.; *Muscles in Space – Shall the Force be with Us?*
12. D. Palli, P. Turano, A. Vignoli, et al.; *Mammographic density and breast cancer prevention: a metabolomic epigenetic and inflammatory markers integrated approach.*
13. A. Vignoli*, A. McCartney et al.; *Metabolomics in breast cancer: a decade in review.*

* First Author or Co-First Author

Attended congresses

CONFERENCE CONTRIBUTIONS

Poster: XLIII National Congress of Magnetic Resonance GIDRM Bari 22-24 September 2014 "*Applications of metabolomics in biomedicine: prospective longitudinal study of patients with chronic obstructive pulmonary disease (COPD)*"

Poster: PhD Day 6 University of Florence Sesto Fiorentino 27 May 2015 *"Nuclear magnetic resonance-based metabolomic approach to study urine of Chronic Inflammatory Rheumatic Disease patients"*

Oral communication: XLV National Congress of Magnetic Resonance GIDRM Modena 5-7 September 2016 *"Serum metabolomic profiles identify ER-positive early breast cancer patients at increased risk of disease recurrence in a multicentre population"*

Poster: 30° Congresso Nazionale S.I.S.A. Roma 20-22 November 2016 "*Metabolomics by nuclear magnetic resonance identifies patients with high risk of death within two years after a cardiovascular event: the case of the Amiflorence II study*"

Workshop: NMR&MS in Metabolomics, University of Padua 3 February 2017

Oral communication: PhD Day 8 University of Florence Sesto Fiorentino 24 May 2017 *"Serum metabolomic profiles identify ER-positive early breast cancer patients at increased risk of disease recurrence: a multicenter population study"*

Oral communication: MOVISS workshop Vorau (At) 20-23 September 2017 *"Serum metabolomic profiles identify ER-positive early breast cancer patients at increased risk of disease recurrence: a multicentre population study"*

Oral communication: Festival della Scienza Genova 4 November 2017 *"Serum metabolomics as a prognostic tool for breast cancer and cardiovascular diseases"*

PUBLISHED CONFERENCE PAPERS

1. Santini, G.; Mores, N.; Vignoli, A.; et al. Effects of treatment and withdrawal with inhaled beclomethasone/formoterol on electronic nose and NMR metabolomic breathprints in patients with COPD. Eur. Respir. J. 2016, 48 (suppl 60), PA1075.
2. Mislang, A. R. A.; Vignoli, A.; Donato, S. D.; et al. Serum metabolomics as biomarkers to differentiate early from metastatic disease and predict relapse in elderly colorectal cancer (CRC) patients. J. Clin. Oncol. 2016, 34 (suppl; abstr 10042).
3. Di Donato, S.; Mislang, A. R.; Vignoli, A.; et al. D20Serum metabolomic as biomarkers to differentiate early from metastatic disease in elderly colorectal cancer (crc) patients. Ann. Oncol. 2016, 27 (suppl_4), iv45-iv45.
4. Hart, C. D.; Vignoli, A.; Tenori, L.; et al. Serum metabolomic profiles identify ER-positive early breast cancer patients at increased risk of disease recurrence in a multicentre population. Ann. Oncol. 2016, 27 (suppl_6).
5. Hart, C. D.; Vignoli, A.; Tenori, L.; Risi, E.; Love, R.; Luchinat, C.; Di Leo, A. A risk score based on preoperative serum metabolomic profiles identifies patients with early breast cancer at increased risk of recurrence in a multicenter population: outcomes by adjuvant online stratification. Asia Pac. J. Clin. Oncol. 2016, 12, 104–168.
6. Tenori, L.; Giusti, B.; Vignoli, A.; et al. Metabolomics by Nuclear Magnetic Resonance identifies patients with high risk of death within two years after a cardiovascular event: The case of the Amiflorence II study. Nutr. Metab. Cardiovasc. Dis. 2017, 27 (1), e39–e40.

Table of contents

Abbreviations and acronyms

1D: One-dimensional
2D: Two-dimensional
ACS: Acute Coronary Syndrome
AD: Alzheimer's Disease
AMI: Acute Myocardial Infarction
AUC: Area Under the receiver operating characteristic Curve
CA: Canonical Analysis
CD: Coeliac Disease
CE: Capillary Electrophoresis
CIRDs: Chronic Inflammatory Rheumatic Diseases
CNS: Central Nervous System
COPD: Chronic Obstructive Pulmonary Disease
COSY: COrrelation SpectroscopY
CPMG: Carr–Purcell–Meiboom–Gill spin-echo sequence
CSF: CerebroSpinal Fluid
DAMA: Diet, physical Activity and MAmmography
EBC: Exhaled Breath Condensate
eBC: early Breast Cancer
FID: Free Induction Decay
GC: Gas Chromatography
GRACE: Global Registry of Acute Coronary Events
H0: Null Hypothesis
HA: Alternative Hypothesis
HC: Healthy Control

HER2: Human Epidermal growth factor Receptor 2
HR: Hazard Ratio
HR-MAS: High Resolution Magic Angle Spinning spectroscopy
HSQC: Heteronuclear Single Quantum Coherence spectroscopy
ICS/LABA: Inhaled Corticosteroid/Long-Acting β2-Agonist
ISS: International Space Station
k-NN: k Nearest Neighbours
LC: Liquid Chromatography
LMO: Leave-More-Out
LOO: Leave-One-Out
mBC: metastatic Breast Cancer
MCI: Mild Cognitive Impairment
mRNA: messenger RiboNucleic Acid
MS: Mass Spectrometry
MSC: Multiple SCLerosis
N: Negative
NMR: Nuclear Magnetic Resonance
NOESY: ^{1}H-Nuclear Overhauser Effect SpectroscopY
OPLS-DA: Orthogonal Projection to Latent Structure Discriminant Analysis
P: positive
PBC: Primary Biliary Cirrhosis
PCA: Principal Component Analysis
PCs: Principal Components
PLS-DA: Partial Least Squares Discriminant Analysis
PQN: Probabilistic Quotient Normalization
ROC: Receiver Operating Characteristic curve
SNPs: Single-Nucleotide Polymorphisms
SVMs: Support Vector Machines
T2: transverse relaxation time
TMSP: Sodium TriMethylSilyl-[2,2,3,3-$^{2}H_{4}$]Propionate
TN: True Negative
TOCSY: Total COrrelation SpectroscopY
TP: True Positive
tRNA: transfer RiboNucleic Acid
UHPLC: Ultra-High Performance Liquid Chromatography

Chapter 1
Introduction

1.1 What is metabolomics?

Biological systems are complex entities composed of dynamic and interrelated genetic, protein, metabolic and cellular components. Environmental and many other external factors exert significant influence; therefore, comprehension of biological systems at a molecular level can be achieved more thoroughly only if they are considered and studied as a whole by combining biology, chemistry, mathematics, statistics, and bioinformatics. In this framework, systems biology aims at modelling complex biological interactions, by integrating data from interdisciplinary fields in a holistic fashion[1].

Omics sciences can be considered as the analytical basis of systems biology, since they enable the global characterization and quantification of many different biological molecules, such as genes, proteins and metabolites, which explain the complex structure, function and dynamics of cells, tissues or organisms[2]. Genomics, the first among all the omic sciences, is the systematic study of all nucleotide sequences, including structural genes, regulatory and non-coding sequences that are present in an organism's genome. Transcriptomics studies the entire pool of mRNA in a cell or organism, which reflects the genes that are actively expressed at any given moment. Proteomics aims at characterizing the complete set of all expressed proteins in a cell, tissue or organism, determining their role in physiological and pathophysiological functions. Metabolomics is one of the latest omic technologies, broadly defined as the comprehensive measurement of the complete ensemble of metabolites present in a biological specimen, the so-called metabolome[3]. The metabolome can be described as a highly complex and finely organized biochemical network in which small molecules interact together, as well as with other biological macromolecules[4]. It is a dynamic and

evolving entity that can be regarded as the downstream end-product of the interaction of genetic expression, transcriptional changes, post-translational modifications of proteins, and various other external factors such as environment, diet, drug administration, diseases, life style and age[5] (Figure 1). In contrast to genomics, which indicates what might happen, metabolomic profiling and phenotyping capture what is actually happening in the body[6]. For this reason, metabolites are considered the most proximal reporters of any disease status or phenotype, with potential for powerful insights into the mechanisms of human health and disease.

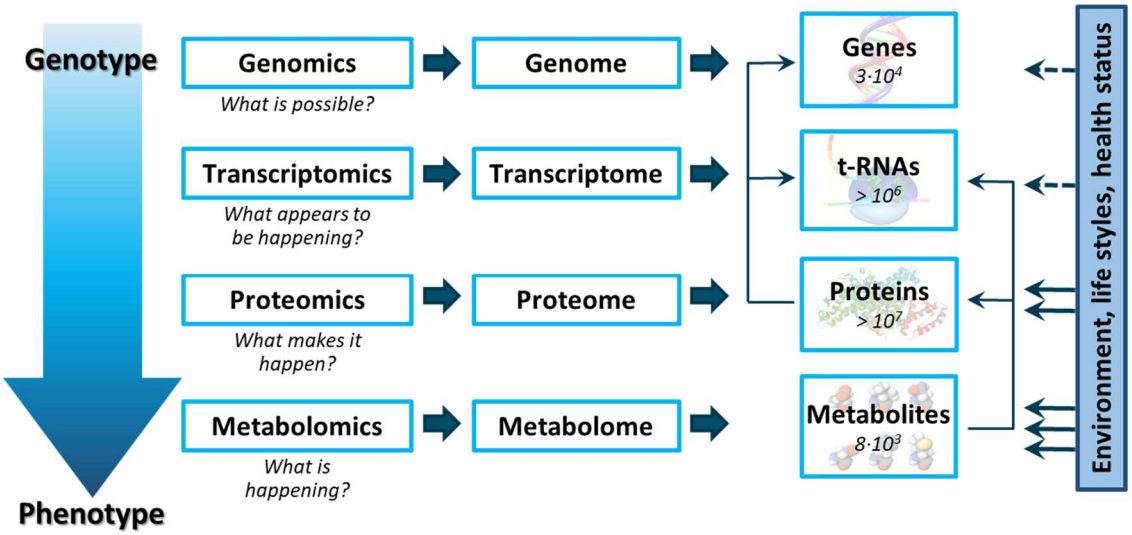

Figure 1. *Diagram illustrating omics sciences. The flow of information proceeds from genes to transcripts, to proteins and finally to metabolites, increasingly affected by external influences. This integrated scheme illustrates a temporal evolution from the genotype to the phenotype.*

Metabolomics is focused on the analysis of intermediates and end-products of metabolism, which comprise carbohydrates, fatty acids, amino acids, nucleotides, organic acids, vitamins, antioxidants, and many other classes of compounds. The total number of these metabolites is relatively small if compared with genes, transcripts or proteins; however, their levels are influenced by several internal stimuli and external perturbations. This makes metabolomics an extremely valuable tool enabling the identification of key players of diseases in the form of endogenous metabolites (gene-derived metabolites) and exogenous metabolites (environmentally derived metabolites), which provides crucial information on the underlying causes of diseases at a molecular level[7].

1.2 Metabolomics: a technique, many approaches

Dependent on the biological question at issue, metabolomic analysis can be addressed with two different methodological approaches: targeted and untargeted (Table 1).
Targeted metabolomics approaches involve the monitoring of a panel of a priori selected metabolites on the basis of known metabolic pathways or pre-identified

biomarkers that are undoubtedly associated with the disease or condition of interest. Therefore, the analytical techniques used should provide selectivity and enough sensitivity to enable the unambiguous absolute quantification of the selected metabolite in the sample.

Conversely, untargeted metabolomics provides a global view of a sample by analyzing all measurable analytes present. This purpose can be achieved via two approaches: metabolic fingerprinting or profiling. Metabolic fingerprinting is a global, rapid evaluation of all detectable metabolites in a biological sample, without identification of single metabolites. This approach is utilized to essentially provide sample classification and not for quantitative purposes. Usually, metabolic fingerprinting aims at discriminating between specimens with different biological statuses (e.g. presence or absence of disease, before or after treatment), in turn characterizing a specific health state with a unique metabolic pattern. Metabolic profiling, in contrast, concerns the quantification of all identified metabolites in a biological sample. This strategy enables the identification of metabolites and metabolic pathways associated with a specific physiological or pathological condition, providing new insights into pathophysiological molecular mechanism of diseases[6].

Table 1. *Metabolomic glossary.*

Term	Definition
Metabolites	Low molecular mass organic molecules (< 2000 g/mol) involved in metabolic processes as substrates or products with different biological functions (i.e. fuel, structure, signaling, catalytic and inhibitory effects on enzymes, defense).
Metabolome	The quantitative ensemble of all metabolites present within an organism, an organ, a biofluid, a tissue or a cell in a particular physiological or developmental state.
Metabolomics	The quantitative measurement of the dynamic multiparametric metabolic response of living systems to pathophysiological stimuli or genetic modifications.
Targeted metabolomics	The measurement of defined groups of biochemically and chemically characterized metabolites undoubtedly associated with a specific metabolic condition.
Untargeted metabolomics	The comprehensive analysis of all the measurable analytes in a sample, including chemical unknowns.
Metabolic fingerprinting	Global, high-throughput, rapid analysis of all metabolites presents in a biological sample to provide sample classification (even without metabolite identification).
Metabolic profiling	The identification and quantification of as many as possible metabolites present in a biospecimen.

1.3 Biological samples

In principle, every biofluid, tissue or cell culture can be utilized for metabolomics analysis; however, urine and blood plasma or serum are by far the most commonly used. They contain hundreds to thousands of metabolites, and can be collected relatively non-invasively, ensuring easy and high-frequency sampling of large cohorts of samples. As systemic biofluids, they are always at dynamic equilibrium with the body; therefore, they rapidly reflect every evolving metabolic changes[8]. Blood is the primary carrier of dissolved gases, nutrients, hormones and body wastes (Table 2).

Table 2. *Chemical classes in the human blood metabolome, data retrieved from the literature[9].*

Compound class	Number	Compound class	Number
Acyl glycines	10	Indoles and indole derivatives	12
Acyl phosphates	10	Inorganic ions and gases	20
Alcohol phosphates	2	Keto acids	8
Alcohols and polyols	40	Ketones	6
Aldehydes	3	Leukotrienes	8
Alkanes and alkenes	10	Minerals and elements	40
Amino acid phosphates	1	Miscellaneous	77
Amino acids	114	Nucleosides	24
Amino alcohols	14	Nucleotides	24
Amino ketones	14	Peptides	21
Aromatic acids	22	Phospholipids	2177
Bile acids	19	Polyamines	11
Biotin and derivatives	2	Polyphenols	22
Carbohydrates	35	Porphyrins	6
Carnitines	22	Prostanoids	23
Catecholamines and derivatives	21	Pterins	14
Cobalamin derivates	4	Purines and purine derivatives	11
Coenzyme A derivatives	1	Pyridoxals and derivatives	7
Cyclin amines	9	Pyrimidines and pyrimidine derivatives	2
Dicarboxylic acids	17	Quinones and derivatives	3
Fatty acids	65	Retinoids	11
Glucoronides	8	Sphingolipids	3
Glycerolipids	1070	Steroids and steroid derivatives	109
Gluycolipids	15	Sugar phosphates	9
Hydroxy acids	129	Tricarboxylic acids	2

Blood plays a key role in the regulation of the pH and ion composition of interstitial fluids, in the defense against pathogens and in the stabilization of body temperature[10].

Because of these complex and fundamental systemic roles, the concentrations of metabolites in blood are strongly controlled by feedback cycles, which regulate and maintain body homeostasis within strict parameters; therefore, they are not subjected to extreme daily variations. Since blood interacts essentially with every living cell in the human body, it offers a snapshot of the state of an organism and provides crucial information for detecting, monitoring and managing virtually all human diseases.
Urine contains more than 2000 different metabolites at variable concentrations, the urine metabolome can be summarized in 24 superclasses (Table 3). Furthermore, fresh urines are characterized by the presence of many cellular and non-cellular components[10]. As urine essentially contains metabolic wastes, urine samples are significantly affected by diet, environment, lifestyle, drug administration and bacterial by-products. Within the same individual, the urinary metabolic profile presents high rates of circadian and day-to-day variability, and therefore, in contrast to blood, urine provides a time-averaged representation of the physiological state. For all the abovementioned reasons, repeated sampling at different times for the same individual (20 samples per subject[11]) represents the best approach for urine studies.

Table 3. *Chemical superclasses in the human urine metabolome, data retrieved from the literature[12].*

Compound Superclass	Number	Compound Superclass	Number
Aliphatic Acyclic Compounds	93	Homogenous Metal Compounds	45
Aliphatic Heteromonocyclic Compounds	43	Homogenous Non-Metal Compounds	15
Aliphatic Heteropolycyclic Compounds	40	Lignans and Norlignans	12
Aliphatic Homomonocyclic Compounds	18	Lipids	866
Aliphatic Homopolycyclic Compounds	5	Mixed Metal/Non-metal Compounds	7
Alkaloids and Derivatives	45	Nucleic Acids and Analogues	49
Amino Acids, Peptides, and Analogues	286	Organic Acids and Derivatives	108
Aromatic Heteromonocyclic Compounds	67	Organic Halides	3
Aromatic Heteropolycyclic Compounds	728	Organometallic Compounds	1
Aromatic Homomonocyclic Compounds	432	Organophosphorus Compounds	17
Aromatic Homopolycyclic Compounds	6	Polyketides	74
Carbohydrates and Carbohydrate Conjugates	116	Tannins	2

Beyond blood and urine, cerebrospinal fluid (CSF) is widely used to study neurological diseases, although its sampling is much more invasive. Cerebrospinal fluid is both produced and resorbed within the central nervous system (CNS). Filling the ventricles and the subarachnoid space of the brain and spinal column, CSF protects the brain from physical shock, it circulates nutrients and chemicals filtered from the blood, and

transports waste products into the venous blood stream[13]. Since CSF composition is directly related to brain metabolic activity, it can be considered by far the ideal specimen for the study of central nervous system (CNS) disorders such as Alzheimer's disease, Parkinson's disease, and multiple sclerosis. The CSF metabolome has been characterized as shown in Table 4.

Table 4. *Chemical classes in the human CSF metabolome, data retrieved from the literature[13].*

Compound class	Number	Compound class	Number
Amino acids	56	Carnitines	5
Minerals and elements	27	Prostanoids	5
Fatty acids	18	Aromatic acids	4
Steroids and steroid derivatives	18	Pyrimidines and their derivatives	4
Hydroxy acids	16	Amino ketones	4
Alcohols and polyols	16	Aldehydes	4
Dicarboxylic acids	13	Leukotrienes	2
Peptides	12	Tricarboxylic acids	2
Carbohydrates	11	Ketones	2
Nucleosides	10	Biotin and derivatives	1
Inorganic ions and gases	10	Porphyrins	1
Cyclic amines	10	Glycolipids	1
Catecholamines and derivatives	9	Amino acids phosphates	1
Pterins	9	Cobalamin derivatives	1
Nucleotides	9	Quinolines	1
Keto-acids	7	Acyl phosphates	1
Indoles and indole derivatives	6	Amino alcohols	1
Purines and purine derivatives	5	Lipids	1

For the sake of completeness, it is important to mention that also saliva proved to be a valuable and very easy accessible biospecimen to monitor overall health status[14], and that the analysis of faecal extracts provides an innovative and non-invasive way to study gut microbiota and to diagnose intestinal diseases or alterations[15].

1.4 Analytical techniques used in metabolomics

The two leading analytical techniques used to perform metabolomic analyses are mass spectrometry (MS) and nuclear magnetic resonance (NMR) spectroscopy. Both techniques yield information about many different molecules in a single measurement, and can be used to determine structures and concentrations of metabolites[16]. Nevertheless, each of technique has its own strengths and limitations (Table 5).

MS determines the molecular composition of biological samples base on the mass-to-charge ratio (m/z) of ionized metabolites. This method often requires the separation of metabolites from the biofluid matrix. As such, MS is coupled with liquid chromatography (LC), gas chromatography (GC), or capillary electrophoresis (CE). Specifically, appropriate phases or columns allow LC-MS to analyze numerous metabolites with molecular characteristics ranging from hydrophilic to hydrophobic, and the use of ultra-high performance liquid chromatography (UHPLC) has lowered the detection limit from the usual nanomolar scale down to femtomolar.

Despite these recent improvements, reproducibility still remains the biggest limitation of MS; for this reason, although overshadowed by MS in terms of sensitivity, NMR spectroscopy offers crucial advantages. NMR data are highly reproducible[17] and intrinsically quantitative over a wide dynamic range; NMR is non-destructive, and enables the analysis of intact tissues. Moreover, it is more suitable for untargeted metabolomics with the aim of characterizing metabolic phenotype of diseases. It is important also to mention that standards of each metabolite to be analyzed at known concentration need to be used for MS experiments to generate calibration curves for absolute quantification; conversely no-standards are needed for NMR, making the analysis straightforward and possibly high throughput.

Table 5. *Advantages and limitations of NMR spectroscopy and MS spectrometry as metabolomic analytical platforms.*

Mass Spectrometry (MS)	Nuclear Magnetic Resonance spectroscopy (NMR)
Advantages	
Sensitivity (1 nM)	Reproducibility
Low sample volumes	Non-destructive
Robust	Robust
Selectivity	Minimal sample preparation
Quantitative	High throughput sample analysis
Low-medium costs	Quantitative
	Analysis of intact tissues
	Not affected by matrix components
Limitations	
Destructive	Low sensitivity (1-10 μM)
Complex sample preparations	High sample volumes (100-700 μL)
No high throughput analysis	Expensive instrumentations
No analysis of intact tissues	
Affected by matrix components	

In the NMR spectra, the integrals of each peak relate directly to the number of nuclei (with nonzero spin) giving rise to the peak, and hence to the relative concentrations of

the molecules in the sample, making NMR an intrinsically quantitative technique. The most important nuclei in biomolecular NMR studies are ^{1}H (proton), ^{13}C, ^{15}N, and ^{31}P. One-dimensional (1D) ^{1}H NMR is the most widely used NMR approach in metabolomics, since the proton is the most sensitive and abundant nucleus; however, multidimensional NMR experiments offer further possibilities that can be sometimes exploited for unambiguous identification of metabolites in complex mixtures like biofluids or tissues.

In conclusion, MS and NMR are two complementary techniques with comparative strengths and weaknesses. NMR represents the first choice to perform untargeted metabolomics with the aim of generating new scientific hypotheses. Conversely, MS is the best technology to confirm or validate a preexisting hypothesis with a targeted approach, since its high sensitivity enables the detection of all metabolites present in a specific metabolic cycle, particularly the ones below the NMR detection limit.

In view of the fact that during my PhD I have been involved in hypothesis-generating studies, the untargeted approach obviously was the one to be chosen, and NMR was the analytical platform utilized for all the analyses.

1.5 NMR-based metabolomic workflow

A workflow scheme of a typical untargeted NMR-based metabolomic study is presented in Figure 2.

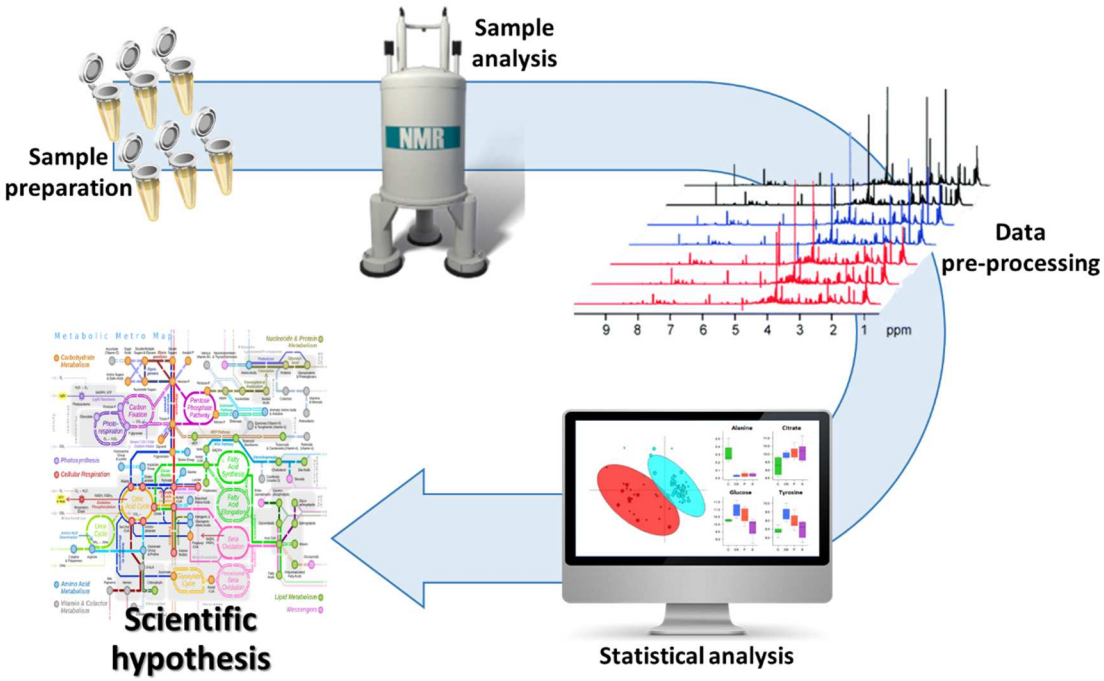

Figure 2. *A typical untargeted NMR metabolomic experimental pipeline.*

Sample collection, handling, storage and preparation constitute the first step of a metabolomic analysis, and the adoption of standard operating procedures is essential

to best maintain sample stability and obtain reproducible results. Thus, specimens that are not collected, stored or processed uniformly can be corrupted and the data obtained from analyses of these samples can be invalid or erroneous.
Sample preparation can vary widely, depend on the chosen analytical technique, and processes such as extraction or buffering could be necessary. The second step involves analysis of the samples by NMR spectroscopy with appropriate pulse sequences.
Before statistical analysis, the analytical data obtained are subjected to pre-processing (alignment, phasing, baseline correction, bucketing) and pre-treatment procedures (normalization, centering, scaling) to make metabolomic features more comparable[18].
Since metabolomics generates large amount of data, multivariate statistical analyses are always performed alongside with the common univariate analyses (i.e. student's t test, analysis of variance, Kruskal–Wallis test, Wilcoxon signed-rank test). Generally, the initial experimental hypothesis guides the selection of the appropriate statistical algorithm. Many pattern recognition methods can be applied to assess how the spectra of biological samples, belonging to the groups of interest, cluster. Principal component analysis (PCA), cluster analysis and correlation analysis are most used methods for unsupervised analyses, together with partial least squares discriminant analysis (PLS-DA), orthogonal projection to latent structure discriminant analysis (OPLS-DA), canonical analysis (CA) and support vector machines (SVMs) for supervised discriminations[6]. The robustness of the calculated models needs also to be checked to avoid overfitting of the data using internal cross-validation procedures, permutation tests or receiver operating characteristic (ROC) curve estimation, or using an external independent validation set when available.
Finally, the statistically significant metabolites among the groups of interest can be placed in metabolic networks, by using on line tools like MetaboAnalyst[19], to enable biological understanding of occurring phenomena and to provide new insights into fundamental mechanisms of diseases.

1.6 State-of-the-art of metabolomics and biomedicine

In the past decades, biomedical research has been led by the fundamental assumption that many chronic or serious pathologies should have genetic origins; therefore, huge efforts aimed at characterizing the whole human genome, transcript profiles and single nucleotide polymorphisms (SNPs) have been made. The Human Genome Project indeed revolutionized biomedical research and provided fundamental insights into biology, but the expected "genetic revolution" has yielded far fewer results than originally expected for diagnosis, prevention and treatment of human diseases[20,21]. This phenomenon could be explained by considering more-recent epidemiological surveys, which have revealed the crucial role of environment on disease development and risk of death, underlying the importance of the epigenome and the microbiome[7,22,23]. Metabolomics, which monitors the global outcome of all influencing

factors (exogenous and endogenous) without making assumptions about the effect of any single contribution to that outcome, overcomes any differences and as such could be a perfect tool to investigate and understand the molecular mechanisms of human health and disease[16]. Unlike genes and proteins, metabolites are easier to correlate with phenotype and serve as direct signatures of biochemical activity, since they play a central role in disease development, cellular signaling and physiological control. For these reasons, many biomedical fields, summarized in three broad areas in Figure 3, could benefit from metabolomic studies.

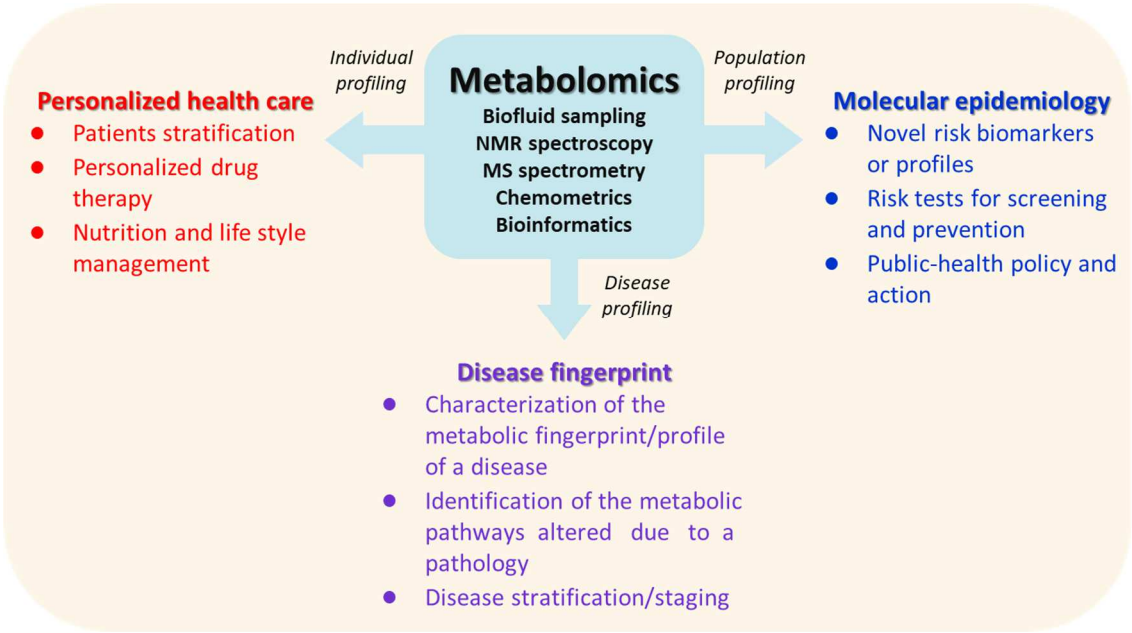

Figure 3. *Applications of metabolomics in biomedical research. Adapted from Nicholson et al.[16].*

Classically, metabolomics is applied to characterize disease metabolic profiles with the intent of discovering new biomarkers and identifying biochemical pathways involved in disease pathogenesis. Metabolomics has already increased our understanding of comprehensive cellular and physiological metabolism helping to identify many unexpected chemical causes for several important chronic and complex diseases, such as cancer[4,24,25], cardiovascular diseases[2,26], and diabetes[27,28]. Furthermore, the metabolomic approach can also offer a cost-effective and productive route to uncover new targets for drug discovery. Actually, not only most prominent diseases such as cardiovascular diseases, hypertension, obesity, or diabetes have undeniable metabolic basis, but also many other chronic and serious illnesses have been found to have unexpected or underappreciated metabolic causes[29–34].

For all the abovementioned research potentials, metabolomics represents a powerful tool in biomedicine with the most ambitious objective of detection of early metabolic perturbations even before the manifestation of disease symptoms, providing new promise for early diagnosis, preventing therapies and precision medicine approaches. The goal of precision medicine is indeed to customize subjects' therapeutical

treatments according to their specific omic-profiles (individual profiling). In current clinical practice, small numbers of molecules have been used to diagnose complex metabolic diseases (e.g. blood glucose for diabetes, blood phenylalanine for phenylketonuria); conversely, current metabolomic technologies go well beyond the scope of standard clinical chemistry techniques and achieve detection of dozens to hundreds of metabolites. Metabolomics enables patient diagnosis and prognosis, prediction of individual response to drug treatment (pharmacometabolomics) and monitoring of therapies and lifestyles interventions; therefore there can be little doubt that metabolomics can play a crucial role into informing the practice of precision medicine[7].

Finally, metabolic profiling of populations could enable the development of the so called 'molecular epidemiology', defined as the ability to assess the susceptibilities of specific groups of individuals to disease[16]. This might allow the development of novel risk tests for screening and prevention, with future implications for health screening programs.

For the sake of completeness, it is important to underline that the use of the metabolomic approach is not confined to human medicine. Several potential applications in the veterinary industry are possible, in particular in the framework of: disease diagnosis and investigation, optimization of health and production, drug discovery and animal welfare[35].

Chapter 2

Aims of the thesis

Metabolomics is an emerging technology that holds promise of powerful insights into the mechanisms of health and disease. In this methodological thesis, different topics will be addressed and discussed with the aim of demonstrating the potential of NMR-based metabolomics in biomedicine, with particular attention paid to:

1) provide a means to predict response and recurrence of diseases. Specifically, robust statistical models were built with the aim of developing novel risk tests for screening and prevention using data from large multicenter studies, regarding breast cancer risk of recurrence in early stage patients, and patient risk of death within 2-years after acute coronary syndrome;
2) provide predictive, prognostic, and diagnostic markers/fingerprints of distinct pathological states, such as primary biliary cirrhosis, Alzheimer's disease, and chronic inflammatory rheumatic diseases, to uncover the underlying molecular mechanisms of diseases, and to enable stratification of patients based on metabolic pathways impacted by the diseases;
3) prove the usefulness of metabolomics in the framework of precision medicine by a) unraveling biomarkers/fingerprints for drug response phenotypes, providing an effective means to predict variation in individual response to treatment (pharmacometabolomics). In particular, the effects of steroid treatment and withdrawal in patients with chronic obstructive pulmonary disease has been assessed; b) describing the molecular individual response to life style interventions, such as the effects of a healthy life style in women at increased risk to develop breast cancer, or to stressful situations, like a 6-months spaceflight; and c) characterizing the human metabolic phenotype, in particular age and sex effects on plasma metabolic phenotype and on metabolite association networks in healthy

subjects. The investigation of how common variables influence the expression of the metabolic phenotype is actually a critical component for development of metabolomics as a population screening and precision medicine platform.

4) Furthermore, the potential applications of metabolomics in veterinary research has been investigated by characterizing the blood metabolic profiles of calves with acute bronchopneumonia and monitoring the effects of boron supplementation on peripartum dairy cows' health as a treatment to prevent the negative energy balance (NEB) at the onset of lactation via blood metabolomic analysis.

Chapter 3
Methodological aspects

3.1 NMR metabolomic analysis

NMR spectroscopy exploits the behavior of molecules when placed in a magnetic field and irradiated with specific radiofrequency waves, to identify different nuclei (with nonzero spin) based on their resonance frequency. One-dimensional (1D) ^{1}H NMR spectroscopy is the most widely used approach in metabolomics; therefore, compared to other applications of NMR, the pulse sequences employed in metabolomics require a lower level of sophistication and relatively more rapid acquisition times.

The main problem that must be addressed in any NMR sequence used for metabolomic scopes is the detection of hydrogen nuclei (protons) of biological molecules in aqueous samples at μM or lower concentrations against a background concentration of 110 M water protons[36]. Thus, suppression of the water signal is definitely required. The most widespread solvent suppression method used is the so-called presaturation: the water resonance is selectively saturated by frequency irradiation with a long (typically 2 s), low power RF pulse before the acquisition phase, thus leading to a suppression of its signal. The big advantage of this technique is the high chemical shift selectivity; conversely, the main disadvantage comes from the long duration of the pulse applied that induced also the saturation of hydrogen atoms in chemical exchange with water (e.g. urea protons) and protons having signals under the water line[36].

According to the properties of the biospecimen under study, different NMR sequences can be used to collect metabolomic data. The most widespread pulse sequence used is 1D ^{1}H-Nuclear Overhauser Effect SpectroscopY (NOESY); NOESY spectra present signals from both low- and relatively high-molecular weight metabolites, providing a highly reproducible, robust and high-quality method to obtain the complete overview of the sample metabolome. As an example, a typical ^{1}H NMR spectrum of urine contains

thousands of sharp lines mainly from low molecular weight metabolites (Figure 4), while blood plasma or serum contain both low and high molecular weight components (Figure 5A): broad signals from macromolecules (e.g. proteins, lipids and lipoproteins) contribute strongly to the NMR profile, with sharp signals from small molecules superimposed on them. The reference compound usually used in aqueous samples is the sodium salt of 3-trimethylsilylpropionic acid (TMSP) with the methylene groups deuterated.

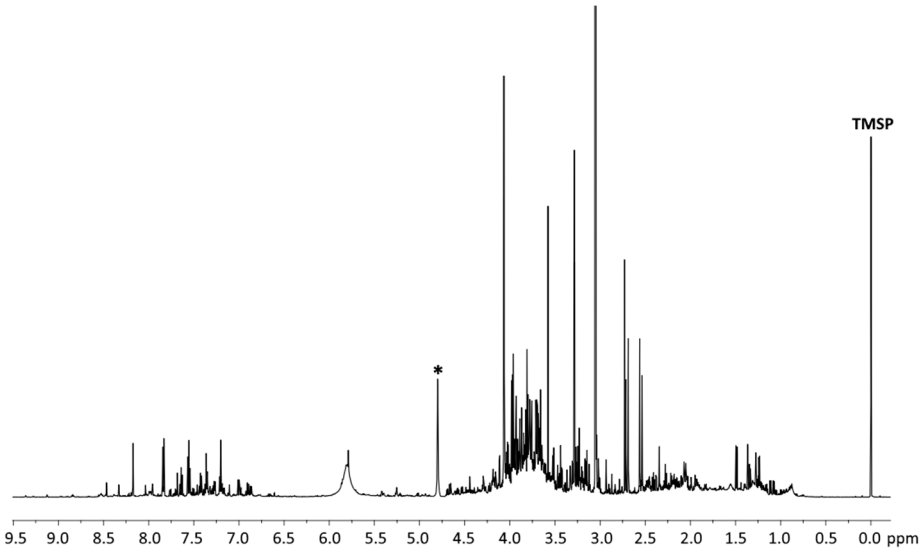

Figure 4. *600 MHz ^{1}H NOESY NMR spectrum of a urine sample. The spectrum is calibrated at the trimethylsilyl-[2,2,3,3-$^{2}H_4$]propionate (TMSP) signal (0.0 ppm). Residual water signal (*) after presaturation is also reported. Only sharp signals due to the presence of low molecular weight metabolites are present.*

Standard NMR pulse sequences can be used, in biofluids like blood plasma, serum and CSF, to selectively highlight the signals from low-molecular weight metabolites or to enhance only the contributions from macromolecules. The ^{1}H Carr–Purcell–Meiboom–Gill (CPMG) spin-echo sequence[37] exploits the different NMR transverse relaxation times of low and high molecular weight molecules to remove signals of macromolecules through T2-spectral editing (Figure 5B). Conversely, the ^{1}H diffusion-edited pulse sequence is routinely used to effectively suppress small molecule resonances on the basis of molecular diffusion coefficients, making it possible to selectively study macromolecule profiles (Figure 5C)[36].

In order to obtain high quality and robust NMR data, exchange data among laboratories, create NMR databases of small biological molecules, and enable the wide diffusion of metabolomics applications, best practices and standard NMR sequences need to be adopted. Therefore, for samples that contain just low molecular weight metabolites, like urine, 1D ^{1}H NOESY spectra are the standard spectra acquired to accomplish a metabolomic analysis; instead, for samples like blood serum or plasma 1D ^{1}H NOESY, ^{1}H CPMG, and ^{1}H diffusion-edited spectra are standardly acquired providing a complete analysis of both low and high molecular weight molecules.

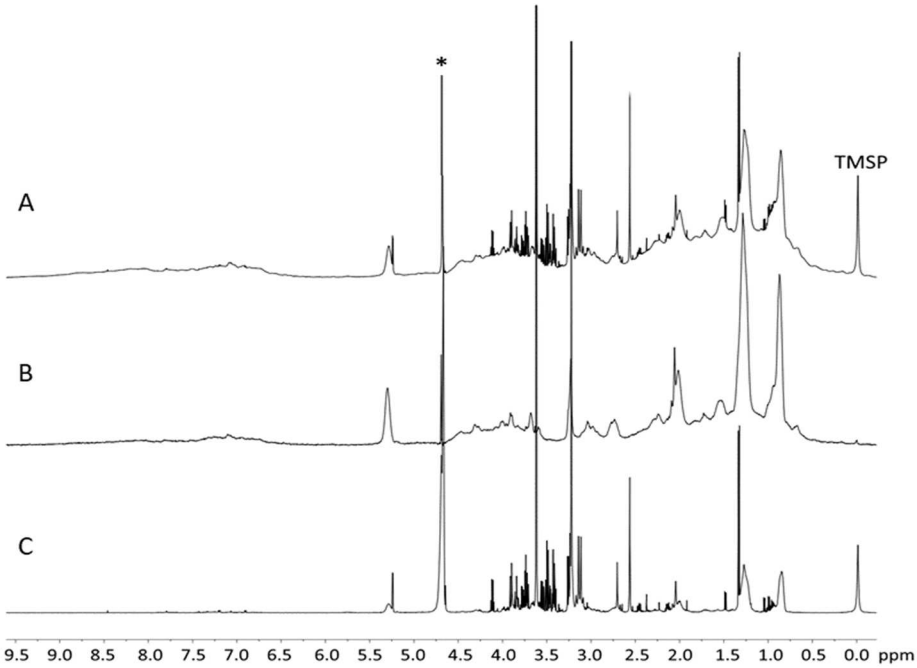

Figure 5. *600 MHz ^{1}H NMR spectra of a serum sample: A) NOESY presat spectrum; B) Diffusion-edited spectrum; C) CPMG spectrum. The spectra are calibrated at the anomeric glucose signal (5.24 ppm). Residual water signal (*) after presaturation is also reported.*

As abovementioned, the use of 2D NMR spectroscopy in metabolomics is limited; usually, only small sample arrays are analyzed with these kinds of approaches with the aim at increasing signal dispersions to simplify the spectra, thereby making spectrum assignment easier. These spectroscopic methods include 2D J-resolved experiments[38] (Figure 6), which provide information on the multiplicity and coupling patterns of resonances, but also correlation spectroscopy (COSY) and total correlation spectroscopy (TOCSY) experiments, which provide spin–spin coupling connectivity, giving information on which protons of a molecule are close in terms of chemical bond[36].

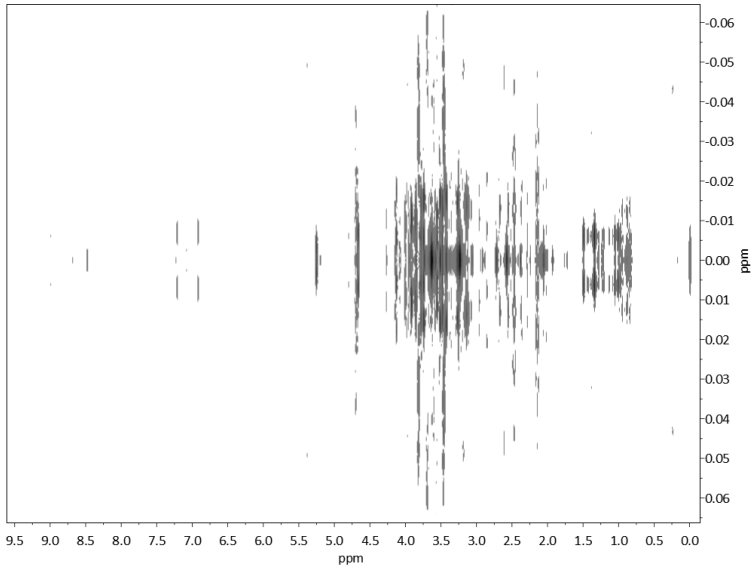

Figure 6. *600 MHz 2D ^{1}H-^{1}H J-resolved NMR spectrum of blood serum.*

Other types of nuclei with spin I = ½, such as naturally abundant ^{13}C, ^{15}N or ^{31}P, can be used to perform heteronuclear experiments, such as the ^{1}H-^{13}C HSQC experiment. These 2D experiments require much longer acquisition times than the standard 1D pulse sequences, and therefore are used only to help identify and assign metabolites in the NMR spectra[39,40].

Furthermore, ^{31}P NMR can be used to study cellular energy states also *in vivo*, and ^{13}C detection enables the study of metabolic reaction rates (fluxes) to elucidate the dynamics and mechanisms of metabolite transformations and regulations (fluxomics)[41].

For the sake of completeness, it is important to mention that NMR metabolomic analysis can be extended also to intact tissues via High Resolution Magic Angle Spinning (HR-MAS) NMR spectroscopy. Indeed, using this technology the effects of line-broadening mechanisms seen in conventional NMR spectra of non-solution state samples are attenuated by the rapid rotation of the sample around an axis that is inclined at an angle of 54.7356° (magic angle) with respect to the external main magnetic field, yielding well-resolved NMR spectra[42].

3.2 Spectral pre-processing and pre-treatment

NMR data pre-processing and pre-treatment can be considered as an intermediate step between recording of raw spectra and performing statistical analysis. These procedures make metabolomic features more comparable, ensuring thus more robust and accurate analyses and modelling.

For NMR data, raw free induction decay (FID) phasing, baseline correction and referencing to an internal standard (usually TMSP at 0.0 ppm or, if there are proteins like albumin in blood that bind TMSP, the anomeric glucose peak at 5.24 ppm) are considered pre-processing procedures.

Binning is the widespread pre-treatment procedure applied to NMR processed data, it is a way to reduce the number of total variables, to cope with subtle chemical shift variability, and to filter noise from the data. NMR spectra are simply subdivided into bins and each bin is integrated to obtain a matrix of variables.

There are many methods for pre-treatment of data matrices of the sort produced by NMR metabolomic spectra; the three most applied ones are centering, normalization and scaling.

Centering is an operation performed across the samples to convert all the concentrations to fluctuations around zero instead of around the mean of the metabolite concentrations by subtracting from each bin the mean of that chemical shift bins (column mean). Therefore, it adjusts for differences in the offset between metabolites present in high and low concentrations.

Metabolite concentrations in biofluids can vary on a large dynamic range and, as in urine, may be subject to significant dilution variations, thus leading to considerable

heterogeneity in the data[43]. Normalization is an operation performed across samples to reduce between-sample variation. The most popular normalization technique is total integral normalization, where each bin of a spectrum is divided by the total spectral intensity of that sample; however, more sophisticated method can be also applied. In particular, Probabilistic Quotient Normalization (PQN)[44] is a more accurate and more robust alternative to the total integral normalization when large variations of dilution occur (e.g. in urine samples). PQN assumes that biologically interesting concentration changes influence only few parts of the NMR spectrum, while dilution effects will affect all signals. PQN involves an integral normalization of each spectrum and the calculation of a reference spectrum, such as a median spectrum. Then, for each bin of each spectrum, the quotient with respect to the reference spectrum is calculated and the median of all quotients is estimated. Finally, all bins of each spectrum are divided by the median quotient[43].

Scaling methods are data pretreatment approaches that divide each variable (bin or metabolite) by a factor, the scaling factor, which is different for each variable. The aim is to adjust for the fold differences between the different metabolites, making profiles more comparable. These methods are often used when, within the same dataset, data from different sources (i.e. metabolomic and clinical data) need to be analyzed.

3.3 Statistical analysis

Since NMR metabolomic analysis generates large amount of complex data, in order to obtain accurate and comprehensive results, statistical matters must constitute a crucial part of a metabolomic study. Multivariate statistical approaches are routinely used to visualize biological data, to identify possible clusters among the conditions of interest, and to build predictive models; conversely, univariate statistical methods are used to identify metabolites and thus metabolic pathways altered in response to physiological or pathophysiological specific conditions.

Multivariate statistical approaches can be divided in two main classes: unsupervised and supervised methods. Unsupervised learning methods are utilized to summarize, explore, and discover clusters or trends in the data unlabeled with any class membership; therefore, no prior assumptions or knowledge of the data are needed[45]. Unsupervised methods represent usually the first step in data analysis, helping to visualize data and to discover possible outliers.

Among the different unsupervised machine learning methods, principal component analysis (PCA)[46] and cluster analysis are the most popular methods. PCA is a dimension reduction technique, which enables to express the variance within a dataset in a new reduced matrix of variables, the principal components (PCs), each of them orthogonal and independent from all the others. Each PC is a linear combination of the original variables (bins), so each successive PC shows the maximum percentage of possible variance, not represented in the previous PCs. As a consequence, while the first

principal components contain the largest percentage of variance and thus the greatest content of meaningful information, the last ones are far less important and express mostly noise.
Geometrically PCA can be viewed as a rotation of the reference system to maximize the data structure and minimize noise: the original data matrix (X) can be described through two new matrices, the score matrix T and the loading matrix P (Equation 1).

$$T = X\,P \tag{1}$$

The score matrix T encloses the coordinates of the original data in the new principal component space, each column represents the coordinates of all the samples along a particular PC. The score matrix T represents a simplified description of the original observations in the new lower dimensional space while maintaining all the relationships present among the original data. The first columns of the matrix T (usually the first two or three), that contain the largest amount of variance, can be plotted together in the so-called score plot (Figure 7A); in this plot each sample is represented by a dot and based on the distances among the dots data distributions, clusters or outliers can be visualized. Similarly, the coefficients of the linear combinations that describe the main components in terms of the experimental variables are arranged in the loading matrix P, these coordinates describe the coefficients responsible for the separation among the groups of interest (Figure 7B).

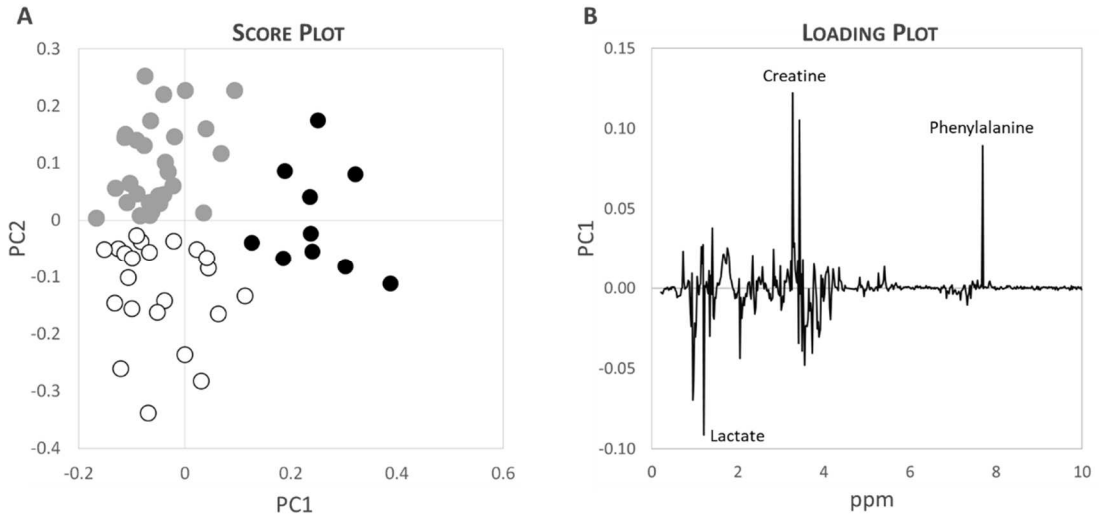

Figure 7. *Example of PCA analysis. A) Score Plot: PC1 vs PC2, each dot in the plot represents a different sample; black dots: group 1; white dots: group 2; gray dots: group 3. B) Loadings Plot of PC1. Most significant metabolites in the score plot showed the highest loadings in the PC1.*

Cluster analysis aims at clustering experimental units into classes according to similarity criteria; classes are built by maximizing homogeneity within each class and inhomogeneity among the different classes. K-means and Hierarchical Cluster Analysis are the main used approaches.

In contrast to the unsupervised methods just described, supervised approaches use *a priori* knowledge to generate models that are tightly focused on the effects of interest. These approaches can be divided in two main classes: projection based methods and machine learning methods. Among the former, Projections to Latent Structures by Partial Least Squares (PLS)[47] is the most widely used method; its robustness in the presence of highly correlated variables and its ability to provide highly predictive models using a small number of latent variables makes it useful to address the study of a large number of systems[48]. PLS can be thought as the supervised extension of PCA, it addresses the data reduction problem in a regression-based framework: instead of describing the maximum variation in the measured data (X), which is the case for PCA, PLS aims at deriving latent variables, analogous to PCs, which maximize the co-variation between the measured data (X) and the response variable (Y) regressed against[49]. This algorithm can be used for classification purposes as PLS discriminant analysis (PLS-DA), using a 'dummy' Y matrix that comprises an orthogonal unit vector for each class. Orthogonal signal correction partial least squares discriminant analysis (O-PLS-DA) is an extension of PLS which uses orthogonal signal correction to maximize the explained covariance between X and Y on the first latent variables (n-1 variables, with n the number of groups of interest), and all the orthogonal (or unrelated) variance in the other following latent variables.

A more sophisticated version of the PLS is the multilevel PLS[50] which enables the analysis of within-subject variability without being confounded with the other variation sources (e.g. matched samples of the same subject at two time-points, or two repeated measurements on the same sample). In a multilevel PLS between-subject variation is separated from the within-subject variation by subtracting the individual specific average, and only the within-subject variation is analyzed.

Reduction techniques like PCA and PLS can be used in combination with Canonical Analysis (CA) to enhance group discriminations. CA finds discriminant projection by maximizing between-class distance and minimizing within-class distance (e.g. maximize the ratio between the two values).

Machine learning supervised methods are widely used for classification and prediction purposes, they enable the resolution of the problem of identifying to which set of groups a new observation belongs (e.g. healthy or diseased), on the basis of an existing training dataset containing observations whose group memberships is known. k-Nearest Neighbours (k-NN)[51], Support Vector Machines (SVMs)[52] and Random Forest (RF)[53] can be considered the most widespread algorithms.

k-NN is probably the simplest non-parametric method to classify a new object into one of k classes. This method works in a local neighborhood around of the considered test object to be classified. The neighborhood is usually determined by the Euclidean distance, and the closest k objects of the training set are used for estimation of the group membership of the new object[54]. As a consequence, k is the fundamental parameter to be set: small k values can lead to the construction of a model subject to

significant statistical fluctuations, while large k values can reduce statistical errors but flatten many details of the distribution (Figure 8A).
SVMs are statistical techniques that enable sample classification based on the boundaries between classes comprising the whole data set. SVMs identifies a line, a plane, or, for more than three dimensions, a hyper-plane that maximizes the separation between the two classes (Figure 8B), creating thus a classifier. The hyper-plane found by the SVMs in the feature space corresponds to a non-linear decision boundary in the input space.

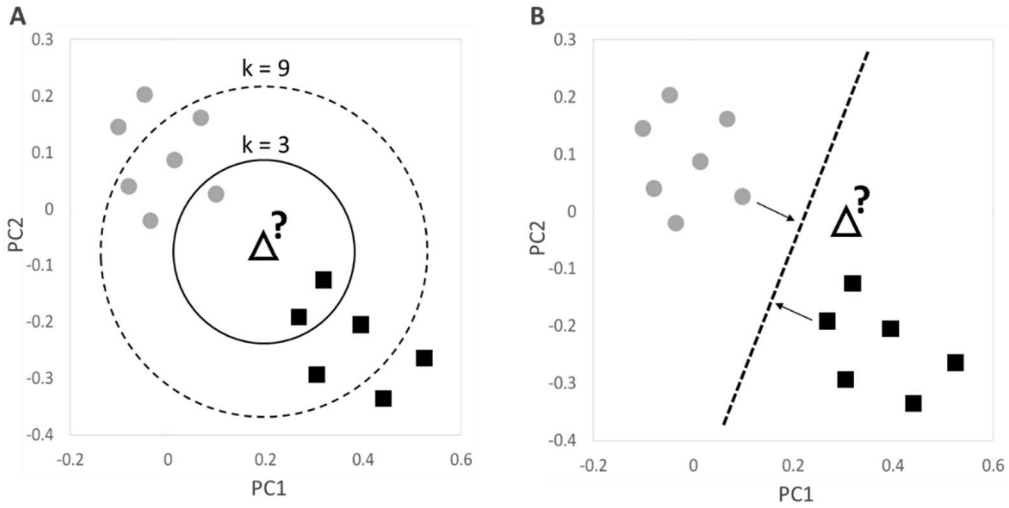

Figure 8: *Classification of an unknown object (white triangle) among two groups (grey dots and black squares) with different methods: A) k-NN classification; B) SVM.*

Random forests is a relatively new and powerful approach for data exploration and predictive modelling. The classification is derived from a randomly grown ensemble (forest) of decision trees based on the following steps: 1) the original data are randomly divided using bootstrapping into a training and test set; 2) an ensemble of decision trees is grown using the training set, where each of the trees is built on randomly selected variables (bins) at each decision node; 3) as soon as all the trees are built an unbiased assessment of the classification error using the out-of-bag samples is performed, enabling the estimation of the model performances[55]. Furthermore, for each sample, the percentage of trees in the forest that assign one sample to a specific class can be inferred as a probability of class belonging, making this approach very useful for predictive modelling purposes.
Modeling results need to be validated by simply using an independent validation set (when available) or with more sophisticated approaches like cross-validation schemes. Cross-validation (CV) techniques create a random internal validation set by removing one (Leave-One-Out, LOO) or many (Leave-Many-Out, LMO) samples from the training set. The model is built on the training set and the removed samples are used to assess the model performances generating a confusion matrix that express sensitivity, specificity, and accuracy. Sensitivity is defined as the ratio between true positives (TP)

and all positives (P), while specificity is the ratio between true negative (TN) and all negatives (N). Accuracy is defined as the ratio between the sum of TP and TN, and the total population analyzed (P+N). Furthermore, permutation tests can be used to calculate the statistical significance of a model.

In order to find a metabolite or panels of metabolites that can be considered possible new biomarkers of a specific pathology or condition under investigation, each metabolite needs to be analyzed independently from all the other without considering any possible interactions. Univariate statistical analysis is the key to achieve this goal: statistical tests, correlation analysis and Receiver Operating Characteristic (ROC) curves are the most used approaches.

On the biological asymptotic assumption that metabolite concentrations are not normally distributed, non-parametric tests must be utilized. Wilcoxon Rank Sum test[56] is the non-parametric analogue of the t-test to compare two groups. The null hypothesis (H0) claims that two randomly selected samples from two populations actually belong to the same population, and as a consequence, their medians are equal; the alternative hypothesis (Ha) states that H0 is false and the two population are distinct, and therefore, their medians are different. It is worth mentioning that this test is nearly as efficient as the t-test on normal distributions, and a variant of this test, the Wilcoxon signed-rank test[57], also exists that is suited when comparing two related samples, matched samples, or repeated measurements on the same sample to assess whether their population median ranks differ. Kruskal-Wallis test[58] (analogue of the parametric analysis of variance) is the extension of the Wilcoxon Rank-Sum test for comparison of three or more groups.

The output of all these tests is a *P*-value: it expresses the probability of obtaining the same as, or of greater magnitude value than, the actual observed results, when the null hypothesis is true. Conventionally, when the *P*-value is less than the significance level of 0.05 or 0.01 the null hypothesis is rejected. However, since *P*-values are strongly dependent on the total number of analyzed samples, usually a huge number in metabolomics, multiple testing corrections need to be adopted: Bonferroni[59] and Benjamini-Hochberg[60] are the most widespread methods.

Furthermore, effect size analysis which is independent of the population size can be also performed. Effect size is a quantitative measure of the strength of a phenomenon and it expresses how different sample means are. For non-parametric data, like metabolite concentrations, Cliff's delta (d) is the utilized test[61], and it measures how often one value in one distribution is higher than the values in the second distribution. Cliff's delta ranges between +1 when all values of one distribution are higher than the ones of the other distribution, and -1 when reverse is true. Two overlapping distributions would have d of 0. According to the usual convention, an absolute value of d (|d|) lower than 0.147 means a negligible effect, |d| lower that 0.33 but larger than 0.147 means a small effect, |d| lower that 0.474 but larger than 0.33 means a medium effect, and |d| higher than 0.474 represents large effects.

ROC curves are graphical representations that illustrate the diagnostic ability of a binary classifier system as its discrimination threshold is varied (Figure 9A). These plots show false positives (1-specificity) on the horizontal axis, and the true positives on the vertical axis (sensitivity). Accuracy is measured by the area under the ROC curve (AUC). An area of 1 represents a perfect test; an area of 0.5 represents a worthless test. Pearson correlations can be calculated to test whether there is an association, understood as linear dependence, between metabolites and clinical data or biological features (Figure 9B). Correlations are expressed by a coefficient (R) which ranges between +1 (totally correlated), 0 (no correlation) and -1 (totally anticorrelated).

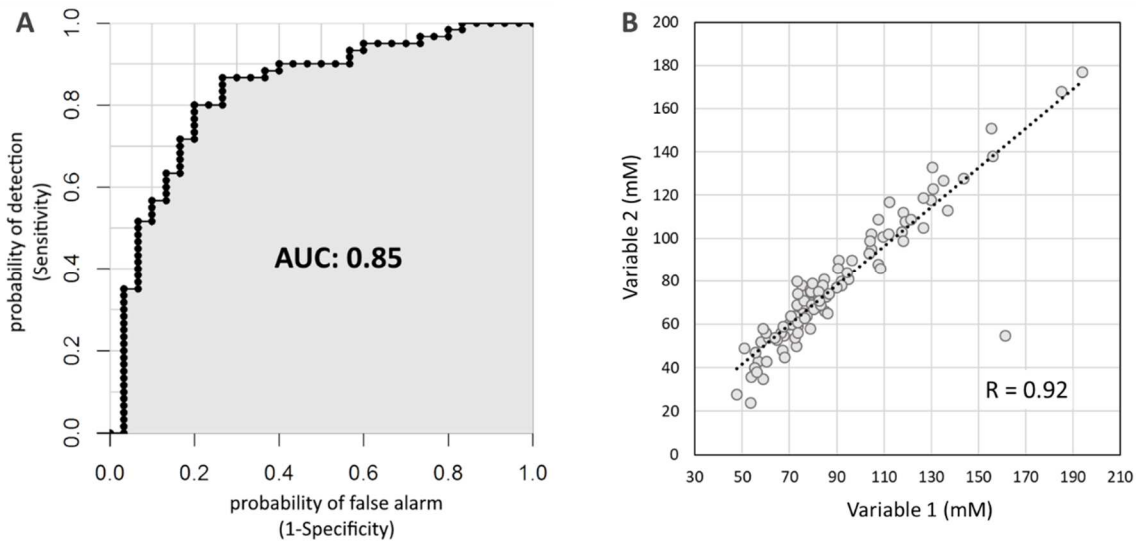

Figure 9. *Univariate statistical analyses: A) ROC curve; B) Pearson correlation of two variables.*

Chapter 4
Results

4.1 Metabolomics in molecular epidemiology

The usefulness of metabolomics for molecular epidemiology to build novel risk tests for screening and prevention is probably the most innovative topic explored in this work of thesis. Our studies demonstrated that the NMR-based metabolomic approach can be successfully applied to build statistical models able to predict the prognosis of early-stage breast cancer (eBC) and acute coronary syndrome (ACS) patients independently from traditional established clinicopathological risk factors.

In the precision medicine era, development of tailored oncological treatment for BC is lagging; moreover, clinical studies have clearly demonstrated that, although adjuvant chemotherapy improves disease free survival, many patients remain disease free after surgery alone[62]. The ability to discern between patients with eBC at high risk of disease recurrence, and those who need to be cured by locoregional therapy alone would represent an invaluable tool for clinicians, offering more aggressive adjuvant therapies to the former group and preventing the latter one from treatments whose benefit-risk ratio is poor. Metabolomics provides the analysis of subjects and their biological idiosyncrasies within the dynamic context of a disease process, considering both the effects that a cancer exerts upon an individual, and the individual upon the cancer, and therefore represents a valuable tool to stratify eBC patients.

We analyzed via NMR serum samples collected in the framework of two phase III breast cancer clinical trials run by the International Breast Cancer Research Foundation in South Asia and Africa for a total of eleven different hospitals involved; for this reason, as far, this study represents the broadest multicenter metabolomic breast cancer study published. The cohort of 699 breast cancer patients enrolled was divided according to the cancer stage in metastatic (109) and early (590) patients, among which 127

developed recurrence in the 6-years after surgery and tamoxifen treatment, and their serum samples were analyzed with the aim of predicting the real risk of disease relapse.

Our results (see paragraph 4.1.1) show not only that the serum metabolomic patterns can discriminate between early and advanced breast cancer patients (90% discrimination accuracy), but also that the score built using our model is prognostic for disease recurrence in a validation set (prediction accuracy 71%, AUC 0.747), independent of traditional risk factors (e.g. hormone receptor status, HER2 status, nodal status, tumor size). All these data confirmed the results published previously by our group in a smaller single center study[63]. Moreover, survival analysis of the early group (see paragraph 4.1.2), subdivided according to primary tumor size (T) and nodal status (N), particularly emphasized the performance of the metabolomic prediction within the T>1N0 group (hazard ratio [HR] 3.5, 95% CI 1.7-7.3; *P*=0.0012), probably the most complex for the decision of recommending - or not - adjuvant therapy.

In the same application field, we investigated the metabolomic fingerprint of acute coronary syndromes (ACS), the most common cause of emergency hospital admission also associated with the highest mortality and morbidity, by analyzing patient serum samples with the aim of evaluating the possible role of NMR metabolomics in the prognosis stratification. For this purpose, 978 serum samples of post ACS patients (samples were collected in the 24-48 h after the cardiovascular event) were analyzed according to their 2-year outcomes: 832 survivors and 146 deaths. We found that the metabolic fingerprint is able to discriminate patients who died within two years after the ACS event from long survivors (see paragraph 4.1.3) with a high accuracy (78.2% discrimination accuracy, 0.859 AUC) and this result was duplicate in a validation set (72.64% predictive accuracy, 0.801 AUC). To the best of our knowledge, this is the first study which assessed the capability of metabolomics to predict mortality in the setting of acute coronary syndromes. Furthermore, the score built using our model showed to be independent from the classical clinical parameters and the widely used GRACE (Global Registry of Acute Coronary Events) score, and to achieve better results in predicting all-cause death within two years from ACS considering both logistic regression and ROC analysis. Using a metabolomic profiling approach, we also found that short survivors are characterized by significantly higher levels of 3-hydroxybutyrate, proline, creatinine, acetate, acetone, formate and mannose, and significantly lower levels of valine and histidine.

Our data support the usefulness of the metabolomic approach to identify a more precise risk profile in ACS patients by identifying a metabolic fingerprint associated with a poor prognosis, and therefore, by recognizing those patients who need to undergo a very early and aggressive treatment.

4.1.1 *Serum metabolomic profiles identify ER-positive early breast cancer patients at increased risk of disease recurrence in a multicentre population*

Christopher D Hart[1]*, Alessia Vignoli[2]*, Leonardo Tenori[2,3], Gemma Uy[4], Ta Van To[5], Clement Adebamowo[6], S Mozammel Hossain[7], Laura Biganzoli[1], Emanuela Risi[1], Richard Love[8]**, Claudio Luchinat[2,9]**, Angelo Di Leo[1]**

*Contributed equally to the work (clinical and methodological first authors).
**Co-senior authors

[1] "Sandro Pitigliani" Medical Oncology Department, Hospital of Prato, Via Suor Niccolina 20, Istituto Toscano Tumori, 59100 Prato, Italy
[2] Magnetic Resonance Center (CERM), University of Florence, Via L. Sacconi 6, 50019 Sesto Fiorentino, Italy
[3] FiorGen Foundation, Via L. Sacconi 6, 50019 Sesto Fiorentino, Italy
[4] Philippine General Hospital, Manila, Philippines.
[5] Hospital K, Hanoi, Vietnam
[6] University College Hospital, Ibadan, Nigeria
[7] Khulna Medical College and Hospital, Khulna, Bangladesh
[8] The International Breast Cancer Research Foundation, USA
[9] Department of Chemistry, University of Florence, Via della Lastruccia 3, 50019 Sesto Fiorentino, Italy

Published in:
Clin. Cancer Res. Off. J. Am. Assoc. Cancer Res. **23**, 1422–1431 (2017).

Candidate's contributions: acquisition of NMR data, statistical analysis and interpretation of data, writing and review of the manuscript.

Personalized Medicine and Imaging

Clinical Cancer Research

Serum Metabolomic Profiles Identify ER-Positive Early Breast Cancer Patients at Increased Risk of Disease Recurrence in a Multicenter Population

Christopher D. Hart[1], Alessia Vignoli[2], Leonardo Tenori[2,3], Gemma Leonora Uy[4], Ta Van To[5], Clement Adebamowo[6], Syed Mozammel Hossain[7], Laura Biganzoli[1], Emanuela Risi[1], Richard R. Love[8], Claudio Luchinat[2,9], and Angelo Di Leo[1]

Abstract

Purpose: Detecting signals of micrometastatic disease in patients with early breast cancer (EBC) could improve risk stratification and allow better tailoring of adjuvant therapies. We previously showed that postoperative serum metabolomic profiles were predictive of relapse in a single-center cohort of estrogen receptor (ER)–negative EBC patients. Here, we investigated this further using preoperative serum samples from ER-positive, premenopausal women with EBC who were enrolled in an international phase III trial.

Experimental Design: Proton nuclear magnetic resonance (NMR) spectroscopy of 590 EBC samples (319 with relapse or ≥6 years clinical follow-up) and 109 metastatic breast cancer (MBC) samples was performed. A Random Forest (RF) classification model was built using a training set of 85 EBC and all MBC samples. The model was then applied to a test set of 234 EBC samples, and a risk of recurrence score was generated on the basis of the likelihood of the sample being misclassified as metastatic.

Results: In the training set, the RF model separated EBC from MBC with a discrimination accuracy of 84.9%. In the test set, the RF recurrence risk score correlated with relapse, with an AUC of 0.747 in ROC analysis. Accuracy was maximized at 71.3% (sensitivity, 70.8%; specificity, 71.4%). The model performed independently of age, tumor size, grade, HER2 status and nodal status, and also of Adjuvant! Online risk of relapse score.

Conclusions: In a multicenter group of EBC patients, we developed a model based on preoperative serum metabolomic profiles that was prognostic for disease recurrence, independent of traditional clinicopathologic risk factors. *Clin Cancer Res; 1–10. ©2016 AACR.*

Introduction

In the treatment of early breast cancer (EBC), risk stratification based on prognostic features is critical to decisions about the appropriate adjuvant strategy, in particular whether or not chemotherapy is warranted. Molecular profiling of the primary tumor has improved on traditional clinicopathologic risk stratification, yet still a significant proportion of "high risk" patients do not relapse and may receive chemotherapy unnecessarily (1–3). In addition to focusing on the characteristics of the primary cancer, an improved method to detect the actual presence of micrometastatic disease would help to identify those who might benefit from adjuvant therapies and those who may not.

Metabolomics is the study of metabolites (small molecules) in blood, tissue, or other biological samples, where the presence and relative concentrations of these molecules can be used as evidence of cellular processes and functions. Given that cancer cells can have significantly altered metabolism, the pattern of metabolites produced can yield a "signature" that may indicate the cancer's presence or behavior (4). Importantly, and in contrast to gene expression profiling as a risk stratifier, this is a signal that originates directly or indirectly from micrometastatic disease, rather than one derived from features of the primary tumor. Furthermore, the surrounding stroma and immune response may also contribute to an altered metabolomic profile, thus offering combined information on residual tumor and host response. A major challenge in metabolomics is detecting this signature against the dynamic sea of metabolic data from normal cellular function.

Several groups including our own have identified a metastatic "signature" in patients with advanced breast cancer, using nuclear magnetic resonance (NMR) spectra or mass spectrometry to analyze the metabolites in biological samples, primarily serum (5–7). We compared the NMR spectra of serum from a group of EBC patients and a group of metastatic breast cancer (MBC) patients and identified a metastatic signature that could differentiate the two groups (5).

[1]"Sandro Pitigliani" Medical Oncology Department, Hospital of Prato, Istituto Toscano Tumori, Prato, Italy. [2]Magnetic Resonance Center (CERM), University of Florence, Sesto Fiorentino, Italy. [3]FiorGen Foundation, Sesto Fiorentino, Italy. [4]Philippine General Hospital, Manila, Philippines. [5]Hospital K, Hanoi, Vietnam. [6]University College Hospital, Ibadan, Nigeria. [7]Khulna Medical College and Hospital, Khulna, Bangladesh. [8]The International Breast Cancer Research Foundation, Madison, Wisconsin. [9]Department of Chemistry, University of Florence, Sesto Fiorentino, Italy.

Note: Supplementary data for this article are available at Clinical Cancer Research Online (http://clincancerres.aacrjournals.org/).

C.D. Hart and A. Vignoli contributed equally to this article.

R.R. Love, C. Luchinat, and A. Di Leo share senior authorship of this article.

Corresponding Author: Angelo Di Leo, Hospital of Prato, Via Suor Niccolina 20, Prato 59100, Italy. Phone: 3905-7480-2520; Fax: 3905-7480-2903; E-mail: angelo.dileo@uslcentro.toscana.it

doi: 10.1158/1078-0432.CCR-16-1153

Translational Relevance

Adjuvant chemotherapy in early breast cancer improves survival by targeting micrometastatic disease. Because of difficulties in detecting such a disease in patients, there is a tendency to overtreat, meaning that many patients receive chemotherapy unnecessarily, with substantial morbidity. We hypothesize that the combined altered cellular behavior of micrometastatic disease, supporting stroma and host response, results in a unique, detectable pattern of metabolites (metabolomic profile) similar to that seen in advanced disease and that it correlates with relapse. Here, using serum taken from premenopausal women enrolled in two phase III trials, and using nuclear magnetic resonance spectroscopy, we show that patients with metabolomic profiles more resembling the metastatic profile have a higher rate of relapse. Metabolomics thus has the potential to identify patients with micrometastatic disease, improve risk stratification, and reduce overprescription of chemotherapy.

From there, we hypothesized that EBC patients with micrometastatic disease may also have features of the metastatic signature in their metabolomic profile, whereas those with no micrometastatic disease would not, and that this signature would predict for relapse. This hypothesis was tested in a follow-up study using serum from a biobank of estrogen receptor–negative (ER^-) patients from the Memorial Sloan Kettering Cancer Center (New York, NY), for whom clinical outcome (relapse at 5 years) was known (8). A model was built in which EBC patients were assigned a metabolomic risk score [Random Forest (RF) risk score], which was a function of the likelihood that they would be misclassified as metastatic based on their serum NMR spectra. Again, we were able to demonstrate that EBC and MBC profiles differed, but importantly, we also demonstrated that the RF risk score could predict relapse, independent of traditional clinicopathologic risk factors, in this single-center group of ER^- EBC women.

In this current study, we aimed to test the RF risk score again as a predictor of relapse in a large group of premenopausal EBC patients with ER-positive (ER^+) disease taking part in a multicenter adjuvant trial.

Patients and Methods

This retrospective study was a collaborative project among the International Breast Cancer Research Foundation, the University of Florence Magnetic Resonance Centre (Florence, Italy), and the Sandro Pitigliani Medical Oncology Department, Hospital of Prato (Prato, Italy). The study protocol received ethics approval from the ethics committee of the Hospital of Prato.

Patient selection

Serum samples for analysis were obtained from a bank of blood samples that had been collected during a phase III adjuvant breast cancer clinical trial (NCT00201851; ref. 9) and a parallel phase III MBC clinical trial (NCT00293540; ref. 10) conducted at centers across South East Asia. Both the trials were run by the International Breast Cancer Research Foundation.

In the adjuvant trial, 740 premenopausal women with stage II–IIIB hormone receptor (HR)–positive breast cancer received surgical oophorectomy at the time of breast cancer surgery (mastectomy), followed by tamoxifen for 5 years, to investigate the hypothesis that surgery performed during the luteal phase of the menstrual cycle would be associated with better outcomes. At the time of enrollment, 231 patients were estimated to be in the luteal phase and were scheduled for immediate surgery; 509 patients were estimated not to be in the luteal phase and were randomized to receive either immediate surgery or surgery scheduled to occur in the predicted mid-luteal phase (9). Blood samples were collected preoperatively in fasted patients on the day of surgery. Frozen sera were initially stored at local sites and then shipped frozen to the United States. Subsequently specimens were shipped still frozen to Italy. No patients were recorded as diabetic. The trial was designed to follow patients for recurrence for at least 6 years, and deidentified clinical outcome data were made available for the purposes of this study. The study was approved at individual participating institutions in the Philippines, Vietnam, and Morocco and/or by supervising Institutional Review Boards for these institutions and at lead investigator's American institutions. The consent processes addressed the use of samples for future research studies.

In the metastatic trial, premenopausal patients with ER^+ MBC were randomized to undergo oophorectomy surgery as palliative endocrine therapy in either the follicular or the luteal phase of the menstrual cycle, followed by tamoxifen (10). Blood samples were collected preoperatively from fasted patients on the day of surgery. Frozen sera were initially stored at local sites and then shipped frozen to the United States. Subsequently specimens were shipped still frozen to Italy. Diabetic status of patients was not recorded.

NMR sample preparation

Frozen serum samples were thawed at room temperature and shaken before use and then were prepared according to standard operating procedures (11).

A total of 300 μL of sodium phosphate buffer (70 mmol/L Na_2HPO_4; 20% (v/v) ^2H_2O; 0.025% (v/v) NaN_3; 0.8% (w/v) sodium trimethylsilyl [2,2,3,3-$^2H_4$]propionate pH 7.4) was added to 300 μL of each serum sample, and the mixture was homogenized by vortexing for 30 seconds. A total of 450 μL of this mixture was transferred into a 4.25-mm NMR tube (Bruker BioSpin srl) for the analysis.

NMR analysis

Monodimensional 1H NMR spectra for all samples were acquired using a Bruker 600 MHz spectrometer (Bruker BioSpin) operating at 600.13 MHz proton Larmor frequency and equipped with a 5-mm CPTCI 1H-13C-31P and 2H-decoupling cryoprobe, including a *z*-axis gradient coil, an automatic tuning-matching, and an automatic sample changer. A BTO 2000 thermocouple served for temperature stabilization at the level of approximately 0.1 K at the sample. Before measurement, samples were kept for at least 3 minutes inside the NMR probehead for temperature equilibration (310 K for serum samples).

According to standard practice (12, 13), three monodimensional 1H NMR spectra with different pulse sequences were acquired for each serum sample, allowing the selective detection of different molecular components:

(i) a standard nuclear Overhauser effect spectroscopy pulse sequence NOESY 1Dpresat (noesygppr1d.comp; Bruker BioSpin) using 64 scans, 98,304 data points, a spectral width of 18,028 Hz, an acquisition time of 2.7 seconds, a relaxation delay of 4 seconds, and a mixing time of 0.1 second was applied to obtain a spectrum in which both signals of metabolites and high molecular weight macromolecules (lipids and lipoproteins) are visible.

(ii) a standard spin echo Carr–Purcell–Meiboom–Gill (CPMG; ref. 14; cpmgpr1d.comp; Bruker BioSpin) pulse sequence with 64 scans, 73,728 data points, a spectral width of 12,019 Hz, and a relaxation delay of 4 seconds was used for the selective observation of low molecular weight metabolites, suppressing signals arising from macromolecules.

(iii) a standard diffusion-edited (ledbgppr2s1d.comp; Bruker BioSpin; ref. 15) pulse sequence, using 64 scans, 98,304 data points, a spectral width of 18,028 Hz, and a relaxation delay of 4 seconds was applied to suppress metabolite signals.

Spectral processing

Free induction decays were multiplied by an exponential function equivalent to a 1.0-Hz line-broadening factor before applying Fourier transformation. Transformed spectra were automatically corrected for phase and baseline distortions and calibrated (anomeric glucose doublet at 5.24 ppm) using TopSpin 3.2 (Bruker Biospin srl). Each 1D spectrum in the range 0.2 to 10.00 ppm was segmented into 0.02-ppm chemical shift bins, and the corresponding spectral areas were integrated using AMIX software (version 3.8.4, Bruker BioSpin). Binning is a means to reduce the number of total variables and to compensate for small shifts in the signals, making the analysis more robust and reproducible (16, 17). Regions between 4.5 and 6.5 ppm containing residual water signal were removed, and the dimension of the system was reduced to 391 bins. The total spectral area was calculated on the remaining bins, and total area normalization was carried out on the data prior to pattern recognition.

Statistical analysis

Statistical analyses were planned prior to specimen retrieval, based on those performed in the previous study, including minimum number of samples required (8). All data analyses were performed using R (18). Principal component analysis (PCA) was used first as an unsupervised exploratory analysis to assess the presence of any clusters or outliers.

To confirm that serum metabolomic profiles can be used to distinguish patients with MBC from those with early disease, an RF classifier (19) was built to separate early and metastatic patients. For the initial model, the group of EBC patients who had relapsed or had minimum 5 years clinical follow-up was randomly split into two groups, to form a training set and a validation set, as in the previous study (8). Briefly, the RF classifier uses data from the metastatic and training set to build an ensemble of decision trees, where each tree contains a random sample of the original data, with only a small number of variables (bins) at each decision node, used to predict whether a sample is early or metastatic. For early patients, a score was created that expresses the extent to which the serum metabolomic profile appears to be metastatic, designated as the "RF risk score." For each patient, three "RF risk scores" were derived using the three types of spectra (NOESY1D, CPMG, and diffusion-edited spectra). For all calculations, the R package "Random Forest" (20) was used to grow a forest of 1,000 trees, using the default settings.

The next step was to test the hypothesis that a metastatic metabolomic signature in early disease would be predictive of relapse and that higher RF relapse scores would correlate with higher risk of developing a relapse. Using ROC analysis, the performance of the RF risk score was compared with actual breast cancer outcome. A prognostic model was created using the CPMG RF risk score, which had the best performance in the training set. To delineate high risk of relapse, a cutoff for the RF risk score was calculated in the training set that optimized accuracy, sensitivity, and specificity, and the performance of the model was subsequently tested in the validation set.

Multivariate analysis of the impact of provenance of the sample was achieved using unsupervised PCA of the spectra. When this impact was found to be significant, the model for relapse prediction was redesigned:

(i) We hypothesized that samples from different clinical sites had been collected or stored following different operating procedures (e.g., longer periods from collection to sera separation and freezing, or different freezing temperatures), and that this may be reflected in the metabolomic spectra. As reported in the literature (11), lactate (coupled with pyruvate and glucose) is the most sensitive marker for sample degradation. To overcome this influence, we removed the bins related to lactate from the data matrix.

(ii) The nonrelapsing patients included in the analysis were restricted to those with a minimum follow-up of 6 years, as HR^+ breast cancer has a relatively steady relapse rate for at least 10 years.

(iii) Finally, we chose to include in the training set only women who had not developed a recurrence, to reduce the likelihood of confounding factors due to the presence of patients with micrometastases in the model. Thus, ROC analysis could only be carried out on the subsequent test set of relapsed and nonrelapsed patients.

Assessment of confounding factors (e.g., age, tumor size, nodal status, etc.) within the spectra was performed by using the multivariate RF classifier analysis to determine whether spectra could be predictive of each factor. The independent prognostic capacity of the redesigned RF risk score model was evaluated in a multivariate analysis controlling for standard prognostic features, which also included an Adjuvant! Online (AoL) risk of relapse score. The AoL score was calculated for 10-year risk of relapse assuming no adjuvant therapy and was used as a surrogate combined clinicopathologic risk.

For the analysis of individual metabolites, the spectral regions related to 22 metabolites were assigned in the ^{1}H CPMG NMR profiles by using matching routines of AMIX 3.8.4 (Bruker BioSpin) in combination with the BBIOREFCODE (Bruker BioSpin) and the Human Metabolome Database (21). The spectral regions were fitted and integrated to obtain the concentration in arbitrary units, and these data were used to compare metabolite concentrations between EBC and MBC patients. Wilcoxon signed-rank test (22) was chosen to perform the analysis on the biological asymptotic assumption that the metabolite concentrations are not normally distributed, and FDR correction was applied using the Benjamini–Hochberg method (23). $P < 0.05$ was deemed significant. Because of the method used to generate spectra, NMR profiles could not be used to measure individual lipid concentrations, nor metabolites in very small concentrations, such as acylcarnitines.

Results

Patients

Serum samples from 675 women with EBC and 125 with MBC were received. Of these, 101 samples were deemed nonevaluable for technical reasons (plasma instead of serum, inadequate amount of serum, hemolysis, and insufficient clinical information), leaving 590 EBC and 109 MBC samples suitable for NMR spectroscopy to build metabolomic profiles. Baseline characteristics are reported in Table 1.

Provenance of samples

EBC samples came from 5 centers in the Philippines and 2 centers in Vietnam; MBC samples came from 5 centers in the Philippines, 3 centers in Bangladesh, and one in Nigeria (Table 2). Notably, no MBC samples came from Vietnam, and only 24 came from Philippine General Hospital in Manila, yet these centers contributed the majority of EBC samples, representing significant imbalance.

Discrimination between EBC and MBC patients

Using the RF classifier for supervised analysis, the metabolomic profiles of 590 EBC and 109 MBC patients were classified, and show significant differential clustering, with near-complete separation of the two groups (Fig. 1). Clustering was achieved by the CPMG, NOESY1D, and diffusion spectra.

As in the previous studies (5, 8), the clustering provided by the CPMG spectra shows the highest accuracy for predicting early or metastatic status, with accuracy of 90.3% [95% confidence interval (CI), 90.2%–90.4%], compared with 86.8% (95% CI, 86.7%–86.8%) for NOESY1D, and 84.4% (95% CI, 84.3%–84.5%) for diffusion edited. Only results for CPMG spectra will be reported from here on.

Relapse prediction by RF score

A metabolomic RF risk score for each EBC sample was generated on the basis of the probability that the NMR spectrum would be classified as metastatic. The initial model was built using the same parameters as in the previous study, using CPMG spectra and only including EBC samples from patients who either relapsed or were relapse free with a minimum of 5 years clinical follow-up data (total 443). The training set consisted of 68 relapsed and 41 nonrelapsed EBC patients chosen at random and all 109 metastatic patients. The validation set consisted of the remaining 124 relapsed and 210 nonrelapsed EBC patients. The AUC obtained for the training set was 0.644, and the accuracy of the RF risk score was maximized using a threshold of 0.18, which yielded sensitivity of 61.3% (95% CI, 60.3%–62.2%), specificity of 61.0% (95% CI, 60.6%–61.3%), and overall accuracy for predicting likelihood of relapse of 61.1% (95% CI, 60.6%–61.6%; Supplementary Fig. S1A). The model was then applied to the validation set, using the RF risk score threshold of 0.18, achieving a sensitivity, specificity, and predictive accuracy of 71.7%, 46.7%, and 62.4%, respectively, and an AUC of 0.631 (Supplementary Fig. S1B).

In view of the low AUC results, investigation of the effect of provenance (collection center) and length of follow-up was carried out.

Exploratory unsupervised PCA of the CMPG spectra showed marked differentiation among the different centers of collection (Supplementary Fig. S2A), with the spectral region of lactate resulting in the most relevant discrimination in the first two principal components. Lactate concentrations, calculated in arbitrary units from the spectra, differed significantly between EBC and MBC patients (Table 3), demonstrating the key role of lactate in both discrimination of EBC and MBC and in the identification of treatment centers. This finding was consistent with our hypothesis regarding differences in storage and handling between treatment centers in our samples.

Relapse prediction by RF score—optimized model

To overcome the influence of lactate, we removed the bins related to this metabolite from the data matrix. The PCA score plot (Supplementary Fig. S2B) calculated using this reduced data matrix shows greatly reduced dispersion of the data points. This observation is confirmed by calculating the generalized variance (24) of the first three PCA components. This value (calculated as the determinant of the covariance matrix) represents the volume of the ellipsoid containing the data. Using the complete data matrix, we obtain a generalized variance of 16.8, whereas for the reduced data matrix, the generalized variance is 11.8, illustrating that removal of the bins corresponding to lactate indeed reduced spreading of the data, thus reducing the location effect.

The EBC cohort was restricted to those with relapse or minimum 6 years follow-up, which reduced the sample size to 319. In this new model, the training set consisted of 85 early patients without relapse (randomly selected) and all 109 metastatic patients. The test set contained 192 early patients that suffered relapse and the remaining 42 relapse-free early patients.

Using the CPMG NMR spectra, the RF classifier discriminated EBC from MBC patients in the training set with sensitivity, specificity, and predictive accuracy of 90.0% (95% CI 89.7%–90.3%), 84.9% (95% CI 84.7%–85.1%), and 87.1% (95% CI 86.9%–87.3%), respectively (Fig. 2A). This new model was then applied to the test set to assess ability to predict relapse, attaining an AUC of 0.747. The accuracy of the RF risk score was maximized using a threshold of 0.235, which yielded sensitivity of 70.8%, specificity of 71.4%, and overall accuracy for predicting likelihood of relapse of 71.3% (Fig. 2B). AUC scores for NOESY1D and diffusion-editing spectra were inferior, at AUC 0.706 and 0.617, respectively.

The AUC score calculated on the RF score was assessed for significance against the null hypothesis of no prediction accuracy in the data, by means of 10,000 randomized class permutation tests. The estimate AUC score obtained after randomization is 0.531 (95% CI, 0.53–0.531), demonstrating the significance of our result (AUC, 0.747; $P = 1.63 \times 10^{-20}$) despite the problems encountered.

Comparison with known prognostic factors

The known prognostic factors age, tumor size (0–2 cm, 2.1–5 cm, >5 cm), nodal status (0, 1–3, >3), histologic grade, and HER2 overexpression were compared with the CPMG RF risk score, calculated on the optimized set, in univariate and multivariate regression analyses (Table 4). We also compared the RF risk score with the 10-year risk of recurrence as calculated by AoL in a separate multivariate analysis. In all cases, the RF risk score maintained independent prognostic value.

Similarly, using RF classification to predict individual prognostic features based on the CPMG NMR spectra, none of these features could be meaningfully discriminated (Supplementary Fig. S3). Only the tumor size showed a weak concordance with the

Table 1. Patients and tumor characteristics for EBC and MBC cohorts, including populations restricted to include only relapsed patients or those with clinical follow-up greater than 5 or 6 years

Characteristic	EBC all	EBC – relapsed or follow-up ≥5 years	EBC – relapsed or follow-up ≥6 years	MBC
Number	590	443	319	109
Age, mean (range)	42 (29–50)	42 (29–50)	42 (29–50)	39 (22–53)
Tumor size, *n* (%)				
<2 cm	35 (5.9)	23 (5.2)	11 (3.5%)	—
2–5 cm	396 (67.1)	285 (64.3)	203 (63.6%)	
>5 cm	159 (27)	135 (30.5)	105 (32.9%)	
Grade, *n* (%)				
I	74 (13)	63 (14)	46 (14)	—
II	300 (51)	224 (51)	162 (51)	
III	115 (19)	89 (20)	73 (23)	
Unknown	101 (17)	67 (15)	38 (12)	
Lymph node status, *n* (%)				
0	248 (42)	166 (37.5)	106 (33)	—
1–3	157 (27)	121 (27.5)	83 (26)	
>3	185 (31)	156 (35)	130 (41)	
HER2, *n* (%)				
Positive	108 (18)	90 (20.5)	76 (24)	—
Negative	388 (66)	298 (67)	210 (66)	
Unknown	94 (16)	55 (12.5)	33 (10)	
ER, *n* (%)				
Positive	552 (93.6)	410 (92.6)	297 (93)	—
Negative	37 (6.3)	32 (7.2)	22 (7)	
Unknown	1 (0.2)	1 (0.2)	0 (0)	
PR, *n* (%)				
Positive	545 (92.4)	405 (91.4)	291 (91)	—
Negative	44 (7.4)	37 (8.4)	28 (9)	
Unknown	1 (0.2)	1 (0.2)	0 (0)	
Treatment arm, *n* (%)				
A	186 (31.5)	142 (32.0)	106 (33.2)	—
B	216 (36.6)	158 (35.7)	111 (34.8)	
C	188 (31.9)	143 (32.3)	102 (32.0)	
Dominant metastatic site, *n* (%)				
Soft tissue	—	—	—	79 (72.5)
Bone				17 (15.6)
Viscera				13 (11.9)
Prior systemic treatment, *n* (%)				
No	—	—	—	69 (63.3)
Yes				40 (36.7)

NOTE: Treatment arm A: not in luteal phase at the time of trial entry, randomized to luteal phase surgery; treatment arm B: not in luteal phase at the time of trial entry, randomized to immediate, non-luteal phase surgery; and treatment arm C: in luteal phase at the time of trial entry, immediate surgery in luteal phase.
Abbreviation: PR, progesterone receptor.

CPMG RF risk score (coefficient of correlation = 0.18; P value corrected with Bonferroni = 0.02).

Metabolite analysis

NMR spectra were analyzed to identify which metabolites were contributing to discrimination of MBC and EBC profiles. In the combined multicenter populations (Table 3), compared with EBC patients, patients with MBC are characterized by higher serum levels (adjusted $P < 0.05$) of citrate, choline, acetate, formate, lactate, glutamate, 3-hydroxybutyrate, phenylalanine, glycine, leucine, alanine, proline, tyrosine, isoleucine, creatine, creatinine, and methionine and lower serum levels (adjusted $P < 0.05$) of glucose and glutamine. In single-center analysis (Supplementary Table S1), citrate, formate,

Table 2. Distribution of EBC and MBC samples by treatment center

Country	Samples, *n*	EBC samples, *n*	MBC samples, *n*
Vietnam, Hanoi - Hospital K	228	228	—
Vietnam, Danang - Danang General	14	14	—
Philippines, Manila - PGH	302	278	24
Philippines, Cebu - Vicente Sotto Hospital	39	26	13
Philippines, Manila - Santo Tomas Hospital	9	3	6
Philippines, Manila - Rizal	20	15	5
Philippines, Manila - East Avenue	29	26	3
Nigeria, Ibadan - University College Hospital	8	—	8
Bangladesh, Dhaka - Dhaka Medical College	15	—	15
Bangladesh, Khulna - Khulna Medical College	28	—	28
Bangladesh, Dhaka - BSMMU	7	—	7
Total	699	590	109

Abbreviations: BSMMU, Bangabandhu Sheikh Mujib Medical University; PGH, Philippine General Hospital.

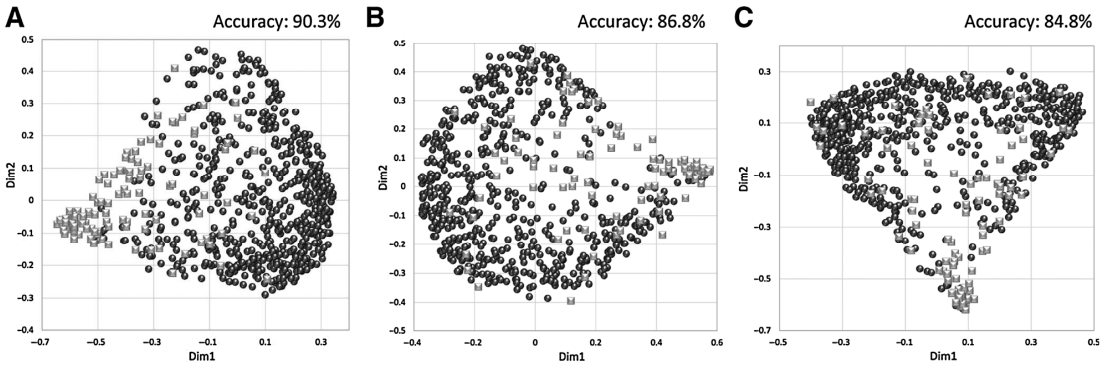

Figure 1.
Clustering of serum metabolomic profiles. Discrimination between EBC (black circles, $n = 590$) and MBC (gray squares, $n = 109$) patients using the RF classifier. **A–C,** CPMG (**A**), NOESY1D (**B**), and diffusion (**C**).

methionine, and phenylalanine were significantly higher in MBC patients. Others were numerically higher, consistent with the multicenter populations, but low patient numbers limit statistical significance.

In the cohort of EBC patients with relapse or follow-up of at least of 6 years (those included in the RF models), the patients who developed a recurrence were characterized by higher serum levels (adjusted $P < 0.05$) of choline, phenylalanine, leucine, histidine, glutamate, glycine, tyrosine, valine, lactate, and isoleucine but lower levels of glutamate (Supplementary Table S2). In the RF risk score algorithm, bins corresponding to phenylalanine, histidine, a lipid fraction (undifferentiated), methionine, glutamate, acetone, and formate carried the most weight in descending order of rank.

Discussion

Risk stratification in EBC for the purpose of deciding whether to recommend adjuvant therapies is of great importance, not least because of the significant toxicity associated with such treatment. For those at low risk of relapse, the risk of harm may outweigh the absolute risk of benefit.

The purpose of adjuvant therapy is to treat suspected residual micrometastatic disease. Yet, current prognostic factors and algorithms, including modern genomic signatures, are extrapolated from features of the primary tumor, surrogate markers for the likelihood of micrometastatic disease being present and progressing to an incurable state. Importantly, however, even among high-risk populations, a substantial proportion of patients is

Table 3. Comparison of individual metabolite concentrations in arbitrary units in the serum NMR spectra of EBC and MBC patients, for all patients included in the study

		All hospitals				
		EBC		MBC		
		Median	MAD	Median	MAD	*P*
Choline		329.82	533.53	1,607.25	1,953.73	2.88E−16
Acetate		272.09	177.43	512.38	220.30	6.11E−14
Formate		10.37	3.00	18.83	8.21	3.63E−20
Lactate		1,240.10	334.19	2,117.70	659.71	1.57E−24
Glutamate		269.60	121.22	431.99	154.55	1.59E−13
3-Hydroxybutyrate		88.30	58.74	134.81	81.05	8.53E−03
Phenylalanine		253.18	71.80	374.63	106.38	1.17E−16
Glycine	Higher	817.54	224.84	1,148.41	314.98	2.69E−14
Leucine	levels in	585.41	178.33	770.75	288.17	4.59E−06
Alanine	MBC	1,920.95	376.40	2,384.07	511.61	1.19E−07
Proline		97.38	30.84	114.99	43.44	5.59E−03
Tyrosine		156.48	36.38	182.26	42.73	4.59E−06
Isoleucine		168.84	35.37	193.65	45.08	9.24E−04
Histidine		162.96	39.65	186.24	47.26	1.60E−03
Creatine		147.90	46.12	167.65	51.09	2.12E−02
Creatinine		194.25	38.19	216.27	48.55	5.59E−03
Methionine		118.72	27.45	127.43	32.47	3.65E−02
Citrate		111.84	22.22	118.77	42.60	>0.05
Valine		1,138.91	171.58	1,169.77	211.08	>0.05
Mannose	Higher	68.19	13.57	64.38	14.09	>0.05
Glucose	levels in	3,275.44	292.23	2,843.51	584.25	3.93E−08
Glutamine	EBC	105.32	40.11	80.67	45.68	3.59E−02

NOTE: Adjusted *P* values are for the significance of any difference between EBC and MBC.
Abbreviation: MAD, median absolute deviation.

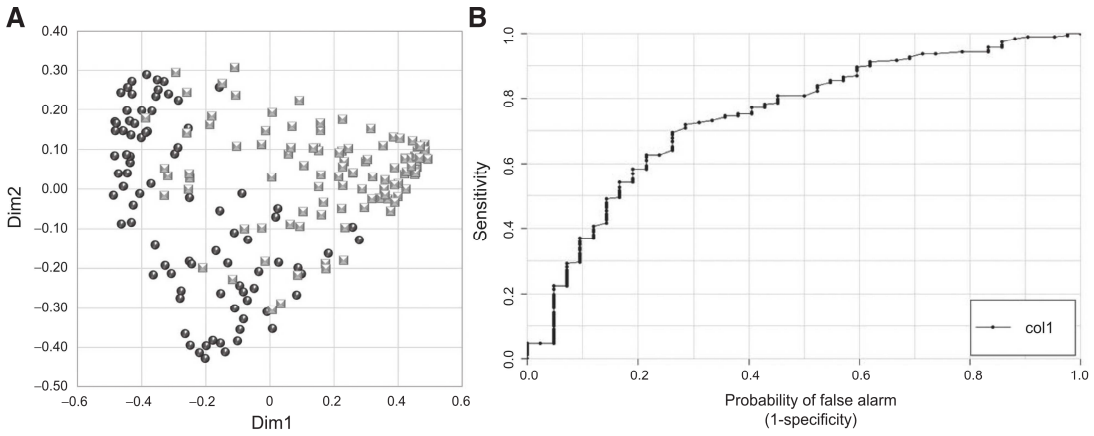

Confusion matrix:

	EBC	MBC
EBC	78	7
MBC	15	94

Confusion matrix:

	EBC No relapse	EBC Relapse
EBC No relapse	70.8	29.2
EBC Relapse	28.6	71.4

Figure 2.

A, discrimination between EBC patients without relapse for at least 6 years (black circles, $n = 85$) and MBC patients (gray squares, $n = 109$) using the RF classifier on CPMG spectra. The confusion matrix is also reported. **B,** prediction of relapse in the test set containing 192 EBC with relapse and 42 EBC without relapse up to 6 years. The ROC and AUC scores are presented for the RF risk score on CPMG spectra. The confusion matrix is also reported.

cured by surgery alone. In the seminal trial of adjuvant CMF versus no further treatment in women with node-positive EBC after primary cancer resection, 22% of untreated patients remained alive and disease free after a median of 28.5 years (1). In another study of ER^+, node positive, EBC patients stratified by Oncotype DX, 60% of those with a high Oncotype recurrence score remained disease free after 6 years, with only tamoxifen as adjuvant therapy (3). These nonrelapsing high-risk patients either had no micrometastatic disease to begin with or were able to control it without the use of chemotherapy. The ability to detect the presence of micrometastatic disease could greatly refine the selection of high-risk patients.

A theoretical advantage of metabolomics as a residual disease detector is its potential to capture not only signals from the micrometastatic disease, but also the surrounding stroma and any inflammatory/immune response. Other liquid biopsies, such as circulating tumor cells or plasma tumor DNA, will miss these host factors, potentially reducing sensitivity.

In this study, we were once again able to identify a metabolomic signal in the sera of EBC patients associated with increased risk of disease recurrence that is independent of standard risk factors, this time in a large, multicenter population. Our previous study was limited to a set of ER^- patients from the MSKCC biobank, with blood draws taken after resection of the primary cancer, but before commencement of adjuvant therapy (8). In the current study, all patients were HR^+, blood samples had been taken preoperatively, and patients came from multiple clinical sites in several countries, making this a new exploratory study rather than a confirmatory one. These differences introduced new challenges.

The effect of serum sample provenance was found to be the most discriminating feature of spectra. Causes for this may be multiple and include differences in the populations, such as diet or ethnicity, but may also reflect non-patient–related factors, such as specimen handling. Delays in centrifugation, insufficient or variable cooling, and unintentional thaw refreeze can affect the metabolic composition dramatically.

As noted in Table 2, only 5 centers collected samples both from EBC and MBC patients, and these samples are very few with respect to the total population of this study, while Vietnam provided a large proportion of EBC samples and no MBC samples. This large discrepancy, and resultant effect on spectra, would therefore be expected to induce an error in the building of the models (i.e., we are discriminating collection centers rather than EBC and MBC). Limiting the model to samples from a single site to control for location gave too few samples for meaningful analysis.

Controlling for lactate, a metabolite associated with suboptimal handling, removed much of the bias associated with location and thus may explain the cause. Lactate may also be affected by other metabolic factors. In this study, all patients were fasted as per preoperative protocol, reducing a dietary effect. Similarly, diabetes can have an effect if uncontrolled; to the best of our knowledge, there were no patients with diabetes in the EBC trial, but these data were lacking from the MBC trial. However, lactate is known to be altered in metastatic disease (7, 8), and indeed in this study, it differed between EBC and MBC patients and relapsing and nonrelapsing patients.

Examination of individual metabolites was performed to compare with results from other studies, but data must be interpreted with caution in light of the strong observed effect of provenance. A comparison of metabolites between EBC and MBC patients from a single center was also included, but small numbers of MBC

Table 4. ORs for prognostic features and RF risk score in the optimized set of EBC patients, using univariate and multivariate analysis

Characteristics	OR (univariate)	P	OR (multivariate)	P	OR (multivariate)	P
Age						
<43	1.0		1.0		—	—
>43	0.5205	5.06E−03	0.5429	0.0536		
Tumor size						
<2 cm	1.0		1.0		—	—
2–5 cm	2.1115	0.2447	3.5484	0.1458		
>5 cm	4.8124	0.0181	6.1417	0.0450		
Grade						
I	1.0		1.0		—	—
II	2.2533	0.0165	2.4557	0.0472		
III	2.2858	0.0319	2.0559	0.1512		
Lymph node status						
0	1.0		1.0		—	—
1–3	4.2742	3.40E−06	3.0661	0.0048		
>3	11.8770	5.57E−15	7.6775	1.38E−07		
HER2						
Negative	1.0		1.0		—	—
Positive	2.3243	5.52E−03	2.4567	0.0170		
ER						
Positive	1.0		1.0		—	—
Negative	0.9522	0.9130	1.3370	0.6822		
PR						
Positive	1.0		1.0		—	—
Negative	2.6099	0.0437	4.3288	0.0320		
Treatment arm						
A	1.0		1.0		—	—
B	0.8449	0.5522	0.7493	0.4606		
C	0.5563	0.0397	0.5666	0.1558		
AoL score						
≤52.7	1.0		—	—	1.0	
52.7–73.7	3.9519	2.04E−06			3.8740	7.13E−06
>73.7	12.9138	1.84E−13			15.308	1.18E−13
RF risk score						
<0.235	1.0		1.0		1.0	
>0.235	2.7991	1.59E−05	3.1224	0.0004	3.4768	7.84E−06

NOTE: AoL score split into tertiles. A multivariate analysis using only RF risk score and AoL score is also reported in the last two columns.
Abbreviation: PR, progesterone receptor.

patients affect statistical significance. Large numbers of metabolites were at significantly higher concentrations in MBC (Table 3), of which nine also correlated with relapse in the refined EBC cohort (Supplementary Table S2). Higher levels of phenylalanine were seen in MBC, in line with other studies (5, 6), and correlated with relapse in EBC. Similarly, higher glutamate in MBC is consistent with Jobard and colleagues' work (6) and correlated positively with relapse in EBC here. Histidine was higher in MBC compared with EBC, but in this case, it is at odds with three other studies (6–8) in which it was lower.

The fact that geographical differences impacted significantly on the construction of a discriminating model is reflective of a broader issue for this approach, related to the need to establish a specific metastatic profile for each new study population. For example, applying the RF risk model created on the MSKCC dataset (8) to the current study population yielded very poor accuracy, due to the fact that differences between samples were far greater than the differences between the respective EBC and MBC cohorts (Supplementary Fig. S4). This greatly limits the transferability of the current approach between populations, until common standard procedures for metabolomics are adopted and a more universal metastatic profile can be established. In this regard, further studies are warranted.

A limitation of the dataset used is the fact that a follow-up time of 5 or 6 years is insufficient to capture all relapses in an HR^+ EBC cohort, where relapse rates remain fairly constant for at least 10 years. Thus, there will be a proportion of EBC patients labeled as nonrelapsed who are in fact destined to relapse. Limiting the EBC cohort to patients with longer follow-up would be expected to improve on this but comes at the expense of a reduced sample size and was not possible here.

All patients in this study received systemic adjuvant endocrine therapy, making it impossible to know whether the therapy was directly responsible for the lack of relapse. An ideal series would have an arm with no intervention, although this is unlikely to be feasible for high-risk patients.

In this study, we were able to detect a signal correlated with recurrence despite the fact that the primary tumor was *in situ* at the time of blood draw. The presence and stage of the primary tumor might be expected to alter the metabolomic profile, and yet, the model predicted poorly for tumor size and nodal status, with little or no correlation. Whether the small correlation with size was as a direct result of the primary tumor or related to the fact that larger tumors are associated with higher risk of relapse, and thus may be a surrogate for presence of micrometastatic disease, is unknown. Part of our hypothesis is that the metabolomic signal correlating with residual disease, and thus relapse, is as much a reflection of the host state as it is of the presence of the tumor cells themselves, and our results support this.

Given the challenges of this study, in particular, the diversity of the populations and the fact that the bulk of the MBC and EBC sera came from different clinical sites, respectively, it is all the more compelling that a signal could be identified that discriminated between early and late breast cancer patients and that the RF risk score, essentially a measure of the "metastatic-ness" of the sera, correlated with relapse. Indeed, we see this study as complementary to the previous one because it suggests that the metabolomic score is relevant in predicting relapse in both ER^- and ER^+ patients, in both a single-center and in a multicenter setting.

What remains to be determined is whether the signal that correlates with relapse is truly a marker of micrometastatic disease or in fact reflective of the biological state of the primary tumor. Tumor-based genomic profiling assays, such as the 21-gene assay or MammaPrint, assess the expression of a number of genes to arrive at a risk of recurrence score, with those genes relating to proliferation playing a significant role. It is possible that differences in tumor gene expression state are also reflected in the metabolome, contributing to the metabolomic profile, in which case the metabolomic signals correlating with relapse may be dependent on the gene expression profile. It is vital then that future studies address this question, to examine whether metabolomics may provide independent, relevant prognostic information in the setting of genomic risk stratification, and we are investigating this currently. Given that a substantial proportion of patients designated as high-risk by genomic assays will not relapse, it would be invaluable to have a biomarker that might identify and restratify these patients. Ideally, this would be performed in prospective trials in which there is prespecified stratification by genomic risk score, where the metabolomic risk score could be tested for prognostic power within each risk group.

Disclosure of Potential Conflicts of Interest

A. Di Leo is a consultant/advisory board member for AstraZeneca, Bayer, Eisai, Genomic Health, Ipsen, Lilly, Novartis, Pfizer, and Pierre Fabre. No potential conflicts of interest were disclosed by the other authors.

Authors' Contributions

Conception and design: T.V. To, L. Biganzoli, R.R. Love, C. Luchinat, A. Di Leo
Development of methodology: L. Tenori, T.V. To, R.R. Love, A. Di Leo
Acquisition of data (provided animals, acquired and managed patients, provided facilities, etc.): A. Vignoli, G.L. Uy, T.V. To, C. Adebamowo, S.M. Hossain, R.R. Love
Analysis and interpretation of data (e.g., statistical analysis, biostatistics, computational analysis): C.D. Hart, A. Vignoli, L. Tenori, T.V. To, L. Biganzoli, R.R. Love, C. Luchinat, A. Di Leo
Writing, review, and/or revision of the manuscript: C.D. Hart, A. Vignoli, L. Tenori, T.V. To, C. Adebamowo, S.M. Hossain, L. Biganzoli, E. Risi, R.R. Love, C. Luchinat, A. Di Leo
Administrative, technical, or material support (i.e., reporting or organizing data, constructing databases): T.V. To, S.M. Hossain, R.R. Love
Study supervision: T.V. To, C. Adebamowo, R.R. Love, C. Luchinat, A. Di Leo

Acknowledgments

We acknowledge and thank the Sandro Pitigliani Foundation and the Breast Cancer Research Foundation for their generous support.

Grant Support

This study was supported by the Breast Cancer Research Foundation (to A. Di Leo). This work has also been partially supported by Fondazione Veronesi through the Post-Doctoral Fellowship-2015 (to L. Tenori).

The costs of publication of this article were defrayed in part by the payment of page charges. This article must therefore be hereby marked *advertisement* in accordance with 18 U.S.C. Section 1734 solely to indicate this fact.

Received May 6, 2016; revised August 24, 2016; accepted August 28, 2016; published OnlineFirst September 20, 2016.

References

1. Bonadonna G, Moliterni A, Zambetti M, Daidone MG, Pilotti S, Gianni L, et al. 30 years' follow up of randomised studies of adjuvant CMF in operable breast cancer: cohort study. BMJ 2005;330:217.
2. Paik S, Shak S, Tang G, Kim C, Baker J, Cronin M, et al. A multigene assay to predict recurrence of tamoxifen-treated, node-negative breast cancer. N Engl J Med 2004;351:2817–26.
3. Albain KS, Barlow WE, Shak S, Hortobagyi GN, Livingston RB, Yeh IT, et al. Prognostic and predictive value of the 21-gene recurrence score assay in postmenopausal women with node-positive, oestrogen-receptor-positive breast cancer on chemotherapy: a retrospective analysis of a randomised trial. Lancet Oncol 2010;11:55–65.
4. Claudino WM, Quattrone A, Biganzoli L, Pestrin M, Bertini I, Di Leo A. Metabolomics: available results, current research projects in breast cancer, and future applications. J Clin Oncol 2007;25:2840–6.
5. Oakman C, Tenori L, Claudino WM, Cappadona S, Nepi S, Battaglia A, et al. Identification of a serum-detectable metabolomic fingerprint potentially correlated with the presence of micrometastatic disease in early breast cancer patients at varying risks of disease relapse by traditional prognostic methods. Ann Oncol 2011;22:1295–301.
6. Jobard E, Pontoizeau C, Blaise BJ, Bachelot T, Elena-Herrmann B, Trédan O. A serum nuclear magnetic resonance-based metabolomic signature of advanced metastatic human breast cancer. Cancer Lett 2014;343:33–41.
7. Asiago VM, Alvarado LZ, Shanaiah N, Gowda GA, Owusu-Sarfo K, Ballas RA, et al. Early detection of recurrent breast cancer using metabolite profiling. Cancer Res 2010;70:8309–18.
8. Tenori L, Oakman C, Morris PG, Gralka E, Turner N, Cappadona S, et al. Serum metabolomic profiles evaluated after surgery may identify patients with oestrogen receptor negative early breast cancer at increased risk of disease recurrence. Results from a retrospective study. Mol Oncol 2015;9:128–39.
9. Love RR, Laudico AV, Van Dinh N, Allred DC, Uy GB, Quang le H, et al. Timing of adjuvant surgical oophorectomy in the menstrual cycle and disease-free and overall survival in premenopausal women with operable breast cancer. J Natl Cancer Inst 2015;107:djv064.
10. Love RR, Hossain SM, Hussain MM, Mostafa MG, Laudico AV, Siguan SS, et al. Luteal versus follicular phase surgical oophorectomy plus tamoxifen in premenopausal women with metastatic hormone receptor-positive breast cancer. Eur J Cancer 2016;60:107–16.
11. Bernini P, Bertini I, Luchinat C, Nincheri P, Staderini S, Turano P. Standard operating procedures for pre-analytical handling of blood and urine for metabolomic studies and biobanks. J Biomol NMR 2011;49:231–43.
12. Beckonert O, Keun HC, Ebbels TMD, Bundy J, Holmes E, Lindon JC, et al. Metabolic profiling, metabolomic and metabonomic procedures for NMR spectroscopy of urine, plasma, serum and tissue extracts. Nat Protoc 2007;2:2692–703.
13. Gebregiworgis T, Powers R. Application of NMR metabolomics to search for human disease biomarkers. Comb Chem High Throughput Screen 2012;15:595–610.
14. Meiboom S, Gill D. Modified spinecho method for measuring nuclear relaxation times. Rev Sci Instrum 1958;29:688–91.
15. Wu DH, Chen A. Three-dimensional diffusion-ordered NMR spectroscopy: the homonuclear COSY-DOSY experiment. J Magn Reson Ser A 1996;123:215–8.
16. Spraul M, Neidig P, Klauck U, Kessler P, Holmes E, Nicholson JK, et al. Automatic reduction of NMR spectroscopic data for statistical and pattern recognition classification of samples. J Pharm Biomed Anal 1994;12:1215–25.

17. Holmes E, Foxall PJ, Nicholson JK, Neild GH, Brown SM, Beddell CR, et al. Automatic data reduction and pattern recognition methods for analysis of 1H nuclear magnetic resonance spectra of human urine from normal and pathological states. Anal Biochem 1994;220:284–96.
18. Ihaka R, Gentleman RR. A language for data analysis and graphics. J Comput Stat Graph 1996;5:299–314.
19. Breiman L. Random forests. Mach Learn 2001;45:5–32.
20. Liaw A, Wiener M. Classification and regression by random forest. R News 2002;2:18–22.
21. Wishart DS, Jewison T, Guo AC, Wilson M, Knox C, Liu Y, et al. HMDB 3.0–The Human Metabolome Database in 2013. Nucleic Acids Res 2013;41:D801–7.
22. Wilcoxon F. Individual comparisons by ranking methods. Biom Bull 1945;1:80.
23. Benjamini Y, Hochberg Y. Controlling the false discovery rate: a practical and powerful approach to multiple testing. J R Stat Soc Ser B Methodol 1995;57:289–300.
24. Bagai OP. The distribution of the generalized variance. Ann Math Stat 1965;36:120–30.

Supplementary materials:

Supplementary figure S1 - Receiver operator characteristic (ROC) analysis of the RF risk score as a predictor of relapse in the initial cohort, for CPMG spectra: A) training set; B) validation set.

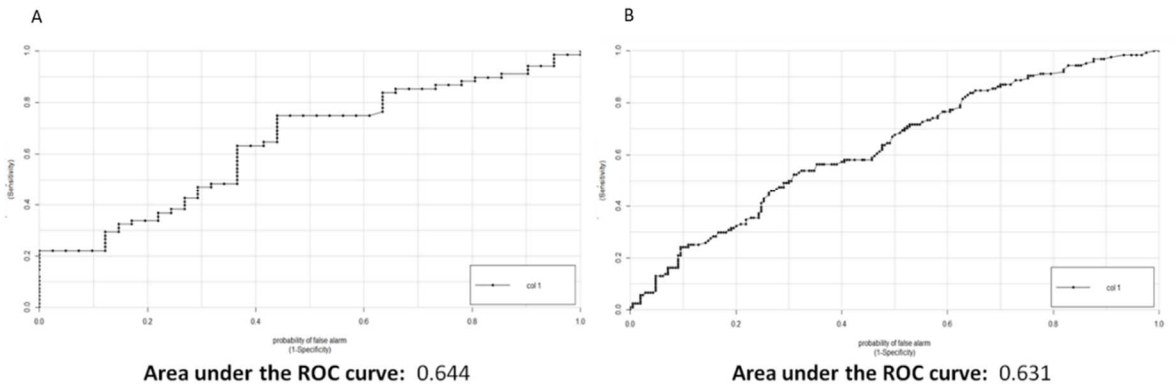

Supplementary figure S2 - Spectral clustering by treatment centre, demonstrated by score plots of the first three components of unsupervised PCA using (A) the entire dataset, and (B) the reduced data-matrix (bins related to lactate removed). In these plots each dot represents a 1H NMR CPMG patient spectrum. The colors represent the sample provenance: red, Vietnam, Hanoi - Hospital K; orange, Philippines, Manila - PGH; yellow, Vietnam, Danang - Danang General; green, Philippines, Cebu - Vicente Sotto Hospital; cyan, Philippines, Manila - Santo Tomaso Hospital; turquoise, Philippines, Manila - Rizal; sky blue, Philippines, Manila - East Avenue; blue, Nigeria, Ibadan - University College Hospital; purple, Bangladesh, Dhaka - Dhaka Medical College; magenta, Bangladesh, Khulna - Khulna Medical College; pink, Bangladesh, Dhara - BSMMU.

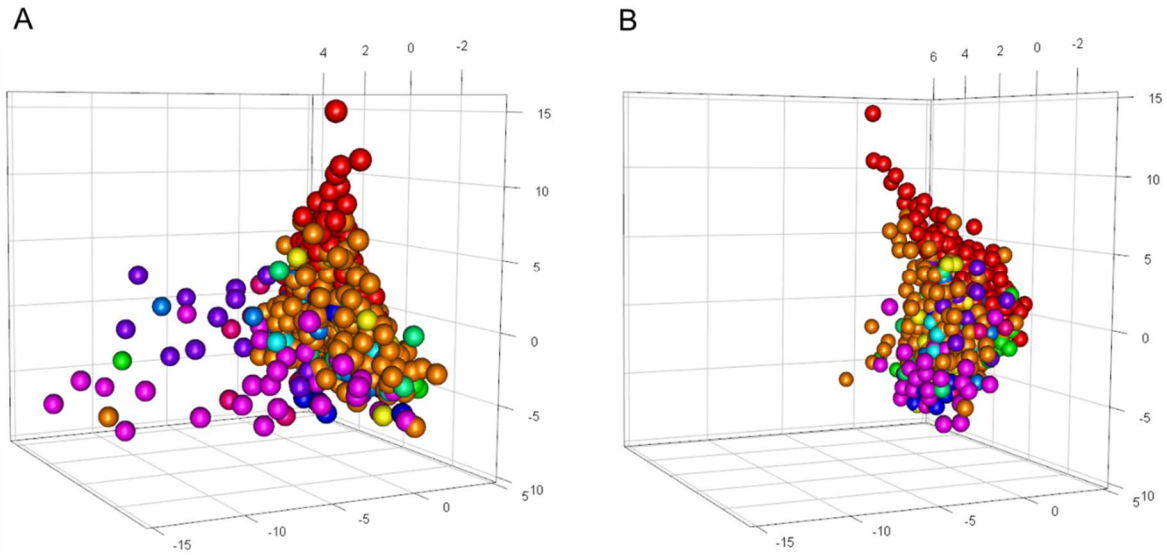

Supplementary figure S3 - Clustering of serum metabolomic profiles using Random Forest classification to discriminate EBC patients according to different clinicopathological parameters. This illustrates the degree to which each parameter influences the spectra. A) Age of patients, divided into two groups using the median age as threshold (red dots - age < 43 years; blue dots - age {greater than or equal to} 43 years); B) HER2 positivity (red dots - HER2 positive; blue dots - HER2 negative); C) Size of the tumor (red dots - size {less than or equal to} 5 cm; blue dots - size > 5 cm); D) Nodal status (red dots - node negative; blue dots - node positive); E) Grade of the tumor (red dots - grade 1; blue dots - grade 2; green dots - grade 3). For each analysis the confusion matrix is also reported.

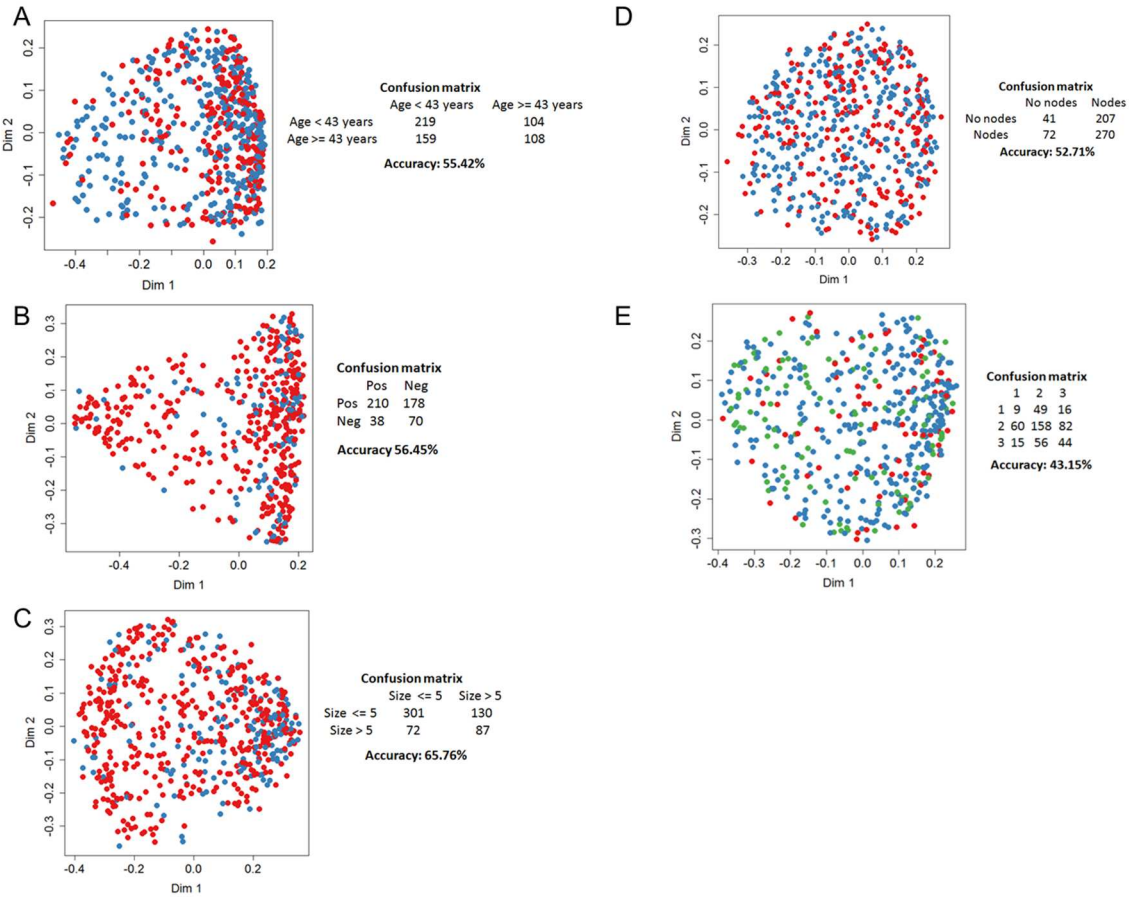

Supplementary figure S4 - Illustration of the significant differences in metabolomic spectra between serum samples from current study and those from the MSKCC cohort used in a previous study. Differences due to location far overwhelm differences between EBC and MBC spectra, and preclude the RF risk score from predicting relapse. A. Clustering of CPMG spectra using first two components of supervised PCA-CA. Each dot represents an EBC patient and each triangle a MBC patients. In red are reported the samples collected for this study and in green the MSKCC samples. The confusion matrix and the accuracy of the discrimination between the samples of the two studies are also reported. B. Predictive ability of the RF risk score developed on the MSKCC data set in the current cohort, using ROC analysis. AUC and the confusion matrix are presented for the CPMG RF scores, calculated using the model built on the MSKCC samples, in the test set.

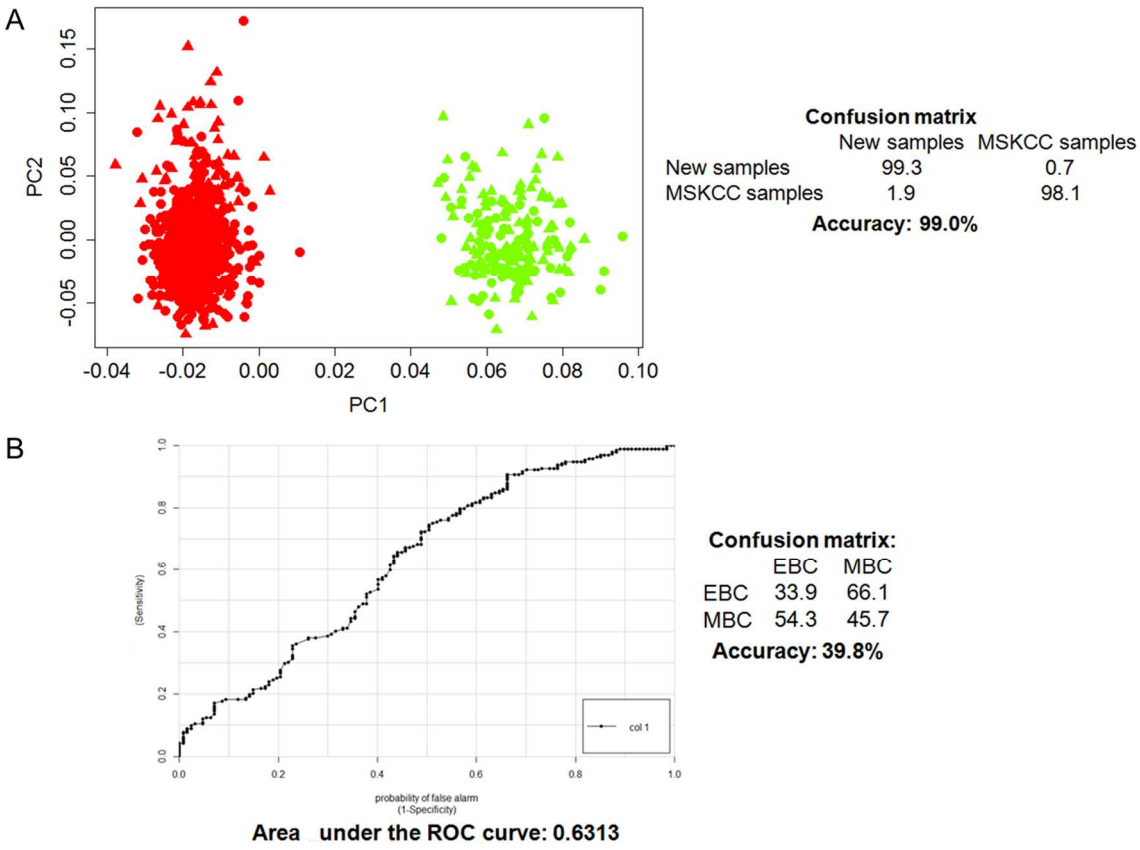

Supplemental Table S1 - Comparison of individual metabolite concentrations in arbitrary units in the serum NMR spectra of EBC and MBC patients, for a single centre (Philippines General Hospital - PGH). Adjusted P-values are for the significance of any difference between EBC and MBC. MAD = median absolute deviation.

		PGH				
		EBC		**MBC**		
		Median	**MAD**	**Median**	**MAD**	**P-value**
Choline	Higher levels in MBC	373.02	530.59	611.49	612.46	> 0.05
Methionine		112.32	25.28	144.36	25.44	2.23E-02
Formate		12.85	3.38	16.18	5.36	4.76E-02
Citrate		104	18.05	129.18	27.65	2.23E-02
Phenylalanine		313.47	78.57	379.41	57.07	2.23E-02
Lactate		1524.8	277.18	1774.02	435.75	> 0.05
Acetate		432.07	160.24	499.07	127.67	> 0.05
Glutamate		383.41	95.27	435.07	135.42	> 0.05
Glycine		965.14	276.75	1094.29	193.79	> 0.05
Leucine		719.97	210.22	811.03	199.2	> 0.05
Alanine		2151.05	368.72	2367.21	449.61	> 0.05
Mannose		67.74	13.79	73.23	17.16	> 0.05
Proline		96.51	25.34	103.75	33.78	> 0.05
Creatinine		189.83	34.73	200.97	62.74	> 0.05
Tyrosine		195.01	45.46	204.89	42.98	> 0.05
Isoleucine		194.88	41.6	198.94	41.48	> 0.05
Valine		1250.74	219.42	1274.87	282.54	> 0.05
Creatine		159	55.47	160.32	31.91	> 0.05
Glucose	Lower levels in MBC	3275.59	395.92	3209.56	433.32	> 0.05
Histidine		193.82	43.51	188.92	43.72	> 0.05
3-hydroxybutyrate		63.66	36.63	61.81	29.25	> 0.05
Glutamine		77.19	36.52	59.7	50.14	> 0.05

Supplementary Table S2 - Comparison of individual metabolite concentrations in arbitrary units in the serum NMR spectra of relapsing and non-relapsing EBC patients. Adjusted P-values for the comparison of relapsing and non-relapsing EBC Adjusted P-values are for the significance of any difference between EBC and MBC. MAD = median absolute deviation.

		EBC with recurrence		**EBC without recurrence**		**Adjusted P-value**
		Median	**MAD**	**Median**	**MAD**	
Phenylalanine	Higher levels in EBC with recurrence	265.537	74.807	191.621	43.661	5.66E-08
Leucine		637.139	192.335	460.075	94.221	1.09E-04
Histidine		173.526	46.016	136.511	23.005	1.09E-04
Glutamate		304.663	112.451	253.009	120.452	4.12E-02
Glycine		818.751	216.682	726.373	169.731	4.12E-02
Tyrosine		166.198	42.299	148.327	25.349	4.36E-03
Acetate		338.31	171.11	305.928	208.532	> 0.05
Formate		11.579	3.381	10.574	3.3	> 0.05
Lactate		1319.428	274.716	1209.747	319.439	4.83E-02
Valine		1176.013	205.037	1091.636	142.323	4.43E-02
Proline		93.228	26.273	86.778	22.181	> 0.05
Isoleucine		172.142	39.988	162.562	29.006	6.76E-03
Alanine		1946.47	399.423	1902.673	343.637	> 0.05
Choline		298.2	459.43	148.25	253.23	4.83E-02
Glucose	Lower levels in EBC with recurrence	3291.47	348.202	3297.304	262.102	> 0.05
Citrate		110.867	22.105	112.61	20.218	> 0.05
Methionine		114.868	25.027	117.193	26.012	> 0.05
Creatine		141.096	43.452	147.571	39.941	> 0.05
Mannose		67.697	13.56	71.275	13.901	> 0.05
Creatinine		185.727	36.025	196.867	35.02	> 0.05
3-Hydroxybutyrate		79.355	51.141	86.638	48.975	> 0.05
Glutamine		93.457	41.566	113.765	52.878	> 0.05

4.1.2 *De-escalating and escalating treatment beyond endocrine therapy in patients with luminal breast cancer*

Amelia McCartney[a], Alessia Vignoli[b], Christopher Hart[c], Leonardo Tenori[b,d], Claudio Luchinat[b,e], Laura Biganzoli[a], Angelo Di Leo[f]

[a] "Sandro Pitigliani" Medical Oncology Department, Hospital of Prato, Istituto Toscano Tumori, Prato, Italy.
[b] Magnetic Resonance Center (CERM), University of Florence, Sesto Fiorentino, Italy.
[c] St Vincents Hospital, 35 Victoria Parade, Fitzroy Victoria 3065, Australia.
[d] FiorGen Foundation, Via L. Sacconi 6, 50019, Sesto Fiorentino, Italy.
[e] Department of Chemistry, University of Florence, Via della Lastruccia 3, 50019, Sesto Fiorentino, Italy.
[f] Sandro Pitigliani" Medical Oncology Department, Hospital of Prato, Istituto Toscano Tumori, Prato, Italy.

Published in:
The Breast. doi:10.1016/j.breast.2017.06.021

Candidate's contributions: statistical analysis and interpretation of data, review of the manuscript.

ARTICLE IN PRESS

The Breast xxx (2017) 1–6

Contents lists available at ScienceDirect

The Breast

journal homepage: www.elsevier.com/brst

De-escalating and escalating treatment beyond endocrine therapy in patients with luminal breast cancer

Amelia McCartney [a], Alessia Vignoli [b], Christopher Hart [c], Leonardo Tenori [b, d], Claudio Luchinat [b, e], Laura Biganzoli [a], Angelo Di Leo [a, *]

[a] "Sandro Pitigliani" Medical Oncology Department, Hospital of Prato, Istituto Toscano Tumori, Prato, Italy
[b] Magnetic Resonance Center (CERM), University of Florence, Sesto Fiorentino, Italy
[c] St Vincents Hospital, 35 Victoria Parade, Fitzroy, Victoria 3065, Australia
[d] FiorGen Foundation, Via L. Sacconi 6, 50019, Sesto Fiorentino, Italy
[e] Department of Chemistry, University of Florence, Via della Lastruccia 3, 50019, Sesto Fiorentino, Italy

ARTICLE INFO

Article history:
Available online xxx

Keywords:
Luminal
Breast cancer
Adjuvant
Chemotherapy
Subtype
Prediction

ABSTRACT

Luminal breast cancers demonstrate significant molecular and clinical heterogeneity, despite the commonality of shared expression of the estrogen receptor (ER). To date, no clinical trial has prospectively investigated the optimal chemotherapy regime according to luminal type, highlighting a paucity of data furthermore required to guide treatment decisions. Current methods of predicting advantage from adjuvant chemotherapy lack refinement and can over-estimate the risk of relapse, inevitably leading to a proportion of patients being unnecessarily exposed to chemotherapy. This paper will explore the evidence behind modalities which may add further value to existing known clinicopathological and molecular profiling techniques in predicting clinical benefit from chemotherapy. Adjuvant chemotherapy regime choice in the context of early luminal breast cancer types will be discussed, and areas for further research and debate identified.

The issue of how best to identify patients who will benefit the most from adjuvant systemic therapy for estrogen receptor (ER) positive early breast cancer remains a conundrum. Adjuvant chemotherapy does not come without a significant price. First, the personal cost to the patient, who is put at risk of serious, potentially life-threatening, toxicities associated with the treatment itself, as well as the additional consequences of lost productivity and possible duress sustained during the (often prolonged) period of treatment and recovery. Second, financially, in the form of the pecuniary cost of the drugs themselves, the fiscal expenditure associated with treatment administration and monitoring, and supportive care required by patients throughout the course of therapy and into long term survivorship. In the setting of disease with a significant likelihood of recurrence, these costs and risks are invariably considered to be outweighed by the potential gain made in terms of disease- and overall survival rates. Conversely, many ER positive early breast cancers have an excellent prognosis, and stand to gain little, if anything, from the addition of adjuvant chemotherapy. Indeed, in these patients, adverse consequence may outweigh any clinical advantage, to potential calamitous effect.

Seminal trials in early breast cancer, involving adjuvant cyclophosphamide, methotrexate and fluorouracil (CMF) chemotherapy versus no further treatment have provided long-term survival data in the setting of early disease [1]. After a median follow up of 28.5 years, whilst CMF bestowed a significant overall risk reduction of disease recurrence in node positive patients, 22% of the untreated patient population remained disease free. Patients with ER negative, node negative disease who did not receive adjuvant systemic therapy demonstrated an even higher disease-free survival rate of 40% after 19.2 years of follow up, which suggests loco-regional treatment alone is sufficient to effect long term disease-free status in a significant proportion of patients. Similar observations were made by the National Surgical Adjuvant Breast and Bowel Project (NSABP) clinical trials group in trial B-13, which randomised ER- and node negative patients to surgery plus adjuvant MF chemotherapy, or surgery alone. After sixteen years of follow up, 63% of the surgery monotherapy arm remained free of recurrence, with an overall survival of 65% [2]. Despite these statistics, many

* Corresponding author. Hospital of Prato, Via Suor Niccolina 20, Prato, 59100, Italy.
E-mail address: angelo.dileo@uslcentro.toscana.it (A. Di Leo).

http://dx.doi.org/10.1016/j.breast.2017.06.021
0960-9776/

Please cite this article in press as: McCartney A, et al., De-escalating and escalating treatment beyond endocrine therapy in patients with luminal breast cancer, The Breast (2017), http://dx.doi.org/10.1016/j.breast.2017.06.021

women are presently still over-treated, notwithstanding evolving knowledge of the clinical and molecular heterogeneity observed in breast cancer. Furthermore, once the decision is made to give chemotherapy, the most appropriate chemotherapy regimen according to intrinsic cancer subtype remains a concept without consensus.

This paper will explore the evidence behind modalities which may add further value to existing known clinicopathological and molecular profiling techniques in predicting clinical benefit from chemotherapy. Adjuvant chemotherapy regime choice in the context of early luminal breast cancer types will be discussed, and areas for further research and debate identified.

At least four intrinsic molecular subtypes of breast cancer have been identified by gene-expression profiling studies [3,4]. Luminal breast cancers, which constitute approximately 60% of all breast cancers, arise from luminal epithelial cells lining the mammary ducts, and demonstrate positive expression of hormonal receptors and other genes involved in ER activation. Luminal A tumours classically exhibit strong expression of ER and progesterone receptor (PgR), a low histological grade and proliferative index, and negative expression of human epidermal growth factor receptor 2 (HER2). In contrast, luminal B subtypes characteristically express pathologically higher tumour grades and Ki67 indices, reflective of a greater proliferative rate. Additionally, they typically display a comparatively weak expression of ER, weak/loss of expression of PgR, and can be either HER2 positive or negative [5]. Perhaps unsurprisingly, a luminal B subtype confers a poorer prognosis than luminal A, although overall, luminal breast cancers are generally associated with a more favourable outlook than their HER2 enriched and ER-negative subtype counterparts [6].

1. Gene signature tests

In the era of personalised medicine, commercially available genomic panel tests have allowed clinicians to characterise tumour gene signatures to form a predictive analysis of clinical outcome [7,8]. Today these predictive models are increasingly utilised in conjunction with clinicopathological prognostic markers, such as patient age, tumour size, grade, nodal status and hormonal and HER2 receptor status, in order to assist clinical decision making. Gene signature tests are particularly influential in guiding treatment recommendations in ER positive, node-negative, HER2 negative cases, wherein the optimal strategy is often unclear [9,10]. Luminal B cancers have predictably high recurrence scores and poor prognostic signatures [11], and as such, coupled with its reputed chemosensitivity, the common practice of offering adjuvant cytotoxic agents to patients with luminal B disease and intermediate-to high-risk clinicopathological features is relatively uncontroversial. In contrast, discriminating between high and low risk luminal A cancers remains a contentious topic, wherein cases of luminal A disease with high clinicopathological or genomic risk factors are often considered for chemotherapy.

Undoubtedly, genomic tools have positively assisted clinical decision making, but there is evidence that genomic assessment may still over-estimate the risk of disease relapse. Retrospective 21 gene assay (Oncotype Dx) analyses of archived tissue obtained in large breast cancer studies have identified a sizeable population of patients who may otherwise have been offered chemotherapy, and consequently over-treated, upon having been deemed at genomic "high risk" of recurrence. In patients enrolled in the NSABP B20 trial, which compared the effect of tamoxifen alone versus tamoxifen plus chemotherapy in ER positive, node negative early breast cancer, 60.5% of those who received tamoxifen alone, who were retrospectively defined as being at high risk of recurrence, remained free of distantly recurrent disease at 10 years [12]. Analogous findings were demonstrated in a node positive population derived from SWOG S8814, a trial that studied the effect of tamoxifen alone versus tamoxifen plus anthracycline-based chemotherapy. In patients with node positive disease who were found to have a high recurrence score, 43% remained event-free at ten years, despite not receiving chemotherapy [13]. The MINDACT trial, which enrolled mainly luminal type cancers, provided the first level IA evidence suggesting it is safe to omit chemotherapy in patients who demonstrate a low 70-gene signature score (MammaPrint) [14]. MINDACT data also elegantly demonstrated that at five years, the majority (90.6%) of patients identified to be at high risk of recurrence according to both clinical and genomic prediction remained free of distant metastases, with a disease free survival rate of 85.3% and overall survival of 94.7%. Undoubtedly, this effect is in part attributable to the adjuvant chemotherapy that this group was universally recommended to receive (3.9% did not receive chemotherapy), Nevertheless, these high rates of survival most likely also reflect the endurance of those patients who were rendered disease-free by surgery alone.

Despite the recent advent of molecular genomic analysis of tumours and ensuing additional enhancement in risk assessment, the ability to identify the subset of early breast cancer patients who harbour micrometastatic disease postoperatively (who would therefore stand to benefit most from systemic adjuvant therapies) continues to be an elusive goal. Tools that may allow clinicians to detect the presence of active micro-metastatic disease may help in refining prognostic assessments.

2. CTCs and ctDNA

Scientific discovery is ongoing into less invasive modalities which may detect malignancy in its early, recurrent and metastatic stages, assess mutational status, as well as predict likelihood of both treatment response and resistance. Peripheral evidence of malignant disease can be assessed in the circulation by way of two sources: circulating tumour cells (CTCs) and circulating tumour DNA (ctDNA), which represents the subset of circulating free DNA that contains the same somatic chromosomal re-arrangements as can be found in the patient's tumour. The comparatively lower tumour burden found in early stage disease correlates with much lower (or absent) concentrations of ctDNA, posing a challenge to investigators – as such, the majority of previous studies have concentrated on metastatic populations. ctDNA has previously been shown to be a sensitive biomarker of metastatic breast cancer, with evidence of correlation between ctDNA levels and treatment response [15]. ctDNA has been detected at high frequencies and levels in patients with metastatic breast cancer, and to a lesser, but still significant, extent in localised disease [16]. In a prospective cohort study of patients receiving neoadjuvant chemotherapy for early breast cancer, mutation tracking in serial plasma samples demonstrated the ability of ctDNA to predict relapse, with a median lead time of 7.9 months over clinically detected relapse [17]. In a small retrospective study of patients with non-metastatic, predominantly node negative, ER positive, HER2 negative breast cancer, elevated plasma ctDNA levels preceded clinical relapse in 86% of patients, with a mean lead time of 11 months. Furthermore, in patients with long-term disease-free survival, ctDNA was undetectable in post operative samples, in contrast with those with established high quantities of ctDNA, which predicted a correlative poor survival [18] (see Table 1).

Detection of CTCs has shown a similar association with poor prognosis in early breast cancer. Prospective collection of peripheral blood samples from chemotherapy-naïve patients with operable Stage I-III breast cancer by one group revealed 24% of those sampled had detectable CTCs, the presence of which predicted a

Please cite this article in press as: McCartney A, et al., De-escalating and escalating treatment beyond endocrine therapy in patients with luminal breast cancer, The Breast (2017), http://dx.doi.org/10.1016/j.breast.2017.06.021

Table 1
ctDNA studies in early breast cancer setting.

	No. pts enrolled	Study design	Clinical setting	% of relapsed pts with detectable ctDNA	Median lead time of ctDNA detection over clinical relapse
Garcia Murillas [17]	55	Prospective	Neoadjuvant, serial ctDNA tracking vs single post surgical sample	80%	7.9 months (range: 0.03–13.6 months)
Olsson [18]	20	Retrospective	Post surgery (no neoadjuvant Rx).	86%	11 months (range: 0–37 months)

decrease of both progression free survival (PFS) and overall survival (OS) [19]. Similarly, in a large prospective trial, the presence of CTCs was found to be an independent prognostic marker for disease-free survival and overall survival. Additionally, higher concentrations of CTCs was associated with worse PFS and OS, as was evidence of persistence of CTCs following adjuvant chemotherapy [20] (see Table 2).

Both ctDNA and CTC extraction and analysis present various technical challenges, but in the future may be used in tandem to inform personalised treatment decisions, as well as to monitor treatment response and detect relapse [21]. Studies into the utility of CTC and ctDNA in the setting of early breast cancer require further validation and expansion, until more robust data is acquired, international recommendations as yet do not support their incorporation into clinical practice [22].

3. Metabolomics

The science of metabolomics comprises the study of metabolic profiles found in biological samples such as tissue, blood, urine or saliva. Metabolites are an inevitable consequence of all cellular metabolic processes, and are in turn shaped by external variables, such age, disease, drugs, hormones, gender and genetic drift. In the context of malignant disease, cancer cells characteristically display altered cellular processes, which give rise to metabolites that differ from normal cells. Correspondingly, the host response to tumour may also alter the metabolite signature. It is possible to perform metabolomic analysis using a range different of platforms, such as gas chromatography-mass spectroscopy, liquid chromatography-mass spectroscopy, and nuclear magnetic resonance spectroscopy (^{1}H NMR). Hundreds of metabolites are measured simultaneously, and contain patterns which form the metabolic signature of the sample, which is more informative than analysing individual metabolites alone [23]. Succinctly, metabolomic signatures illustrate the dynamic effect that cancer exerts upon the host, and vice versa. This offers a potential advantage over other liquid biopsies, such as ctDNA, which cannot account for or quantify the effect the host brings to bear upon the malignancy – metabolomics not only can potentially identify signals directly caused by the presence of micro-metastatic disease, but can also detect changes in the microenvironment consistent with host inflammatory or immune response.

Our group has previously showed that metabolomic patterns have the ability to differ between early and advanced breast cancer patients [24]. Serum samples collected from early breast cancer patients pre- and post-operatively were assessed for metabolomic patterns by ^{1}H NMR, with metastatic patients serving as controls. A measurement of metabolomic risk was calculated for each early patient. Different metabolomic patterns were observed between groups, with preoperative patients correctly distinguished from the metastatic controls with 75% sensitivity, 69% specificity and 72% predictive accuracy. Surgical excision of the primary tumour also demonstrated a shift in metabolomic expression: of 22 patients initially classified as high risk, 19 (86%) exhibited a reduction in metabolomic risk post operatively.

Further validation was found by our group in a retrospective study derived from serum collected and banked from a larger cohort of ER negative early breast cancer patients [25]. A Random Forest (RF) classification algorithm was built to discriminate between early breast cancer patients and metastatic controls. Metabolomic profiles correctly distinguished between early breast cancer and metastatic disease in 83.7% of cases. A subset of patients with early disease was classified as metastatic by their RF risk score; this was taken as a surrogate indicator of the presence of micro-metastatic disease. To test this hypothesis, the metabolomic risk classifier was compared to actual recurrence rates observed over time. The early breast cancer cohort was broken into two groups: the training set, upon which all initial analyses were conducted, and the independent set, which allowed for data reproduction subsequent to primary analyses. Clinical relapse was predicted by the prognostic risk model with 90% sensitivity, 67% specificity and 73% predictive accuracy in the training set, with similar results observed in the independent set (82% sensitivity, 72% specificity, 75% predictive accuracy). It is important to note that the majority of the early breast cancer cohort received chemotherapy, which in clinical practice may have mitigated the overall rate of relapse, thus leading to an under-estimation of the strength of predictive scores.

Finally, our group sought to test a metabolomic predictive score within an ER positive cohort, utilising archived serum samples collected preoperatively during parallel adjuvant and metastatic breast cancer multicentre trials conducted in South-East Asia [26]. The majority of serum derived for the adjuvant study was collected

Table 2
CTC studies in early breast cancer setting.

	Total pts enrolled, no with CTCs detected (%)	Study design	Clinical setting	PFS probability in CTC positive pts vs (CTC negative pts)	OS probability in CTC positive pts vs (CTC negative pts)
Lucci [19]	302, 73 (24%)	Prospective	Chemotherapy naïve cohort	One or more CTCs subgroup: 87% (99%)[a] Two or more CTCs: 79% (98%)[a] Three or more CTCs: 69% (97%)[a]	One or more CTCs subgroup: 94% (99%)[a] Two more more CTCs: 89% (99%)[a] Three more more CTCs: 81% (99%)[a]
Rack [20]	Pre chemo: 2026, 435 (21.5%) Post chemo: 1492, 330 (22.1%)	Prospective	Analysed before and after adjuvant chemotherapy	88.1% (93.7%)[b]	93.2% (97.3%)[b]

[a] Measured at 2 years.
[b] Measured at 36 months.

Please cite this article in press as: McCartney A, et al., De-escalating and escalating treatment beyond endocrine therapy in patients with luminal breast cancer, The Breast (2017), http://dx.doi.org/10.1016/j.breast.2017.06.021

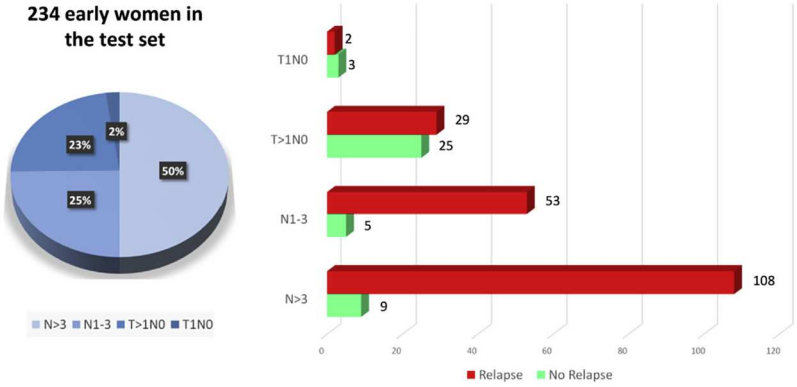

Fig. 1. T and N stages in early test set (N = 234).

from a population at predominantly high clinicopathological risk of relapse (see Fig. 1), with each subject analysed for metabolomic signatures and stratified according to predicted risk of recurrence (see Fig. 2).

Within the adjuvant training set, metabolomic profiles demonstrated 84.9% accuracy in discriminating between patients with early and metastatic breast cancer. The test set recurrence risk score correlated with clinical relapse, with accuracy maximised at 71.3%, sensitivity 70.8% and specificity 71.4%. The model also performed independently of clinicopathological factors such as age, tumour size and grade, nodal status, HER2 status, and also of the computational risk of relapse score estimated by Adjuvant!Online. Survival analysis of the adjuvant group, subdivided according to primary tumour size (T) and nodal status (N), particularly emphasised the performance of metabolomic prediction within the T > 1N0 group. Metabolomic high risk-classified patients had a poorer survival outcome compared to low risk patients (hazard ratio [HR] 3.5, 95% CI 1.7–7.3; P = 0.0012) (see Fig. 3).

One limitation of this study was the follow up period of this dataset, which was restricted to five or six years, increasing the likelihood that the model's ability to predict relapse was not fully realised. Relapses often occur later in ER positive cancer, therefore a proportion of relapses theoretically predicted by metabolomic signature may not have been captured as events within the follow up period.

In summary, methods that may detect signals of active micrometastatic disease, such as CTCs, ctDNA and metabolomics, are still in the stages of development, but results thus far are promising. Integrating these approaches with standard clinicopathological and genomic assessment of patients in prospectively designed studies would appear to be the next logical step, so that greater sophistication and accuracy is added to the current practice of prognostic risk assessment.

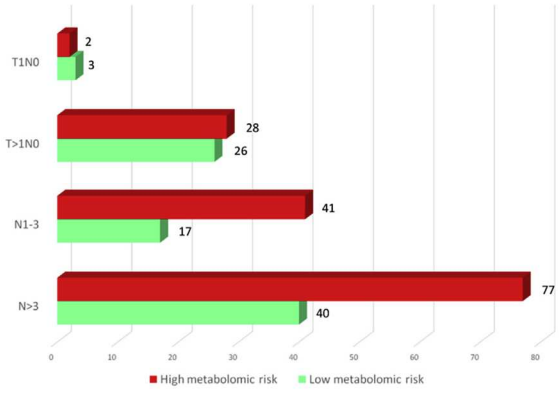

Fig. 2. Metabolomic risk according to T and N group classification.

4. Which adjuvant chemotherapy is best for luminal breast cancer?

Luminal A breast cancer, and its associated low-proliferative, generally well-differentiated pathology, is largely regarded as a malignancy with relative insensitivity to chemotherapy, and a favourable prognostic outlook. It is difficult to justify instituting adjuvant chemotherapy in cases of luminal A disease with uniformly low clinicopathologic and genomic risk factors, due to the competing concern that toxicities of treatment will outweigh the very small potential benefit stood to gain from chemotherapy. Nevertheless, a subset of luminal A tumours present with a considerable burden of nodal disease, and others exhibit a genomic profile suggestive of a high risk of recurrence, whilst clinicopathologic features simultaneously suggest otherwise. Until further refinement is added to prognostic and predictive methods, it will remain common practice to recommend chemotherapy to such patients, along with the majority of luminal B cases. The question as to which regimen is optimal for luminal types remains unanswered, as to date, no prospective trial has specifically assessed the benefit of chemotherapy for each luminal subtype [27].

A previous retrospective analysis of clinical outcome according to intrinsic breast cancer subtype failed to meet statistical significance with regards to substitution of anthracyclines in luminal subtypes [28]. Nevertheless, a trend towards better survival in luminal B types treated with anthracycline was observed, with relatively no difference observed for luminal A disease, suggesting the latter represents a group wherein omission of anthracyclines may be safely realised. Similarly in other analyses, the observed benefit derived from taxane-based regimes was limited to luminal B disease, and not established in luminal A subtypes [29,30]. Meta-analyses performed by the Early Breast Cancer Trialists' Collaborative Group (EBCTCG) demonstrated clinical benefit from chemotherapy (both taxane and anthracycline based regimes) for ER positive tumours [31]. However, the group did not have

Please cite this article in press as: McCartney A, et al., De-escalating and escalating treatment beyond endocrine therapy in patients with luminal breast cancer, The Breast (2017), http://dx.doi.org/10.1016/j.breast.2017.06.021

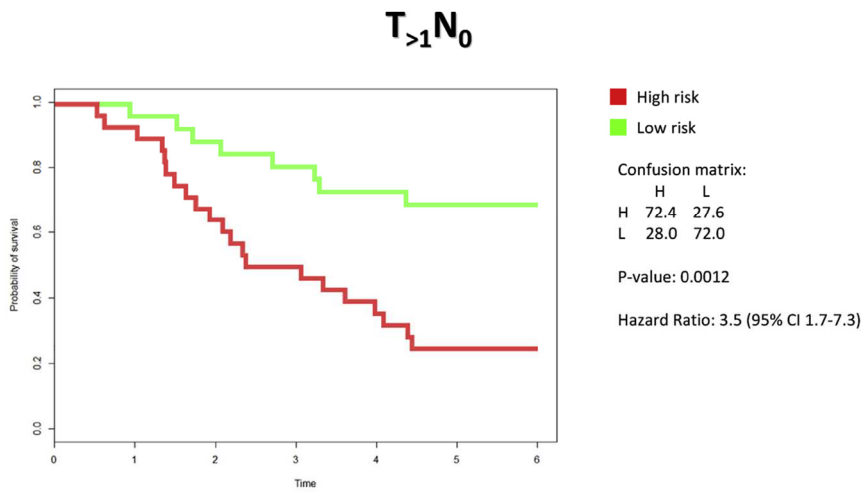

Fig. 3. Kaplan-Meier curve demonstrating probability of disease-free survival within the T > 1N0 group, according to estimated metabolomic risk.

sufficient data to split the cohort of ER positive tumours into luminal A-like and luminal B-like cases.

Our group collected retrospective subgroup analyses of luminal-like subtypes in adjuvant chemotherapy trials, to explore the question as to whether escalation to newer generation regimens may offer significant improvements in survival that in turn may justify the cost of potential toxicity [32]. This strictly exploratory, hypothesis-generating review was limited by way of marked heterogeneity of the included trials, and as such, definitive statistical and theoretical conclusions were not drawn. Nevertheless, for luminal A-like disease, the choice of chemotherapy regime did not appear to make a difference to outcome – raising the premise that there may be potential for less toxic regimens to offer as much benefit in luminal A patients as newer generation regime. It is important to note that this review only compared between chemotherapy regimes within luminal groups, and as such, did not evaluate the potential benefit of receiving chemotherapy versus endocrine therapy alone/omission of chemotherapy. Relapses otherwise prevented by the cytotoxic effect of chemotherapy typically tend to occur early, within the first five years following treatment, so it is unlikely that the lack of observed benefit from newer agents in luminal A tumours was attributable to a limited follow up time. In contrast, luminal B-like disease showed a consistent trend in favour of the incorporation of taxanes, supporting the edict that the more proliferative, aggressive luminal B subtype will benefit more from newer agents. This assessment served only to generate hypotheses - prospective, predictive data is required to guide treatment decisions according to luminal subtype.

5. Dose dense regimes

To date, no published prospective data exists regarding the value of dose-dense regimes in ER positive cancer according to luminal status, with this critical sub-group analysis absent from various seminal trials in the area [33–36]. Retrospective analysis of NCIC CTG MA.21, a trial that compared various dose-dense, dose-intense regimes to doxorubicin, cyclophosphamide and paclitaxel (AC-T) showed intrinsic subtypes defined by PAM50 were not predictive of treatment benefit between regimens [37]. Multivariate analysis revealed that only non-luminal subtypes showed benefit from a taxane within the dose-dense regimens, leading the authors to suggest that taxanes may even pose potential harm to luminal type patients. It is important to acknowledge, however, that this subgroup analysis was post-hoc and showed only borderline statistical significance. Furthermore, combining both luminal types in this analysis would likely lead to the statistical perception of taxanes being of poor utility due to the inclusion of luminal A subtypes in that group.

Due to insufficient data, breast cancer treatment is yet to reach the point of didactic tailoring of treatment according to luminal type. There is no strong evidence in favour of anthracycline and taxane combinations in luminal A cancer, so in cases wherein patients with luminal A disease have a strong inclination toward less toxic regimens, such treatment preferences can be respected with some confidence that the patient is at low risk of suffering consequent harm. Correspondingly, in most luminal B cancers, regimens containing both an anthracycline and taxane appear to be the most appropriate choice, but again, further assessment of existing data, as well as prospective enquiry, would be an effective step towards arriving at a definitive consensus.

Disclosure of potential conflicts of interest

A. Di Leo is a consultant/advisory board member for AstraZeneca, Bayer, Eisai, Genomic Health, Ipsen, Lilly, Novartis, Pfizer, and Pierre Fabre. No potential conflicts of interest were disclosed by the other authors.

References

[1] Bonadonna G, Moliterni A, Zambetti M, Daisone MG, Pilotti S, Gianni L, et al. 30 years' follow up of randomised studies of adjuvant CMF in operable breast cancer: cohort study. BMJ 2005 Jan 29;330(7485):217. http://dx.doi.org/10.1136/bmj.38314.622095.8F. Epub 2005 Jan 13.

[2] Fisher B, Jeong J-H, Anderson S, Dignam J, Fisher ER, Wolmark N, et al. Treatment of axillary lymph-node negative, estrogen receptor-negative breast cancer: updated findings from National Surgical Adjuvant Breast and Bowel Project clinical trials. J Natl Cancer Inst 2004;96:1823–31. http://dx.doi.org/10.1016/S0140-6736(04)16981-X.

[3] Sørlie T, Perou CM, Tibshirani R, Aas T, Geisler S, Johnsen H, et al. Gene expression patterns of breast carcinomas distinguish tumor subclasses with clinical implications. Proc Natl Acad Sci 2001 Sep 11;98:10869–74. http://

Please cite this article in press as: McCartney A, et al., De-escalating and escalating treatment beyond endocrine therapy in patients with luminal breast cancer, The Breast (2017), http://dx.doi.org/10.1016/j.breast.2017.06.021

dx.doi.org/10.1073/pnas.191367098.
[4] Cancer Genome Atlas Network. Comprehensive molecular portraits of human breast tumours. Nature 2012;490:61–70. http://dx.doi.org/10.1038/nature11412.
[5] Cheang MC, Chia SK, Voduc D, Gao D, Leung S, Snider J, et al. Ki67 index, HER2 status, and prognosis of patients with luminal B breast cancer. J Natl Cancer Inst 2009 May 20;101:736–50. http://dx.doi.org/10.1093/jnci/djp082. Epub 2009 May 12.
[6] Sotiriou C, Neo SY, McShane LM, Korn EL, Long PM, Jazaeri A, et al. Breast cancer classification and prognosis based on gene expression profiles from a population-based study. Proc Natl Acad Sci U. S. A 2003;100:10393–8. http://dx.doi.org/10.1073/pnas.1732912100. Epub 2003 Aug 13.
[7] Paik S, Shak S, Tang G, Kim C, Baker J, Cronin M, et al. A multigene assay to predict recurrence of tamoxifen-treated, node negative breast cancer. N Engl J Med 2004;351:2817–26. http://dx.doi.org/10.1056/NEJMoa041588. Epub 2004 Dec 10.
[8] van de Vijver MJ, He YD, van't Veer L, Dai H, Hart AA, Voskuil DW, et al. A gene-expression signature as a predictor of survival in breast cancer. N Engl J Med 2002;347:1999–2009. http://dx.doi.org/10.1056/NEJMoa021967.
[9] Levine MN, Julian JA, Bedard PL, Eisen A, Trudeau ME, Higgins B, et al. Prospective evaluation of the 21-gene recurrence score assay for breast cancer decision making in Ontario. J Clin Oncol 2016;34:1065–71. http://dx.doi.org/10.1200/JCO.2015.62.8503. Epub 2015 Nov 23.
[10] Kuijer A, Straver M, den Dekker B, van Bommel ACM, Elias SG, Smorenburg CH, et al. Impact of 70-gene signature use on adjuvant chemotherapy decisions in patients with estrogen receptor-positive early breast cancer: results of a prospective cohort study. J Clin Oncol 2017;35. Epub 2017 March 13.
[11] Fan C, Oh DS, Wessels L, Weigelt B, Nuyten DS, Nobel AB, et al. Concordance among gene-expression-based predictors for breast cancer. N Engl J Med 2006;355:560–9. http://dx.doi.org/10.1056/NEJMoa052933.
[12] Paik S, Tang G, Shak S, Kim C, Baker J, Kim W, et al. Gene expression and benefit of chemotherapy in women with node-negative, estrogen-positive breast cancer. J Clin Oncol 2006;24:3726–34. http://dx.doi.org/10.1200/JCO.2005.04.7985. Epub 2006 May 23.
[13] Albain KS, Barlow WE, Shak S, Hortobagyi GN, Livingston RB, Yeh IT, et al. Prognostic and predictive value of the 21-gene recurrence score assay in a randomized trial of chemotherapy for postmenopausal, node-positive, estrogen receptor-positive breast cancer. Lancet Oncol 2010;11:55–65. http://dx.doi.org/10.1016/S1470-2045(09)70314-6. Epub 2009 Dec 10.
[14] Cardoso F, van't Veer LJ, Bogaerts J, Slaets L, Viale G, Delaloge S, et al. 70-gene signature as an aid to treatment decisions in early-stage breast cancer. N Engl J Med 2016;375:717–29. http://dx.doi.org/10.1056/NEJMoa1602253.
[15] Dawson SJ, Tsui DWY, Murtaza M, Biggs H, Rueda OM, Chin SF, et al. Analysis of circulating tumor DNA to monitor metastatic breast cancer. N Engl J Med 2013;368:1199–209. http://dx.doi.org/10.1056/NEJMoa1213261. Epub 2013 Mar 13.
[16] Bettegowda C, Sausen M, Leary RJ, Kinde I, Wang Y, Agrawal N, et al. Detection of circulating tumor DNA in early- and late-stage human malignancies. Sci Transl Med 2014;6:224ra24. http://dx.doi.org/10.1126/scitranslmed.3007094.
[17] Garcia-Murillas I, Schiavon G, Weigelt B, Ng C, Hrebien S, Cutts RJ, et al. Mutation tracking in circulating tumor DNA predicts relapse in early breast cancer. Sci Transl Med 2015;7:302ra133. http://dx.doi.org/10.1126/scitranslmed.aab0021.
[18] Olsson E, Winter C, George A, Chen Y, Howlin J, Tang MH, et al. Serial monitoring of circulating tumor DNA in patients with primary breast cancer for detection of occult metastatic disease. EMBO Mol Med 2015;7:1034–47. http://dx.doi.org/10.15252/emmm.201404913.
[19] Lucci A, Hall CS, Lodhi AK, Bhattacharyya A, Anderson AE, Xiao L, et al. Circulating tumour cells in non-metastatic breast cancer: a prospective study. Lancet Oncol 2012;13:688–95. http://dx.doi.org/10.1016/S1470-2045(12)70209-7. Epub 2012 Jun 6.
[20] Rack B, Schindlbeck C, Juckstock J, Andergassen U, Hepp P, Zwingers T, et al. Circulating tumor cells predict survival in average-to-high risk breast cancer patients. J Natl Cancer Inst 2014;106. http://dx.doi.org/10.1093/jnci/dju066. dju066.
[21] Ignatiadis M, Dawson S-J. Circulating tumour cells and circulating tumour DNA for precision medicine: dream or reality? Ann Oncol 2014;25:2304–13. http://dx.doi.org/10.1093/annonc/mdu480. Epub 2014 Oct 21.
[22] Harris LN, Ismaila N, McShane LM, Hayes DF. Use of biomarkers to guide decisions on adjuvant systemic therapy for women with early-stage invasive breast cancer: American Society of Clinical Oncology clinical practice guideline. J Clin Oncol 2016;34:1134–50. http://dx.doi.org/10.1200/JOP.2016.010868. Epub 2016 Mar 8.
[23] Claudino WM, Quattrone A, Biganzoli L, Pestrin M, Bertini I, Di Leo A. Metabolomics: available results, current research projects in breast cancer, and future applications. J Clin Oncol 2007;25:2840–6. http://dx.doi.org/10.1200/JCO.2006.09.7550. Epub 2007 May 14.
[24] Oakman C, Tenori L, Claudino WM, Cappadona S, Nepi S, Battaglia A, et al. Identification of a serum-detectable metabolomic fingerprint potentially correlated with the presence of micrometastatic disease in early breast cancer patients at varying risks of disease relapse by traditional prognostic methods. Ann Oncol 2011;22:1295–301. http://dx.doi.org/10.1093/annonc/mdq606. Epub 2011 Jan 3.
[25] Tenori L, Oakman C, Morris PG, Gralka E, Turner N, Cappadona S, et al. Serum metabolomic profiles evaluated after surgery may identify patients with oestrogen receptor negative early breast cancer at increased risk of disease recurrence. Results from a retrospective study. Mol Oncol 2015;9:128–39. http://dx.doi.org/10.1016/j.molonc.2014.07.012. Epub 2014 Aug 10.
[26] Hart CD, Vignoli A, Tenori L, Uy GL, Van To T, Adebamowo C, et al. Serum metabolomic profiles identify ER-positive early breast cancer patients at increased risk of disease recurrence in a multi center population. Clin Cancer Res 2016:1–10. http://dx.doi.org/10.1158/1078-0432.CCR-16-1153. Epub 2017 Jan 12.
[27] Coates AS, Colleoni M, Goldhirsch A. Is adjuvant chemotherapy useful for women with luminal A breast cancer? J Clin Oncol 2012;30:1260–3. http://dx.doi.org/10.1200/JCO.2011.37.7879. Epub 2012 Feb 21.
[28] Cheang MCU, Voduc KD, Dongsheng T, Jiang S, Leung S, Chia SK, et al. Responsiveness of intrinsic subtypes to adjuvant anthracycline substitution in the NCIC.CTG MA.5 randomized trial. Clin Cancer Res 2012;18:2402–12. http://dx.doi.org/10.1158/1078-0432.CCR-11-2956. Epub 2012 Feb 20.
[29] Hugh J, Hanson J, Cheang MC, Nielsen TO, Perou CM, Dumontet C, et al. Breast cancer subtypes and response to docetaxel in node-positive breast cancer: use of an immunohistochemical definition in the BCIRG 001 trial. J Clin Oncol 2009;27:1168–76. http://dx.doi.org/10.1200/JCO.2008.18.1024. Epub 2009 Feb 9.
[30] Penault-Llorca F, André F, Sagan C, Lacroix-Triki M, Denoux Y, Verriele V, et al. Ki67 expression and docetaxel efficacy in patients with estrogen receptor-positive breast cancer. J Clin Oncol 2009;27:2809–15. http://dx.doi.org/10.1200/JCO.2008.18.2808. Epub 2009 Apr 20.
[31] Early Breast Cancer Trialists' Collaborative Group (EBCTCG). Comparisons between different polychemotherapy regimes for early breast cancer: meta-analyses of long-term outcome among 100 000 women in 123 randomised trials. Lancet 2012;379:432–44. http://dx.doi.org/10.1016/S0140-6736(11)61625-5. Epub 2011 Dec 6.
[32] Hart CD, Sanna G, Siclari O, Biganzoli L, Di Leo A. Defining optimal duration and predicting benefit from chemotherapy in patients with luminal-like subtypes. Breast 2015;24:S136–42. http://dx.doi.org/10.1016/j.breast.2015.07.033. Epub 2015 Aug 29.
[33] Citron ML, Berry DA, Cirrincione C, Hudis C, Winer EP, Gradishar WJ, et al. Randomized trial of dose-dense versus conventionally scheduled and sequential versus concurrent combination chemotherapy as postoperative adjuvant treatment of node-positive primary breast cancer: first report of intergroup trial C9741/Cancer and Leukemia Group B trial 9741. J Clin Oncol 2003;21:1431–9. http://dx.doi.org/10.1200/JCO.2003.09.081. Epub 2003 Feb 13.
[34] Sparano JA, Wang M, Martino S, Jones V, Perez EA, Saphner T, et al. Weekly paclitaxel in the adjuvant treatment of breast cancer. N Engl J Med 2008;358:1663–71. http://dx.doi.org/10.1056/NEJMoa0707056.
[35] Venturini M, Del Mastro L, Aitini E, Baldini E, Caroti C, Contu A, et al. Dose-dense chemotherapy in early breast cancer patients: results from a randomized trial. J Natl Cancer Inst 2005;23:1724–33. http://dx.doi.org/10.1093/jnci/dji398.
[36] Del Mastro L, De Placido S, Bruzzi P, De Laurentiis M, Boni C, Cavazzini G, et al. Fluorouracil and dose-dense chemotherapy in adjuvant treatment of patients with early-stage breast cancer: an open-label, 2x2 factorial, randomised phase 3 trial. Lancet 2015;385:1863–72. http://dx.doi.org/10.1016/S0140-6736(14)62048-1. Epub 2015 Mar 2.
[37] Liu S, Chapman JA, Burnell MJ, Levine MN, Pritchard KI, Whelan TJ, et al. Prognositic and predictive investigation of PAM50 subtypes in the NCIC CTG MA.21 phase III chemotherapy trial. Breast Cancer Res Treat 2015;149:439–48. http://dx.doi.org/10.1007/s10549-014-3259-1. Epub 2015 Jan 1.

Please cite this article in press as: McCartney A, et al., De-escalating and escalating treatment beyond endocrine therapy in patients with luminal breast cancer, The Breast (2017), http://dx.doi.org/10.1016/j.breast.2017.06.021

4.1.3 *NMR-based Metabolomics identifies high risk of death patients within two years after acute coronary syndrome. Metabolomics in the AMI-Florence II study*

Alessia Vignoli[a]*, Leonardo Tenori[b]*, Betti Giusti[c], Panteleimon G. Takis[d], Serafina Valente[c], Nazario Carabba[c], Daniela Balzi[e], Alessandro Barchielli[e], Niccolò Marchionni[c], Gian Franco Gensini[f], Rossella Marcucci[c], Claudio Luchinat[a,g]**, Anna Maria Gori[c]**

*Contributed equally to the work. **Co-senior authors

[a] Magnetic Resonance Center (CERM), University of Florence, Sesto Fiorentino, Italy
[b] Department of Clinical and Experimental Medicine, University of Florence, Florence, Italy
[c] Careggi Hospital, Florence, Italy
[d] Giotto Biotech S.r.l., Sesto Fiorentino, Italy
[e] Unit of Epidemiology, ASL 10, Florence, Italy
[f] Centro Studi Medicina Avanzata (CESMAV) Florence, Italy, Florence, Italy
[g] Department of Chemistry, University of Florence, Sesto Fiorentino, Italy

Submitted

Candidate's contributions: statistical analysis and interpretation of data, writing and review of the manuscript.

NMR-based Metabolomics identifies high risk of death patients within two years after acute coronary syndrome

Metabolomics in the AMI-Florence II study

Abstract

Background. Risk stratification and management of patients continue to be challenging despite considerable efforts made in the last decades by many clinicians and researchers.

Objectives. The aim of this study was to investigate the metabolomic fingerprint of acute coronary syndromes using nuclear magnetic resonance spectroscopy of patient serum samples and to evaluate the possible role of metabolomics in the prognostic stratification of ACS patients.

Methods. 978 ACS patients were enrolled for the study, among these 146 patients died, whereas 832 survived within 2 years from the ACS. Serum samples were analyzed via high resolution 1H-NMR and the spectra were used to characterized the metabolic fingerprint of patients. Multivariate statistics were used to create a prognostic model for the prediction of death within 2 years from the cardiovascular event.

Results. In the training set, metabolomics showed significant differential clustering of the two outcomes cohorts. A prognostic risk model predicted death with 76.9% sensitivity, 79.5% specificity, and 78.2% predictive accuracy, and an area under the ROC curve of 0.859. These results were reproduced in a validation set, obtaining 72.6% sensitivity, 72.64% specificity and 72.64% predictive accuracy. The known prognostic factors (i.e. GRACE score, age, sex, Killip class, etc.) were compared by regression analyses with the metabolomic RF risk score, calculated on the validation set. In the univariate analysis, many prognostic factors were statistically associated with the outcomes, but the RF score shows the *P*-value by far more significant (*P*=2.65e-12). Moreover, in the multivariate regression only age, Killip class and RF score still remain statistically significant, demonstrating their independence from the other variables.

Conclusions. Discrimination between patients with different outcomes after an ACS is demonstrated for the first time using metabolic profiling technologies, which seem to be more accurate than the standard stratification based on clinical and biohumoral parameters.

Condensed Abstract

Risk stratification and management of patients continue to be challenging despite considerable efforts made in the last decades. In 978 ACS patients from AMI Florence II Study, the metabolic fingerprint was evaluated by high resolution 1H-Nuclear Magnetic Resonance. The multivariable prognostic risk model, which included metabolic fingerprint and clinical variables, predicted death with higher accuracy than the model including only clinical variables.

Discrimination between patients with different outcomes after an ACS is demonstrated for the first time using metabolic profiling technologies, which seem to be more accurate than the standard stratification based on clinical and biohumoral parameters.

Keywords

Acute coronary syndrome, nuclear magnetic resonance, serum, metabolomics, biomarker, prognosis

Abbreviations and Acronyms

CVDs = cardiovascular diseases
ACS = acute coronary syndrome
NMR = nuclear magnetic resonance
MI = myocardial infarction
RF = random forest
ROC = receiver operating characteristics
AUC = area under the curve
PCI = percutaneous coronary intervention
NOESY = nuclear Overhauser effect spectroscopy pulse sequence
CPMG = Carr-Purcell-Meiboom-Gill pulse sequence

Introduction

Among Cardiovascular diseases (CVDs), acute coronary syndrome (ACS) represents the most common cause of emergency hospital admission and it is associated with the highest mortality and morbidity (1, 2). The prognosis is directly associated with timely initiation of revascularization, and misdiagnosis or late diagnosis may have unfavorable clinical implications. Established risk stratification tools such as the Global Registry of Acute Coronary Events (GRACE) and the Thrombolysis In Myocardial Infarction (TIMI) risk scores are derived from demographic, clinical, laboratory, and electrocardiogram (ECG)-related variables (3, 4). These do not incorporate the use of newer biomarkers, which could represent different pathophysiologic processes and provide complementary prognostic information, thereby improving risk stratification beyond traditionally used variables.

In the last years, several studies evaluated the potential clinical usefulness of new biomarkers able to identify patients who underwent a poor outcome. In particular, high levels of inflammatory markers such as C-Reactive Protein (CRP) and Interleukin-8 (IL-8) had long-term prognostic utility in patients with acute coronary syndrome that undergone coronary revascularization (5, 6).

However, no conclusive and consistent data about the prognostic utility of measuring the inflammatory markers in the early phase of the acute coronary syndrome are available in literature.

A number of studies have evidenced that a global approach such as genomics, proteomics and metabolomics may represent a valid strategy for improving the knowledge of pathophysiological mechanism and for identifying ACS patients at high risk.

Metabolomics analysis by nuclear magnetic resonance (NMR) is a high-throughput and high-reproducible analysis, as demonstrated by numerous ring trials performed over the years by many different NMR laboratories (7, 8), which gives qualitative and quantitative information on the hundreds of different small molecules present in a biological sample (9), and may provide a global picture of a wide range of metabolic processes underlying complex and multifactorial diseases such as acute coronary syndromes. During the last years the metabolomic approach was applied to identify a risk profile in heart failure patients (10, 11), atrial fibrillation patients (12) and diabetic patients (13). In the setting of ACS, few case-control studies characterized the metabolic biosignature of Myocardial Ischemia (14, 15), identified altered signatures in lipid metabolism in patients with angina or MI with respect to control subjects (16) or microbial metabolites in urine associated with coronary heart disease (17).

Risk stratification should identify individuals at high risk requiring more intensive therapy or conversely, patients with a favorable prognosis could avoid drug overuse and associated side effects. In this framework, the aim of the present study is to evaluate the impact of metabolomics profile on the occurrence of cardiovascular death in ACS patients after percutaneous coronary intervention.

Methods

This study was part of a collaborative project between the Department of Medical and Surgical Critical Care of the University of Florence and the University of Florence Magnetic Resonance Centre (CERM).

Study population

The study population comprised a group of 978 out of 1496 patients admitted to the Coronary Unit of the Careggi University Hospital, Florence, Italy from April 2008 to April 2009 enrolled on the frame of the Florence Acute Myocardial Infarction-2 (AMI-Florence 2) registry (18). In the present study, we evaluated 978 patients (345 females and 633 males, median age 74), among them 146 patients died within two years from the ACS event (dead patients) and 832 patients survived for at least two years (survivor patients), the two-year vital status was assessed by consulting the registry office of the city of residence. Thirty-five percent of the AMI-Florence 2 population was excluded from this study for the lack of good quality blood sample (never thawed before) for the metabolomic analyses; however, according to a standard power analysis (19) using a t-test as the test statistics, and fixing an alpha level of 0.05 for a significant comparison, 146 dead and 832 survivors demonstrated to be enough to detect small-medium effects (Cohen's d~0.25) with a statistical power of 80%. Blood samples were collected in the 24-48 h after PCI and overnight fasting. All information about inclusion criteria and treatments of the patients are detailed in depth in the Supplementary Materials.

All subjects gave informed consent; the study protocol complies with the Declaration of Helsinki, and received the approval by the local ethics committee.

NMR analyses

Samples were prepared following the standard protocols detailed by Bernini *et al*. (20). According to standard practice (21, 22), all spectra were acquired at 310 K using a Bruker 600 MHz spectrometer (Bruker BioSpin), and for each serum sample three monodimensional 1H NMR spectra, namely NOESY, CPMG and Diffusion-edited spectra, were acquired allowing the selective detection of different molecular weight metabolites. A detailed description about sample preparation and experiments is presented in the Supplementary Materials.

Each 1D spectrum in the range 0.2-10.00 ppm was segmented into 0.02 ppm chemical shift bins and the corresponding spectral areas were integrated using AMIX software (version 3.8.4, Bruker BioSpin). Binning is a mean to reduce the number of total variables, to compensate for subtle signal shifts, and filter noise in the spectra, making the analysis more robust and reproducible (23, 24). The region between 4.5 and 5.0 ppm containing the residual water signal was removed and the dimension of the system was reduced to 466 bins. The total spectral area was calculated on the remaining bins and total area normalization was carried out on the data prior to pattern recognition.

Statistical analysis

Data analyses were performed using the open source software R. For the demographic and baseline characteristics, the t-test was used for comparison between groups and the chi-square test for comparison between categorical variables.

For the multivariate data analyses of the NMR data the group of 978 patients was randomly split into two independent cohorts: a training set constituted by 80 survivors and 40 dead patients (25), and a validation set constituted by all the remaining patients (106 dead patients and 752 survivor patients).

The initial analysis was restricted to the training set and the first step was to establish if serum metabolomic profiles could distinguish between dead and survivor patients within two years from the cardiovascular event, for this purpose, a Random Forest (RF) classifier (26) was built (considering for each sample all spectrum, thus, no choice of particular metabolite has been performed). The percentage of trees in the forest that assign one sample to a specific class can be inferred as a probability of class belonging, and it gives an unbiased assessment of the classification error using the out-of-bag samples (27).

The RF classifier uses data from the training set to build an ensemble of decision trees. Each tree is used to predict whether a sample is associated with death or survival. For each patient, a score was created that expresses the extent to which the serum metabolomic profile appears to be similar to the one of patients with a negative outcome, designated as the 'RF risk score'. This score is based on the percentage of trees in the ensemble that misclassify the sample as belonging to the cohort of dead patients. For each patient, three RF scores were derived using the three types of spectra acquired. For all calculations, the R package 'Random Forest' (26) was used to grow a forest of 2000 trees, using the default settings.

The next step was to test the hypothesis that a metabolomic signature similar to the one of dead patients would be really predictive of death within two years from the CV event. Using receiver operating characteristics (ROC) analysis ("colAUC" function of the R package "caTools") and Harrell's c index ("cindex" function on the R package "dynpred"), the performance of the RF risk scores were compared with the actual outcome. To delineate high risk of death, a cut-off for the RF risk score was calculated in the training set that optimized accuracy, sensitivity and specificity, and the performance of the model was subsequently tested in the validation set.

The independent prognostic capacity of the RF risk score model was evaluated in comparison with standard prognostic features in a multivariate logistic regression, using the standard R function "glm".

The spectral regions related to the metabolites were assigned in the CPMG NMR spectra by using matching routines of AMIX 3.8.4 (Bruker BioSpin) in combination with the BBIOREFCODE (Bruker BioSpin), and freely available dataset i.e. Human Metabolome DataBase (HMDB) (28). The metabolites quantification was determined by an in-house developed software in MATLAB programming suite (version R2014b).

Our algorithm is based upon the unconstrained non-linear minimization (fitting) of the metabolite NMR signals, employing a combination of lorentzian-gaussian functions. By this approach, each NMR region of interest is decomposed and deconvoluted into its component parts, and then integrated to obtain the metabolite concentrations in arbitrary units (Supplementary Figure 1). Wilcoxon signed-rank test (29) was chosen to infer differences between the metabolites concentrations of the outcomes groups on the biological assumption that metabolite concentrations are not normally distributed, and false discovery rate correction was applied using the Benjamini-Hochberg method (30). An adjusted p-value < 0.05 was deemed significant. Effect size using Cliff's delta (31) was calculated by means of the R package "effsize".
The statistical approach described above was also used to build gender-specific statistical models based on NOESY spectra.
NMR and clinical data will freely available in the Open-Access Database Repository MetaboLights from October 2017 with the accession number MTBLS395 (http://www.ebi.ac.uk/metabolights).

Results

Demographic and clinical characteristics of the enrolled patients are shown in Table 1. In Supplementary Table 1 the characteristics of patients according to gender are also reported.

NMR spectra

For each sample three NMR metabolomic profiles were obtained using NOESY, CPMG, and Diffusion-edited sequences (Supplementary Figure 2). According to the peculiar characteristics of each NMR experiment high and low molecular weight metabolites can be detected. An exploratory Principal Component Analysis of the dataset is reported in Supplementary Figure 3.

Discrimination of the outcomes and the RF scores in the training set

Using the Random Forest classifier, the metabolomic profiles of 80 survivors and 40 dead patients (training set) were classified, and showed significant differential clustering, with a good separation of the two groups using each type of NMR spectra NOESY (Figure 1A), CPMG (Supplementary Figure 4A), and Diffusion (Supplementary Figure 4B).
Using ROC analyses, the areas under the curve (AUC) obtained were 0.859 for NOESY spectra (Figure 1B), 0.857 and 0.775 for CPMG and Diffusion editing spectra, respectively (Supplementary Figure 4 C-D). NOESY and CPMG models showed approximately the same performances, and the discrimination between the two outcome groups can be ascribed to both low (mostly) and high molecular weight metabolites. Thus, it was decided to use the NOESY spectra in the further analyses because they contain both high and low molecular weight metabolite information.

The NOESY RF risk score was thus optimized in the training set choosing the best threshold for the maximization of sensitivity and specificity in the outcome discrimination. A threshold of ≥ 0.454 was set optimizing accuracy, sensitivity and specificity; this optimized threshold yielded 76.9% (95% CI 76.5-77.3%) sensitivity, 79.5% (95% CI 78.4-80.6%) specificity, and 78.2% (95% CI 77.6-78.7%).
Moreover, the NOESY RF model demonstrated to be robust with respect to different strategies of model-validation, indeed, with a 100 cycles of classical Monte Carlo cross-validation scheme with 80-20 % splitting of the data (training set, validation set) a mean AUC of 0.805 (95% CI, 0.795-0.814) was obtained. Furthermore, the model was robust with respect to the origin of samples: using samples coming from the Careggi University Hospital as training set and the other samples as validation set (and vice-versa) affected only slightly the AUC obtained (Supplementary Figure 5).

Outcome prediction by NOESY RF score in a validation set of patients
The validation set (106 dead patients and 752 survivor patients) was evaluated using an unsupervised analysis. Spectra of the validation samples were classified as either 'dead' or 'survivor' using the optimized NOESY RF risk score model derived from the training set. Comparison between metabolomic classification and actual outcome demonstrated high correlation with AUC of 0.801 (Figure 1C). Using the threshold maximized in the training set we obtained 72.60% sensitivity, 72.64% specificity and 72.64% overall predicting accuracy.
The AUC score calculated on the Random Forest score was assessed for significance against the null hypothesis of no prediction accuracy in the data, by means of 10,000 randomized class-permutation test: the estimate AUC score obtained after randomization is 0.570 (95% CI 0.569-0.571), demonstrating the significance of our result (AUC 0.801, p-value of 2.21·10-06).
For the sake of completeness, comparison between actual outcome and the metabolomic classification with CPMG and Diffusion editing models were also performed, results are reported in Supplementary Figure 4 E-F.

Comparison of the NOESY RF score with known prognostic factors and the GRACE score
The known prognostic factors age, sex, previous CABG, previous PCI, heart failure, atrial fibrillation, cerebrovascular disease, diabetes, creatinine concentration, killip class, and acute coronary syndrome classification were compared with the NOESY RF risk score, calculated on the validation set, in univariate and multivariate regression analyses, and the results are displayed in Table 2. A similar analysis using age as a continuous variable has been performed, details are reported in the Supplementary Materials.
In the univariate analysis, many prognostic factors were statistically associated with the outcomes, but the NOESY RF score shows the P-value by far more significant (p = 2.00·10-16). Moreover, in the multivariate regression only the age, the killip class and

the RF score remain statistically significant, demonstrating their independence with respect to the other variables. Interestingly, also in this cohort the smoker's paradox, already described by other several studies (32), has been observed.
Moreover, using the ROC analysis, the NOESY RF score performance was tested against some well-known parameters that are commonly measured in the clinical practice (training and validation set were considered together and in these analyses were included only patients from whom all the clinical parameters were available). As displayed in Figure 2, our score showed the best AUC 0.767, and only age showed a comparable result (AUC 0.738) in predicting death within 2 years from the CV event.
Furthermore, the performance of our approach was also tested in two distinct sub-groups of patients, divided according to the ACS severity (STEMI and NSTEMI). The results, reported in the Supplementary Materials (Supplementary Figure 6), demonstrated that our approach is marginally affected by these two subcategories.
The performances of the NOESY RF score in predicting two-year outcomes were also compared with the ones of the Global Registry of Acute Coronary Events (GRACE) hospital discharge risk score (33) for those patients for which all clinical parameters, needed to calculate the GRACE score, were available (84.5% of patients). Results (Harrell's c index and AUC), displayed in Supplementary Table 2, demonstrated that the NOESY RF score played slightly better both in the training and in the validation sets, confirming undoubtedly how the metabolomic approach here described could be useful for risk stratification in the setting of post ACS patients. Moreover, calculations to create a combined score (GRACE + NOESY RF scores) were performed (Supplementary Figure 7): the combined model, obtained via a linear combination, showed improved results with respect to the two separated ones in both training and validation sets.

Metabolites analysis
An analysis of the NMR spectra was conducted to identify which metabolites are statistically different between dead and survivor patients. All patients (training and validation sets) were included in the analysis. We observed that patients with worst prognosis are characterized by significantly (adjusted p-value < 0.05) higher levels of 3-hydroxybutyrate, proline, creatinine, acetate, acetone, formate and mannose, and significantly lower levels of valine and histidine (Table 2).
Metabolite analysis replicated in training and validation sets separately are provided in the Supplementary Materials (Supplementary Figure 8).

Gender-specific RF models
The presence of gender-specific differences in human metabolism is well-known and the nuclear magnetic resonance metabolomics is sensitive to these differences (34). Therefore, we decided to build two different RF models for females and males to obtain an outcome clusterization and prediction unbiased by gender.

For each gender-specific group using the Random Forest classifier, the metabolomic NOESY1D profiles of 60 survivors and 30 dead patients were classified. Both gender models showed significant differential clustering, with a good separation of the two outcomes groups (Figure 3 A, D).

Using the NOESY NMR spectra of the female and male cohorts separately, the Random Forest classifier discriminated dead from survivor patients in the training set with area under the curve (AUC) of 0.786 and 0.834, respectively (Figure 3 B, E). Thresholds of ≥ 0.46 for the female cohort and ≥ 0.476 for the male cohort were set in the training set by optimizing accuracy, sensitivity, and specificity and the results for both cohorts are shown in Supplementary Table 3.

Applying these models to the validation set of female and male cohorts we attained an AUC of 0.782 and 0.821 respectively (Figure 3 C, F) and using the threshold maximized in the training set we obtained 74.7% and 73.4% overall accuracy for predicting the likelihood of outcome of in female and male cohorts respectively (details in Supplementary Table 3).

By analyzing the spectra of the female and the male cohorts, we observed that female dead patients were characterized by higher levels of creatinine, whereas male dead patients were characterized by higher levels of 3-hydroxybutyrate, proline, creatinine and formate, and significantly lower levels of histidine and valine.

Discussion

In ACS patients enrolled in the AMI Florence 2 Study we found a metabolic fingerprint which is able to discriminate patients who died within two years after the CV event from survivors with a high accuracy (0.859 AUC) and this result was duplicate in a validation set (0.801 AUC). Moreover, gender-specific Random Forest models were built: for males, the ability of predicting the outcomes showed better results (77.2% accuracy for male and 74.5% accuracy for female), and this evidence is confirmed also in the validation set. To the best of our knowledge, this is the first study which assessed the capability of metabolomic assay to predict mortality in the setting of acute coronary syndromes.

The metabolic fingerprint can be deemed as a holistic super-biomarker with a discriminative and predictive power undoubtedly higher than the simple sum of the few quantified metabolites (35). ACS, as the majority of human diseases, has a multifactorial aetiology and a complex physiopathology that alter concurrently several metabolic pathways (36); therefore, the metabolic fingerprint, composed by the superimposition of all the visible signals of the low and high molecular weight endogenous metabolites, represents an optimal level at which to analyze pathological changes in biological systems (37), indeed it takes into account all metabolite variations even the slightly ones.

The NOESY RF score, based on the metabolic fingerprint here presented, showed to be independent from the classical clinical parameters and the widely used GRACE score,

and to achieve better results in predicting all-cause death within two years from ACS considering both logistic regression and ROC analysis.

In this substantial cohort of ACS patients of the AMI Florence 2 Registry we found that dead patients are characterized by significantly higher levels of 3-hydroxybutyrate, proline, creatinine, acetate, acetone, formate and mannose, and significantly lower levels of valine and histidine.

It has been demonstrated that the lifestyle and medication administered to a patient influence the molecular signatures in plasma/serum samples, and the relative metabolite concentrations reflect tissue lesions and organ dysfunctions. In this framework, previous studies have underlined the usefulness of metabolomics of serum/plasma in determining the individual's disease risk, prognosis, and therapeutic options in different clinical settings (27, 38–40). For instance, sera of heart failure patients possess a strong signature of the disease, estimation of the HF-related metabolic disturbance and a better prognostic value than conventional biomarkers (11, 39).

In a prospective study of three population-based cohorts from Finland, and free of CVD at baseline (41) the metabolomic analysis had evidenced that circulating phenylalanine, monounsaturated and polyunsaturated fatty acids were strongly predictive of cardiovascular risk as the conventional lipid risk factors, and were markers of CVD onset during a long-term follow-up (more than a decade).

In our study, we do not find any role for these metabolites in predicting mortality. However, the different study populations (CVD free vs ACS patients) with different lifestyle and dietary habits, may explain the different molecular signature.

The usefulness of the metabolomic approach was also demonstrated in a general cohort of patients at risk for cardiovascular events undergoing cardiac catheterization (42), as baseline plasma metabolomic profiles independently predicted cardiovascular death after adjustment for multiple clinical covariates. In this study, a significant predictive role for 5 metabolomic factors, including the branched-chain amino acids and related catabolites, was demonstrated. Consistently, in the present study we found that higher levels of valine are protective factors in ACS patients. At variance with our study, increased concentrations of branched-chain amino acids levels in coronary artery patients compared with control subjects were shown (43) and high levels of these essential aminoacids (AA) significantly correlated with the severity of CAD (44). However, these studies were case-control studies and did not evaluate CAD patients in the acute phase of the disease. The pathways of the branched-aminoacids in humans are very complex and it is likely that in ACS patients an altered metabolic pathway of these aminoacids may represent a prognostic risk factor.

Our study, performed in a large sample population of ACS patients, followed for 2 years, provided new data about the role of high 3-hydroxybutyrate circulating levels on post-ACS mortality. A previous paper, which evaluated the ketone bodies in the urine of 5 ACS patients demonstrated that ketone bodies and particularly 3-hydroxybutyrate

were altered during the acute event (45). Furthermore, it has been demonstrated that high levels of 3-hydroxybutyrate are associated with high prevalence of heart failure and diabetes (46). In insulin deficiency, when the release of free fatty acids from adipose tissues exceeds the capacity of the tissues to metabolize them, severe and potentially fatal diabetic ketoacidosis can occur where blood 3-hydroxybutyrate levels can reach up to 25 mM (47). However, it remains unclear whether the elevation of ketone bodies represents an adaptive mechanism required to maintain cell metabolism or if it actually contributes to the disease progression.

As expected, patients with worst prognosis showed higher level of serum creatinine, a well-known marker of renal insufficiency. Indeed, it has already been demonstrated that the elevated admission serum creatinine levels are associated with impaired myocardial flow and poor prognosis on one-year mortality (48, 49).

Previous studies evidenced an interaction between gender and adverse cardiovascular events in CAD patients (50–52) as MI morbidity and mortality resulted to be higher in women than in men. Consistently, our results demonstrated a higher prevalence of cardiovascular mortality in women than in men (19.4% vs 12.5%). The excess risk of mortality in women could be ascribed to the differences in cardiovascular risk factor i.e. age, hypertension, diabetes and co-morbidities prevalence. Accordingly, in our study, females show higher median age and higher prevalence of hypertension, atrial fibrillation and heart failure with respect to males.

Building gender-specific models has enabled to obtain an improvement of the outcome prediction in the male cohort, but not in the female one. Thus, male metabolic fingerprint seems to show a higher association with cardiovascular mortality with respect the female one. However, it needs to be consider that the female cohort is less numerous than the male cohort and this may affect the predictive capability of the model; therefore, to build robust gender-specific models wider cohorts of patients are needed.

Conclusions

In conclusion, our data support the usefulness of the metabolomic approach to identify a more precise risk profile in ACS patients. The metabolomic analysis by NMR enables fast, approachable and reproducible characterization of the ACS metabolic fingerprint associated with a poor prognosis improving the cardiovascular risk assessment, beyond that achieved by established risk factors, and most likely identify those patients who need to undergo a very early and aggressive treatment.

Although our study has several strengths, including the number of patients studied, the two-year follow-up, and the analysis replication in a validation set, some limitations should also be considered: NMR is less sensitive than mass spectrometry (even if it is more suitable for metabolic fingerprinting), sample collections were done only in the acute phase of the disease, and lack a further validation set obtained from an independent population. Moreover, the biggest obstacle to the translation of

metabolomics in clinical practice is the acquisition of standard operating procedures for sample collection and storage, only in this possible future scenario this approach could be successfully translated in very large multicenter studies.

Perspectives

Competency in medical knowledge:

NMR metabolomics has the potential to identify patients with high risk of death within two years from ACS, and thus to improve prognostic risk stratification and management of ACS patients.

Translational outlook:

Additional clinical studies on multicenter cohorts are still needed to fully translate the present results into a standard clinical tool and to build a comprehensive clinical/metabolomic integrated model that will predict outcomes in ACS patients with higher accuracy.

References

1. Wright RS, Anderson JL, Adams CD, et al. 2011 ACCF/AHA focused update incorporated into the ACC/AHA 2007 Guidelines for the Management of Patients with Unstable Angina/Non-ST-Elevation Myocardial Infarction: a report of the American College of Cardiology Foundation/American Heart Association Task Force on Practice Guidelines developed in collaboration with the American Academy of Family Physicians, Society for Cardiovascular Angiography and Interventions, and the Society of Thoracic Surgeons. J AmCollCardiol 2011;57:e215–e367.
2. Mozaffarian D, Benjamin EJ, Go AS, et al. Heart disease and stroke statistics--2015 update: a report from the American Heart Association. Circulation 2015;131:e29-322.
3. Granger CB, Goldberg RJ, Dabbous O, et al. Predictors of hospital mortality in the global registry of acute coronary events. Arch. Intern. Med. 2003;163:2345–2353.
4. Antman EM, Cohen M, Bernink PJ, et al. The TIMI risk score for unstable angina/non-ST elevation MI: A method for prognostication and therapeutic decision making. JAMA 2000;284:835–842.
5. Cavusoglu E, Marmur JD, Yanamadala S, et al. Elevated baseline plasma IL-8 levels are an independent predictor of long-term all-cause mortality in patients with acute coronary syndrome. Atherosclerosis 2015;242:589–594.
6. Emerging Risk Factors Collaboration, Kaptoge S, Di Angelantonio E, et al. C-reactive protein concentration and risk of coronary heart disease, stroke, and mortality: an individual participant meta-analysis. Lancet Lond. Engl. 2010;375:132–140.
7. Gallo V, Intini N, Mastrorilli P, et al. Performance Assessment in Fingerprinting and Multi Component Quantitative NMR Analyses. Anal. Chem. 2015;87:6709–6717.

8. Dumas ME, Maibaum EC, Teague C, et al. Assessment of Analytical Reproducibility of 1H NMR Spectroscopy Based Metabonomics for Large-Scale Epidemiological Research: the INTERMAP Study. Anal. Chem. 2006;78:2199–2208.
9. Eckhart AD, Beebe K, Milburn M. Metabolomics as a key integrator for "omic" advancement of personalized medicine and future therapies. Clin. Transl. Sci. 2012;5:285–288.
10. Zordoky BN, Sung MM, Ezekowitz J, et al. Metabolomic fingerprint of heart failure with preserved ejection fraction. PloS One 2015;10:e0124844.
11. Tenori L, Hu X, Pantaleo P, et al. Metabolomic fingerprint of heart failure in humans: a nuclear magnetic resonance spectroscopy analysis. Int. J. Cardiol. 2013;168:e113-115.
12. Alonso A, Yu B, Qureshi WT, et al. Metabolomics and Incidence of Atrial Fibrillation in African Americans: The Atherosclerosis Risk in Communities (ARIC) Study. PloS One 2015;10:e0142610.
13. Liu X, Gao J, Chen J, et al. Identification of metabolic biomarkers in patients with type 2 diabetic coronary heart diseases based on metabolomic approach. Sci. Rep. 2016;6:30785.
14. Bodi V, Sanchis J, Morales JM, et al. Metabolomic profile of human myocardial ischemia by nuclear magnetic resonance spectroscopy of peripheral blood serum: a translational study based on transient coronary occlusion models. J. Am. Coll. Cardiol. 2012;59:1629–1641.
15. Ali SE, Farag MA, Holvoet P, Hanafi RS, Gad MZ. A Comparative Metabolomics Approach Reveals Early Biomarkers for Metabolic Response to Acute Myocardial Infarction. Sci. Rep. 2016;6:36359.
16. Park JY, Lee S-H, Shin M-J, Hwang G-S. Alteration in metabolic signature and lipid metabolism in patients with angina pectoris and myocardial infarction. PloS One 2015;10:e0135228.
17. von Zur Muhlen C, Schiffer E, Zuerbig P, et al. Evaluation of urine proteome pattern analysis for its potential to reflect coronary artery atherosclerosis in symptomatic patients. J. Proteome Res. 2009;8:335–345.
18. Cesari F, Marcucci R, Gori AM, et al. Reticulated platelets predict cardiovascular death in acute coronary syndrome patients. Insights from the AMI-Florence 2 Study. Thromb. Haemost. 2013;109:846–853.
19. Cohen J. Statistical power analysis for the behavioral sciences. L. Erlbaum Associates; 1988. Available at: http://books.google.it/books?id=8wBHAAAAMAAJ.
20. Bernini P, Bertini I, Luchinat C, Nincheri P, Staderini S, Turano P. Standard operating procedures for pre-analytical handling of blood and urine for metabolomic studies and biobanks. J. Biomol. NMR 2011;49:231–243.

21. Beckonert O, Keun HC, Ebbels TMD, et al. Metabolic profiling, metabolomic and metabonomic procedures for NMR spectroscopy of urine, plasma, serum and tissue extracts. Nat. Protoc. 2007;2:2692–2703.
22. Gebregiworgis T, Powers R. Application of NMR metabolomics to search for human disease biomarkers. Comb. Chem. High Throughput Screen. 2012;15:595–610.
23. Spraul M, Neidig P, Klauck U, et al. Automatic reduction of NMR spectroscopic data for statistical and pattern recognition classification of samples. J Pharm Biomed Anal 1994;12:1215–1225.
24. Holmes E, Foxall PJ, Nicholson JK, et al. Automatic data reduction and pattern recognition methods for analysis of 1H nuclear magnetic resonance spectra of human urine from normal and pathological states. Anal Biochem 1994;220:284–296.
25. Kotsiantis S, Kanellopoulos D, Pintelas P. Handling imbalanced datasets: A review. GESTS Int. Transter Sci. Eng. CompugResearchGate 2005;30:25–36.
26. Breiman L. Random Forests. Mach. Learn. 2001;45:5–32.
27. Tenori L, Oakman C, Morris PG, et al. Serum metabolomic profiles evaluated after surgery may identify patients with oestrogen receptor negative early breast cancer at increased risk of disease recurrence. Results from a retrospective study. Mol. Oncol. 2015;9:128–139.
28. Wishart DS, Jewison T, Guo AC, et al. HMDB 3.0--The Human Metabolome Database in 2013. Nucleic Acids Res. 2013;41:D801–D807.
29. Wilcoxon F. Individual Comparisons by Ranking Methods. Biom. Bull. 1945;1:80.
30. Benjamini Y, Hochberg Y. Controlling the false discovery rate: a practical and powerful approach to multiple testing. J. R. Stat. Soc. Ser. B Methodol. 1995:289–300.
31. Cliff N. Ordinal Methods for Behavioral Data Analysis. Mahwah, N.J: Psychology Press; 1996.
32. Robertson JO, Ebrahimi R, Lansky AJ, Mehran R, Stone GW, Lincoff AM. Impact of Cigarette Smoking on Extent of Coronary Artery Disease and Prognosis of Patients With Non–ST-Segment Elevation Acute Coronary Syndromes: An Analysis From the ACUITY Trial (Acute Catheterization and Urgent Intervention Triage Strategy). JACC Cardiovasc. Interv. 2014;7:372–379.
33. Tang EW, Wong C-K, Herbison P. Global Registry of Acute Coronary Events (GRACE) hospital discharge risk score accurately predicts long-term mortality post acute coronary syndrome. Am. Heart J. 2007;153:29–35.
34. Kochhar S, Jacobs DM, Ramadan Z, Berruex F, Fuerholz A, Fay LB. Probing gender-specific metabolism differences in humans by nuclear magnetic resonance-based metabonomics. Anal. Biochem. 2006;352:274–281.
35. Vignoli A, Rodio DM, Bellizzi A, et al. NMR-based metabolomic approach to study urine samples of chronic inflammatory rheumatic disease patients. Anal. Bioanal. Chem. 2016:1–9.

36. Nicholson JK, Holmes E, Wilson ID. Gut microorganisms, mammalian metabolism and personalized health care. Nat. Rev. Microbiol. 2005;3:431–438.
37. Li J, Brazhnik O, Kamal A, et al. Metabolic Profiling - Its Role in Biomarker Discovery and Gene Function Analysis. In: Harrigan G, Goodacre R, editors. Kluwer Academic Publishers, 2003:293–309.
38. Basak T, Varshney S, Hamid Z, Ghosh S, Seth S, Sengupta S. Identification of metabolic markers in coronary artery disease using an untargeted LC-MS based metabolomic approach. J. Proteomics 2015;127:169–177.
39. Cheng M-L, Wang C-H, Shiao M-S, et al. Metabolic disturbances identified in plasma are associated with outcomes in patients with heart failure: diagnostic and prognostic value of metabolomics. J. Am. Coll. Cardiol. 2015;65:1509–1520.
40. Hart CD, Vignoli A, Tenori L, et al. Serum Metabolomic Profiles Identify ER-Positive Early Breast Cancer Patients at Increased Risk of Disease Recurrence in a Multicenter Population. Clin. Cancer Res. Off. J. Am. Assoc. Cancer Res. 2017;23:1422–1431.
41. Würtz P, Havulinna AS, Soininen P, et al. Metabolite profiling and cardiovascular event risk: a prospective study of 3 population-based cohorts. Circulation 2015;131:774–785.
42. Shah SH, Sun J-L, Stevens RD, et al. Baseline metabolomic profiles predict cardiovascular events in patients at risk for coronary artery disease. Am. Heart J. 2012;163:844–850.e1.
43. Yang RY, Wang SM, Sun L, et al. Association of branched-chain amino acids with coronary artery disease: A matched-pair case-control study. Nutr. Metab. Cardiovasc. Dis. NMCD 2015;25:937–942.
44. Bhattacharya S, Granger CB, Craig D, et al. Validation of the association between a branched chain amino acid metabolite profile and extremes of coronary artery disease in patients referred for cardiac catheterization. Atherosclerosis 2014;232:191–196.
45. Martin-Lorenzo M, Zubiri I, Maroto AS, et al. KLK1 and ZG16B proteins and arginine-proline metabolism identified as novel targets to monitor atherosclerosis, acute coronary syndrome and recovery. Metabolomics Off. J. Metabolomic Soc. 2015;11:1056–1067.
46. Soininen P, Kangas AJ, Würtz P, Suna T, Ala-Korpela M. Quantitative serum nuclear magnetic resonance metabolomics in cardiovascular epidemiology and genetics. Circ. Cardiovasc. Genet. 2015;8:192–206.
47. Cahill GF, Veech RL. Ketoacids? Good medicine? Trans. Am. Clin. Climatol. Assoc. 2003;114:149-161-163.
48. Zhao L, Wang L, Zhang Y. Elevated admission serum creatinine predicts poor myocardial blood flow and one-year mortality in ST-segment elevation myocardial infarction patients undergoing primary percutaneous coronary intervention. J. Invasive Cardiol. 2009;21:493–498.

49. Cakar MA, Gunduz H, Vatan MB, Kocayigit I, Akdemir R. The Effect of Admission Creatinine Levels on One-Year Mortality in Acute Myocardial Infarction. Sci. World J. 2012;2012:e186495.
50. Vaccarino V, Abramson JL, Veledar E, Weintraub WS. Sex differences in hospital mortality after coronary artery bypass surgery: evidence for a higher mortality in younger women. Circulation 2002;105:1176–1181.
51. Löwel H, Meisinger C, Heier M, et al. [Sex specific trends of sudden cardiac death and acute myocardial infarction: results of the population-based KORA/MONICA-Augsburg register 1985 to 1998]. Dtsch. Med. Wochenschr. 1946 2002;127:2311–2316.
52. Kunadian V, Qiu W, Lagerqvist B, et al. Gender Differences in Outcomes and Predictors of All-Cause Mortality After Percutaneous Coronary Intervention (Data from United Kingdom and Sweden). Am. J. Cardiol. 2016.

List of Figures and Tables

CENTRAL ILLUSTRATION

Title: Metabolomics as tool to improve the risk of death stratification in ACS patients

Legend: ACS is a generic term that encompasses the different clinical manifestations of ischemic heart disease. Although current patient management procedures have resulted in a reduction of hospital mortality for the acute phase, the first-year mortality is still increasing. Therefore, new methods of risk assessment and stratification are required. Applying NMR-based metabolomic approach is possible to identify ACS patients with an adverse prognosis within the first two years after the cardiovascular event with 78% accuracy. The results are also reproduced in an independent test set obtaining an AUC of 0.801, and 72.64% accuracy.

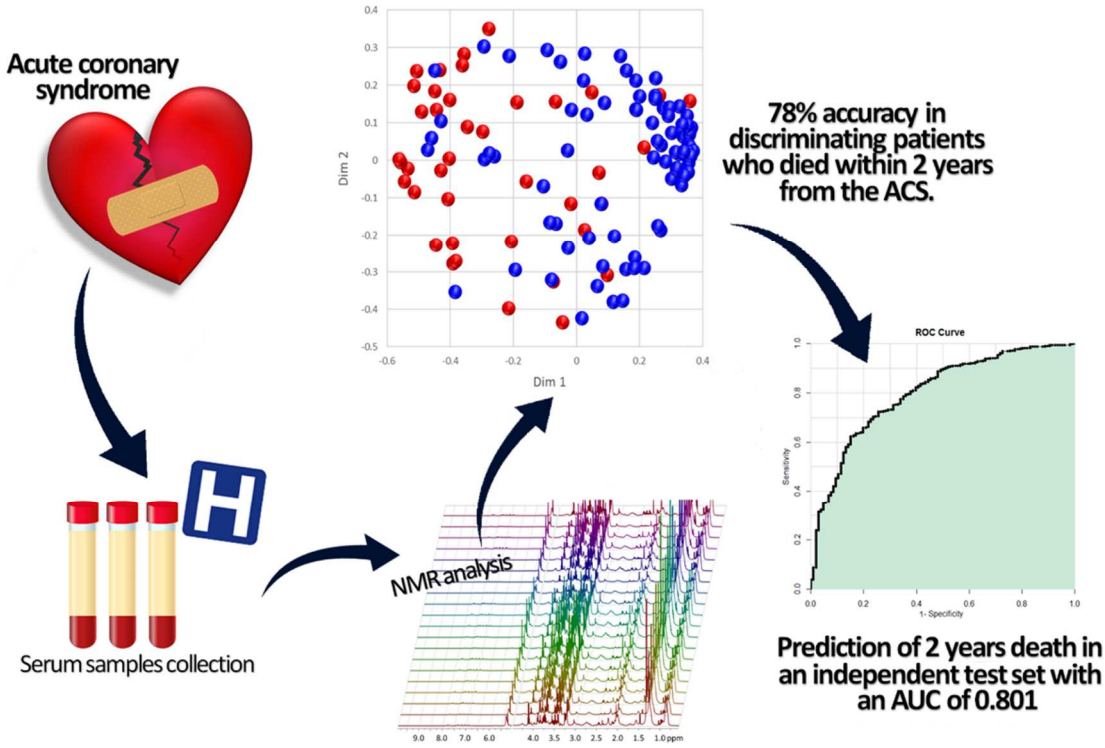

FIGURE 1

Title: Clusterization of serum metabolomic profiles and comparisons between metabolomic classification and outcomes in the training set and the validation set.

Legend: A) Discrimination between survivor (blue dots, n = 80) and dead (red dots, n = 40) patients using the Random Forest classifier on NOESY spectra in the training set. The ROC curves and the AUC scores are presented for B) Training set; C) Validation test.

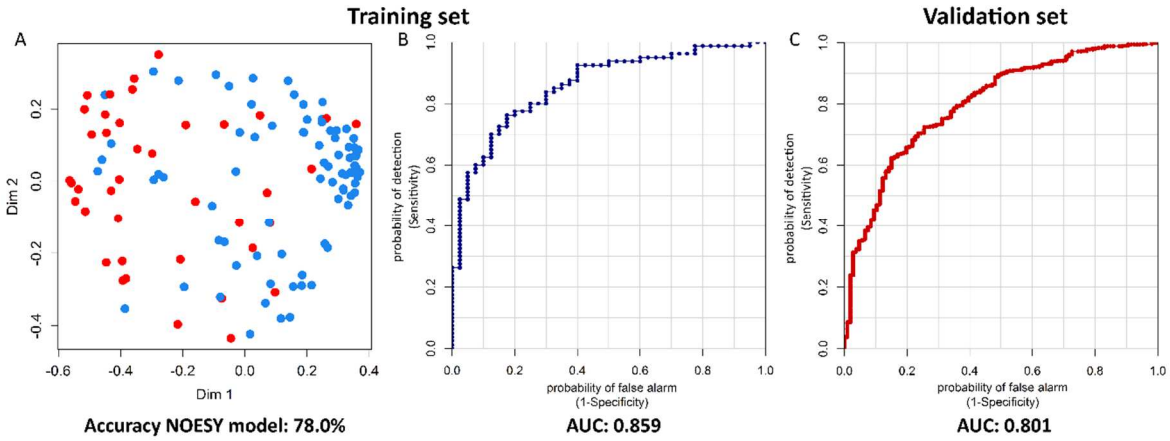

FIGURE 2

Title: NOESY RF score and clinical parameters ROC curves.

Legend: The ROC curves and the AUC scores are presented for NOESY RF score, age, heart frequency, diastolic pressure, systolic pressure, glycemia, creatinine, platelets, troponine max and creatine kinase-MB max.

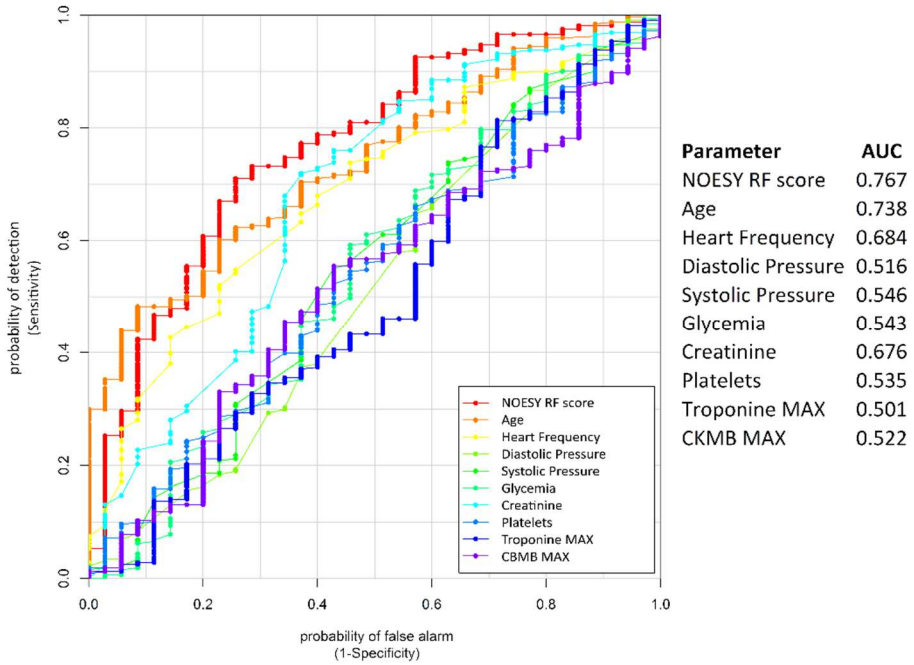

Parameter	AUC
NOESY RF score	0.767
Age	0.738
Heart Frequency	0.684
Diastolic Pressure	0.516
Systolic Pressure	0.546
Glycemia	0.543
Creatinine	0.676
Platelets	0.535
Troponine MAX	0.501
CKMB MAX	0.522

FIGURE 3

Title: Gender-specific models and predictions using NOESY1D spectra

Legend: Clusterization of serum metabolomic profiles discriminating between survivor (blue dots) and dead (red dots) patients using the Random Forest classifier for A) male; D) female. Comparison between metabolomic classification and outcomes in the training set: the ROC curves and the AUC scores are presented for B) male; E) female. Prediction of outcomes in the validation set: the ROC and the AUC scores are presented for C) male; F) female.

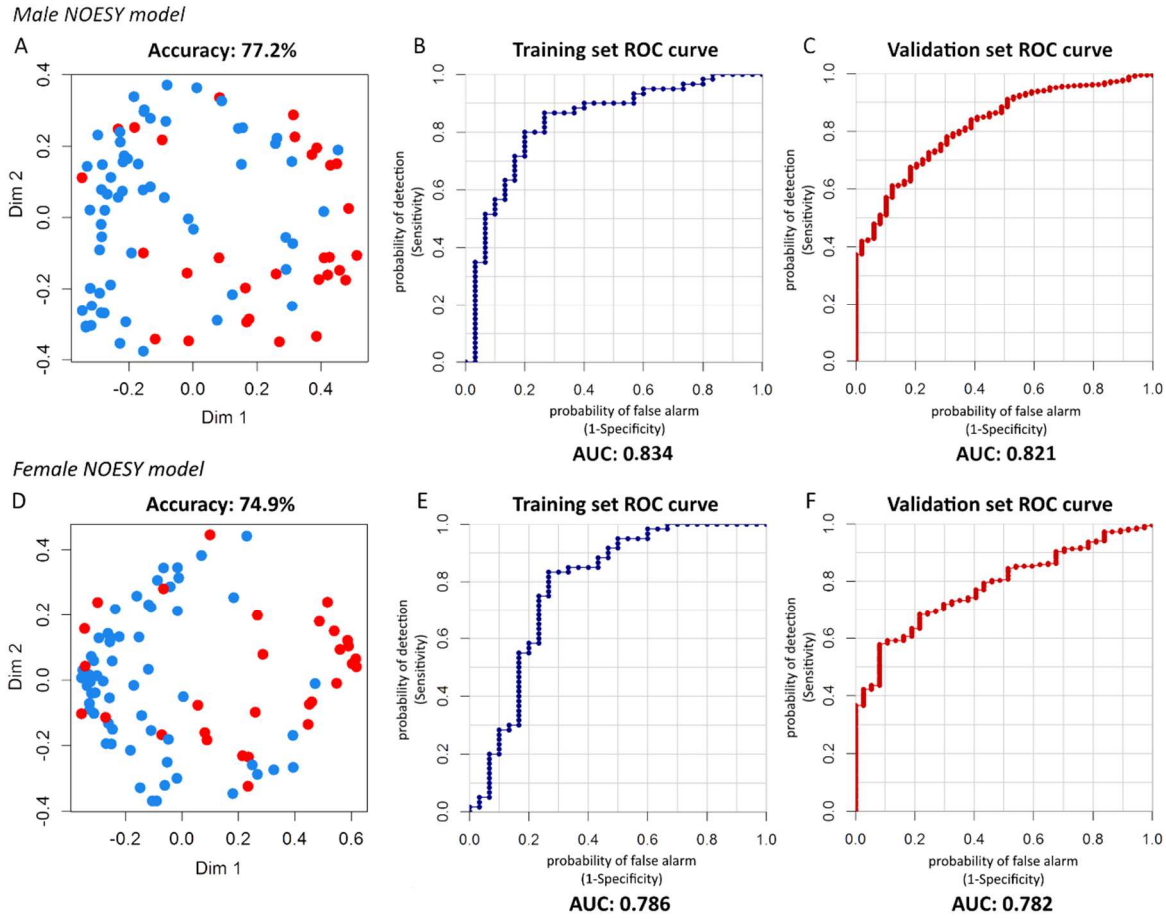

TABLE 1 **Demographic and Clinical Characteristics**

	Survivor patients (832)	Dead patients (146)	P-value
Demographic characteristics,			
Age (years), median (IQR)	72 (62-80)	82 (78-83)	< 2.20E-16
Gender, females, n (%)	278 (33.4)	67 (45.9)	4.86E-03
Cardiovascular risk factors, n (%)			
Hypertension	537 (64.5)	104 (71.2)	1.21E-01
Dyslipidemia	294 (35.3)	32 (21.9)	3.55E-03
Current smokers	226 (27.2)	20 (13.7)	1.45E-04
Ex-smokers	21 (2.5)	8 (5.5)	4.01E-01
CAD	220 (26.4)	17 (11.6)	5.03E-04
Diabetes	197 (23.7)	61 (41.8)	6.32E-06
Medical history, n (%)			
Myocardial infarction	164 (19.7)	48 (32.9)	5.23E-04
Angina, onset > 1 month	119 (14.3)	24 (16.4)	8.96E-01
Angina, onset ≤ 1 month	149 (17.9)	15 (10.3)	3.78E-02
CABG	41 (4.9)	10 (6.8)	4.39E-01
PCI	136 (16.3)	32 (21.9)	1.20E-01
Chronic heart failure	33 (4.0)	26 (17.8)	2.62E-10
Atrial fibrillation	42 (5.0)	21 (14.4)	4.60E-05
Cerebrovascular disease	50 (6.0)	28 (19.2)	1.28E-07
Presentation features			
ACS classification, STEMI, n (%)	343 (41.2)	35 (24.0)	1.15E-04
Killip II-IV, n (%)	114 (13.7)	61 (41.8)	6.33E-16
Creatinine > 1.2 mg/dL, n (%)	129 (15.5)	54 (37.0)	4.08E-09
Heart rate (bpm), median (IQR)	80 (67-91)	90 (80-105)	3.66E-06
Positive peak troponine max, n (%)	804 (96.6)	143 (97.9)	6.98E-01
Positive peak CK-MB max, n (%)	422 (50.7)	50 (32.2)	1.88E-03

CAD = coronary artery diseases; CABG = coronary artery bypass grafting; PCI = percutaneous coronary intervention; ACS = acute coronary syndrome; STEMI = ST-segment elevation myocardial infarction; CK-MB = creatine kinase-MB

TABLE 2 **Association with the Outcome: unadjusted and adjusted Odds Ratios**

	Odds ratio (univariate)	P-value	Odds ratio (multivariate)	P-value
Age				
68 -79	4.1579	9.09e-04	1.7916	3.15e-01
> 79	14.112	8.01e-11	4.7021	7.96e-03
Male sex	0.5644	6.30e-03	0.6785	2.74e-01
Hypertension	1.2710	2.86e-01	0.3745	1.04e-02
Dyslipidemia	0.5380	1.26e-02	0.3412	1.62e-02
Smoking habits				
Yes	0.3028	2.56e-04	0.7043	4.42e-01
Ex-smokers	0.9612	9.44e-01	6.78e-08	9.83e-01
CAD	0.4101	4.22e-03	1.2303	6.33e-01
Previous CABG	1.4639	3.43e-01	1.9080	3.87e-01
Previous PCI	1.2995	3.20e-01	1.5356	4.14e-01
Heart failure	4.9639	2.65e-07	2.0267	1.57e-01
Atrial fibrillation	2.5118	6.43e-03	1.0956	8.60e-01
Cerebrovascular disease	3.9224	2.15e-06	1.8436	1.90e-01
Diabetes	2.4871	2.17e-05	1.8466	8.09e-02
Creatinine (>1.2 mg/dL)	2.9582	1.73e-06	1.3379	4.43e-01
Killip class				
II	3.7494	6.58e-07	1.2553	6.09e-01
III	5.8838	9.66e-08	5.6398	3.74e-04
IV	10.383	9.95e-02	19.4783	5.70e-02
ACS classification				
STEMI	0.5379	7.66e-03	0.7458	4.28e-01
Random Forest Risk Score				
≥ 0.454	7.0378	2.00e-16	3.3625	1.26e-03

Correlation with the outcome for prognostic features and RF risk score in the validation set, using univariate and multivariate analysis. Age split into tertiles. Abbreviations as in Table 1. In the multivariate odd ratios all the variable were included together in the analysis.

TABLE 3 Univariate Metabolites Analyses

Assigned metabolites	Dead cohort	Survivor cohort	Adjusted p-value	Effect size (Cliff's delta)	Fold change
Acetate	97.14 ± 66.16	78.27 ± 47.94	3.10e-02	0.167	0.312
Acetone	913.9 ± 819.93	747.66 ± 564.49	4.10e-02	0.163	0.290
Alanine	1384.39 ± 319.37	1499.65 ± 368.9	1.32e-01	-0.144	-0.115
Citrate	100.18 ± 39.36	89.58 ± 30.12	1.82e-01	0.138	0.161
Creatine	101.15 ± 78.45	103.11 ± 60.2	1.00e+00	0.016	-0.028
Creatinine	265.11 ± 107.24	198.4 ± 56.18	1.48e-11	0.373	0.418
Formate	11.04 ± 3.5	9.48 ± 3.26	1.46e-04	0.234	0.221
Glucose	3034.26 ± 1143.89	2758.32 ± 755.37	1.79e-01	0.139	0.138
Glutamate	175.21 ± 108.52	205.48 ± 106.61	1.00e+00	-0.099	-0.230
Glutamine	201.64 ± 66.5	189.8 ± 45.97	1.00e+00	0.103	0.087
Glycine	494.25 ± 170.9	528.65 ± 159.84	1.00e+00	-0.079	-0.097
Histidine	106.22 ± 21.98	114.64 ± 22.04	4.92e-04	-0.221	-0.110
Isobutyrate	35.54 ± 14.59	30.36 ± 12.47	9.05e-02	0.150	0.227
Isoleucine	150.73 ± 41.74	163.78 ± 42.15	1.11e-01	-0.147	-0.120
Lactate	1594.03 ± 575.05	1536.27 ± 419.58	1.00e+00	0.007	0.053
Leucine	482.98 ± 151.7	523.63 ± 120	9.86e-01	-0.106	-0.117
Mannose	122.14 ± 54.41	105.44 ± 34.71	8.33e-03	0.185	0.212
Methionine	115.76 ± 42.64	110.98 ± 35.8	1.00e+00	0.058	0.061
Phenylalanine	234.35 ± 65.27	228.57 ± 59.25	8.20e-01	0.110	0.036
Proline	158.42 ± 94.5	114.52 ± 59.5	2.97e-07	0.295	0.468
Tyrosine	167.18 ± 44.94	170.61 ± 37.32	1.00e+00	-0.043	-0.029
Valine	1016.1 ± 250.83	1127.15 ± 237.85	4.69e-06	-0.270	-0.150
3-hydroxybutyrate	488.44 ± 526.3	319.89 ± 310.27	1.17e-03	0.211	0.611

List of metabolites assigned in the serum NMR spectra, reported as median with median absolute deviation (arbitrary units). A p-value adjusted with Bonferroni < 0.05 deemed significant. The Cliff's delta and the fold change for each metabolite are also reported.

Supplementary materials

Supplementary methods

Study population

The study population comprised a group of 978 out of 1496 patients admitted to the Coronary Unit of the Careggi University Hospital, Florence, Italy from April 2008 to April 2009 enrolled on the frame of the Florence Acute Myocardial Infarction-2 (AMI-Florence 2) registry.

The AMI-Florence Registry prospectively included all patients who arrived alive to the emergency departments of one of the six participating hospitals in the Florence health district with a suspected STEMI between March 2000 and February 2001. All patients fulfilling the diagnostic criteria for acute or sub-acute (symptom onset ≤ 24 or > 24 hours, respectively) STEMI were screened for enrolment in the registry, without any exclusion criteria. The AMI-Florence 2 registry is a second-wave survey of the AMI-Florence registry, and was extended to include all cases of suspected ACS arriving alive to any of the six hospitals, with no exclusion criteria (AMI-Florence 2 included both STEMI and NSTEMI cases).

ACS was diagnosed according to criteria established by the European Society of Cardiology (1). Briefly, AMI was defined as typical rise and gradual fall of troponin, or more rapid rise and fall of CK-MB, defined as > 99% of normal levels (troponin T >0.05 ng/mL; CK-MB >10 ng/mL), with at least one of the following: acute onset of typical ischaemic chest pain; some Q waves in V1-V3 , 30 ms Q waves 1 mm in two contiguous leads; ST- segment elevation or depression in 2 leads, 0.2 mV in V1-V3, >0.1 mV in other leads. Unstable angina was defined as a history of new-onset, more frequent, more persistent or rest episode of chest pain, without typical changes of myocardial enzymes and with ECG evidence of myocardial ischaemia (transient ST segment displacement >0.1 mV during chest pain). All patients underwent coronary angiography performed by the Judkins' technique and PCI. Before PCI, all patients received a loading dose of 500 mg of acetylsalicylic acid (ASA) and 300 mg of clopidogrel, followed by 100 (15.9%) or 325 mg (84.1%) of ASA daily and 75 mg of clopidogrel daily. The use of glycoprotein (GP)IIb/IIIa inhibitors was at discretion of the operator and was carried out in 48.5% of patients. Unfractioned heparin 70IU/kg was used in all patients during PCI as anticoagulant. Clinical follow-up information was obtained by contacting all the patients at 24 months, and source documents of potential events were recorded.

Current smoking status was determined at the time of blood collection. The subjects were classified as having hypertension according to the guidelines of European Society of Hypertension/ European Society of Cardiology (2) or if they reported taking antihypertensive medications, as verified by the physician. Diabetic subjects were defined in agreement with the American Diabetes Association (3) or on the basis of self-report data (if confirmed by medication or chart review). Dyslipidemia was defined according to the Third report of the National Cholesterol Education Program (NCEP-III) (4) or if they reported taking antidyslipidaemic drugs, as verified by the physician. A positive family history was defined as the presence of at least one first-degree relative who had developed CAD before the age of 55 years for men and 65 years for women.

In-hospital data collection

A web-based form was used to collect information on demographics, medical history, clinical and ECG characteristics, treatment and outcomes during hospitalization, and prescriptions at

discharge. Time intervals from onset of symptoms to hospital admission and revascularization were recorded. The Coordinating Centre periodically reviewed data for inconsistencies, and, when necessary, queries were sent to local investigators for further checks before data processing. Completeness of enrolment was periodically checked by comparing hospital discharge data for Acute Coronary Syndromes ICD9-CM codes (primary diagnosis: 410.*, 411.* and 413.*, or 427.5 associated with 410.*, 411.*, 413.* as secondary diagnosis; asterisks indicates only three ICD 9 digits, irrespective of the other digits (fourth and fifth)) from hospitals in the area with data of patients actually entered. When a discharge record could not be tracked in the study database, the original clinical record was checked, and, if enrolment criteria were met, the case was eventually included. Therefore, the series enrolled is population-based and fully representative of incident AMI cases in the area over the study period.

Follow-up data collection
Two-year vital status was assessed by consulting the registry office of the city of residence.

Serum sample collection and storage
Blood withdrawals were obtained drew by trained medical personnel and, serum samples were obtained by centrifuging blood sample at 2,000 g for 10 min a 4°C and then stored in aliquots at -80°C until analysis.

NMR sample preparation
Frozen serum samples were thawed at room temperature and shaken before use. The NMR samples were prepared according to the standard operating procedures (5). A total of 300 μL of a sodium phosphate buffer (10.05 g Na2HPO4·7H2O; 0.2 g NaN3; 0.4 g sodium trimethylsilyl [2,2,3,3-2H4]propionate (TMSP) in 500 mL of H2O with 20% (v/v) 2H2O; pH 7.4) was added to 300 μL of each serum sample, and the mixture was homogenized by vortexing for 30 s. A total of 450 μL of this mixture was transferred into a 4.25 mm NMR tube (Bruker BioSpin srl) for the analysis.

NMR spectra acquisition and processing
Monodimensional 1H NMR spectra for all samples were acquired using a Bruker 600 MHz spectrometer (Bruker BioSpin) operating at 600.13 MHz proton Larmor frequency, and equipped with a 5 mm CPTCI 1H-13C-31P and 2H-decoupling cryoprobe including a z axis gradient coil, an automatic tuning-matching (ATM) and an automatic sample changer. A BTO 2000 thermocouple served for temperature stabilization at the level of approximately 0.1 K at the sample. Before measurement, samples were kept for at least 3 minutes inside the NMR probehead, for temperature equilibration at 310 K.
According to standard practice, for each serum samples three monodimensional 1H NMR spectra with different pulse sequences were acquired:

(i) a standard nuclear Overhauser effect spectroscopy pulse sequence NOESY 1Dpresat (noesygppr1d.comp; Bruker BioSpin), using 64 scans, 98304 data points, a spectral width of 18028 Hz, an acquisition time of 2.7 s, a relaxation delay of 4 s and a mixing time of 0.1 s, was applied to obtain a spectrum in which both signals of low molecular weight metabolites and high molecular weight aggregates (lipids and lipoproteins) are visible.

(ii) a standard spin echo Carr-Purcell-Meiboom-Gill (CPMG) (6) (cpmgpr1d.comp; Bruker BioSpin) pulse sequence, with 64 scans, 73728 data points, a spectral width of 12019 Hz and a relaxation delay of 4 s, was used for the selective observation of low molecular weight metabolites, suppressing signals arising from high molecular weight aggregates.

(iii) a standard diffusion-edited (7) (ledbgppr2s1d.comp; Bruker BioSpin) pulse sequence, using 64 scans, 98304 data points, a spectral width of 18028 Hz and a relaxation delay of 4 s, was applied to suppress the signals of low molecular weight metabolites.

Free induction decays were multiplied by an exponential function equivalent to a 1.0 Hz line-broadening factor before applying Fourier transformation. Transformed spectra were automatically corrected for phase and baseline distortions and calibrated (anomeric glucose doublet at 5.24 ppm) using TopSpin 3.2 (Bruker Biospin srl).

Each 1D spectrum in the range 0.2-10.00 ppm was segmented into 0.02 ppm chemical shift bins and the corresponding spectral areas were integrated using AMIX software (version 3.8.4, Bruker BioSpin). Binning is a mean to reduce the number of total variables, to compensate for subtle signal shifts, and filter noise in the spectra, making the analysis more robust and reproducible (8, 9). The region between 4.5 and 5.0 ppm containing the residual water signal was removed and the dimension of the system was reduced to 466 bins. The total spectral area was calculated on the remaining bins and total area normalization was carried out on the data prior to pattern recognition.

Statistical analysis

Data analyses were performed using the open source software R. For the demographic and baseline characteristics, the t-test was used for comparison between groups and the chi-square test for comparison between categorical variables.

For the multivariate data analyses of the NMR data the group of 978 patients was randomly split into two independent cohorts: a training set constituted by 80 survivors and 40 dead patients (10), and a validation set constituted by all the remaining patients (106 dead patients and 752 survivor patients).

The initial analysis was restricted to the training set and the first step was to establish if serum metabolomic profiles could distinguish between dead and survivor patients within two years from the cardiovascular event, for this purpose, a Random Forest (RF) classifier (11) was built. The percentage of trees in the forest that assign one sample to a specific class can be inferred as a probability of class belonging, and it gives an unbiased assessment of the classification error using the out-of-bag samples (12).

The RF classifier uses data from the training set to build an ensemble of decision trees. Each tree is used to predict whether a sample is associated with positive or negative outcome. For each patient, a score was created that expresses the extent to which the serum metabolomic profile appears to be similar to the one of patients with a negative outcome, designated as the 'RF risk score'. This score is based on the percentage of trees in the ensemble that misclassify the sample as belonging to the cohort of patients with a negative outcome. For each patient, three RF scores were derived using the three types of spectra acquired. For all calculations, the R package 'Random Forest' (11) was used to grow a forest of 2000 trees, using the default settings.

The next step was to test the hypothesis that a metabolomic signature similar to the one of patients with a negative outcome would be really predictive of death within two years from

the CV event. Using receiver operating characteristics (ROC) analysis ("colAUC" function of the R package "caTools") and Harrell's c index ("cindex" function on the R package "dynpred"), the performance of the RF risk scores were compared with the actual outcome. To delineate high risk of death, a cut-off for the RF risk score was calculated in the training set that optimized accuracy, sensitivity and specificity, and the performance of the model was subsequently tested in the validation set. Sensitivity, specificity, and accuracy were calculated according to the standard definition of, respectively: proportion of death patients that are correctly identified as such with respect to the total death patients; proportion of alive patients that are correctly identified as such with respect to the total alive patients; proportion of correctly classified individuals (both death and alive) that are correctly identified with respect to the total cohort.

Supplementary Results

Exploratory unsupervised analysis of the dataset

Principal Component Analysis (PCA) was performed as first exploratory analysis. It is apparent that no unsupervised discrimination between the main hospital (Careggi University Hospital) and the other centers is present. The score plot of the first two principal components is provided (Supplementary Figure 3).

Distinct metabolomic models calculated according to ACS severity

Patients enrolled in this study were 378 STEMI and 600 NSTEMI. Using a Random Forest classifier, it is possible to discriminate between these two subgroups with 66.5% accuracy (Supplementary Figure 6), indicating that the serum metabolic fingerprint is weakly affected by the ACS severity. The possible implications of these differences due to sub-phenotypes of STEMI and NSTEMI has been further investigated by building two distinct models for the outcome prediction: 100 cycles of classical Monte Carlo cross-validation scheme with 80-20 % splitting of the data (training set, validation set) have been performed for each sub-group, and a mean AUC of 0.829 (95% CI, 0.812-0.846) and of 0.784 (95% CI, 0.774-0.794) were obtained for STEMI and NSTEMI, respectively. Comparing these results with the mean cross-validated AUC obtained using all the dataset together (AUC 0.805), we can conclude that the division of patients according to severity contributes only marginally to the metabolomic fingerprint associated with the outcome, and, as a consequence, that the prognostic value of the metabolic fingerprint reported here is not just a proxy of the clinical status, but a real instrument able to improve the risk stratification in the framework of post ACS patients.

Comparison of the NOESY RF score with age as a continuous variable

Logistic analysis was performed also using age as a continuous variable. In this case, an odd ratio of 1.11 and a *P*-value of 1.12e-14 in the univariate analysis (multivariate results: odd ratio 1.07 and *P*-value 4.07e-05) was obtained. The effect of using age as a continuous variable on the odd ratios and *P*-values of the other significant variables is only marginal (NOESY RF score odd ratio 3.21 and *P*-value 2E-03; Killip class III odd ratio 5.02 and *P*-value 9e-04).

SUPPLEMENATRY TABLE 1 **Demographic and Clinical Characteristics divided according to gender**

	Male		Female		P-value M *vs* F
	Survivor patients (554)	Dead patients (79)	Survivor patients (278)	Dead patients (67)	
Age (years), median (IQR)	70 (59-77)	81 (76-87)	77 (70-84)	83 (80-88)	2.2E-16
Cardiovascular risk factors, n (%)					
Hypertension	340 (61.4)	52 (65.8)	197 (70.9)	52 (77.6)	1.15E-03
Dyslipidemia	191 (29.0)	18 (22.8)	103 (37.1)	14 (20.9)	7.78E-01
Current smokers	186 (33.6)	15 (19.0)	40 (14.4)	5 (7.5)	1.46E-20
Ex-smokers	13 (2.9)	5 (6.3)	8 (2.9)	3 (4.5)	1.09E-01
CAD	160 (28.9)	9 (11.4)	60 (21.6)	8 (2.9)	3.14E-02
Diabetes	121 (21.8)	35 (44.3)	76 (27.3)	26 (38.8)	1.21E-01
Medical history, n (%)					
Myocardial infarction	109 (19.7)	32 (40.5)	55 (19.8)	16 (23.9)	5.51E-01
Angina, onset > 1 month	76 (13.7)	14 (17.7)	43 (15.5)	10 (14.9)	1.00E+00
Angina, onset ≤ 1 month	108 (19.5)	9 (11.4)	41 (14.7)	6 (9.0)	6.27E-02
CABG	31 (5.6)	7 (8.9)	10 (3.6)	3 (4.5)	1.71E-01
PCI	96 (17.3)	23 (29.1)	40 (14.4)	9 (13.4)	7.77E-02
Chronic heart failure	17 (3.1)	11 (13.9)	16 (5.8)	15 (22.4)	6.73E-03
Atrial fibrillation	19 (3.4)	8 (10.1)	23 (8.3)	13 (19.4)	3.20E-04
Cerebrovascular disease	31 (5.6)	14 (17.7)	19 (6.8)	14 (20.9)	2.24E-01
Presentation features					
ACS classification, STEMI, n (%)	250 (45.1)	17 (21.5)	93 (33.4)	18 (26.9)	2.68E-03
Killip II-IV, n (%)	59 (10.7)	29 (36.7)	53 (19.1)	32 (47.8)	2.16E-05
Creatinine > 1.2 mg/dL, n (%)	85 (15.3)	32 (40.5)	44 (15.8)	22 (32.8)	1.00E+00
Heart rate (bpm), median (IQR)	77.5 (65-89)	89 (80-100)	83 (70-98)	94 (80-106)	3.36E-05
Peak troponine max, n (%)	532 (96.0)	78 (98.7)	272 (97.8)	65 (97.0)	1.00E+00
Peak CK-MB max, n (%)	297 (53.6)	31 (39.2)	125 (45.0)	19 (28.4)	2.89E-03

CAD = coronary artery diseases; CABG = coronary artery bypass grafting; PCI = percutaneous coronary intervention; ACS = acute coronary syndrome; STEMI = ST-segment elevation myocardial infarction; CK-MB = creatine kinase-MB

SUPPLEMENTARY TABLE 2 **Comparison between NOESY RF and GRACE scores.**

	NOESY RF score	GRACE score
Training set,		
AUC	0.843	0.815
Harrell's c index	0.806	0.776
Test set,		
AUC	0.801	0.750
Harrell's c index	0.789	0.740

AUC: area under the ROC curve

SUPPLEMENTARY TABLE 3 **Results for the gender-specific models**

	Male cohort	Female cohort
Training set, % (95% CI)		
Sensitivity	83.3% (95% CI 82.6-83.6%)	84.6% (95% CI 84.2-84.9%)
Specificity	74.2% (95% CI 73.2-75.2%)	70.0% (95% CI 68.7-71.3%)
Accuracy	77.2% (95% CI 76.5-77.9%)	74.9% (95% CI 74.0-75.7%)
Test set, %		
Sensitivity	73.1%	68.8%
Specificity	73.5%	75.7%
Accuracy	73.4%	74.7%

CI = confidence interval

SUPPLEMENTARY FIGURE 1. Upper: The NMR spectrum region with the above study metabolite annotated. Below: Our algorithm metabolites NMR signals deconvolution. Firstly, all NMR peaks in the above study NMR spectral region are fitted and the fitting procedure residuals are identified. Finally, the metabolite's NMR peaks (or part of them) of our interest are extracted and integrated, resulting to the metabolite's quantification with high level of accuracy. The figures are reported for A) acetone; B) phenylalanine.

A)

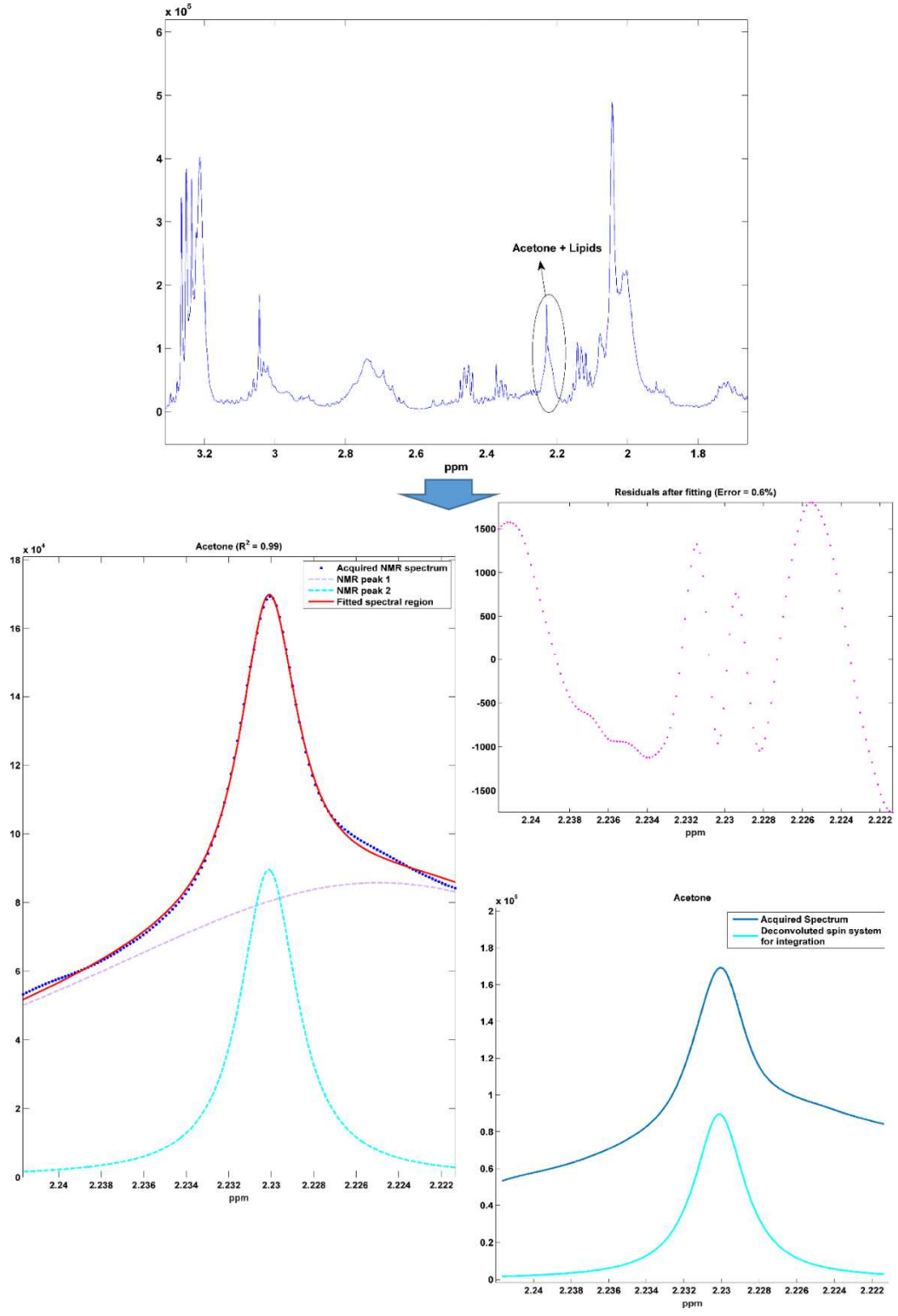

B)

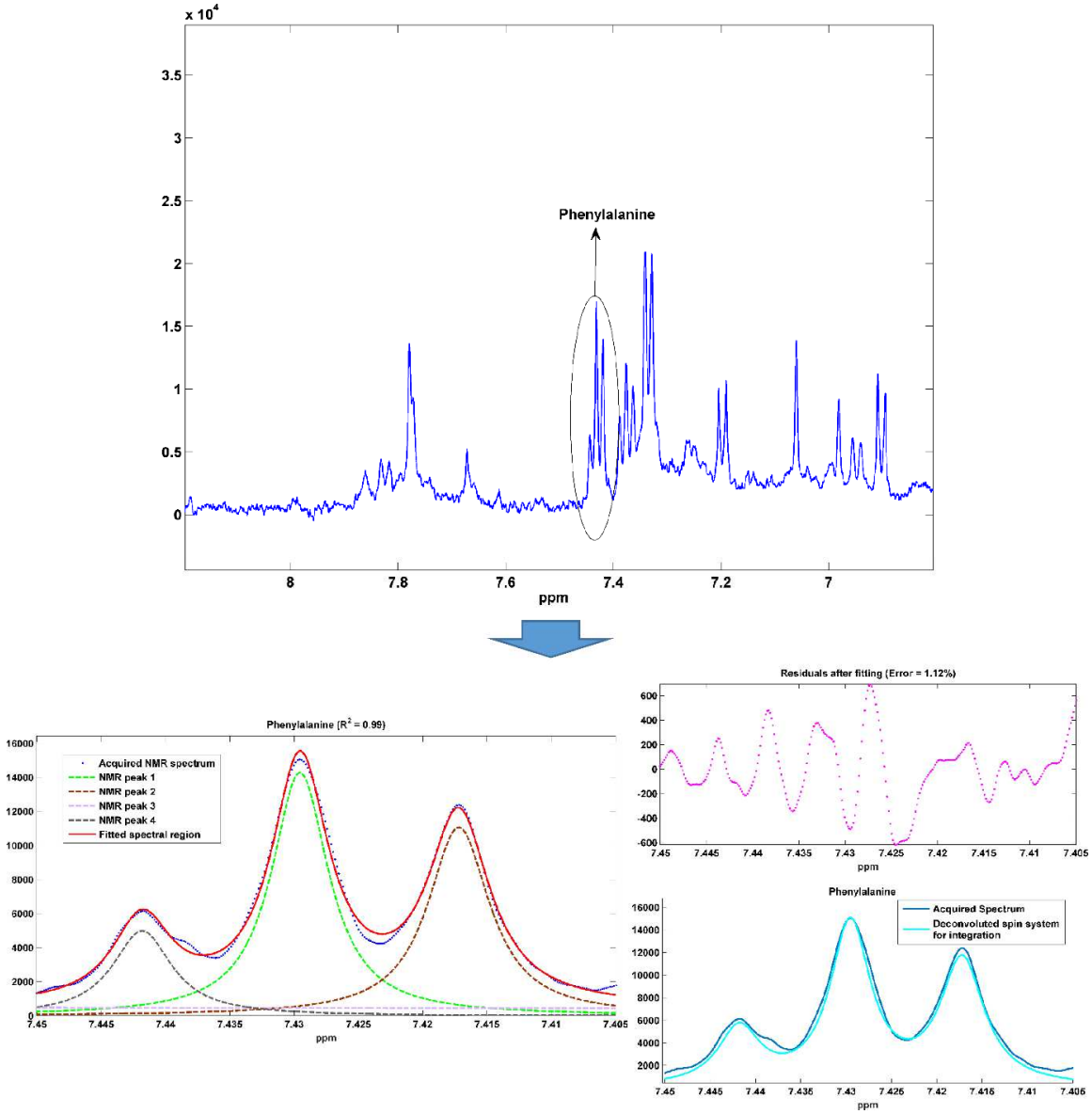
x 10^4
Phenylalanine
ppm
Phenylalanine (R^2 = 0.99)
Acquired NMR spectrum
NMR peak 1
NMR peak 2
NMR peak 3
NMR peak 4
Fitted spectral region
Residuals after fitting (Error = 1.12%)
Phenylalanine
Acquired Spectrum
Deconvoluted spin system for integration

SUPPLEMENTARY FIGURE 2. Metabolomic profiles for one randomly selected patient from each group of outcomes. For each patients NOESY, CPMG, and Diffusion spectra are displayed.

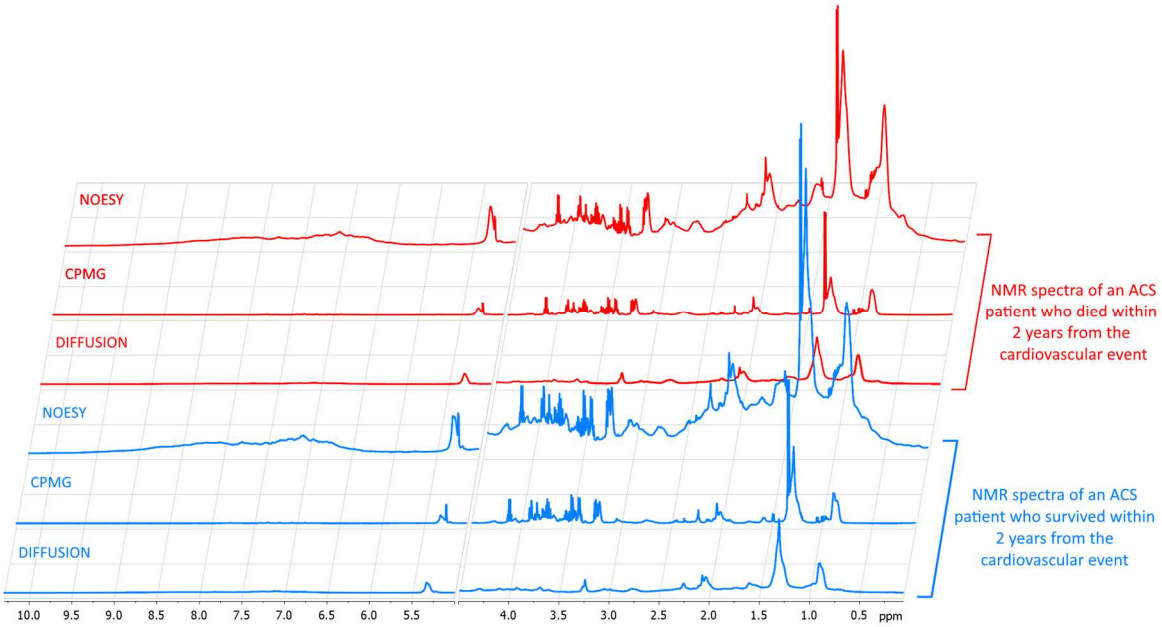

SUPPLEMENTARY FIGURE 3. Discrimination between Careggi University Hospital (blue dots, n = 579) and other centers (orange dots, n = 399) using Principal Component Analysis.

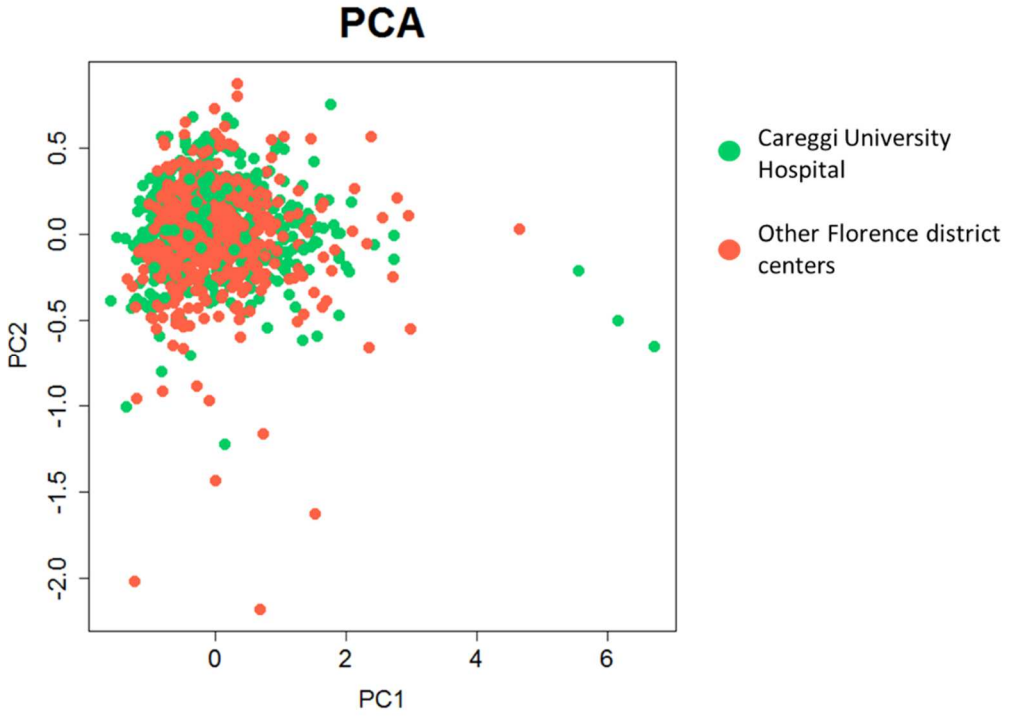

SUPPLEMENTARY FIGURE 4. Discrimination between survivor (blue dots, n = 80) and dead (red dots, n = 40) patients using the Random Forest classifier in the training set. A) CPMG; B) Diffusion. The ROC curves and the AUC scores in the training set are presented for C) CPMG; D) Diffusion. The ROC curves and the AUC scores in the validation set are presented for E) CPMG; F) Diffusion.

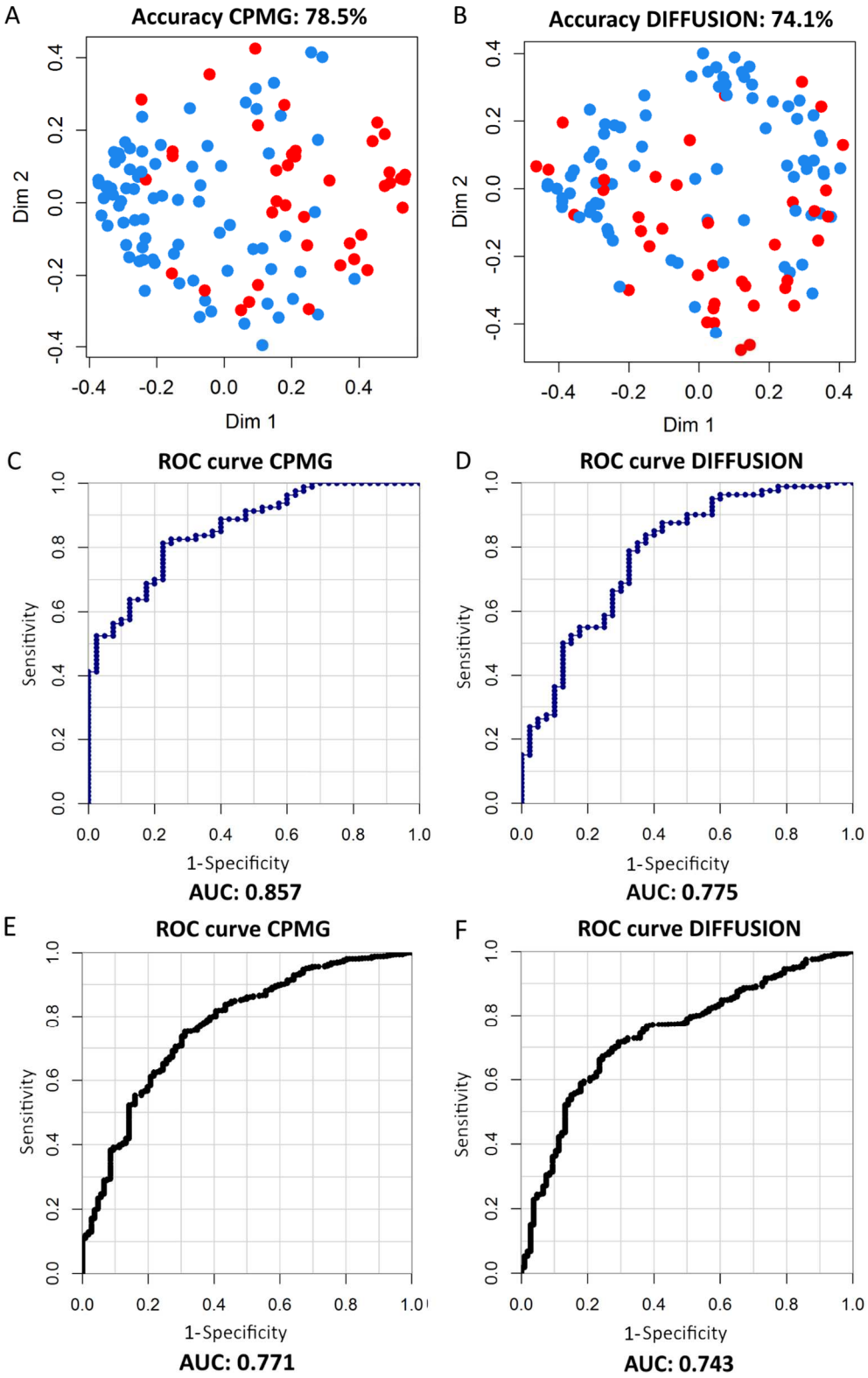

SUPPLEMENTARY FIGURE 5. Receiver Operating Characteristic Curves and the corresponding Area are reported for two models: Model 1, A) Training set: Careggi University Hospital; B) Validation set: Other Hospitals. Model 2, C) Training set: Other Hospitals; B) Validation set: Careggi University Hospital.

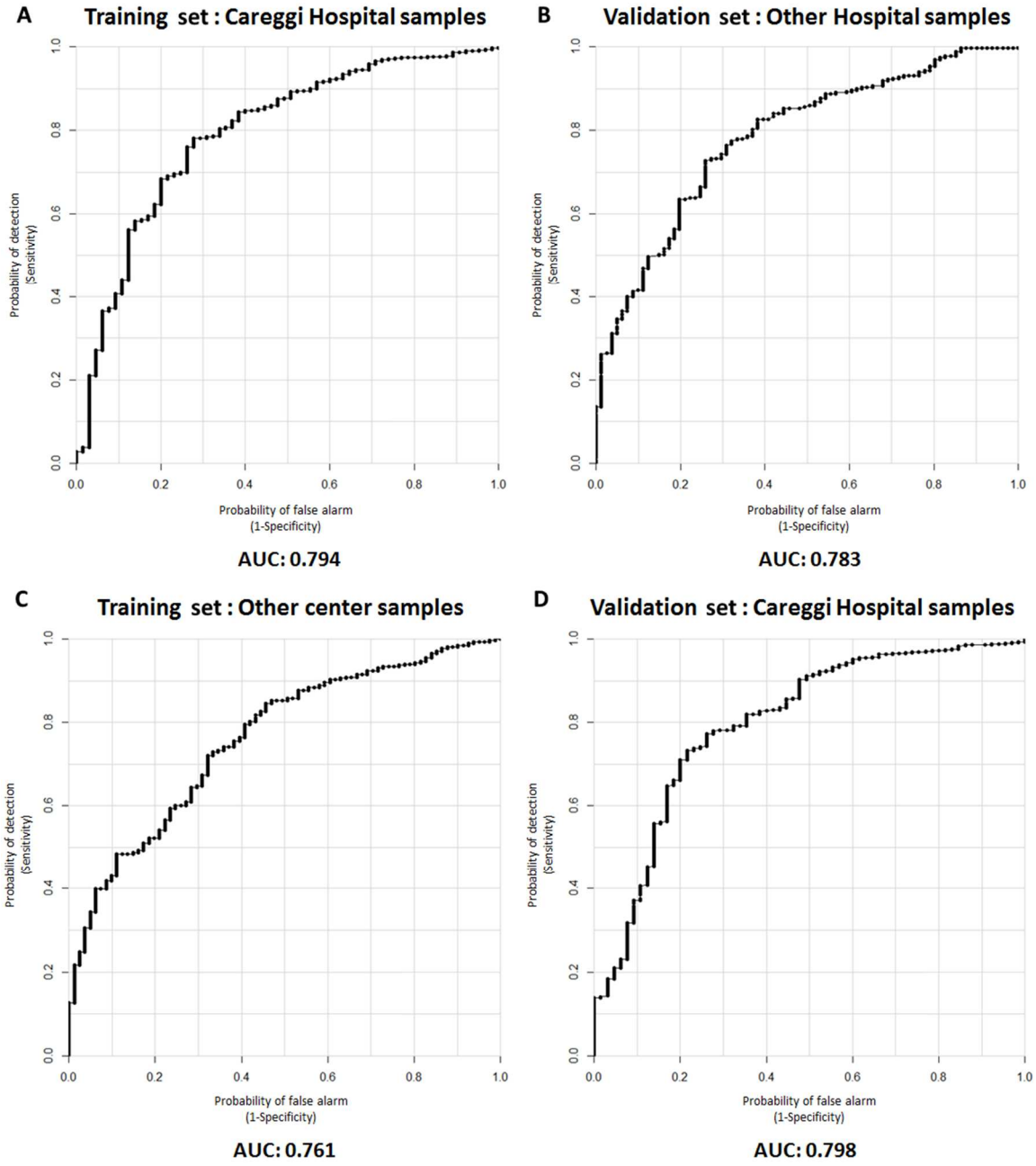

SUPPLEMENTARY FIGURE 6. Discrimination between NSTEMI (blue dots, n = 600) and STEMI (red dots, n = 378) patients using the Random Forest. Discrimination accuracy is 66.5%.

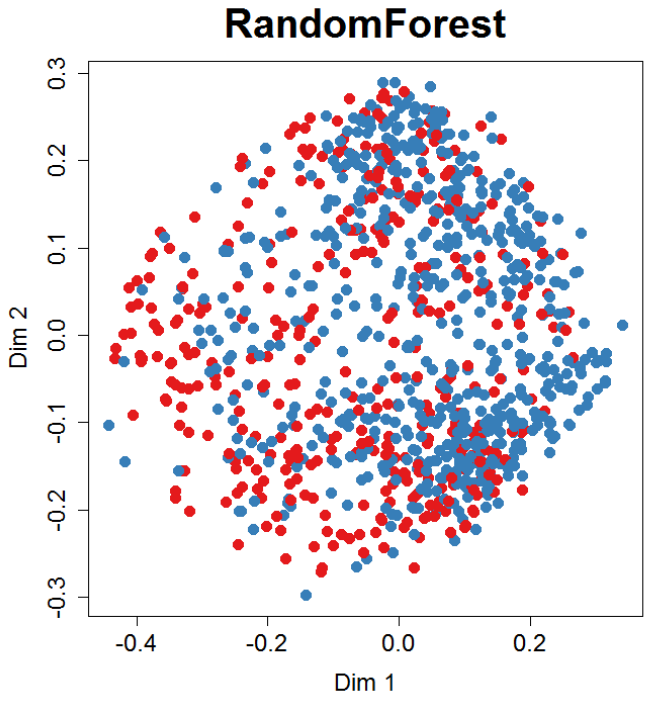

SUPPLEMENTARY FIGURE 7. Linear combined model (NOESY RF + GRACE score). ROC curve and AUC are reported for: A) training set; B) validation set.

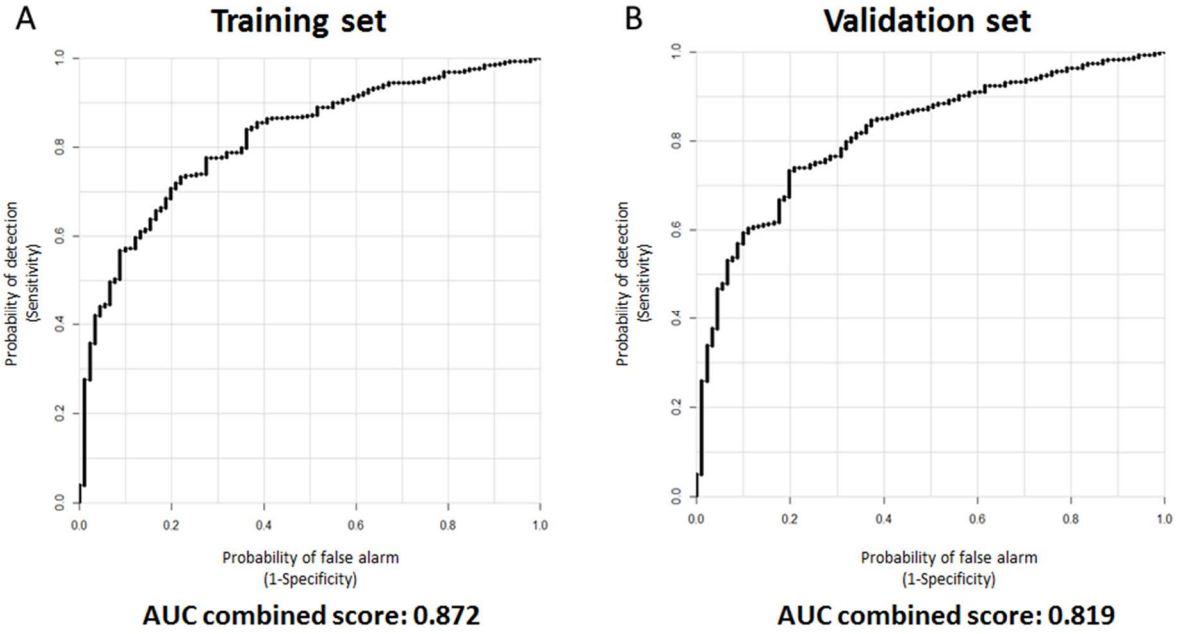

SUPPLEMENTARY FIGURE 8. Metabolite concentrations in: A) All dataset; B) Training set; C) Validation set. Metabolites are reported as log2 of the Fold Change, and positive values mean higher concentrations in dead patients. Green bars represent statistically significant *P*-values (P<0.05 after correction), conversely red bars mean not significant *P*-values.

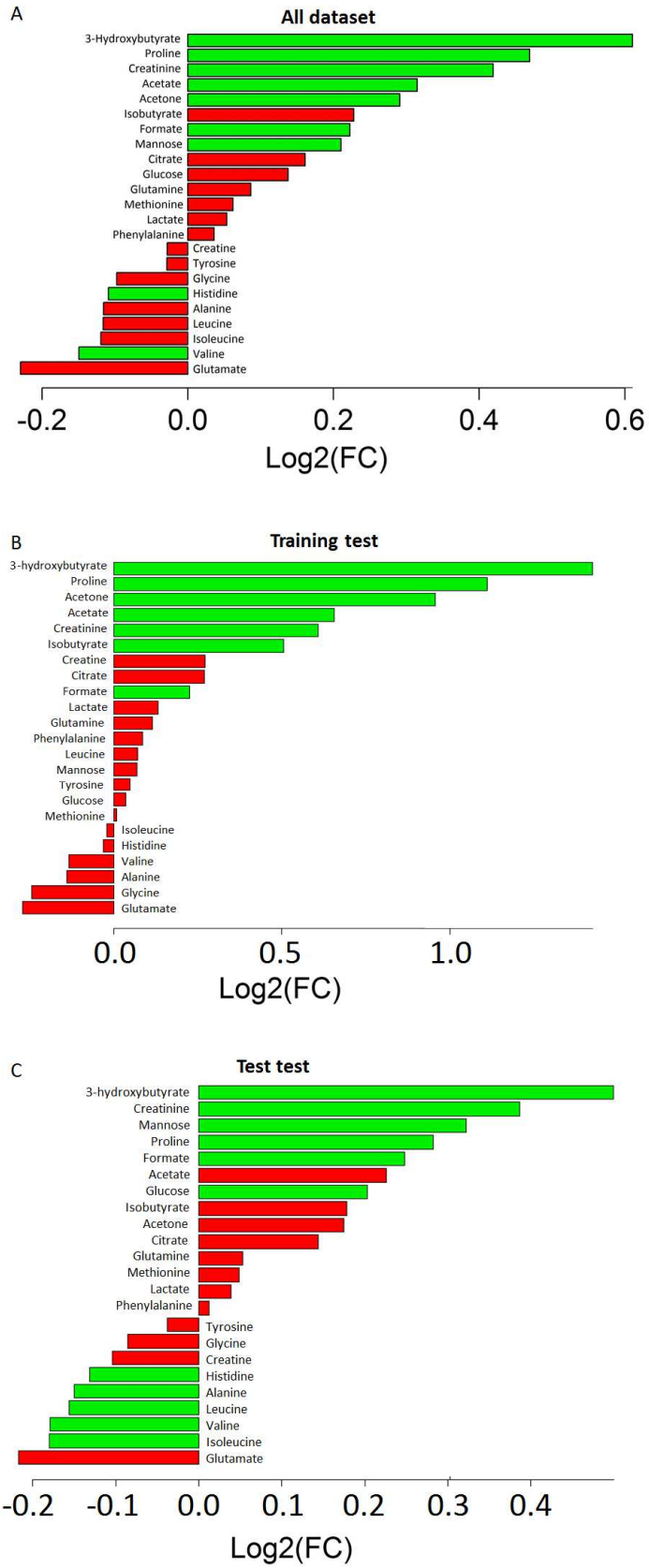

References

1. Hamm CW, Bassand J-P, Agewall S, et al. ESC Guidelines for the management of acute coronary syndromes in patients presenting without persistent ST-segment elevation: The Task Force for the management of acute coronary syndromes (ACS) in patients presenting without persistent ST-segment elevation of the European Society of Cardiology (ESC). Eur. Heart J. 2011;32:2999–3054.
2. Cifkova R, Erdine S, Fagard R, et al. Practice guidelines for primary care physicians: 2003 ESH/ESC hypertension guidelines. J. Hypertens. 2003;21:1779–1786.
3. Expert Committee on the Diagnosis and Classification of Diabetes Mellitus. Report of the expert committee on the diagnosis and classification of diabetes mellitus. Diabetes Care 2003;26 Suppl 1:S5-20.
4. Wilkins LW&. Third Report of the National Cholesterol Education Program (NCEP) Expert Panel on Detection, Evaluation, and Treatment of High Blood Cholesterol in Adults (Adult Treatment Panel III) Final Report. Circulation 2002;106:3143–3143.
5. Bernini P, Bertini I, Luchinat C, Nincheri P, Staderini S, Turano P. Standard operating procedures for pre-analytical handling of blood and urine for metabolomic studies and biobanks. J. Biomol. NMR 2011;49:231–243.
6. Meiboom S, Gill D. Modified Spin-Echo Method for Measuring Nuclear Relaxation Times. Rev. Sci. Instrum. 1958;29:688–691.
7. Wu DH, Chen A. Three-dimensional diffusion-ordered NMR spectroscopy: The homonuclear COSY-DOSY experiment. J Magnen Reson A 1996;123:215–218.
8. Spraul M, Neidig P, Klauck U, et al. Automatic reduction of NMR spectroscopic data for statistical and pattern recognition classification of samples. J Pharm Biomed Anal 1994;12:1215–1225.
9. Holmes E, Foxall PJ, Nicholson JK, et al. Automatic data reduction and pattern recognition methods for analysis of 1H nuclear magnetic resonance spectra of human urine from normal and pathological states. Anal Biochem 1994;220:284–296.
10. Kotsiantis S, Kanellopoulos D, Pintelas P. Handling imbalanced datasets: A review. GESTS Int. Transter Sci. Eng. CompugResearchGate 2005;30:25–36.
11. Breiman L. Random Forests. Mach. Learn. 2001;45:5–32.
12. Tenori L, Oakman C, Morris PG, et al. Serum metabolomic profiles evaluated after surgery may identify patients with oestrogen receptor negative early breast cancer at increased risk of disease recurrence. Results from a retrospective study. Mol. Oncol. 2015;9:128–139.

4.2 Characterizing the metabolic signature of diseases

In the last years, metabolomics has already proved to be useful in the characterization of several important chronic and complex diseases by analyzing samples from human origins. Exploring pathologies through this holistic approach can shed new light on their mechanisms and their impact on humans, discovering new possible biomarkers and identifying biochemical pathways involved in disease pathogenesis. In this thesis, NMR-based metabolomics has been used to characterize disease signatures using biological samples. Three different studies are presented in this section.

Alzheimer's disease (AD) is an irreversible neurodegenerative disorder that slowly destroys memory, thinking skills, and eventually the ability to accomplish even the simplest daily tasks. It is the most common neurodegenerative disease, affecting about 5% to 7% of the population over 60 years of age[64]. The need to identify novel molecular targets for AD to use in early diagnosis, prognosis, prediction of the disease evolution, and therapeutics is crucial[65]; therefore, to effectively address all these challenges detailed information about the underlying molecular biochemistry of AD are required. In our study (see paragraph 4.2.1), for the first time to the best of our knowledge, we performed a comparative analysis of the CSF metabolome with an untargeted NMR-based approach in a cohort of patients showing a typical protein CSF AD profile (altered CSF levels of Aβ42, total tau and phosphorylated tau proteins), both at pre-dementia (MCI-AD, 19 patients) and dementia (AD, 41 patients) stages, and of patients with MCI not due to AD (MCI with normal CSF profile, MCI-MCI, 21 patients), with the aim of identifying the metabolomic pattern correlating with the CSF AD biomarker profile.

Our results confirm the usefulness of CSF metabolomics to discriminate AD from MCI-MCI patients (sensitivity 76%, specificity 81%, accuracy 78%), and introduce also the evaluation of MCI-AD patients, as metabolically intermediate. A panel of seven metabolites (creatine, acetoacetate, 3-methyl-2-oxovalerate, 3-hydroxybutyrate, pyruvate, valine, and glycine) has been found lower in MCI-MCI with respect to AD patients. These data allowed us to confirm in AD the shift of the brain metabolism from glucose to ketone bodies, probably the first evidence of AD that precedes the onset of any functional impairment or neurological damage, and also to identify alterations in the metabolism of creatine and 3-methyl-2-oxovalerate. Interestingly, MCI-AD patients showed intermediate trends, indicating that the progression from MCI-MCI to AD is a sort of continuum metabolic spectrum. These data are particularly interesting if compared with the CSF core biomarker concentrations: using the available biomarkers the MCI-AD group can be considered identical to overt AD though they are still in a pre-dementia stage, while this is not true from the point of view of CSF metabolome.

In the second study presented in this section, we adopt an untargeted metabolomic approach to investigate the influence of chronic inflammatory rheumatic diseases (CIRDs) on the urine metabolome by the comparison with healthy controls and another immuno-mediated disorder, the multiple sclerosis (MSC) (see paragraph 4.2.2). The

pathological mechanisms of rheumatic diseases are complex involving both genetic and environmental factors; furthermore, their underlying mechanisms remain still poorly understood. Urines collected from 39 CIRDs patients, 25 healthy subjects and 26 MSC patients were analyzed using ^{1}H NMR spectroscopy, and the NMR spectra were examined using PLS-DA. Clear discriminations between CIRDs patients and healthy controls (average diagnostic accuracy 83.5%±1.9%), as well as between CIRDs patients and MSC patients (diagnostic accuracy 81.1%±1.9%), were obtained; conversely, no statistically significant discrimination between CIRDs and MSC patients has been found. Furthermore, we have also identified several metabolites down-regulated in the urine of CIRDs patients: significantly lower urinary levels ($p < 0.05$) of leucine, valine, alanine, 3-hydroxyisobutyric acid, 3-hydroxyisovaleric acid, glycine, citric acid, creatinine, hippuric acid and methylnicotinamide relative to controls were observed. Some of these metabolites (leucine, alanine, 3-hydroxyisobutyric acid, citric acid, 3-hydroxyisovaleric acid and creatinine) were also significantly lower in CIRDs urines comparing to the MSC ones. These data can provide new insights to better clarify the pathophysiological mechanisms underlying these disorders, identifying anomalous metabolic traits like alterations in the protein metabolism and muscle turnover, and the presence of other connected pathologies.

Finally, the last study here presented (see paragraph 4.2.3) concerned the characterization of the metabolic signature of primary biliary cirrhosis (PBC), a chronic autoimmune liver disease characterized by ongoing inflammatory destruction of the interlobular bile ducts, eventually leading to chronic cholestasis and biliary cirrhosis, by comparing PBC patients and healthy controls (HC). Secondly, this study aims at evaluating the possible association between the metabolomic profile of PBC and celiac disease (CD) patients. Serum and urine samples of 23 PBC patients, 21 CD patients and 19 sex-matched healthy controls (HC) were analyzed for our purposes. PBC can be discriminated with respect to HC with 76.9-83.1% accuracies using serum and 78.1% accuracy using urine; moreover, PBC patient sera were characterized by altered levels (*P*-value <0.05) of citrate, lactate, lysine, phenylananine, proline, pyruvate, serine and tyrosine, and PBC urines showed lower levels of hippuric acid, p-cresolsulfate, pyruvate and trigonelline with respect to HC. Several hypotheses can be made to explain these results: since the liver plays a central role in the aromatic amino-acid catabolism, the hepatic function impairment probably caused the alterations of the aromatic amino acid levels; moreover, the evidence of an impaired energy metabolism in PBC can be probably associated with altered gut microbiota.

PBC can be also discriminated with respect to CD with 78.2-88.3% accuracy for serum and 78.1% accuracy for urine, indicating thus two distinct metabolic signatures for these associated pathologies. In particular, PBC patients feature higher levels of cholesterol and high-density lipoprotein-cholesterol (HDL-C) with respect to CD patients. These differences are a clear result of a marked and opposite alterations in the lipid metabolism in these two disorders.

4.2.1 *Cerebrospinal fluid metabolic profile correlates with Alzheimer's core biomarkers*

Alessia Vignoli[1*], Silvia Paciotti[2*], Leonardo Tenori[3], Paolo Eusebi[2], Leonardo Biscetti[2], Davide Chiasserini[2,4], Paola Turano[1,5], Claudio Luchinat[1,5§], Lucilla Parnetti[2§]

*Contributed equally to the work. §Co-senior authors

[1] Magnetic Resonance Center (CERM), University of Florence, Sesto Fiorentino, Italy
[2] Lab of Clinical Neurochemistry, Section of Neurology, University of Perugia
[3] Department of Experimental and Clinical Medicine, University of Florence, Florence, Italy
[4] Oncoproteomics Laboratory, VU University Medical Center, De Boelelaan 1117, 1081HV, Amsterdam, The Netherlands
[5] Department of Chemistry, University of Florence, Sesto Fiorentino, Italy

Submitted

Candidate's contributions: acquisition of NMR data, statistical analysis and interpretation of data, writing and review of the manuscript.

Cerebrospinal fluid metabolic profile correlates with Alzheimer's core biomarkers

Abstract

Background: Metabolomics can identify different biochemical alterations in Alzheimer disease (AD). Metabolomic studies on AD patients using Nuclear Magnetic Resonance (NMR) spectroscopy are lacking. We sought for CSF metabolomic profile in AD patients characterized according to CSF AD biomarkers (Aβ42, p-tau, and t-tau), both at pre-dementia (mild cognitive impairment due to AD, MCI-AD) and dementia stage (ADdem), and in patients with MCI not due to AD (non-pathological CSF biomarker profile, MCI-MCI) using an untargeted NMR-based approach.

Methods: 1H NMR analysis was performed on CSF samples collected from 41 AD-dem patients, 19 MCI-AD and 21 MCI -MCI.

Results: In all NMR-spectra, 27 metabolites were identified. Metabolomic profiles well discriminated ADdem from MCI-MCI (Sens 76%, Spec 81%, Acc 78%). ADdem patients showed significantly higher levels of creatine, 3-methyl-2-oxovalerate, 3-hydroxybutyrate, pyruvate, acetoacetate, valine and glycine as compared to MCI-MCI, while in MCI-AD the concentrations showed intermediate values. The combination of pyruvate, creatine and 3-methyl-2-oxovalerate gave the best discrimination between ADdem and MCI-MCI (81%, Spec 75%, AUC=0.87). This metabolite-based model classified as ADdem 10 out of 13 MCI-AD who developed dementia during the follow-up (median 2 years follow up), while 3 out of 4 MCI-AD who did not convert to dementia were classified as MCI-MCI.

Conclusions: The CSF metabolomic profile is different in ADdem patients as compared to patients with non-pathological CSF AD biomarker profile and it is significantly associated with the dementia stage. Our data also suggest the possible role of the metabolomic profile as prognostic factor of conversion to dementia in MCI-AD patients. This issue deserves further investigation.

Keywords: Alzheimer's disease, Metabolomics, Nuclear Magnetic Resonance, Cerebrospinal fluid, Aβ, total tau and phosphorylated tau.

Introduction

Alzheimer's disease (AD) is a progressive neurodegenerative disorder, representing the commonest cause of dementia in older people (1). The pathophysiological changes that lead to cognitive decline, functional and behavioral impairment in AD patients, take place several years before the clinical symptoms appear (2). Variations in the levels of CSF core AD biomarkers total tau (t-tau), phosphorylated tau (p-tau) and amyloid beta 1-42 peptide (Aβ42) reflect the key aspects of disease pathogenesis (i.e. neuronal degeneration, tangles formation and aggregation and deposition of amyloid plaques) (3). AD patients typically show low concentrations of CSF Aβ42 and high concentrations of t-tau and p-tau already during the preclinical asymptomatic phase of AD (4–6). In clinical practice, abnormal CSF core AD biomarkers levels allow to identify patients affected by AD even in the prodromal phase (7).

Very little is known about the molecular pathways involved in the onset and progression of AD. In this framework, metabolomics may provide an interesting approach to identify alterations in multiple biochemical networks over the course of AD. Metabolomics enables the identification, quantification and characterization of the complete ensemble of metabolites present in a biological specimen. Nuclear Magnetic Resonance spectroscopy (NMR) is one of the main analytical techniques for metabolomics. NMR metabolomics approach has proved to be useful as diagnostic (8–11), prognostic (12, 13) and theragnostic (14) tool in different pathological conditions. Previous studies, performed both in animal models (15–18) and in human-derived samples like plasma, saliva, CSF and brain (19–25), have shown that metabolomics can provide powerful insights into the biochemical mechanisms of the AD clinical spectrum. So far, the available metabolomic studies on CSF have been performed by means of mass spectrometry (19, 26, 27), while no data have been reported for NMR in AD.

Differently to a classical analytical approach focused on target diagnostic parameters, NMR metabolomics is an untargeted method, which provides a comprehensive picture of the most abundant metabolites in the metabolome of a sample (concentrations > 1 μM).

Since the complex metabolic changes associated with AD progression, namely calcium dysregulation, mitochondrial dysfunction, oxidative stress, inflammation, altered cell signaling and lipid homeostasis (28–31), may occur prior to the development of clinical symptoms, metabolomics in conjunction with the available biomarkers for AD diagnosis could give a richer information on the pathophysiological processes taking place during disease development. Encouraging data have been provided by investigations carried out in AD patients: CSF AD biomarkers have been found to be related to several metabolic derangements both in pre-dementia (mild cognitive impairment, MCI) and in dementia phases (32).

To the best of our knowledge, this is the first study in which the CSF metabolome assessed by means of an untargeted NMR-based approach is evaluated in a cohort of

patients with a typical protein biomarker CSF AD profile based Aβ42, p-tau, and t-tau levels, both at pre-dementia (MCI-AD) and dementia (ADdem) stage, and patients with MCI not due to AD (MCI with normal CSF profile, MCI-MCI). The aim is to find out if a specific metabolomic pattern is associated with the CSF AD biomarker profile.

Methods and Materials

Patient cohort

The patients included in this study were consecutively enrolled at the Center of Memory Disturbances of the University of Perugia. According to NIA-AA criteria (33, 34), the cohort was composed of 41 patients affected by dementia diagnosed as high likelihood of AD pathophysiology (ADdem) (34), 19 MCI patients with CSF AD-like profile (MCI due to AD, MCI-AD)(33), and 21 MCI patients with normal CSF profile (MCI-MCI). Patients underwent clinical and neuropsychological assessments once a year (follow-up ranging from 1 to 4 years, median: 2 years).

At baseline, clinical examination, extensive neuropsychological testing including Mini-Mental State Examination (MMSE), blood chemistry and brain MRI scan (for excluding other causes of cognitive deficits) were carried out in all subjects included in the study. During the follow up, 13 out of 19 MCI-AD patients progressed to dementia according to the clinical and neuropsychological evaluation.

All the procedures were performed following the Helsinki Declaration and in agreement with the local Ethics Committee policy. All patients and/or their legal representatives gave informed written consent for the lumbar puncture.

CSF sampling

CSF collection was performed according to previously published procedures (35) and following international guidelines (36, 37). Briefly 12mL of CSF were collected via lumbar puncture in sterile polypropylene tubes (Sarstedt), centrifuged at room temperature for 10min (2000× g), and divided into 0.5mL aliquots. Tubes were frozen at –80° C pending analysis.

CSF Aβ42, t-tau and p-tau were measured with ELISA assays (Innotest β Amyloid 1–42, hTAU-Ag, p-TAU 181 Ag; Fujirebio, Gent, Belgium) (38).

NMR sample preparation

No standard operating procedures (SOPs) are available for CSF NMR sample preparation; since in CSF both high and low molecular weight metabolites are present, samples were prepared according to blood serum/plasma SOPs (39). Frozen CSF samples were thawed at room temperature and thoroughly mixed before use. A total of 350 µL of a sodium phosphate buffer (10.05 g Na2HPO4·7H2O; 0.2 g NaN3; 0.4 g sodium trimethylsilyl-[2,2,3,3-2H4]-propionate (TMSP) in 500 mL of H2O with 20% (v/v) 2H2O; pH 7.4) was added to 350 µL of each sample, and the mixture was vortexed

for 30 s. A total of 600 μL of each mixture was transferred into a 5 mm NMR tube (BrukerBioSpinsrl) for the analysis.

NMR analysis

Monodimensional 1H NMR spectra for all samples were acquired using a Bruker 600 MHz spectrometer (BrukerBioSpin) operating at 600.13 MHz proton Larmor frequency and equipped with a 5mm PATXI 1H-13C-15N and 2H-decoupling probe including a z axis gradient coil, an automatic tuning-matching (ATM) and an automatic and refrigerated (6°C) sample changer (SampleJet). A BTO 2000 thermocouple served for temperature stabilization at the level of approximately 0.1 K at the sample. Before measurement, samples were kept for at least 5 min inside the NMR probehead, for temperature equilibration at 310 K.

Water suppressed Carr–Purcell–Meiboom–Gill (CPMG) (40) spin echo pulse sequence (RD-90°-(τ-180°-τ)n-acq) with a total spin echo (2nτ) of 80 ms was used in order to obtain monodimensional 1H-NMR spectra in which broad signals from high molecular weight metabolites are attenuated (Supplementary Figure 1). 256 FIDs were collected into 73728 data points over a spectral width of 12019 Hz, with a relaxation delay (RD) of 4 s and acquisition time (acq) of 3.1 s.

Spectral Processing

Free induction decays were multiplied by an exponential function equivalent to a 0.3 Hz line-broadening factor before applying Fourier transform. Transformed spectra were automatically corrected for phase and baseline distortions and calibrated (TMSP signal 0.0 ppm) using TopSpin 3.2 (BrukerBiospin).

Each 1D CSF spectrum in the range between 0.5 and 10.00 ppm was segmented into 0.02 ppm chemical shift bins and the corresponding spectral areas were integrated using AMIX software (version 3.8.4, BrukerBioSpin). Binning is a mean to reduce the number of total variables, to compensate for subtle signal shifts, and filter noise in the spectra, making the analysis more robust and reproducible (41, 42). Regions between 4.2 and 5.5 ppm containing residual water signal were removed and the dimension of the system was reduced to 411 bins. The total spectral area was calculated on the remaining bins and total area normalization was carried out on the data prior to pattern recognition.

Statistical analysis

All data analyses were performed using R, an open source software for the statistical analysis of data (43, 44). Multivariate analysis was conducted on processed data; instead, univariate analysis was performed on the whole spectra.

Data reduction was carried out by means of projection into a Partial Least Square (PLS) subspace, only the first 30 components were retained in the model and the canonical analysis (CA) was applied to obtain the supervised separation of the analyzed groups.

For the purpose of classification, we used the K-nearest neighbors (k-NN) method (k=5) applied on the PLS-CA scores (8). Accuracy, sensitivity and specificity for the different classifications were assessed by means of a Monte Carlo cross-validation scheme (R script in-house developed). Briefly, 90% of the data were randomly chosen at each iteration as a training set to build the model. Then the remaining 10% was tested, and sensitivity, specificity and accuracy for the classification were assessed. The procedure was repeated 100 times to derive the average discrimination accuracy for each group of subjects.

The spectral regions related to the metabolites were assigned in the NMR profiles by using matching routines of AMIX 3.8.4 (BrukerBioSpin) in combination with the BBIOREFCODE (BrukerBioSpin), a freely available dataset i.e. Human MetabolomeDataBase (HMDB) (45), and published literature when available. The metabolites quantification was determined by an in-house developed software (Takis et al. in preparation) in MATLAB programming suite (Mathworks, MATLAB version R2014b). Our algorithm is based upon the unconstrained non-linear minimization of the metabolites NMR signals, employing a combination of lorentzian-gaussian functions By this approach, each NMR complex region (i.e. overlapping signals including macromolecules broad 1H NMR peaks, baseline distortions) of our interest is decomposed into its component parts, where the metabolites NMR peaks are deconvoluted and integrated, resulting into the accurate metabolite's concentration determination. These concentrations were analyzed to determine the discriminating metabolites between the groups of patients. Wilcoxon–Mann–Whitney test (46) was chosen to infer differences between the groups on the biological assumption that metabolite concentrations are not normally distributed, and false discovery rate correction was applied using the Benjamini-Hochberg method (47). An adjusted P-value < 0.05 was deemed significant.

The prognostic role of biomarkers was tested with logistic regression; the results were evaluated with receiver operating characteristics (ROC) analysis.

Moreover, the Pearson correlations among the clinical variables and CSF metabolites were calculated using the function "corr.test" implemented in the R-library "psych". The levelplot of the correlation matrix was built using the R-function "levelplot", implemented in the "lattice" package.

Results

Cohort characteristics

Demographic data, MMSE score and CSF protein biomarkers levels of the cohort are reported in Table 1. As the classification criterion of the patients was based on the CSF profile, as expected, CSF biomarkers were substantially similar in MCI-AD and ADdem and significantly different from MCI-MCI. Likewise, the lowest MMSE scores were observed in the ADdem group.

NMR analysis

1H NMR CSF metabolomic profiles were obtained for all patients included in the study using the CPMG sequence (Supplementary Figure 1) in order to suppress broad resonances originating from large macromolecules. This procedure improves the baseline by avoiding the use of filtration or extraction methods, thus facilitating the quantification process. In all NMR spectra 27 metabolites, representing ~80% of all quantifiable peaks present in each CSF spectrum, were unambiguously identified (Supplementary Figure 2) and quantitated in arbitrary units.

Correlations between clinical data and metabolite concentrations were calculated (Figure 1, Supplementary Table 1). Among all metabolites, creatinine showed the highest correlations with t-tau and p-tau, and 3-methyl-2-oxovalerate presented the highest anticorrelations with Aβ42/p-tau and Aβ42/t-tau ratios.

Comparative metabolomic analysis

Using a PLS-CA-kNN model, the CSF metabolomic profiles of ADdem and MCI-MCI patients were classified, and showed significant differential clustering (Figure 2), with a remarkable separation of the two groups yielding 76% sensitivity (95% CI 73-79%), 81% specificity (95% CI 79-83%), and 78% accuracy (95% CI 75-80%). The discrimination accuracy obtained with the PLS-CA model was validated in a permutation test obtaining a P-value of 0.01.

An analysis of the concentrations of the metabolites assigned in the NMR spectra was conducted to identify which metabolites are statistically different between the two groups of patients: ADdem patients were characterized by significantly (adjusted P-value< 0.05) higher levels of seven metabolites: creatine, 3-methyl-2-oxovalerate, 3-hydroxybutyrate, pyruvate, acetoacetate, valine, and glycine; moreover, the pyruvate/lactate ratio was significantly more elevated in ADdem patients (Table 2).

Pairwise discrimination, using the PLS-CA model, of MCI-MCI vs. MCI-AD, and ADdem vs. MCI-AD did not reach statistical significance (respectively, 51% and 43% discrimination accuracy). Interestingly, however, the metabolites showing higher levels in ADdem with respect to MCI-MCI exhibit intermediate levels in the MCI-AD group (Figure 3, Supplementary Table 2).

Using the most significant metabolites to discriminate AD from MCI-MCI

A classification model able to discriminate ADdem from MCI-MCI was built using a logistic regression based on creatine, pyruvate, and 3-methyl-2-oxovalerate concentrations. These metabolites were chosen on the basis of the P-values being the three most statistically significant metabolites (adjusted P-value <0.05) in the MCI-MCI vs. ADdem comparison.

The area under the ROC curve (AUC) for each metabolite separately was found to be 0.83 for creatine, 0.77 for pyruvate, and 0.79 for 3-methyl-2-oxovalerate; interestingly, the combined model reached an AUC of 0.87 (Figure 3). Using this combination of

metabolites, 81% sensitivity, 75% specificity, and 79% accuracy were obtained setting a threshold of 0.64 on the fitted values obtained by logistic regression, thus maximizing both sensitivity and specificity.

This metabolite-based model was used to analyze the MCI-AD group (considering only the 17 patients for whom follow up information was available): 65% of the patients were classified as ADdem and 35% as MCI-MCI. These results are particularly interesting if the follow up information is considered: indeed, 10 out of 13 patients classified as ADdem by the model had developed ADdem at follow up, and 3 out of 4 patients classified as MCI-MCI did not show an evolution of the disease at follow up, despite the positivity of CSF biomarkers. These data suggest that the metabolomic profile, obtained through this metabolite-based model, could predict whether a patient classified as MCI-AD could progress to dementia or not.

Discussion

CSF AD biomarkers (i.e. Aβ1-42, t-tau, p-tau) have been defined as "the CSF AD signature" (48), since they are found altered independently of the stage of the disease, including preclinical and prodromal phases. Their robustness justifies their use for diagnostic purposes in routine clinical work, where it is mandatory to formulate an early and accurate AD diagnosis, in view of forthcoming disease-modifying drugs. The untargeted metabolomic approach represents an important source for anchoring the CSF AD signature to a restricted panel of metabolites characterizing AD also in its prodromal phase.

By using NMR, we investigated the CSF metabolomic pattern in a cohort of patients characterized according to CSF AD biomarkers and clinical follow-up.

The CSF metabolomic profile well discriminated ADdem from MCI-MCI, albeit, as expected, with lower accuracy than AD core biomarkers. Conversely, CSF metabolomic profile poorly discriminated MCI-AD patients from MCI-MCI, indicating a largely overlapping metabolomic picture in these two conditions. Twenty-seven metabolites were clearly identified and quantified in each analyzed CSF sample, and the univariate analysis of their concentrations enables the identification of those significantly different in ADdem as compared to MCI-MCI patients. ADdem patients showed higher levels of creatine, 3-methyl-2-oxovalerate, 3-hydroxybutyrate, pyruvate, pyruvate/lactate ratio, acetoacetate, valine, and glycine (Table 2). Interestingly, MCI-AD patients showed intermediate values of metabolite concentrations (Supplementary Table 2).

Based on CSF Aβ42, t-tau and p-tau profile (representing the pathophysiological fingerprint of Alzheimer's pathology), the MCI-AD group is similar to ADdem, while CSF metabolomic pattern shows a sort of dynamic pattern from MCI-AD to ADdem. Of interest, the combination of pyruvate, creatine and 3-methyl-2-oxovalerate classified the MCI-AD patients in agreement with the clinical follow-up. These data allowed us to hypothesize that the metabolomic profile may reflect the risk of progression to

dementia in prodromal AD, thus assuming the role of prognostic marker of conversion from MCI-AD status to AD dementia. Further investigations are needed to confirm this hypothesis.

The concomitant increase of pyruvate, pyruvate/lactate ratio and ketone bodies (i.e. 3-hydroxybutyrate and acetoacetate) found in the ADdem group might be explained considering the reduction of the cerebral oxidative metabolism, a largely documented event already present in the early stage of disease (49–53). The decline in glucose metabolism in specific brain regions is associated with decreased expression of glycolytic enzymes and reduced activity of the pyruvate dehydrogenase complex (54, 55), which is responsible for the conversion of pyruvate in Acetyl-CoA (51). The alteration of cerebral metabolism is also accompanied by the activation of alternative compensatory metabolic pathways utilizing less usual substrates such as ketone bodies (56), thus explaining the increase of 3-hydroxybutyrate and acetoacetate concentrations found in CSF of ADdem group.

Creatine levels were also significantly higher in ADdem patients vs. MCI-MCI. The presence of creatine deposits has been observed in brain of transgenic AD mice and in post-mortem brain of AD patients (57, 58). Although the mechanism that causes creatine deposits is still unknown, it has been hypothesized that it might be the consequence of an altered creatine kinase (CK) activity (58). CK is a key enzyme in the brain energetic metabolism, and observations of aberrant CK activity in brain of AD patients have been previously reported (59, 60), thus suggesting a direct link between perturbed energy state, creatine metabolism and Alzheimer's pathology.

Of interest, from our data creatine appears as an unsuspected progression marker of Alzheimer's disease: creatine itself well discriminated ADdem vs MCI-MCI, and the three metabolite-based model showed high efficiency in predicting MCI-AD progression to dementia.

Glycine and valine also showed increased values in ADdem with respect to MCI-MCI and MCI-AD patients. Alterations of amino acids levels in AD patients have already been reported (27, 61–63). Conversely, no available data can help in interpreting the higher levels of 3-methyl-2-oxovalerate we found in ADdem group, where its concentration was significantly associated with Aβ42/t-tau and Aβ42/p-tau ratios.

Limitations of our study are the small sample size of the subjects studied, and the lack of a validation set by an independent population. However, the accurate clinical and biochemical characterization of the patients included and the availability of follow up information, partly counteract the abovementioned limitations.

In conclusion, the data obtained from this NMR-based investigation assessing the CSF metabolome in patients classified according to their CSF AD profile, show a panel of seven metabolites significantly increased in Alzheimer's dementia patients with respect to non- Alzheimer's patients. Furthermore, the use of a three-metabolite model (creatine, pyruvate, 3-methyl-2-oxovalerate) may predict dementia progression (or

may support the prediction of dementia progression) in MCI-AD subjects, who show an intermediate metabolomic profile.

References

1. Alzheimer's Association (2016): 2016 Alzheimer's disease facts and figures. Alzheimers Dement J Alzheimers Assoc. 12: 459–509.
2. Morris JC, Price JL (2001): Pathologic correlates of nondemented aging, mild cognitive impairment, and early-stage Alzheimer's disease. J Mol Neurosci MN. 17: 101–118.
3. Blennow K, Hampel H, Weiner M, Zetterberg H (2010): Cerebrospinal fluid and plasma biomarkers in Alzheimer disease. Nat Rev Neurol. 6: 131–144.
4. Mattsson N, Zetterberg H, Hansson O, Andreasen N, Parnetti L, Jonsson M, et al. (2009): CSF biomarkers and incipient Alzheimer disease in patients with mild cognitive impairment. JAMA J Am Med Assoc. 302: 385–393.
5. Shaw LM, Vanderstichele H, Knapik-Czajka M, Clark CM, Aisen PS, Petersen RC, et al. (2009): Cerebrospinal fluid biomarker signature in Alzheimer's disease neuroimaging initiative subjects. Ann Neurol. 65: 403–413.
6. Visser PJ, Verhey F, Knol DL, Scheltens P, Wahlund L-O, Freund-Levi Y, et al. (2009): Prevalence and prognostic value of CSF markers of Alzheimer's disease pathology in patients with subjective cognitive impairment or mild cognitive impairment in the DESCRIPA study: a prospective cohort study. Lancet Neurol. 8: 619–627.
7. Dubois B, Feldman HH, Jacova C, Hampel H, Molinuevo JL, Blennow K, et al. (2014): Advancing research diagnostic criteria for Alzheimer's disease: the IWG-2 criteria. Lancet Neurol. 13: 614–629.
8. Calabrò A, Antonio, Gralka E, Luchinat C, Saccenti E, Tenori L (2014): A Metabolomic Perspective on Coeliac Disease. Autoimmune Dis. 2014: e756138.
9. Tenori L, Hu X, Pantaleo P, Alterini B, Castelli G, Olivotto I, et al. (2013): Metabolomic fingerprint of heart failure in humans: a nuclear magnetic resonance spectroscopy analysis. Int J Cardiol. 168: e113-115.
10. Clish CB (2015): Metabolomics: an emerging but powerful tool for precision medicine. Cold Spring Harb Mol Case Stud. 1. doi: 10.1101/mcs.a000588.
11. Johnson CH, Ivanisevic J, Siuzdak G (2016): Metabolomics: beyond biomarkers and towards mechanisms. Nat Rev Mol Cell Biol. 17: 451–459.
12. Hart CD, Vignoli A, Tenori L, Uy GL, Van To T, Adebamowo C, et al. (2017): Serum Metabolomic Profiles Identify ER-Positive Early Breast Cancer Patients at Increased Risk of Disease Recurrence in a Multicenter Population. Clin Cancer Res Off J Am Assoc Cancer Res. 23: 1422–1431.
13. Tenori L, Giusti B, Vignoli A, Gori AM, Luchinat C, Grifoni E, et al. (2017): Metabolomics by Nuclear Magnetic Resonance identifies patients with high risk of death within two years after a cardiovascular event: The case of the amiflorence II study. Nutr Metab Cardiovasc Dis. 27: e39–e40.

14. Wishart DS (2016): Emerging applications of metabolomics in drug discovery and precision medicine. Nat Rev Drug Discov. 15: 473–484.
15. Dedeoglu A, Choi J-K, Cormier K, Kowall NW, Jenkins BG (2004): Magnetic resonance spectroscopic analysis of Alzheimer's disease mouse brain that express mutant human APP shows altered neurochemical profile. Brain Res. 1012: 60–65.
16. Marjanska M, Curran GL, Wengenack TM, Henry P-G, Bliss RL, Poduslo JF, et al. (2005): Monitoring disease progression in transgenic mouse models of Alzheimer's disease with proton magnetic resonance spectroscopy. Proc Natl Acad Sci U S A. 102: 11906–11910.
17. Salek RM, Xia J, Innes A, Sweatman BC, Adalbert R, Randle S, et al. (2010): A metabolomic study of the CRND8 transgenic mouse model of Alzheimer's disease. Neurochem Int. 56: 937–947.
18. Trushina E, Nemutlu E, Zhang S, Christensen T, Camp J, Mesa J, et al. (2012): Defects in mitochondrial dynamics and metabolomic signatures of evolving energetic stress in mouse models of familial Alzheimer's disease. PloS One. 7: e32737.
19. Trushina E, Dutta T, Persson X-MT, Mielke MM, Petersen RC (2013): Identification of altered metabolic pathways in plasma and CSF in mild cognitive impairment and Alzheimer's disease using metabolomics. PloS One. 8: e63644.
20. Sato Y, Suzuki I, Nakamura T, Bernier F, Aoshima K, Oda Y (2012): Identification of a new plasma biomarker of Alzheimer's disease using metabolomics technology. J Lipid Res. 53: 567–576.
21. Greenberg N, Grassano A, Thambisetty M, Lovestone S, Legido-Quigley C (2009): A proposed metabolic strategy for monitoring disease progression in Alzheimer's disease. Electrophoresis. 30: 1235–1239.
22. Han X, Rozen S, Boyle SH, Hellegers C, Cheng H, Burke JR, et al. (2011): Metabolomics in early Alzheimer's disease: identification of altered plasma sphingolipidome using shotgun lipidomics. PloS One. 6: e21643.
23. Sato Y, Nakamura T, Aoshima K, Oda Y (2010): Quantitative and wide-ranging profiling of phospholipids in human plasma by two-dimensional liquid chromatography/mass spectrometry. Anal Chem. 82: 9858–9864.
24. Paglia G, Stocchero M, Cacciatore S, Lai S, Angel P, Alam MT, et al. (2016): Unbiased Metabolomic Investigation of Alzheimer's Disease Brain Points to Dysregulation of Mitochondrial Aspartate Metabolism. J Proteome Res. 15: 608–618.
25. Trushina E, Mielke MM (2014): Recent advances in the application of metabolomics to Alzheimer's Disease. Biochim Biophys Acta. 1842: 1232–1239.
26. Czech C, Berndt P, Busch K, Schmitz O, Wiemer J, Most V, et al. (2012): Metabolite Profiling of Alzheimer's Disease Cerebrospinal Fluid. PLOS ONE. 7: e31501.
27. Ibáñez C, Simó C, Martín-Álvarez PJ, Kivipelto M, Winblad B, Cedazo-Mínguez A, Cifuentes A (2012): Toward a predictive model of Alzheimer's disease progression using capillary electrophoresis-mass spectrometry metabolomics. Anal Chem. 84: 8532–8540.

28. Supnet C, Bezprozvanny I (2010): Neuronal calcium signaling, mitochondrial dysfunction and Alzheimer's disease. J Alzheimers Dis JAD. 20: S487–S498.
29. Di Paolo G, Kim T-W (2011): Linking Lipids to Alzheimer's Disease: Cholesterol and Beyond. Nat Rev Neurosci. 12: 284–296.
30. Bagyinszky E, Giau VV, Shim K, Suk K, An SSA, Kim S (2017): Role of inflammatory molecules in the Alzheimer's disease progression and diagnosis. J Neurol Sci. 376: 242–254.
31. Magi S, Castaldo P, Macrì ML, Maiolino M, Matteucci A, Bastioli G, et al. (2016): Intracellular Calcium Dysregulation: Implications for Alzheimer's Disease. BioMed Res Int. 2016: 6701324.
32. Kaddurah-Daouk R, Zhu H, Sharma S, Bogdanov M, Rozen SG, Matson W, et al. (2013): Alterations in metabolic pathways and networks in Alzheimer's disease. Transl Psychiatry. 3: e244.
33. Albert MS, DeKosky ST, Dickson D, Dubois B, Feldman HH, Fox NC, et al. (2011): The diagnosis of mild cognitive impairment due to Alzheimer's disease: recommendations from the National Institute on Aging-Alzheimer's Association workgroups on diagnostic guidelines for Alzheimer's disease. Alzheimers Dement J Alzheimers Assoc. 7: 270–279.
34. McKhann GM, Knopman DS, Chertkow H, Hyman BT, Jack CR, Kawas CH, et al. (2011): The diagnosis of dementia due to Alzheimer's disease: recommendations from the National Institute on Aging-Alzheimer's Association workgroups on diagnostic guidelines for Alzheimer's disease. Alzheimers Dement J Alzheimers Assoc. 7: 263–269.
35. Chiasserini D, Biscetti L, Farotti L, Eusebi P, Salvadori N, Lisetti V, et al. (2016): Performance Evaluation of an Automated ELISA System for Alzheimer's Disease Detection in Clinical Routine. J Alzheimers Dis JAD. 54: 55–67.
36. Teunissen CE, Petzold A, Bennett JL, Berven FS, Brundin L, Comabella M, et al. (2009): A consensus protocol for the standardization of cerebrospinal fluid collection and biobanking. Neurology. 73: 1914–1922.
37. del Campo M, Mollenhauer B, Bertolotto A, Engelborghs S, Hampel H, Simonsen AH, et al. (2012): Recommendations to standardize preanalytical confounding factors in Alzheimer's and Parkinson's disease cerebrospinal fluid biomarkers: an update. Biomark Med. 6: 419–430.
38. Parnetti L, Chiasserini D, Eusebi P, Giannandrea D, Bellomo G, De Carlo C, et al. (2012): Performance of aβ1-40, aβ1-42, total tau, and phosphorylated tau as predictors of dementia in a cohort of patients with mild cognitive impairment. J Alzheimers Dis JAD. 29: 229–238.
39. Bernini P, Bertini I, Luchinat C, Nincheri P, Staderini S, Turano P (2011): Standard operating procedures for pre-analytical handling of blood and urine for metabolomic studies and biobanks. J Biomol NMR. 49: 231–243.

40. Meiboom S, Gill D (1958): Modified Spin-Echo Method for Measuring Nuclear Relaxation Times. Rev Sci Instrum. 29: 688–691.
41. Spraul M, Neidig P, Klauck U, Kessler P, Holmes E, Nicholson JK, et al. (1994): Automatic reduction of NMR spectroscopic data for statistical and pattern recognition classification of samples. J Pharm Biomed Anal. 12: 1215–1225.
42. Holmes E, Foxall PJ, Nicholson JK, Neild GH, Brown SM, Beddell CR, et al. (1994): Automatic data reduction and pattern recognition methods for analysis of 1H nuclear magnetic resonance spectra of human urine from normal and pathological states. Anal Biochem. 220: 284–296.
43. Ihaka R, Gentleman R (1996): R: A Language for Data Analysis and Graphics. J Comput Stat Graph. 5: 299–314.
44. R Core Team (2014): R: A language and environment for statistical computing. . Retrieved from http://www.R-project.org/.
45. Wishart DS, Lewis MJ, Morrissey JA, Flegel MD, Jeroncic K, Xiong Y, et al. (2008): The human cerebrospinal fluid metabolome. J Chromatogr B. 871: 164–173.
46. Mann HB, Whitney DR (1947): On a test of whether one of two random variables is stochastically larger than the other. Ann Math Stat. 18: 50–60.
47. Benjamini Y, Hochberg Y (1995): Controlling the False Discovery Rate: A Practical and Powerful Approach to Multiple Testing. J R Stat Soc Ser B Methodol. 57: 289–300.
48. Blennow K, Dubois B, Fagan AM, Lewczuk P, de Leon MJ, Hampel H (2015): Clinical utility of cerebrospinal fluid biomarkers in the diagnosis of early Alzheimer's disease. Alzheimers Dement J Alzheimers Assoc. 11: 58–69.
49. Schubert D (2005): Glucose metabolism and Alzheimer's disease. Ageing Res Rev, Stress, Neuropeptides and Age-Related Diseases. 4: 240–257.
50. Blass JP (2000): The mitochondrial spiral. An adequate cause of dementia in the Alzheimer's syndrome. Ann N Y Acad Sci. 924: 170–183.
51. Yao J, Rettberg JR, Klosinski LP, Cadenas E, Brinton RD (2011): Shift in Brain Metabolism in Late Onset Alzheimer's Disease: Implications for Biomarkers and Therapeutic Interventions. Mol Aspects Med. 32: 247–257.
52. Mosconi L, Pupi A, De Leon MJ (2008): Brain glucose hypometabolism and oxidative stress in preclinical Alzheimer's disease. Ann N Y Acad Sci. 1147: 180–195.
53. Parnetti L, Gaiti A, Polidori MC, Brunetti M, Palumbo B, Chionne F, et al. (1995): Increased cerebrospinal fluid pyruvate levels in Alzheimer's disease. Neurosci Lett. 199: 231–233.
54. Imahori K (2010): The biochemical study on the etiology of Alzheimer's disease. Proc Jpn Acad Ser B Phys Biol Sci. 86: 54–61.
55. Sorbi S, Bird ED, Blass JP (1983): Decreased pyruvate dehydrogenase complex activity in Huntington and Alzheimer brain. Ann Neurol. 13: 72–78.

56. Henderson ST (2008): Ketone bodies as a therapeutic for Alzheimer's disease. Neurother J Am Soc Exp Neurother. 5: 470–480.
57. Gallant M, Rak M, Szeghalmi A, Del Bigio MR, Westaway D, Yang J, et al. (2006): Focally elevated creatine detected in amyloid precursor protein (APP) transgenic mice and Alzheimer disease brain tissue. J Biol Chem. 281: 5–8.
58. Bürklen TS, Schlattner U, Homayouni R, Gough K, Rak M, Szeghalmi A, Wallimann T (2006): The Creatine Kinase/Creatine Connection to Alzheimer's Disease: CK Inactivation, APP-CK Complexes, and Focal Creatine Deposits. J Biomed Biotechnol. 2006. doi: 10.1155/JBB/2006/35936.
59. Burbaeva GS, Aksenova MV, Makarenko IG (1992): Decreased Level of Creatine Kinase BB in the Frontal Cortex of Alzheimer Patients. Dement Geriatr Cogn Disord. 3: 91–94.
60. Pettegrew JW, Panchalingam K, Klunk WE, McClure RJ, Muenz LR (1994): Alterations of cerebral metabolism in probable Alzheimer's disease: a preliminary study. Neurobiol Aging. 15: 117–132.
61. Fonteh AN, Harrington RJ, Tsai A, Liao P, Harrington MG (2007): Free amino acid and dipeptide changes in the body fluids from Alzheimer's disease subjects. Amino Acids. 32: 213–224.
62. Jiménez-Jiménez FJ, Molina JA, Gómez P, Vargas C, de Bustos F, Benito-León J, et al. (1998): Neurotransmitter amino acids in cerebrospinal fluid of patients with Alzheimer's disease. J Neural Transm Vienna Austria 1996. 105: 269–277.
63. Enche Ady CNA, Lim SM, Teh LK, Salleh MZ, Chin A-V, Tan MP, et al. (2017): Metabolomic-guided discovery of Alzheimer's disease biomarkers from body fluid. J Neurosci Res. n/a-n/a.

List of Figures and Tables

Figure 1. Correlations among clinical data (Aβ42 peptide, protein t-tau and p-tau, mini-mental state examination score, age, Aβ42/p-tau and Aβ42/t-tau ratios) and metabolite concentrations reported as level plot.

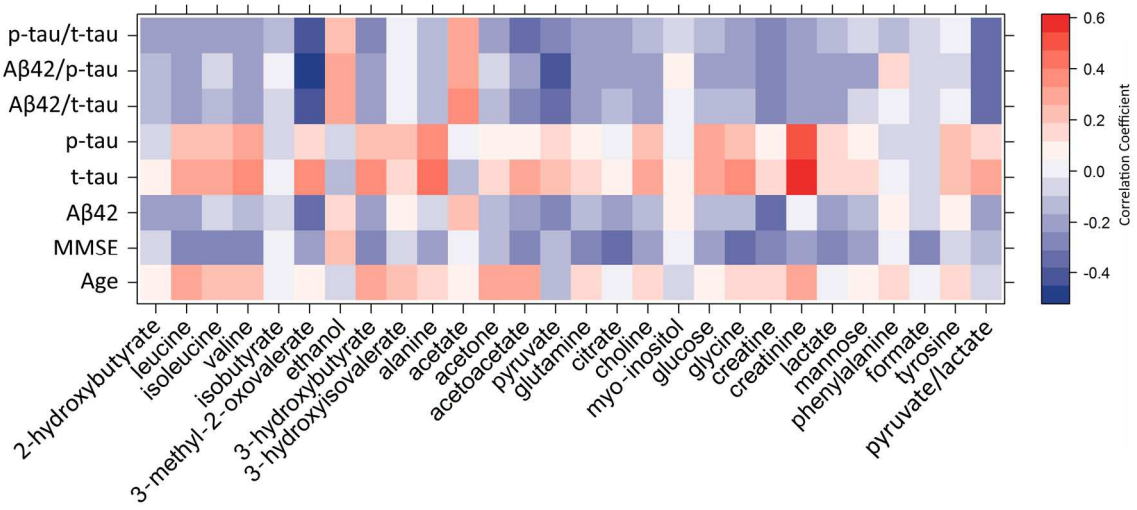

Figure 2. Clustering in the first two components of the PLS-CA model on NMR CSF profiles of ADdem patients (41 red dots) and MCI-MCI patients (21 green dots).

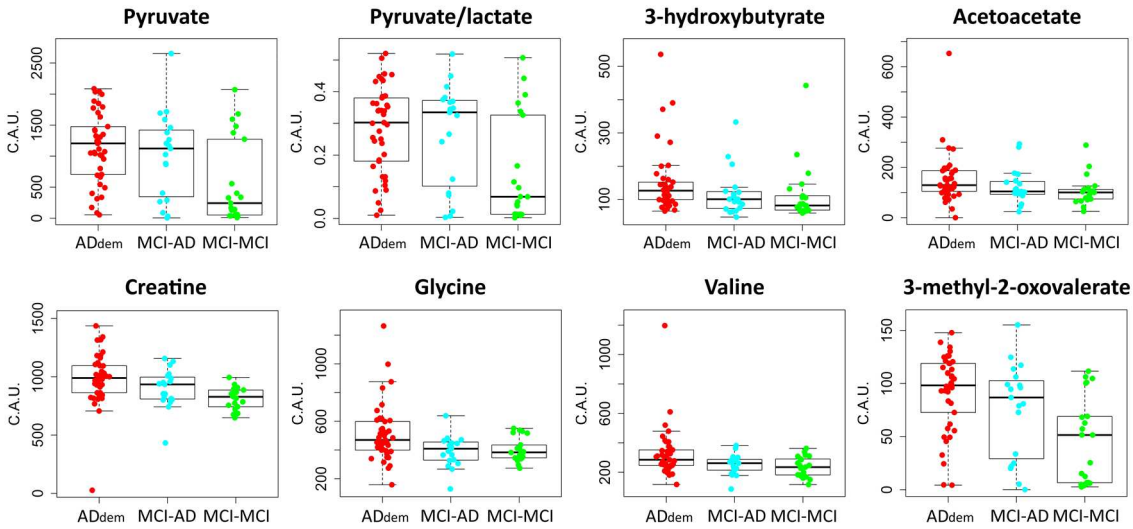

Figure 3. Box plot showing levels of representative metabolites in ADdem (red), MCI-AD (cyan), and MCI-MCI patients (green).

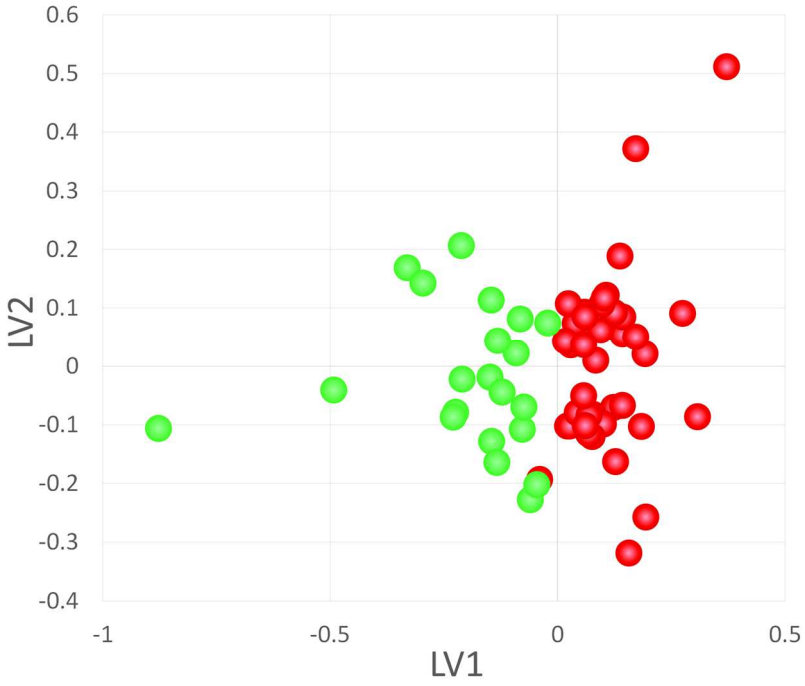

Figure 4. The Receiver Operating Characteristic (ROC) curve of the creatine-pyruvate-3-methyl-2-oxovalerate model. The area under the ROC curve (AUC) is also reported.

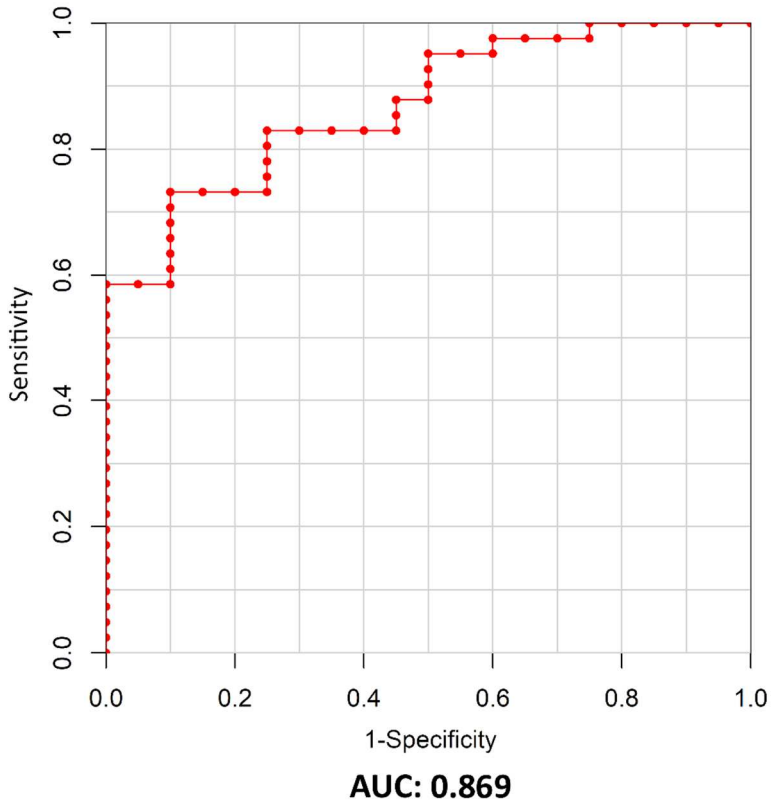

Table 1. Clinical, demographic and biomarker feature of the patients

	MCI-MCI	**MCI-AD**	**ADdem**
No (M/F)	21 (15/6)	19 (9/10)	41 (16/25)
MMSE	26.3 ± 2.2	24.1 ± 2. 6	16.6 ± 4.0
Aβ42 (pg/mL)	1010 ± 392	407 ± 92	478 ± 150
t-Tau (pg/mL)	288 ± 125	680 ± 271	782 ± 361
p-Tau (pg/mL)	51 ± 16	108 ± 54	108 ± 57

mean ± SD

Table 2. Comparison of CSF metabolite concentrations in ADdem and MCI-MCI patients (Wilcoxon test)

	ADdem (median ± MAD)	**MCI-MCI (median ± MAD)**	***P*-value**	**Adjusted *P*-value**	**Effect size (Cliff's Δ)**
Creatine	990 ± 116	828 ± 71	*P*< 0.0001	0.0002	0.6632
3-methyl-2-oxovalerate	98 ± 21	51 ± 45	0.0002	0.0036	0.5563
Pyruvate/lactate	0.3 ± 0.1	0.07 ± 0.06	0.0014	0.0109	0.489
Pyruvate	1204 ± 428	243 ± 205	0.0015	0.0109	0.4866
3-hydroxybutyrate	127 ± 27	82 ± 16	0.0043	0.022	0.4402
Acetoacetate	130 ± 37	101 ± 22	0.0045	0.022	0.4379
Valine	285 ± 53	235 ± 56	0.0058	0.0241	0.4262
Glycine	470 ± 79	383 ± 44	0.0067	0.0243	0.4193
Acetate	846 ± 462	1706 ± 812	0.0172	0.0553	-0.3705
Citrate	2588 ± 373	2322 ± 369	0.0269	0.073	0.3449
Leucine	475 ± 88	427 ± 71	0.0302	0.073	0.338
Mannose	281 ± 53	233 ± 39	0.0302	0.073	0.338
Alanine	342 ± 75	307 ± 48	0.0741	0.1389	0.2799
Ethanol	32 ± 15	64 ± 52	0.0693	0.1389	-0.2846
Glucose	9117 ± 811	8829 ± 558	0.0766	0.1389	0.2776
Lactate	3862 ± 370	3569 ± 373	0.0626	0.1389	0.2915
Acetone	347 ± 72	294 ± 53	0.1339	0.2103	0.2358
Glutamine	1248 ± 94	1179 ± 53	0.1378	0.2103	0.2334
Isoleucine	89 ± 22	76 ± 22	0.146	0.2116	0.2288
2-hydroxybutyrate	193 ± 40	162 ± 36	0.1726	0.2383	0.2149
Isobutyrate	182 ± 20	171 ± 18	0.2362	0.3114	0.187
Creatinine	1258 ± 133	1196 ± 118	0.2607	0.315	0.1777
Formate	151 ± 25	139 ± 13	0.2544	0.315	0.18
Phenylalanine	202 ± 25	189 ± 33	0.2735	0.3173	0.1731
Myo-inositol	731 ± 137	764 ± 126	0.4692	0.5234	-0.115
3-hydroxyisovalerate	213 ± 40	213 ± 47	0.6473	0.6473	0.0732
Choline	240 ± 71	251 ± 75	0.6263	0.6473	0.0778
Tyrosine	138 ± 34	129 ± 30	0.6473	0.6473	0.0732

Supplementary materials

Supplementary Figure 1. CPMG spin-echo pulse sequence (cpmgpr1d.comp; Bruker BioSpin) used for CSF sample acquisitions.

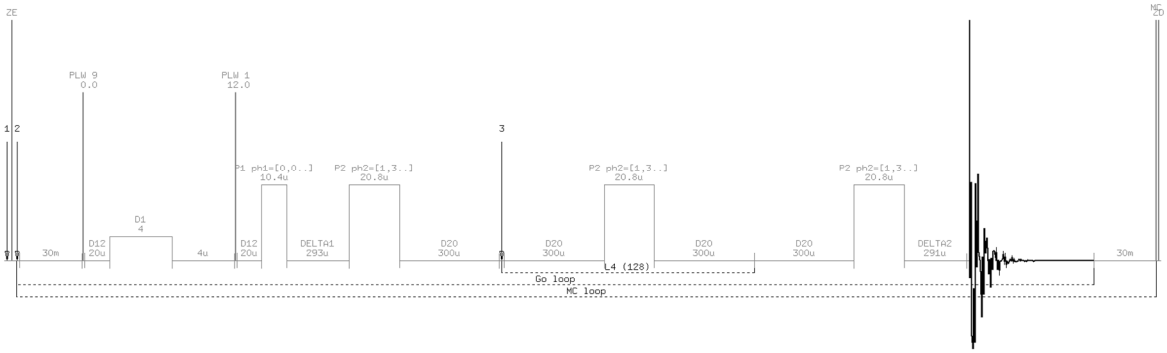

Supplementary Figure 2. A CPMG spectrum of CSF sample with the metabolites assigned and quantified for all samples. A) Aliphatic region of the spectrum; B) Aromatic region of the spectrum, the area in the box is magnified for clarity.

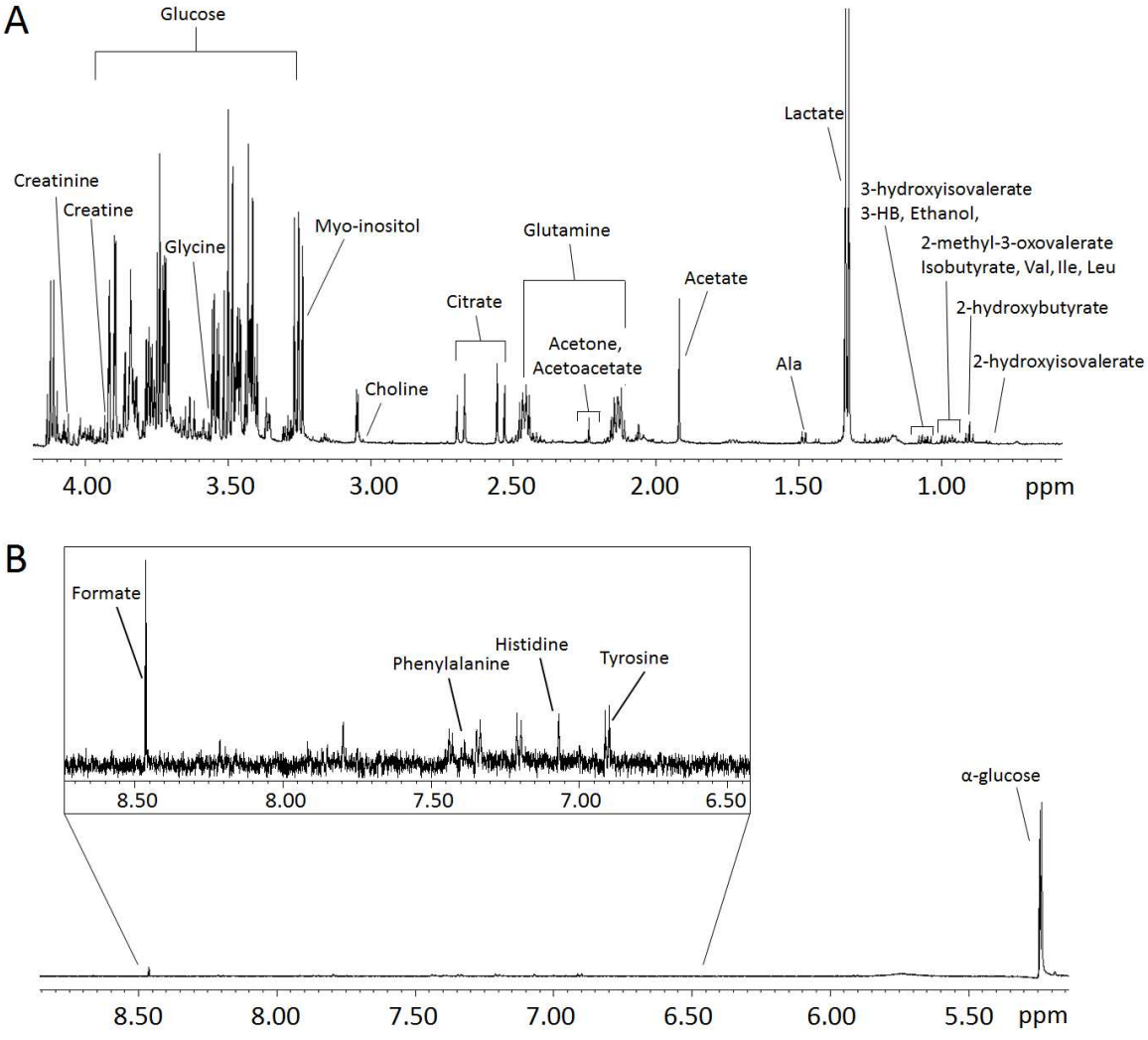

Supplementary Table 1. Linear correlation among metabolite concentrations and clinical data.

Metabolite	Age	MMSE	Abeta 42	t-tau	p-tau	Abeta 42/t-tau	Abeta 42/p-tau
2-hydroxybutyrate	0.082 (4.68E-01)	-0.088 (4.33E-01)	-0.177 (1.15E-01)	0.066 (5.65E-01)	-0.108 (3.47E-01)	-0.157 (1.66E-01)	-0.095 (4.08E-01)
leucine	0.246 (2.65E-02)	-0.288 (9.22E-03)	-0.216 (5.32E-02)	0.32 (4.03E-03)	0.134 (2.44E-01)	-0.235 (3.68E-02)	-0.193 (9.11E-02)
isoleucine	0.182 (1.05E-01)	-0.267 (1.61E-02)	-0.08 (4.78E-01)	0.33 (2.93E-03)	0.206 (7.10E-02)	-0.148 (1.94E-01)	-0.094 (4.13E-01)
valine	0.223 (4.58E-02)	-0.304 (5.74E-03)	-0.154 (1.71E-01)	0.397 (2.88E-04)	0.229 (4.37E-02)	-0.225 (4.63E-02)	-0.167 (1.44E-01)
isobutyrate	0.009 (9.39E-01)	-0.011 (9.22E-01)	-0.072 (5.25E-01)	-0.009 (9.34E-01)	-0.136 (2.36E-01)	-0.076 (5.05E-01)	0.006 (9.59E-01)
3-methyl-2-oxovalerate	0.04 (7.21E-01)	-0.274 (1.33E-02)	-0.346 (1.55E-03)	0.366 (9.12E-04)	0.151 (1.88E-01)	-0.46 (1.97E-05)	-0.45 (3.64E-05)
ethanol	-0.075 (5.06E-01)	0.245 (2.73E-02)	0.161 (1.50E-01)	-0.147 (1.95E-01)	-0.052 (6.50E-01)	0.321 (3.97E-03)	0.322 (3.99E-03)
3-hydroxybutyrate	0.323 (3.25E-03)	-0.181 (1.05E-01)	-0.095 (3.96E-01)	0.286 (1.05E-02)	0.129 (2.61E-01)	-0.167 (1.40E-01)	-0.162 (1.57E-01)
3-hydroxyisovalerate	0.219 (4.99E-02)	-0.055 (6.23E-01)	0.04 (7.22E-01)	0.168 (1.39E-01)	0.106 (3.54E-01)	-0.008 (9.41E-01)	0.023 (8.40E-01)
alanine	0.141 (2.11E-01)	-0.208 (6.20E-02)	-0.066 (5.60E-01)	0.422 (1.07E-04)	0.325 (3.68E-03)	-0.149 (1.90E-01)	-0.138 (2.29E-01)
acetate	0.085 (4.51E-01)	0.088 (4.37E-01)	0.248 (2.53E-02)	-0.183 (1.06E-01)	-0.074 (5.22E-01)	0.356 (1.27E-03)	0.32 (4.27E-03)
acetone	0.321 (3.52E-03)	-0.071 (5.30E-01)	-0.006 (9.59E-01)	0.118 (3.00E-01)	0.022 (8.49E-01)	-0.057 (6.17E-01)	-0.034 (7.66E-01)
acetoacetate	0.31 (4.81E-03)	-0.222 (4.65E-02)	-0.176 (1.17E-01)	0.273 (1.51E-02)	0.066 (5.68E-01)	-0.237 (3.54E-02)	-0.193 (8.96E-02)
pyruvate	-0.106 (3.48E-01)	-0.205 (6.60E-02)	-0.305 (5.61E-03)	0.284 (1.11E-02)	0.122 (2.89E-01)	-0.393 (3.47E-04)	-0.384 (5.15E-04)
glutamine	0.116 (3.03E-01)	-0.293 (8.03E-03)	-0.121 (2.82E-01)	0.157 (1.66E-01)	0.07 (5.40E-01)	-0.189 (9.53E-02)	-0.187 (1.01E-01)
citrate	-0.013 (9.11E-01)	-0.306 (5.40E-03)	-0.2 (7.34E-02)	0.091 (4.25E-01)	-0.045 (6.94E-01)	-0.169 (1.37E-01)	-0.184 (1.06E-01)
choline	0.139 (2.17E-01)	-0.164 (1.44E-01)	-0.048 (6.72E-01)	0.27 (1.62E-02)	0.208 (6.73E-02)	-0.146 (1.99E-01)	-0.2 (7.98E-02)
myo-inositol	-0.042 (7.07E-01)	0.052 (6.47E-01)	0.068 (5.44E-01)	0.016 (8.87E-01)	-0.182 (1.11E-01)	0.041 (7.22E-01)	0.101 (3.79E-01)
glucose	0.037 (7.42E-01)	-0.251 (2.41E-02)	-0.128 (2.55E-01)	0.31 (5.51E-03)	0.167 (1.44E-01)	-0.134 (2.38E-01)	-0.167 (1.43E-01)
glycine	0.107 (3.41E-01)	-0.361 (9.24E-04)	-0.104 (3.54E-01)	0.372 (7.24E-04)	0.166 (1.47E-01)	-0.155 (1.73E-01)	-0.16 (1.62E-01)
creatine	0.14 (2.12E-01)	-0.313 (4.50E-03)	-0.343 (1.73E-03)	0.132 (2.46E-01)	0.12 (2.95E-01)	-0.307 (5.93E-03)	-0.299 (7.78E-03)
creatinine	0.28 (1.13E-02)	-0.183 (1.01E-01)	-0.013 (9.08E-01)	0.527 (5.99E-07)	0.406 (2.24E-04)	-0.197 (8.15E-02)	-0.188 (9.93E-02)
lactate	-0.002 (9.84E-01)	-0.247 (2.64E-02)	-0.181 (1.06E-01)	0.185 (1.02E-01)	0.06 (6.03E-01)	-0.191 (9.21E-02)	-0.201 (7.73E-02)
mannose	0.05 (6.58E-01)	-0.189 (9.04E-02)	-0.085 (4.49E-01)	0.146 (1.99E-01)	0.022 (8.46E-01)	-0.081 (4.78E-01)	-0.198 (8.18E-02)
phenylalanine	0.165 (1.41E-01)	0.016 (8.89E-01)	0.077 (4.96E-01)	0.006 (9.58E-01)	-0.054 (6.36E-01)	0.015 (8.97E-01)	0.136 (2.36E-01)
formate	0.044 (6.96E-01)	-0.264 (1.72E-02)	-0.064 (5.67E-01)	-0.063 (5.82E-01)	-0.085 (4.61E-01)	-0.09 (4.28E-01)	-0.082 (4.74E-01)
tyrosine	0.125 (2.66E-01)	-0.101 (3.69E-01)	0.05 (6.60E-01)	0.267 (1.72E-02)	0.156 (1.74E-01)	-0.01 (9.31E-01)	-0.016 (8.89E-01)
pyruvate/lactate	-0.064 (5.70E-01)	-0.193 (8.51E-02)	-0.279 (1.15E-02)	0.301 (6.98E-03)	0.158 (1.68E-01)	-0.392 (3.55E-04)	-0.379 (6.20E-04)

Coefficient of correlation (*P*-value)

Supplementary Table 2. CSF metabolite concentrations in ADdem, MCI-MCI, and MCI-AD patients.

Metabolite	**ADdem (median ± MAD)**	**MCI-MCI (median ± MAD)**	**MCI-AD (median ± MAD)**
Creatine	989.57 ± 116.17	828.44 ± 70.57	934.63 + 107.34
3-methyl-2-oxovalerate	98.21 ± 20.79	51.43 ± 44.92	86.81 + 26.91
Pyruvate	1204.3 ± 427.97	243.24 ± 205.11	1123.22 + 466.71
Pyruvate/lactate	0.3 ± 0.1	0.07 ± 0.06	0.33 + 0.08
3-hydroxybutyrate	126.73 ± 27.03	82.17 ± 15.91	100.94 + 26.25
Acetoacetate	129.52 ± 36.83	100.55 ± 22.28	104.26 + 30.90
Valine	285.28 ± 52.64	234.84 ± 55.79	261.43 + 39.54
Glycine	469.64 ± 79.16	383.07 ± 43.97	409.01 + 62.24
Acetate	846.01 ± 462.16	1705.86 ± 811.89	854.96 + 369.88
Citrate	2588.44 ± 373.32	2321.74 ± 369.48	2436.26 + 306.62
Leucine	474.96 ± 87.73	426.87 ± 70.67	440 + 40.56
Mannose	281.3 ± 53.11	232.88 ± 38.78	232.8 + 72.89
Alanine	341.93 ± 74.68	306.9 ± 48.15	305.64 + 63.31
Ethanol	32.36 ± 14.82	64.16 ± 51.76	45.39 + 32.90
Glucose	9117.47 ± 811.19	8828.65 ± 558.32	8759.28 + 927.47
Lactate	3862.04 ± 369.66	3568.53 ± 373.38	3632.1 + 322.84
Acetone	347.05 ± 72.2	293.53 ± 52.73	287.63 + 60.04
Glutamine	1248.17 ± 93.69	1179.44 ± 53.35	1197.66 + 80.21
Isoleucine	88.53 ± 21.61	76.25 ± 22.3	76.75 + 15.33
2-hydroxybutyrate	193.28 ± 40.31	162.2 ± 35.86	165.09 + 30.00
Isobutyrate	182.28 ± 19.7	171.43 ± 18.37	170.95 + 22.86
Creatinine	1257.53 ± 133.42	1196.19 ± 117.83	1262.72 + 126.58
Formate	151.39 ± 25.38	139.47 ± 13.1	137.08 + 24.93
Phenylalanine	202.29 ± 25.21	188.77 ± 32.72	179.31 + 23.59
Myo-inositol	730.75 ± 136.96	763.61 ± 126.11	744.55 + 120.44
3-hydroxyisovalerate	213.19 ± 39.93	213.37 ± 47.2	186.77 + 54.90
Choline	240.14 ± 71.36	251.16 ± 74.75	250.49 + 51.26
Tyrosine	138.08 ± 33.59	128.85 ± 30.11	131.95 + 27.36

4.2.2 *NMR-based metabolomics approach to study urines of chronic inflammatory rheumatic diseases patients*

Alessia Vignoli[1,#], Donatella Maria Rodio[2,#], Anna Bellizzi[3,#], Anatoly Petrovich Sobolev[4,#], Elena Anzivino[2], Monica Mischitelli[2], Leonardo Tenori[5], Federico Marini[6], Roberta Priori[7], Rossana Scrivo[7], Guido Valesini[7]*, Ada Francia[8], Manuela Morreale[8], Maria Rosa Ciardi[2], Marco Iannetta[2], Cristiana Campanella[9], Donatella Capitani[4,] Claudio Luchinat[1,10], Valeria Pietropaolo[2], Luisa Mannina[9,4]

[#]Contributed equally to the work

[1] Magnetic Resonance Center (CERM), University of Florence, Sesto Fiorentino, Italy
[2] Department of Public Health and Infectious Diseases, Sapienza University of Rome, Rome, Italy
[3] Department of Public Health and Infectious Diseases, Institute Pasteur, Cenci-Bolognetti Foundation, Sapienza University of Rome, Rome, Italy
[4] Institute of Chemical Methodologies, "Annalaura Segre" Magnetic Resonance Laboratory, CNR, Rome, Italy
[5] FiorGen Foundation, Sesto Fiorentino, Italy
[6] Department of Chemistry, Sapienza University of Rome, Rome, Italy
[7] Department of Internal Medicine and Medical Specialties, Rheumatology Unit, Sapienza University of Rome, Rome, Italy
[8] Department of Department of Neurology and Psychiatry, Sapienza University of Rome, Rome, Italy
[9] Department of Drug Chemistry and Technologies, Sapienza University of Rome, Rome, Italy
[10] Department of Chemistry, University of Florence, Sesto Fiorentino, Italy

Published in:
Anal. Bioanal. Chem. **409,** 1405–1413 (2017).

Candidate's contributions: statistical analysis and interpretation of data, writing and review of the manuscript.

Anal Bioanal Chem
DOI 10.1007/s00216-016-0074-z

RESEARCH PAPER

NMR-based metabolomic approach to study urine samples of chronic inflammatory rheumatic disease patients

Alessia Vignoli[1] · Donatella Maria Rodio[2] · Anna Bellizzi[3] · Anatoly Petrovich Sobolev[4] · Elena Anzivino[2] · Monica Mischitelli[2] · Leonardo Tenori[5] · Federico Marini[6] · Roberta Priori[7] · Rossana Scrivo[7] · Guido Valesini[7] · Ada Francia[8] · Manuela Morreale[8] · Maria Rosa Ciardi[2] · Marco Iannetta[2] · Cristiana Campanella[9] · Donatella Capitani[4] · Claudio Luchinat[1,10] · Valeria Pietropaolo[2] · Luisa Mannina[9,4]

Received: 21 July 2016 / Revised: 5 October 2016 / Accepted: 31 October 2016

Abstract The nuclear magnetic resonance (NMR)-based metabolomic approach was used as analytical methodology to study the urine samples of chronic inflammatory rheumatic disease (CIRD) patients. The urine samples of CIRD patients were compared to the ones of both healthy subjects and patients with multiple sclerosis (MS), another immuno-mediated disease. Urine samples collected from 39 CIRD patients, 25 healthy subjects, and 26 MS patients were analyzed using ^{1}H NMR spectroscopy, and the NMR spectra were examined using partial least squares-discriminant analysis (PLS-DA). PLS-DA models were validated by a double cross-validation procedure and randomization tests. Clear discriminations between CIRD patients and healthy controls (average diagnostic accuracy 83.5 ± 1.9%) as well as between CIRD patients and MS patients (diagnostic accuracy 81.1 ± 1.9%) were obtained. Leucine, alanine, 3-hydroxyisobutyric acid, hippuric acid, citric acid, 3-hydroxyisovaleric acid, and creatinine contributed to the discrimination; all of them being in a lower concentration in CIRD patients as compared to controls or to MS patients. The application of NMR metabolomics to study these still poorly understood diseases can be useful to better clarify the pathologic mechanisms; moreover, as a holistic approach, it allowed the detection of, by means of anomalous metabolic traits, the presence of other pathologies or pharma-

Alessia Vignoli, Donatella Maria Rodio, Anna Bellizzi and Anatoly Petrovich Sobolev contributed equally to this work.

Electronic supplementary material The online version of this article (doi:10.1007/s00216-016-0074-z) contains supplementary material, which is available to authorized users.

✉ Guido Valesini
guido.valesini@uniroma1.it

[1] Magnetic Resonance Center (CERM), University of Florence, Via Luigi Sacconi, 50019 Sesto Fiorentino, Italy

[2] Department of Public Health and Infectious Diseases, Sapienza University of Rome, Piazzale Aldo Moro 5, 00185 Rome, Italy

[3] Department of Public Health and Infectious Diseases, Institute Pasteur, Cenci Bolognetti Foundation, Sapienza University of Rome, Viale Regina Elena 291, 00161 Rome, Italy

[4] Institute of Chemical Methodologies, "Annalaura Segre" Magnetic Resonance Laboratory, CNR, Via Salaria Km 29,300, 00015 Monterotondo, Italy

[5] FiorGen Foundation, Via Luigi Sacconi 6, 50019 Sesto Fiorentino, Italy

[6] Department of Chemistry, Sapienza University of Rome, Piazzale Aldo Moro 5, 00185 Rome, Italy

[7] Department of Internal Medicine and Medical Specialties, Rheumatology Unit, Sapienza University of Rome, Viale del Policlinico 155, 00161 Rome, Italy

[8] Department of Neurology and Psychiatry, Sapienza University of Rome, Piazzale Aldo Moro 5, 00185 Rome, Italy

[9] Department of Drug Chemistry and Technologies, Sapienza University of Rome, Piazzale Aldo Moro 5, 00185 Rome, Italy

[10] Department of Chemistry, University of Florence, Via della Lastruccia, 3-13, 50019 Sesto Fiorentino, Italy

Published online: 30 November 2016

ceutical treatments not directly connected to CIRDs, giving comprehensive information on the general health state of individuals.

Keywords Nuclear magnetic resonance spectroscopy · Metabolomics · Urine · Multivariate data analysis · Chronic inflammatory rheumatic diseases

Abbreviations

CIRDs	Chronic inflammatory rheumatic diseases
COSY	Correlation spectroscopy
CSF	Cerebrospinal fluid
HMBC	Heteronuclear multiple bond correlation
HPLC	High-performance liquid chromatography
HSQC	Heteronuclear single quantum coherence
MS	Multiple sclerosis
NMR	Nuclear magnetic resonance
PLS-DA	Partial least squares-discriminant analysis
TMSP	Trimethylsilyl propionate
UTIs	Urinary tract infections
VIP	Variable importance in projection

Introduction

Metabolomics, one of the "omics" sciences, is concerned with the identification, quantification, and characterization of the complete set of low molecular weight metabolites, called metabolome, present in a biological specimen [1]. Metabolome is a dynamic and evolving entity that can be regarded as the downstream end product of the interaction between genome, transcriptome, and proteome, influenced by the environment, diet, drugs, diseases, lifestyle, and age [2]. Nuclear magnetic resonance (NMR)-based metabolomics has been applied in many research fields such as food chemistry [3], biological chemistry [4], and medicine [5–7]. Considering the complexity and multiplicity of human pathologies, only few applications of NMR metabolomic approach have been reported so far especially in the areas of biomedical research focused on nutritional studies [8], diagnosis of diseases [9, 10], identification of biomarkers, and definition of pathological status [11, 12]. One major application of metabolomics is the analysis of biological fluids, such as human urine, serum, and saliva, which are easily obtained and readily used for disease diagnosis and in clinical trials for the monitoring of drug therapy. With respect to a classical analytical approach focused on target diagnostic parameters, every application of metabolomics is untargeted, showing a comprehensive picture of metabolome with a high possibility to meet with the unexpected or even unknown metabolic changes, and new markers of pathology can be discovered as a result of the metabolomic analysis.

In this applicative paper, for the first time, we adopt a metabolomic approach to investigate the influence of chronic inflammatory rheumatic diseases (CIRDs) on urine metabolome. Human urine is very complex in composition, containing thousands of different compounds, and the changes of these metabolites reflect the biochemical changes in a living system [5–7].

CIRDs are a group of multisystem diseases characterized by inflammation, immunological abnormalities, swelling, and pain in joints or muscles. More than 100 types of diseases are classified as rheumatic diseases, including rheumatoid arthritis, ankylosing spondylitis, psoriatic arthritis, and osteoarthritis. The pathologic mechanisms of rheumatic diseases are complex, involving both genetic and environmental factors. Although the rheumatic diseases have been studied for decades, the underlying mechanisms remain still poorly understood [13].

We applied an NMR metabolomic analytical approach to compare the urine samples of CIRD patients with those of healthy subjects and to find out potential biomarkers of pathology. Taking into account that CIRD pathology is immuno mediated, it was interesting to compare a urine metabolome of CIRD patients with another immuno-mediated disease. Therefore, we exploited the same NMR analytical approach to make a comparison between the urine samples of CIRD and multiple sclerosis (MS) patients.

Materials and methods

Volunteer recruitment and sample collection

Adult volunteers (35 males and 55 females, mean age 44 with a standard deviation of ±14) participated in this study. Thirty-nine patients (11 males and 28 females, mean age 54 with a standard deviation of ±12) were affected by CIRDs. The control group consisted of 25 healthy subjects (13 males and 12 females, mean age 35 with a standard deviation of ±7) from the staff of the Department of Public Health and Infectious Diseases and Department of Drug Chemistry and Technologies, Sapienza University of Rome. Twenty-six patients (11 males and 15 females, mean age 37 with a standard deviation of ±9) were diagnosed as having MS.

First-morning preprandial urine void was used for the collection period. Patients were supplied with appropriate collection instructions and information on fasting, diet, and medication restrictions. The urine samples were collected without preservative into prelabeled sterile collection cups, and aliquots were immediately frozen and stored at −80 °C until the analysis. Additionally, all volunteers were asked to record their dietary intake and the use of any medication (either

prescribed or self-administered) on the day before each visit and to fast from midnight until urine collection in following morning.

The study was carried out in accordance with the ethical standards of the institutional research committee and with the 1964 Helsinki Declaration and its later amendments. Informed consent was obtained from each participant included in the study.

NMR sample preparation

Fresh urine is characterized by the presence of human cells (erythrocytes, leucocytes, urothelial cells, epithelial cells), bacteria, fungi, sperm counts, non-cellular components (mucus filaments, cylinders, cylindroids, pseudocylinders, crystals, urates). To avoid the presence of particulate components and cellular enzyme leakage in the NMR samples that will affect the spectral quality, the optimized standard protocol [14] for NMR analysis was followed. Frozen aliquots (1 mL) were thawed at room temperature. Urine samples were shaken before use, and 790 μL was centrifuged at 14,100*g* for 5 min at room temperature. Seven hundred microliters of the supernatant was added to 78 μL of potassium phosphate buffer (37 mM KH_2PO_4, 63 mM K_2HPO_4, 30 mM NaN_3, and 10 mM sodium trimethylsilyl [2,2,3,3-$^2H_4$] propionate (TMSP) in 100% D_2O, pH 7.4). Seven hundred microliters of the mixture was put into 5-mm NMR tubes.

NMR measurements

^{1}H NMR experiments were recorded at 300 K on a Bruker Avance 600 spectrometer (Bruker BioSpin GmbH, Rheinstetten, Germany) operating at the proton Larmor frequency of 600.13 MHz (B_0 = 14.1 T) and equipped with a Bruker multinuclear Z gradient 5-mm probe head. For each urine sample, a 1D NMR spectrum was acquired with water peak suppression during relaxation delay (4 s) using the zgpr standard presaturation pulse Bruker sequence.

In order to obtain the spectra of good quality, a standard sample for setting and adjustment signal line shape was regularly used. For each analyzed sample, we used a protocol that assure appropriate line width for standard signal TMSP, residual water signal suppression, and baseline correction. Moreover, the reproducibility was verified by comparing the spectra of the same sample obtained at beginning and at the end of the experimental design.

The ^{1}H spectra of the urine samples were acquired using the following conditions: number of scans 256, $\pi/2$ pulse ~10–12 μs, time domain (TD) 64 K data points, relaxation delay plus acquisition time 6.73 s, and spectral width 20 ppm. Total acquisition time for each sample was 29 min. ^{1}H NMR spectra were obtained by the Fourier transformation of the free induction decay, applying an exponential multiplication with a line-broadening factor of 0.3 Hz and a zero filling (size = 64 K) procedure. ^{1}H NMR spectra were manually phased. Chemical shifts were referenced internally to the singlet methyl resonance of TMSP at 0.00 ppm.

The baseline was corrected using the Cubic Spline Baseline Correction routine in the Bruker TopSpin software (version 1.3).

Two-dimensional NMR experiments, namely ^{1}H–^{1}H correlation spectroscopy (COSY), ^{1}H–^{13}C heteronuclear single quantum coherence (HSQC), and ^{1}H–^{13}C heteronuclear multiple bond correlation (HMBC), were performed using the same experimental conditions previously reported. The HSQC experiments were performed using a coupling constant ($^1J_{C–H}$) of 150 Hz, and the ^{1}H–^{13}C HMBC experiments were performed using a delay of 80 ms for the evolution of long-range couplings.

Signals were assigned using both 2D NMR experiments and matching routines of AMIX 3.8.4 (Bruker BioSpin) in combination with the BIOREFCODE reference database (Bruker BioSpin) and freely available databases like Urine Metabolome Database (UMDB) [15].

Spectral processing for statistical analysis

For the multivariate statistical analysis, each ^{1}H spectrum was segmented into 0.02-ppm chemical shift bins in the range between 0.5 and 10.00 ppm using AMIX, so that an integral of each bin represents a new point in the binned spectrum. Bins of urea (5.68–5.92 ppm) and water (4.61–4.95 ppm) were excluded. The regions around citric acid (2.65–2.73 and 2.51–2.59 ppm) and the creatinine (4.04–4.10 and 3.02–3.08 ppm) resonances were combined to account for shifting signals. This binning method reduced each spectrum to 436 variables.

The binned spectra were normalized to be comparable. Normalization is a preprocessing method, which accounts for different dilutions of samples by scaling the spectra to the same virtual overall concentration. In our case, all the spectra were normalized using probabilistic quotient normalization (PQN) [16]. This method is based on the calculation of the most probable dilution factor by looking at the distribution of the quotients obtained, dividing the amplitudes of the acquired spectra by those of a reference spectrum. The median spectrum of the control samples was used as reference.

For the univariate analysis, after PQN normalization of the spectra, each spectral region related to the metabolites assigned in the ^{1}H NMR profiles was aligned, by a simple horizontal rigid shift, in a way that the corresponding peaks of interest resulted superimposed and then were integrated. In this way, it is possible to reduce the selected ppm intervals and to improve the precision in the integration by compensating the variations in peak position in the different urine spectra due to pH and ionic strength variability. The obtained integrals represent the concentrations of metabolites in arbitrary units. The whole procedure was performed using an R script developed in-house.

Statistical analysis

Data analyses were performed using R, an open source software for the statistical analysis of data [17], and in-house routines running under a MATLAB environment (The MathWorks, Natick, MA). In particular, in order to assess whether the metabolic profiles of CIRD patients vary with respect to the metabolic profiles of healthy subjects or to those of MS patients, a classification analysis was conducted by means of the partial least squares–discriminant analysis (PLS-DA) algorithm, considering all possible pairs of conditions (control vs CIRD, control vs MS, and CIRD vs MS). PLS-DA operates classification by building a PLS regression model between the independent matrix X containing the spectral profiles and the dummy binary vector encoding for class membership as Y response: if a bipolar coding is used, so that the two classes are indicated by −1 and +1, respectively, a threshold value of zero is adopted to decide whether a sample belongs to one category or another on the basis of the predicted Y values.

The statistical significance of the classification models obtained in the study was assessed using a double cross-validation approach with eight cancelation groups in the outer and seven in the inner loops; the procedure was repeated 100 times, and the results were averaged. Moreover, for each comparison, the accuracy calculated by the double cross-validation approach was checked for significance against the empirical distribution of three figures of merit (number of misclassifications, area under the ROC curve, and discriminant Q^2) under the null hypothesis (no discrimination), by means of a randomization test with 1000 permutations.

Based on the calculated models, the multivariate search for candidate biomarkers was carried out by inspecting the values of variable importance in projection (VIP) scores and of the rank products, as estimated by the double cross-validation procedure.

For the univariate analysis, metabolite concentrations in arbitrary units were analyzed to determine the discriminating metabolites among the healthy group and the two groups of patients diagnosed of having immuno-mediated diseases (see Electronic Supplementary Material (ESM) Table S1). Statistical significance of each metabolite in the comparisons was assigned using the univariate non-parametric Kruskal-Wallis test [18], on the biological assumption that metabolites are not normally distributed. Because a statistical test was executed for each assigned metabolite, the Benjamini and Hochberg correction was used to control for the risk of false discoveries (type I errors) and to adjust all the p values, taking into account the multiple comparisons performed (i.e., each test for each variable) [19]. An adjusted p value <0.05 was deemed statistically relevant.

Results

The ^{1}H NMR spectra of the urine samples of CIRD patients and healthy subjects are reported in Fig. 1. The ^{1}H NMR spectrum of a urine sample can be considered as its metabolic

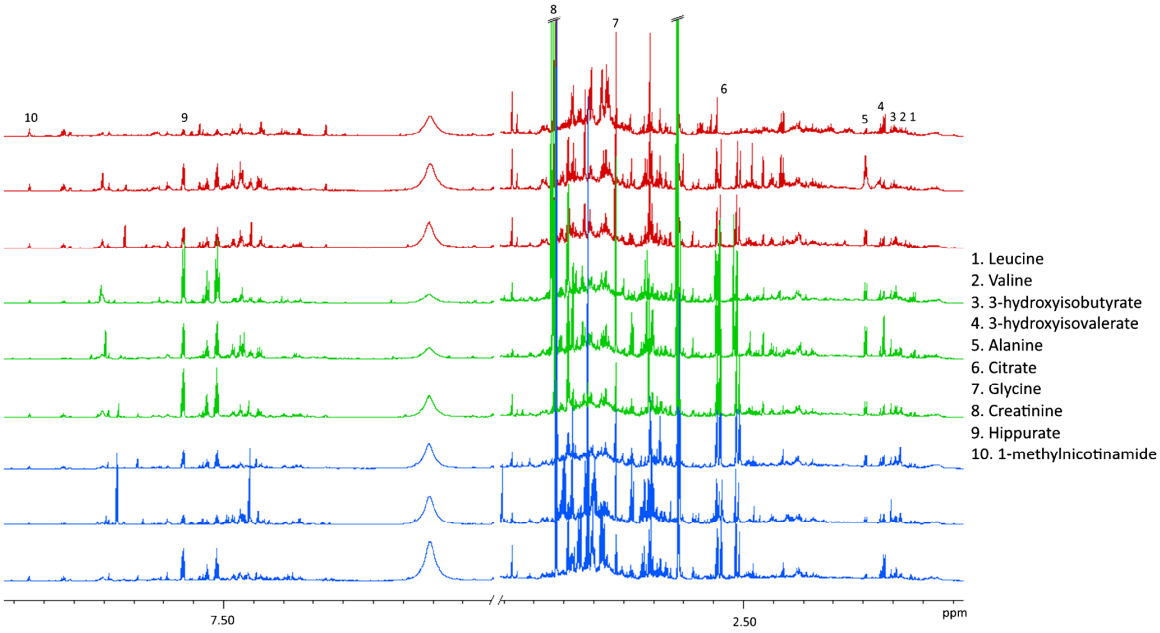

Fig. 1 ^{1}H spectra (600 MHz) of urine samples at 300 K of CIRD patients (*red*), healthy controls (*green*), and MS patients (*blue*). For each group, three representative spectra are reported. For the comparisons, the signals that discriminate between CIRD and MS patients and healthy controls are shown

fingerprint as such, even without statistical treatment, can be used in a preliminary *visual analysis* to obtain some important information. Comparing the ^{1}II NMR spectrum of a given urine sample to a control one, it is possible to reveal the presence of *anomalous* metabolites. For instance, the ^{1}H spectrum of the urine sample of CIRD patient (see ESM Fig. S1b) showed the presence of anomalous signals. These signals were assigned to derivatives of isonicotinic acid using 2D experiments (see ESM Fig. S2). The presence of these compounds was due to the intake of isoniazid, the hydrazide of isonicotinic acid, as confirmed by the medical information. The ^{1}H spectrum of another urine sample of CIRD patient (see ESM Fig. S1c) showed signals at 5.24 ppm and in the 3–4 ppm range characteristic of glucose, suggesting a diabetic disease, which was then confirmed by medical information.

After this visual analysis that allowed to exclude outlier resonances from the statistical analysis, the ^{1}H spectra were assigned (see ESM Table S2), confirming the presence of the following metabolites in all urine samples: 1-methylnicotinamide, hippuric acid, phenylacetylglycine, trigonelline, pyruvic acid, alanine, choline, citric acid, creatinine, dimethylamine, glycine, 3-hydroxyisovaleric acid, 3-hydroxyisobutyric acid, isoleucine, lactic acid/threonine, leucine, and valine.

The entire ^{1}H spectra were analyzed using the bucketing procedure described above, and the PQN-normalized data were submitted to PLS-DA. At first, the NMR data from 25 urine samples of controls and 39 urine samples of CIRD patients were used to build a PLS-DA model to differentiate the two types of individuals. The optimal model (3 LV) correctly identified 75.6 ± 2.9% of 39 CIRD patients and 95.9 ± 0.7% of 25 controls with an overall diagnostic accuracy of 83.5 ± 1.9%, as evaluated from the results on the outer loop of the double cross-validation procedure. The obtained discrimination between the two categories can be observed in Fig. 2, where the projection of the samples onto the first two latent variables of the model is reported. This discrimination appeared to be statistically significant in terms of all the three figures of merit considered (number of misclassifications, area under the ROC curve, and discriminant Q^2). Indeed, the comparison of the results obtained on the data in double cross-validation and the empirical distribution of the indices under the null hypothesis, estimated by the randomization tests (Fig. 3), show in all cases a significant discrimination ($p < 0.001$).

Inspection of the VIP scores and of the rank product values after double cross-validation suggests that the metabolites mostly involved in the differentiation between CIRD patients and controls are creatinine, citric acid, phenylalanine, glycine, hippuric acid, lactic acid, and trigonelline.

A further validation of these results was obtained by univariate inspection of the metabolites, which evidenced that the patients with CIRD featured significantly lower levels ($p < 0.05$) of leucine, valine, alanine, 3-hydroxyisobutyric acid, 3-hydroxyisovaleric acid, hippuric acid, glycine, citric acid, creatinine, and methylnicotinamide relative to controls (ESM Fig. S3).

Samples of patients with CIRD were also compared with patients with another immune-mediated disease, MS, an inflammatory demyelinating condition of the central nervous system of unknown etiology [20]. NMR data from urine samples of 39 patients with CIRD and of 26 patients with MS (see ^{1}H NMR spectra in Fig. 1) were used to build and validate a PLS-DA model (optimal complexity 4 LV), which showed an overall classification accuracy of 81.1 ± 1.9%, as evaluated on the outer double cross-validation loop. In detail, this analysis correctly identified 77.5 ± 3.1% of 39 patients with CIRD and 86.5 ± 3.7% of 26 patients with MS. A graphical representation of the discriminant ability of the model is shown in Fig. 4, where the projection of the samples onto the space spanned by the first

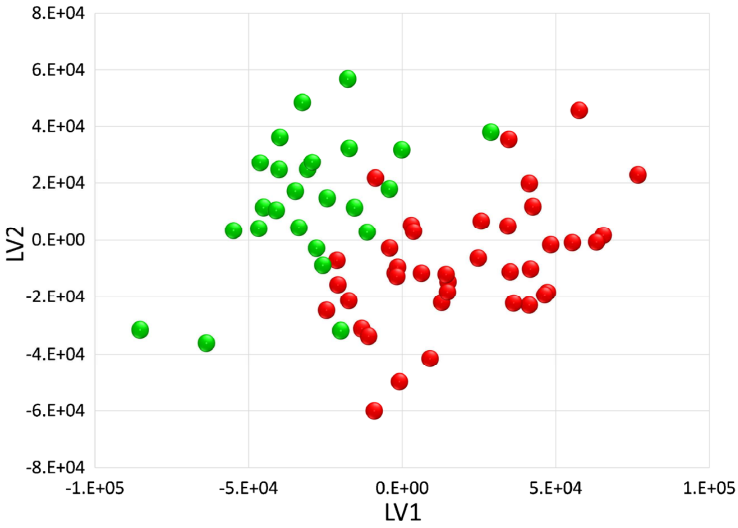

Fig. 2 PLS-DA score plot of CIRD patients and healthy subjects. Projection of the samples onto the space spanned by the two significant latent variables of the model (*green* and *red circles*)

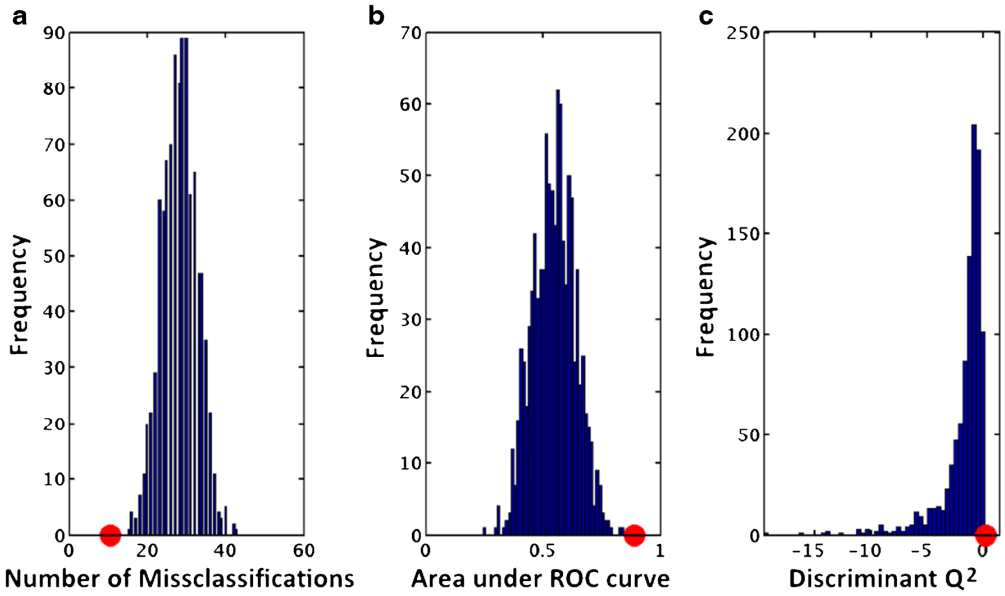

Fig. 3 PLS-DA of CIRD patients and healthy subjects. Comparison between the average values of the number of misclassification, area under the ROC curve, and discriminant Q^2 in double cross-validation (*red dots* in panels **a**–**c**, respectively) and their distributions under the null hypothesis, estimated by randomization tests with 1000 permutations (*blue* histograms)

two latent vectors is reported. The statistical significance of the observed discrimination was tested by comparing the average number of misclassifications, area under the ROC curve, and discriminant Q^2 to their distribution under the null hypothesis, estimated by means of permutation tests, and in all cases, the observed differences appeared to be meaningful ($p < 0.001$).

Also in this case, a multivariate evaluation of candidate biomarkers was carried out by inspecting the values of VIP scores and rank product. Both indices agreed in identifying creatinine, citric acid, phenylalanine, glycine, hippuric acid, lactic acid, trigonelline, and isoleucine as the variables contributing the most to the observed discrimination. In particular, a further univariate inspection of the NMR data showed that the patients with CIRD featured significantly lower levels ($p < 0.05$) of leucine, alanine, 3-hydroxyisobutyric acid, citric acid, 3-hydroxyisovaleric acid, dimethylamine, and creatinine relative to MS patients (ESM Fig. S4).

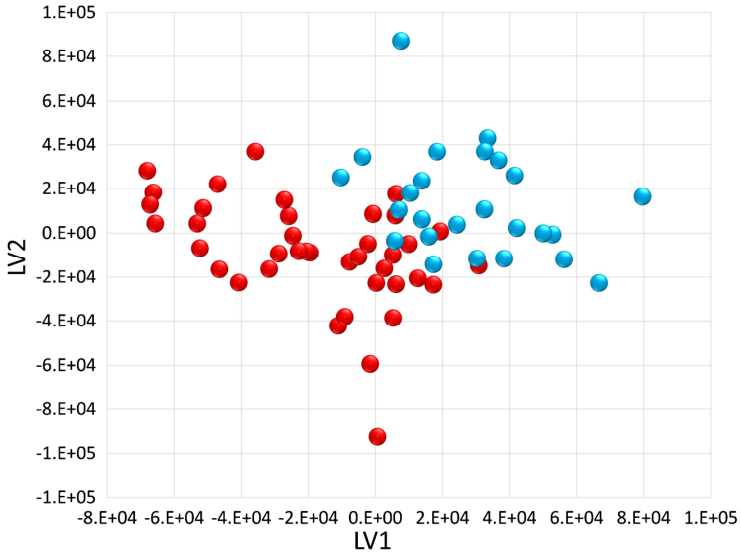

Fig. 4 PLS-DA score plot of CIRD and MS patients. Projection of the samples onto the space spanned by the first two significant latent variables of the model (*red* and *blue circles*)

PLS-DA were also performed using a subgroup of CIRD patients better matched for age and gender (21 CIRD patients (47 years of age), 9 males and 12 females) with respect to controls and MS patients. The results obtained were comparable with the ones reported above (83.2 ± 2.6 and 85.0 ± 2.4% for the discrimination against MS patients and controls, respectively), demonstrating that the not well-matched groups are not an issue. Moreover, the metabolites identified as significantly contributing to the model were consistent to those previously identified.

A PLS-DA for CIRD patients was also performed using, as input data only, the statistically significant metabolites as an alternative to the whole NMR spectral profile. The results obtained (79.8 ± 1.9 and 83.2 ± 1.9 % for the discrimination of CIRD patients against MS patients and controls, respectively) were only slightly lower than those obtained using the NMR fingerprint, confirming the relevance of these metabolites.

Lastly, PLS-DA was carried out on the NMR data from 25 control urine samples and from 26 urine samples of patients with MS to check whether any significant metabolic difference could be evidenced between them. The PLS analysis correctly identified 60.5 ± 7.8% of 25 controls and 47.8 ± 5.5% of 26 patients with MS. The overall accuracy was only 54.1 ± 4.4%, showing that in this dataset, no discrimination is possible between the two groups. Moreover, with reference to univariate inspection of the metabolites, there are no metabolites that differ significantly between MS patients and controls.

Discussion

In the present study, we report the results obtained, applying the NMR-based metabolomic approach to study the urine samples of chronic inflammatory rheumatic disease patients compared to the samples of controls or MS patients. NMR spectroscopy of urine yielded a fairly accurate discrimination between patients with CIRD and healthy controls and between CIRD patients and MS patients, but not for the comparison between MS patients and healthy subjects. These results suggest that CIRD patients (but not MS patients) feature a distinct metabolic fingerprint in urine (Table 1). Urine samples from CIRD patients featured significantly lower levels ($p < 0.05$) of leucine, valine, alanine, 3-hydroxyisobutyric acid, 3-hydroxyisovaleric acid, glycine, citric acid, creatinine, hippuric acid, and methylnicotinamide relative to controls. Some of these metabolites (leucine, alanine, 3-hydroxyisobutyric acid, citric acid, 3-hydroxyisovaleric acid, and creatinine) were also significantly lower in CIRD patients compared with MS patients.

Previous studies, also performed using NMR metabolomics, have shown that the serum metabolic fingerprint in patients with CIRD is clearly distinct from that of healthy controls due to the presence of inflammatory processes [21]. If we compare the trend of the metabolites measured in our study with those reported for serum in Priori et al.'s review for murine models [10] and in the study of Zabek and coworkers on 20 women with RA [22], it can be noted that both studies converge on the presence of high concentrations of citrate in the patients' sera (see ESM Table S3). Moreover, our results seem to reflect the same trend seen in sera by Zabek, this finding may be explained by an alteration of the homeostasis that gives a decrease to the increment of these metabolites in sera and, therefore, a decrease of their levels of excretion. Nevertheless, these assumptions need further investigations.

It is noteworthy that the downregulation of 1-methylnicotinamide, citric acid, creatinine, and hippuric acid observed in the urine samples of CIRD patients has been also reported by Nevedomskaya and coworkers [23] in the case of urinary tract infections (UTIs), a complex disorder for which diagnostics is not straightforward. Clearly, the infections induce changes in the urinary metabolic patterns, contributing to the determination of the urine metabolic fingerprint. The downregulation of some metabolites in the urine samples of CIRD patients could be a consequence of UTI, since a higher

Table 1 Summary of the statistical results relative to the comparison between CIRD patients and healthy subjects, between CIRD and MS patients, and between MS patients and healthy subjects

Comparison	Diagnostic accuracy (%)	Number of LV used in the optimized model	Fraction of total variation of Y (%)	Statistically relevant metabolites ($p < 0.05$)
CIRD patients vs. healthy subjects	83.5 ± 1.9	3	75.3	Leucine, valine, alanine, 3-hydroxyisobutyric acid, hippuric acid, glycine, citric acid, creatinine, 3-hydroxyisovaleric acid, and methylnicotinamide
CIRD vs. MS patients	81.1 ± 1.9	4	74.1	Leucine, alanine, 3-hydroxyisobutyric acid, citric acid, dimethylamine, creatinine, and 3-hydroxyisovaleric acid
MS patients vs. healthy subjects	54.1 ± 4.4	2	33.1	None of the metabolites assigned

incidence of urinary tract infections among rheumatoid arthritis patients with respect to general population has been demonstrated [24].

In the literature, it has been reported that CIRD patients present low body mass [25] and muscle weakness [26]. We can hypothesize that low levels of valine and leucine, essential amino acids, are due to an increased demand for muscle turnover since these amino acids are utilized in the synthesis of muscle proteins.

Moreover, we also find out a lowering creatinine level in CIRD patients as compared with controls and MS patients. This result could be explained by a reduced carnitine palmitoyltransferase I activity that induced the decrease of the muscle mass and the increase of the muscle turnover observed in CIRD patients, in particular in the case of rheumatoid arthritis patients [27, 28]. This finding could be an interesting remark also because Kapoor and coworkers have shown that creatinine in urine raises up only in patients who have a good response to the antitumor necrosis factor therapy [29], so creatinine concentration could be a useful biomarker in the follow-up of the therapy.

Our data show a decrease in the urinary citric acid levels in patients with CIRD. This phenomenon may be due to the presence of a pathology called distal renal tubular acidosis (dRTA). dRTA, characterized by an inappropriately high urine pH (usually >5.5), hypokalemia, and hypocitraturia, has a variety of etiologies including inflammatory autoimmune diseases, typically Sjögren's syndrome but also rheumatoid arthritis [30].

Our data on urine analyses do not permit a clear discrimination between MS patients and healthy controls; moreover, there are no assigned metabolites that differ in a statistically relevant way between these two groups, even if previous studies showed the presence of the particular MS metabolic fingerprint in serum [31, 32] and in cerebrospinal fluid (CSF) [33]. However, CSF is a biofluid located in the region of the body in which the inflammatory process due to the pathology takes place; thus, its biochemical composition is likely to be more influenced by inflammation. The studies related to the serum have shown alterations regarding oxypurine, nitrate, and nitrite determined by HPLC and phosphocholine and glucose determined by NMR. Oxypurine, nitrate, and nitrite are not detectable by NMR, whereas phosphocholine and glucose are not normally present in urine. This can explain why the metabolic urine fingerprint in MS patients is not clearly distinct from that in healthy subjects in our dataset.

Conclusions

In the present work, we have presented a novel application of the NMR-based analytical approach to discriminate the metabolic fingerprints of the urine samples of CIRD patients from those of both healthy controls and MS patients. We have also identified several metabolites downregulated in the urine samples of CIRD patients: significantly lower urinary levels ($p < 0.05$) of leucine, valine, alanine, 3-hydroxyisobutyric acid, 3-hydroxyisovaleric acid, glycine, citric acid, creatinine, hippuric acid, and methylnicotinamide relative to controls were observed. Some of these metabolites (leucine, alanine, 3-hydroxyisobutyric acid, citric acid, 3-hydroxyisovaleric acid, and creatinine) were also significantly lower in the urine samples of CIRD patients compared to those of MS ones. Although none of these metabolites has sufficient diagnostic power by itself, each of them contributes to the metabolic fingerprint of the disease. The metabolic fingerprint can be considered as a sort of holistic biomarker with a discriminative power higher than the simple sum of the few quantified metabolites. The fact that there are many small differences and large overlaps between the identified metabolites is common in the major part of real cases: often, it is too optimistic to search for a single discriminant biomarker that can identify and provide an adequate measure of a disease or a clinical condition. This is because most human diseases have a multifactorial etiology and a complex physiopathology; consequently, there will be an alteration of several metabolic products [34]. The metabolic fingerprint composed by the superimposition of all the visible signals of the low molecular weight endogenous metabolites takes into account all those variations even if few metabolites are (slightly) significant. The fingerprint can be, therefore, a useful tool, like in the present case, to discriminate with high accuracy between healthy subjects and patients. This innovative approach of course needs to be validated on larger cohorts before being translated in the clinical routine. These results may allow for the development of novel approaches to the optimization of therapy and of robust, standardized protocols for biofluids of interest, critical to allow for safe comparisons among different patient groups and diseases. Moreover, the opportunity given by NMR to detect early metabolic perturbations even before the appearance of disease symptoms can provide new possibilities for early diagnosis, prevention therapies, and precision medicine approach to design an effective treatment protocol.

Acknowledgements This study has been developed within the "Unità di Metabolomica: Studi su Alimenti, Nutraceutici e Fluidi biologici" of the Sapienza University of Rome. This work has been partially supported by Fondazione Veronesi that granted L.T. through the Post-Doctoral Fellowship 2015 and by Ateneo 2015 (Sapienza University of Rome prot C26A15CJ98).

Compliance with ethical standards The study received the approval by the local ethics committee in accordance with local requirements, and at the time of the collection, informed consent was obtained from each participant enrolled in the study.

Conflict of interest The authors declare that they have no competing interests.

References

1. Wishart DS, Jewison T, Guo AC, Wilson M, Knox C, Liu Y, et al. HMDB 3.0—the Human Metabolome Database in 2013. Nucleic Acids Res. 2013;41:D801–7. doi:10.1093/nar/gks1065.
2. Slupsky CM, Rankin KN, Wagner J, Fu H, Chang D, Weljie AM, et al. Investigations of the effects of gender, diurnal variation, and age in human urinary metabolomic profiles. Anal Chem. 2007;79:6995–7004. doi:10.1021/ac0708588.
3. Liquid state ^{1}H high field NMR in food analysis. http://www.sciencedirect.com/science/article/pii/S0079656512000209. Accessed 7 July 2016.
4. Pelantová H, Bártová S, Anýž J, Holubová M, Železná B, Maletínská L, et al. Metabolomic profiling of urinary changes in mice with monosodium glutamate-induced obesity. Anal Bioanal Chem. 2015;408:567–78. doi:10.1007/s00216-015-9133-0.
5. Assfalg M, Bertini I, Colangiuli D, Luchinat C, Schäfer H, Schütz B, et al. Evidence of different metabolic phenotypes in humans. Proc Natl Acad Sci. 2008;105:1420–4. doi:10.1073/pnas.0705685105.
6. Bernini P, Bertini I, Luchinat C, Nepi S, Saccenti E, Schäfer H, et al. Individual human phenotypes in metabolic space and time. J Proteome Res. 2009;8:4264–71. doi:10.1021/pr900344m.
7. Ghini V, Saccenti E, Tenori L, Assfalg M, Luchinat C. Allostasis and resilience of the human individual metabolic phenotype. J Proteome Res. 2015. doi:10.1021/acs.jproteome.5b00275.
8. Jones DP, Park Y, Ziegler TR. Nutritional metabolomics: progress in addressing complexity in diet and health. Annu Rev Nutr. 2012;32:183–202. doi:10.1146/annurev-nutr-072610-145159.
9. Bertini I, Calabrò A, De Carli V, Luchinat C, Nepi S, Porfirio B, et al. The metabonomic signature of celiac disease. J Proteome Res. 2008;8:170–7. doi:10.1021/pr800548z.
10. Priori R, Scrivo R, Brandt J, Valerio M, Casadei L, Valesini G, et al. Metabolomics in rheumatic diseases: the potential of an emerging methodology for improved patient diagnosis, prognosis, and treatment efficacy. Autoimmun Rev. 2013;12:1022–30. doi:10.1016/j.autrev.2013.04.002.
11. Tenori L, Oakman C, Morris PG, Gralka E, Turner N, Cappadona S, et al. Serum metabolomic profiles evaluated after surgery may identify patients with oestrogen receptor negative early breast cancer at increased risk of disease recurrence. Results from a retrospective study. Mol Oncol. 2015;9:128–39. doi:10.1016/j.molonc.2014.07.012.
12. Bernini P, Bertini I, Luchinat C, Tenori L, Tognaccini A. The cardiovascular risk of healthy individuals studied by NMR metabonomics of plasma samples. J Proteome Res. 2011;10:4983–92. doi:10.1021/pr200452j.
13. Wang L, Wu L-F, Lu X, Mo X-B, Tang Z-X, Lei S-F, et al. Integrated analyses of gene expression profiles digs out common markers for rheumatic diseases. PLoS ONE. 2015;10:e0137522. doi:10.1371/journal.pone.0137522.
14. Bernini P, Bertini I, Luchinat C, Nincheri P, Staderini S, Turano P. Standard operating procedures for pre-analytical handling of blood and urine for metabolomic studies and biobanks. J Biomol NMR. 2011;49:231–43. doi:10.1007/s10858-011-9489-1.
15. Bouatra S, Aziat F, Mandal R, Guo AC, Wilson MR, Knox C, et al. The human urine metabolome. PLoS ONE. 2013;8:e73076. doi:10.1371/journal.pone.0073076.
16. Dieterle F, Ross A, Schlotterbeck G, Senn H. Probabilistic quotient normalization as robust method to account for dilution of complex biological mixtures. Application in 1H NMR metabonomics. Anal Chem. 2006;78:4281–90. doi:10.1021/ac051632c.
17. Ihaka R, Gentleman R. R: a language for data analysis and graphics. J Comput Stat Graph. 1996;5:299–314.
18. Kruskal WH, Wallis WA. Use of ranks in one-criterion variance analysis. J Am Stat Assoc. 1952;47:583. doi:10.2307/2280779.
19. Benjamini Y, Hochberg Y. Controlling the false discovery rate: a practical and powerful approach to multiple testing. J R Stat Soc Ser B Methodol. 1995;57:289–300.
20. Hassan-Smith G, Wallace GR, Douglas MR, Sinclair AJ. The role of metabolomics in neurological disease. J Neuroimmunol. 2012;248:48–52. doi:10.1016/j.jneuroim.2012.01.009.
21. Young SP, Kapoor SR, Viant MR, Byrne JJ, Filer A, Buckley CD, et al. The impact of inflammation on metabolomic profiles in patients with arthritis. Arthritis Rheum. 2013;65:2015–23. doi:10.1002/art.38021.
22. Zabek A, Swierkot J, Malak A, Zawadzka I, Deja S, Boguniа-Kubik K, et al. Application of 1H NMR-based serum metabolomic studies for monitoring female patients with rheumatoid arthritis. J Pharm Biomed Anal. 2016;117:544–50. doi:10.1016/j.jpba.2015.10.007.
23. Nevedomskaya E, Pacchiarotta T, Artemov A, Meissner A, van Nieuwkoop C, van Dissel JT, et al. 1H NMR-based metabolic profiling of urinary tract infection: combining multiple statistical models and clinical data. Metabolomics. 2012;8:1227–35. doi:10.1007/s11306-012-0411-y.
24. Puntis D, Malik S, Saravanan V, Rynne M, Heycock C, Hamilton J, et al. Urinary tract infections in patients with rheumatoid arthritis. Clin Rheumatol. 2012;32:355–60. doi:10.1007/s10067-012-2129-7.
25. Munro R, Capell H. Prevalence of low body mass in rheumatoid arthritis: association with the acute phase response. Ann Rheum Dis. 1997;56:326–9.
26. Willer B, Stucki G, Hoppeler H, Brühlmann P, Krähenbühl S. Effects of creatine supplementation on muscle weakness in patients with rheumatoid arthritis. Rheumatol Oxf Engl. 2000;39:293–8.
27. Krähenbühl S, Willer B, Brühlmann P, Hoppeler H, Stucki G. Carnitine homeostasis in patients with rheumatoid arthritis. Clin Chim Acta. 1999;279:35–45. doi:10.1016/S0009-8981(98)00161-2.
28. van Wietmarschen HA, Dai W, van der Kooij AJ, Reijmers TH, Schroën Y, Wang M, et al. Characterization of rheumatoid arthritis subtypes using symptom profiles, clinical chemistry and metabolomics measurements. PLoS ONE. 2012;7:e44331. doi:10.1371/journal.pone.0044331.
29. Kapoor SR, Filer A, Fitzpatrick MA, Fisher BA, Taylor PC, Buckley CD, et al. Metabolic profiling predicts response to anti-tumor necrosis factor α therapy in patients with rheumatoid arthritis. Arthritis Rheum. 2013;65:1448–56. doi:10.1002/art.37921.
30. Mount D, Sayegh MH, Singh AK. Core concepts in the disorders of fluid, electrolytes and acid–base balance. New York: Springer Science & Business Media; 2012.
31. Dickens AM, Larkin JR, Griffin JL, Cavey A, Matthews L, Turner MR, et al. A type 2 biomarker separates relapsing-remitting from secondary progressive multiple sclerosis. Neurology. 2014;83:1492–9.
32. Tavazzi B, Batocchi AP, Amorini AM, Nociti V, D'Urso S, Longo S, et al. Serum metabolic profile in multiple sclerosis patients. Mult Scler Int. 2011;2011:e167156. doi:10.1155/2011/167156.
33. Reinke SN, Broadhurst DI, Sykes BD, Baker GB, Catz I, Warren KG, et al. Metabolomic profiling in multiple sclerosis: insights into biomarkers and pathogenesis. Mult Scler J. 2014;20:1396–400. doi:10.1177/1352458513516528.
34. Nicholson JK, Holmes E, Wilson ID. Gut microorganisms, mammalian metabolism and personalized health care. Nat Rev Microbiol. 2005;3:431–8.

Supplementary materials:

Fig. S1 600 MHz, ^{1}H spectrum at 300 K of: a, an urine control sample; b, urine sample with anomalous metabolite signals at 8.63 – 8.73 ppm, and 7.77 – 7.80 ppm, labelled by asterisks; c, urine sample containing an "anomalous" concentration of glucose

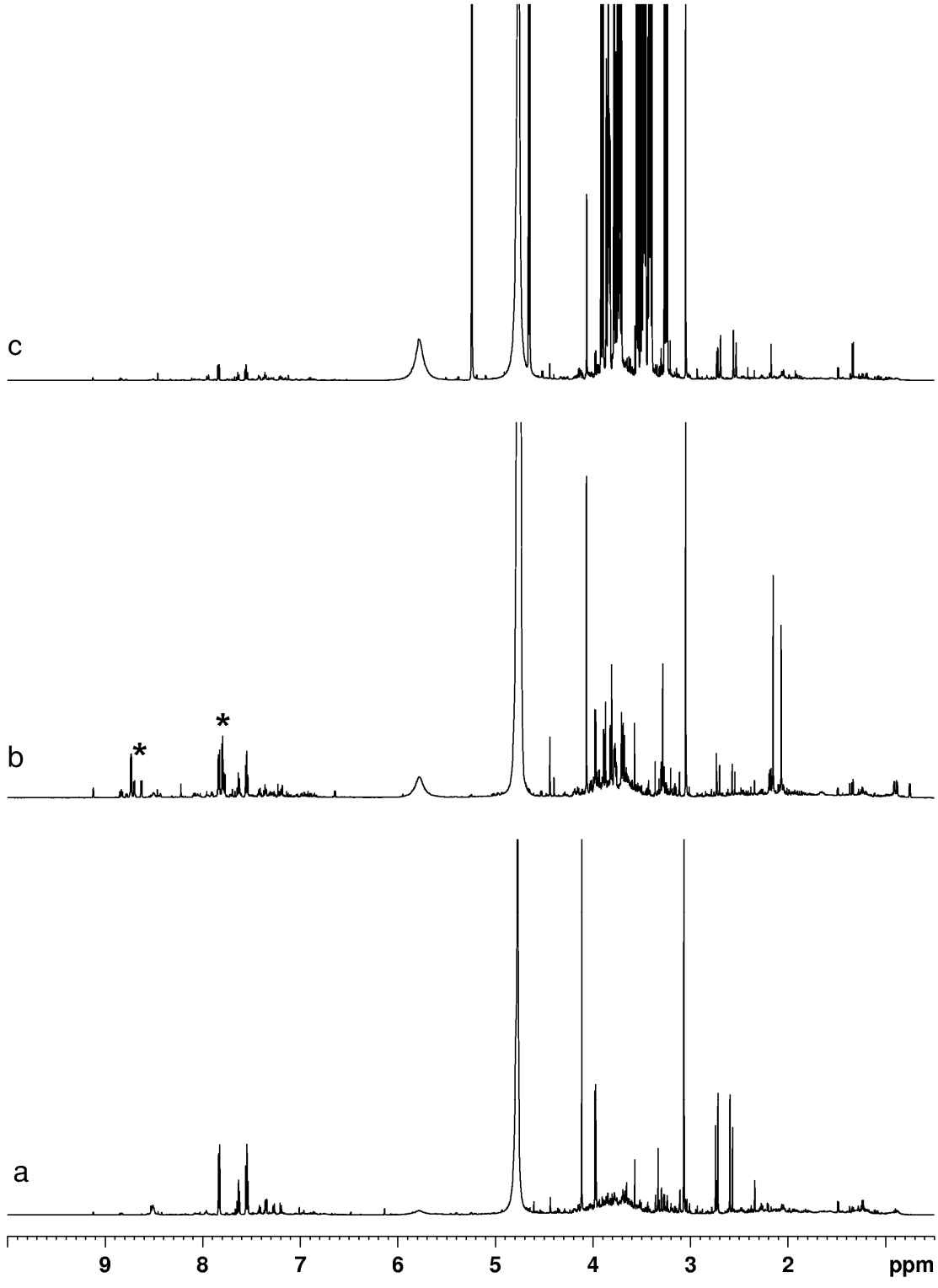

Fig. S2 ^{1}H and ^{13}C NMR spectral assignments of isonicotinic acid derivatives in a urine sample a) ^{1}H-^{1}H COSY, b) ^{1}H-^{13}C HSQC, c) ^{1}H-^{13}C HMBC spectra with the assignments

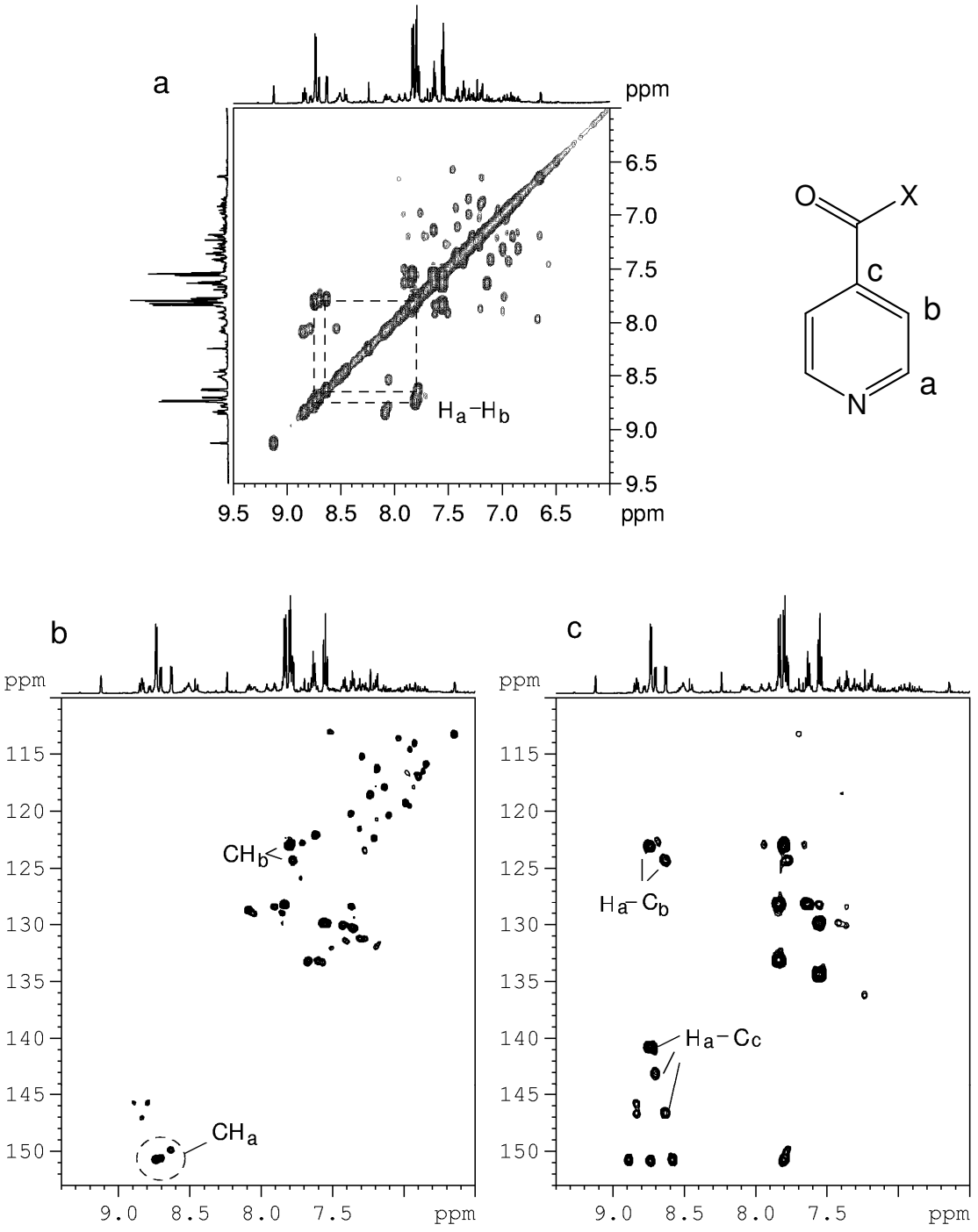

Fig. S3 Metabolites with –Log2(FC) negative values had a higher concentrations in CIRDs patients with respect to healthy subjects. Metabolites with –Log2(FC) positive values had higher concentration in healthy subjects. Green bars represented metabolites whose concentration is significantly different (p-value<0.05) in the comparison, red bars represented metabolite values that were not statistically relevant

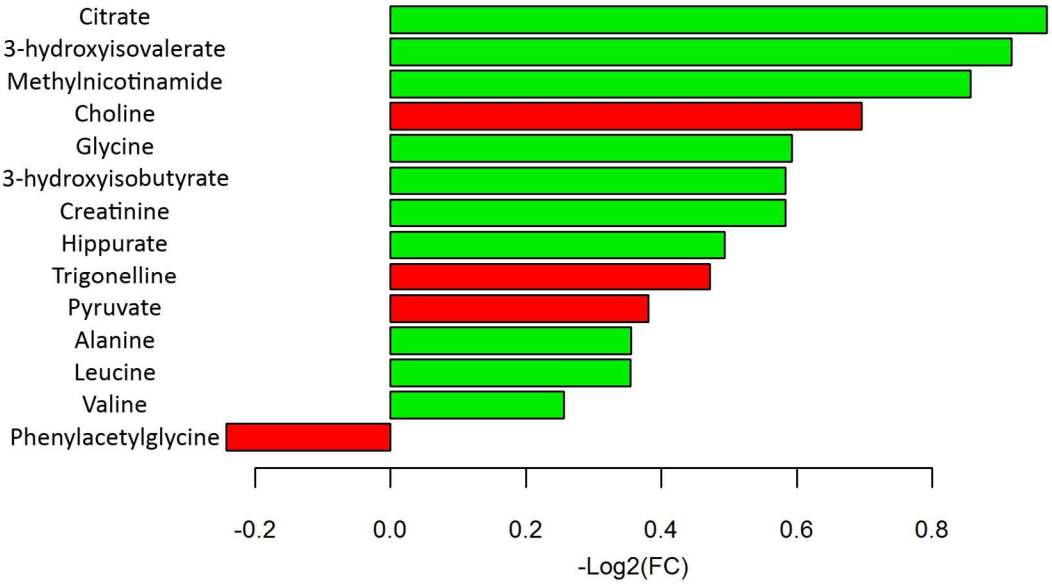

Fig. S4 Metabolites with –Log2(FC) negative values had a higher concentrations in CIRDs patients with respect to MS patients. Metabolites with –Log2(FC) positive values had higher concentration in MS patients. Green bars represented metabolites whose concentration is significantly different (p-value<0.05) in the comparison, red bars represented metabolite values that were not statistically relevant

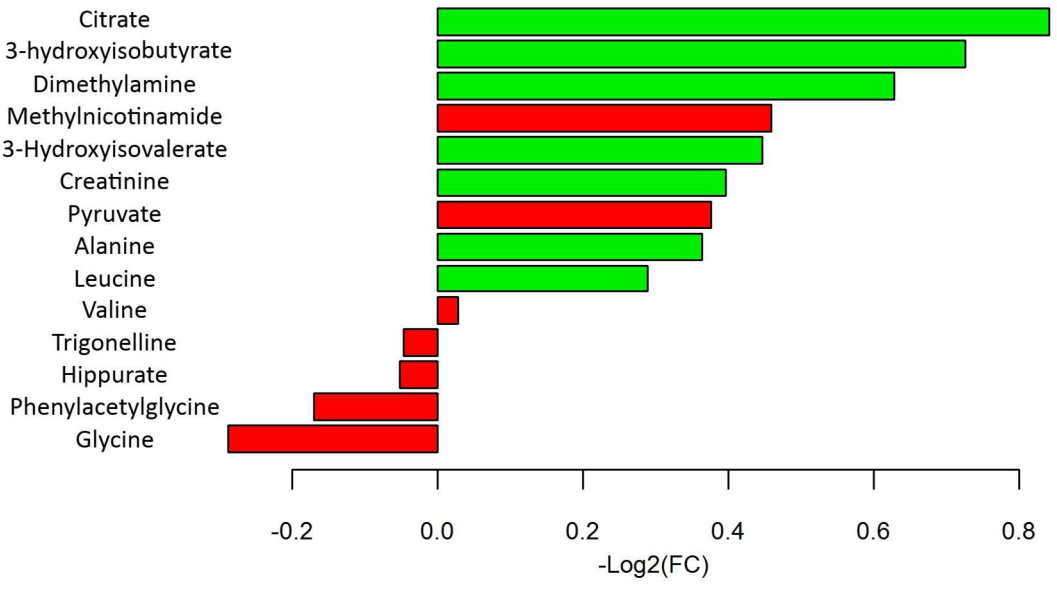

Table S1 Metabolites concentrations in CIRDs, MS and healthy subjects urine. In the table are reported the concentrations ± the standard deviation and the p-values of the two comparisons obtained using the univariate non-parametric Kruskal test and corrected with the Benjamini & Hochberg correction

Metabolite	MSI level of identification	Database	Compound ID	CIRDS patients	Healthy controls	MS patients	P-value CIRDs-Healthy	P-value CIRDs-MS
Leucine	1	HMDB	HMDB00687	1772.869±647.247	2489.196±830.276	2426.316±1083.581	0.00561	0.014165857
Valine	1	HMDB	HMDB00883	1435.753±477.87	2039.967±720.712	1863.898±970.841	0.00743	>0.05
3-hydroxyisobutyrate	1	HMDB	HMDB00023	4364.931±2395.114	6894.304±4133.196	7055.09±2780.217	0.00561	0.001281092
3-hydroxyisovalerate	1	HMDB	HMDB00754	9345.936±6751.704	14029.772±6634.506	12768.988±6914.728	0.00363	0.017569329
Lactate+Threonine	1 1	HMDB HMDB	HMDB00190 HMDB00167	70824.576±21299.354	100587.226±41807.128	108960.244±58092.789	0.00288	0.000214879
Alanine	1	HMDB	HMDB00161	11439.198±4254.088	17536.63±10406.739	14521.975±5866.745	0.03802	0.047270204
Pyruvate	1	HMDB	HMDB00243	32645.587±23293.979	37429.859±25314.147	42709.918±35862.018	>0.05	>0.05
Citrate	1	HMDB	HMDB00094	203681.163±132610.983	326917.957±125691.858	333706.621±164790.688	0.00363	0.003908777
Dimethylamine	1	HMDB	HMDB00087	50662.026±33562.293	132900.262±68436.558	76643.072±68501.723	0.01066	0.001183167
Glycine	1	HMDB	HMDB00123	90004.678±81017.342	141997.331±186599.617	99531.512±43796.302	0.03802	0.038582387
Creatinine	1	HMDB	HMDB00562	687138.069±207065.716	1030807.66±283657.874	896230.85±170012.242	0.00003	0.001183167
Trigonelline	1	HMDB	HMDB00875	36834.268±20907.842	51548.27±29968.347	37177.211±22265.853	>0.05	>0.05
Phenylacetylglycine	1	HMDB	HMDB00821	115309.539±60309.865	67263.51±35546.488	109533.985±58585.367	>0.05	>0.05
Hippurate	1	HMDB	HMDB00714	194139.822±99576.228	271654.526±153714.621	223967.978±230450.519	0.04639	>0.05
1-Methylnicotinamide	1	HMDB	HMDB00699	1014.968±720.1	1552.247±811.814	1463.085±1159.77	0.01340	>0.05
Choline	1	HMDB	HMDB00097	23791.244±19715.502	33442.096±25979.563	34108.335±29081.941	>0.05	>0.05
Dimethylglycine	1	HMDB	HMDB00092	10994.946±10574.255	13319.12±1941.038	12816.905±7978.645	>0.05	>0.05

Table S2 Metabolites assigned in the ^{1}H NMR spectra of urines

Metabolite	Group	^{1}H, ppm	Multiplicity, *J* Hz	^{13}C, ppm
Alanine	CH_3	1.49	d: 7.2	17.3
	CH	3.79		51.8
Choline	$N(CH_3)_3$	3.23	s	55.1
	β–CH_2	3.52		68.5
	α–CH_2	4.06		56.8
Citric A	α,γ-CH	2.55	d: 16.1	45.9
	α',γ'-CH	2.70	d: 16.1	45.9
	β–C			76.5
	COOH			179.7
	COOH			182.5
Creatinine	N-CH_3	3.05	s	31.3
	N-CH_2	4.07	s	57.4
	N=C			169.8
	COO			189.4

Dimethylamine	$N\text{-}CH_3$	2.74	s	35.8
Glycine	CH_2	3.57	s	42.7
	COOH			173.5
Hippuric A	Phe, *o*-CH	7.83	d	128.17
	Phe, *m*-CH	7.55	t	129.9
	Phe, *p*-CH	7.63	t	133.2
	CH_2-NH	3.97	d: 5.8	45.0
3-Hydroxyisobutyric A	CH_3	1.07	d:7.1	
	CH	2.49		
	CH_2		3.55; 3.70	
3-Hydroxyisovaleric A	CH_3	1.27	s	29.1
	C(OH)			70.9
	CH_2	2.37	s	50.5
Isoleucine	δCH_3	0.94		
	γCH_3	1.01		
	γCH_2		1.23; 1.45	
	βCH	1.98		
	αCH	3.63		
Lactic A	CH_3	1.34	d: 6.8	21.2
	CH	4.12	q	69.7
Leucine	CH_3	0.97		
	γ-CH	1.68		
	β-CH_2	1.73		
	α-CH	3.72		
1-Methylnicotinamide	2-CH	9.27	s	
	4-CH	8.96	d: 6.1	
	5-CH	8.18		
	6-CH	8.89	d: 8.2	
	$N\text{-}CH_3$	4.48	s	
Phenylacetylglycine	Phe, *m*-CH	7.42		130.0
	Phe, *o*-CH	7.36		130.2
	Phe, *p*-CH	7.36		128.3
	Phe, C-1			136.1
	CH_2-Phe	3.66		43.4
	CH_2-NH	3.79		44.5
Pyruvic A	CH_3	2.37		
Threonine	CH_3	1.34	d: 6.8	20.6
	β–CH	4.28		67.1
	α–CH	3.60		61.6
Trigonelline	2-CH	9.12	s	146.9

Valine	4-CH	8.83	d: 7.3	145.7
	5-CH	8.08	dd: 8.6; 7.3	128.7
	6-CH	8.84	d: 8.6	147
	N-CH_3	4.44	s	49.3
	γ-CH_3	1.05	d	
	γ'-CH_3	0.97	d	
	β-CH	2.27		
	α-CH	3.62		

Table S3. Comparison of the trend of common metabolites among urine, serum and CSF for CIRDs patients, MS patients and healthy controls

	CIRDs vs Healthy			**MS vs Healthy**	
	Urine	Serum (Priori et al. 2013)	Serum (Zabek et a. 2016)	CSF (Reinke et al. 2014)	Serum (Dickens al. 2014; Tavazzi et al. 20
Alanine	↓	↑	↓		
Lactate	↓	↑	↓	↓	
Leucine	↓	↑	↓		
Citrate	↓	↑	↑	↓	
Creatinine	↓		↓	↑	↑
Glycine	↓	↑			

4.2.3 *The metabolic signature of Primary Biliary Cirrhosis and its comparison with Coeliac Disease*

Alessia Vignoli[*], Beatrice Orlandini[§], Leonardo Tenori[†], Maria Rosa Biagini[§], Daniela Renzi[§,¥], Stefano Milani[§], Claudio Luchinat[*,ǂ], Antonio Calabrò[§,¥]

[*] Magnetic Resonance Center (CERM), University of Florence, Sesto Fiorentino, Italy
[§] Department of Experimental and Clinical Biomedical Sciences, University of Florence, Italy
[†] Department of Experimental and Clinical Medicine, University of Florence, Firenze, Italy
[¥] Tuscany Referral Center for Adult Coeliac Disease, Florence, Italy
[ǂ] Department of Chemistry, University of Florence, Sesto Fiorentino, Italy

To be submitted

Candidate's contributions: acquisition of NMR data, statistical analysis and interpretation of data, writing and review of the manuscript.

The metabolic signature of Primary Biliary Cirrhosis and its comparison with Coeliac Disease

Abstract

Background & Aims

Primary biliary cirrhosis (PBC) is a chronic autoimmune liver disease characterized by ongoing inflammatory destruction of the interlobular bile ducts, eventually leading to chronic cholestasis and biliary cirrhosis. This study primarily aimed at defining the metabolomic signature of PBC comparing PBC patients and healthy controls (HC). The second study purpose was to evaluate the possible association between the metabolomic profile of patients with PBC and celiac disease (CD).

Methods

23 PBC patients, 21 CD patients and 19 sex-matched healthy controls (HC) participated in the study and both serum and urine samples were collected. Monodimensional ^{1}H-NMR spectra for all samples were acquired and multivariate statistical analyses were used to evaluate the differences among the three clusters' spectra and provide information about the involved metabolites.

Results

The classification accuracies to discriminate PBC and HC groups were 76.9-83.1% for serum and 78.1% for urine. PBC patient sera were characterized by altered levels (*P*-value <0.05) of citrate, lactate, lysine, phenylananine, proline, pyruvate, serine and tyrosine. Moreover, PBC patients urines showed lower levels (*P*-value <0.05) of hippuric acid, p-cresolsulfate, pyruvate and trigonelline with respect to HC. In this study, we compare for the first time, the NMR metabolomic profiles of patients with PBC and CD, revealing significant differences.

Conclusions

Our results show that PBC displays a unique metabolomic fingerprint, and it is possible to speculate about an impaired energy metabolism in PBC, probably associated with altered gut microbiota. These data could provide clues for the comprehension of the PBC pathogenetic mechanism and the detection of novel therapeutical targets.

Keywords

Primary Biliary Cirrhosis, Coeliac Disease, Metabolomics, NMR, Metabolites

Introduction

Primary biliary cirrhosis (PBC) is a chronic cholestatic liver disease characterized by a slowly progressive immune-mediated inflammation of the small intrahepatic bile ducts that leads to their destruction. Bile ducts loss decreases bile secretion and causes retention of several toxins, inducing hepatic damages that could proceed from fibrosis to cirrhosis and subsequent liver failure[1–3]. PBC mainly affects middle-aged women (female:male ratio is established as at least 9:1)[3] and at the moment of diagnosis patients are frequently asymptomatic or suffer from fatigue and pruritus[2].

Associated autoimmune diseases are frequently reported in the literature (up to 84% of the cases), especially thyroiditis, rheumatoid arthritis, Sjögren's syndrome and coeliac disease (CD)[1,4]. In a 1999 study[5] the frequent combination between PBC and CD, an immune-mediated enteropathy triggered by the ingestion of gluten in genetically susceptible subjects, was reported. However, more insights on metabolic and pathophysiological mechanisms that are common or different in these two diseases are still needed.

In this framework, metabolomics could be a powerful tool: metabolites are the most sensitive reporters of any disease status or phenotype, indeed, even slight alterations on metabolic fluxes have significant effects on metabolites concentrations[6]. As a consequence, metabolomics is already be applied extensively to develop personalized diagnostic, prognostic and therapeutic approaches[7,8], to monitor disease progression, treatment efficacy or predisposition to drug-related side effects[9–14].

In this paper, we report the results obtained by applying the NMR-based metabolomic approach to determinate the serum and urine metabolic profile of PBC patients and, for the first time, to compare the serum and urine global metabolomic profiles of patients with PBC and CD.

Methods

Study Population and Sample Collections

Twenty-three adults with a clinical and/or histological diagnosis of PBC (20 females, 3 males, mean age 56 years) participated in the study. Two of them suffered from potential coeliac disease (PCD), one from CD and one patient was diagnosed with PBC-autoimmune hepatitis overlap syndrome. Two of the followings three criteria were required for PBC diagnosis: anti-mitochondrial antibodies (AMAs) ≥1:40, serum alkaline phosphatase (ALP) 1.5 times upper limit of normal, liver histology with nonsuppurative destructive cholangitis and destruction of interlobular bile ducts. CD diagnosis was based on positive serology, anti-endomysium (EMA) and anti-tissue transglutaminase antibodies (tTGA), and typical mucosal atrophy at the duodenal biopsies. Small intestinal mucosal damage was graduated according to the classification of Marsh modified by Oberhuber[15]. PCD diagnosis was considered when patients presented a positive serology, genetic susceptibility (i.e. DQ2 and/or DQ8 haplotype) with normal (Marsh 1) or almost normal (Marsh 1 or 2) small intestinal

mucosal architecture. CD and PCD were analyzed at the time of diagnosis, before starting a gluten-free diet. Twenty-one adults with CD (17 females, 4 males, mean age 56 years) were recruited for the study. Nineteen healthy controls (HC) (17 females, 2 males, mean age 46) were selected, after confirmation of negative EMA, tTGA and silent medical history for gastrointestinal and autoimmune diseases.
Serum and urine samples were collected from PBC, CD, PCD patients and HC. Each subject had fasted overnight, urine and serum were collected pre-prandial in the morning, and immediately frozen and stored at - 80 °C until used. All information about sample collections are detailed in depth in the Supplemental Materials.
Written informed consent was obtained from all enrolled patients and healthy controls and the study protocol was approved by the local ethical committee.

Patients Characteristics

Characteristics of the 63 PBC, CD patients and HC patients were analyzed. A high female prevalence of PBC patients was noticed (86,9%), according to the previous data of the literature. PBC, CD patients and HC were matched for sex and age. The median age of patients was 56 years for PBC (interquartile range (IQR) 48-66 years) and CD (IQR 48,5-59,6 years) patients, while HC were 46 year old (IQR 39-53 years). Biopsy was performed in 9 patients, two were diagnosed as stage I, one as stage II, five as stage IV. Based on clinical and transient elastography assessment (Fibroscan) three other patients were attributed to stage I, two patients to stage II-III and two to stage IV. PBC patient characteristics are summarized in Table 1.

NMR analyses

Serum and urine samples were prepared following the standard protocols detailed by Bernini et al.16. According to standard practice[17,18], all serum spectra were acquired at 310 K using a Bruker 600 MHz spectrometer, and for each serum sample three monodimensional 1H-NMR spectra, namely NOESY, CPMG and Diffusion-edited spectra, were acquired allowing the selective detection of different molecular weight metabolites. Instead, urine monodimensional 1H NMR spectra were acquired with presaturation water peak suppression using a standard NOESY 1Dpresat samples at 300 K. A detailed description about sample preparation and experiments is presented in the Supplemental Materials.
Each 1D spectrum in the range between 0.2 and 10.00 ppm was segmented into 0.02 ppm chemical shift bins and the corresponding spectral areas were integrated using AMIX software (version 3.8.4, Bruker BioSpin). Binning is a means to reduce the number of total variables and to compensate for small shifts in the signals, making the analysis more robust and reproducible[19,20]. Regions between 6.5 and 4.2 ppm containing residual water signal were removed and the dimension of the system was reduced to 375 bins. The total spectral area was calculated on the remaining bins and total area normalization was carried out on the serum data prior to pattern

recognition; instead, for urine spectra probabilistic quotient normalization[21] was chosen, because it performs well even when large variations of dilution occur.

Statistical analyses

All data analyses were performed using R, an open source software for statistical analysis[22]. Multivariate data analysis was conducted on processed data and univariate statistical analysis was carried out on whole spectra by combining established methods.

Principal component analysis (PCA) was use as dimension reduction technique and as a preparation of the data table before further statistical analyses. Data reduction was carried out by means of projection into a PCA subspace, only the first 25 components, explaining 99.9% of the variance in the data, were retained in the model and the canonical analysis (CA) was applied to obtain the supervised separation of the analyzed groups.

For the purpose of classification we used the K-nearest neighbors (k-NN) method (k=5) applied on the PCA-CA scores[23]. All the accuracies reported and the confusion matrix for the different classifications were assessed by means of 100 cycles of a Monte Carlo cross-validation scheme (MCCV, R script in-house developed). Briefly, 90% of the data were randomly chosen at each iteration as a training set to build the model. Then the remaining 10% was tested and sensitivity, specificity and accuracy for the classification were assessed. The procedure was repeated 100 times to derive an average discrimination accuracy for each group of subjects.

The spectral regions related to the metabolites were assigned in the 1H-NMR profiles by using matching routines of AMIX 3.8.4 (Bruker BioSpin) in combination with the BBIOREFCODE (Bruker BioSpin), freely available database[24], and published literature when available. These spectral regions were integrated to obtain the concentrations of metabolites in arbitrary units and the concentrations were analyzed to determine the discriminating metabolites among PBC patients, CD patients and healthy subjects. Wilcoxon–Mann–Whitney test[25] was chosen to infer differences among the groups on the biological assumption that metabolite concentrations are not normally distributed, a *P*-value <0.05 was deemed significant.

Results

The clusterizations of PBC, CD patients and HC for the four sets of experiments (serum CPMG, NOESY, and Diffusion-edited, and urine NOESY) are shown in Figure 1 and Figure 2.

The PCA-CA models applied demonstrated to be effective for the discrimination between the 19 PBC patients and the 20 HC using each set of experiment, even if the best clusterization was provided by serum CPMG spectra. The classification accuracies obtained for each experiment are reported in Table 2: the existence of a metabolic

fingerprint of primary biliary cirrhosis in both serum and urine is clearly demonstrated.

In the comparison between the serum CPMG spectra of PBC patients and HC, higher levels of phenylalanine, tyrosine, serine, proline, lysine, lactate, citrate and pyruvate could be recorded in patients with PBC (P-value < 0.05) (Figure 3A). Lower levels of hippuric acid, trigonelline, p-cresolsulfate and pyruvate, instead, were demonstrated in PBC patients versus HC using urine samples (Figure 3B).

To assess the capability of metabolomic profiles to discriminate between PBC and CD patients, the NMR data of 20 PBC samples and of 21 CD samples were analyzed using PCA-CA analysis, as previously described. The classification accuracies estimated for each of the four experiments are reported in Table 3. In this comparison, the serum Diffusion-edited spectra showed the best clusterization results. Data showed that PBC and CD have two different and distinguishable metabolic fingerprints on both serum and urine spectra. In particular, citrate, pyruvate, serine and phenylalanine levels were found to be higher in CD patients rather than PBC patients using CPMG spectra.

In order to better understand the metabolic differences among PBC, CD and HC, the Diffusion-edited spectra was then analyzed, which is known to provide relevant information on lipoprotein lipids and subclasses (Supplemental Figure 1). PBC patients featured lower levels of cholesterol (C18) as compared with HC (*P*-value 0.0182). More relevant differences were remarkable comparing PBC and CD patients: cholesterol (C18) and $-N(CH_3)_3$ groups in molecules containing the choline moiety were found significantly higher in PBC patients (*P*-values are respectively 0.0027 and 0.0072).

Interestingly, three patients suffering from both diseases (PBC and CD) were used as independent test set: on serum CPMG spectra using the classification model (PCA-CA-kNN) applied to the three groups (PBC, CD, HC) these three patients with both diseases were placed in the metabolic region between PBC and CD (total discrimination accuracy of 71.9%) (Supplemental Figure 2). The same result was obtained with the other serum NMR spectra. With urine samples, instead, one patient was misclassified as healthy, confirming the evidence that the metabolic fingerprint of these two diseases is weaker in urine than in serum.

Discussion

The liver plays a critical role in human metabolism, regulating homeostasis and the synthesis, metabolism and catabolism of many products. For this reason, metabolomics has been used for detecting alterations of metabolic profiles in several liver diseases[26–28]. In the present study, we applied NMR-based metabolomics to study serum and urine samples obtained from PBC patients, healthy controls and CD patients. To the best of our knowledge this is the first study analyzing systematically the metabolomic profile of PBC and CD patients.

Our study shows that the 1H NMR metabolic profiles of PBC patients and healthy controls are definitely different, obtaining 83.1%, 79.6%, and 76.9% discrimination

accuracies with CPMG, NOESY, and Diffusion spectra respectively using serum, and 78.1% accuracy using urine.

Compared to healthy controls, the CPMG serum metabolic profiles of PBC patients show increased levels of phenylalanine, tyrosine, serine, proline, lysine, lactate, citrate and pyruvate. The lowest discrimination accuracy is obtained from urine NOESY spectra, as expected from the higher day-to-day variability of the urine metabolic profiles[29,30]. Despite this, a PBC urine fingerprint can be defined, characterized by lower levels of hippuric acid, trigonelline, p-cresolsulfate and pyruvate. Even if there is not a unique possible interpretation, several hypotheses can be proposed to explain these results.

1) The liver plays a central role in the aromatic amino-acid catabolism and in our study PBC patients present increased level of two of these amino-acids: phenylalanine and tyrosine. These aminoacids are metabolically closely related, indeed, phenylalanine is converted to tyrosine by the hepatic enzyme phenylalanine hydroxylase[31]. The observed imbalance in serum amino-acids levels, as highlighted by the decrease in the ratio between branched chain amino acids and aromatic amino acids (BCAA/AAA ratio in PBC and healthy controls respectively: 2.18 and 3.11) could be related to the hepatic function impairment. These results are consistent with previous studies[32,33], which revealed that during a hepatic failure BCAA blood levels decrease while the levels of AAA increase, and hypothesized that the cause of these abnormalities is a reduction in the insulin/glucagon ratio disturbing the balance between anabolism and catabolism.

2) The increased serum levels of lactate and pyruvate could be explained with an impairment of the mitochondrial respiratory chain. As described in a previous study, the autoantibodies AMAs typical of PBC, seem to have direct effects in muscle metabolism leading to an excessive use of the anaerobic respiration[34]. The inability to adapt and compensate acidosis possibly induces systemic lactic acidosis that potentially correlated with fatigue, a frequent symptom in PBC patients. The hypothesis of a peripheral mechanism in the development of fatigue in PBC patients is further supported by the high levels of tyrosine found in serum; indeed, tyrosine is a key precursor in the biosynthesis of neurotransmitters (like dopa, dopamine, epinephrine and norepinephrine) and its reduction is associated with fatigue[35]. Moreover, fatigue symptoms improve only marginally after liver transplantation, most likely indicating that the cognitive symptoms operate outside the liver[36].

3) It is interesting to underline that PBC patients show a reduction in the urinary excretion levels of three metabolites directly produced by the intestinal microbiota: p-cresol, a uremic toxin that represents the end-product of the catabolism of tyrosine and phenylalanine[37,38], hippuric acid, obtained by the conjugation of benzoic acid with glycine[39], and trigonelline. This evidence could indicate an alteration of the gut microbiota metabolism. Previous studies reported changes in colonic/fecal microbiota of cirrhotic patients[40], and immune responses involving the microbiota have been

proposed as relevant in the pathogenesis of PBC[41]; therefore, our results could be considered as a sort of direct consequences of these processes.

Bertini et al.[9,10,42] have extensively described the metabolic signature of CD (overt and potential) applying the same NMR-metabolomic approach here described, and identifying important alterations of the metabolic profiles of patients with respect to controls, especially for what concerns energy and ketone body metabolism, and gut microbiota alterations. In this study, we established a significant differential clustering comparing PBC and CD metabolic profiles. Interestingly, the discrimination accuracy in this comparison using serum samples increases upon going from CMPG to NOESY, to Diffusion-edited spectra, a trend opposed of what emerged comparing PBC with HC. Actually, Diffusion-edited spectra model ensures the highest accuracy in discriminating PBC and CD, and from the spectra analysis emerged that PBC patients feature higher levels of cholesterol and high-density lipoprotein-cholesterol (HDL-C) with respect to CD patients. These differences are a clear result of an opposite alterations in the lipid metabolism: PBC, indeed, is characterized by a marked increment of the enterohepatic circulation of various compounds, especially of lipid moieties, and several studies have demonstrated that cholesterol metabolism is markedly impaired both for synthesis and biliary elimination in PBC patients[1,43]. Conversely, not only untreated coeliac disease patients are associated with lower concentrations of total cholesterol and high-density lipoprotein-cholesterol, but it seems that a reduction in serum HDL-C level is present even in the absence of gastrointestinal symptoms[44,45]. Therefore, HDL-C could be a key biomarker for the early diagnosis of CD and for the follow-up of the patients after gluten free diet treatment[44–46]. Nonetheless, the underlying mechanisms remain still poorly understood: intestinal malabsorption, reduction of the cholesterogenesis, reduction in cholesterol-transporting lipoproteins, decreased apolipoprotein (Apo)-AI secretion from the altered small bowel mucosa, increased biliary secretion and high fecal elimination of cholesterol have all been proposed as explanations of this phenomenon[45,46].

Nevertheless, it was possible to identify differences also analyzing low molecular weight metabolites: the serum concentrations of citrate, pyruvate, serine and phenylalanine resulted appreciably higher in PBC patients with respect to CD. In particular, the differences related to pyruvate and citrate could indicate a different impairment in the energetic metabolism in the two diseases.

In conclusion, in the present work we have demonstrated the presence of a clear metabolic fingerprint in serum and urine of PBC patients that is able to discriminate them from healthy controls. Our results show that the PBC NMR metabolomic profiles differ markedly from those of CD patients, indicating that these two pathologies, whose association is well established4, are characterized by different metabolic alterations. Undoubtedly, our results require validation in a larger independent cohort of patients to confirm their reproducibility. Moreover, all PBC patients in this study received

systemic therapy, making it impossible to know whether the therapy was directly responsible for changes in PBC metabolic fingerprint. An ideal series would have an arm with no intervention, although this is unlikely to be feasible because patients are often treated also before the final diagnosis.

References

1. Kaplan MM. Primary Biliary Cirrhosis. N Engl J Med. 1996;335(21):1570-1580. doi:10.1056/NEJM199611213352107.
2. Kaplan MM, Gershwin ME. Primary Biliary Cirrhosis. N Engl J Med. 2005;353(12):1261-1273. doi:10.1056/NEJMra043898.
3. Smyk DS, Rigopoulou EI, Pares A, et al. Sex Differences Associated with Primary Biliary Cirrhosis. J Immunol Res. 2012;2012:e610504. doi:10.1155/2012/610504.
4. Kingham J, Parker D. The association between primary biliary cirrhosis and coeliac disease: a study of relative prevalences. Gut. 1998;42(1):120-122.
5. Sørensen HT, Thulstrup AM, Blomqvist P, et al. Risk of primary biliary liver cirrhosis in patients with coeliac disease: Danish and Swedish cohort data. Gut. 1999;44(5):736-738. doi:10.1136/gut.44.5.736.
6. Brown M, Dunn WB, Ellis DI, et al. A metabolome pipeline: from concept to data to knowledge. Metabolomics. 2005;1(1):39-51. doi:10.1007/s11306-005-1106-4.
7. Koen N., Du Preez I. Metabolomics and Personalized Medicine. Adv Protein Chem Struct Biol. 2015. doi:10.1016/bs.apcsb.2015.09.003.
8. Vignoli A, Rodio DM, Bellizzi A, et al. NMR-based metabolomic approach to study urine samples of chronic inflammatory rheumatic disease patients. Anal Bioanal Chem. 2017;409(5):1405-1413. doi:10.1007/s00216-016-0074-z.
9. Bertini I, Calabrò A, De Carli V, et al. The Metabonomic Signature of Celiac Disease. J Proteome Res. 2008;8(1):170-177. doi:10.1021/pr800548z.
10. Bernini P, Bertini I, Calabrò A, et al. Are Patients with Potential Celiac Disease Really Potential? The Answer of Metabonomics. J Proteome Res. 2010;10(2):714-721. doi:10.1021/pr100896s.
11. Lindon JC, Holmes E, Nicholson JK. Metabonomics and its role in drug development and disease diagnosis. Expert Rev Mol Diagn. 2004;4(2):189-199. doi:10.1586/14737159.4.2.189.
12. Andrew Clayton T, Lindon JC, Cloarec O, et al. Pharmaco-metabonomic phenotyping and personalized drug treatment. Nature. 2006;440(7087):1073-1077. doi:10.1038/nature04648.
13. Tenori L, Oakman C, Morris PG, et al. Serum metabolomic profiles evaluated after surgery may identify patients with oestrogen receptor negative early breast cancer at increased risk of disease recurrence. Results from a retrospective study. Mol Oncol. 2015;9(1):128-139. doi:10.1016/j.molonc.2014.07.012.
14. Hart CD, Vignoli A, Tenori L, et al. Serum Metabolomic Profiles Identify ER-Positive Early Breast Cancer Patients at Increased Risk of Disease Recurrence in a

Multicenter Population. Clin Cancer Res. September 2016. doi:10.1158/1078-0432.CCR-16-1153.

15. Oberhuber G. Histopathology of celiac disease. Biomed Pharmacother Biomedecine Pharmacother. 2000;54(7):368-372. doi:10.1016/S0753-3322(01)80003-2.
16. Bernini P, Bertini I, Luchinat C, et al. Standard operating procedures for pre-analytical handling of blood and urine for metabolomic studies and biobanks. J Biomol NMR. 2011;49(3-4):231-243. doi:10.1007/s10858-011-9489-1.
17. Beckonert O, Keun HC, Ebbels TMD, et al. Metabolic profiling, metabolomic and metabonomic procedures for NMR spectroscopy of urine, plasma, serum and tissue extracts. Nat Protoc. 2007;2(11):2692-2703.
18. Gebregiworgis T, Powers R. Application of NMR metabolomics to search for human disease biomarkers. Comb Chem High Throughput Screen. 2012;15(8):595-610.
19. Spraul M, Neidig P, Klauck U, et al. Automatic reduction of NMR spectroscopic data for statistical and pattern recognition classification of samples. J Pharm Biomed Anal. 1994;12(10):1215-1225.
20. Holmes E, Foxall PJ, Nicholson JK, et al. Automatic data reduction and pattern recognition methods for analysis of 1H nuclear magnetic resonance spectra of human urine from normal and pathological states. Anal Biochem. 1994;220(2):284-296.
21. Dieterle F, Ross A, Schlotterbeck G., et al. Probabilistic Quotient Normalization as Robust Method to Account for Dilution of Complex Biological Mixtures. Application in 1H NMR Metabonomics. Anal Chem. 2006;78(13):4281-4290. doi:10.1021/ac051632c.
22. Ihaka R, Gentleman R. R: A Language for Data Analysis and Graphics. J Comput Stat Graph. 1996;5:299-314.
23. Cover T, Hart P. Nearest neighbor pattern classification. Inf Theory IEEE Trans On. 1967;13(1):21-27.
24. Wishart DS, Jewison T, Guo AC, et al. HMDB 3.0--The Human Metabolome Database in 2013. Nucleic Acids Res. 2013;41(D1):D801-D807. doi:10.1093/nar/gks1065.
25. Mann HB, Whitney DR. On a test of whether one of two random variables is stochastically larger than the other. Ann Math Stat. 1947;18(1):50-60.
26. Kalhan SC, Guo L, Edmison J, et al. Plasma metabolomic profile in nonalcoholic fatty liver disease. Metabolism. 2011;60(3):404-413. doi:10.1016/j.metabol.2010.03.006.
27. Beyoğlu D, Idle JR. The metabolomic window into hepatobiliary disease. J Hepatol. 2013;59(4):842-858. doi:10.1016/j.jhep.2013.05.030.
28. Huang Q, Tan Y, Yin P, et al. Metabolic characterization of hepatocellular carcinoma using nontargeted tissue metabolomics. Cancer Res. 2013;73(16):4992-5002. doi:10.1158/0008-5472.CAN-13-0308.

29. Ghini V, Saccenti E, Tenori L, et al. Allostasis and Resilience of the Human Individual Metabolic Phenotype. J Proteome Res. 2015;14(7):2951-2962. doi:10.1021/acs.jproteome.5b00275.
30. Maher AD, Zirah SFM, Holmes E, et al. Experimental and analytical variation in human urine in 1H NMR spectroscopy-based metabolic phenotyping studies. Anal Chem. 2007;79(14):5204-5211.
31. Dejong CHC, Poll MCG van de, Soeters PB, et al. Aromatic Amino Acid Metabolism during Liver Failure. J Nutr. 2007;137(6):1579S-1585S.
32. Fischer JE, Yoshimura N, Aguirre A, et al. Plasma amino acids in patients with hepatic encephalopathy. Effects of amino acid infusions. Am J Surg. 1974;127(1):40-47.
33. Qi S-W, Tu Z-G, Peng W-J, et al. 1H NMR-based serum metabolic profiling in compensated and decompensated cirrhosis. World J Gastroenterol WJG. 2012;18(3):285-290. doi:10.3748/wjg.v18.i3.285.
34. Griffiths L, Jones DE. Pathogenesis of Primary Biliary Cirrhosis and Its Fatigue. Dig Dis. 2014;32(5):615-625. doi:10.1159/000360515.
35. ter Borg PC, Fekkes D, Vrolijk JM, et al. The relation between plasma tyrosine concentration and fatigue in primary biliary cirrhosis and primary sclerosing cholangitis. BMC Gastroenterol. 2005;5:11. doi:10.1186/1471-230X-5-11.
36. Pells G, Mells GF, Carbone M, et al. The impact of liver transplantation on the phenotype of primary biliary cirrhosis patients in the UK-PBC cohort. J Hepatol. 2013;59(1):67-73. doi:10.1016/j.jhep.2013.02.019.
37. Dou L, Bertrand E, Cerini C, et al. The uremic solutes p-cresol and indoxyl sulfate inhibit endothelial proliferation and wound repair. Kidney Int. 2004;65(2):442-451. doi:10.1111/j.1523-1755.2004.00399.x.
38. Vanholder R, Smet RD, Lesaffer G. p-Cresol: a toxin revealing many neglected but relevant aspects of uraemic toxicity. Nephrol Dial Transplant. 1999;14(12):2813-2815. doi:10.1093/ndt/14.12.2813.
39. Wikoff WR, Anfora AT, Liu J, et al. Metabolomics analysis reveals large effects of gut microflora on mammalian blood metabolites. Proc Natl Acad Sci. 2009;106(10):3698-3698.
40. Quigley EMM. Is the gut microbiota disturbed in chronic liver disease? Clin Liver Dis. 2015;5(4):94-95. doi:10.1002/cld.456.
41. Bogdanos D-P, Baum H, Okamoto M, et al. Primary biliary cirrhosis is characterized by IgG3 antibodies cross-reactive with the major mitochondrial autoepitope and its Lactobacillus mimic. Hepatol Baltim Md. 2005;42(2):458-465. doi:10.1002/hep.20788.
42. Calabrò A, Antonio, Gralka E, et al. A Metabolomic Perspective on Coeliac Disease. Autoimmune Dis. 2014;2014:e756138. doi:10.1155/2014/756138.

43. Puppo MD, Kienle MG, Crosignani A, et al. Cholesterol metabolism in primary biliary cirrhosis during simvastatin and UDCA administration. J Lipid Res. 2001;42(3):437-441.
44. Capristo E, Addolorato G, Mingrone G, et al. Low-serum high-density lipoprotein-cholesterol concentration as a sign of celiac disease. Am J Gastroenterol. 2000;95(11):3331-3332. doi:10.1111/j.1572-0241.2000.03329.x.
45. Lewis NR, Sanders DS, Logan RFA, et al. Cholesterol profile in people with newly diagnosed coeliac disease: a comparison with the general population and changes following treatment. Br J Nutr. 2009;102(4):509–513. doi:10.1017/S0007114509297248.
46. Capristo E, Malandrino N, Farnetti S, et al. Increased Serum High-density Lipoprotein-Cholesterol Concentration in Celiac Disease After Gluten-free Diet Treatment Correlates With Body Fat Stores: J Clin Gastroenterol. 2009;43(10):946-949. doi:10.1097/MCG.0b013e3181978e4d.

List of Figures and Tables

Figure 1. PCA-CA-kNN score plots, discrimination between PBC (red dots, n = 20) and healthy controls (blue dots, n = 19). A) CPMG serum samples; B) NOESY1D serum samples; C) Diffusion-edited serum samples; D) NOESY1D urine samples.

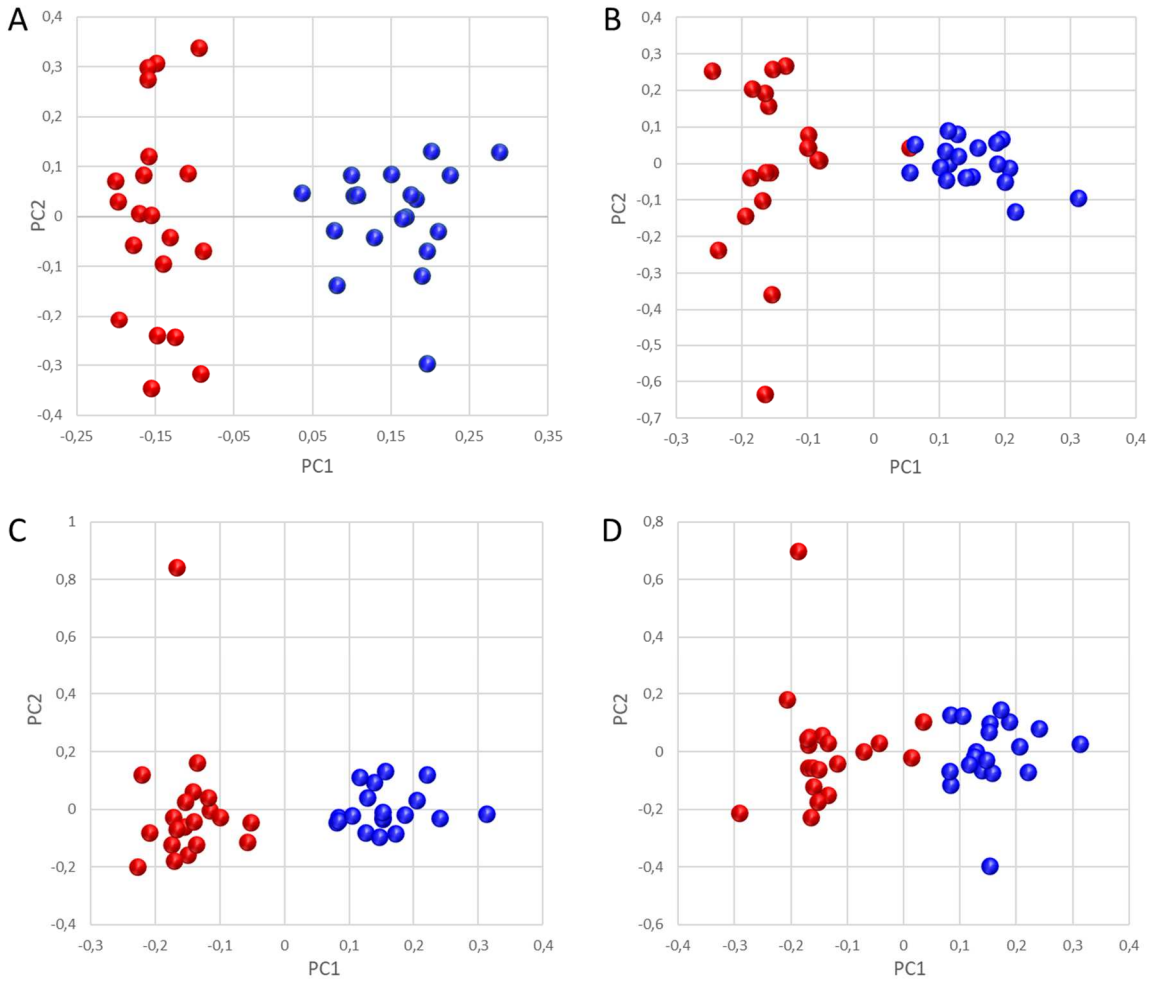

Figure 2. PCA-CA-kNN score plots, discrimination between PBC patients (red dots, n = 20) and CD patients (blue dots, n = 21). A) CPMG serum samples; B) NOESY1D serum samples; C) Diffusion-edited serum samples; D) NOESY1D urine samples.

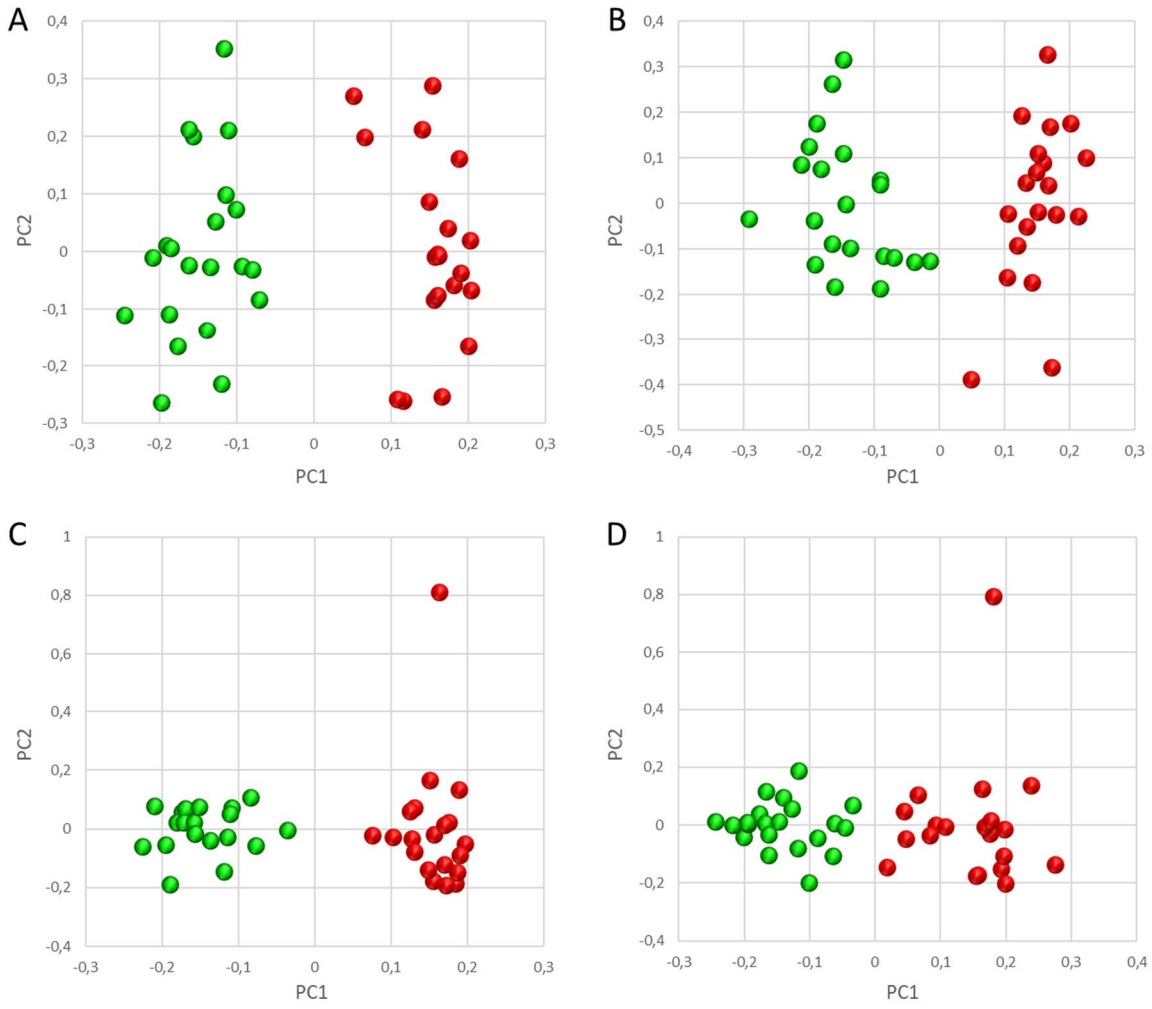

Figure 3. Metabolites with $-Log_2(FC)$ negative values had higher concentrations in PBC patients with respect to healthy subjects. Green bars represented metabolites whose concentration is significantly different (*P*-value <0.05) in the comparison, red bars represented metabolite values that were not statistically relevant. A) serum analysis; B) urine analysis.

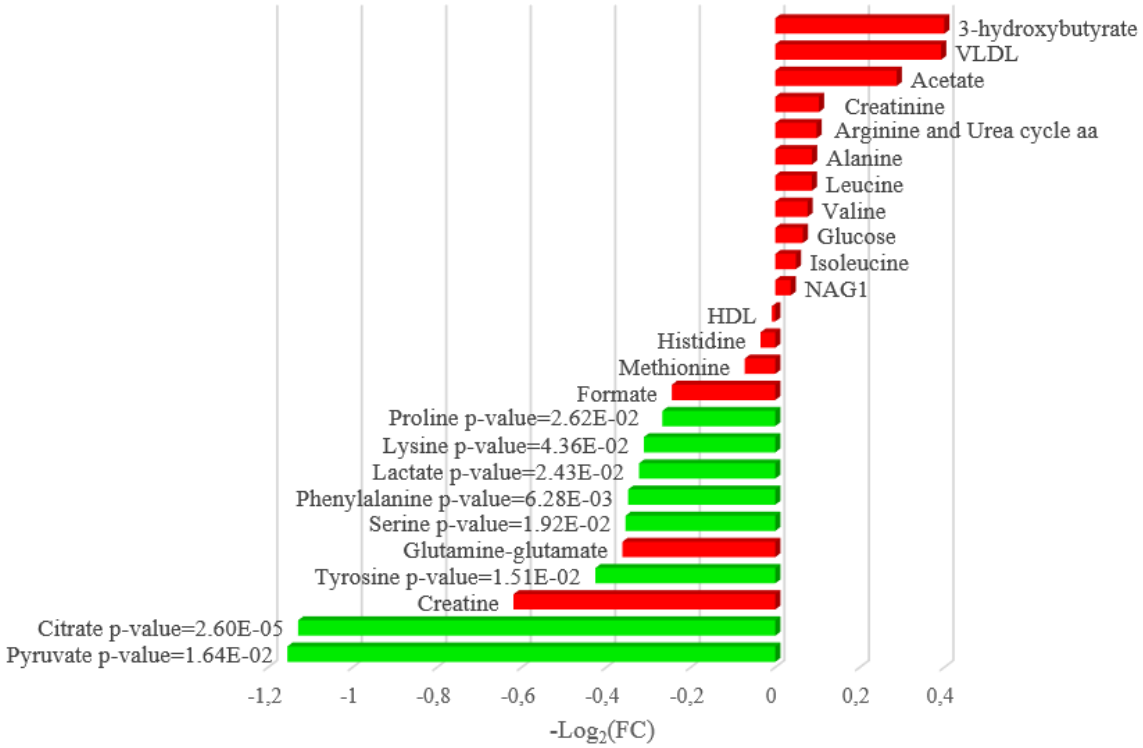

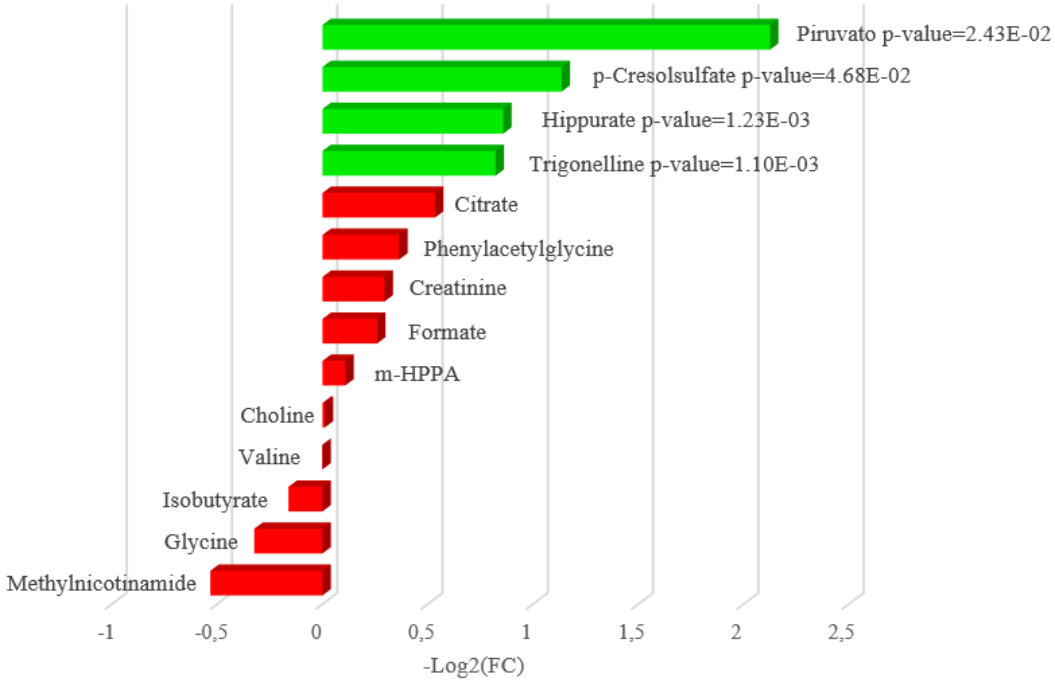

Table 1. PBC patients and their characteristics. IQR= interquartile range; GGT = gamma-glutamyl transferase, ALP= alkaline phosphatase; AST= aspartate transaminase, ALT= alanine transaminase, anti-mitochondrial antibodies

	PBC *(n = 23)*
Sex (M/F) *(n)*	4/19
Age (median, IQR) *(years)*	56 (48-66)
Haemoglobin (median IQR) *(g/dL)*	12,45 (11,175-13,45)
Total Bilirubin (median, IQR) *(mg/dL)*	0,985 (0,52-1,685)
Conjugated Bilirubin (median, IQR) *(mg/dL)*	0,325 (0,2-1,14)
γGT (median, IQR) *(U/L)*	128 (40-194)
ALP (median, IQR) *(U/L)*	217,5 (151-323,75)
AST (median, IQR) *(UI/L)*	56 (25-120)
ALT (median, IQR) *(UI/L)*	67 (25-110)
AMAs (median, IQR) *(n)*	1/320 (1/240-1/480)

Table 2. Cross-validation classification results obtained using CPMG, NOESY, Diffusion-edited serum spectra and NOESY urine spectra of PBC patients and healthy controls (HC).

	Sensitivity	Specificity	Accuracy
PBC - HC		Serum CPMG spectra	
	77.3% (95% CI 76.7-78.0%)	89.3% (95% CI 88.8-89.8%)	83.1% (95% CI 82.7-83.6%)
		Serum NOESY spectra	
	75.4% (95% CI 74.8-76.0%)	84.2% (95% CI 83.5-84.8%)	79.6% (95% CI 79.3-80.1%)
		Serum Diffusion-edited spectra	
	70.5% (95% CI 69.7-71.2%)	83.7% (95% CI 83.1-84.2%)	76.9% (95% CI 76.4-77.4%)
		Urine NOESY spectra	
	74.8% (95% CI 74.2-75.4%)	81.6% (95% CI 81.0-82.2%)	78.1% (95% CI 77.7-78.6%)

Table 3. Cross-validation classification results obtained using CPMG, NOESY, Diffusion-edited serum spectra and NOESY urine spectra of PBC patients and CD patients.

	Sensitivity	Specificity	Accuracy
PBC - CD		Serum CPMG spectra	
	91.8% (95% CI 91.4-92.2%)	65.2% (95% CI 64.4-66.0%)	78.2% (95% CI 77.8-78.6%)
		Serum NOESY spectra	
	85.3% (95% CI 84.8-85.8%)	84.3% (95% CI 83.7-84.8%)	84.8% (95% CI 84.4-85.2%)
		Serum Diffusion-edited spectra	
	89.3% (95% CI 88.8-89.8%)	87.3% (95% CI 86.8-87.8%)	88.3% (95% CI 88.0-88.6%)
		Urine NOESY spectra	
	87.3% (95% CI 86.8-87.8%)	69.4% (95% CI 68.7-70.1%)	78.1% (95% CI 77.7-78.7%)

Supplementary materials

Sample Collections

Venous blood samples were collected into plastic serum tube (6 mL), with increased silica act clot activator, silicone-coated interior (Becton Dickinson, Plymouth, U.K.). Clotting was obtained by standing tubes vertically at room temperature (22 °C) for 60 min. Tubes were centrifuged at 1,800 RCF for 10 min at room temperature. Within 15 min of centrifugation, the supernatant (serum) was transferred in 500 µL aliquots to prelabeled 1 mL cryovials (Bruker BioSpin, Milan, Italy). Three aliquots per patient were immediately frozen and stored at - 80 °C until used.

First morning pre-prandial urine void was used for the collection period. Patients were supplied with appropriate collection instructions and information on fasting, diet and medication restrictions when necessary. The urine samples were collected into prelabeled sterile collections cups. One milliliter of urine sample was transferred into prelabeled 1 mL sterile cryovials (Nalgene, Rochester, NY). Three aliquots per patient were immediately frozen and stored at - 80 °C until used.

NMR samples preparation

Frozen urine and serum samples were thawed at room temperature and shaken before use, both kinds of biological specimens were prepared according to standard operating procedures[1]. A total of 300 µL of a phosphate sodium buffer (10.05 g $Na_2HPO_4 \cdot 7H_2O$; 0.2 g NaN_3; 0.4 g sodium trimethylsilyl [2,2,3,3-$^2H_4$]propionate (TMSP) in 500 mL of H2O with 20% (v/v) ^2H_2O; pH 7.4) was added to 300 µL of each serum sample, and the mixture was homogenized by vortexing for 30 s. A total of 450 µL of this mixture was transferred into a 4.25 mm NMR tube (Bruker BioSpin srl) for analysis.

Urine NMR samples were prepared centrifuging 630 µL of each sample at 14,000 RCF for 5 minutes. 540 µL of the supernatant were added to 60 µL of phosphate potassium buffer (1.5 M K_2HPO_4, 100% (v/v) ^2H_2O, 10 mM sodium trimethylsilyl [2,2,3,3-$^2H_4$]propionate (TMSP) pH 7.4). A total of 450 µL of each of the mixtures was transferred into a 4.25 mm NMR tube (Bruker BioSpin srl) for analysis.

NMR analyses

Monodimensional ^1H NMR spectra for all samples were acquired using a Bruker 600 MHz spectrometer (Bruker BioSpin) operating at 600.13 MHz proton Larmor frequency and equipped with a 5mm CPTCI ^1H-^{13}C-^{31}P and ^2H-decoupling cryoprobe including a z axis gradient coil, an automatic tuning-matching (ATM) and an automatic sample changer. A BTO 2000 thermocouple served for temperature stabilization at the level of approximately 0.1 K at the sample. Before measurement, samples were kept for at least 3 minutes inside the NMR probehead, for temperature equilibration (310 K for serum samples, 300 K for urine samples). According to common practices[2,3], for each serum samples three monodimensional ^1H NMR spectra with different pulse sequences were acquired allowing the selective detection of different molecular components:

(i) a standard nuclear Overhauser effect spectroscopy pulse sequence NOESY 1Dpresat (noesygppr1d.comp; Bruker BioSpin) pulse sequence, using 64 scans, 98,304 data points, a spectral width of 18,028 Hz, an acquisition time of 2.7 s, a relaxation delay of 4 s and a

mixing time of 0.1 s, was applied to obtain a spectrum in which both signals of metabolites and high molecular weight macromolecules (lipids and lipoproteins) are visible.

(ii) a standard spin echo Carr-Purcell-Meiboom-Gill (CPMG)[4] (cpmgpr1d.comp; Bruker BioSpin) pulse sequence applied to a standard 1D sequence, with 64 scans, 73,728 data points, a spectral width of 12,019 Hz and a relaxation delay of 4 s, was used for the selective observation of low molecular weight metabolites, suppressing signals arising from macromolecules.

(iii) a standard Diffusion-edited[5] (ledbgppr2s1d.comp; Bruker BioSpin) pulse sequence, using 64 scans, 98,304 data points, a spectral width of 18,028 Hz and a relaxation delay of 4 s, was applied to suppress metabolites signals.

For each urine sample, one monodimensional ^{1}H NMR spectra was acquired with presaturation water peak suppression using a standard NOESY 1Dpresat pulse sequences (noesygppr1d.comp; Bruker BioSpin), using 64 scans, 64k data points, a spectral width of 12019 Hz, an acquisition time of 2.7 s, a relaxation delay of 4 s and a mixing time of 100 ms.

Spectral Processing

Free induction decays were multiplied by an exponential function equivalent to a 1.0 Hz line-broadening factor before applying Fourier transform. Transformed spectra were automatically corrected for phase and baseline distortions and calibrated (glucose doublet at 5.24 ppm for serum, and TMSP singlet at 0.00 ppm for urine) using TopSpin 3.2 (Bruker Biospin srl). Each 1D spectrum in the range between 0.2 and 10.00 ppm was segmented into 0.02 ppm chemical shift bins and the corresponding spectral areas were integrated using AMIX software (version 3.8.4, Bruker BioSpin). Binning is a means to reduce the number of total variables and to compensate for small shifts in the signals, making the analysis more robust and reproducible[6,7]. Regions between 6.5 and 4.2 ppm containing residual water signal were removed and the dimension of the system was reduced to 375 bins. The total spectral area was calculated on the remaining bins and total area normalization was carried out on the data of serum prior to pattern recognition, instead for urine spectra probabilistic quotient normalization (PQN)[8] was chosen, because it performs well even when large variations of dilution occur.

References

1. Bernini P, Bertini I, Luchinat C, et al. Standard operating procedures for pre-analytical handling of blood and urine for metabolomic studies and biobanks. J Biomol NMR. 2011;49(3-4):231-243. doi:10.1007/s10858-011-9489-1.
2. Beckonert O, Keun HC, Ebbels TMD, et al. Metabolic profiling, metabolomic and metabonomic procedures for NMR spectroscopy of urine, plasma, serum and tissue extracts. Nat Protoc. 2007;2(11):2692-2703.
3. Gebregiworgis T, Powers R. Application of NMR metabolomics to search for human disease biomarkers. Comb Chem High Throughput Screen. 2012;15(8):595-610.
4. Meiboom S, Gill D. Modified Spin-Echo Method for Measuring Nuclear Relaxation Times. Rev Sci Instrum. 1958;29(8):688-691.
5. Wu DH, Chen A. Three-dimensional diffusion-ordered NMR spectroscopy: The homonuclear COSY-DOSY experiment. J Magnen Reson A. 1996;123:215-218.

6. Spraul M, Neidig P, Klauck U, et al. Automatic reduction of NMR spectroscopic data for statistical and pattern recognition classification of samples. J Pharm Biomed Anal. 1994;12(10):1215-1225.
7. Holmes E, Foxall PJ, Nicholson JK, et al. Automatic data reduction and pattern recognition methods for analysis of 1H nuclear magnetic resonance spectra of human urine from normal and pathological states. Anal Biochem. 1994;220(2):284-296.
8. Dieterle F, Ross A, Schlotterbeck G., et al. Probabilistic Quotient Normalization as Robust Method to Account for Dilution of Complex Biological Mixtures. Application in 1H NMR Metabonomics. Anal Chem. 2006;78(13):4281-4290. doi:10.1021/ac051632c.

Supplemental Figure 1. The Diffusion-edited NMR spectral characteristics and the metabolic contents of a serum sample. Despite the broad overall peaks and the overlap of the resonances, the spectra provide information on lipoproteins as indicated in figure. In red are highlighted the signals whose values are statistically relevant in the comparison between PBC and CD patients.

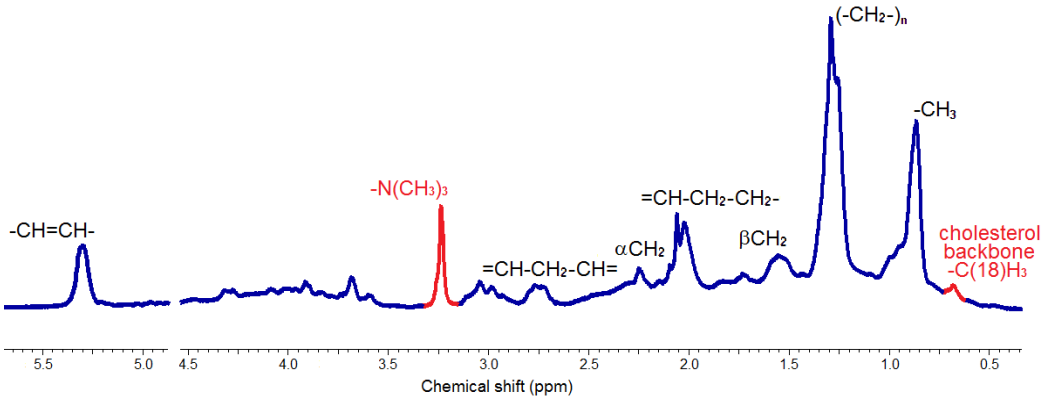

Supplemental Figure 2. PCA-CA-kNN score plots using CPMG spectra as input variables considering all the three groups: PBC patients (red), CD patients (green) and healthy controls (blue). Yellow triangles represent the patients that suffer for both diseases, these samples are placed in the PCA-CA-kNN subspace in the region between PBC and CD samples.

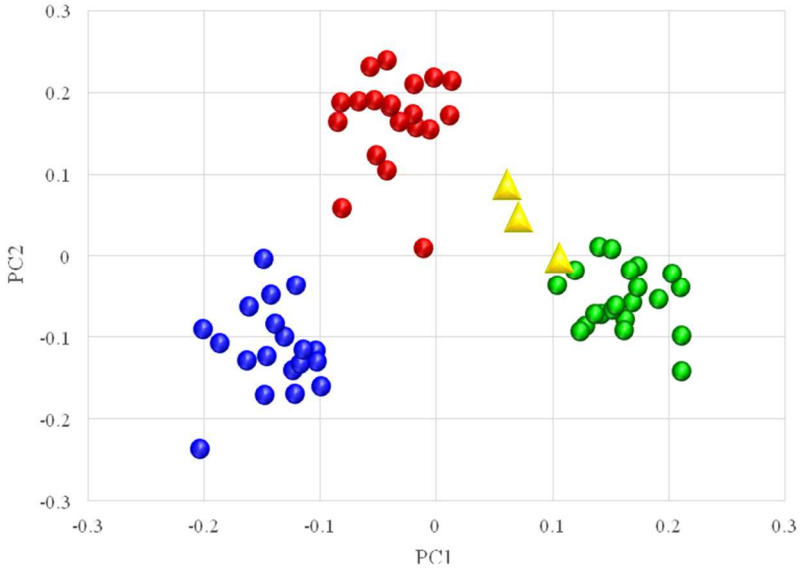

4.3 Metabolomics as a tool for precision medicine

The goal of precision medicine is to customize disease prevention and clinical care strategies base on individual variability in response to environment, lifestyle, genetics, and molecular phenotype. Since metabolomics through biofluid analysis monitors the global outcome of all factors influencing the individual phenotype, it represents a valuable and promising tool for that goal. This kind of metabolomics application has been investigated in two different ways in this thesis: the first two studies proposed in this section contribute to the characterization of the human metabolic phenotype; while, the second two studies demonstrate how it is possible to use metabolomics to monitor patient responses to drug administrations and life interventions.

The comprehension of how common variables affect the expression of the individual metabolic phenotype is of paramount importance for development of metabolomics as a population screening and precision medicine platform. In the first study here presented, in a cohort of 844 adult healthy volunteers age and sex effects on plasma metabolic phenotype and on the probabilistic network constructions of an array of 22 quantified metabolites have been investigated (see paragraph 4.3.1). Our results show not only that is possible to discriminate individuals upon sex and age with a classical multivariate approach, but also that plasma-metabolite networks can be associated with sex and age differences. Statistically significant sex differences in metabolite concentrations and connections were observed, implying variations in many metabolic pathways (aminoacyl-tRNA biosynthesis, nitrogen, valine, leucine and isoleucine, arginine and proline, D-Glutamine and D-glutamate metabolisms). Moreover, alterations of the aminoacyl-tRNA metabolism and the shrinkage of the number of network connectivities were found to be associated with age in both sex groups.

Furthermore, in the second study here proposed, we explored how strong and prolonged stressful conditions can affect the plasma metabolomic phenotype (see paragraph 4.3.2). This metabolomic investigation is part of the Sarcolab study[66], designed to disentangle the various constituents of muscle weakness, elucidate the myotendinous and neuromuscular adaptations to long-term spaceflight, and address the molecular metabolic pathways in skeletal muscle and in the blood affected in astronauts during their missions on the international space station (ISS). We analyzed the plasma samples of two astronauts collected prior to the mission, immediately after the spaceflight and two weeks after the mission, and we could identify pronounced differences between them for what concern aminoacidic and energetic metabolisms. Crew member A, who was under a milder physical activity plan than crew member B, showed increased levels of glucose, pyruvate and pyruvate/lactate ratio, which can be understood as the metabolic consequences of muscle wasting, since it has been proposed that muscle disuse atrophy shifts metabolism towards glycolysis and gluconeogenesis. Interestingly, the metabolic profiles of the two individuals appeared distinct already before launch; then, they responded to the space mission stress, even

if in two different ways, moving toward different metabolic positions, and finally both reverted to their initial metabolic spaces two weeks after the spaceflights. This behavior is consistent with the resilience of the individual metabolic phenotype already described in urine[11].

The third study presented in this section showed how a breathomic approach can be successfully combined with classic diagnostic techniques to monitor the effects of steroid treatment and withdrawal in chronic obstructive pulmonary disease (COPD) patients (see paragraph 4.3.3). Exhaled breath condensate (EBC) metabolomics in combination with exhaled breath analysis with two different e-noses, sputum cell counts, prostaglandin-E2 and 15-F2t-isoprostane in sputum supernatants and EBC, fraction of exhaled nitric oxide, and spirometry were used to follow 14 COPD patients at 4 visits in a timeframe of 10 weeks. At visit 1 patients were administered for at least 8 weeks with a combination of inhaled fluticasone propionate (steroid drug formulated in microparticles) and salmeterol, the therapy was then changed in a combination of inhaled beclomethasone (steroid drug formulated in nanoparticles) and formoterol for two weeks (visit 2). The steroid drug was then suspended for 4 weeks (visit 3) and finally the combination of inhaled beclomethasone/formoterol was reintroduced once again for 4 weeks (visit 4). Three independent breathomic techniques (carbon polymer sensor e-nose, quartz crystal sensor e-nose, NMR-based metabolomics) showed that extrafine beclomethasone/formoterol short-term treatment was associated with different breathprints compared with regular fluticasone propionate/formoterol, and a multidimensional, integrated, model including all analyses performed improves the ability of identifying pharmacological treatment-induced effects compared with a monodimensional model based on standard pulmonary function testing. Therefore, this study provides the first prospective evidence of the effects of pharmacological treatment and steroid withdrawal on breathomics in COPD patients, and it represents a rational basis for large, randomized, controlled, pharmacological trials.

Finally, NMR-based metabolomic analysis has been performed to evaluate the impact of the effects of specific life style interventions, inspired by The European Code Against Cancer, in a cohort of women with high mammographic density, and therefore, higher risk to develop breast cancer (see paragraph 4.3.4). Plasma samples of 321 women were collected and analyzed at baseline and at follow up after four different life style interventions (diet, physical activity, diet + physical activity, control). Each intervention arm was compared at baseline and at follow up using two approaches: PCA-CA models to discover interindividual variations and mPLS to unravel intraindividual variability at the two-time points, obtaining statistically significant accuracies. Furthermore, our data demonstrated for the first time that the information of the mammographic density in a certain way is included in the plasma metabolic fingerprint. Indeed, we discriminated high and low breast density with 70% accuracy and 4 metabolites (leucine, isoleucine, valine and glucose) correlated with the density in a statistically relevant way.

4.3.1 *Age and sex effects on plasma metabolite association networks in healthy subjects*

A. Vignoli[1], L. Tenori[2], C. Luchinat[1,3], E. Saccenti[4]

[1] Magnetic Resonance Center (CERM), University of Florence, Via Luigi Sacconi 6, 50019, Sesto Fioren-tino (FI), Italy
[2] Department of Clinical and Experimental Medicine, University of Florence, Firenze, Italy
[3] Department of Chemistry, University of Florence, Sesto Fiorentino, Italy
[4] Laboratory of Systems and Synthetic Biology, Wageningen University & Research, Wageningen, The Netherlands.

Submitted

Candidate's contributions: statistical analysis and interpretation of data, writing and review of the manuscript.

Age and sex effects on plasma metabolite association networks in healthy subjects

Abstract

In the era of precision medicine, the analysis of simple information like sex and age can increase the potential to better diagnose and treat conditions that occur more frequently in one of the two sexes, present sex-specific symptoms and outcomes, or are characteristic of a specific age group. In this framework metabolomics and networks analyses could be important instruments for the molecular characterization of sex and age differences. We investigate the probabilistic network constructions of experimentally identified relationships within an array of 22 plasma metabolites, and applied a differential network approach to analyze sex and age differences in a cohort of 844 adult healthy volunteers.

Our results show that plasma-metabolite networks can be associated with sex and age differences. Significant sex differences in whole-spectrum fingerprints, metabolite concentrations and connections were observed implying variations in many metabolic pathways (aminoacyl-tRNA biosynthesis, nitrogen, valine, leucine and isoleucine, arginine and proline, D-Glutamine and D-glutamate metabolisms). Alterations of the aminoacyl-tRNA metabolism and the shrinkage of the number of network connectivities were found to be associated with age in both sex groups.

Our results demonstrate that the characterization of metabolite–metabolite association networks is a powerful tool to characterize the human phenotype at a molecular level.

Keywords

NMR, Metabolomics, Network analysis, Metabolism

INTRODUCTION

Simple type information like sex and age can prove valuable information within a precision medicine approach to investigate and to define disease risk and susceptibility in the human population. Although the molecular mechanisms may be not fully understood, it has been long known that differences between the two sexes affect manifestation, epidemiology and pathophysiology of many widespread diseases and, therefore, require different approaches to health care[1]: for instance, drug efficacy and toxicity profiles are affected by sexual dimorphisms[2].

Age differences in the metabolic phenotype have been previously explored: Chiu et al.[3] investigated the age-related metabolic changes in healthy children throughout early childhood; Yu et. al analyzed the serum metabolome and its association with age[4]. Moreover, the metabolic effects of chronological and physiological aging in correlation with blood leukocyte telomere length and epigenetic data were also investigated[5–7]. Age-related considerations are increasingly being taken into account in medical therapy, such as in the case of cancer treatment[8]; but while sexual dimorphisms is a dichotomic variable providing a clear discrimination of the groups of interest, age and ageing are elusive concepts and new insight into systemic metabolic patterns associated with this variable are needed. Indeed, not only the definition of young and old and the discriminant among them depends on socioeconomic and geographical considerations, but the metabolomics study of aging requires large-scale longitudinal studies with replication due to the high variability observed among subjects in term of metabolic phenotypes[8–13].

In this study, we take a systems biology approach to investigate sex and age-specific differences in the plasma metabolite profiles of healthy subjects by considering a group of young and middle aged healthy subjects of both sexes derived from a larger cohort of healthy blood donor volunteers who were analyzed for their plasma metabolite concentration profiles using Nuclear Magnetic Resonance (NMR) spectroscopy. Consistent with previous observations of sex specific differences at the metabolic level[14] we performed the analysis separately for males and females to minimize confounding effects.

In contrast with other age-related metabolomics studies, our data analysis strategy combines standard univariate and multivariate analysis[15] to explore the patterns of variation of metabolites among the two age classes together with advanced metabolite-metabolite association network analysis and inference.

Networks and network analysis are fundamental tools in systems biology and are being exploited more and more often to analyze, understand and interpret the complex patterns observed in metabolomics data[13,14,16,17]. The rationale is that metabolite concentrations change in an orchestrated fashion in such a way that the association among metabolite inferred from measured concentrations in biofluids can be considered, to some extent, related to the underlying structure of the biological networks. Moreover, since metabolite concentrations can change rapidly in response

to perturbations of the system, they can be considered proximal reporters of a pathophysiological status.
The utility of network-based approaches to analyze metabolomics data relies on these two key concepts, and networks are best exploited when compared across different conditions in a so called differential-network analysis approach: different network characteristics and different patterns of association between metabolites can highlight possibly affected molecular mechanisms, such as those that can be expected to be altered when considering young and old subjects.

MATERIALS AND METHODS

Data description

The study population consists of 844 adult healthy volunteers (661 males, 183 females, median age 41±12 years) recruited in collaboration with the Tuscany section of the Italian Association of Blood Donors (AVIS) in the Transfusion Service of the Pistoia Hospital (Ospedale del Ceppo, AUSL 3 - Pistoia, Italy). NMR spectra, and associated clinical data were retrieved from the Open-Access Database Repository MetaboLights[18] with the accession number MTBLS147 (http://www.ebi.ac.uk/metabolights). Twenty samples from the original dataset were excluded from this analysis because sex or age information were missing. Age distributions for both sexes are reported as histograms in the Supplementary Figure 1.

Statistical analysis

All data analyses were performed using the open source software R[19]. Multivariate analysis was conducted on both spectral bins and integrated peak area corresponding to metabolite concentrations; instead, univariate analysis was performed only on metabolite concentrations.
Data reduction was carried out by means of projection into a PCA subspace, the minimum number of components that maximized the accuracy was retained in the model and the canonical analysis (CA) was applied to obtain the supervised separation of the groups of interest.
The k-Nearest Neighbors (k-NN) method (k=9) applied on the PCA-CA scores was used for classification[20]. All the accuracies reported and the confusion matrix for the different classifications were assessed by means of 100 cycles of a Monte Carlo cross-validation scheme (MCCV, R script in-house developed). Briefly, 90% of the data were randomly chosen at each iteration as a training set to build the model. Then the remaining 10% was tested and sensitivity, specificity and accuracy for the classification were assessed. The procedure was repeated 100 times to derive an average discrimination accuracy for each group of interest. Sensitivity, specificity and accuracy are given together with the standard error calculated over 10^2 repetitions of the Monte Carlo samplings. Moreover, the accuracies calculated were assessed for

significance against the null hypothesis of no prediction accuracy in the data, by means of 10^2 randomized class-permutation test.
The spectral regions related to the metabolites were assigned in the spectra by using matching routines of AMIX 3.8.4 (Bruker BioSpin) in combination with the BBIOREFCODE (Bruker BioSpin), freely available dataset i.e. Human Metabolome DataBase (HMDB)[21,22] and published literature when available. The metabolites quantification was determined by an in-house developed software in MATLAB programming suite (Mathworks, MATLAB version R2014b). Our algorithm is based upon the unconstrained non-linear minimization (fitting) of the metabolites NMR signals, employing a combination of lorentzian-gaussian functions. By this approach, each NMR region of interest is decomposed and deconvoluted into its component parts, and then integrated to obtain the metabolite concentrations in arbitrary units. These concentrations were analyzed to determine the discriminating metabolites between the groups of interest. Wilcoxon signed-rank test[23] was chosen to infer differences between the groups on the biological assumption that metabolite concentrations are not normally distributed, and false discovery rate correction was applied using the Bonferroni method[24]. An adjusted P-value < 0.05 was deemed significant. Cliff's delta[25] was calculated using the R package "effsize".

Network Analysis
Network reconstruction
Three different methods were used to infer metabolite-metabolite association networks together with the standard correlation approach A brief description of the methods is presented here: we refer to the original publications for more details[17,26,27]. All methods were applied using default parameters.

Method based on correlations (CORR)
The association between any pair of metabolites is measured through the absolute value of Pearson's correlation.

The CLR algorithm
The CLR (Context Likelihood of Relatedness) algorithm[28] uses mutual information (MI) as a measure of the similarity between the profiles of any two metabolites in the data which is then compared against the local context for each possible interaction: in this way possible spurious (indirect) associations are removed. This result in a weighted adjacency matrix that can be transformed into a binary adjacency matrix imposing a threshold of 0 on its entries.

The ARACNE algorithm
As CLR, ARACNE (Algorithm for the Reconstruction of Accurate Cellular Networks)[29] uses MI as a measure of the similarity between two chosen variables. The properties of

MI are used to prune the network of spurious interactions. Specifically, edges for which the null hypothesis of mutual independence cannot be ruled out at a given confidence level are removed from the network.

The PCLRC algorithm

PCLRC[17] is based on a modification of the CLR algorithm (using correlation instead of MI to measure similarity between metabolite profiles) and on iteratively sampling the dataset resulting in a weighted adjacency matrix containing an estimate of the association likeliness between any two metabolites. An R implementation of this algorithm is available at semantics.systemsbiology.nl.

Construction of plasma metabolite networks

The plasma metabolite-metabolite association networker taking a wisdom of crowd approach as detailed in reference[13]. For each set of samples (Males, Females, Old M, Young M, Old F, Young F) adjacency matrices (aij)m (with m=1,2 ,... 4) were obtained using the above described methods. The entries of such matrices matrix are real numbers in the range [-1, 1] for correlation matrices, in the [0, +∞] range for mutual information matrices, or [0, 1] for probabilistic networks, indicating the strength or the likelihood of the metabolite-metabolite associations. These matrices are binarized to 0 and 1 imposing a threshold on the values[9–11,13]:

$$\{a_{ij}\} \rightarrow \begin{cases} 1 & \text{if } a_{ij} > \tau_m \\ 0 & \text{otherwise} \end{cases} \quad (1)$$

The values of τ_m tm depends on the method considered: 0 for ARACNE and CLR, 0.95 for PCLRC, and 0.6 for the correlation map, as previously detailed[26]. The four networks were then superimposed

$$\{a_{ij}\} \rightarrow \sum_{m=1}^{4} \{a_{ij}\}_m \quad (2)$$

The final adjacency matrix, representing the metabolite network was defined by retaining only those links inferred by three or more methods, as suggested in ref 26

$$\{a_{ij}\} \rightarrow \begin{cases} 1 & \text{if } a_{ij} \geq 3 \\ 0 & \text{otherwise} \end{cases} \quad (3)$$

In total, six networks were defined: Males, Females, Old M, Young M, Old F, and Young F. Network vertexes are colored according to their modularity calculated using the R

package "igraph". The modularity of each graph with respect to vertex types measures how separated are the different vertex types from each other. It defined as

$$Q = \frac{1}{2m}\sum_{i,j}^{m}\left(A_{ij} - \frac{k_i \cdot k_j}{2m}\right) \cdot \delta(c_i c_j) \quad (4)$$

here m is the number of edges, Aij is the element of the A adjacency matrix in row i and column j, ki is the degree of i, kj is the degree of j, ci is the type (or component) of i, cj that of j, the sum goes over all i and j pairs of vertices, and delta(x,y) is 1 if x=y and 0 otherwise.

Enrichment analysis

Metabolic pathway analysis (MetPA) was performed using MetaboAnalyst 3.0[30] server (http://www.metaboanalyst.ca/): this tool combines functional enrichment analysis and network topology analysis to help identify metabolic pathways that are most likely to be associated with the condition under study. For the over-representation analysis, hypergeometric test was chosen and the pathway topology analysis was based on the relative-betweeness centrality.

Ethical Issues

The original data were collected in accordance with the 1964 Helsinki declaration and its later amendments.

RESULTS AND DISCUSSION

Sex related effects on blood metabolite profiles

Discrimination analysis among the NMR profiles of males and females was performed using PCA-CA-kNN (Figure 1A). The data set was unbalanced, with far more males (n = 661) than females (n = 163). This is not surprising and it reflects the sex bias observed in Italy among blood donors where more males than females donate blood[31]. To avoid the bias resulting from different sample size, analysis was performed by resampling n = 150 subjects from both the male and female groups and taking the average over 102 repetitions.

We obtained excellent discrimination between the plasma profiles of males and females (see Table 1), a result in line with previous observations[14]. Discrimination accuracy was also high when only a reduced set of 22 quantified metabolites was used, indicating that sex-specific biological information is thoroughly represented by a limited number of metabolites, consistently to what observed in the case of metabolite and metabolic profiling in urines[13].

Upon univariate analysis, the concentration levels of several metabolites were found to be statistically different between males and female (P-value<0.05 after Bonferroni correction): creatine showed higher levels in females; instead, phenylalanine, glutamine, proline, histidine, glutamate, tyrosine, valine, propylene glycol, leucine, isoleucine, creatinine, and acetone were higher in males (Table 2). Higher levels of creatinine in males has been reported since long time and has been found to relate to muscle mass. Overall we observed systematic higher plasma concentrations of amino acids in males which may be linked to differences in muscle mass metabolism[32].

We also performed metabolic pathway analysis on the metabolites whose concentration were observed to be different in males and females and we found statistically significant P-values for the aminoacyl-tRNA biosynthesis, nitrogen, valine, leucine and isoleucine, arginine and proline, D-Glutamine and D-glutamate metabolisms (Table 3). Variation in amino acids levels is consistent with differential regulation and activity of the aminoacyl-tRNA biosynthesis, a metabolic pathway directly involved in the protein synthesis.

Our results are in line with those of Krumsiek and coworkers[14], who addressed sex-specific differences in the metabolism of healthy subjects, although two different analytical approach were applied (Mass Spectrometry vs NMR spectroscopy) and the study sizes were different. Interestingly, in the present work creatinine and tyrosine trends are consistent with their findings but in contrast with what reported by Dunn et al. in their UK population study[33] where they observed lower levels of creatinine and tyrosine in males. Moreover, we did not observe sex-related differences in glucose and lactate plasma levels.

Sex related effects on plasma metabolite association networks

Plasma metabolite-metabolite association networks were estimated taking a so called "wisdom of crowd" approach, i.e. combing the results of four different methods to avoid bias induced by the choice of a particular method, following an established practice[13,26,34]. Sex specific networks are shown in Figure 2A (males) and 2B (females). Networks were arranged and colored according to metabolite modularity. In both sex-specific networks two aminoacidic clusters are visible; moreover, in males also metabolites related to glucose/energetic metabolism formed a cluster. These evidences are in line with those observed by Krumsiek and coworkers[14].

We observed that, in general, the female-specific network is less densely connected that the males-specific network (Figure 3) and this different topology is likely to reflect underlying metabolic differences but it could be also affected by the differences in the sample size. Highly connected metabolites, the so called "hubs" play a special role in biological network and network analysis since in many cases, for example in gene co-expression and regulatory networks[35,36], metabolic networks, protein–protein interaction networks[37–39], and cell–cell interaction networks[40], there is evidence of few highly connected nodes (in this case metabolites) that are considered to play crucial

biological roles; for instance it has been shown that, in yeast, proteins that are highly connected are essential for survival[35,37].

Consistently with previous approaches[41], at a first stage, we considered as hubs those metabolites with degree larger than 5 and clustering coefficient <0.03. In male-specific networks only leucine, glucose, lactate, valine, acetoacetate, and creatinine satisfied these selection criterion, while in the female-specific network only valine was found to be a hub according to this classification. Interestingly, valine is a hub metabolite in both networks, yet it resulted more connected in males than in females (9 vs 5 connections); 4 connections are in common (Ile, Leu, Phe, and Tyr) while citrate is a connection found only in females, and acetoacetate, creatinine, creatine, acetone, and histidine are connected with valine only in males. It is worth of noting that citrate excretion levels differ significantly in males and females, and in particular the sex differences increase with age[42]. We used high connectivity and low clustering coefficient to exclude metabolites that could be highly interconnected because participating to same molecular machine, such as amino acids deriving from protein metabolism and catabolism, while focus on metabolites that could be pivotal in discriminating between males and females network topology. Indeed, according to this criterion BCAA such as isoleucine and leucine, whose levels are also dependent of protein intake, are excluded. The hub metabolites in the male-specific network are enriched for propanoate metabolism and for the valine, leucine and isoleucine degradation. Branched chain amino acids (BCAA) cannot be synthesized de novo, so their homeostasis is maintained by degradation and dietary intake only[43], which we speculate may be differentially regulated in males and females given the different connectivity observed in the sex-specific networks. Whether protein metabolism and degradation is different in males and females is an open question, and there are conflicting results given also the different methodologies used in such studies. However, the present results seem to suggest the existence of sex-specific differences in protein metabolism: whether these differences are due to different body mass composition or being attributable to sex hormones as suggested[44,45] has to be ascertained.

Propionate and BCAA metabolism overlap at the gene level with BCAA metabolic genes contributing to propanoate pathway enrichment; propanoate is involved in BCAA metabolism but is also involved in the short-chain fatty acid metabolism, and this result can be reconciled with the hypothesis of sexual dimorphism in human lipid metabolism[46].

Similarly to[41] we also analyzed the networks using a hub definition of connectivity greater than 5 without considering the clustering coefficient, and we focused solely on those metabolites for which the difference Δ between a metabolite connectivity in the male and female specific network was larger than 2. In addition to the valine, leucine and isoleucine catabolism and propanoate metabolism we found three other pathways associated with sex-specific metabolite connectivity differences, namely synthesis and degradation of ketone bodies, aminoacyl-tRNA biosynthesis, and pyruvate metabolism.

That ketone bodies catabolism emerges as a discriminant between males and females is interesting; blood samples have been collected after overnight fasting, and it is known that during short term fasting the decrease of plasma glucose and the increase of ketone body levels are greater in females than in males[47–51] and evidences have been given for the existence of sexual dimorphism for what concerns lipid metabolism in response to short-term fasting[47]. However, as for the case of protein metabolism, the causes are not known and a role of sexual hormones has been proposed[47]. Since aminoacyl-tRNA is the obligatory precursor of protein synthesis[52], the sexual dimorphism highlighted by sex- specific network analysis further supports the hypothesis that protein metabolism and degradation is different in males and females. Pyruvate is produced during glycolysis and it has been suggested that females have a significantly lower overall capacity for aerobic oxidation and for anaerobic glycolysis than males[53,54].

Age effects on blood metabolite networks

While sexual dimorphism provides a clear discriminant for a comparative analysis, dividing the population under investigation in age groups is less straightforward. According to the World Health Organization[55], the chronological age of 65 years is used for the definition of 'elderly' or older person. However, in this study the cohort is made of blood donor volunteers, and in Italy the maximum age for blood donation is set to 65. Here, the average age is 41±11 years for males and 42±12 years for females; we are thus in the presence of a relatively young, healthy, and homogenous population. To set boundaries for discriminant analysis we take a pragmatic approach, by taking the lower (L) and upper (U) tertiles of the age distribution and labelling as Old those individual with age > U and as YOUNG those with age < L. For males we had L = 35 and U = 45 years, and for females L = 37 and U =48 .

Discriminant analysis was performed using PCA-CA-kNN on these age-defined groups (Figure 1C-F). As shown in Table 1 we found good discrimination accuracy between the two age classes, with discrimination higher in males than in females. This can be due to the smaller sample size in the case of females (661 males vs 183 females) which can affect the discrimination power of the statistical model, or reflecting the fact that males age faster than females[56] resulting in larger age related differences in males in respect with females.

The univariate analysis of the metabolite concentrations (arbitrary units) was also presented for both age-comparisons: acetate, and histidine exhibited statistically higher concentrations in Young males; conversely, alanine and creatine were elevated in Old males (Table 5). These metabolites were associated with the aminoacyl-tRNA biosynthesis (Table 3). For the female cohort, glucose, glutamine, glycine, tyrosine, and creatine presented statistically higher concentrations in Old females (Table 6) and these metabolites were related with aminoacyl-tRNA biosynthesis and nitrogen metabolism (Table 3). The role of the aminoacyl-tRNA metabolic pathway in

individuals with different age, independent of sex, could be related to the so called codon restriction theory of aging[57,58]. This theory is based on the hypothesis that the readability of codons progressively decreases with the age, resulting in inefficient and inaccurate protein synthesis.

The analysis of the metabolite connectivity (Δ degree) was also performed for the comparison Young males vs Old males, and Young females vs Old females. For males 3-hydroxybutyrate, proline, citrate, and creatinine showed increased connectivity in the young cohort (Δ ≥ 2); instead, acetone, leucine, and propylene glycol decreased their connectivity with age (Figure 3B). Isoleucine, phenylalanine, glycine, glutamine, glutamate, formate, creatine, and acetoacetate did not display any connectivity variations in the male cohort (Δ = 0). MetPA results suggested that changing in metabolite connectivities were associated with the synthesis and degradation of ketone bodies and arginine and proline metabolism; instead, glutamine and glutamate metabolism was associated with the metabolites with Δ = 0 (Table 4).

For females, isoleucine, alanine, tyrosine, 3-hydroxybutyrate, proline, leucine and glucose were found to be more connected in the young cohort (Δ ≥ 2); instead, glutamine and creatine did not exhibit any changes in connectivity (Figure 3C). MetPA showed statistically significant results only for the metabolites that changed in connectivity. Indeed, they resulted associated with the valine, leucine and isoleucine biosynthesis and degradation, and with the aminoacyl-tRNA biosynthesis (Table 4).

As a general remark, we can observe a shrinkage of the number of connections in the older individuals, both for males (Figure 2C and E) and females (Figure 2D and F). Older males showed two hubs (valine and acetone) that are not present in younger ones; conversely, no hubs were found in females independent of age. Interestingly, Soltow et al.[59] in their study on metabolism and ageing in common marmosets (Callithrix jacchus, a premiere primate model for studies of aging) reported that metabolite connectivity decreases with age and this result is line with what we are reporting in this paper. These evidences could indicate that further efforts in this direction and using these types of analyses (global metabolic profiling combined with network analysis) in well-designed models may reveal biomarkers associated with age-related phenotype and disease.

CONCLUSIONS

In conclusion, we have presented the network constructions of experimentally identified relationships between metabolites, and applied a differential network approach to analyze sex and age differences in a cohort of healthy subjects. Our results show significant differences between males and females for what concerns both metabolite concentrations and connections implying variations in the metabolic pathways, especially for what concerns the aminoacyl-tRNA biosynthesis, nitrogen, valine, leucine and isoleucine, arginine and proline, D-Glutamine and D-glutamate

metabolisms. Moreover, we found an alteration of the aminoacyl-tRNA metabolism, and a decrease of the connectivity with age in both sex groups, demonstrating that this evidence is peculiar of ageing even if the biological meaning of our result needs to be further investigated.

Although the age range is limited and sex is unequally biased towards males, this study provides important information on how common variables influence expression of the metabolic phenotype. Both age and sex are recognized confounders, understanding these differences will be a critical component for development of metabolomics as a population screening and precision medicine platform.

Acknowledgements

We acknowledge AVIS Toscana (in the person of the Luciano Franchi and Donata Marangio), AVIS Pistoia (in the person of Alessandro Pratesi), and the technical staff of Transfusion Service of the Pistoia Hospital for volunteer recruitment and sample collection.

This work was partly supported by the European Commission-funded INFECT project (Contract No. 305340) and the H2020 project PhenoMeNal (Grant 654241).

Author Contributions

The authors' responsibilities were as follows: CL, ES, LT, and AV assisted in the study design. ES, and AV performed statistical data analyses. CL, ES, LT, and AV interpreted the data, prepared the manuscript, and were responsible for its final content. All authors read and approved the final version of the manuscript.

Conflicts of Interest

The authors declare no competing financial, and non-financial interests.

REFERENCES

(1) Regitz-Zagrosek, V. Sex and gender differences in health. EMBO Rep. 2012, 13 (7), 596–603.

(2) Gandhi, M.; Aweeka, F.; Greenblatt, R. M.; Blaschke, T. F. Sex differences in pharmacokinetics and pharmacodynamics. Annu. Rev. Pharmacol. Toxicol. 2004, 44, 499–523.

(3) Chiu, C.-Y.; Yeh, K.-W.; Lin, G.; Chiang, M.-H.; Yang, S.-C.; Chao, W.-J.; Yao, T.-C.; Tsai, M.-H.; Hua, M.-C.; Liao, S.-L.; et al. Metabolomics Reveals Dynamic Metabolic Changes Associated with Age in Early Childhood. PloS One 2016, 11 (2), e0149823.

(4) Yu, Z.; Zhai, G.; Singmann, P.; He, Y.; Xu, T.; Prehn, C.; Römisch-Margl, W.; Lattka, E.; Gieger, C.; Soranzo, N.; et al. Human serum metabolic profiles are age dependent. Aging Cell 2012, 11 (6), 960–967.

(5) Menni, C.; Kastenmüller, G.; Petersen, A. K.; Bell, J. T.; Psatha, M.; Tsai, P.-C.; Gieger, C.; Schulz, H.; Erte, I.; John, S.; et al. Metabolomic markers reveal novel pathways of ageing and early development in human populations. Int. J. Epidemiol. 2013, 42 (4), 1111–1119.

(6) Jové, M.; Maté, I.; Naudí, A.; Mota-Martorell, N.; Portero-Otín, M.; De la Fuente, M.; Pamplona, R. Human Aging Is a Metabolome-related Matter of Gender. J. Gerontol. A. Biol. Sci. Med. Sci. 2016, 71 (5), 578–585.

(7) Zhao, J.; Zhu, Y.; Uppal, K.; Tran, V. T.; Yu, T.; Lin, J.; Matsuguchi, T.; Blackburn, E.; Jones, D.; Lee, E. T.; et al. Metabolic profiles of biological aging in American Indians: the Strong Heart Family Study. Aging 2014, 6 (3), 176–186.

(8) Repetto, L.; Venturino, A.; Fratino, L.; Serraino, D.; Troisi, G.; Gianni, W.; Pietropaolo, M. Geriatric oncology: a clinical approach to the older patient with cancer. Eur. J. Cancer Oxf. Engl. 1990 2003, 39 (7), 870–880.

(9) Assfalg, M.; Bertini, I.; Colangiuli, D.; Luchinat, C.; Schafer, H.; Schutz, B.; Spraul, M. Evidence of different metabolic phenotypes in humans. Proc.Natl.Acad.Sci.U.S.A 2008, 105 (1091–6490 (Electronic)), 1420–1424.

(10) Bernini, P.; Bertini, I.; Luchinat, C.; Nepi, S.; Saccenti, E.; Schafer, H.; Schutz, B.; Spraul, M.; Tenori, L. Individual human phenotypes in metabolic space and time. J ProteomeRes 2009, 8 (1535–3893 (Print)), 4264–4271.

(11) Ghini, V.; Saccenti, E.; Tenori, L.; Assfalg, M.; Luchinat, C. Allostasis and Resilience of the Human Individual Metabolic Phenotype. J. Proteome Res. 2015.

(12) Mäkinen, V.-P.; Ala-Korpela, M. Metabolomics of aging requires large-scale longitudinal studies with replication. Proc. Natl. Acad. Sci. U. S. A. 2016, 113 (25), E3470.

(13) Saccenti, E.; Menichetti, G.; Ghini, V.; Remondini, D.; Tenori, L.; Luchinat, C. An entropy based network representation of the individual metabolic phenotype. J. Proteome Res. 2016.

(14) Krumsiek, J.; Mittelstrass, K.; Do, K. T.; Stückler, F.; Ried, J.; Adamski, J.; Peters, A.; Illig, T.; Kronenberg, F.; Friedrich, N.; et al. Gender-specific pathway differences in the human serum metabolome. Metabolomics Off. J. Metabolomic Soc. 2015, 11 (6), 1815–1833.

(15) Saccenti, E.; van Duynhoven, J.; Jacobs, D. M.; Smilde, A. K.; Hoefsloot, H. C. J. Strategies for individual phenotyping of linoleic and arachidonic Acid metabolism using an oral glucose tolerance test. PloS One 2015, 10 (3), e0119856.

(16) Krumsiek, J.; Suhre, K.; Illig, T.; Adamski, J.; Theis, F. J. Gaussian graphical modeling reconstructs pathway reactions from high-throughput metabolomics data. BMC Syst. Biol. 2011, 5, 21.

(17) Saccenti, E.; Suarez-Diez, M.; Luchinat, C.; Santucci, C.; Tenori, L. Probabilistic Networks of Blood Metabolites in Healthy Subjects As Indicators of Latent Cardiovascular Risk. J. Proteome Res. 2014.

(18) Kale, N. S.; Haug, K.; Conesa, P.; Jayseelan, K.; Moreno, P.; Rocca-Serra, P.; Nainala, V. C.; Spicer, R. A.; Williams, M.; Li, X.; et al. MetaboLights: An Open-Access Database Repository for Metabolomics Data. Curr. Protoc. Bioinforma. 2016, 53, 14.13.1-18.

(19) Ihaka, R.; Gentleman, R. R: A Language for Data Analysis and Graphics. J Comput Stat Graph 1996, 5, 299–314.

(20) Cover, T.; Hart, P. Nearest neighbor pattern classification. Inf. Theory IEEE Trans. On 1967, 13 (1), 21–27.

(21) Wishart, D. S.; Tzur, D.; Knox, C.; Eisner, R.; Guo, A. C.; Young, N.; Cheng, D.; Jewell, K.; Arndt, D.; Sawhney, S.; et al. HMDB: the Human Metabolome Database. Nucleic Acids Res. 2007, 35 (Database issue), D521-526.

(22) Wishart, D. S.; Jewison, T.; Guo, A. C.; Wilson, M.; Knox, C.; Liu, Y.; Djoumbou, Y.; Mandal, R.; Aziat, F.; Dong, E.; et al. HMDB 3.0--The Human Metabolome Database in 2013. Nucleic Acids Res. 2013, 41 (D1), D801–D807.

(23) Wilcoxon, F. Individual Comparisons by Ranking Methods. Biom. Bull. 1945, 1 (6), 80.

(24) Bonferroni, C. E. Il calcolo delle assicurazioni su gruppi di teste. In Studi in Onore del Professore Salvatore Ortu Carboni; Rome, 1935; pp 13–60.

(25) Cliff, N. Ordinal Methods for Behavioral Data Analysis; Psychology Press: Mahwah, N.J, 1996.

(26) Suarez-Diez, M.; Saccenti, E. Effects of Sample Size and Dimensionality on the Performance of Four Algorithms for Inference of Association Networks in Metabonomics. J. Proteome Res. 2015, 14 (12), 5119–5130.

(27) Suarez-Diez, M.; Adam, J.; Adamski, J.; Chasapi, S. A.; Luchinat, C.; Peters, A.; Prehn, C.; Santucci, C.; Spyridonidis, A.; Spyroulias, G. A.; et al. Plasma and Serum Metabolite Association Networks: Comparability within and between Studies Using NMR and MS Profiling. J. Proteome Res. 2017.

(28) Faith, J. J.; Hayete, B.; Thaden, J. T.; Mogno, I.; Wierzbowski, J.; Cottarel, G.; Kasif, S.; Collins, J. J.; Gardner, T. S. Large-scale mapping and validation of Escherichia coli transcriptional regulation from a compendium of expression profiles. PLoS Biol. 2007, 5 (1), e8.

(29) Margolin, A. A.; Nemenman, I.; Basso, K.; Wiggins, C.; Stolovitzky, G.; Dalla Favera, R.; Califano, A. ARACNE: an algorithm for the reconstruction of gene regulatory networks in a mammalian cellular context. BMC Bioinformatics 2006, 7 Suppl 1, S7.

(30) Xia, J.; Sinelnikov, I. V.; Han, B.; Wishart, D. S. MetaboAnalyst 3.0--making metabolomics more meaningful. Nucleic Acids Res. 2015, 43 (W1), W251-257.

(31) Bani, M.; Giussani, B. Gender differences in giving blood: a review of the literature. Blood Transfus. 2010, 8 (4), 278–287.

(32) Honda, T.; Kobayashi, Y.; Togashi, K.; Hasegawa, H.; Iwasa, M.; Taguchi, O.; Takei, Y.; Sumida, Y. Associations among circulating branched-chain amino acids and tyrosine with muscle volume and glucose metabolism in individuals without diabetes. Nutr. Burbank Los Angel. Cty. Calif 2016, 32 (5), 531–538.

(33) Dunn, W. B.; Lin, W.; Broadhurst, D.; Begley, P.; Brown, M.; Zelena, E.; Vaughan, A. A.; Halsall, A.; Harding, N.; Knowles, J. D.; et al. Molecular phenotyping of a UK population: defining the human serum metabolome. Metabolomics Off. J. Metabolomic Soc. 2015, 11, 9–26.

(34) Marbach, D.; Costello, J. C.; Küffner, R.; Vega, N. M.; Prill, R. J.; Camacho, D. M.; Allison, K. R.; DREAM5 Consortium; Kellis, M.; Collins, J. J.; et al. Wisdom of crowds for robust gene network inference. Nat. Methods 2012, 9 (8), 796–804.

(35) Carter, S. L.; Brechbühler, C. M.; Griffin, M.; Bond, A. T. Gene co-expression network topology provides a framework for molecular characterization of cellular state. Bioinforma. Oxf. Engl. 2004, 20 (14), 2242–2250.

(36) Stuart, J. M.; Segal, E.; Koller, D.; Kim, S. K. A gene-coexpression network for global discovery of conserved genetic modules. Science 2003, 302 (5643), 249–255.

(37) Jeong, H.; Mason, S. P.; Barabási, A. L.; Oltvai, Z. N. Lethality and centrality in protein networks. Nature 2001, 411 (6833), 41–42.

(38) Rzhetsky, A.; Gomez, S. M. Birth of scale-free molecular networks and the number of distinct DNA and protein domains per genome. Bioinforma. Oxf. Engl. 2001, 17 (10), 988–996.

(39) Yook, S.-H.; Oltvai, Z. N.; Barabási, A.-L. Functional and topological characterization of protein interaction networks. Proteomics 2004, 4 (4), 928–942.

(40) Hartwell, L. H.; Hopfield, J. J.; Leibler, S.; Murray, A. W. From molecular to modular cell biology. Nature 1999, 402 (6761 Suppl), C47-52.

(41) Lu, X.; Jain, V. V.; Finn, P. W.; Perkins, D. L. Hubs in biological interaction networks exhibit low changes in expression in experimental asthma. Mol. Syst. Biol. 2007, 3 (1), n/a-n/a.

(42) Caudarella, R.; Vescini, F.; Buffa, A.; Stefoni, S. Citrate and mineral metabolism: kidney stones and bone disease. Front. Biosci. J. Virtual Libr. 2003, 8, s1084-1106.

(43) Wanders, R. J. A.; Duran, M.; Loupatty, F. J. Enzymology of the branched-chain amino acid oxidation disorders: the valine pathway. J. Inherit. Metab. Dis. 2012, 35 (1), 5–12.

(44) Phillips, S. M.; Atkinson, S. A.; Tarnopolsky, M. A.; MacDougall, J. D. Gender differences in leucine kinetics and nitrogen balance in endurance athletes. J. Appl. Physiol. Bethesda Md 1985 1993, 75 (5), 2134–2141.

(45) McKenzie, S.; Phillips, S. M.; Carter, S. L.; Lowther, S.; Gibala, M. J.; Tarnopolsky, M. A. Endurance exercise training attenuates leucine oxidation and BCOAD activation during exercise in humans. Am. J. Physiol. Endocrinol. Metab. 2000, 278 (4), E580-587.

(46) Mittendorfer, B. Sexual dimorphism in human lipid metabolism. J. Nutr. 2005, 135 (4), 681–686.

(47) Mittendorfer, B.; Horowitz, J. F.; Klein, S. Gender differences in lipid and glucose kinetics during short-term fasting. Am. J. Physiol. Endocrinol. Metab. 2001, 281 (6), E1333-1339.

(48) Paula, F. J.; Pimenta, W. P.; Saad, M. J.; Paccola, G. M.; Piccinato, C. E.; Foss, M. C. Sex-related differences in peripheral glucose metabolism in normal subjects. Diabete Metab. 1990, 16 (3), 234–239.

(49) Yki-Järvinen, H. Sex and insulin sensitivity. Metabolism. 1984, 33 (11), 1011–1015.

(50) Rizza, R. A.; Mandarino, L. J.; Gerich, J. E. Dose-response characteristics for effects of insulin on production and utilization of glucose in man. Am. J. Physiol. - Endocrinol. Metab. 1981, 240 (6), E630–E639.

(51) Zderic, T. W.; Coggan, A. R.; Ruby, B. C. Glucose kinetics and substrate oxidation during exercise in the follicular and luteal phases. J. Appl. Physiol. 2001, 90 (2), 447–453.

(52) Chow, L. S.; Albright, R. C.; Bigelow, M. L.; Toffolo, G.; Cobelli, C.; Nair, K. S. Mechanism of insulin's anabolic effect on muscle: measurements of muscle protein synthesis and breakdown using aminoacyl-tRNA and other surrogate measures. Am. J. Physiol. - Endocrinol. Metab. 2006, 291 (4), E729–E736.

(53) Green, H. J.; Fraser, I. G.; Ranney, D. A. Male and female differences in enzyme activities of energy metabolism in vastus lateralis muscle. J. Neurol. Sci. 1984, 65 (3), 323–331.

(54) Russ, D. W.; Lanza, I. R.; Rothman, D.; Kent-Braun, J. A. Sex differences in glycolysis during brief, intense isometric contractions. Muscle Nerve 2005, 32 (5), 647–655.

(55) WHO | Proposed working definition of an older person in Africa for the MDS Project http://www.who.int/healthinfo/survey/ageingdefnolder/en/ (accessed Feb 8, 2017).

(56) Blagosklonny, M. V. Why men age faster but reproduce longer than women: mTOR and evolutionary perspectives. Aging 2010, 2 (5), 265–273.

(57) Strehler, B.; Hirsch, G.; Gusseck, D.; Johnson, R.; Bick, M. Codon-restriction theory of aging and development. J. Theor. Biol. 1971, 33 (3), 429–474.

(58) Timiras, P. S. Physiological Basis of Aging and Geriatrics, Fourth Edition; CRC Press, 2007.

(59) Soltow, Q. A.; Jones, D. P.; Promislow, D. E. L. A Network Perspective on Metabolism and Aging. Integr. Comp. Biol. 2010, 50 (5), 844–854.

List of Figures and Tables

Figure. 1 Clustering in the first two components of the PCA-CA models on NMR plasma metabolite concentration profiles of: A) male (blue dots) and female (pink dots); B) young (light blue) and old (dark blue) male subjects; C) young (light pink) and old (dark pink) female subjects. Discrimination accuracy obtained using kNN for each different model are given in table 1.

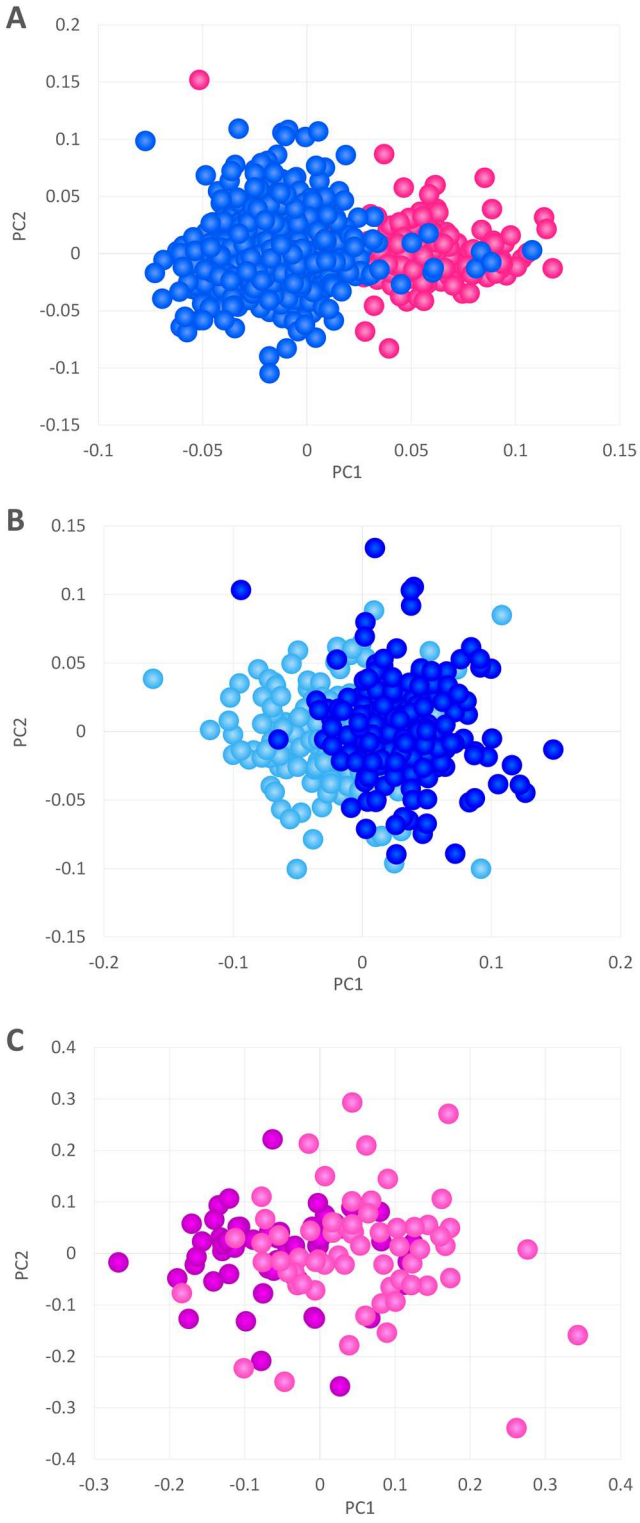

Figure. 2 Metabolite-metabolite association networks reconstructed from the plasma metabolite concentration profiles of: A) males; B) females; C) Young males; D) Young females; E) Old males and F) Old females. Vertexes are colored according to metabolite modularity.

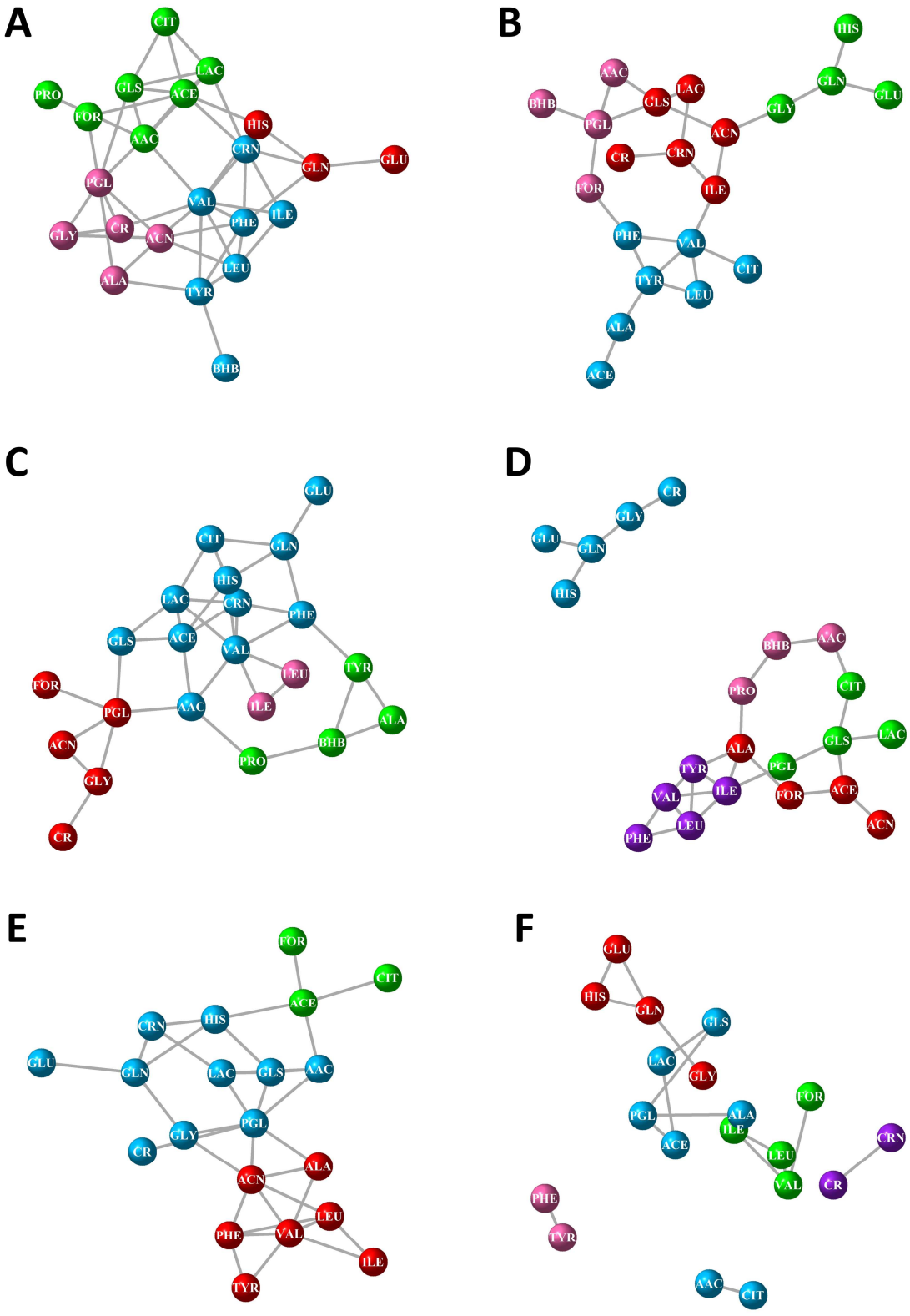

Figure. 3 Differences in metabolite connectivity (node degree) between A) males and females; B) young and old males and C) young and old females

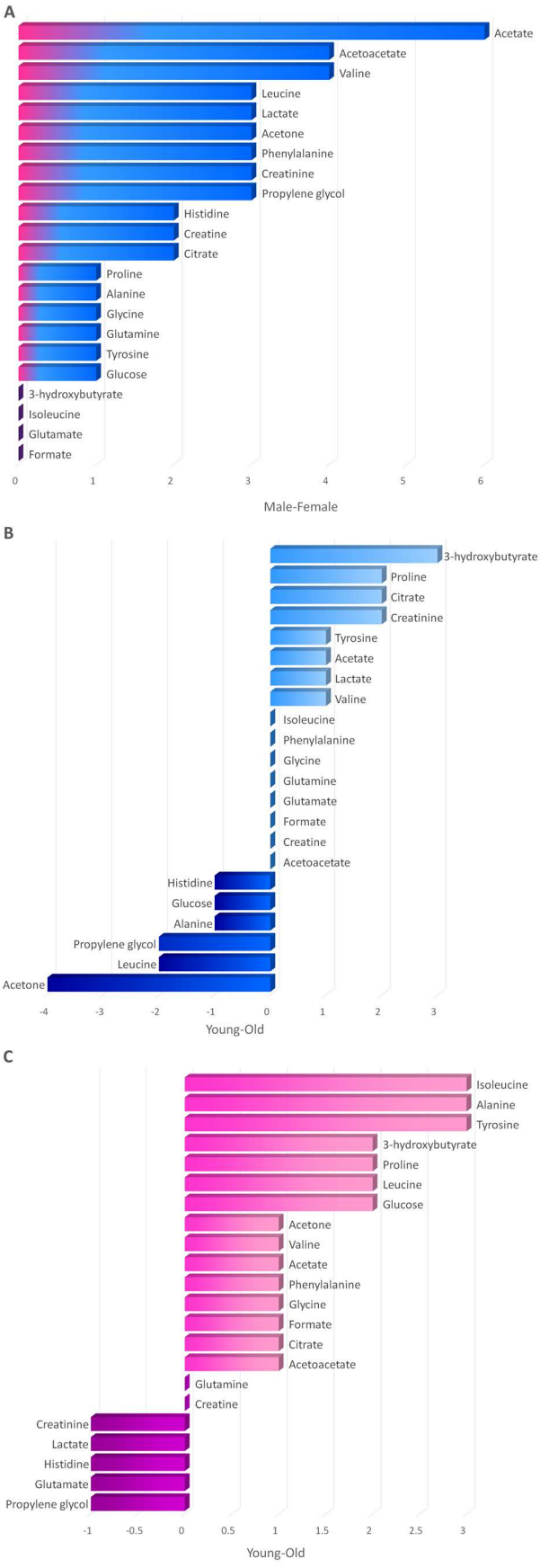

Table 1. The average Accuracy, Sensitivity and Specificity are given together with the standard error calculated over 102 repetitions of the Monte Carlo samplings. The significance (P-value) is assessed by mean of permutation test.

PCA-CA-kNN Model	Accuracy	Sensitivity	Specificity	*P-value*
Full CPMG NMR spectra				
Males *vs* Females	0.90±0.01	0.90±0.02	0.89±0.02	<0.01
Young *vs* Old Males	0.70±0.01	0.70±0.02	0.71±0.02	<0.01
Young *vs* Old Females	0.60±0.04	0.56±0.05	0.64±0.05	0.02
Quantified metabolites in CPMG NMR spectra				
Males *vs* Females	0.79±0.03	0.81±0.03	0.78±0.02	<0.01
Young *vs* Old Males	0.65±0.01	0.64±0.02	0.66±0.02	<0.01
Young *vs* Old Females	0.65±0.03	0.68±0.03	0.62±0.04	<0.01

Table 2. Pairwise comparison of plasma metabolite concentration in males and females using Wilcoxon test. A positive log2(FC) indicates higher concentrations in females.

	P-value	Adjusted P-value	Cliff's Δ	log2(FC)
3-hydroxybutyrate	5.83E-02	1.00E+00	-6.75E-02	0.00E+00
Acetate	3.30E-01	1.00E+00	-4.70E-02	-7.12E-02
Acetoacetate	8.50E-01	1.00E+00	-9.12E-03	7.29E-02
Acetone	1.65E-11	3.62E-10	-3.25E-01	-6.04E-01
Alanine	5.23E-03	1.15E-01	-1.35E-01	-8.61E-02
Citrate	3.80E-01	1.00E+00	4.24E-02	6.27E-02
Creatine	2.95E-23	6.48E-22	4.79E-01	9.33E-01
Creatinine	2.08E-52	4.58E-51	-7.35E-01	-4.40E-01
Formate	3.05E-02	6.70E-01	-1.04E-01	-5.18E-02
Glucose	7.96E-01	1.00E+00	-1.25E-02	-1.34E-03
Glutamate	1.77E-03	3.90E-02	-1.51E-01	-1.92E-01
Glutamine	3.93E-04	8.64E-03	-1.71E-01	-1.26E-01
Glycine	7.19E-01	1.00E+00	1.74E-02	8.34E-03
Histidine	1.58E-04	3.48E-03	-1.82E-01	-1.67E-01
Isoleucine	7.07E-29	1.55E-27	-5.38E-01	-3.48E-01
Lactate	9.91E-01	1.00E+00	5.54E-04	9.93E-03
Leucine	2.11E-29	4.65E-28	-5.43E-01	-3.19E-01
Phenylalanine	3.38E-05	7.45E-04	-2.00E-01	-8.79E-02
Proline	6.44E-05	1.42E-03	-1.93E-01	-1.59E-01
Propylene glycol	4.87E-10	1.07E-08	-3.00E-01	-2.41E-01
Tyrosine	4.41E-10	9.70E-09	-3.01E-01	-1.99E-01
Valine	1.05E-14	2.32E-13	-3.73E-01	-2.28E-01

Table 3. Significant results for pathway analysis performed on the sets of metabolites whose adjusted P-value were find statically significant between the groups.

Pathway Name	**Match Status**	***P*-value**	**Adjusted *P*-value**	**FDR**
Males *vs* Females				
Aminoacyl-tRNA biosynthesis	8/75	6.93E-10	5.55E-08	5.55E-08
Nitrogen metabolism	4/39	3.79E-05	3.00E-03	1.52E-03
Valine, leucine and isoleucine biosynthesis	3/27	3.34E-04	2.61E-02	8.91E-03
Arginine and proline metabolism	4/77	5.56E-04	4.28E-02	1.11E-02
Valine, leucine and isoleucine degradation	3/40	1.08E-03	8.24E-02	1.73E-02
D-Glutamine and D-glutamate metabolism	2/11	1.44E-03	1.08E-01	1.92E-02
Young *vs* Old Males				
Aminoacyl-tRNA biosynthesis	3/75	2.78E-04	2.22E-02	2.09E-02
Young *vs* Old Females				
Nitrogen metabolism	3/39	3.85E-05	3.08E-03	3.08E-03
Aminoacyl-tRNA biosynthesis	3/75	2.78E-04	2.20E-02	1.11E-02

Table 4. Significant results for pathway analysis performed on the sets of metabolites whose connectivity was found to vary (Δ ≥ 2) or being the same (Δ = 0) in the differential network analysis.

	Match Status	*P*-value	Adjusted *P*-value	FDR
Δ ≥ 2 Males *vs* Females				
Propanoate metabolism	4/35	1.71E-05	1.37E-03	1.37E-03
Synthesis and degradation of ketone bodies	2/6	3.38E-04	2.67E-02	8.66E-03
Aminoacyl-tRNA biosynthesis	4/75	3.56E-04	2.78E-02	8.66E-03
Pyruvate metabolism	3/32	4.33E-04	3.34E-02	8.66E-03
Valine, leucine and isoleucine degradation	3/40	8.44E-04	6.41E-02	1.35E-02
Δ ≥ 2 Young *vs* Old Males				
Synthesis and degradation of ketone bodies	2/6	7.74E-05	6.19E-03	6.19E-03
Arginine and proline metabolism	2/77	1.39E-02	1.00E+00	5.58E-01
Δ = 0 Young *vs* Old Males				
D-Glutamine and D-glutamate metabolism	2/11	5.24E-04	4.09E-02	1.40E-02
Δ ≥ 2 Young *vs* Old Females				
Aminoacyl-tRNA biosynthesis	5/75	5.15E-07	4.12E-05	4.12E-05
Valine, leucine and isoleucine biosynthesis	2/27	2.46E-03	1.94E-01	9.83E-02
Valine, leucine and isoleucine degradation	2/40	5.37E-03	4.19E-01	1.43E-01

Table 5. Pairwise comparison of plasma metabolite concentration in young and old male subjects using Wilcoxon test. A positive log2(FC) indicates higher concentrations in young male.

	P-value	Adjusted P-value	Cliff's Δ	log2(FC)
3-hydroxybutyrate	1.97E-01	1.00E+00	-5.21E-02	0.00E+00
Acetate	1.15E-03	2.53E-02	1.72E-01	1.60E-01
Acetoacetate	5.32E-01	1.00E+00	-3.32E-02	4.33E-02
Acetone	5.25E-02	1.00E+00	-1.03E-01	-2.26E-01
Alanine	1.15E-04	2.54E-03	-2.04E-01	-1.27E-01
Citrate	1.00E-02	2.20E-01	-1.36E-01	-9.21E-02
Creatine	1.88E-05	4.13E-04	-2.27E-01	-3.91E-01
Creatinine	2.98E-01	1.00E+00	5.51E-02	4.07E-02
Formate	2.10E-01	1.00E+00	6.64E-02	3.74E-02
Glucose	3.07E-03	6.76E-02	-1.57E-01	-5.91E-02
Glutamate	3.09E-01	1.00E+00	5.39E-02	1.01E-01
Glutamine	7.12E-02	1.00E+00	-9.56E-02	-7.56E-02
Glycine	4.00E-02	8.80E-01	1.09E-01	6.69E-02
Histidine	1.98E-04	4.36E-03	1.97E-01	1.65E-01
Isoleucine	9.44E-01	1.00E+00	3.71E-03	4.63E-04
Lactate	5.78E-01	1.00E+00	-2.95E-02	-2.73E-03
Leucine	1.26E-01	1.00E+00	8.12E-02	2.88E-03
Phenylalanine	9.38E-01	1.00E+00	-4.13E-03	-2.17E-02
Proline	5.28E-01	1.00E+00	3.34E-02	7.14E-03
Propylene_glycol	8.33E-02	1.00E+00	9.18E-02	6.71E-02
Tyrosine	1.99E-04	4.38E-03	-1.97E-01	-1.24E-01
Valine	1.82E-01	1.00E+00	7.07E-02	3.50E-02

Table 6. Pairwise comparison of plasma metabolite concentration in young and old female subjects using Wilcoxon test. A positive log2(FC) indicates higher concentrations in young female.

	P-value	Adjusted P-value	Cliff's Δ	log2(FC)
3-hydroxybutyrate	7.52E-01	1.00E+00	2.14E-02	0.00E+00
Acetate	1.72E-01	1.00E+00	-1.41E-01	-1.96E-01
Acetoacetate	5.42E-03	1.19E-01	-2.87E-01	-3.43E-01
Acetone	6.57E-01	1.00E+00	-4.61E-02	-4.77E-02
Alanine	3.31E-03	7.28E-02	-3.04E-01	-2.40E-01
Citrate	2.74E-02	6.03E-01	-2.28E-01	-9.92E-02
Creatine	3.33E-07	7.33E-06	-5.27E-01	-7.54E-01
Creatinine	7.55E-01	1.00E+00	-3.25E-02	2.62E-02
Formate	7.77E-01	1.00E+00	-2.95E-02	-7.13E-02
Glucose	6.60E-04	1.45E-02	-3.52E-01	-1.49E-01
Glutamate	9.69E-01	1.00E+00	4.28E-03	1.69E-01
Glutamine	1.26E-03	2.77E-02	-3.33E-01	-2.21E-01
Glycine	7.00E-06	1.54E-04	-4.64E-01	-2.58E-01
Histidine	6.03E-02	1.00E+00	-1.94E-01	-1.75E-01
Isoleucine	7.33E-01	1.00E+00	3.55E-02	7.60E-03
Lactate	3.01E-01	1.00E+00	-1.07E-01	-1.72E-01
Leucine	3.27E-01	1.00E+00	-1.02E-01	-6.79E-02
Phenylalanine	1.93E-01	1.00E+00	-1.35E-01	-9.14E-02
Proline	4.32E-01	1.00E+00	-8.14E-02	-1.53E-02
Propylene glycol	3.59E-01	1.00E+00	-9.50E-02	-6.36E-02
Tyrosine	1.57E-03	3.45E-02	-3.27E-01	-3.19E-01
Valine	2.99E-01	1.00E+00	-1.08E-01	-7.38E-02

Supplementary materials

Supplementary Figure 1. Age distribution for: A) Female; B) Male. Median age, mean age and standard deviation are also reported.

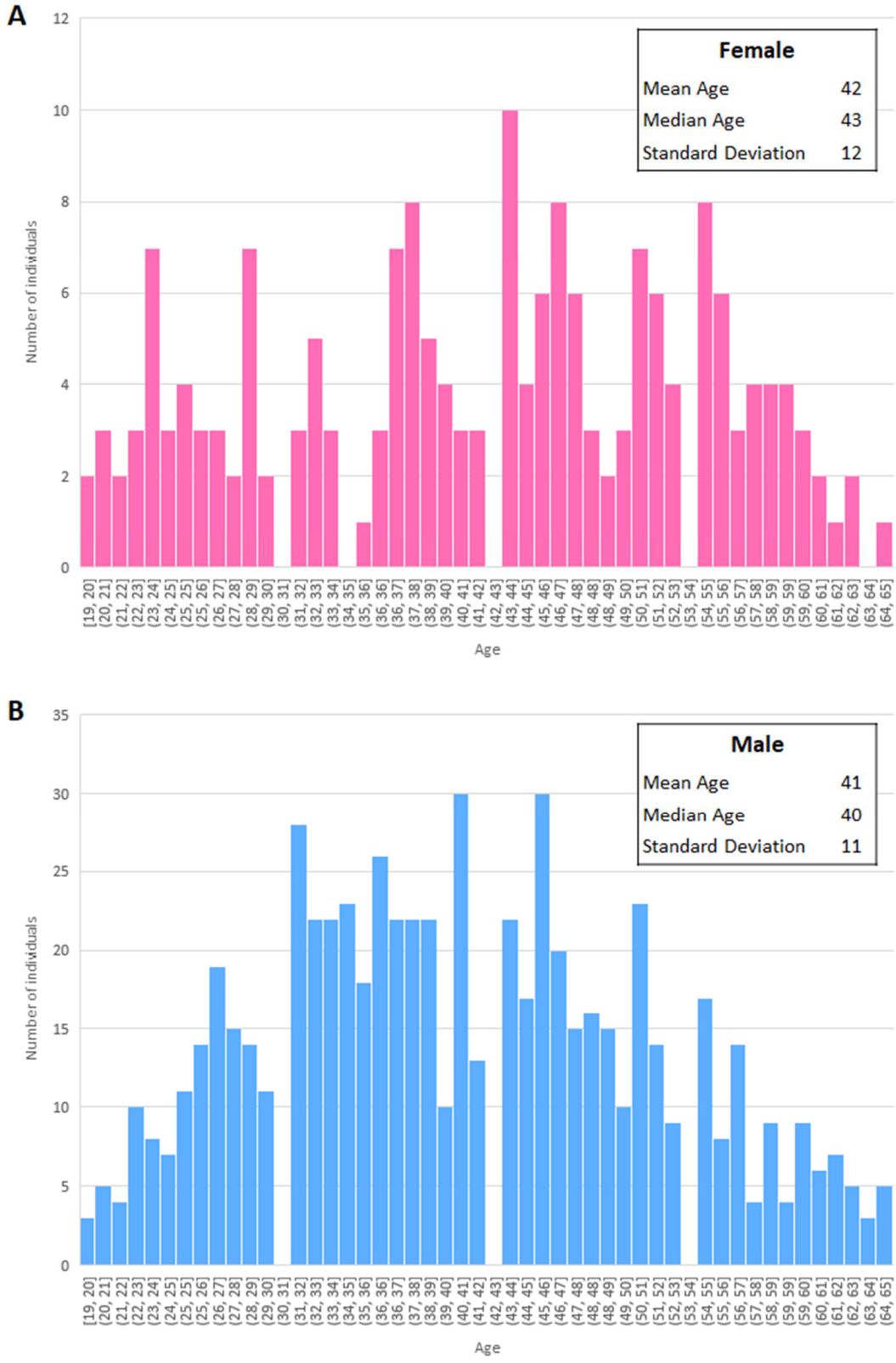

4.3.2 *Muscle in Space – Shall the Force be with Us?*

Jörn Rittweger[1,2], Kirsten Albracht[3], Martin Flück[4], Severin Ruoss[4], Lorenza Brocca[5], Emanuela Longa[5], Manuela Moriggi[6], Olivier Seynnes[7], Irene Di Giulio[8], Leonardo Tenori[9], Alessia Vignoli[10], Miriam Capri[11], Cecilia Gelfi[12], Claudio Luchinat[10], Claudio Francheschi[11], Roberto Bottinelli[5], Paolo Cerretelli[6], Marco Narici[13]

1 Institute of Aerospace Medicine, German Aerospace Center (DLR), Cologne, Germany
2 Department of Pediatrics and Adolescent Medicine, University of Cologne, Cologne, Germany
3 Faculty of Medical Engineering and Technomathematics, FH Aachen University of Applied Sciences, Aachen, Germany
4 Department of Orthophedics, University of Zürich, Zürich, Switzerland
5 Institute of Human Physiology, University of Pavia, Pavia, Italy
6 CNR-IBFM, Segrate (MI), Italy; CONI, Roma, Italy
7 Department of Physical Performance, Norwegian School of Sport Sciences, Oslo, Norway
8 Centre of Human and Aerospace Physiological Sciences, King's College London, London, United Kingdom
9 Department of Experimental and Clinical Medicine, University of Florence, Italy
10 CERM Centro di Ricerca di Risonanze Magnetiche, Florence, Italy
11 Department of Experimental, Diagnostic and Specialty Medicine, University of Bologna, Bologna, Italy
12 Department of Biomedical Sciences for Health, University of Milan, Milano, Italy
13 School of Graduate Entry Medicine and Health, University of Nottingham, Nottingham, United Kingdom

Working draft

Candidate's contributions: acquisition of NMR data, statistical analysis and interpretation of data, writing and review of the metabolomic section of the manuscript.

Muscles in Space – Shall the Force be with Us?

Introduction

Physical deconditioning has been known to occur as a result of space flight since the days of Skylab and Mir studies. Lower limb muscles, in particular, undergo rapid wasting (1) and loss of function (2). Most affected is the triceps surae muscle (3), where 20% fiber atrophy occur after 6 months of space flight (4). In the ground-based models of spaceflight (e.g. bedrest), this muscle wasting is associated with decreases in the fascicles' pennation angle and length (5, 6). Alterations of muscle architecture directly affect the mechanical output and therefore are potential contributors to muscle weakness. Moreover, immobilization is also leading to reductions in the muscle fibers' specific force and power, and to reductions in myosin heavy chain (MCH) concentration (7). All of these factors can independently alter the mechanical characteristics of the lower limb muscles and hamper force output.

Countermeasure exercises on board the international space station (ISS) are nowadays mandatory for the crew. Countermeasures aiming at muscle involve exercises with the advanced resistive exercise device (aRED) and the treadmill with vibration isolation system (TVIS). Effects of strength training upon skeletal muscle on Earth have been studied extensively (8), but relatively little is known about the molecular events in disuse or in spaceflight. It is therefore an open question in how far the training loads in space are helpful to maintain the lower limb musculature. As a window into the muscle's loading history, we were interested in the behavior of the costameric proteins (9-15), which anchor the sarcomeres to extracellular matrix (ECM) receptors (16-18). Integrin-linked focal adhesion kinase (FAK) is a mechanically regulated costamere component that controls the turnover of focal adhesion in a fiber type-specific manner together with its natural inhibitor FRNK (13, 16, 19). Herein, the content of post-translation modification of tyrosine 397 (Y397) is a critical event, which is affecting the activity of FAK (20-22).

Thus, the Sarcolab study has been designed to 1) disentangle the various constituents of muscle weakness, to 2) elucidate the myotendinous and neuromuscular adaptations to long-term spaceflight, and to 3) address the molecular and metabolic pathways in skeletal muscle and in the blood affected in astronauts during their missions on the international space station (ISS). The general hypothesis of the Sarcolab study is that both alterations in the physiological cross section as well as in single fiber mechanics are involved in the space-related muscle weakness. Moreover, the study also aims to assess messenger RNA and proteomic data in order to generate new hypotheses, and to screen for systemic consequences related to muscle metabolism. After initial data assessment in two astronauts, the study has now been enlarged into a 3-agency study

(Sarcolab-3). The present paper now highlights the salient findings from the two astronauts of the Sarcolab pilot study.

Results

Analyses on the two astronaut enrolled in this study (crew member A and B) were performed at three time points: before the space flight (baseline), at post-flight 1 (PF-1, at 0 to 4 days after landing) and at post-flight 2 (PF-2, at 15 days after landing).

On-board Exercise Training: Crew member A performed fewer treadmill sessions than B (90 vs. 114), ran with lower pull-down force (median of 55.9% vs 85.6% of body weight), ran at slower speed (median 11.3 vs. 12.9 km/hr), and covered a shorter distance than B, both per running session (median 4.7 vs. 5.8 km) as well as cumulated for the 6-month space sojourn (442 vs. 572 km, Figure 1). Crew member A also trained less with the aRED, performing fewer heel raise sessions (54 vs. 98) with fewer repetitions (median 30 vs. 48) and at lower resistive load (median 122% vs. 221% of body weight). Thus, B was generally training more vigorously than A, which was in particular true for the resistive elements of the countermeasure exercises.

Muscle function: During post-flight session 1 (PF-1, performed 0 to 4 days after return to Earth), plantar flexor muscle strength was reduced by 30.6% in crew member A, whereas B depicted little or no change from baseline (Figure 2). However, very notably, the rate of force development was profoundly compromised in both crew members, and perhaps even more so in B, during both post-flight testing sessions.

Muscle size and architecture: Volume, pennation angle and fascicle length were all substantially reduced in the medial gastrocnemius (GM) muscle at PF-1 in crew member A (Table 1). Such changes were much less pronounced in B. However, the physiological cross-sectional area (pCSA) was affected to comparable extent in both crew members at PF-1 (Table 1). At PF-2, pCSA of the GM muscle had recovered in B, but not in A.

Fiber type, fiber size & fiber mechanics: As expected for soleus muscles, the analysis of myosin heavy chain isoform (MHC) distribution showed almost homogeneous MHC-1 content in the samples of both crew members. No shift in MHC relative content was observed post flight. Cross sectional area of individual muscle fibers (CSA_SF) declined at PF-1 in crew member A by -45%, but only by -23% in B (Figure 2).

Functional analysis could be performed pre- and post-flight in crew member A only. All fibers analyzed contained MHC-1, i.e. were type 1 fibers. As expected, specific force (Po/CSA) was lower post-flight than pre-flight (-27%), but unloaded shortening velocity (Vo) was unchanged. Interestingly, actin sliding velocity (Vf) on myosin extracted from single muscle fibers of crew member A was not different pre- vs post-

flight. Taken together, Vo and Vf finding suggest no alteration in the acto-myosin kinetics post-flight and no alteration of myosin at molecular level.

Skeletal muscle proteomic analysis: From 1100 spots detected in the 2D-DIGE gel, 900 were included in the base set for statistical analysis. The Principal Component Analysis (PCA) of the muscle tissue from both crew members provided an overview of spot distributions and yielded two components (PCA1 and PCA2) that explain 59.2% and 25.9%, respectively, of the global variation (supplementary Figure 1). Interestingly, differences between baseline and PF-1 are concordant for both crew members with regards to PCA2. However, the differences between baseline and PF-2 were discordant between crew members with regards to PCA1; the protein data set at PF-2 appears more similar to baseline in crew member B.

Proteomic analyses followed by paired one-way ANOVA and Tukey tests ($\alpha = 0.01$) indicated significant differences between baseline and PF-1 in 32 and 39 spots in crew member A and B, respectively. When comparing baseline to PF-2, 37 spots were changed in crew member A and 24 spots were changed in crew member B (Figure 3).

Concerning contractile proteins, PF-1 samples revealed alterations in troponin I and troponin T in both crew members, but only crew member B revealed some moderate changes in Actin and tropomyosin. More specifically, crew member A demonstrated distinct increases in troponin I fast (TNNI2) and in two proteoforms of troponin T fast (TNNT3), and decreases in two proteoforms of troponin T slow (TNNT1). Notably, where PF-1 changes in the troponins were observed in B, they were in the opposite direction in crew member A. At PF-2, some moderate decreases in Actin proteoforms (ACTA1) were observed in both crew members.

Proteins involved in anaerobic metabolism were also affected by space flight. In crew member A there were decreases in four different proteoforms of glycogen phosphorylase (PYGM) at PF-1, as well as increases in glycerol-3-phosphate dehydrogenase (GPDI) and one beta-enolase proteoform (ENO3). By contrast, B depicted increases in glyceraldehyde-3-phosphatase dehydrogenase (GAPDH), phosphoglycerate mutase 2 (PGAM2), alpha-enolase (ENO1), three proteoforms of ENO3 and pyruvate kinase (PKM). At PF-2, two of the PYGM proteoforms were recovered in A, but decreases in two proteoforms of fructose-bisphosphate aldolase A (ALDOA) and L-lactate dehydrogenase A chain (LDHA) occurred at that time. Thus, dysregulation of glycogen metabolism and accumulation of specific enolase proteoforms appeared and persisted post-flight in crew member A, whereas crew member B adapted metabolically to space flight by increasing anaerobic metabolism.

Concerning aerobic metabolism, enzymes involved in malate shuttle, in oxidative phosphorylation and in lipid metabolism were down-regulated in both crew members at PF-1 and persisting at PF-2. In crew member A, this encompassed virtually all enzymes, except for NADH dehydrogenase iron-sulfur protein 3 (NDUFS3) was up-regulated. Crew member B depicted a very similar response as A, except that NDUFS3

was down- rather than up-regulated. Thus, aerobic metabolism seemed comparably compromised in both crew members.
Enzymes involved in high energy phosphate transfer likewise depicted a down-regulation in both crew members post-flight. This was more pronounced in crew member A than B, and A also tended to better recover these changes at PF-2. The enzymes affected involved four proteoforms of creatine kinase M-type (CKM) and creatine kinase S-type (CKMT2). Thus, the dysregulation of enzymes involved in high energy phosphate production appeared to be a consequence of the severe impairment of aerobic metabolism.

Costameric protein expression: All costameric proteins of interest were detectable in soleus muscle at baseline (Supplementary Figures 2 to 4). Gamma-vinculin was more abundant than meta-vinculin (Supplementary Figure 2). At PF-1, protein concentrations of FAK (normalized to actin) was reduced in crew members A and B by -60% and -44%, respectively, and FRNK by -60% and -67 (Table 2, Supplementary Figure 3). By contrast, FAK and FRNK concentrations were both increased above baseline levels at PF-2 (Table 2, Supplementary Figure 3). Importantly, FAK-pY397 concentration was reduced in crew member A at PF-1, but increased in B (Supplementary Figure 3). These findings suggest that loading forces in space were near-normal in crew member B, but substantially reduced in A.
Concentration of the meta-vinculin proteoform and tenascin-C was increased at PF-1 in crew member A by 786% and 2781% respectively, but both were slightly reduced in crew member B (Supplementary Figures 2 and 4). At PF-2, these proteins resumed to near baseline levels in crew member A, but were increased in crew member B (Supplementary Figure 2). The concentration of gamma-vinculin was only marginally affected by space flight (Table 2).
The meta-vinculin:gamma-vinculin ratio was comparable in crew members A and B at baseline (0.06 vs. 0.06). It depicted 8-fold and 5-fold increases in crew member A at PF-1 and PF-2, respectively, but no changes in crew member B (Supplementary Table 1). The FRNK:FAK ratio, by contrast, was greater at baseline in crew member A than in crew member B (2.01 vs. 0.58). It was unchanged in crew member A after spaceflight, but depicted a moderate decrement in B.

Intracellular signaling pathways controlling muscle mass and metabolism: The response to spaceflight of the two major catabolic systems was studied on mRNA level in both crew members by assessing expression of MuRF-1 and atrogin-1, the two major markers of the ubiquitin proteasome activity, and of p62 and Beclin-1, two of the markers of activity of autophagy. Whereas atrogin-1 expression was upregulated post-flight in both crew members, MuRF-1 expression was highly up-regulated in crew member A, but not in crew member B. Beclin-1 was upregulated in both crew members post-flight, whereas p62 was up-regulated in crew member A only.

At PF-2, expression of all of these markers was lower than at PF-1. In crew member A, recovery towards normal activation was somewhat less complete, especially for Murf-1. The results suggest a higher activation of both catabolic systems and a slower recovery towards normal values in crew member A.
PGC-1alpha is a master controller of mitochondrial biosynthesis and oxidative metabolism. It was surprisingly up-regulated post flight in both crew members and did not go back to normal expression even at PF-2. SREBP-1 is a transcription factor controlling lipid synthesis. It was upregulated in crew member B only.
NRF2 is a transcription factor involved in the response to injury and inflammation, and thus also in sensing the level of intracellular ROS and stimulates synthesis of antioxidant defense systems. Its increase occurred in crew member B only. No complete recovery of pre-flight expression was observed at PF-2.

Plasma Metabolomics: Twenty metabolites were assigned and quantified in the spectra, the levels of the statistically significant metabolites (plasma amino acids, glucose, lactate, pyruvate, and pyruvate/lactate ratio) are reported along with their *P*-values in Figure 4, compared with a cohort of control subjects. All metabolite levels investigated at baseline were comparable with the control group, except for isoleucine that was elevated and alanine that was at the upper control margin at PF-1 in crew member A. Serum alanine was increased in this crew member post flight (in both PF-1 and PF-2 $P < 0.01$), but, conversely from isoleucine, was not normalized at PF-2. Moreover, crew member A depicted elevated serum levels of glucose and pyruvate, as well as an elevated pyruvate-lactate ratio on day PF-1 (all $P < 0.01$).
In crew member B, serum levels were generally within the control margins. The only exceptions were alanine, phenylalanine and tyrosine, which were all increased at PF-1 ($P < 0.01$), but not at PF-2.

Discussion

The present study provides a comprehensive account of how different two different individuals can respond to the same stimulus of spaceflight. Whilst crew member A exhibited the expected neuromuscular responses, namely decrements in plantar flexor muscle volume, altered architecture, reductions in contractile protein composition, downgraded fiber contractility, and thus overall muscle strength, crew member B was much less affected after 6 months in Space. It has to be considered here that the loading levels achieved by crew member B are rarely achieved by other crew members in Space. It is therefore tempting to ascribe the salient differences between A and B to the loading forces. Moreover, it seems reasonable to ascribe the divergent muscle proteomic responses in both crew members (contractile proteins & aerobic metabolism affected in crew member A, but almost not in B), as well as differences in the systemic metabolic profiles (greater effects upon energy and protein metabolism

in A than in B) to the different countermeasure regimens. These findings therefore demonstrate the partial effectiveness of current ISS countermeasures. However, the 23% decrement in muscle fiber CSA that was still occurring in crew member B, the fact that rate of torque development, aerobic metabolism as well as high phosphate energy transfer were still compromised in crew member B suggest that complete preservation of the musculature in Space is not yet achievable.

It is also intriguing that the response of the two load-dependent parameters, pY397-FAK and meta-vinculin concentration (12, 13) reflected the diverging responses of the two crew members in muscle mass and strength, but not FAK or FRNK. Explaining these differences by the loading during on-board countermeasure exercises seems straightforward, and thereby corroborate the idea of a load-regulated costamere turnover that is mediated by the FAK system.

By contrast, expression of FAK and FRNK proteins demonstrated a consistent down-regulation at PF-1. These replicates earlier findings in anti-gravity muscles of rats and human (11-13), implicating a requirement of gravitational loading for maintaining the expression of the gene products of the FAK gene (i.e. PTK2). It has been previously demonstrated that immobilization-related decrement in pY397-FAK is related to a reduction of FAK content at the sarcolemma (12), while pY397-FAK concentration during recovery from immobilization remains low independent of alterations in FAK protein (12). The present novel observations support that the phenomenon of muscle unloading is associated with a net reduction in the capacity for regulation of costamere turnover (10). Consistently with this notion, the concentration of both FAK and FRNK, in vastus lateralis muscle increased two weeks after return to Earth being indicative of regulation towards a reestablishment of adhesion sites in the sarcolemma with return of load-bearing muscle activity.

Alterations in the costameric factors FAK-pY397 and meta-vinculin were associated with alterations in tenascin-c expression, which typically is up-regulated by muscle loading (23, 24) (compare supplementary Figures 2 to 4). All these factors were considerably less affected in crew member B, who experienced greater loading during on-board exercising (Figure 1). Collectively the tenascin-C alterations suggest a protection of the soleus muscle in crew member one to the injuring consequence of high forces during reentry into the gravitational field of the Earth .

Surprisingly, the present results did not show a shift in MHC isoform content toward a fast phenotype, and likewise no increase in Vo of individual muscle fibers. Thus, no compensation for the lost muscle mass could be provided by these mechanisms. Notably, the muscle wasting appears to be at least partly due to activation of muscle proteolysis, i.e. through activation of ubiquitine proteasome and autophagy. This interpretation is also supported by the observation that crew member A had greater activation of these catabolic pathways than crew member B after spaceflight.

It is a bit surprising to see that muscular aerobic metabolism was affected in both crew members, given the time and distance covered during treadmill exercise. Moreover, the

increase in pGC-1alpha expression in both crew members is somewhat counterintuitive, as a down-regulation following disuse in soleus muscle of mice (25) and in VL muscle of humans (26) have been previously observed. The lower expression of PGC-1alpha has been considered a relevant cause of muscle atrophy in disuse (25-27). The origin of the higher expression of PGC-1alpha following space-flight is unclear. It could be due to reloading after flight and before biopsy. An alternative possibility is that the countermeasures in flight successfully prevented PGC-1alpha down-regulation, possibly preventing metabolic alterations in muscle too. PGC-1alpha is believed to be responsible for the metabolic response to endurance training.

It is also of interest that SREBP1 expression was increased in the soleus muscle in both crew members after space flight. As SREBP1 is a master control of lipid metabolism and increases lipid synthesis, it seems possible that weightlessness may increase intramuscular lipid accumulation. Furthermore, it is interesting that NRF2, a transcription factor sensitive to intracellular ROS and simultaneously a stimulator of antioxidant defense systems, was elevated in crew member B but not in crew member A. Redox imbalance could be expected on the basis of previous observations in humans (Dalla Libera et al) (26) and mice (25). However, to see the NRF2 increment in crew member B only speaks against a higher redox imbalance as a side-effect of muscle atrophy. An alternative explanation might be that NRF2 increase is a compensatory antioxidant response in crew member B, which does not occur in crew member A.

Pronounced differences between the two crew members were also present in their metabolomic profiles. Whilst post-flight changes in crew member B can be related more to energy metabolism than to aminoacids metabolism, the opposite was true for crew member A. Previous reports suggest that myofibrillar breakdown (assessed via urine 3-methylhistidine) is un-affected by spaceflight (28), which was also confirmed in the present study (data not shown). Moreover, the increases of glucose, pyruvate and pyruvate/lactate ratio in crew member A can be understood as the metabolic consequences of muscle wasting, and it has been proposed that muscle disuse atrophy shifts metabolism towards glycolysis and gluconeogenesis (29). Interestingly, both crew members' metabolic profiles appeared distinct already before launch: PCA showed that the two crew members were located in different regions of the metabolic distribution space before the space mission; then, they responded to the space mission stress, even if in two different ways, moving toward different positions at PF-1, and finally both reverted to their initial metabolic spaces at PF-2 (Supplementary Figure 5). This behavior is consistent with the observed metabolic resilience already described in urine of healthy controls (30).

In conclusion, this observational study in two ISS crew members has shown that single fiber mechanics seems to be a better explanation for post-flight muscle weakness than muscle architecture. However, the present data still support an important contribution to muscle strength by muscle size and architecture. Countermeasure exercises seem to have been remarkably effective in crew member B, albeit not fully. Altogether, results

indicate a crucial role for force loading to constitute effective on-board exercises. Finally, proteomic assessment of muscle tissue and metabolomic blood analyses have greatly helped to widen the view in this study, and to understand that exercise may have benefits in space that go far beyond mere maintenance of muscle mass.

Methods

Subjects and testing schedule: Two crew members of equal sex, A and B, were tested pre-flight and post-flight (Supplementary Table 2), and in between accomplished their ISS mission of 6 months, respectively. Information on in-flight countermeasure exercise performance on advanced resistive exercise device (aRED) and on the T2 Colbert treadmill was obtained via data sharing with NASA. For the heel raise exercises on aRED, the total number of repetitions was computed, and the peak and average load during each session was selected and normalized to body weight. For T2 treadmill exercises, the distance, speed, exercise time and the bungee load at rest were extracted. Two-way ANOVA was performed to test for time effects and differences between astronauts.

Metabolomic profiles: for the control cohort, plasma samples were collected from 79 healthy volunteers from two centers, 56 of which collected in collaboration with the Tuscanian section of the Italian Association of Blood Donors (AVIS) in the Transfusion Service of Pistoia Hospital (Ospedale del Ceppo, AUSL 3 - Pistoia, Italy), and 23 samples were from young healthy subjects collected in Bologna (in the framework of the project PRIN2009CB4C9F with ethical approval EM 157/2011/U at S.Orsola-Malpighi hospital, Bologna). Specifically, 6 healthy volunteers were recruited at 4 different times (up to 7 months, one dropped out at a specific time, thus 23 samples were obtained). No differences in the time series were evidenced (data not shown) and all samples were merged to obtain a more heterogenous population.

Muscle biopsy: Approximately 50 mg of tissue were harvested from the soleus muscle with a 11G ACECUT automatic biopsy system (TSK Laboratory, Oisterwijk, the Netherlands). A lateral approach was chosen approximately 2 cm below the distal end of the lateral gastrocnemius muscle. Before the incision, the skin was razed and disinfected appropriately, and 2 mL of local anesthetic (Lidocain 1%) was injected into the skin and the fascia. Samples were divided, shock-frozen in liquid nitrogen and aliquoted within 10 min after the biopsy.

Costameric protein biochemistry: Biopsies were sectioned and protein was extracted with the help of a rotorstat mixer (Kinematica, Lucerne, Switzerland) using RIPA buffer, and total protein quantified essentially as described (13). Homogenate corresponding to 10 microgram total protein was separated on 7.5% SDS-PAGE gels,

blotted onto nitrocellulose membrane and subjected to immunological protein detection as described (13) using the following antibodies: 1: 1000 dilution of polyclonal FAK antiserum Lulu (16), 1:500 of monoclonal Tenascin-C serum B28:13 (31), 1:100 of monoclonal antiserum against gamma-vinculin and meta-vinculin (gift of Dr. M. A. Glukhova, Paris, France) (13). Detection of pY397-FAK content was carried out based on immune-precipitation of soluble proteins in homogenate corresponding to 1 mg total protein essentially as described (13). Samples being derived from the three samples of each subject were analyzed in adjacent lanes of the same SDS-PAGE gel. Equal loading and blotting was verified based on the signal intensity of the actin band on the Ponceau S-stained nitrocellulose membrane after blotting signal intensity was assessed from background-corrected band intensities using PxI system (Syngene) as described (32).

Skeletal muscle proteomics: Protein extraction: for 2-dimensional difference in gel electrophoresis (2D-DIGE) and immunoblot assays, each sample from each subject was suspended in lysis buffer (7 M urea, 2 M thiourea, 4% CHAPS, 30 mM Tris, and 1 mM PMSF) and solubilized by sonication on ice. Proteins were selectively precipitated using PlusOne 2D-Clean up Kit (GE Healthcare, Little Chalfont, UK) in order to remove non protein impurities, and re-suspended in lysis buffer. The pH of the protein extracts was adjusted to pH 8.5 by addition of 1 M NaOH. Protein concentrations were determined by PlusOne 2D-Quant Kit (GE Healthcare). 2D-DIGE: Protein minimal labeling with cyanine dyes (Cy3 and Cy5), 2D separation, and analyses were performed as described previously (for crew members A and B; SOL biopsy pre-flight, immediately post-flight and 15 days post-flight) (15). Briefly, proteins extracted (50 μg) from each individual samples were labeled with Cy5, while internal standards were generated by pooling (50 μg) individual samples that were Cy3-labeled. Samples were separated on 3–10 nonlinear immobilized pH gradient (IPG) strips; the adopted gradient enables separation of protein isoforms in the first dimension, providing a detailed pattern of the muscle proteome. Each individual sample was run in triplicate (analytical replicates) to minimize the inter-gel variability and to increase the reliability of the results. Image analysis was performed using DeCyder 7.0 software (GE Healthcare). Statistically significant differences of 2D-DIGE data were computed by paired one-way ANOVA coupled to Tukey's multiple group comparison test; the significance level was set at $p < 0.01$. In addition, the false discovery rate (FDR) was applied as a multiple testing correction method to keep the overall error rate as low as possible (Hochberg, Y. B. Y. (2000). Educ. Behav. Stat. 25, 60–83). Two independent analyses were performed. Proteins of interest were identified by mass spectrometry. Protein identification by mass spectrometry: proteins were identified by peptide mass fingerprinting (PMF) utilizing a matrix-assisted laser desorption/ionization (MALDI) time-of-flight (ToF) mass spectrometer (Ultraflex III ToF/ToF; Bruker Daltonics, Bremen, Germany), as previously described (33). In particular, search was carried out

by correlation of uninterpreted spectra to Mammalia entries in NCBInr 20090430 database (8 483 808 sequences; 2 914 572 939 residues). In cases where this approach was unsuccessful, additional searches were performed using electrospray ionization-MS/MS, as previously described (34).

Metabolomics: Blood sampling was obtained both from astronauts and control cohort. Ethylenediaminetetraacetic acid (EDTA) was always used as anticoagulant, but the effects of its presence were eliminated as previously described (35). Frozen plasma samples were thawed at room temperature, shaken before use, and NMR samples were prepared according to the standard operating procedures (36) . A total of 300 µL of a sodium phosphate buffer (10.05 g $Na_2HPO_4 \cdot 7H_2O$; 0.2 g NaN_3; 0.4 g sodium trimethylsilyl [2,2,3,3-$2H_4$]propionate (TMSP) in 500 mL of H_2O with 20% (v/v) 2H2O; pH 7.4) was added to 300 µL of each plasma sample, and the mixture was homogenized by vortexing for 30 s. A total of 450 µL of this mixture was transferred into a 4.25 mm NMR tube for the analysis.

^1H NMR spectra were acquired at 310 K using a Bruker 600 MHz spectrometer (Bruker BioSpin): water suppressed Carr–Purcell–Meiboom–Gill (CPMG) (37) spin echo pulse sequence (RD-90°-(τ-180°-τ)n-acq) with a total spin echo (2nτ) of 80 ms was used in order to obtain monodimensional 1H NMR spectra in which broad signals from high molecular weight metabolites (i.e. proteins and lipoproteins) are attenuated. 64 FID were collected into 73728 data points over a spectral width of 12019 Hz, with a relaxation delay of 4 s and acquisition time of 3.1 s. Free induction decays were multiplied by an exponential function equivalent to a 1.0 Hz line-broadening factor before applying Fourier transformation. Transformed spectra were automatically corrected for phase and baseline distortions and calibrated (anomeric glucose doublet at 5.24 ppm) using TopSpin 3.2 (Bruker Biospin GmbH, Germany).

All metabolomic data analyses were performed using R (40). The spectral regions related to metabolites were assigned in the ^1H-NMR profiles by using matching routines of AMIX 3.8.4 in combination with the BBIOREFCODE (Bruker BioSpin GmbH, Germany), freely available datasets (e.g. the Human Metabolome DataBase -HMDB-Wishart et al.,(41, 42)), and published literature when available. Metabolite concentrations in arbitrary units were obtained integrating the related spectral regions. Principal component analysis (PCA) was used as a first unsupervised exploratory analysis to compare metabolic profiles of astronauts and healthy volunteers, monitoring how the two astronaut profiles move in the PCA metabolic space at the three different time points; moreover, PCA enables the assessment of the homogeneity or the presence of any outliers in plasma samples of volunteers that come from two different collection centers.

For the univariate statistical analysis, the concentrations of each metabolite in the astronaut samples were compared with the healthy volunteers distributions using a modified Z-score calculated on Median Absolute Deviation (MAD), on the biological

assumption that metabolite concentrations are not parametrically distributed (43). P-values < 0.01 were deemed significant and P-values < 0.05 near-significant.

Acknowledgments
The study has been supported by the European Space Agency, with great help from Patrik Sundblad, Simone Thomas and Marine le-Gouic. Peter Gauger and Wolfram Sies have been instrumental in preparation of human testing devices. Asa Beijer has helped with pre-processing of the muscle samples.

Competing interests
The authors declare no conflicts of interest.

Contributions
R.B., P.C., and M.N. designed the study. Human physiology experiments were performed by J.R., K.A., O.S., I.D.G., and M.N.. Laboratory analyses were performed by M.F., L.B., E.L., M.M., C.M., M.C., A.V., L.T., C.L., and C.G.. J.R., R.B. and M.N. wrote the manuscript with input and editing from all authors.

Funding
The study was supported by internal funding from DLR (cost object 2475 115 'effects of microG'). The study was supported by RFO (Ricerca Fondamentale Orientata) funds to MC.

References
1. Convertino VA. Physiological adaptations to weightlessness: Effects on exercise and work performance. Exerc Sport Sci Rev. 1990;18 (119):166.
2. Narici M, Kayser B, Barattini P, Cerretelli P. Effects of 17-day spaceflight on electrically evoked torque and cross-sectional area of the human triceps surae. Eur J Appl Physiol. 2003;90(3-4):275-82.
3. Fitts RH, Riley DR, Widrick JJ. Physiology of a microgravity environment invited review: microgravity and skeletal muscle. J Appl Physiol (1985). 2000;89(2):823-39.
4. Fitts RH, Trappe SW, Costill DL, Gallagher PM, Creer AC, Colloton PA, et al. Prolonged Space Flight-Induced Alterations in the Structure and Function of Human Skeletal Muscle Fibres. J Physiol. 2010.
5. de Boer MD, Seynnes OR, di Prampero PE, Pisot R, Mekjavic IB, Biolo G, et al. Effect of 5 weeks horizontal bed rest on human muscle thickness and architecture of weight bearing and non-weight bearing muscles. Eur J Appl Physiol. 2008;104(2):401-7.

6. de Boer MD, Maganaris CN, Seynnes OR, Rennie MJ, Narici MV. Time course of muscular, neural and tendinous adaptations to 23 day unilateral lower-limb suspension in young men. J Physiol. 2007;583(Pt 3):1079-91.
7. D'Antona G, Pellegrino MA, Adami R, Rossi R, Carlizzi CN, Canepari M, et al. The effect of ageing and immobilization on structure and function of human skeletal muscle fibres. J Physiol (Lond). 2003;552(Pt 2):499-511.
8. Hoppeler H, Baum O, Lurman G, Mueller M. Molecular mechanisms of muscle plasticity with exercise. Compr Physiol. 2011;1(3):1383-412.
9. Chopard A, Pons F, Marini JF. Vinculin and meta-vinculin in fast and slow rat skeletal muscle before and after hindlimb suspension. Pflugers Arch. 2002;444(5):627-33.
10. Chopard A, Arrighi N, Carnino A, Marini JF. Changes in dysferlin, proteins from dystrophin glycoprotein complex, costameres, and cytoskeleton in human soleus and vastus lateralis muscles after a long-term bedrest with or without exercise. Faseb J. 2005;19(12):1722-4.
11. Salanova M, Gelfi C, Moriggi M, Vasso M, Vigano A, Minafra L, et al. Disuse deterioration of human skeletal muscle challenged by resistive exercise superimposed with vibration: evidence from structural and proteomic analysis. Faseb J. 2014;28(11):4748-63.
12. Li R, Narici MV, Erskine RM, Seynnes OR, Rittweger J, Pisot R, et al. Costamere remodeling with muscle loading and unloading in healthy young men. J Anat. 2013;223(5):525-36.
13. Klossner S, Li R, Ruoss S, Durieux AC, Fluck M. Quantitative changes in focal adhesion kinase and its inhibitor, FRNK, drive load-dependent expression of costamere components. Am J Physiol Regul Integr Comp Physiol. 2013;305(6):R647-57.
14. Rindom E, Vissing K. Mechanosensitive Molecular Networks Involved in Transducing Resistance Exercise-Signals into Muscle Protein Accretion. Front Physiol. 2016;7:547.
15. Moriggi M, Vasso M, Fania C, Capitanio D, Bonifacio G, Salanova M, et al. Long term bed rest with and without vibration exercise countermeasures: Effects on human muscle protein dysregulation. Proteomics. 2010;10(21):3756-74.
16. Fluck M, Ziemiecki A, Billeter R, Muntener M. Fibre-type specific concentration of focal adhesion kinase at the sarcolemma: influence of fibre innervation and regeneration. J Exp Biol. 2002;205(Pt 16):2337-48.
17. Samarel AM. Costameres, focal adhesions, and cardiomyocyte mechanotransduction. Am J Physiol Heart Circ Physiol. 2005;289(6):H2291-301.
18. Grounds MD, Sorokin L, White J. Strength at the extracellular matrix-muscle interface. Scand J Med Sci Sports. 2005;15(6):381-91.

19. Miyamoto S, Teramoto H, Coso OA, Gutkind JS, Burbelo PD, Akiyama SK, et al. Integrin function: molecular hierarchies of cytoskeletal and signaling molecules. J Cell Biol. 1995;131(3):791-805.
20. Schlaepfer DD, Mitra SK, Ilic D. Control of motile and invasive cell phenotypes by focal adhesion kinase. Biochim Biophys Acta. 2004;1692(2-3):77-102.
21. Li S, Kim M, Hu YL, Jalali S, Schlaepfer DD, Hunter T, et al. Fluid shear stress activation of focal adhesion kinase. Linking to mitogen-activated protein kinases. J Biol Chem. 1997;272(48):30455-62.
22. Durieux AC, D'Antona G, Desplanches D, Freyssenet D, Klossner S, Bottinelli R, et al. Focal adhesion kinase is a load-dependent governor of the slow contractile and oxidative muscle phenotype. J Physiol. 2009;587(Pt 14):3703-17.
23. Fluck M, Chiquet M, Schmutz S, Mayet-Sornay MH, Desplanches D. Reloading of atrophied rat soleus muscle induces tenascin-C expression around damaged muscle fibers. Am J Physiol Regul Integr Comp Physiol. 2003;284(3):R792-801.
24. Jarvinen TA, Jozsa L, Kannus P, Jarvinen TL, Hurme T, Kvist M, et al. Mechanical loading regulates the expression of tenascin-C in the myotendinous junction and tendon but does not induce de novo synthesis in the skeletal muscle. J Cell Sci. 2003;116(Pt 5):857-66.
25. Cannavino J, Brocca L, Sandri M, Bottinelli R, Pellegrino MA. PGC1-alpha over-expression prevents metabolic alterations and soleus muscle atrophy in hindlimb unloaded mice. J Physiol. 2014;592(20):4575-89.
26. Brocca L, Cannavino J, Coletto L, Biolo G, Sandri M, Bottinelli R, et al. The time course of the adaptations of human muscle proteome to bed rest and the underlying mechanisms. J Physiol. 2012;590(20):5211-30.
27. Cannavino J, Brocca L, Sandri M, Grassi B, Bottinelli R, Pellegrino MA. The role of alterations in mitochondrial dynamics and PGC-1alpha over-expression in fast muscle atrophy following hindlimb unloading. J Physiol. 2015;593(8):1981-95.
28. Stein TP, Schluter MD. Human skeletal muscle protein breakdown during spaceflight. Am J Physiol. 1997;272(4 Pt 1):E688-95.
29. Stein TP, Wade CE. Metabolic consequences of muscle disuse atrophy. J Nutr. 2005;135(7):1824S-8S.
30. Ghini V, Saccenti E, Tenori L, Assfalg M, Luchinat C. Allostasis and Resilience of the Human Individual Metabolic Phenotype. Journal of proteome research. 2015;14(7):2951-62.
31. Brellier F, Martina E, Degen M, Heuze-Vourc'h N, Petit A, Kryza T, et al. Tenascin-W is a better cancer biomarker than tenascin-C for most human solid tumors. BMC Clin Pathol. 2012;12:14.
32. Fluck M, Ruoss S, Mohl CB, Valdivieso P, Benn MC, von Rechenberg B, et al. Genomic and lipidomic actions of nandrolone on detached rotator cuff muscle in sheep. J Steroid Biochem Mol Biol. 2017;165(Pt B):382-95.

33. Vigano A, Vasso M, Caretti A, Bravata V, Terraneo L, Fania C, et al. Protein modulation in mouse heart under acute and chronic hypoxia. Proteomics. 2011;11(21):4202-17.
34. Capitanio D, Vasso M, Fania C, Moriggi M, Vigano A, Procacci P, et al. Comparative proteomic profile of rat sciatic nerve and gastrocnemius muscle tissues in ageing by 2-D DIGE. Proteomics. 2009;9(7):2004-20.
35. Bernini P, Bertini I, Luchinat C, Tenori L, Tognaccini A. The cardiovascular risk of healthy individuals studied by NMR metabonomics of plasma samples. Journal of proteome research. 2011;10(11):4983-92.
36. Bernini P, Bertini I, Luchinat C, Nincheri P, Staderini S, Turano P. Standard operating procedures for pre-analytical handling of blood and urine for metabolomic studies and biobanks. Journal of biomolecular NMR. 2011;49(3-4):231-43.
37. Meiboom S, Gill D. Modified spin-echo method for measuring nuclear relaxation times. The Review of scientific instruments. 1958;29:688-91.
38. Spraul M, Neidig P, Klauck U, Kessler P, Holmes E, Nicholson JK, et al. Automatic reduction of NMR spectroscopic data for statistical and pattern recognition classification of samples. Journal of pharmaceutical and biomedical analysis. 1994;12(10):1215-25.
39. Holmes E, Foxall PJ, Nicholson JK, Neild GH, Brown SM, Beddell CR, et al. Automatic data reduction and pattern recognition methods for analysis of 1H nuclear magnetic resonance spectra of human urine from normal and pathological states. Anal Biochem. 1994;220(2):284-96.
40. Ihaka R, Gentleman R. R: a language for data analysis and graphics. Journal of computational and graphical statistics. 1996;5(3):299-314.
41. Wishart DS, Tzur D, Knox C, Eisner R, Guo AC, Young N, et al. HMDB: the Human Metabolome Database. Nucleic acids research. 2007;35(Database issue):D521-6.
42. Bouatra S, Aziat F, Mandal R, Guo AC, Wilson MR, Knox C, et al. The human urine metabolome. PLoS ONE. 2013;8(9):e73076.
43. Iglewicz B, Hoaglin DC. How to detect and handle outliers: Asq Press; 1993.

List of Figures and Tables

Figure 1: Survey of the load and distance per treadmill session, and the load and number of heel raise exercise with aRED for crew member A (red) and B (green) during their sojourn on the ISS.

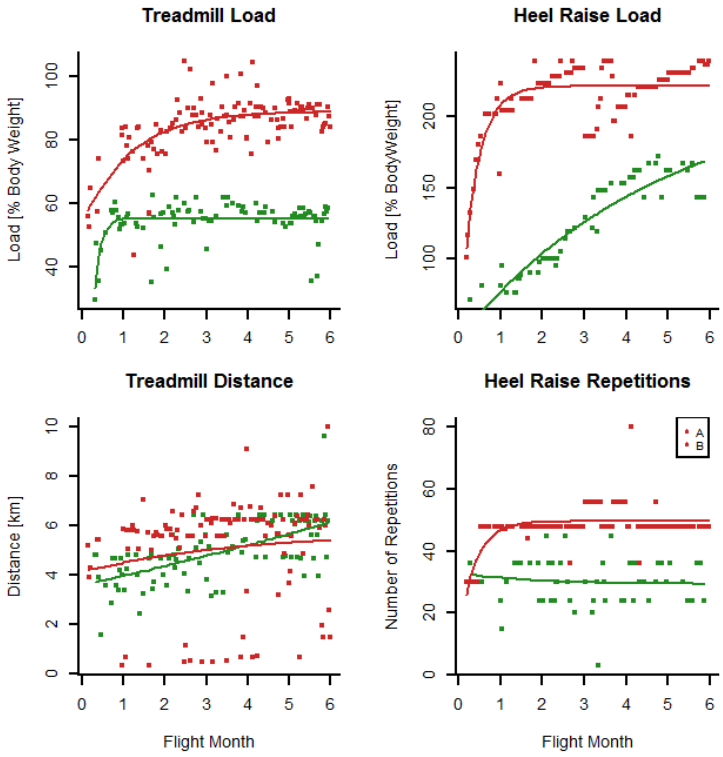

Figure 2: Effects of spaceflight upon muscle function, given in percent changes from baseline, for crew member A and B.

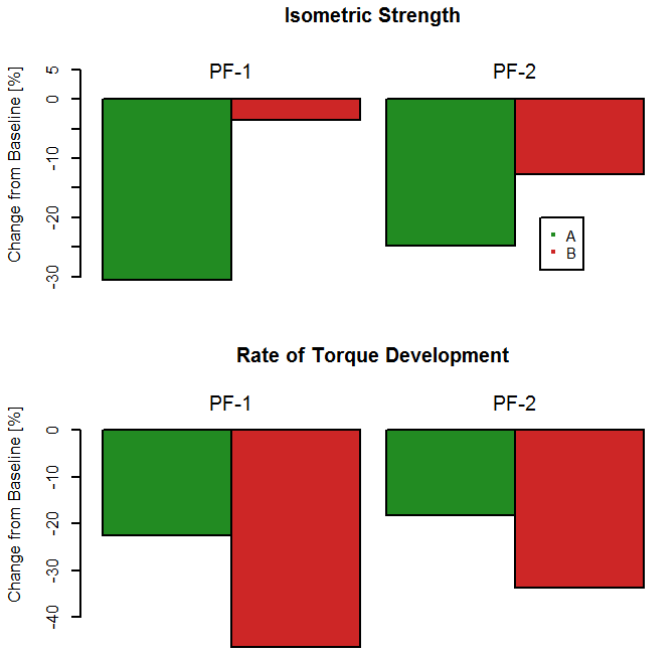

Figure 3: Proteomic analysis in human skeletal muscle. Histograms of differential protein expression in soleus muscle between baseline versus PF-1 (colored bars) and baseline versus PF-2 (striped bars) in crew member A (green bars) and B (red bars), as detected by 2D DIGE analysis. Proteins significantly altered (paired one-way ANOVA and Tukey, α=0.01) are indicated by their gene name and expressed as a percent of spot volume variation. (A) Contractile proteins; (B) Metabolism.

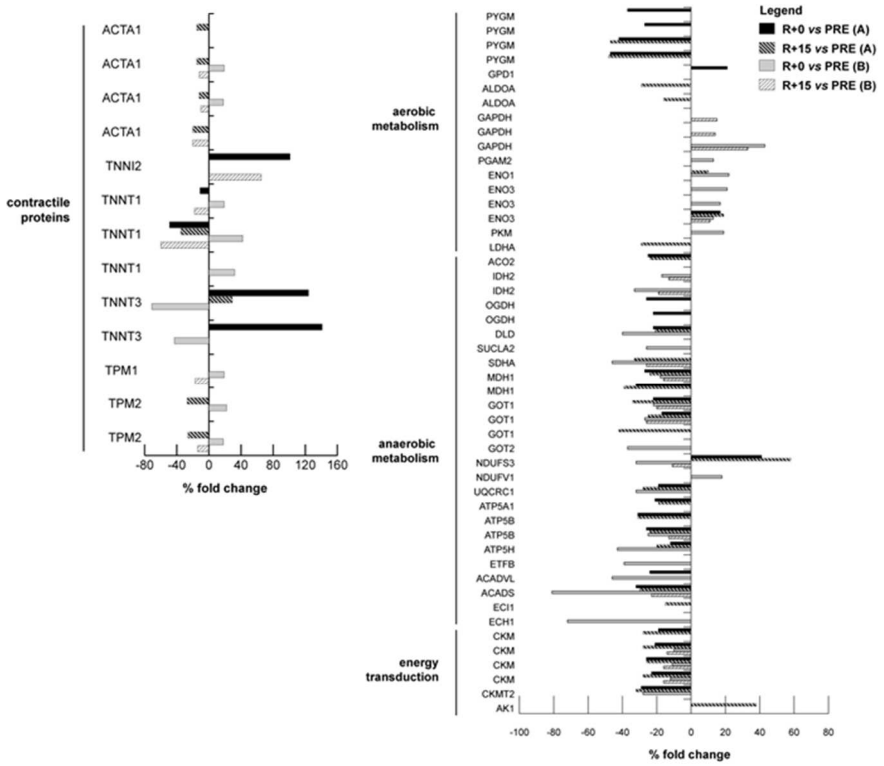

Figure 4: Metabolomic analysis. Panels (A,B) show amino acid and energetic metabolites, respectively, in box plot analysis and in arbitrary units (C.A.U.) concentrations of the most significant metabolites. Astronaut A and B are represented by green and red colors, respectively. Circle, triangle and square represent baseline, PF-1 and PF-2, respectively. Gray circles represent the control cohort (76 volunteers). Significant (p<0.01) and barely significant (p<0.05) p-values are also reported.

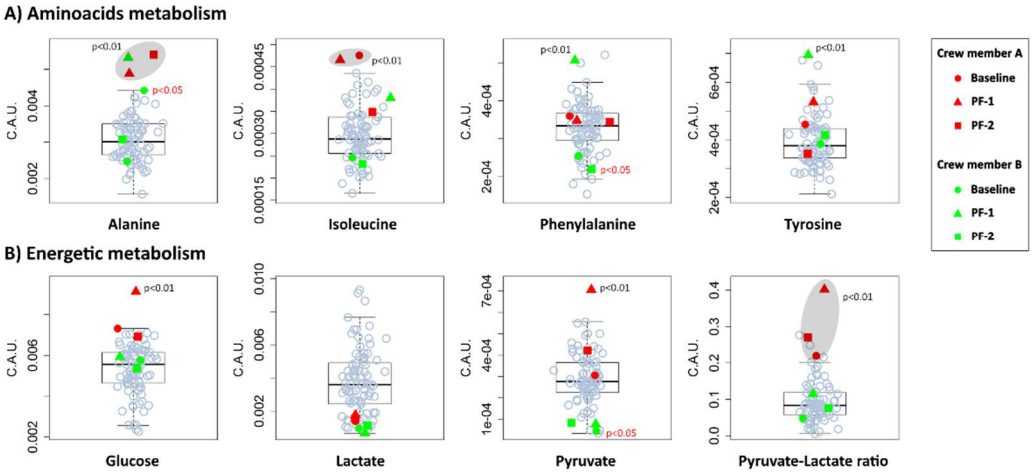

Table 1: Changes in muscle size and architecture for testing sessions post-flight 1 (PF-1, at 0 to 4 days after landing) and post-flight session 2 (PF-2, at 15 days after landing)

		Crew Member	**PF-1**	**PF-2**
Medial Gastrocnemius Muscle	Volume	A	-18.1%	-10.7%
		B	-11.8%	-1.2%
	Pennation angle	A	-23.2%	-13.1%
		B	+3.7%	+3.3%
	Fascicle length	A	-7.6%	-0.6%
		B	-1.3%	-0.6%
	Physiological CSA	A	-11.4%	-10.2%
		B	-10.7%	-0.6%
Soleus Muscle	Volume	A	-21.1%	-16.6%
		B	-9.4%	-7.4%
	Pennation Angle	A		
		B	-2.9%	+6.2%
	Fascicle length	A		
		B	+0.6%	+1.7%
	Physiological CSA	A		
		B	-9.9%	-8.9%

Table 2: Summary of expressional alterations in costameric proteins.

	PF-1		***PF-2***	
Parameter	***Crew member A***	***Crew member B***	***Crew member A***	***Crew member B***
FAK-pY397	-92%	11%	-54%	28%
FAK	-60%	-44%	112%	88%
FRNK	-60%	-67%	124%	26%
FAK-p85	-75%	-35%	257%	5%
Gamma-vinculin	5%	-17%	4%	23%
Meta-vinculin	786%	-26%	-24%	116%
Tenascin-C	2781%	-14%	-40%	64%

Supplementary materials:

Supplementary Table 1: Relationships between costameric gene products, which relate to fast fiber types. Note the considerable increase in meta- per gamma-vinculin content in crew member A after space flight, and the relative stability of this ratio in crew member B.

	Baseline	***PF-1***	***PF-2***
FRNK per FAK			
Crew member A	2.01	1.98	2.09
Crew member B	0.58	0.34	0.23
meta-vinculin per gamma-vinculin			
Crew member A	0.06	0.47	0.34
Crew member B	0.05	0.05	0.08

Supplementary Table 2: Testing schedule. Baseline dates are relative to launch (L), and post-flight dates are relative to return to Earth (R+0 = landing day).

Crew Member	**Test**	**Baseline**	**Post-Flight 1 (PF-1)**	**Post-Flight 2 (PF-2)**
A	Blood Sample & Biopsy	L-79	R+0	R+15
	Magnetic Resonance Imaging	L-79	R+3	R+15
	Plantar flexor testing	L-79	R+1	R+15
B	Blood Sample & Biopsy	L-76	R+0	R+15
	Magnetic Resonance Imaging	L-76	R+3	R+15
	Plantar flexor testing	L-76	R+4	R+15

Supplementary Figure 1:

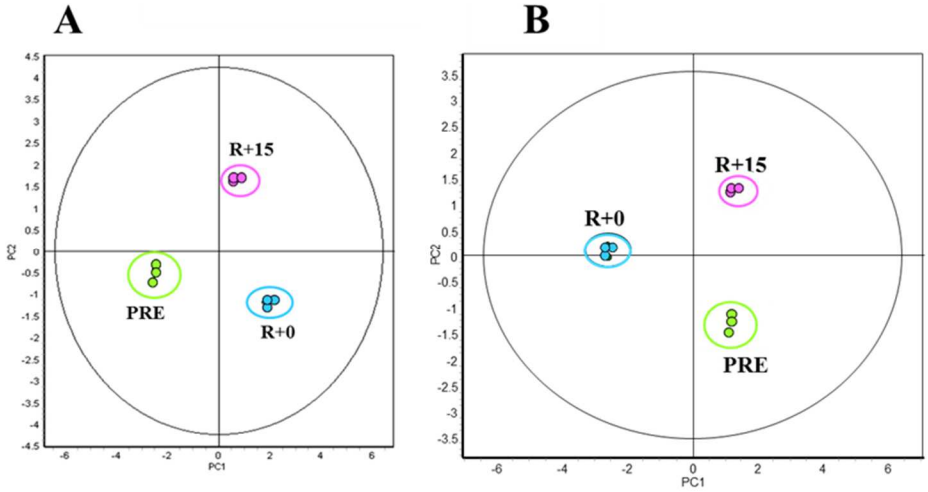

Supplementary figure 2:

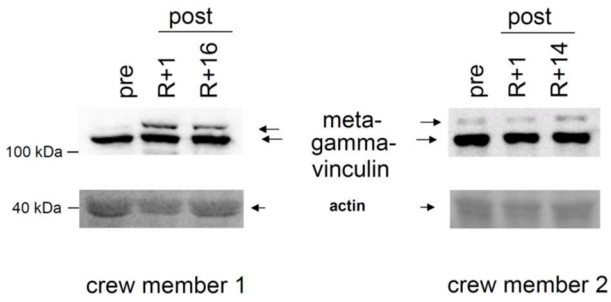

Supplementary figure 3:

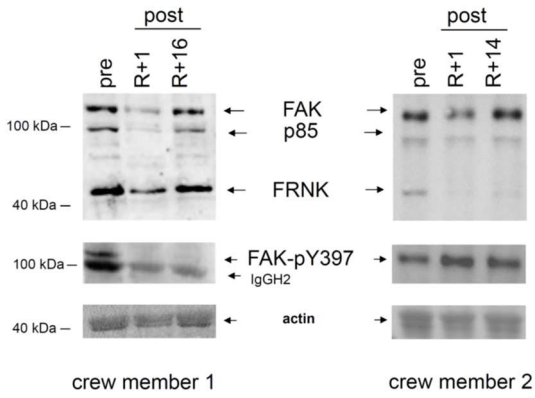

Supplementary figure 4:

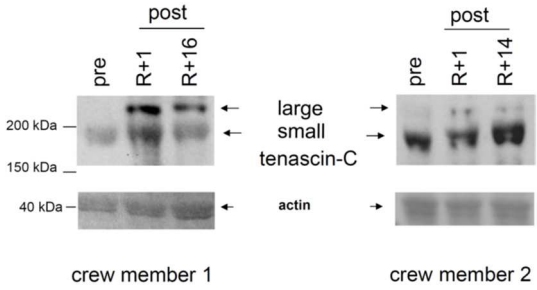

Supplementary figure 5:

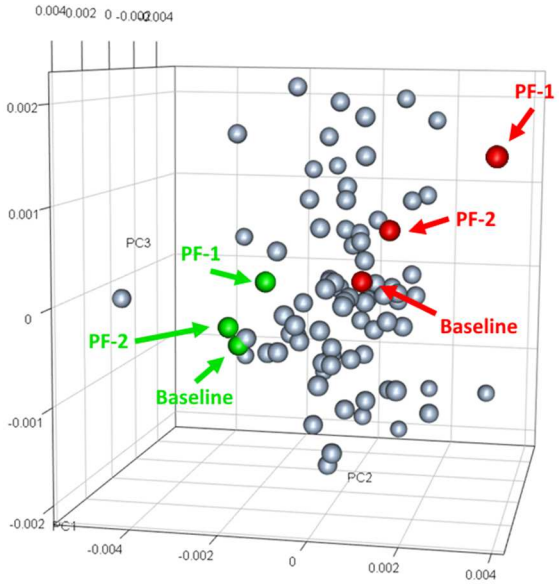

4.3.3 *Breathomics for assessing the effects of treatment and withdrawal with inhaled Beclomethasone/Formoterol in patients with COPD*

[1,*]Paolo Montuschi, M.D., [1,*]Giuseppe Santini, B.Sci., [1,*]Nadia Mores, M.D., [2,*]Alessia Vignoli, M.Sci., [3]Francesco Macagno, M.D., [4]Rugia Shoreh, PhD, [2]Leonardo Tenori, PhD, [5]Gina Zini, M.D., [3]Leonello Fuso, M.D., [6]Chiara Mondino, M.D., [7]Corrado Di Natale, PhD, PhD, [7]Arnaldo D'Amico, PhD, [2]Claudio Luchinat, PhD, [8]Peter J. Barnes, DM, [2]Tim Higenbottam, M.D.

*Contributed equally to the work

[1] Department of Pharmacology, Faculty of Medicine, Catholic University of the Sacred Heart, University Hospital Agostino Gemelli Foundation, Rome, Italy
[2] Department of Chemistry "Ugo Schiff", Magnetic Resonance Center (CERM), University of Florence, Italy,
[3] Department of Internal Medicine and Geriatrics, Catholic University of the Sacred Heart, University Hospital Agostino Gemelli Foundation, Rome, Italy,
[4] Department of Drug Sciences, Faculty of Pharmacy, University "G. d'Annunzio", Chieti, Italy, Chieti, Italy,
[5] Department of Hematology, Faculty of Medicine, Catholic University of the Sacred Heart, University Hospital Agostino Gemelli Foundation, Rome, Italy,
[6] Department of Allergology, 'Bellinzona e Valli' Hospital, Bellinzona, Switzerland
[7] Department of Electronic Engineering, University of Tor Vergata, Rome, Italy,
[8] Airway Disease Section, Imperial College, Faculty of Medicine, National Heart and Lung Institute, London, United Kingdom,
[9] Faculty of Pharmaceutical Medicine, Royal College of Physicians, London, United Kingdom

Submitted

Candidate's contributions: acquisition of NMR data, statistical analysis and interpretation of data, writing and review of the manuscript.

BREATHOMICS FOR ASSESSING THE EFFECTS OF TREATMENT AND WITHDRAWAL WITH INHALED BECLOMETHASONE/FORMOTEROL IN PATIENTS WITH COPD

ABSTRACT

Prospective pharmacological studies on breathomics in COPD are not available. We assessed the effects of steroid treatment and withdrawal of an extrafine inhaled corticosteroid (ICS)- long-acting β2-agonist (LABA) fixed dose combination (FDC) in a multidimensional classification model including breathomics.

A pilot study was undertaken in 14 COPD patients on inhaled fluticasone propionate/salmeterol FDC (500/50 μg b.i.d.) maintenance treatment (visit 1). Patients received 2-week inhaled beclomethasone dipropionate/formoterol FDC (100/6 μg b.i.d.) (visit 2), 4-week formoterol (6 μg b.i.d.) (visit 3), and 4-week beclomethasone/formoterol (100/6 μg b.i.d.) (visit 4). Exhaled breath analysis with two different e-noses and exhaled breath condensate (EBC) NMR-based metabolomics were performed. Sputum cell counts, sputum supernatant and EBC prostaglandin-E_2 and 15-F_{2t}-isoprostane, fraction of exhaled nitric oxide, and spirometry were measured.

Three independent breathomic techniques showed that extrafine beclomethasone/formoterol short-term treatment was associated with different breathprints compared with regular fluticasone propionate/formoterol. Either ICS/LABA FDC treatment versus formoterol alone was associated with increased $FEF_{25\%-75\%}$ and FEV_1/FVC (P=0.008-0.029). The multidimensional model distinguished fluticasone propionate/salmeterol versus beclomethasone/formoterol, fluticasone propionate/salmeterol versus formoterol, and formoterol versus beclomethasone/formoterol (accuracy>70%, P<0.01).

Breathomics could be used for assessing ICS treatment and withdrawal in COPD patients. Large, controlled trials are required to clarify the biological implications of breathomic changes.

INTRODUCTION

Respiratory inflammation has a central role in the pathophysiology of COPD. Inhaled corticosteroids (ICS) are the principal anti-inflammatory treatment for COPD [1], but little is known about the pattern of inflammatory markers which are affected by this pharmacotherapy. While ICS are generally effective in asthma, their anti-inflammatory efficacy in COPD is not clearly established [2].

Electronic noses (e-noses), consisting of cross-reactive chemical sensor arrays for the detection of volatile chemical species [3], discriminate between patients with COPD, asthmatic patients, healthy smokers and healthy non-smokers [4], and predict oral corticosteroid responsiveness in patients with asthma [5]. E-nose breathprints are associated with airway inflammatory markers, including sputum eosinophils and neutrophils, in COPD patients and can be useful for subphenotyping [6,7]. Metabolomics is a global approach to understanding regulation of metabolic pathways and metabolic networks of a biological system [7]. Nuclear magnetic resonance (NMR)-based metabolomic analysis of exhaled breath condensate (EBC), the liquid fraction of exhaled breath, is suitable for identifying and quantifying semi-volatile/non-volatile small molecular weight metabolites and has been applied to the assessment of airway inflammation in COPD patients [9-11]. Published prospective clinical studies on effects of pharmacological treatment on e-nose breathprints in COPD patients are not available.

We aimed to assess the effects of treatment and steroid withdrawal of an extrafine ICS/long-acting β_2-agonist (LABA) fixed dose combination (FDC) on breathprints and non-invasive inflammatory outcomes in COPD patients; to compare accuracy of a multidimensional classification model versus a standard spirometry-based model.

METHODS

Study subjects

Fourteen COPD non-smokers or ex-smokers diagnosed for at least one year with stable mild, moderate or severe airflow limitation (GOLD stage I-III, baseline forced expiratory volume in one second (FEV_1) > 30% predicted value, FEV_1/forced vital capacity (FVC) < 70%), who were on a fixed dose combination (FDC) of fluticasone propionate/salmeterol delivered via a dry powder inhaler [DPI] at a constant dose of 500/50 µg b.i.d. for at least 8 weeks, were studied. Diagnosis of COPD was based on GOLD guideline criteria [1].

COPD patients had negative reversibility test to 400 µg of inhaled salbutamol (<12% or 200 mL increase in FEV_1), no history of asthma and atopic disease, negative skin prick test results, no upper respiratory tract infections in the previous 3 weeks, and were excluded from the study if they had used systemic corticosteroids in the previous 4 weeks.

Study design

This was a single centre, prospective, open label, pilot, proof-of-concept, pharmacological study of steroid withdrawal and treatment in COPD patients on maintenance treatment with inhaled fluticasone propionate/salmeterol at full doses (visit 1). Study duration was 10 weeks including 4 visits (Figure 1). Patients received inhaled beclomethasone/formoterol FDC for 2 weeks (100/6 μg 2 puffs b.i.d. via pressurized metered dose inhaler [pMDI]) (visit 2), inhaled formoterol alone for 4 weeks (6 μg 2 puffs b.i.d. via pMDI) (visit 3), and inhaled beclomethasone/formoterol FDC for 4 weeks (visit 4) (Figure 1). Breathomics included analysis of exhaled breath gaseous phase with two different e-noses, and NMR-based metabolomics of exhaled breath condensate (EBC). Sputum cell counts, prostaglandin (PG)-E_2 and 15-F_{2t}-isoprostane in sputum supernatants and EBC, and fraction of exhaled nitric oxide (F_ENO) were also measured (see also online supplementary material).

Informed consent was obtained from patients. The study was approved by the Ethics Committee of the Catholic University of the Sacred Heart, Rome, Italy (EudraCT: 2012-001749-42).

Pulmonary function

Spirometry was performed with a Pony FX spirometer (Cosmed, Rome, Italy) and the best of three consecutive maneuvers chosen.

F_ENO measurement

F_ENO was measured with the NIOX system (Aerocrine, Stockholm, Sweden) with a single breath on-line method at constant flow of 50 mL/sec according to American Thoracic Society guidelines [12,13]. F_ENO measurements were obtained before spirometry.

Collection of exhaled breath

Exhaled breath was collected from each subject at 8.30 a.m. No food or drinks were allowed at least 12 hours prior to collection of exhaled breath.

Exhaled breath was collected as previously described [4,14] and based on recent ERS technical standard [3]. Subjects were asked to breathe tidally volatile organic compound (VOC)-filtered air for 5 minutes, while wearing a nose-clip, into a 2-way non-rebreathing valve with an inspiratory VOC filter and an expiratory silica reservoir to reduce sample water vapor [15]. Then, subjects were asked to inhale to maximal inspiration and perform a FVC maneuver into a Tedlar bag. Two consecutive samples were collected 15 min apart and immediately analyzed.

Electronic noses

The first sample was analyzed with a commercially available e-nose (Cyranose 320, Sensigent, Baldwin Park, USA) [4,16], which consists of an array of 32 cross-reactive

carbon black polymer composite sensors and detects resistance variations; the second sample was analyzed with an e-nose prototype (Ten 2011, University of Rome Tor Vergata, Italy) [17] which consists of an array of 8 cross-reactive quartz microbalance gas sensors coated by molecular films of metallo-porphyrins and detects frequency variations [17]. Breathprints were analyzed by pattern recognition algorithms (see supplementary material) [18].

Ambient VOCs were subtracted from measures and results were automatically adjusted for ambient VOCs.

EBC sampling

Before EBC collection, subjects refrained from eating for at least 3 h. EBC was collected using a condenser (Ecoscreen, Jaeger, Hoechberg, Germany) [9], in a windowless clinic facility without disinfectant dispensers (see online supplementary material) [9]. Samples were snap frozen in liquid nitrogen to immediately 'quench' metabolism and preserve the metabolite concentrations.

Metabolomic analysis of EBC with NMR spectroscopy

^{1}H-NMR spectra for EBC samples were acquired using a Bruker 600 MHz spectrometer operating at 600.13 MHz using standard nuclear Overhauser effect spectroscopy (NOESY) experiments and standard protocols for sample preparation [19]. Signals of interest were assigned on template one-dimensional NMR profiles and integrated to calculate their relative concentrations [10,19,20]. Multilevel partial least square (PLS) analysis was used to analyze EBC spectra from the same subject obtained at paired visits. (see also online supplementary material).

Measurement of PGE_2 and 15-F_{2t}-isoprostane in sputum supernatants and EBC

PGE_2 and 15-F_{2t}-isoprostane concentrations in sputum supernatants and EBC were measured with radioimmunoassays developed in our laboratory, previously validated and compared with gas chromatography/mass spectrometry and high performance liquid chromatography [21,22].

Skin testing

Atopy was assessed by skin prick tests for common aeroallergens (Stallergenes, Antony, France) [23].

Multivariate data analysis

E-nose and NMR spectroscopy data analysis requires multivariate statistical algorithms [18,24]. Multilevel partial least square analysis was used for data reduction; the K-nearest neighbors method, applied on the multilevel PLS scores, was used for classification purposes [18,24]. The global classification accuracy was assessed by means of Monte Carlo cross-validation scheme. The threshold for significant

classification was set at a value of 70% [25]. Correlations among multidimensional data, shown as a heatmap, were calculated using the algorithm implemented in the R-library "psych" [26,27], based on a correlation matrix built using the R-function "heatmap.2", implemented in the "gplots" package [28]. (see online supplementary material).

Statistical analysis

Data were expressed as mean ± SEM or medians and interquartile ranges (25^{th} and 75^{th} percentiles), after assessing for normality with the D'Agostino-Pearson omnibus normality test. Depending on data distribution, repeated-measures ANOVA or Friedman test or Wilcoxon test were used for assessing within-group pharmacological treatment effect. Correlation was expressed as a Pearson coefficient. Significance was defined as a value of $P < 0.05$.

RESULTS

Study subjects

The mean age of the subjects (2 females and 12 males) enrolled in this study was 73.6 ± 1.8 years. Patients smoke a mean of 64.3 ± 1.8 pack-year and, according to the airflow limitation severity, were classified as GOLD I (4 patients), II (5 patients), and III (5 patients). Information about common aeroallergens, history of atopy, sputum eosinophils at visit 1 are detailed in Table 1.

Pulmonary function testing

Higher mean percentage of predicted pre-bronchodilator (forced expiratory flow at 25% to 75% of forced vital capacity ($FEF_{25\%-75\%}$) and absolute values were observed after 2-week inhaled beclomethasone/formoterol FDC treatment (visit 2) compared with 4-week treatment with inhaled formoterol alone (visit 3) ($P = 0.029$ and $P = 0.026$, respectively) (Figure 2A and 2B; Supplementary Table 1).

Mean pre-bronchodilator FEV_1/FVC ratio was higher on maintenance treatment with inhaled fluticasone propionate/salmeterol FDC (visit 1) compared with post-treatment with inhaled formoterol alone (visit 3) ($P = 0.008$) (Supplementary Table 1).

Higher mean pre-bronchodilator peak expiratory flow (PEF) percentage predicted and absolute values were observed after 2-week beclomethasone/formoterol FDC (visit 2) compared with those observed after 4-week treatment with formoterol alone (visit 1) ($P = 0.044$ and $P = 0.033$, respectively) (Figure 2C and 2D; Supplementary Table 1). No within-group differences in post-bronchodilator functional parameters were observed (Supplementary Table 2).

Electronic nose

E-nose analysis with either e-nose was successfully performed in all 14 subjects at all

visits. A total of 56 breathprints for each e-nose was collected. Fifteen out of 32 carbon polymer sensors showed significant mean differences between maintenance treatment with inhaled fluticasone propionate/salmeterol FDC (visit 1) and after 4-week treatment with beclomethasone/formoterol FDC (visit 4), whereas 7 sensors showed significant mean differences between fluticasone propionate/salmeterol maintenance treatment (visit 1) and 2-week treatment with beclomethasone/formoterol (visit 2) (Table 2).

Consistent with carbon polymer sensor behaviour, two quartz crystal sensors showed significant differences between maintenance treatment with fluticasone propionate/salmeterol (visit 1) and 4-week beclomethasone/formoterol treatment (visit 4); sensor 3 and 4 showed significant differences between fluticasone propionate/salmeterol maintenance treatment (visit 1) and 2-week treatment with beclomethasone/formoterol (visit 2) (Table 3).

There was no difference in sensor response using either e-nose when other paired visits were compared (Table 2 and 3).

Metabolomic analysis of EBC with NMR spectroscopy

A total of 56 EBC NMR spectra obtained from 14 study subjects across visits were analyzed (Supplementary Figure 1). EBC metabolomics with NMR spectroscopy discriminated between maintenance treatment with fluticasone propionate/salmeterol FDC (visit 1) and treatment with beclomethasone/formoterol FDC for 4 weeks (visit 4) (accuracy = 72%, P = 0.01) (Supplementary Figure 2). Formate levels were higher at visit 1 (694.9 ± 360.5 arbitrary units, median ± median absolute deviation [MAD]) than at visit 4 (409.2 ± 224.8 arbitrary units, P = 0.029) (Supplementary Figure 3A and 3B, s-Table 3). Other paired comparisons showed accuracy below the significant threshold set at 70% (s-Table 4). After 4-week treatment with beclomethasone/formoterol FDC (visit 4), EBC acetate levels were lower than those measured after 4-week treatment with formoterol alone (visit 3) (P = 0.009) (s-Table 3). Several EBC metabolites, including formate, phenol, methanol, trimethylamine, acetone, acetoine, acetate, n-butyrate, lactate, 3-hydroxyisovalerate, ethanol, propionate, and leucine-o-butyrate were identified (Figure 3). Apart from formate and acetate, their levels were similar across visits (s-Table 3).

Fraction of exhaled nitric oxide (F_ENO)

There was no within-group difference in F_ENO concentrations in patients with COPD (overall P = 0.35) (s-Table 5).

Measurement of PGE_2 and 15-F_{2t}-isoprostane in sputum supernatants and EBC

PGE_2 concentrations were detected in 49 out of a total of 56 sputum supernatant samples. Compared with formoterol alone post-treatment values (visit 3), lower sputum PGE_2 concentrations were observed after 4-week treatment with

beclomethasone/formoterol FDC (visit 4) (P = 0.008) and on maintenance treatment with fluticasone propionate/salmeterol FDC (visit 1) (P = 0.021) (Supplementary Table 6). These data suggest that treatment with ICS FDC, containing either fluticasone propionate or beclomethasone, reduces PGE_2 sputum concentrations. There was no between-visit differences in EBC PGE_2 or sputum and EBC 15-F_{2t}-isoprostane concentrations (Supplementary Table 6).

Sputum cell analysis

Eight patients with COPD had a complete set of sputum slides (visit 1 to visit 4) (Supplementary Table 7). No patient with COPD had sputum eosinophilia, as defined by sputum cell counts > 3%, at visit 1 (screening visit). There was no within-group difference in sputum cell counts (Supplementary Table 7). Percentage sputum cell counts in all valid sputum slides are shown in Supplementary Table 8.

Correlations

Responses within each individual e-nose and between e-noses were correlated, whereas EBC metabolites detected by NMR spectroscopy were not correlated with either e-noses, except EBC phenol which was correlated with 16 carbon polymer sensors (Figure 4, and online supplementary material). In EBC, there was a correlation between PGE_2 and formate ($r = 0.78$, $P = 5.06^{-11}$), acetone ($r = 0.63$, $P = 1.64^{-6}$), lactate ($r = 0.64$, $P = 6.03^{-7}$), n-butyrate ($r = 0.82$, $P = 5.89^{-13}$), propionate ($r = 0.59$, $P = 8.26^{-6}$), and acetate ($r = 0.71$, $P = 1.23^{-8}$) (Figure 4). Quartz crystal sensor 4 ($r = -0.35$, $P = 0.023$) and 7 ($r = -0.31$, $P = 0.041$) negatively correlated with sputum neutrophils. These showed negative correlation with FEV_1/FVC ($r = -0.34$; $P = 0.028$) (Figure 4, and online supplementary material).

Multidimensional integrated model for assessment of pharmacological treatment

In the 14 COPD study subjects, multidimensional pairwise discrimination models were built. The models discriminated between maintenance treatment with fluticasone propionate/salmeterol (visit 1) versus 4-week treatment with formoterol alone (visit 3) (accuracy = 71.5%, $P < 0.01$); the univariate analysis showed differences in sputum supernatant PGE_2 and FEV_1/FVC ratio (Table 4); between maintenance treatment with fluticasone propionate/salmeterol (visit 1) versus 4-week treatment with beclomethasone/formoterol (visit 4) (accuracy = 82.5%, $P < 0.01$); the univariate analysis showed differences in EBC formate, e-noses, and EBC PGE_2 (Table 4); between 4-week treatment with formoterol alone (visit 3) versus 4-week treatment with beclomethasone/formoterol (visit 4) (accuracy = 74.6%, $P < 0.01$); the univariate analysis showed differences in sputum PGE_2 and EBC acetate (Table 4). The multidimensional models showed higher accuracies than the models based on spirometry alone (s-Table 9).

DISCUSSION

The principal messages of the present study are: 1) breathomics can be successfully applied to assessment of effects of treatment and steroid withdrawal with ICS/LABA in patients with COPD; 2) breathomic results are confirmed by the concordance of three different breathomic techniques (carbon polymer sensor e-nose, quartz crystal sensor e-nose, NMR-based metabolomics) applied to the gaseous and aerosol particle (EBC) phase of the exhaled breath. These techniques provide complementary information; 3) a multidimensional, integrated, model including breathomics, improves the ability of identifying pharmacological treatment-induced effects compared with a monodimensional model based on standard pulmonary function testing.

We show that short-term treatment with extrafine beclomethasone/formoterol FDC pMDI is associated with different breathprints as compared with regular fluticasone propionate/formoterol FDC DPI in patients with COPD. These results might suggest that various ICS/LABA formulations have different effects on breathomic outcomes, although the biological implications of these findings are unknown and have to be defined.

Treatment with either ICS/LABA FDC versus inhaled formoterol alone was associated with a slight, but significant, increase in small airway function as reflected by $FEF_{25\%-75\%}$ and FEV_1/FVC values, whereas higher PEF values were observed after beclomethasone/formoterol (visit 2) than on regular fluticasone propionate/salmeterol (visit 1), suggesting that treatment-induced e-nose breathprint variations parallel the observed functional changes only to a limited extent. Interestingly, functional effects were observed after only 4-week treatment with inhaled beclomethasone/formoterol, a relatively short duration of treatment for COPD trials, and in patients with COPD who had normal sputum eosinophils, negative reversibility test to bronchodilators, negative skin prick tests, and no history of atopy, thus, excluding an asthma component, on which ICS are generally more effective.

The strong correlation between most sensors within each individual e-nose indicates a high degree of sensor redundancy, whereas a similar behaviour of e-nose based on different technologies confirms the results of the exhaled breath analysis. Of note, quartz crystal sensors, but not carbon polymer sensors, showed correlation with sputum neutrophils. On the other hand, the lack of correlation between EBC metabolites detected by NMR spectroscopy and either e-noses suggests that a comprehensive breathomics approach might be complementary and increase the level of information. In EBC, there was a correlation between PGE_2, an eicosanoid which can have potent pro-inflammatory effects in the airways [29,30], and formate ($r = 0.78$), acetone ($r = 0.63$), lactate ($r = 0.64$), n-butyrate ($r = 0.82$), propionate ($r = 0.59$), and acetate ($r = 0.71$) suggesting that these EBC metabolites might reflect respiratory inflammation.

Unlike a standard model based on spirometry, the multidimensional model used in our study was able to distinguish between pharmacological treatments (accuracy > 70%) in 3 out of 6 possible paired comparisons. This might increase the chance of detecting drug effects in COPD patients. In line with an anti-inflammatory effect of ICS, sputum concentrations of PGE_2, the key between-treatment discriminating outcome measure, were lower after treatment with either ICS/LABA FDC compared with formoterol alone. By contrast, other inflammatory outcomes, including sputum neutrophil cell counts, EBC PGE_2, and sputum and EBC 15-F_{2t}-isoprostane, showed steroid resistance. Elevated EBC formate and acetate levels have been reported in COPD patients compared with healthy subjects [9,31]. Interestingly, we found reduced EBC levels of these metabolites after beclomethasone/formoterol treatment.

Study strengths rely on the fact that this is the first prospective evidence of the effects of pharmacological treatment and steroid withdrawal on breathomics in COPD patients, the multidimensional, non-invasive, approach to drug assessment requiring a systems medicine-based data analysis, and the use of complementary breathomics techniques. The limited number of study subjects, the open-label, uncontrolled, design of the pharmacological study, the short duration of treatment/withdrawal phases, the lack of training and testing validation and external validation cohorts, represent limitations which preclude definitive conclusions.

In conclusion, breathomics can be used for assessing the effects of treatment and steroid withdrawal with ICS/LABA in patients with COPD. The present pilot, proof-of-concept, study provides a rational basis for large, randomized, controlled, pharmacological trials in patients with COPD using a similar multidimensional approach.

Acknowledgements

This work was supported by Chiesi Farmaceutici, as an Investigator Initiated Trial, and by Catholic University of the Sacred Heart, Rome, Italy, Academic Grant 2013.

References

1. Global initiative for chronic obstructive lung disease (GOLD). Global strategy for the diagnosis, management, and prevention of chronic obstructive pulmonary disease (updated 2017). Available at: www.goldcopd.org. Date last accessed: June 4 2017.
2. Barnes PJ. Inhaled corticosteroids in COPD: a controversy. *Respiration* 2010; 80: 89-95.
3. Horváth I, Barnes PJ, Loukides S, *et al*. A European Respiratory Society technical standard: exhaled biomarkers in lung disease. *Eur Respir J* 2017; 49(4). pii: 1600965. doi: 10.1183/13993003.00965-2016

4. Fens N, Zwinderman AH, van der Schee MP, *et al*. Exhaled breath profiling enables discrimination of chronic obstructive pulmonary disease and asthma. *Am J Respir Crit Care Med* 2009; 180: 1076-1082.
5. van der Schee MP, Palmay R, Cowan JO, *et al*. Predicting steroid responsiveness in patients with asthma using exhaled breath profiling. Predicting steroid responsiveness in patients with asthma using exhaled breath profiling. *Clin Exp Allergy* 2013; 43:1217-1225.
6. Fens N, de Nijs SB, Peters S, *et al*. Exhaled air molecular profiling in relation to inflammatory subtype and activity in COPD. *Eur Respir J* 2011; 38:1301-1309.
7. Fens N, van Rossum AG, Zanen P, *et al*. Subphenotypes of mild-to-moderate COPD by factor and cluster analysis of pulmonary function, CT imaging and breathomics in a population-based survey. *COPD* 2013; 10: 277-285.
8. Rochfort S. Metabolomics reviewed: a new "omics" platform technology for systems biology and implications for natural products research. *J Nat Prod* 2005; 68: 1813-1820.
9. De Laurentiis G, Paris D, Melck D, *et al*. Metabonomic analysis of exhaled breath condensate in adults by nuclear magnetic resonance spectroscopy. *Eur Respir J* 2008; 32: 1175-1183.
10. Motta A, Paris D, Melck D, *et al*. Nuclear magnetic resonance-based metabolomics of exhaled breath condensate: methodological aspects. *Eur Respir J* 2012; 39: 498-500.
11. Airoldi C, Ciaramelli C, Fumagalli M, *et al*. ^{1}H NMR to explore the metabolome of exhaled breath condensate in α1-antitrypsin deficient patients: a pilot study. *J Proteome Res* 2016; 15: 4569-4578.
12. ATS/ERS recommendations for standardized procedures for the online and offline measurement of exhaled lower respiratory nitric oxide and nasal nitric oxide, 2005. American Thoracic Society; European Respiratory Society. *Am J Respir Crit Care Med* 2005; 171: 912-930.
13. Dweik RA, Boggs PB, Erzurum SC, *et al*; American Thoracic Society Committee on interpretation of exhaled nitric oxide levels (F_ENO) for clinical applications. An official ATS clinical practice guideline: interpretation of exhaled nitric oxide levels (F_ENO) for clinical applications. *Am J Respir Crit Care Med* 2011; 184: 602-615.
14. Bofan M, Mores N, Baron M, *et al*. Within-day and between-day repeatability of measurements with an electronic nose in patients with COPD. *J Breath Res* 2013; 7(1): 017103.
15. Röck F, Barsan N, Weimar U. Electronic nose: current status and future trends. *Chem Rev* 2008; 108: 705-711.
16. Lewis NS. Comparisons between mammalian and artificial olfaction based on arrays of carbon black-polymer composite vapor detectors. *Acc Chem Res* 2004; 37: 663-672.

17. Montuschi P, Santonico M, Mondino C, *et al*. Diagnostic performance of an electronic nose, fractional exhaled nitric oxide, and lung function testing in asthma. *Chest* 2010; 137: 790-796.
18. Bishop C.M. Pattern Recognition and Machine Learning. Springer, 2006.
19. Bertini I, Luchinat C, Miniati M, *et al*. Phenotyping COPD by ^{1}H NMR metabolomics of exhaled breath condensate. *Metabolomics* 2014; 10:0. doi:10.1007/s11306-013-0572-3.
20. Montuschi P, Paris D, Melck D, *et al*. NMR spectroscopy metabolomic profiling of exhaled breath condensate in patients with stable and unstable cystic fibrosis. *Thorax* 2012; 67: 222-228.
21. Wang Z, Ciabattoni G, Créminon C, *et al*. Immunological characterization of urinary 8-epi-prostaglandin $F_{2\alpha}$ excretion in man. *J Pharmacol Exp Ther* 1995; 275: 94-100.
22. Montuschi P, Ragazzoni E, Valente S, *et al*. Validation of 8-isoprostane and prostaglandin E_2 measurements in exhaled breath condensate. *Inflamm Res* 2003; 52: 502-507.
23. Montuschi P, Mondino C, Koch P, *et al*. Effects of a leukotriene receptor antagonist on exhaled leukotriene E_4 and prostanoids in children with asthma. *J Allergy Clin Immunol* 2006; 118: 347-353.
24. Wilson AD, Baietto M. Applications and advances in electronic-nose technologies. *Sensors (Basel)* 2009; 9: 5099-5148.
25. Bijlsma S, Bobeldijk I, Verheij ER, *et al*. Large-scale human metabolomics studies: a strategy for data (pre-) processing and validation. *Anal Chem* 2006; 78: 567-574.
26. Hahsler M, Hornik K, Buchta C. Getting things in order: an introduction to the R package seriation. *Journal of Statistical Software* 2008; 25: 1-34.
27. Revelle W. An overview of the psych package. Package "psych" (version 1.6.9). Published on September 17 2016.

Available at: https://cran.r-project.org/web/packages/psych/vignettes/overview.pdf. Date last accessed: 4 June 2017.

28. Warnes GR, Bolker B, Bonebakker L, *et al*. Various R programming tools for plotting data. Package "gplots" (version 3.0.1). Published on March 30 2016. Available at: https://cran.r-project.org/web/packages/gplots/gplots.pdf.
29. Holden NS, Rider CF, Bell MJ, *et al*. Enhancement of inflammatory mediator release by beta$_2$-adrenoceptor agonists in airway epithelial cells is reversed by glucocorticoid action. *Br J Pharmacol* 2010; 160: 410-420.
30. Clarke DL, Belvisi MG, Smith SJ, *et al*. Prostanoid receptor expression by human airway smooth muscle cells and regulation of the secretion of granulocyte colony-stimulating factor. *Am J Physiol Lung Cell Mol Physiol* 2005; 288: L238-250.
31. De Laurentiis G, Paris D, Melck D, *et al*. Separating smoking-related diseases using NMR-based metabolomics of exhaled breath condensate. *J Proteome Res* 2013; 12: 1502-1511.

List of Figures and Tables

Table 1. Subject characteristics*

	COPD patients
n	14
Age, years	73.6 ± 1.8
Gender, females/males	2/14
Pack-years	64.3 ± 8.1
GOLD I/II/III, airflow limitation severity	4/5/5
§Skin prick tests, positive/negative	0/14
History of atopy, positive/negative	0/14
#Sputum eosinophils ≥ 3% at visit 1	0/14

*Data are expressed as numbers or mean ± SEM. §Common aeroallergens were tested. #Expressed as percentage of total non-squamous cells.

Table 2. Carbon polymer sensor e-nose response*. The behaviour of each sensor (sensor 1 - sensor 32) is shown. Sensors whose mean values differ across visits are shown in bold.

Sensor 1				
V1	V2	V3	V4	P value
2.507±0.2171	2.843±0.1636	2.891±0.2411	3.208±0.1857	0.0480
V1 vs V4				0.0055
Sensor 2				
V1	V2	V3	V4	P value
1.664±0.1427	1.891±0.0979	1.934±0.1537	2.181±0.1260	0.0212
V1 vs V2				0.0364
V1 vs V4				0.0053
Sensor 3				
V1	V2	V3	V4	P value
2.527±0.2057	2.768±0.1549	2.868±0.2432	3.183±0.1993	n.s.
Sensor 4				
V1	V2	V3	V4	P
1.447±0.1191	1.640±0.0891	1.693±0.1378	1.926±0.1249	0.0209
V1 vs V4				0.0040
Sensor 5				
V1	V2	V3	V4	P value
11.27±1.195	12.86±0.8729	13.38±1.261	16.70±2.785	n.s.
Sensor 6				

V1	V2	V3	V4	P value
6.574±0.7314	7.547±0.5477	7.757±0.8441	8.510±0.6821	n.s.
Sensor 7				
V1	V2	V3	V4	P value
0.001109±0.0962	0.001253±0.0678	0.001265±0.1008	0.001409±0.0763	0.0409
V1 vs V4				0.0053
Sensor 8				
V1	V2	V3	V4	P value
0.6803±0.05038	0.7709±0.03499	0.7732±0.05597	0.8569±0.05064	0.0259
V1 vs V2				0.0216
V1 vs V4				0.0058
Sensor 9				
V1	V2	V3	V4	P value
2.154±0.2058	2.462±0.1496	2.542±0.2280	2.811±0.1892	n.s.
Sensor 10				
V1	V2	V3	V4	P value
1.283±0.1128	1.474±0.08070	1.492±0.1259	1.649±0.1020	n.s.
Sensor 11				
V1	V2	V3	V4	P value
1.277±0.1155	1.429±0.0759	1.460±0.1267	1.607±0.0973	n.s.
Sensor 12				
V1	V2	V3	V4	P value
1.321±0.1193	1.487±0.0781	1.559±0.1282	1.715±0.0970	0.0300
V1 vs V4				0.0046
Sensor 13				
V1	V2	V3	V4	P value
1.036±0.0877	1.185±0.0624	1.196±0.0981	1.315±0.0757	n.s.
Sensor 14				
V1	V2	V3	V4	P value
0.8994±0.0752	1.014±0.0542	1.048±0.0820	1.163±0.0604	0.0258
V1 vs V4				0.0051
Sensor 15				
V1	V2	V3	V4	P value
2.225±0.1933	2.513±0.1338	2.577±0.2234	2.881±0.1799	0.045
V1 vs V4				0.0071
Sensor 16				
V1	V2	V3	V4	P value
1.241±0.1085	1.405±0.0809	1.447±0.1203	1.577±0.0962	0.0100
V1 vs V4				0.0094
Sensor 17				
V1	V2	V3	V4	P value
1.430±0.1237	1.603±0.0880	1.637±0.1437	1.804±0.1222	n.s.

Sensor 18				
V1	V2	V3	V4	P
2.643±0.2480	3.000±0.1781	3.093±0.2729	3.385±0.2228	n.s.
Sensor 19				
V1	V2	V3	V4	P value
0.9070±0.0727	1.033±0.0569	1.075±0.0908	1.172±0.0648	0.0273
V1 vs V2				0.0320
V1 vs V4				0.0052
Sensor 20				
V1	V2	V3	V4	P
2.341±0.2267	2.658±0.1648	2.702±0.2400	2.910±0.1990	n.s.
Sensor 21				
V1	V2	V3	V4	P
0.8288±0.0683	0.9423±0.0510	0.9509±0.0762	1.057±0.0597	0.0362
V1 vs V2				0.0307
V1 vs V4				0.0062
Sensor 22				
V1	V2	V3	V4	P value
1.004±0.0863	1.132±0.0594	1.132±0.0935	1.233±0.0767	n.s.
Sensor 23				
V1	V2	V3	V4	P value
9.586±0.9759	10.94±0.7091	11.47±1.157	13.26±1.443	n.s.
Sensor 24				
V1	V2	V3	V4	P value
1.403±0.1185	1.597±0.0943	1.704±0.1439	1.904±0.0872	0.0084
V1 vs V2				0.0404
V1 vs V4				0.0030
V2 vs V4				0.0365
Sensor 25				
V1	V2	V3	V4	P value
1.426±0.1198	1.618±0.0865	1.635±0.1300	1.849±0.1003	0.0286
V1 vs V2				0.0494
V1 vs V4				0.0051
Sensor 26				
V1	V2	V3	V4	P value
0.003672±0.3577	0.004201±0.2878	0.004370±0.4194	0.004926±0.4143	n.s.
Sensor 27				
V1	V2	V3	V4	P value
0.0005989± 0.0456	0.0006938± 0.0359	0.0007088± 0.0597	0.0007838± 0.0412	0.0182
V1 vs V2				0.0170
V1 vs V4				0.0013
Sensor 28				

V1	V2	V3	V4	P value
0.004238±0.4047	0.004810±0.2025	0.004937±0.4320	0.005434±0.3809	n.s.
Sensor 29				
V1	V2	V3	V4	P value
2.228±0.2167	2.521±0.1581	2.573±0.2285	2.890±0.2030	n.s.
Sensor 30				
V1	V2	V3	V4	P value
0.9987±0.0863	1.151±0.0666	1.170±0.0987	1.301±0.0946	n.s.
Sensor 31				
V1	V2	V3	V4	P value
15.13±1.761	17.41±1.240	18.35±2.133	24.58±6.076	n.s.
Sensor 32				
V1	V2	V3	V4	P value
0.6599±0.0538	0.7333±0.0397	0.7486±0.0599	0.8363±0.0437	0.0426
V1 vs V4				0.0066

*Data, expressed as mean ± SEM, are relative changes in sensor resistance [(Rmax-R0)/R0] (µOhms). Intra-group, between-visit comparisons were performed with ANOVA for repeated measures. If overall P was lower than 0.05, considered significant, paired t test was performed. Abbreviations: n.s., not significant; V, visit.

Table 3. Quartz crystal sensor e-nose response*. The behavior of each sensor (sensor 1 - sensor 8) is shown. Sensors whose mean values differ across visits are shown in bold.

Sensor 1				
V1	V2	V3	V4	P value
21.5 (14.75-31)	30 (19-38)	27.5 (21.75-36.75)	30.5 (22.75-38.25)	n.s.
Sensor 2				
V1	V2	V3	V4	P value
19 (14-29)	27.5 (20.5-32.75)	25 (21.5-35.25)	30.5 (25.5-38)	0.0092
V1 vs V4				0.0329
Sensor 3				
V1	V2	V3	V4	P value
49 (38.25-76.25)	79.5 (57-105.8)	66.5 (53.5-106.5)	89 (65.5-101)	n.s.
V1 vs V2				0.0279
Sensor 4				
V1	V2	V3	V4	P value
31 (26.75-48)	48.5 (37.25-58.25)	44 (36-66.75)	54.4 (43.5-67)	0.0523
V1 vs V2				0.0445
V1 vs V4				0.0413
Sensor 5				
V1	V2	V3	V4	P value
12.5 (9-16.8)	19 (13.3-22.5)	15.5 (12.5-25.5)	19.5 (15.8-24.3)	n.s.
Sensor 6				
V1	V2	V3	V4	P value
24 (18.8-33.3)	29.5 (23.3-43.8)	36 (25-41)	32 (24.8-45)	n.s.
Sensor 7				
V1	V2	V3	V4	P value
20.5 (15.3-32)	29 (22.3-38)	29 (25.8-41.3)	32.5 (29-36.8)	n.s.
Sensor 8				
V1	V2	V3	V4	P value
30.5 (20.3-44.5)	42 (32.5-55.3)	30 (27.5-48.3)	41.5 (29.5-49.5)	n.s.

*Data, expressed as median and interquartile range, are relative changes in sensor frequency [(ƒmax-ƒ0)/ƒ0] (Hz). Intra-group, between-visit comparisons were performed with Friedman's test. If overall P was lower than 0.05, considered significant, Wilcoxon matched-pairs signed rank test was performed. Abbreviation: n.s., not significant; V, visit.

Table 4. Classification accuracies with 95% confidence interval and P values among different pharmacological treatments from visit 1 to visit 4 based on multidimensional PLS models in 14 patients with COPD. The significant variables in the univariate analysis of each experimental technique are also reported (Wilcoxon signed-rank test P values).

Comparison	Overall accuracy (P value)	Model quality	Variable		P value
Visit 1 vs. Visit 2	66.4% (CI 95% 66.0-66.9%) (P = 0.12)	AUC 0.714 Youden's J 0.294	Carbon polymer sensor e-nose	Sensor2	0.036
				Sensor8	0.021
				Sensor19	0.032
				Sensor21	0.031
				Sensor24	0.040
				Sensor25	0.049
				Sensor27	0.017
			Quartz crystal sensor e-nose	Sensor 3	0.028
				Sensor 4	0.044
			Spirometry	PEF, % pred	0.033
				PEF	0.044
Visit 1 vs. Visit 3	71.5% (CI 95% 71.1-72.0%) (P < 0.01)	AUC 0.704 Youden's J 0.446	Eicosanoids	PGE_2 in sputum supernatants	0.021
			Spirometry	FEV_1/FVC, %	0.008
Visit 1 vs. Visit 4	82.5% (CI 95% 82.0-83.0%) (P < 0.01)	AUC 0.857 Youden's J 0.666	NMR spectroscopy	Formate in EBC	0.029
			Carbon polymer sensor e-nose	Sensor1	0.006
				Sensor2	0.005
				Sensor4	0.004
				Sensor7	0.005
				Sensor8	0.006
				Sensor12	0.005
				Sensor14	0.005
				Sensor15	0.007
				Sensor16	0.009
				Sensor19	0.005
				Sensor21	0.006
				Sensor24	0.003
				Sensor25	0.005
				Sensor27	0.001
				Sensor32	0.007
			Quartz crystal sensor e-nose	Sensor 2	0.032
				Sensor 4	0.041
Visit 2 vs. Visit 3	59.9% (CI 95% 58.8-61.1%) (P = 0.23)	AUC 0.571 Youden's J 0.134	Spirometry	$FEF_{25\%-75\%}$, L	0.029
				$FEF_{25\%-75\%}$, % pred	0.026
Visit 2 vs. Visit 4	59.8% (CI 95% 58.2-61.3%) (P = 0.12)	AUC 0.556 Youden's J 0.214	Carbon polymer sensor e-nose	Sensor 24	0.037
Visit 3 vs. Visit 4	74.6% (CI 95% 73.9-75.2%) (P < 0.01)	AUC 0.760 Youden's J 0.454	Eicosanoids	PGE_2 in sputum supernatants	0.008
			NMR spectroscopy	Acetate	0.009

Abbreviations: AUC, area under the curve; EBC, exhaled breath condensate; $FEF_{25\%-75\%}$, forced expiratory flow at 25%-75% of the forced vital capacity; FEV_1, forced expiratory volume in one second; FVC, forced vital capacity; NMR, nuclear magnetic resonance; PEF, peak expiratory flow; PGE_2, prostaglandin E_2; % pred, percentage of predicted value; PLS, partial least squares.

Figure 1. Study design and detail of interventions. At screening visit (visit 1), treatment with a constant dose of inhaled fluticasone propionate/salmeterol xinafoate fixed dose combination (FDC) (500/50 µg b.i.d. via a dry powder inhaler) for at least 8 weeks was switched to an extrafine formulation of inhaled beclomethasone dipropionate (BDP)/formoterol fumarate (FOR) FDC (100/6 µg 2 puffs b.i.d. via a pressurized metered dose inhaler [pMDI]). After a run-in phase of 2 weeks, the FDC containing beclomethasone was suspended (visit 2, baseline visit), while maintaining formoterol alone (6 µg 2 puffs b.i.d. via pMDI). After 4 weeks of beclomethasone withdrawal (visit 3, post-withdrawal visit), treatment with inhaled beclomethasone/formoterol FDC at the same dose (100/6 µg 2 puffs b.i.d. via pMDI) was reintroduced. Exhaled breath sampling for e-nose analysis, measurement of fraction of exhaled nitric oxide (F_ENO), exhaled breath condensate (EBC) collection, pulmonary function tests (PFT), and sputum induction were performed at each visit. Study duration was 10 weeks.

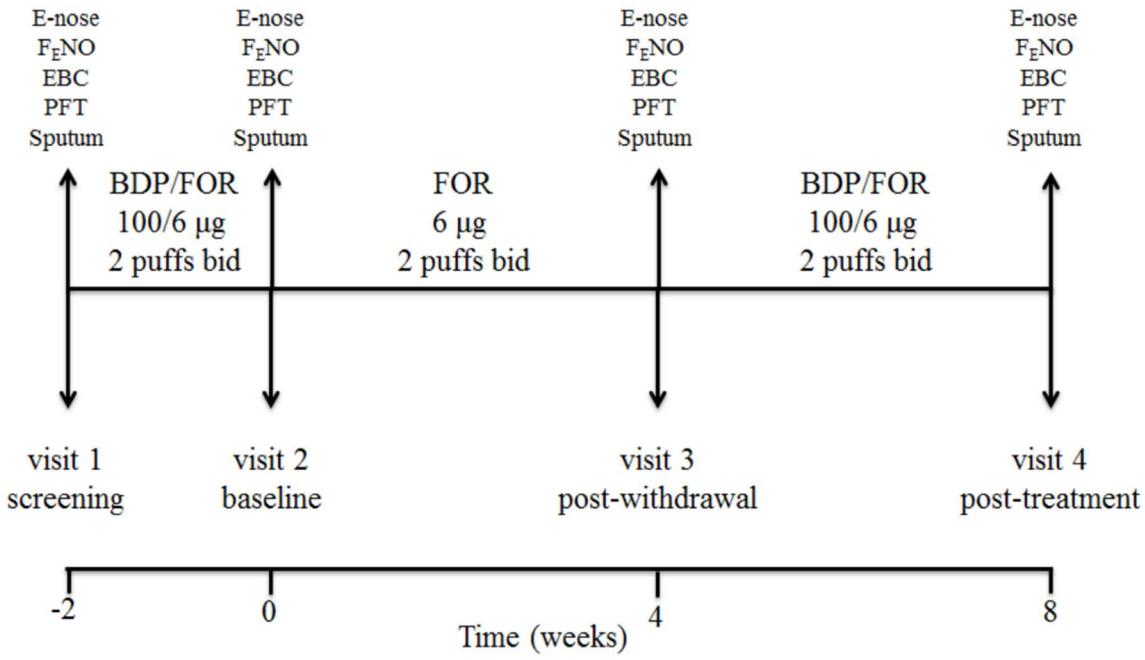

Figure 2. Pre-bronchodilator forced expiratory flow at the 25%-75% of the forced vital capacity ($FEF_{25\%-75\%}$) and peak expiratory flow (PEF) values in 14 patients with COPD at visit 1 (V1) to visit 4 (V4). A) $FEF_{25\%-75\%}$ percentage predicted values; B) absolute $FEF_{25\%-75\%}$ values; C) PEF percentage predicted values; D) absolute PEF values. Mean values ± SEM are shown.

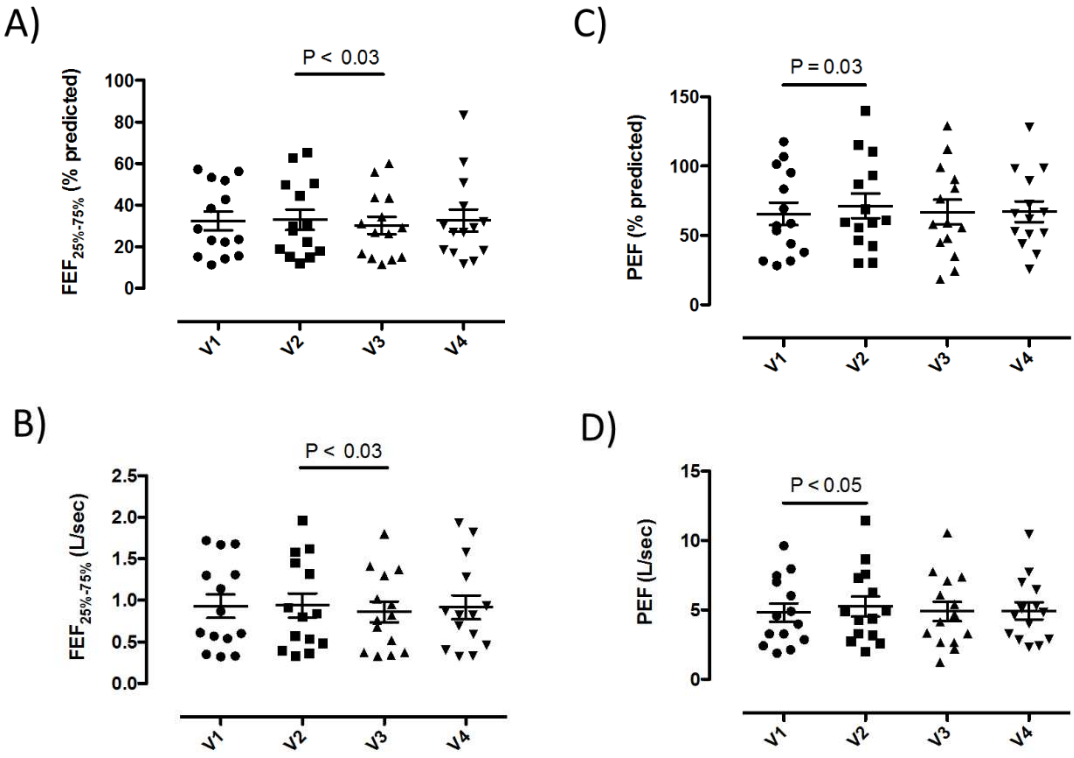

Figure 3. An example of EBC NMR spectrum at 600 MHz. All metabolites assigned and quantified are reported in figure.

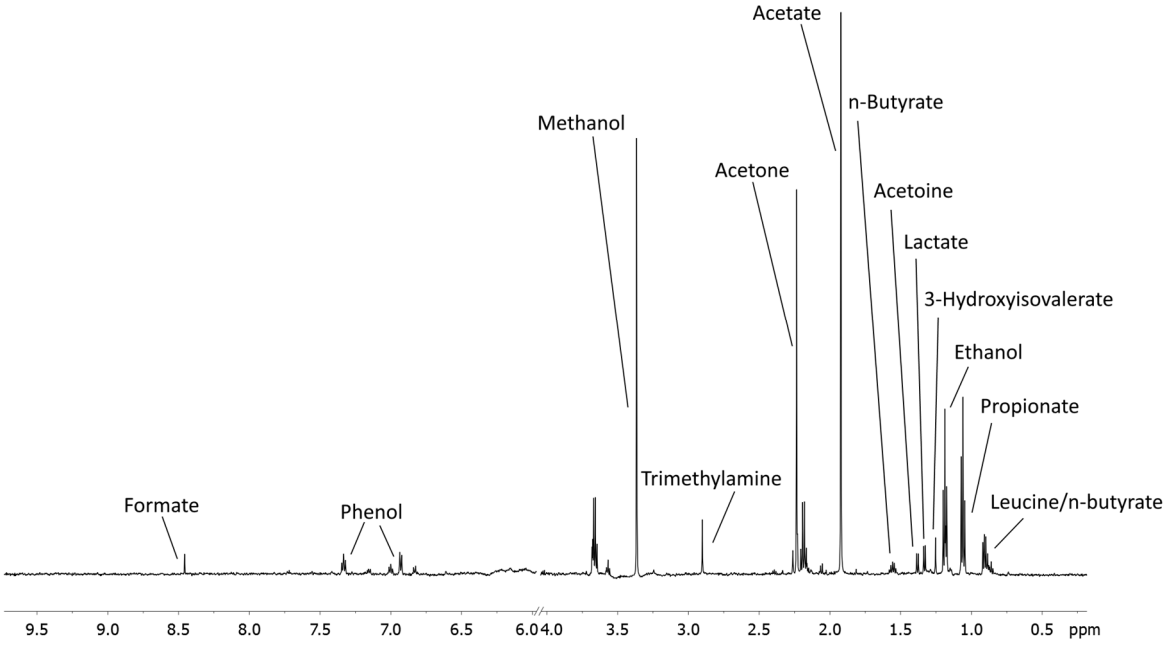

Figure 4. Heatmap showing correlations between study outcome measures in 14 patients with COPD at visit 1 to visit 4 (n = 56). R values are shown as different degree of colour intensity (red, positive correlations; blue, negative correlation).

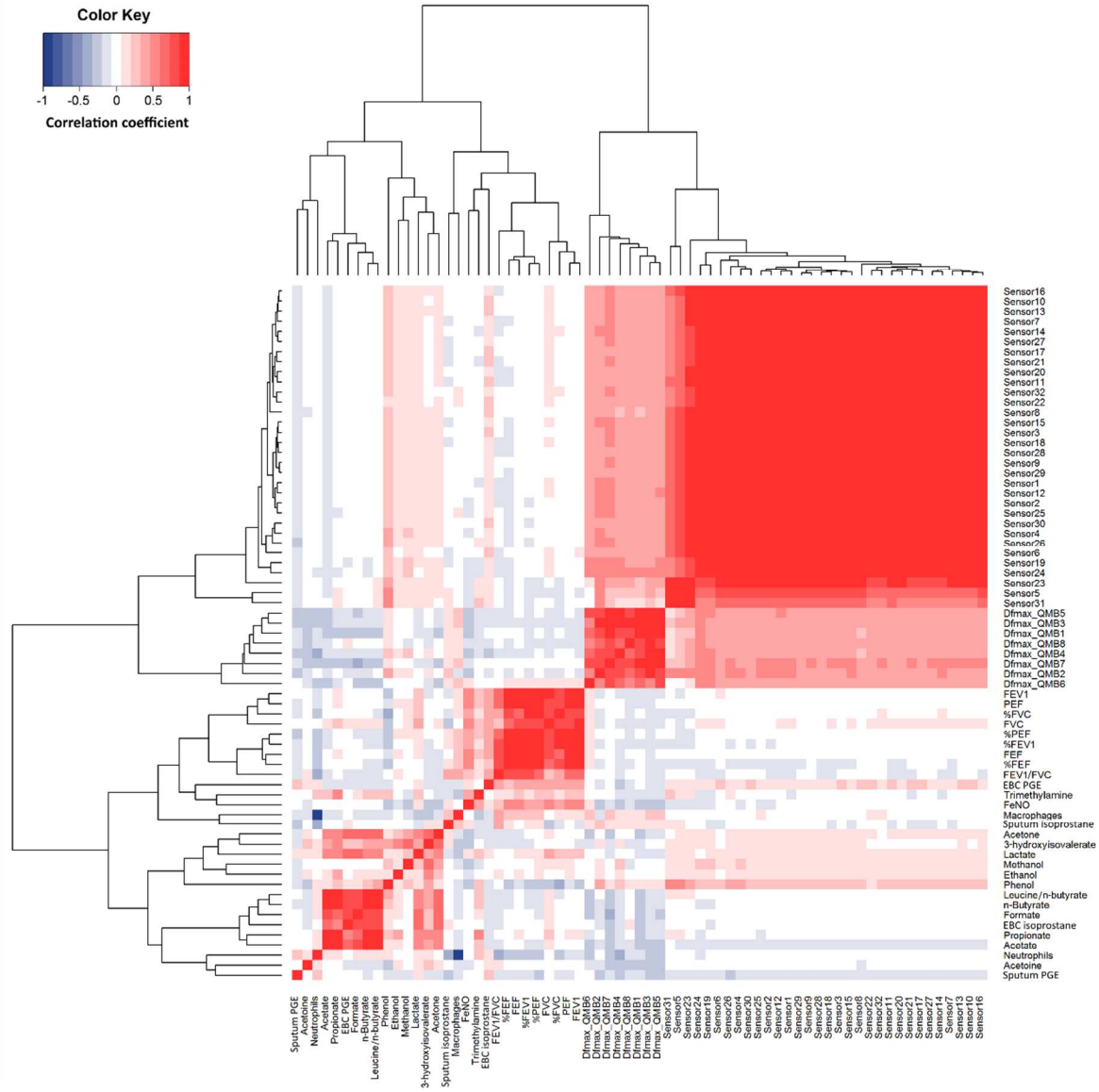

Supplementary materials:

SUPPLEMENTARY METHODS

Study subjects

Subjects were on maintenance treatment with inhaled fluticasone propionate/salmeterol at a constant dose of 500/50 μg b.i.d. delivered via a dry powder inhaler (DPI) for at least 8 weeks. Patients were recruited at the outpatient clinic, Respiratory Medicine Unit, and Clinical Pharmacology Unit, Catholic University of the Sacred Heart, University Hospital Agostino Gemelli Foundation, Rome, Italy.

Study design

Treatment with an extrafine beclomethasone/formoterol fixed dose combination (FDC) was suspended and reintroduced as described in Figure 1 (main manuscript).

At visit 1, patient treatment, consisting of a constant dose of inhaled fluticasone propionate/salmeterol xynafoate FDC (500/50 μg b.i.d. via DPI) for at least 8 weeks, was switched to an extrafine formulation of inhaled beclomethasone/formoterol FDC (100/6 μg 2 puffs b.i.d. via pressurized metered dose inhaler [pMDI]). After 2-week treatment (visit 2), FDC containing beclomethasone was suspended, while maintaining formoterol alone (6 μg 2 puffs b.i.d. via pMDI). After 4 weeks of beclomethasone withdrawal (visit 3), treatment with inhaled extrafine beclomethasone/formoterol FDC at the same dose (100/6 μg 2 puffs b.i.d. via pMDI) was reintroduced and maintained for 4 weeks (visit 4). Study duration was 10 weeks. Study design and details of intervention are shown in Figure 1 (main manuscript). At each visit, interventions were performed in the following order: fraction of exhaled nitric oxide (F_ENO) measurement, exhaled breath sampling for e-nose analysis, exhaled breath condensate (EBC) collection, pulmonary function tests, and sputum induction. Skin prick testing was performed at visit 1.

Before breath sampling, subjects were asked to refrain from eating and drinking (except water) for at least 12 h and to stop short-acting bronchodilators for at least 12 h and long-acting bronchodilators for at least 24 h. Breath sampling and e-nose analysis was performed in a windowless conference facility in the Clinical Pharmacology Unit, University Hospital Agostino Gemelli Foundation, Catholic University of the Sacred Heart, controlled by a central ventilation system and without disinfectant dispensers or person traffic.

Collection of exhaled breath

Exhaled breath was collected through mixed expiratory sampling in which total breath, including dead space air, is collected. An equilibration phase (wash-in) with volatile organic compound (VOC)-filtered room air was performed before breath sampling to reduce the interference of ambient VOCs [1,2]. Subjects were asked to breathe tidally VOC-filtered air for 5 minutes, while wearing a nose-clip, into a 2-way non-rebreathing valve with an inspiratory VOC filter and an expiratory silica reservoir to reduce sample water vapor as this could affect sensor response [3,4]. Then, subjects were asked to inhale to maximal inspiration and perform a FVC manoeuvre into a Tedlar bag against an expiratory resistance of 20 cmH_2O to close the soft palate and obtain an expiratory flow of 0.1-0.2 L/s [1,2]. This breath sampling procedure minimizes the effect of ambient VOCs on e-nose analysis.

Electronic nose analysis

The setup for e-nose analysis used in this study consists of a commercially available e-nose (Cyranose 320®, Sensigent, Baldwin Park, USA, formerly manufactured by Smiths Detection, Pasadena, USA) [1,5] and a prototype e-nose (Ten 2011, University of Rome Tor Vergata, Italy) [6]. The commercially available e-nose consists of an array of 32 chemical sensors made from composites of an inorganic conductor (carbon black) and insulating organic polymers [5]. The measurement is based on a resistance variation in each chemical sensor when exposed to breath VOCs. E-nose analysis was performed immediately after breath sample collection. Each breath sample was analyzed 5 times with the same e-nose. Data from the first measure were discarded as suggested by the manufacturer and reported in previous studies [1,7]; the second e-nose measure was used for data analysis [2]. E-nose responses for each sensor (changes in resistance) were stored in the e-nose in-built database, copied into a Matlab file and analyzed offline with a pattern recognition algorithm [2]. Algorithms were created using principle component analysis (PCA) and multilevel partial least square (PLS) analysis. The K-nearest neighbours method, applied on the multilevel PLS scores, was used for classification purposes. Only the first few principal components were used to avoid errors of the first degree. Component number was chosen based on those required to describe 99.9% of the dataset variance. T-test was used to identify discriminating principle components, with a P value < 0.1 considered significant, which were then analyzed with canonical discriminant analysis. The Monte Carlo cross-validation scheme was used to calculate the cross-validated sensitivity, specificity and global classification accuracy of the algorithm as the limited sample size precluded training and testing validation. The analysis was performed with SPSS (version 17.0, SPSS Inc., Chicago, IL, USA).

The second e-nose, which detects frequency variations, contains an array of eight quartz microbalance (QMB) gas sensors coated by molecular films of metallo-porphyrins [6]. Sensors detect the amount of molecules absorbed in a sensitive film through the changes of resonant frequency that is proportional to the absorbed mass [6].

EBC sampling

The condenser has a saliva trap to reduce the chance of salivary contamination [8]. Under our experimental conditions, no effect of salivary contamination or cleaning solution on EBC profiles has been observed [8-10]. Subjects were asked to wash their mouth thoroughly before collecting EBC, to breathe tidally through a mouthpiece into a two-way non-rebreathing valve for 15 minutes wearing a nose-clip, and to stop breathing into the mouthpiece and swallow every time they felt salivation. An average of 1.5 ± 0.2 mL (mean ± SD) of EBC was collected in 15 minutes of tidal breathing. EBC sampling was performed as previously described [8]. EBC was immediately transferred into 10 mL glass vials, closed with 20 mm butyl rubber lined with polytetrafluoroethylene septa and crimped with perforated aluminum seals [8]. Before sealing, volatile substances were removed from samples by a gentle nitrogen gas flow for 3 min [8]. Previous experiments showed no difference with spectra acquired after a variable time of nitrogen exposure (1, 3, 5, 10, 15 and 20 min) [9]. However, as 1-min interval appeared to be too short to avoid systematic errors, a 3-min interval was chosen. Samples were not dried out to avoid their precipitation, with a possible loss of nonvolatile compounds, and/or formation of aggregates upon dissolving the dried condensate for NMR measurements. Sealed samples

were then frozen in liquid nitrogen, so as to immediately "quench" metabolism and preserve the metabolite concentrations [6,9]. Samples were stored at -80°C until metabolomic analysis.

Metabolomic analysis of EBC with NMR spectroscopy

EBC samples, stored at -80°C, were thawed at room temperature. Sample aliquots (630 µL) were then centrifuged at 14000 rpm for 10 minutes. Sample aliquots of the supernatant (540 µL) were mixed with 55 µL of $^{2}H_2O$ and 5 µL of buffer phosphate (0.2 M Na_2HPO_4, 0.2 M NaH_2PO_4 in 100% $^{2}H_2O$, pH 7) containing 30 mM NaN_3 and 10 mM sodium 3-trimethylsilyl [2,2,3,3-2H4] propionate (TMSP). Then, 450 µL of mixture were pipetted into 4.25 mm NMR tube (Bruker BioSpin) [11].

^{1}H-NMR spectra were acquired using a Bruker 600 MHz spectrometer (Bruker BioSpin) operating at 600.13 MHz proton Larmor frequency and equipped with a 5 mm CPTCI ^{1}H-^{13}C/^{31}P-^{2}H cryo-probe including a z-axis gradient coil, an automatic tuning-matching (ATM), and an automatic sample changer [11].

A PT 100 thermocouple served for temperature stabilization at the level of approximately 0.1 K at the sample. Before measurement, samples were kept for at least 3 min inside the NMR probe head for temperature equilibration (300 K). For each sample, a one-dimensional NMR spectrum was acquired with water peak suppression using a standard pulse sequence (NOESY presat), using 512 free induction decays (FIDs), 64 k data points, a spectral width of 12019 Hz, an acquisition time of 2.7 s, a relaxation delay of 4 s, and a mixing time of 100 ms [11].

Free induction decays were multiplied by an exponential function equivalent to 1.0 Hz line-broadening factor before applying Fourier transform. Transformed spectra were manually corrected for phase and baseline distortions, and calibrated (TMSP peak at 0.00 ppm) using TopSpin (Bruker). Each one-dimensional spectrum in the range of 0.02–10 ppm was segmented into 0.02-ppm chemical shift buckets, and the corresponding spectral areas, after scaling, were used as input variables for the subsequent statistical analysis [11]. Regions between 6.0 and 4.5 ppm, containing residual water signals, were removed. Probabilistic quotient normalization (PQN) algorithm [12] was chosen to normalize the spectra, because it is a more accurate and robust alternative to the total area scaling, and PQN performs well even when large variations of dilution occur. Signals were assigned on template one dimensional NMR profiles by using matching routines of AMIX 3.8.4 (Bruker BioSpin) in combination with the BIOREFCODE reference database (Bruker BioSpin), and publicly available databases like HMDB (Human Metabolome DataBase) [13].

All data analyses were performed using R, an open source software for the analysis of statistical data [14]. Multivariate data analyses were conducted on processed data by combining established methods. Data reduction was obtained by means of multilevel Partial Least Square Analysis (mPLS) using the algorithm implemented in the R-library "plsgenomics" and the standard R function "cancor".

For the purpose of classification, we used the K-nearest neighbors (k-NN) method (k = 3) applied on the multilevel PLS scores [16]. All the accuracies reported and the confusion matrix for the different classifications were assessed by means of 100 cycles of a Monte Carlo cross-validation scheme (MCCV, R script in-house developed) [17]. Briefly, 90% of the data were randomly chosen at each iteration as a training set to build the model. Then the remaining 10% was tested and sensitivity, specificity and accuracy for the classification were assessed.

For the univariate analysis, after PQN normalization of the spectra, each spectral region related to the metabolites assigned in the ^{1}H NMR profiles was aligned, by a simple horizontal rigid shift, in a way that the corresponding peaks of interest resulted superimposed. Then, they were integrated reducing the selected ppm intervals, and improving the precision in the integration by compensating the variations in peaks position in the different EBC samples. The obtained integrals represent the metabolite concentrations in arbitrary units. The whole procedure was performed using a R script developed in house. EBC metabolite concentrations at each visit were determined. Statistical significance was assessed using the univariate non-parametric Wilcoxon signed-rank test [18]. A P value < 0.05 was deemed statistically significant.
To evaluate the discrimination power of the integrated model containing all the different analytical approaches used in this study, paired visit comparisons were performed using data matrices created by binding together all the different variables obtained from the various techniques (EBC NMR-spectroscopy, spirometry, carbon polymer sensor e-nose, quartz crystal sensor e-nose, eicosanoids and FeNO measurements). On this dataset, the same multivariate statistical approach previously described was applied (multilevel PLS and cross-validation using kNN). Furthermore, the accuracies calculated were assessed for significance against the null hypothesis of no prediction accuracy in the data by means of 10^2 randomized class-permutations test [19].

Measurement of PGE_2 and 8-isoprostane in sputum supernatants and EBC
PGE_2 and 8-isoprostane concentrations in sputum supernatants and EBC were measured with radioimmunoassays developed in our laboratory that were previously validated and compared with gas chromatography/mass spectrometry (GC/MS) and high performance liquid chromatography (HPLC) [20,21].

Multivariate data analysis
To investigate the correlations among the different analytical approaches used in this study, a matrix with data from all techniques was created and then its correlation matrix was calculated using the algorithm implemented in the R-library "psych" [22,23]. The heatmap of the correlation matrix was built using the R-function "heatmap.2", implemented in the "gplots" package [24]. This function reordered the rows and columns of the correlation matrix according to the restrictions imposed by the dendrogram, calculated on the basis of the Euclidean distance among the data and using the R-function "hclust".

Statistical analysis
Data were expressed as mean ± SEM or medians and interquartile ranges (25^{th} and 75^{th} percentiles), after assessing for normality with the D'Agostino-Pearson omnibus normality test. Depending on data distribution, repeated-measures ANOVA or Friedman test were used for assessing within-group pharmacological treatment effect. If overall statistical significance was observed, unpaired t test and Mann-Whitney U test were used for comparing groups for normally distributed and nonparametric data, respectively. Correlation was expressed as a Pearson coefficient. Significance was defined as a value of P value < 0.05.

RESULTS

Pulmonary function testing

All patients with COPD performed spirometry at all visits. There was no missing data. Results of pulmonary function tests show higher mean absolute and percentage of predicted pre-bronchodilator $FEF_{25\%-75\%}$ values after treatment with inhaled beclomethasone/formoterol FDC in microparticle formulation (visit 2) compared with inhaled formoterol alone in microparticle formulation (visit 3) (Figure 2A and 2B). These data suggest that inhaled ultrafine beclomethasone/formoterol FDC improves small airway function as reflected by $FEF_{25\%-75\%}$ values. This might be particularly relevant as this functional effect is observed after only 4-week treatment with inhaled beclomethasone/formoterol, a relatively short duration of treatment for COPD trials, and in view of the fact that all patients with COPD included in our study had normal sputum eosinophils, negative reversibility test to bronchodilators, negative skin prick tests, and no history of atopy, thus, excluding an asthma component, on which ICS are generally more effective.

An effect of ICS on small airway function is also suggested by a higher mean pre-bronchodilator FEV_1/FVC ratio at visit 1 (COPD patients were on inhaled fluticasone/salmeterol FDC at full doses) compared with visit 3 (post-treatment with inhaled formoterol alone) (s-Table 1).

Higher mean absolute and percentage of pre-bronchodilator PEF predicted values were observed after 4-week treatment with inhaled beclomethasone/formoterol (visit 2) compared with visit 1 (s-Table 1, Supplementary Figure 2C and 2D). These data might be the consequence of a higher lung deposition of the ultrafine drug formulation delivered through pMDI, resulting in a greater anti-inflammatory and/or bronchodilating effect of inhaled beclomethasone/formoterol combination in the small airways compared with inhaled fluticasone/salmeterol in standard formulation delivered through DPI (s-Table 1).

Electronic nose

E-nose analysis with carbon polymer sensor e-nose and quartz crystal sensor e-nose was performed in all 14 subjects at all 4 visits for a total of 56 breathprints for each e-nose. Results are shown in Table 2 and 3. Data were normally distributed and expressed as mean ± SEM. Mean values (n = 14) for each single sensor at each visit (V1-V4) are shown. Within- group differences were assessed by ANOVA for repeated measures and paired t test using GraphPad Prism software.

Regarding analysis with carbon polymer sensor e-nose, mean ΔR values in 15 out of 32 sensors showed significant differences between visit 1 (screening visit) and visit 4 (post-treatment visit) (sensor 1, 2, 4, 7, 8, 12, 14, 15, 16, 19, 21, 24, 25, 27, 32) and mean ΔR values in 7 sensors showed significant differences between visit 1 and visit 2 (sensor 2, 8, 19, 21, 24, 25, 27).

As all patients with COPD were on a constant dose of a FDC of inhaled fluticasone/salmeterol 500/50 µg one puff b.i.d. via DPI (Seretide® or Aliflus Diskus®) for at least 8 weeks before study enrolment, these data indicate that the FDC of inhaled beclomethasone/formoterol (Foster®) via pMDI at a dose of two puffs of 100/6 µg b.i.d. has a different effect on carbon polymer sensor e-nose breathprints. However, the pathophysiological and clinical implications of these differences are currently unknown and require further study.

There was no difference in the relative change in resistance [(Rmax-R0)/R0] of any sensor between visit 2 (baseline visit) and visit 3 (post-withdrawal visit). These data suggest a similar

effect of inhaled ultrafine beclomethasone/formoterol and inhaled ultrafine formoterol alone on e-nose breathprints in patients with mild to severe COPD. This evidence is reinforced by similar results obtained with the quartz crystal sensor e-nose, based on a different technology (see below).

There was no difference in the behaviour of all sensors between visit 2 (baseline visit) and visit 4 (post-treatment visit).

Consistent with carbon polymer sensor behaviour, two quartz crystal sensors showed significant differences between visit 1 and visit 4, whereas between-visit difference in sensor 3 (P = 0.056) and 5 (P = 0.059) response was close to statistical significance. Sensor 3 and 4 showed significant differences between visit 1 and visit 2, whereas between-visit differences in sensor 2 (P = 0.054) and 5 (P = 0.093) approached statistical significance (Table 3).

These results are consistent with and confirm those obtained with the carbon polymer sensor array, an e-nose based on a different technology (see above), indicating a robust methodology.

Metabolomic analysis of EBC with NMR spectroscopy

EBC samples obtained from 14 patients with COPD at visit 1 to visit 4 for a total of 56 EBC samples were analyzed with NMR spectroscopy as described in Methods. There was no missing data.

When EBC spectra were analyzed with multilevel PLS, that is analysis of pairs of spectra from the same subject at two different visits, comparison between visit 1 and visit 4 showed a classification accuracy of 72% (Supplementary Figure 2).

These data indicate that regular treatment with inhaled fluticasone/salmeterol (COPD patients were on this FDC at a constant full dose, delivered through DPI, for at least 8 weeks) is associated with a different EBC metabolite profile compared with that observed after 4-week treatment with inhaled beclomethasone/formoterol in microparticle formulation delivered through pMDI. The pathophysiological meaning and possible implications of these results require further research.

Regarding the other paired comparisons, classification accuracy was below 70% (s-Table 4). The lack of between visit differences in EBC metabolite profiles, apart from visit 1 vs visit 4, could be due to high intragroup inter-individual variability in EBC metabolites which might mask pharmacological treatment-induced differences.

Among metabolites responsible for discrimination between visit 1 and visit 4, formate was the only one with a P-value < 0.05. EBC formate levels were lower at visit 4 (409.1551 ± 333.2239, relative intensity) compared with those observed at visit 1 (694.9539 ± 534.4349, relative intensity; P = 0.029) (Supplementary Figure 3A and 3B). EBC formate levels were also lower at visit 4 (409.1551 ± 333.2239, relative intensity) compared with those observed at visit 2 (695.1441 ± 770.2066, relative intensity; P = 0.049), although accuracy of classification between visit 2 and visit 4 based on EBC NMR spectroscopy did not reach the significant threshold of 0.7 (0.63) (s-Table 4). Moreover, at visit 4 EBC acetate levels were lower than those measured at visit 3 (P = 0.01) (s-Table 3). The pathophysiological meaning and possible implications of these findings require further research.

Measurement of fraction of exhaled nitric oxide (F_ENO)

Measurement of F_ENO was performed in all subjects at each visit. There was no missing data.

There was no within-group difference in F_ENO concentrations in patients with COPD (overall P = 0.3529) (s-Table 5).
However, in the 8 patients with COPD who had elevated F_ENO concentrations (> 20 ppb), median F_ENO was lower after treatment with beclomethasone/formoterol FDC (visit 4) than after treatment with formoterol alone (visit 3) (26.6 (12.8-34.) ppb vs 14.9 (13.1-25.7) ppb), although this difference was not statistically significant (P = 0.2334).
In the same group of patients with COPD and elevated F_ENO, the difference in median F_ENO concentrations after treatment with fluticasone/salmeterol FDC (visit 1) (27.2 (23.2-29.3) ppb) and after treatment with beclomethasone/formoterol FDC (visit 2) (19.7 (12.8-34.7) ppb) was very close to statistical significance (P = 0.0584, Wilcoxon matched-pairs signed rank test). Taken together, this evidence might suggest a selective effect of inhaled beclomethasone on F_ENO in those patients with COPD who have higher F_ENO concentrations at baseline. As patients with COPD at visit 1 were on a constant full dose of inhaled fluticasone, delivered through DPI, for at least 2 months, further reduction in F_ENO concentrations after 4-week treatment with inhaled beclomethasone (visit 2), might reflect a greater anti-inflammatory effect of the microparticle formulation.

Measurement of PGE_2 in sputum supernatants

PGE_2 concentrations were detected in 49 out of a total of 56 sputum samples. In 7 samples, sputum PGE_2 concentrations were undetectable. One patient with COPD had undetectable sputum PGE_2 concentrations at all visits (4 samples) and was excluded from statistical analysis. At the other 3 undetectable samples, an arbitrary concentration value of 1 pg/mL, corresponding to 50% of the analytical technique detection limit (2 pg/mL), was assigned.
Median sputum PGE_2 concentrations in patients with COPD at visit 1 to visit 4 are shown in s-Table 6.
Compared with visit 3, lower sputum PGE_2 concentrations were observed at visit 4 (P = 0.008) and at visit 3 (P = 0.021) (s-Table 6).
Median sputum PGE_2 concentrations at visit 2 (post-treatment with inhaled beclomethasone/formoterol) were lower (3.75 (1.98-54.9) pg/mL) than those observed at visit 3 (post-treatment with inhaled formoterol alone) (40.1 (8.3-47.0) pg/mL), although this difference was not statistically significant (P = 0.21), likely due to the high inter-individual variability.
These data suggest that treatment with ICS combinations, containing both fluticasone propionate and beclomethasone, reduces sputum concentrations of PGE_2, an eicosanoid which has pro-inflammatory effects in the airways.

Measurement of 15-F_{2t}-isoprostane in sputum supernatants

15-F_{2t}-isoprostane concentrations were detected in 30 out of a total of 56 sputum samples. In 26 samples, sputum 8-isoprostane concentrations were undetectable. Five patients with COPD had undetectable sputum 15-F_{2t}-isoprostane concentrations at all visits (20 samples) and were excluded from statistical analysis. At the other 6 undetectable samples, an arbitrary concentration value of 1 pg/mL, corresponding to 50% of the analytical technique detection limit (2 pg/mL), was assigned.
Median sputum 15-F_{2t}-isoprostane concentrations in patients with COPD at visit 1 to visit 4 are shown in s-Table 6.

There was no within-group difference in sputum 15-F_{2t}-isoprostane concentrations (P = 0.84) (s-Table 6) suggesting that this biomarker of oxidative stress is resistant to ICS treatment in line with previous studies [24].

Measurement of PGE_2 in EBC

PGE_2 concentrations were detected in 43 out of a total of 56 EBC samples. In 13 samples, EBC PGE_2 concentrations were undetectable. Two patients with COPD had undetectable EBC concentrations at all visits (8 samples) and were excluded from statistical analysis. At the other 5 undetectable samples, an arbitrary concentration value of 1 pg/mL, corresponding to 50% of the analytical technique detection limit (2 pg/mL), was assigned.

Median EBC PGE_2 concentrations in patients with COPD at visit 1 to visit 4 are shown in Table 4. There was no within-group difference in EBC PGE_2 concentrations (P = 0.19) (s-Table 6).

Measurement of 15-F_{2t}-isoprostane in EBC

15-F_{2t}-isoprostane concentrations were detected in 46 out of a total 56 EBC samples. In 10 samples, EBC 15-F_{2t}-isoprostane concentrations were undetectable. At these samples, an arbitrary concentration value of 1 pg/mL, corresponding to 50% of the analytical technique detection limit (2 pg/mL), was assigned.

Median EBC 15-F_{2t}-isoprostane concentrations in patients with COPD at visit 1 to visit 4 are shown in s-Table 6.

There was no within-group difference in EBC 15-F_{2t}-isoprostane concentrations (P = 0.60) (s-Table 6) suggesting that this biomarker of oxidative stress is resistant to ICS treatment in line with previous studies [25].

Sputum cell analysis

Sputum was successfully induced and collected in all patients at all visits. Fifty-six sputum samples were collected. Corresponding cytospins were prepared and slides were stained with May-Grunwald-Giemsa as described Methods. Sputum slides were read as described in Methods. Thirteen sputum slides were discarded because of high salivary squamous cells (> 30% of total sputum cells). No patient with COPD had sputum eosinophilia, as defined by sputum cell counts > 3%, at visit 1 (screening visit).

Medians and interquartile range of sputum cell types are shown in s-Table 7. Neutrophils were the predominant cell types in sputum obtained from patients with COPD.

Within-group comparison was performed with Friedman test in the eight patients who had a complete set of sputum slides (visit 1 to visit 4).

There was no within-group difference in neutrophil, macrophage, eosinophil, basophil, bronchial epithelial cell counts (s-Table 8). Basophil and bronchial epithelial cell counts are not shown in Table 5 as counts were mostly 0.

Correlations

Correlations between multidimensional variables in 14 patients with COPD at visit 1 to visit 4 (n = 56) are shown as a heatmap (Figure 4).

There was a negative correlation between quartz crystal sensor 4 (r = -0.35, P = 0.023) and 7 (r = -0.31, P = 0.041) and sputum neutrophil cell counts (Figure 4). Negative correlations

between quartz crystal sensor 3 (r = -0.26, P = 0.88), 5 (r = -0.29, P = 0.056) and 6 (r = -0.27, P = 0.075) and sputum neutrophils were close to statistical significance.
Apart from carbon polymer sensor 2 (r = 0.31, P = 0.021), 3 (r = 0.30, P = 0.026), 4 (r = 0.35, P = 0.007), 5 (r = 0.51, P = 6.58^{-5}), 6 (r = 0.27, P = 0.048), 9 (r = 0.31, P = 0.019), 12 (r = 0.28, P = 0.037), 15 (r = 0.31, P = 0.022), 18 (r = 0.27, P = 0.042), 19 (r = 0.29, P = 0.031), 23 (r = 0.45, P = 0.001), 25 (r = 0.31, P = 0.022), 26 (r = 0.35, P = 0.007), 28 (r = 0.29, P = 0.028), 29 (r = 0.32, P = 0.016), 30 (r = 0.32, P = 0.015), 31 (r = 0.51, P = 6.89^{-5}), which were correlated with EBC phenol concentrations, there was no correlation between carbon polymer sensors and other outcome measures, including pulmonary function tests, sputum neutrophil and macrophages cell counts, PGE_2 concentrations in sputum supernatants and EBC, and 15-F_{2t}-isoprostane concentrations in sputum supernatants and EBC (Figure 4).
FEV_1/FVC values were negatively correlated with sputum neutrophil cell counts (r = -0.34; P = 0.028) (Figure 4). Negative correlations between sputum neutrophils and FEV_1 percentage of predicted values (r = -0.30, P = 0.053) and $FEF_{25\%-75\%}$ percentage of predicted values (r = -027, P = 0.075) were close to statistical significance (Figure 4).
There was a correlation between EBC PGE_2 and formate (r = 0.78, P = 5.06^{-11}), acetone (r = 0.63, P = 1.64^{-6}), lactate (r = 0.64, P = 6.03^{-7}), n-butyrate (r = 0.82, P = 5.89^{-13}), propionate (r = 0.59, P = 8.26^{-6}), and acetate (r = 0.71, P = 1.23^{-8}) concentrations in EBC, suggesting that these EBC metabolites might be suitable as inflammatory outcome measures.

Multidimensional integrated model for assessment of pharmacological treatment
In the 14 COPD study subjects, multidimensional pairwise discrimination models were built (Table 4). The multidimensional models discriminated between visit 1 versus visit 3 (accuracy = 71.5%, P < 0.01), mainly based on sputum supernatant PGE_2 and FEV_1/FVC ratio; between visit 1 versus visit 4 (accuracy = 82.5%, P < 0.01), mainly based on EBC formate, e-noses, and EBC PGE_2; between visit 3 versus visit 4 (accuracy = 74.6%, P < 0.01), mainly based on sputum PGE_2 and EBC acetate concentrations.
The multidimensional models showed higher accuracy than the models based on spirometry alone (s-Table 9). The sensitivity and specificity reported in s-Table 9 follow the standard definitions of proportion of true positives and proportion of true negatives, respectively. It is worth noting that they appear equal for all the comparisons. Furthermore, scores plot from PLS analysis are centrosymmetric. This seeming uncommon behaviour is fully understandable given the pairwise nature of the analyses performed. In a multilevel PLS, between subject variation is separated from within subject variation by subtracting the individual specific average. In the two class cases, this construction leads to a matrix with a two-block structure with opposite signs, thus producing symmetric PLS scores. During cross-validation, when a multilevel PLS model is built from the training set, the entire variation splitting procedure is performed [26,27]. The procedure should, therefore, be adapted to keep the paired data structure both in the training and in the test set. As a result, complete individuals are left out of the training set (per individual validation, not per sample). At each step, if a sample of one individual is mistaken, inevitably the other is mistaken in the opposite way, leading to a fully symmetric confusion matrix. Of course, this symmetry is broken when considering more than just two time points.

DISCUSSION

Correlations

In the EBC, the strong correlations between PGE_2 and small molecular weight metabolites detected by NRM spectroscopy are unlikely to be explained by individual variability in aerosol particle formation [28] as there was no correlation EBC 15-F_{2t}-isoprostane and EBC metabolites nor between EBC PGE_2 and EBC 15-F_{2t}-isoprostane.

Persistent neutrophilic airway inflammation is a typical characteristic of COPD, which persists even after smoking cessation and sputum neutrophil cell counts are a direct measure of airway inflammation which can be used for assessing the anti-inflammatory effects of drugs [29]. We report a negative correlation between the response of some quartz crystal sensors, in terms of relative changes in sensor frequency [(ƒmax-ƒ0)/ƒ0] (Hz), and sputum neutrophil cell counts. These data suggest that the quartz crystal sensor e-nose is potentially useful for assessing neutrophilic airway inflammation and that the higher neutrophilic airway inflammation the lower e-nose response.

The response of 15 out of 32 carbon polymer sensors was correlated with EBC phenol concentrations. However, the biological meaning of these data has to be defined. There was no correlation between any carbon polymer sensor and the inflammatory outcomes measured in this study, including sputum neutrophil and macrophages cell counts, PGE_2 concentrations in sputum supernatants and EBC, 15-F_{2t}-isoprostane concentrations in sputum supernatants and EBC. However, these findings do not exclude the potential utility of carbon polymer sensor e-nose for assessing airway inflammation as 1) inflammation that characterizes COPD is a complex, heterogeneous, pathophysiological process involving many mediators, whereas only a limited number of inflammatory outcomes was measured in the present study; 2) correlations were studied in 14 patients with COPD considering all 4 visits (n = 56) in a time frame of 10 weeks during which pharmacological treatment was changed three times: this might have caused different effects on e-nose sensors and inflammatory outcome measure, thus, resulting in non-significant correlations.

REFERENCES

1. Fens N, Zwinderman AH, van der Schee MP, de Nijs SB, Dijkers E, Roldaan AC, Cheung D, Bel EH, Sterk PJ. Exhaled breath profiling enables discrimination of chronic obstructive pulmonary disease and asthma. Am J Respir Crit Care Med 2009; 180: 1076-1082.
2. Bofan M, Mores N, Baron M, Dabrowska M, Valente S, Schmid M, Trové A, Conforto S, Zini G, Cattani P, Fuso L, Mautone A, Mondino C, Pagliari G, D'Alessio T, Montuschi P. Within-day and between-day repeatability of measurements with an electronic nose in patients with COPD. J Breath Res 2013; 7(1): 017103.
3. Röck F, Barsan N, Weimar U. Electronic nose: current status and future trends. Chem Rev 2008; 108: 705-711.
4. Wilson AD, Baietto M. Applications and advances in electronic-nose technologies. Sensors (Basel) 2009; 9: 5099-5148.
5. Lewis NS. Comparisons between mammalian and artificial olfaction based on arrays of carbon black-polymer composite vapor detectors. Acc Chem Res 2004; 37: 663-672.
6. Montuschi P, Santonico M, Mondino C, Pennazza G, Mantini G, Martinelli E, Capuano R, Ciabattoni G, Paolesse R, Di Natale C, Barnes PJ, D'Amico A. Diagnostic performance of an

electronic nose, fractional exhaled nitric oxide, and lung function testing in asthma. Chest 2010; 137: 790-796.

7. Dragonieri S, Schot R, Mertens BJ, Le Cessie S, Gauw SA, Spanevello A, Resta O, Willard NP, Vink TJ, Rabe KF, Bel EH, Sterk PJ.. An electronic nose in the discrimination of patients with asthma and controls. J Allergy Clin Immunol. 2007; 120: 856-862.
8. Montuschi P, Paris D, Melck D, Lucidi V, Ciabattoni G, Raia V, Calabrese C, Bush A, Barnes PJ, Motta A. NMR spectroscopy metabolomic profiling of exhaled breath condensate in patients with stable and unstable cystic fibrosis. Thorax 2012; 67: 222-228.
9. De Laurentiis G, Paris D, Melck D, Maniscalco M, Marsico S, Corso G, Motta A, Sofia M. Metabonomic analysis of exhaled breath condensate in adults by nuclear magnetic resonance spectroscopy. Eur Respir J 2008; 32: 1175-1183.
10. Motta A, Paris D, Melck D, de Laurentiis G, Maniscalco M, Sofia M, Montuschi P. Nuclear magnetic resonance-based metabolomics of exhaled breath condensate: methodological aspects. Eur Respir J 2012; 39: 498-500.
11. Bertini I, Luchinat C, Miniati M, Monti S, Tenori L. Phenotyping COPD by ^{1}H NMR metabolomics of exhaled breath condensate. Metabolomics 2014; 10:0. doi:10.1007/s11306-013-0572-3.
12. Dieterle F, Ross A, Schlotterbeck G., Senn H. Probabilistic quotient normalization as robust method to account for dilution of complex biological mixtures. Application in ^{1}H NMR metabonomics. Anal Chem 2006; 78: 4281–4290.
13. Wishart DS, Tzur D, Knox C, Eisner R, Guo AC, Young N, Cheng D, Jewell K, Arndt D, Sawhney S, Fung C, Nikolai L, Lewis M, Coutouly MA, Forsythe I, Tang P, Shrivastava S, Jeroncic K, Stothard P, Amegbey G, Block D, Hau DD, Wagner J, Miniaci J, Clements M, Gebremedhin M, Guo N, Zhang Y, Duggan GE, Macinnis GD, Weljie AM, Dowlatabadi R, Bamforth F, Clive D, Greiner R, Li L, Marrie T, Sykes BD, Vogel HJ, Querengesser L.. HMDB: the Human Metabolome Database. Nucleic Acids Res 2007; 35(Database issue): D521-526.
14. Ihaka R, Gentleman R. R: A Language for Data Analysis and Graphics. J Comput Stat Graph 1996; 5:299–314.
15. Cover T, Hart P. Nearest neighbor pattern classification. Inf Theory IEEE Trans On 1967; 13: 21–27.
16. Bijlsma S, Bobeldijk I, Verheij ER, Ramaker R, Kochhar S, Macdonald IA, van Ommen B, Smilde AK. Large-scale human metabolomics studies: a strategy for data (pre-) processing and validation. Anal Chem 2006; 78: 567-574.
17. Boulesteix A-L. Package "WilcoxCV". Available at: https://cran.r-project.org/web/packages/WilcoxCV/WilcoxCV.pdf
18. Wilcoxon F. Individual comparisons by ranking methods. Biom Bull 1945; 1: 80.
19. Alonso A, Marsal S, Julià A. Analytical methods in untargeted metabolomics: state of the art in 2015. Front Bioeng Biotechnol 2015;3:23.
20. Wang Z, Ciabattoni G, Créminon C, Lawson J, Fitzgerald GA, Patrono C, Maclouf J. Immunological characterization of urinary 8-epi-prostaglandin $F_{2\alpha}$ excretion in man. J Pharmacol Exp Ther 1995; 275: 94-100.
21. Montuschi P, Ragazzoni E, Valente S, Corbo G, Mondino C, Ciappi G, Ciabattoni G. Validation of 8-isoprostane and prostaglandin E_2 measurements in exhaled breath condensate. Inflamm Res 2003; 52: 502-507.

22. Hahsler M, Hornik K, Buchta C. Getting things in order: an introduction to the R package seriation. Journal of Statistical Software 2008; 25: 1-34.
23. Revelle W. An overview of the psych package. Package "psych" (version 1.6.9). Published on September 17 2016. Available at: https://cran.r-project.org/web/packages/psych/vignettes/overview.pdf.
24. Gregory R. Warnes, Ben Bolker, Lodewijk Bonebakker, et al. Various R programming tools for plotting data. Package "gplots" (version 3.0.1). Published on March 30 2016. Available at: https://cran.r-project.org/web/packages/gplots/gplots.pdf.
25. Montuschi P, Collins JV, Ciabattoni G, Lazzeri N, Corradi M, Kharitonov SA, Barnes PJ. Exhaled 8-isoprostane as an in vivo biomarker of lung oxidative stress in patients with COPD and healthy smokers. Am J Respir Crit Care Med 2000; 162: 1175-1177.
26. van Velzen EJ, Westerhuis JA, van Duynhoven JP, van Dorsten FA, Hoefsloot HC, Jacobs DM, Smit S, Draijer R, Kroner CI, Smilde AK. Multilevel data analysis of a crossover designed human nutritional intervention study. J. Proteome Res. 2008; 7: 4483–4491.
27. Westerhuis JA, van Velzen EJ, Hoefsloot HC, Smilde AK. Multivariate paired data analysis: multilevel PLSDA versus OPLSDA. Metabolomics 2010; 6: 119–128.
28. Effros RM, Biller J, Foss B, Hoagland K, Dunning MB, Castillo D, Bosbous M, Sun F, Shaker R. A simple method for estimating respiratory solute dilution in exhaled breath condensates. Am J Respir Crit Care Med 2003; 168:1500-1505.
29. Simpson JL, Powell H, Baines KJ, Milne D, Coxson HO, Hansbro PM, Gibson PG. The effect of azithromycin in adults with stable neutrophilic COPD: a double blind randomised, placebo controlled trial. PLoS One 2014;9(8):e105609.

s-Figure 1. Nuclear Overhauser effect spectroscopy (NOESY) ^{1}H-NMR spectra of exhaled breath condensate samples obtained from one randomly selected COPD study subject at visit 1 (red), visit 2 (green), visit 3 (light blue), and visit 4 (purple).

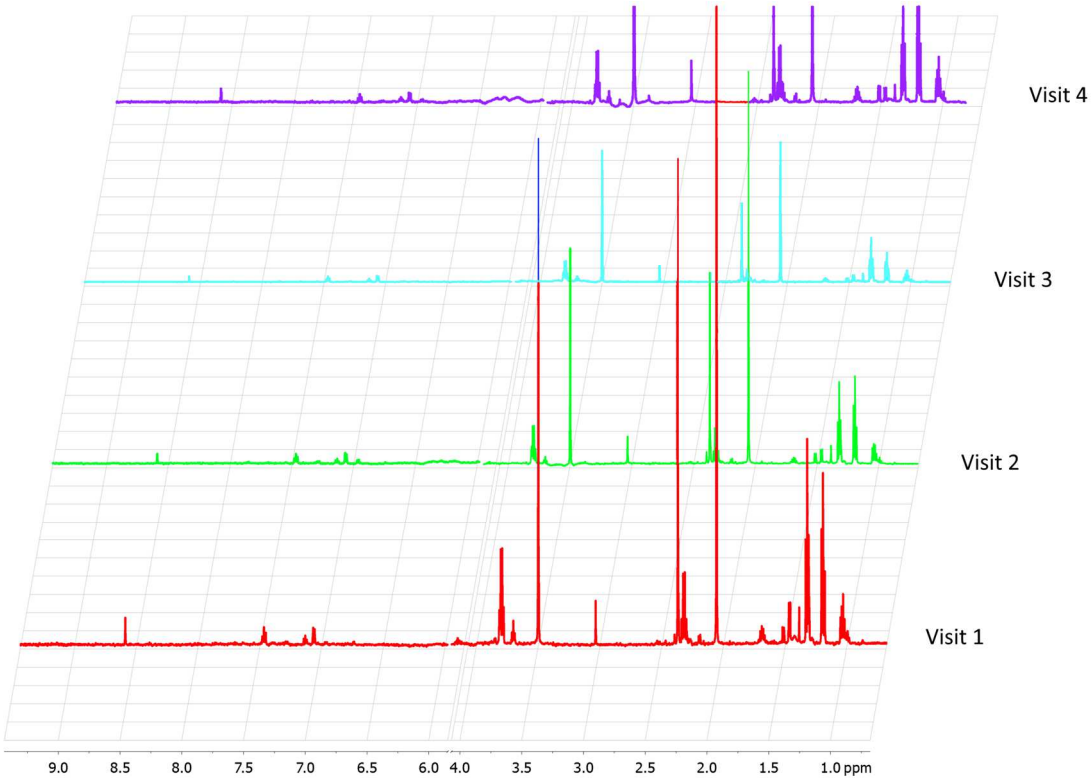

s-Figure 2. Pairwise partial least square (PLS) analysis of exhaled breath condensate in 14 subjects with COPD at visit 1 (red dots) and visit 4 (blue dots) (classification accuracy = 0.72, P = 0.01).

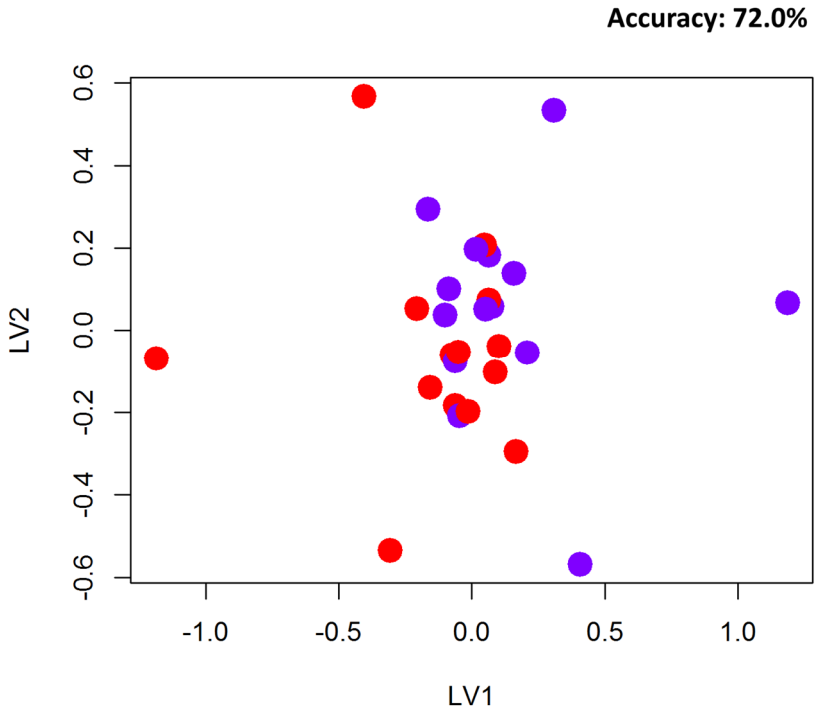

s-Figure 3. A) Formate peak in exhaled breath condensate (EBC) NMR spectra obtained from 14 patients with COPD at visit 1 (red lines) and visit 4 (green lines). B) Box-and-Whiskers plot of formate levels in EBC obtained by analysing NMR spectra from 14 patients with COPD at visit 1 and visit 4. Median arbitrary units and median absolute deviation are shown.

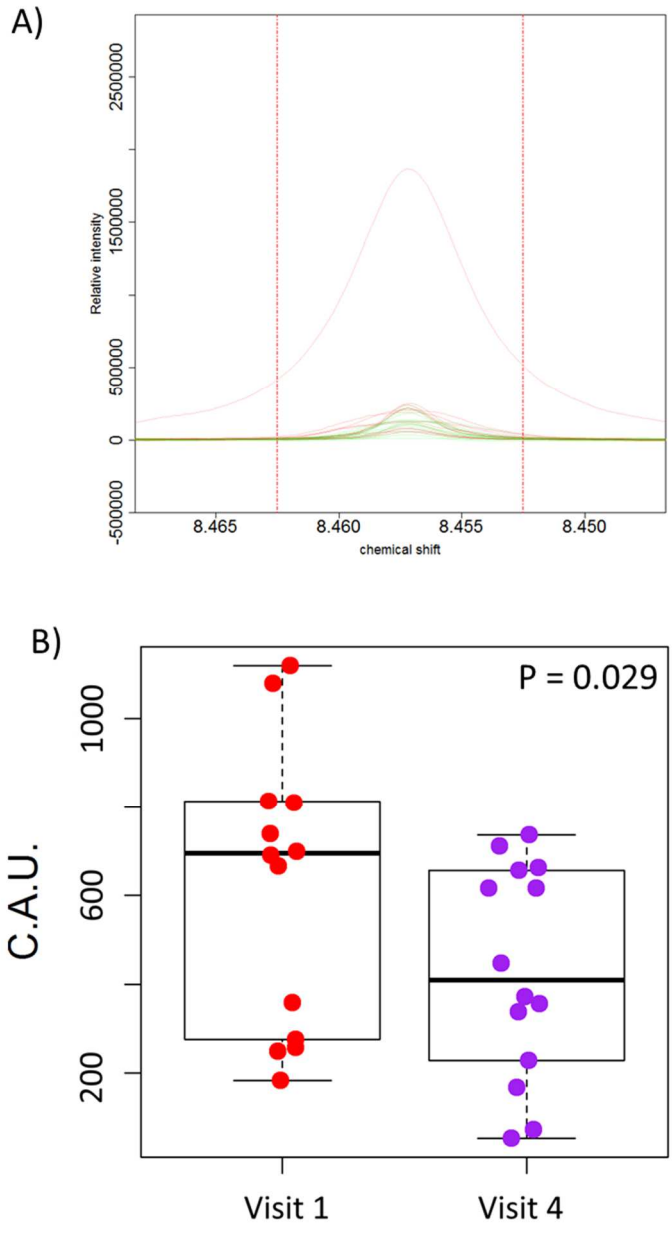

s-Table 1. Lung function tests, pre-bronchodilator values*

	V1 Screening (n = 14)	V2 Baseline (n = 14)	V3 Post-withdrawal (n = 14)	V4 Post-treatment (n = 14)	P value
FEV1, L	1.66 ± 0.21	1.68 ± 0.22	1.65 ± 0.21	1.67 ± 0.21	0.907
FEV1, % predicted	61.8 ± 6.9	62.7 ± 7.0	61.9 ± 6.7	62.4 ± 6.5	0.962
FVC, L	2.80 ± 0.28	2.86 ± 0.28	2.92 ± 0.28	2.91 ± 0.28	0.440
FVC, % predicted	79.9 ± 6.3	81.8 ± 5.9	84.0 ± 6.0	83.3 ± 5.5	0.534
FEV1/FVC, %	58.1 ± 3.21	57.2 ± 3.1	55.3 ± 3.21	56.3 ± 3.3	0.008
PEF, L/sec	4.81 ± 0.652	5.24 ± 0.722	4.89 ± 0.70	4.93 ± 0.62	0.044
PEF, % predicted	65.5 ± 8.12	71.3 ± 8.92	66.8 ± 8.8	67.2 ± 7.4	0.033
FEF25%-75%, L/sec	0.92 ± 0.14	0.94 ± 0.153	0.86 ± 0.133	0.92 ± 0.14	0.029
FEF25%-75%, % predicted	32.4 ± 4.6	32.9 ± 4.93	30.2 ± 4.23	32.6 ± 5.4	0.026

*Data are expressed as numbers or mean ± SEM. Within-group comparisons were performed with ANOVA for repeated measures and paired t test. P < 0.05 was considered significant.
1: V1 vs V3; 2: V1 vs V2; 3: V2 vs V3.
Abbreviations: FEF25%-75%, forced expiratory flow at 25%-75% of the forced vital capacity; FEV1, forced expiratory volume in one second; FVC, forced vital capacity; PEF, peak expiratory flow; V, visit.

s-Table 2. Lung function tests, post-bronchodilator values*

	V1 (n = 14)	V2 (n = 14)	V3 (n = 14)	V4 (n = 14)	P Value
FEV1, L	1.77 ± 0.22	1.80 ± 0.22	1.79 ± 0.22	1.79 ± 0.22	0.902
FEV1, % predicted	66.2 ± 7.0	67.6 ± 7.2	67.0 ± 7.0	66.4 ± 7.0	0.854
FVC, L	2.98 ± 0.28	3.01 ± 0.28	3.07 ± 0.26	3.06 ± 0.28	0.547
FVC, % predicted	85.3 ± 6.2	86.4 ± 6.0	88.7 ± 5.9	87.5 ± 5.6	0.587
FEV1/FVC, %	58.3 ± 3.3	58.5 ± 3.3	56.5 ± 3.1	56.7 ± 3.3	0.110
PEF, L/sec	5.38 ± 0.72	5.29 ± 0.64	5.19 ± 0.70	5.12 ± 0.71	0.427
PEF, % predicted	73.1 ± 8.9	72.4 ± 7.9	70.9 ± 8.70	69.4 ± 8.50	0.437
FEF25%-75%, L/sec	0.99 ± 0.15	1.03 ± 0.16	0.96 ± 0.15	0.96 ± 0.16	0.447
FEF25%-75%, % predicted	34.7 ± 4.8	36.3 ± 5.2	33.7± 4.9	34.0 ± 5.5	0.493

*Data are expressed as numbers or mean ± SEM. Within-group comparisons were performed with ANOVA for repeated measures and paired t test. P < 0.05 was considered significant.
Abbreviations: FEF25%-75%, forced expiratory flow at 25%-75% of the forced vital capacity; FEV1, forced expiratory volume in one second; FVC, forced vital capacity; PEF, peak expiratory flow; V, visit.

s-Table 3. Paired comparison of exhaled breath condensate (EBC) metabolite concentrations at each visit using Wilcoxon signed-rank test. Metabolite concentrations are reported as median arbitrary units ± median absolute deviation (MAD).

	Visit 1	**Visit 2**	**Visit 3**	**Visit 4**	**Visit 1 *vs* 2**	**Visit 1 *vs* 3**	**Visit 1 *vs* 4**	**Visit 2 *vs* 3**	**Visit 2 *vs* 4**	**Visit 3 *vs* 4**
Metabolite	Median ± MAD	Median ± MAD	Median ± MAD	Median ± MAD	P value	P value	P value	P value	P value	P value
Acetate	7322.51 ± 3372.29	8634.57 ± 6598.25	10385.09 ± 4929.83	4683.2 ± 1518.54	0.95	0.33	0.33	0.95	0.12	0.01
Acetoine	706.10 ± 482.55	512.18 ± 215.73	730.90 ± 311.39	546.27 ± 360.24	0.12	0.54	0.27	0.09	0.54	0.12
Acetone	6152.10 ± 3456.11	6072.73 ± 1730.04	6850.06 ± 2420.90	6579.12 ± 2468.53	0.81	1.00	0.22	0.58	0.63	0.17
3-Hydroxyisovalerate	326.31 ± 64.86	351.19 ± 45.66	388.33 ± 44.43	376.95 ± 89.09	0.71	0.30	0.58	0.33	0.81	0.33
Ethanol	488.16 ± 99.84	538.82 ± 201.68	754.17 ± 384.75	544.54 ± 238.66	1.00	0.06	0.95	0.39	0.95	0.08
Formate	694.95 ± 360.47	695.14 ± 519.50	424.52 ± 131.84	409.16 ± 224.76	0.86	0.67	0.03	0.17	0.05	0.05
Lactate	444.24 ± 158.85	284.10 ± 92.29	352.78 ± 142.45	289.46 ± 115.33	0.95	0.95	0.12	0.95	0.12	0.30
Leucine/n-butyrate	1431.78 ± 482.18	2484.15 ± 1743.00	2002.49 ± 896.17	1583.98 ± 537.93	0.50	0.12	0.67	0.71	0.12	0.06
Methanol	14225.48 ± 7044.87	16268.66 ± 7711.03	11570.77 ± 2751.26	14358.75 ± 8341.86	1.00	0.36	0.95	0.81	0.63	0.67
n-butyrate	664.07 ± 198.96	1572.65 ± 1205.33	1099.32 ± 468.94	766.91 ± 251.52	0.22	0.14	0.86	0.71	0.12	0.17
Phenol	443.05 ± 224.90	325.68 ± 204.11	354.39 ± 158.40	335.79 ± 204.24	0.22	0.76	0.36	0.07	0.63	0.39
Proprionate	1542.86 ± 739.74	2394.86 ± 1967.45	2519.65 ± 1754.52	988.23 ± 706.23	0.46	0.12	0.58	0.46	0.46	0.09
Trimethylamine	364.99 ± 260.65	343.87 ± 262.45	348.39 ± 210.49	301.78 ± 195.88	0.76	0.36	0.86	0.39	0.90	0.46

s-Table 4. Classification accuracies and P values among different pharmacological treatments from visit 1 to visit 4 based on a monodimensional PLS model built on EBC NMR spectroscopy data in 14 patients with COPD. The significant variables in the univariate analysis are also reported (Wilcoxon signed-rank test P values).

Abbreviations: EBC, exhaled breath condensate; NMR, nuclear magnetic resonance; PLS, partial least squares.

Comparison	**Overall accuracy**	**Variable (P value)**
Visit 1 vs. Visit 2	42.0% (P > 0.05)	-
Visit 1 vs. Visit 3	55.3% (P > 0.05)	-
Visit 1 vs. Visit 4	72.0% (0.01)	Formate (0.029)
Visit 2 vs. Visit 3	53.3% (P > 0.05)	-
Visit 2 vs. Visit 4	63.3% (P > 0.05)	-
Visit 3 vs. Visit 4	57.3% (P > 0.05)	Acetate (0.009)

s-Table 5. F_ENO values in 14 patients with COPD at visit 1 to visit 4.*

	V1 (n = 14)	V2 (n = 14)	V3 (n = 14)	V4 (n = 14)	Overall P value
F_ENO (ppb)	21.9 (12.7-28)	17.6 (12.3-20.3)	18.5 (11.8-29)	13.2 (11.8-21.7)	0.35

*Data are expressed as medians and interquartile ranges. Within-group comparisons were performed with Friedman test and Wilcoxon matched-pairs signed rank test. Abbreviations: F_ENO, fraction of exhaled nitric oxide; V, visit.

s-Table 6. PGE_2 and 15-F_{2t}-isoprostane concentrations in sputum and EBC*.

	V1	V2	V3	V4	Overall P value
n	13	13	13	13	
Sputum PGE_2 (pg/mL)	18.6 (2-24.6)[1]	3.8 (2-54.9)	40.1 (8.3-47)[1,2]	10.4 (3.5-20.8)[2]	0.04
	V1	V2	V3	V4	Overall P value
n	9	9	9	9	
Sputum 15-F_{2t}-isoprostane (pg/mL)	25 (9.9-45.5)	25.5 (13.2-45.4)	33.2 (7.7-41.5)	13.5 (7.8-26.2)	0.84
	V1	V2	V3	V4	Overall P value
n	12	12	12	12	
EBC PGE_2 (pg/mL)	18.7 (10.6-30.4)	19.1 (11.9-55.1)	14.7 (7-26.1)	11.3 (4-18.7)	0.19
	V1	V2	V3	V4	Overall P value
n	14	14	14	14	
EBC 15-F_{2t}-isoprostane (pg/mL)	18.3 (1.4-37)	24 (9.7-35.7)	20.8 (15.1-32.8)	21.3 (8.1-32.7)	0.60

*Data are expressed as median and interquartile range. Within-group, between-visit comparisons were performed with Friedman's test. If overall P was lower than 0.05, considered significant, Wilcoxon matched-pairs signed rank test was performed. [1]: P = 0.021; [2]: P = 0.008.

One patient with COPD had undetectable sputum PGE_2 concentrations at all visits (4 samples). Five patients with COPD had undetectable sputum 15-F_{2t}-isoprostane concentrations at all visits (20 samples). Two patients with COPD had undetectable EBC PGE_2 concentrations at all visits (8 samples). At undetectable samples, an arbitrary concentration value of 1 pg/mL, corresponding to 50% of the analytical technique detection limit (2 pg/mL), was assigned. Abbreviations: EBC, exhaled breath condensate; PGE_2, prostaglandin E_2; V, visit.

s-Table 7. Within-group comparison of percentage sputum cell counts in the 8 patients with COPD who had a complete set of sputum slides (visit 1 to visit 4)*.

	V1	V2	V3	V4	P value
n	8	8	8	8	
Neutrophils, %	82.5 (57.3-91.6)	85.5 (77.6-95.5)	86.5 (72.3-93.9)	83.3 (68.4-89.6)	0.55
Macrophages, %	10.5 (4.1-39.8)	11.3 (2.8-17.4)	10 (1.7-15)	7.8 (4.4-18)	0.91
Eosinophils, %	0 (0-0.5)	0 (0-0.8)	0.5 (0-2.9)	0.5 (0-3.3)	0.20
Lymphocytes, %	0 (0-0.4)	0 (0-0.5)	0 (0-0.4)	0 (0-0.4)	0.87

*Data are expressed as medians and interquartile range. Percentage of basophil and bronchial epithelial cell counts was 0 and is not shown. Within-group comparisons were performed with Friedman test. Abbreviation: V, visit.

s-Table 8. Percentage sputum cell counts in all valid sputum slides (n = 43)*.

	V1	V2	V3	V4	P value
n	10	12	11	10	
Neutrophils, %	85.8 (67.8-93.4)	87.5 (78-96)	87 (73-89)	83.5 (72.1-90.8)	n.s.
Macrophages, %	10.5 (2.9-25.3)	7.8 (1.8-17.4)	11 (3-13.5)	7.8 (4-18)	n.s.
Eosinophils, %	0.3 (0-0.6)	0 (0-1)	0 (0-1)	0.5 (0-2.8)	n.s.
Lymphocytes, %	0 (0-0.1)	0 (0-0.4)	0 (0-0)	0 (0-1)	n.s.

*Data are expressed as medians and interquartile range. Thirteen sputum slides were excluded due to squamous cell counts > 30%. Sputum cell counts are expressed as a percentage of total non-squamous cells. Percentage of basophils and bronchial epithelial cells was 0. Comparisons were performed with Mann-Withney test. Abbreviations: n.s., not significant for all comparisons within the group; V, visit.

s-Table 9. Comparison between a multidimensional integrated model including breathomics and a model based on spirometry alone used for assessing the effects of pharmacological treatment in 14 patients with COPD.

	Spirometry-based model					**Multidimensional integrated model**				
Comparison	**AUC**	**P-value***	**OR**	**Sensitivity**	**Specificity**	**AUC**	**P-value***	**OR**	**Sensitivity**	**Specificity**
Visit 1 vs. Visit 2	0.689	P = 0.06	3.45	0.650	0.650	0.714	P = 0.12	3.90	0.664	0.664
Visit 1 vs. Visit 3	0.704	P = 0.07	3.54	0.653	0.653	0.704	P < 0.01	6.29	0.715	0.715
Visit 1 vs. Visit 4	0.561	P = 0.90	0.34	0.367	0.367	0.857	P < 0.01	22.2	0.825	0.825
Visit 2 vs. Visit 3	0.729	P = 0.03	6.36	0.716	0.716	0.571	P = 0.23	2.23	0.599	0.599
Visit 2 vs. Visit 4	0.648	P = 0.43	0.85	0.480	0.480	0.556	P = 0.12	2.21	0.598	0.598
Visit 3 vs. Visit 4	0.658	P = 0.11	3.16	0.640	0.640	0.760	P < 0.01	8.63	0.746	0.746

Abbreviations: AUC, area under the curve; OR, odds ratio.

*P-values have been obtained through 100 fold permutation tests and are referred to the AUC values.

4.3.4 *Mammographic density and breast cancer prevention: a metabolomic epigenetic and inflammatory markers integrated approach*

Benedetta Bendelli[1], Claudio Luchinat[2], Giovanna Masala[1], Domenico Palli[1], Paola Turano[2], Alessia Vignoli[2]

(Tentative author list in alphabetic order)

[1] Molecular and Nutritional Epidemiology Unit, Cancer Research and Prevention Institute (ISPO), Florence, Italy
[2] Magnetic Resonance Center (CERM), University of Florence, Via Luigi Sacconi 6, 50019, Sesto Fioren-tino (FI), Italy

Working draft

Candidate's contributions: acquisition of NMR data, statistical analysis and interpretation of data, writing and review of the manuscript.

Mammographic density and breast cancer prevention: a metabolomic epigenetic and inflammatory markers integrated approach

Introduction

High mammographic breast density (MBD) is an established risk factor for breast cancer (BC); beside genetic and hormonal causes, high fat diet seems to correlate with high MBD. Furthermore, healthy diet and regular physical activity (PA) resulted to be positively associated with MBD and reduced BC risk.

This study, called DAMA (Diet, physical Activity and MAmmography), is a factorial randomized trial involving healthy nonsmoking postmenopausal women not using hormone replacement therapy and having MBD >50%, is aimed at evaluating the ability of a 24-month intervention based on moderate-intensity PA and/or dietary modification focused on plant foods with a low glycemic load, low in saturated fats and alcohol, and rich in olive oil, antioxidants and fiber, to reduce the percent MBD. Metabolomics, epigenetics and inflammatory markers are the techniques chosen to characterize the effects of these life style interventions in these women.

Patients and Methods

Study population

For the metabolomic part of the DAMA study 321 women were enrolled, and subjected to four different arms of treatment: no treatment (controls), diet, physical activity, and diet coupled with physical activity. At the baseline and after the treatment (follow up) plasma EDTA samples were collected (Figure 1).

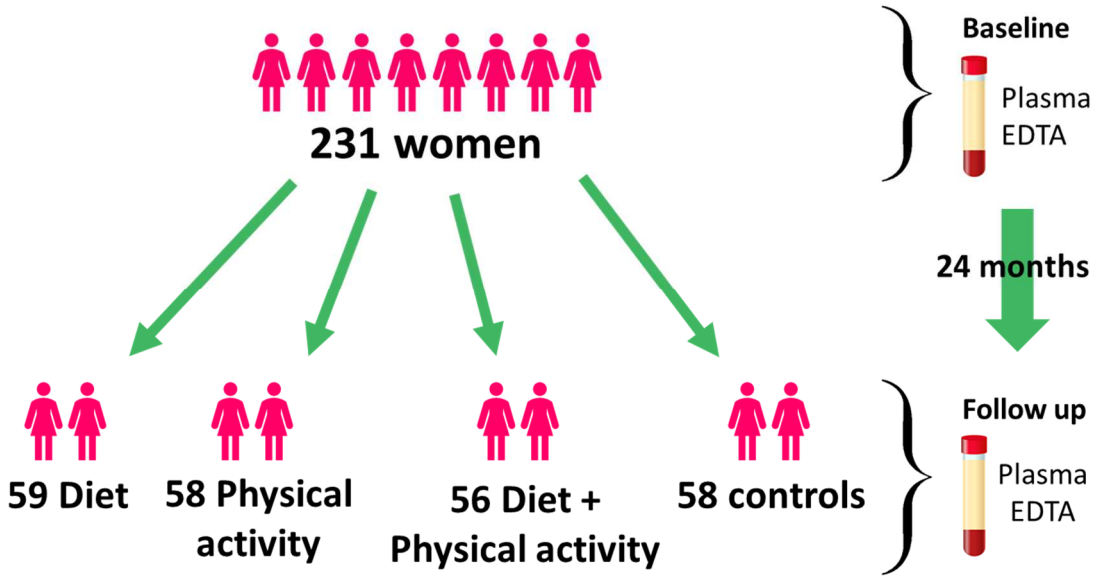

Figure 1. The experimental design

Unfortunately, 9 samples did not meet the quality requisites requested for a high quality metabolomic analysis (i.e. samples were hemolyzed), therefore they were excluded and the NMR analyses were performed on the remaining 453 samples.

NMR analyses

All plasma samples were analyzed following the standard operating procedures (1): frozen plasma samples were thawed at room temperature and shaken before use, a total of 350 µL of a sodium phosphate buffer (10.05 g $Na_2HPO_4 \cdot 7H_2O$; 0. 2g NaN_3; 0.4 g sodium trimethylsilyl [2,2,3,3-$^2H_4$]propionate (TMSP) in 500 mL of H_2O with 20% (v/v) ^2H_2O; pH 7.4) was added to 350 µL of each sample, and the mixture was homogenized by vortexing for 30 s. A total of 600 µL of this mixture was transferred into a 5 mm NMR tube for the NMR analysis, and for each plasma sample three different monodimensional 1H NMR spectra were acquired:

1) a standard nuclear Overhauser effect spectroscopy pulse sequence NOESY 1Dpresat (32 scans, 98304 data points, spectral width of 18028 Hz, acquisition time of 2.7 s, relaxation delay of 4 s and mixing time of 0.01 s) was applied to obtain spectra in which signals of both low and high molecular weight metabolites are visible.
2) a standard spin echo Carr-Purcell-Meiboom-Gill (2) (CPMG) pulse sequence (32 scans, 73728 data points, spectral width of 12019 Hz, total spin echo ($2n\tau$) of 80 ms, acquisition time of 3.1 s, and relaxation delay of 4 s) was used for the selective observation of low molecular weight metabolites.
3) a standard diffusion-edited pulse sequence (3) (32 scans, 98304 data points, spectral width of 18028 Hz, acquisition time of 2.7 s, and relaxation delay of 4 s) was applied to detect selectively high molecular weight metabolites.

Free induction decays were multiplied by an exponential function equivalent to a 0.3 Hz line-broadening factor before applying Fourier transform. Transformed spectra were automatically corrected for phase and baseline distortions and calibrated (anomeric glucose signal 5.24 ppm) using TopSpin 3.2.

Each 1D spectrum in the range 0.2-10.00 ppm was segmented into 0.02 ppm chemical shift bins and the corresponding spectral areas were integrated using AMIX software (version 3.8.4, Bruker BioSpin). Binning is a mean to reduce the number of total variables, to compensate for subtle signal shifts, and filter noise in the spectra, making the analysis more robust and reproducible (4,5). The region between 4.19 and 5.11 ppm containing the residual water signal and the regions containing EDTA signals (3.59-3.65 ppm, 3.09-3.25 ppm, 2.69-2.73 ppm, and 2.57-2.59 ppm) were removed and the dimension of the system was reduced to 432 bins.

Statistical analysis

Data analyses were performed using the open source software R (6). Multivariate analysis was conducted on processed data. Data reduction was carried out by means of

projection into a principal component analysis (PCA) subspace, only the minimum number of components that maximized the accuracy were retained in the model and the canonical analysis (CA) was applied to obtain the supervised separation of the groups of interest. For the purpose of classification, K-nearest neighbors (k-NN) method (k=5) applied on the PCA-CA scores was used. Accuracy, sensitivity and specificity for the different classifications were assessed by means of 100 cycles of a Monte Carlo cross-validation scheme (MCCV, R script in-house developed). Briefly, 90% of the data were randomly chosen at each iteration as a training set to build the model, the remaining 10% was tested and sensitivity, specificity and accuracy for the classification were assessed.

Multilevel partial least square analysis (mPLS)(7) was used to analyze the spectra from the same subject obtained at paired visits, using the algorithm implemented in the R-library "plsgenomics" and the standard R function "cancor". Accuracy, sensitivity and specificity were assessed by means of a Monte Carlo cross-validation scheme.

Metabolites were assigned in the CPMG NMR spectra by using matching routines of AMIX 3.8.4 (Bruker BioSpin) in combination with the BBIOREFCODE (Bruker BioSpin), and freely available dataset i.e. Human Metabolome DataBase (HMDB)(8). Metabolites quantification was determined on the whole spectra by an in-house developed software in MATLAB programming suite (Takis *et al.*, in preparation). This algorithm is based upon the unconstrained non-linear minimization (fitting) of the metabolite NMR signals, employing a combination of Lorentzian-Gaussian functions. By this approach, each NMR region of interest is decomposed and deconvoluted into its component parts, and then integrated to obtain the metabolite concentrations in arbitrary units. Kruskal-Wallis (9) or Wilcoxon signed-rank test (10) were chosen to infer differences between the metabolites concentrations of groups on the biological assumption that metabolite concentrations are not normally distributed, and false discovery rate correction was applied using the Benjamini-Hochberg method (11). An adjusted P-value < 0.05 was deemed significant.

Results

Multivariate statistical analyses

Differences among patients who underwent treatments and the other ones have been investigated: no statistically significant accuracies for both no physical activity vs physical activity (Figure 2) and diet vs no diet (Figure 3) comparisons were found using all the three typologies of NMR spectra acquired.

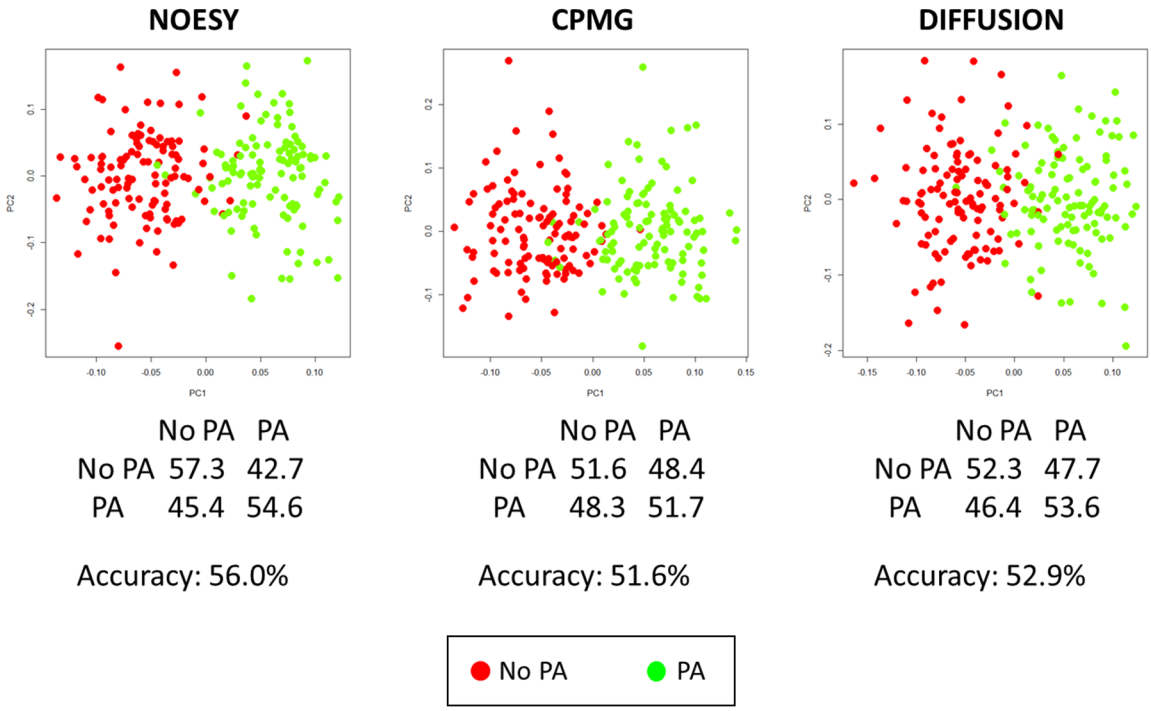

Figure 2. PCA-CA score plots of the first two principal components for the comparison between subjects that did not perform physical activity (No PA, red dots) and subjects that practiced physical activity (PA, green dots) are reported for each kind of NMR spectra: NOESY, CPMG, and Diffusion.

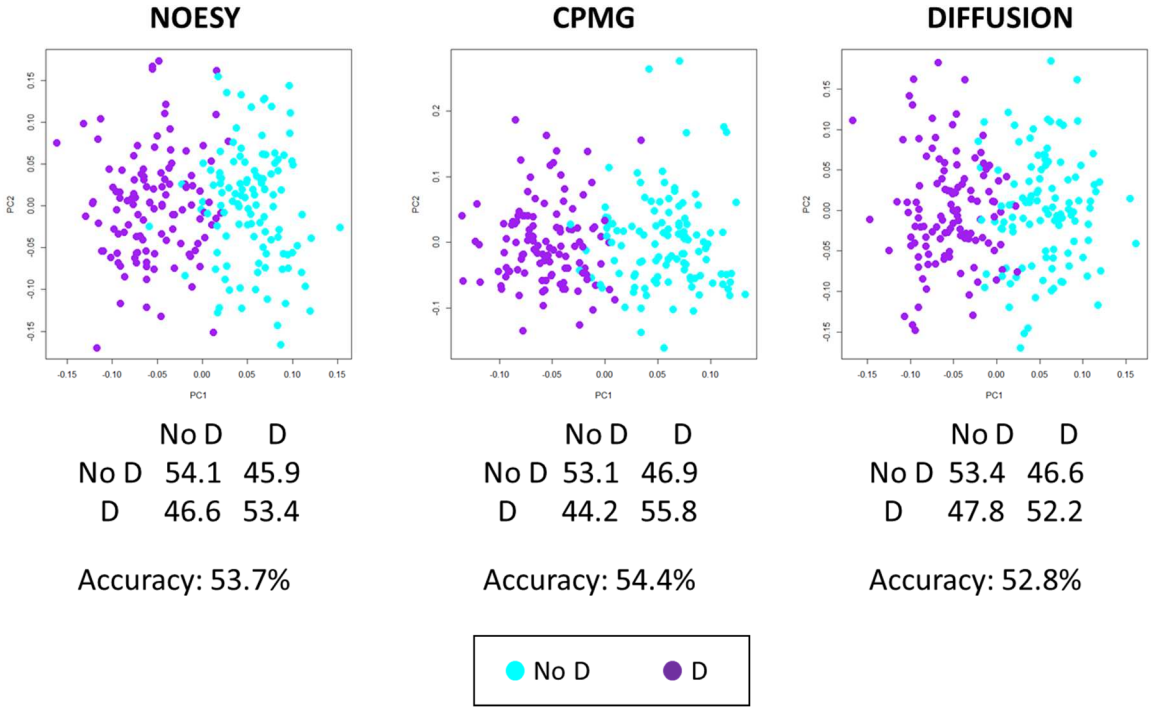

Figure 3. PCA-CA score plots of the first two principal components for the comparison between subjects that did not follow a specific diet (No D, cyan dots) and subjects that adopted the DAMA diet (D, purple dots) are reported for each kind of NMR spectra: NOESY, CPMG, and Diffusion.

Intervention arms were also compared pairwise obtaining weak discrimination accuracies, the comparison diet vs physical activity using diffusion spectra with 59.4% discrimination accuracy showed the best results. Each intervention arm was compared at baseline and follow up using two approaches: PCA-CA models to discover interindividual variations and mPLS to unravel intraindividual variability at the two-time points. Results are reported in Table 1.

Table 1. Comparisons of each intervention arm at baseline and follow up.

Baseline vs Follow up		**PCA-CA model**	**multilevel PLS model**
Control	NOESY	70.7%	82.5%
	CPMG	75.8%	89.2%
	Diffusion	56.7%	63.8%
Diet	NOESY	72.9%	87.1%
	CPMG	80.0%	84.7%
	Diffusion	68.8%	83.9%
Physical activity	NOESY	69.4%	80.0%
	CPMG	72.8%	88.9%
	Diffusion	67.4%	79.5%
Physical activity + Diet	NOESY	69.2%	88.0%
	CPMG	83.3%	87.4%
	Diffusion	63.1%	74.0%

Univariate statistical analyses

In each CPMG spectrum 24 metabolites (leucine, isoleucine, valine, isobutyrate, 3-hydroxybutyrate, alanine, acetate, acetone, acetoacetate, pyruvate, glutamine, citrate, glycine, glycerol, creatine, creatinine, lactate, proline, threonine, glucose, tyrosine, histidine, phenylalanine, formate) were unambiguously assigned and quantified. Only acetone levels showed to be statistically higher in the comparison between no physical activity vs physical activity at follow up (*P*-value 0.02), no statistical significance was found comparing diet vs no diet at follow up. No statistically significant metabolites were found for the same comparisons considering the differences between follow up and baseline. No statistically significant metabolite was found comparing metabolite concentrations among intervention arms; the same analysis was performed considering the differences of follow up and baseline for each metabolite concentration but no statistical significance was found. Conversely, statistically significant metabolites were found comparing each subject of each intervention arm at baseline and follow up: controls (Table2), diet (Table 3), physical activity (Table 4), and physical activity+diet (Table 5).

Table 2. Pairwise comparison of metabolites at baseline and follow up for the controls.

Controls baseline vs follow up				
	P-value	**P-value adjusted**	**Effect size**	**log2(FC)**
Leucine	6.37E-01	9.12E-01	0.0078	0.0137
Isoleucine	2.03E-01	4.44E-01	-0.0893	-0.0067
Valine	6.59E-01	9.12E-01	0.0658	-0.0245
isobutyrate	1.98E-01	4.44E-01	0.1273	-0.0217
3-hydroxybutyrate	2.35E-01	4.69E-01	-0.0618	-0.1671
Alanine	2.07E-02	1.46E-01	0.2192	-0.1599
Acetate	6.00E-01	9.12E-01	0.0365	0.0158
Acetone	3.75E-01	6.93E-01	-0.1049	0.0233
acetoacetate	7.42E-02	2.97E-01	-0.1899	0.4053
Glutamine	1.59E-01	4.25E-01	-0.0991	0.0199
Citrate	8.59E-01	9.31E-01	0.0078	-0.0329
Glycine	7.54E-01	9.12E-01	0.0215	0.0077
Glycerol	9.31E-01	9.31E-01	-0.0356	0.0336
Creatine	1.53E-01	4.25E-01	-0.0801	0.153
Creatinine	5.29E-01	9.06E-01	-0.0124	-0.0359
Lactate	7.20E-01	9.12E-01	0.0422	-0.0018
Threonine	6.07E-02	2.91E-01	-0.1979	0.0946
Glucose	9.02E-02	3.09E-01	0.0957	-0.0184
Tyrosine	2.43E-02	1.46E-01	0.1758	-0.1713
Histidine	9.13E-01	9.31E-01	-0.0238	-0.0104
phenylalanine	7.60E-01	9.12E-01	0.0348	-0.0457
Formate	1.52E-07	3.66E-06	0.6783	-0.5065
Pyruvate	1.95E-02	1.46E-01	-0.256	0.2318
Proline	8.47E-01	9.31E-01	0.0055	-0.0942

Table 3. Pairwise comparison of metabolites at baseline and follow up for the diet group.

Diet baseline vs follow up				
	P-value	**P-value adjusted**	**Effect size**	**log2(FC)**
Leucine	6.37E-01	9.12E-01	0.0078	0.0137
Isoleucine	2.03E-01	4.44E-01	-0.0893	-0.0067
Valine	6.59E-01	9.12E-01	0.0658	-0.0245
Isobutyrate	1.98E-01	4.44E-01	0.1273	-0.0217
3-hydroxybutyrate	2.35E-01	4.69E-01	-0.0618	-0.1671
Alanine	2.07E-02	1.46E-01	0.2192	-0.1599
Acetate	6.00E-01	9.12E-01	0.0365	0.0158
Acetone	3.75E-01	6.93E-01	-0.1049	0.0233
Acetoacetate	7.42E-02	2.97E-01	-0.1899	0.4053
Glutamine	1.59E-01	4.25E-01	-0.0991	0.0199
Citrate	8.59E-01	9.31E-01	0.0078	-0.0329
Glycine	7.54E-01	9.12E-01	0.0215	0.0077
Glycerol	9.31E-01	9.31E-01	-0.0356	0.0336
Creatine	1.53E-01	4.25E-01	-0.0801	0.153
Creatinine	5.29E-01	9.06E-01	-0.0124	-0.0359
Lactate	7.20E-01	9.12E-01	0.0422	-0.0018
Threonine	6.07E-02	2.91E-01	-0.1979	0.0946
Glucose	9.02E-02	3.09E-01	0.0957	-0.0184
Tyrosine	2.43E-02	1.46E-01	0.1758	-0.1713
Histidine	9.13E-01	9.31E-01	-0.0238	-0.0104
Phenylalanine	7.60E-01	9.12E-01	0.0348	-0.0457
Formate	1.52E-07	3.66E-06	0.6783	-0.5065
Pyruvate	1.95E-02	1.46E-01	-0.256	0.2318
Proline	8.47E-01	9.31E-01	0.0055	-0.0942

Table 4. Pairwise comparison of metabolites at baseline and follow up for the physical activity group.

Physical activity baseline vs follow up				
	P-value	**P-value adjusted**	**Effect size**	**log2(FC)**
Leucine	9.97E-01	9.97E-01	-0.0389	5.00E-04
Isoleucine	7.78E-01	9.39E-01	-0.0389	0.0055
Valine	8.10E-01	9.39E-01	-0.0019	-0.0343
isobutyrate	7.23E-01	9.39E-01	-0.0571	0.0622
3-hydroxybutyrate	6.92E-01	9.39E-01	-0.0134	0.1699
Alanine	8.61E-01	9.39E-01	0.0121	0.0227
Acetate	4.12E-01	8.78E-01	0.111	-0.2056
Acetone	5.60E-01	8.96E-01	0.0057	0.0088
acetoacetate	6.85E-03	5.48E-02	-0.2736	0.3146
Glutamine	1.52E-01	7.31E-01	-0.081	0.0253
Citrate	4.03E-01	8.78E-01	0.1008	-0.0483
Glycine	3.14E-01	8.78E-01	-0.0179	-0.022
Glycerol	4.75E-01	8.78E-01	-0.0574	-0.0102
Creatine	2.48E-01	8.78E-01	0.0472	-0.0567
Creatinine	3.85E-01	8.78E-01	0.0338	-0.0241
Lactate	4.60E-01	8.78E-01	-0.0835	0.1652
Threonine	9.84E-01	9.97E-01	-0.023	-0.0254
Glucose	4.51E-01	8.78E-01	0.0644	-0.0101
Tyrosine	5.99E-01	8.98E-01	-0.058	0.0316
Histidine	8.61E-01	9.39E-01	0.0099	0.0282
phenylalanine	5.33E-01	8.96E-01	-0.0201	-0.0055
Formate	2.95E-09	7.08E-08	0.7315	-0.5673
Pyruvate	6.68E-03	5.48E-02	-0.3045	0.2525
Proline	6.95E-02	4.17E-01	-0.132	0.1731

Table 5. Pairwise comparison of metabolites at baseline and follow up for the physical activity+diet group.

Physical activity + diet baseline vs follow up				
	P-value	**P-value adjusted**	**Effect size**	**log2(FC)**
Leucine	7.79E-01	8.99E-01	0.0565	-5.09E-02
Isoleucine	4.79E-01	6.76E-01	0.082	-0.0168
Valine	8.24E-01	8.99E-01	-0.0043	0.0176
Isobutyrate	5.66E-02	2.27E-01	-0.199	0.263
3-hydroxybutyrate	3.05E-01	6.09E-01	0.0255	0.0551
Alanine	3.63E-01	6.30E-01	0.0764	-0.0206
Acetate	8.70E-01	9.08E-01	-0.0136	0.0816
Acetone	8.06E-02	2.77E-01	-0.042	-0.0768
Acetoacetate	5.56E-02	2.27E-01	-0.1379	0.167
Glutamine	4.39E-02	2.27E-01	-0.1471	0.0279
Citrate	2.29E-02	1.83E-01	-0.1617	0.0139
Glycine	9.70E-01	9.70E-01	0.0221	-0.0542
Glycerol	1.48E-01	3.96E-01	-0.1729	0.2525
Creatine	7.92E-01	8.99E-01	-0.036	0.1458
Creatinine	6.06E-01	7.66E-01	-0.0221	0.0302
Lactate	1.95E-01	4.69E-01	0.1154	-0.1489
Threonine	1.48E-01	3.96E-01	-0.1008	0.187
Glucose	3.68E-01	6.30E-01	0.0532	-0.0418
Tyrosine	1.79E-02	1.83E-01	0.2046	-0.2563
Histidine	4.48E-01	6.72E-01	-0.0638	0.0295
Phenylalanine	6.01E-01	7.66E-01	-0.0129	0.0094
Formate	8.81E-08	2.11E-06	0.6423	-0.4761
Pyruvate	2.49E-01	5.44E-01	-0.1431	0.127
Proline	4.19E-01	6.70E-01	-0.0522	-0.0194

Baseline clinical data vs metabolomics data

Any possible clusterization of NMR spectra at baseline due to different breast density percentage according to the Volpara method (VBD) (Figure 4), body mass index (BMI) (Figure 5), and age (Figure 6) was assessed.

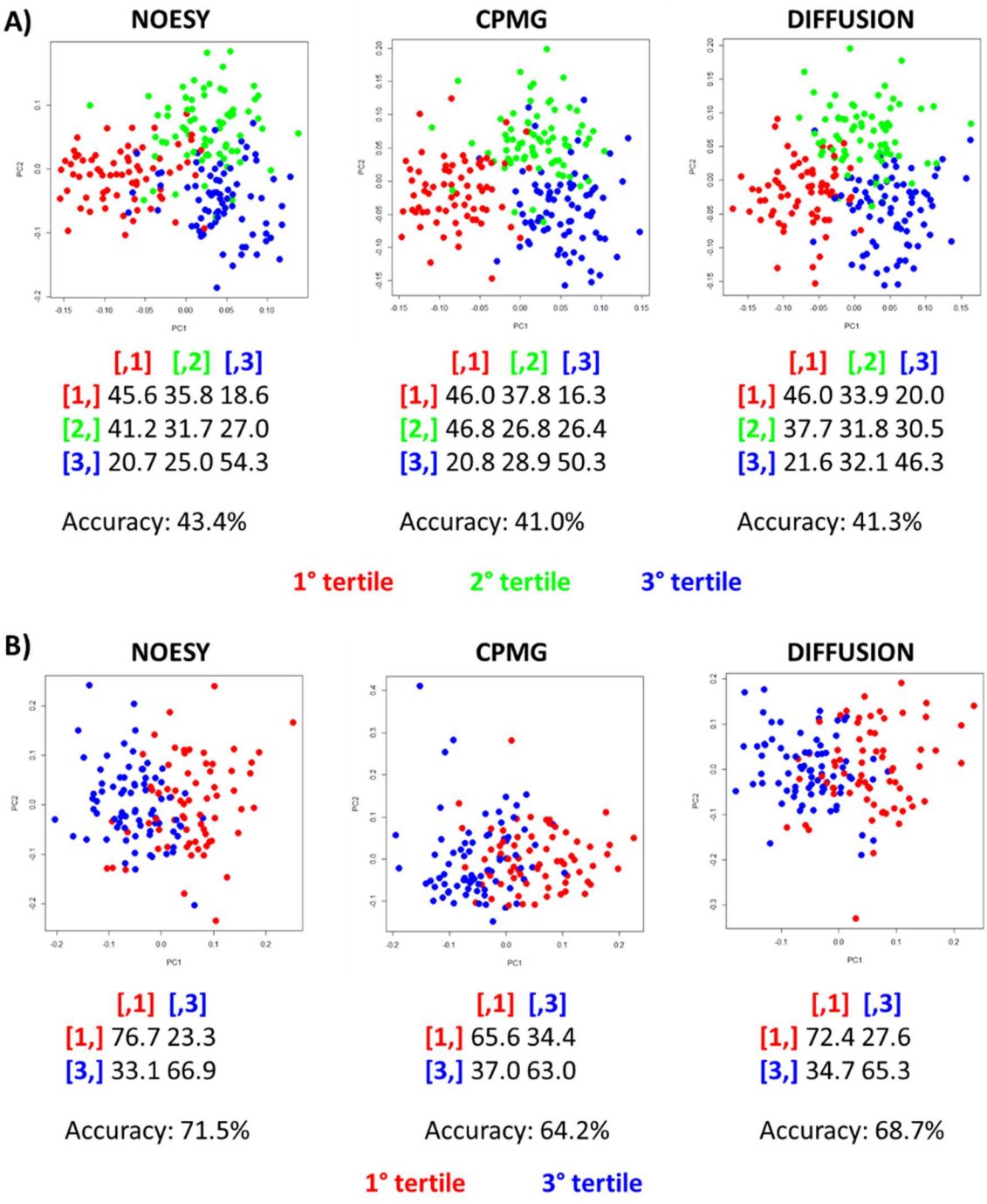

Figure 4. PCA-CA score plots of the first two principal components for the comparison between VBD groups: A) all tertiles; B) 1° vs 3° tertiles.

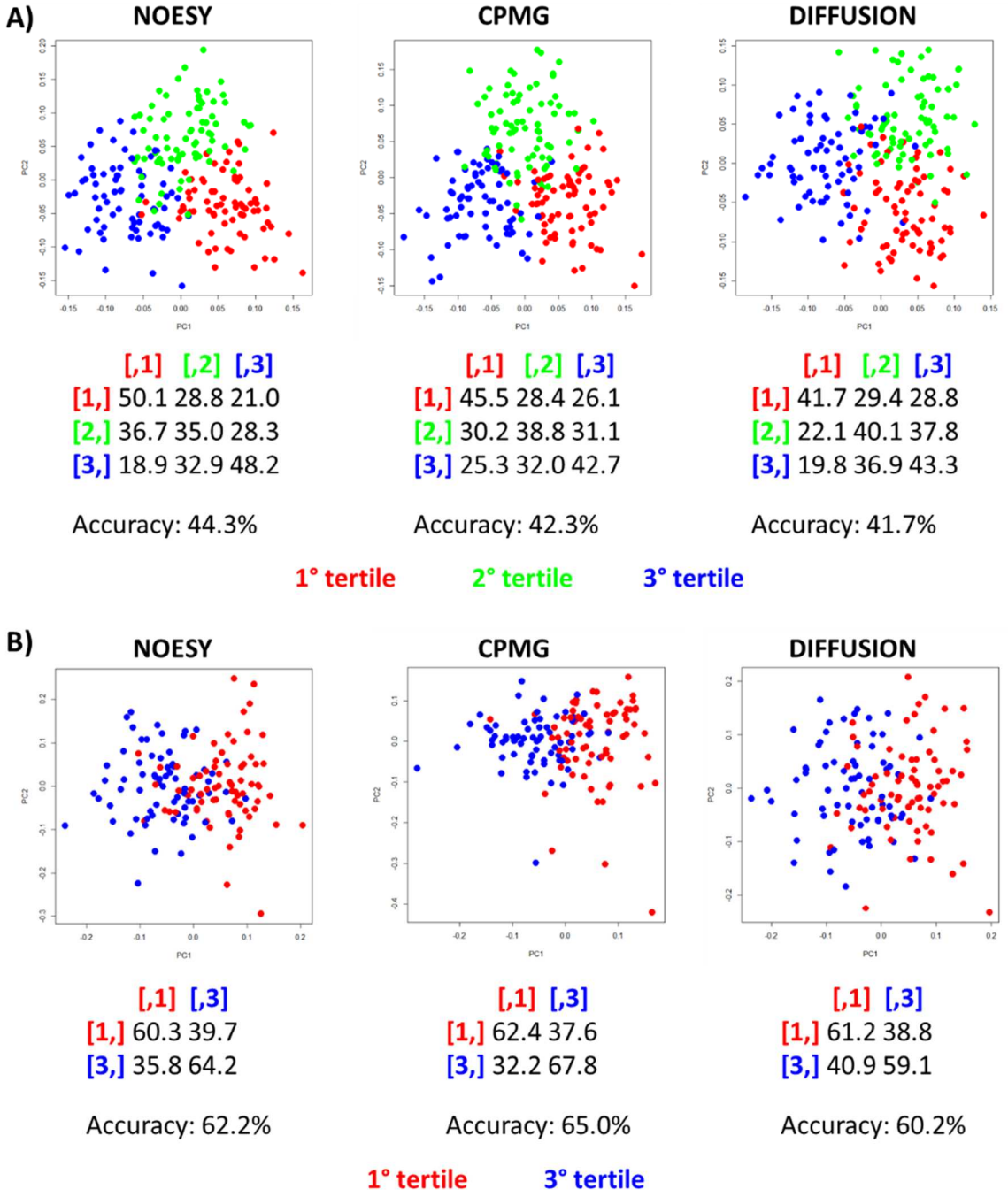

Figure 5. PCA-CA score plots of the first two principal components for the comparison between BMI groups: A) all tertiles; B) 1° vs 3° tertiles.

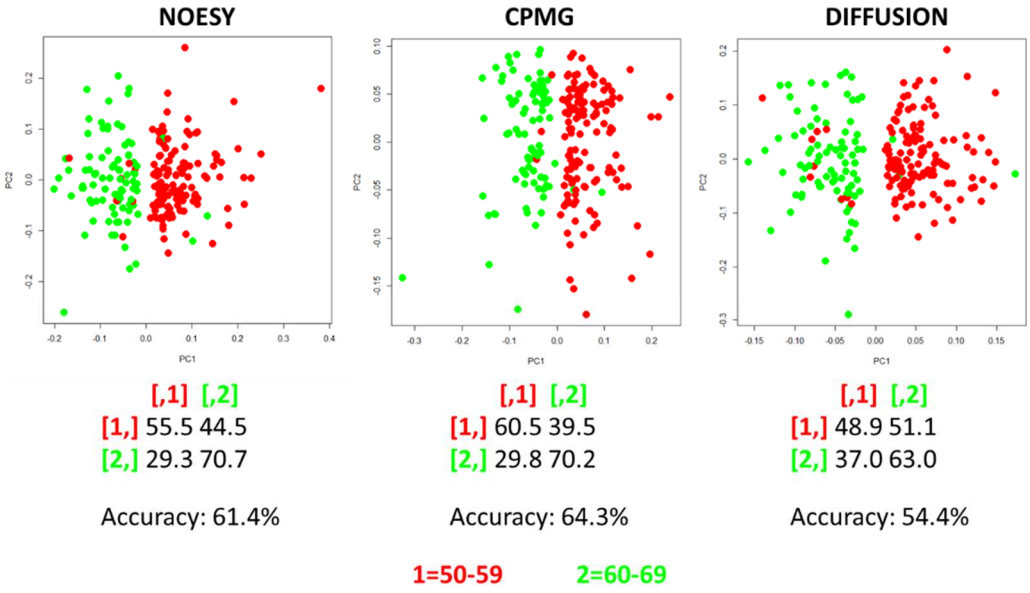

Figure 6. PCA-CA score plots of the first two principal components for the comparison between age groups: 50-59 vs 60-69 groups.

Considering baseline metabolite concentrations, for the VBD leucine, isoleucine, valine, and glucose showed statistically significant P-values and statistically significant correlations (Figure 7).

A) Metabolite univariate analysis

	P-value	P-value adjusted
leucine	7.66E-05	1.60E-03
isoleucine	2.86E-03	1.71E-02
valine	1.23E-03	9.85E-03
Isobutyrate	4.56E-01	6.45E-01
3-hydroxybutyrate	3.65E-01	6.17E-01
alanine	5.73E-02	1.53E-01
acetate	1.62E-01	3.24E-01
acetone	3.59E-02	1.22E-01
acetoacetate	5.13E-01	6.48E-01
glutamine	9.91E-01	9.91E-01
citrate	4.57E-01	6.45E-01
glycine	1.58E-02	7.58E-02
glycerol	7.24E-01	7.90E-01
creatine	1.09E-01	2.39E-01
creatinine	4.07E-02	1.22E-01
lactate	5.04E-01	6.48E-01
threonine	3.86E-01	6.17E-01
glucose	1.33E-04	1.60E-03
tyrosine	3.29E-02	1.22E-01
histidine	8.70E-02	2.09E-01
phenylalanine	6.76E-01	7.90E-01
formate	2.39E-01	4.41E-01
pyruvate	7.24E-01	7.90E-01
proline	8.74E-01	9.12E-01

B) Metabolite correlations with VBD

	Coeff. Of correlation	P-value
leucine	-2.54E-01	1.51E-04
isoleucine	-2.54E-01	1.54E-04
valine	-2.68E-01	6.05E-05
Isobutyrate	-5.39E-02	4.29E-01
3-hydroxybutyrate	-6.83E-02	3.15E-01
alanine	-1.54E-01	2.32E-02
acetate	1.46E-01	3.09E-02
acetone	-1.42E-01	3.60E-02
acetoacetate	-2.49E-02	7.15E-01
glutamine	-2.03E-02	7.65E-01
citrate	9.40E-02	1.67E-01
glycine	1.47E-01	3.04E-02
glycerol	-1.48E-02	8.28E-01
creatine	-4.70E-02	4.90E-01
creatinine	-1.96E-01	3.60E-03
lactate	3.18E-02	6.40E-01
threonine	-2.55E-02	7.08E-01
glucose	-2.85E-01	1.94E-05
tyrosine	-1.55E-01	2.22E-02
histidine	-1.83E-01	6.79E-03
phenylalanine	-1.12E-01	9.96E-02
formate	-1.37E-01	4.35E-02
pyruvate	5.97E-02	3.80E-01
proline	7.30E-03	9.15E-01

Figure 7. A) Metabolite univariate analysis among three VBD tertiles (Kruskal test has been used); B) Pearson correlation between metabolite concentrations and VBD.

Only citrate is significant in the BMI comparison, and no significance was found in the age analysis.

Correlations among metabolites and lipid blood fractions (total cholesterol, HDL cholesterol, and triglycerides) were investigated (Figure 8). Interestingly, many metabolites showed statistically significant correlations; in particular, branched amino acids and glucose (significant in the VBD analysis) correlated with triglycerides concentrations and anticorrelated with HDL cholesterol concentrations. Acetone, the unique metabolite significant in the comparison between physical activity vs no physical activity, also showed the same trend.

A)

Correlation P-values

	Col	Col_HDL	TG
leucine	9.84E-03	2.74E-03	4.51E-09
isoleucine	4.23E-02	6.27E-07	0.00E+00
valine	2.49E-04	2.60E-05	2.13E-14
Isobutyrate	8.13E-02	9.00E-01	9.37E-01
3-hydroxybutyrate	1.41E-01	1.49E-01	2.55E-02
alanine	6.32E-02	2.41E-02	5.37E-11
acetate	6.17E-01	9.55E-01	1.00E-03
acetone	3.63E-04	8.50E-07	0.00E+00
acetoacetate	9.92E-01	2.14E-01	9.91E-05
glutamine	7.56E-01	5.47E-01	1.32E-02
citrate	1.27E-01	2.71E-01	1.58E-01
glycine	7.93E-04	9.97E-01	4.15E-01
glycerol	9.39E-01	9.21E-01	2.50E-01
creatine	5.85E-03	3.24E-02	1.77E-02
creatinine	6.32E-01	1.68E-01	2.58E-06
lactate	4.69E-01	6.44E-01	2.35E-03
threonine	2.69E-02	1.64E-05	0.00E+00
glucose	2.14E-04	6.14E-02	1.38E-09
tyrosine	9.77E-01	2.59E-01	4.32E-05
histidine	3.95E-01	4.20E-01	8.93E-02
phenylalanine	5.16E-02	3.29E-01	1.50E-01
formate	3.88E-01	2.17E-03	6.60E-01
pyruvate	7.24E-01	3.76E-01	1.06E-06
proline	5.67E-01	7.44E-01	2.20E-02

B)

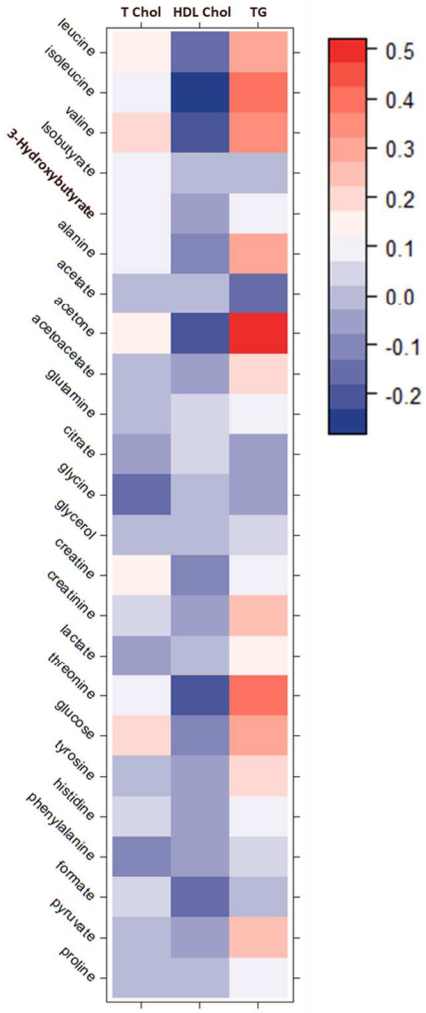

Figure 8. Correlations among metabolite concentrations and lipid blood fractions

Conclusions

- No statistically significant differences can be found comparing the interventions arms at follow up. Conversely, each interventions arm compared at baseline and follow up with the mPLS algorithm showed high discrimination accuracies.

- Lowering of formate levels has been observed at follow up in each group. Formate production is strictly connected to folate metabolism, as formate is the only non-folate-linked intermediate of folate cycle, and homocysteine production. Furthermore, folic acid is often administered to post-menopausal women to contrast hot flashes, probably indicating a metabolic deficiency. Therefore, further investigation on this metabolite need to be performed.
- Using baseline mammographic density already available, we demonstrated for the first time that this information in present in the plasma metabolic fingerprint. Indeed, we discriminated high and low breast density with 70% accuracy.
- Four metabolites (leucine, isoleucine, valine and glucose) showed statistically significant correlation with breast density, indicating that this characteristic could be correlated with metabolic alterations and moreover, that metabolomic could represent a promising tool to monitor the efficacy of possible treatments.
- The metabolomic data coupled with epigenetic and inflammatory markers, that will be soon available, could contribute to provide further insight into the pathogenesis of BC and may allow the development of novel strategies for primary prevention of breast cancer in high-MBD women.

References

1. Bernini P, Bertini I, Luchinat C, Nincheri P, Staderini S, Turano P. Standard operating procedures for pre-analytical handling of blood and urine for metabolomic studies and biobanks. J BiomolNMR [Internet]. 2011 Mar 5;(1573–5001 (Electronic)). Available from: PM:21380509
2. Carr HY, Purcell EM. Effects of Diffusion on Free Precession in Nuclear Magnetic Resonance Experiments. Phys Rev. 1954 May 1;94(3):630–8.
3. Wu DH, Chen A. Three-dimensional diffusion-ordered NMR spectroscopy: The homonuclear COSY-DOSY experiment. J Magnen Reson A. 1996;123:215–8.
4. Spraul M, Neidig P, Klauck U, Kessler P, Holmes E, Nicholson JK, et al. Automatic reduction of NMR spectroscopic data for statistical and pattern recognition classification of samples. J Pharm Biomed Anal. 1994;12(10):1215–25.
5. Holmes E, Foxall PJ, Nicholson JK, Neild GH, Brown SM, Beddell CR, et al. Automatic data reduction and pattern recognition methods for analysis of 1H nuclear magnetic resonance spectra of human urine from normal and pathological states. Anal Biochem. 1994;220(2):284–96.
6. Ihaka R, Gentleman R. R: A Language for Data Analysis and Graphics. J Comput Stat Graph. 1996;5:299–314.
7. Westerhuis JA, van Velzen EJ, Hoefsloot HC, Smilde AK. Multivariate paired data analysis: multilevel PLSDA versus OPLSDA. Metabolomics. 2010 Mar;6(1573–3890 (Electronic)):119–28.

8. Wishart DS, Jewison T, Guo AC, Wilson M, Knox C, Liu Y, et al. HMDB 3.0--The Human Metabolome Database in 2013. Nucleic Acids Res. 2013 Jan 1;41(D1):D801–7.
9. Kruskal WH, Wallis WA. Use of ranks in one-criterion variance analysis. J Am Stat Assoc. 1952;47(260):583–621.
10. Wilcoxon F. Individual Comparisons by Ranking Methods. Biom Bull. 1945 Dec;1(6):80.
11. Benjamini Y, Hochberg Y. Controlling the false discovery rate: a practical and powerful approach to multiple testing. J R Stat Soc Ser B Methodol. 1995;289–300.

4.4 Veterinary metabolomics

Although so far human medicine has mainly led metabolomic research, also several potential applications for metabolomics in veterinary are possible for what concerns investigation of disease mechanisms and pathogeneses, disease diagnosis, optimization of health, nutrition and production, monitoring of pharmaceutical treatments, and drug discovery. In this work of thesis two metabolomic veterinary studies are presented demonstrating the usefulness of this approach in this field.

In the first study proposed, NMR-based metabolomics has been used to reveal new potential biomarkers for acute calf bronchopneumonia (see paragraph 4.4.1), one of the main health issues in dairy calves for which no gold standard method of diagnosis is available. Blood plasma water and lipid extracts of 50 diseased and 10 healthy dairy calves were analyzed; our results showed that the groups of interest have two distinguishable metabolic fingerprints using both water soluble (95.2% accuracy) and lipid extracts (97.7% accuracy). Furthermore, alterations in several metabolites (2-methylglutarate, phenylalanine, phosphatidylcholine, ethanol, dimethylsulfone, propionate, acetate, allantoin, free cholesterol, cholesterol-C18, fatty acids) resulted to be associated with processes involved in the pathogenesis of acute bronchopneumonia (oxidant stress, energy deficit, and surfactant insufficiency), contributing to the understanding of the pathophysiological mechanisms of that disease in calves.

In the second study, parameters of production, biochemical profile, plasma NMR-based metabolomics, abundance of mRNA of gluconeogenic enzymes and lipid oxidation genes were used to investigate the effects of dietary boron supplementation on peripartum dairy cows' health to prevent negative energy balance related diseases at the onset of lactation in the transition period, roughly defined as three weeks prior to calving until three weeks after calving, (see paragraph 4.4.2). This cow pathological condition, which comprises glucose deficit, excessive lipolysis and ketogenesis, can lead to serious metabolic disorders impairing health and productivity of transition dairy cows.

For our aim, four different groups of dairy cows, control group (21 cows), experimental group 1 fed with diet containing 60 ppm boron (24 cows), experimental group 2 fed with diet containing 120 ppm boron (18 cows), experimental group 3 fed with diet containing 180 ppm boron (21 cows), at three specific time points (pre-partum, partum, post-partum) were studied. Relevant differences have been observed among the control group and the three experimental groups at post-partum, but also statistically significant results were found comparing each group at the three time points. Our data support the evidence that dietary boron appears to be effective in minimizing negative energy balance, preventing metabolic disorders and improving animal health; in particular, the lipid soluble metabolome seems to be the most affected by the boron administration, confirming its lipotropic effect.

4.4.1 *Plasma metabolomics in calves with acute bronchopneumonia*

A. Basoglu[1], N. Baspinar[2], L. Tenori[3], A. Vignoli[4], R. Yildiz[5]

[1] Department of Internal Medicine, Faculty of Veterinary Medicine, Selcuk University, Aleaddin Keykubat Campus 42250 Selcuklu, Konya, Turkey
[2] Department of Biochemistry, Faculty of Veterinary Medicine, Selcuk University, Aleaddin Keykubat Campus 42250 Selcuklu, Konya, Turkey
[3] Consorzio Interuniversitario Risonanze Magnetiche di Metallo Proteine (CIRMMP), University of Flo-rence, Via Luigi Sacconi 6, 50019, Sesto Fiorentino (FI), Italy
[4] Magnetic Resonance Center (CERM), University of Florence, Via Luigi Sacconi 6, 50019, Sesto Fiorentino (FI), Italy
[5] Department of Internal Medicine, Faculty of Veterinary Medicine, Mehmet Akif Ersoy University, Istiklal Campus 15030 Burdur, Turkey

Published
Metabolomics **12**, 128 (2016).

Candidate's contributions: acquisition of NMR data, statistical analysis and interpretation of data, writing and review of the manuscript.

Metabolomics (2016)12:128
DOI 10.1007/s11306-016-1074-x

ORIGINAL ARTICLE

Plasma metabolomics in calves with acute bronchopneumonia

Abdullah Basoglu[1] · Nuri Baspinar[2] · Leonardo Tenori[3] · Alessia Vignoli[4] · Ramazan Yildiz[5]

Received: 18 April 2016 / Accepted: 27 June 2016

Abstract
Background Bovine respiratory disease is one of the main health issues in dairy calves. Inflammatory lung diseases are highly complex with respect to pathogenesis and relationships between inflammation, clinical disease and response to treatment. Metabolomics may offer the potential to identify biomarkers that define calf bronchopneumonia in terms of combined clinical, physiological and patho-biological abnormalities. While metabolomic studies are often encountered in childhood pneumonia, there is no knowledge related to the same approach to calf pneumonia.
Objective The aim of this first study was to reveal the new potential biomarkers for acute calf bronchopneumonia by single proton (^{1}H) Nuclear magnetic resonance (NMR) based quantitative metabolomics.
Methods Fifty dairy calves with acute bronchopneumonia presented for treatment to the teaching hospital, and ten healthy dairy calves belonging the teaching farm were used. Laboratory (hematological: complete blood count and blood gas analysis, and biochemical analysis related to health profile) were performed. NMR spectra of the all samples (50 diseased + 10 healthy water soluble extracts, 50 diseased + 10 healthy lipid extracts) were acquired using a standard Nuclear Overhauser Effect Spectroscopy pulse sequence.
Results NMR based metabolomics analysis showed that calves suffering from bronchopneumonia and healthy calves have two different and distinguishable metabolic fingerprints using both water soluble and lipid extracts. Alterations in metabolites, increases in 2-methyl glutarate, phenylalanine, phosphatidylcholine, and decreases in ethanol, dimethylsulfone, propionate, acetate, allantoin, free cholesterol, cholesterol (–C18), were meaningful for pathogenic mechanisms of calf bronchopneumonia.
Conclusion The NMR based metabolomics may contribute to better understanding bronchopneumonia in calves.

Keywords Metabobolomics · NMR · Calf · Bronchopneumonia

1 Introduction

In human medicine, pneumonia represents one of the leading causes of infantile morbidity and mortality, especially in developing countries. Pneumonia remains the leading cause of death in young children globally and improved diagnostics are needed to better identify cases

Electronic supplementary material The online version of this article (doi:10.1007/s11306-016-1074-x) contains supplementary material, which is available to authorized users.

✉ Abdullah Basoglu
abbasoglu@selcuk.edu.tr

[1] Department of Internal Medicine, Faculty of Veterinary Medicine, Selcuk University, Aleaddin Keykubat Campus, Selcuklu, 42250 Konya, Turkey

[2] Department of Biochemistry, Faculty of Veterinary Medicine, Selcuk University, Aleaddin Keykubat Campus, Selcuklu, 42250 Konya, Turkey

[3] Consorzio Interuniversitario Risonanze Magnetiche di Metallo Proteine (CIRMMP), University of Florence, Via Luigi Sacconi 6, 50019 Sesto Fiorentino, FI, Italy

[4] Magnetic Resonance Center (CERM), University of Florence, Via Luigi Sacconi 6, 50019 Sesto Fiorentino, FI, Italy

[5] Department of Internal Medicine, Faculty of Veterinary Medicine, Mehmet Akif Ersoy University, Istiklal Campus, 15030 Burdur, Turkey

Published online: 12 July 2016

and reduce case fatality (Laiakis et al. 2010). Most clinical chemistry tests available today rely on old technologies that measure only a single chemical in blood, urine or other biofluids, and these tests are neither sensitive nor specific for any particular disease (Atzei et al. 2011). Biomarkers in pneumonia can fall into some different categories: microorganisms and their derivatives (conserved bacterial genomic sequence), endotoxin; inflammation mediators (IL-1β, IL-6, IL-8, IL-10); inflammation response proteins (C-reactive protein, long pentraxin 3, procalcitonin, pro-adrenomedullin, soluble form of triggering receptor expressed in myeloid cell-1); and stress-sensing proteins (copeptin, cortisol) (Cheng et al. 2013). Sophisticated large-scale analytical methods to quantify gene expression (transcriptomics), proteins (proteomics), lipids (lipidomics) and metabolites (metabolomics) in the lungs, blood and urine are now available to identify biomarkers that define disease in terms of combined clinical, physiological and patho-biological abnormalities (Wheelock et al. 2013). Metabolomics could be used as the 'gold standard' for clinical validation of novel biomarkers (Mussap et al. 2013). Recent reports have suggested that metabolomics analysis using nuclear magnetic resonance (NMR) and mass spectrometry (MS) approaches may provide clinicians with the opportunity to identify new biomarkers that may predict progression to more severe disease, such as sepsis, which kills many patients each year. However, although several experimental and clinical metabolomics studies have been conducted assessing the application of the science to acute lung diseases, only incremental progress has been made (Stringer et al. 2016).

In veterinary medicine, bovine respiratory disease (BRD) complex, a multi-factorial disease resulting from a combination of calf management, and pathogen factors (including bacteria and viruses), is an important health issue in dairy calves (Mosier 2014; Smith 2015). Calf raisers know that respiratory disease is one of the main disease entities they encounter. Acute bronchopneumonia prevalence in calves ranges from 0 to 52 %, with many cases occurring before weaning, and with BRD being associated with increased calf death rates (Guterbock 2014). In dairy calves, bronchopneumonia, sometimes called *enzootic pneumonia,* is most common in housed calves. The median farm-level incidence of producer-identified respiratory disease is 3–17 % (range: up to 91 %). Respiratory disease in dairy calves can have a negative impact on their subsequent growth and productivity. Calves treated for respiratory disease in the first 90 days of life were 2.5 times more likely to die before weaning than calves that were not treated (Friton et al. 2005; Smith 2015). A difference in metabolomics between healthy individuals and those with critical illness is not surprising. The next step is to determine if, among patients presenting with a serious infection, metabolomics may help identify those destined to fare poorly from those who will recover (Seymour et al. 2013). Thus, the metabolomic status is needed in calves with acute bronchopneumonia. For this purpose, this study was designed to assess the clinical utility of measuring metabolomics by NMR spectroscopy.

2 Materials and methods

2.1 Animals

Fifty clinically ill Holstein dairy calves aged 1–2 month-old (at approximately 45 days of age, main 5 days of disease duration) presented for treatment to the teaching hospital, were subjects of study. Calves were considered suitable for inclusion in the study if they had sufficient clinical and laboratory data at admission to suggest acute bronchopneumonia. Respiratory clinical scoring described by McGuirk and Peek (2014) was used to determine the bronchopneumonia level in ill calves. Ten healthy Holstein dairy calves belonging to the Farm of Faculty of Veterinary Medicine, aged 1–2 month-old served as controls. According to the Cohen formulation of power calculation (Cohen 1988), and using a *t* test as model, these numbers of patients and controls are sufficient to detect large effects ($d \sim 0.8$) at a significance level of 0.05 with a statistical power of 80 %.

2.2 Routine laboratory analysis

Blood was drawn from the jugular vein into heparin-coated and non-heparinized tubes, before therapeutic treatment. Complete blood count (blood cells, MCV, hematocrit, hemoglobin, MCV, MCH, MCHC) (Hemocell Counter MS4e, Melet Schloesing Laboratories, France) and blood gas analysis (pH, pO_2, pCO_2, HCO_3, base excess, O_2 saturation) (Gem Premier 3000, Instrumentation Laboratory, USA) were measured in calves when presented to the hospital. Serum and plasma samples were stored at −80 °C until analysis. Serum total protein, albumin, lactate, creatinine, total bilirubin, glucose, BUN, ALP, AST, GGT, CK, Na, K, Ca, Mg concentrations were measured by spectrometer (BT 3000 Italy).

2.3 Metabolomic evaluation

2.3.1 Sample preparation for ^{1}H-NMR spectroscopy

NMR measurements were performed at CERM/CIRMMP center of the ESFRI Instruct, University of Florence in Florence/Italy. Sample preparation for ^{1}H-NMR spectroscopy: Plasma samples were thawed on ice and extracted using a dual methanol-chloroform extraction (for protein precipitation and separation of hydrophilic and lipophilic fractions) as

previously described (Stringer et al. 2011). This eliminates macromolecules (e.g., proteins) and establishes a fused metabolic profile for water-soluble and lipid metabolites. Briefly, 0.5 ml of ice cold plasma was mixed with 1 ml of chloroform:methanol (1:1 vol/vol) and centrifuged. The supernatant (organic phase) was collected, and the pellet was resuspended with 0.5 ml of chloroform/methanol and centrifuged. The supernatants were combined, and 0.5 ml of ice-cold water was added to 'wash out' remaining water-soluble metabolites from the organic phase. After 15 min at −20 °C, the upper (aqueous) phase was removed and added to the remaining pellet (to wash out remaining water-soluble metabolites from the pellet), 1 ml of water was added, and the sample was centrifuged and freeze-dried overnight. The lipid rich methanol-chloroform fraction (bottom phase after low temperature exposure) was evaporated using a high-speed vacuum centrifuge.

The dried water-soluble extracts were dissolved in 700 μL of $^{2}H_2O$, centrifuged, and 600 μL were transferred into 5 mm NMR tubes (Bruker BioSpin srl) for the analysis. The dried lipid extracts were dissolved in 800 μL of $CDCl_3$, centrifuged and 600 μL were transferred into 5 mm NMR tubes (Bruker BioSpin srl) for the analysis.

2.3.2 NMR analysis

Monodimensional ^{1}H NMR spectra for all samples were acquired using a Bruker 600 MHz spectrometer (Bruker BioSpin) operating at 600.13 MHz proton Larmor frequency and equipped with a 5 mm PATXI 1H-13C-15 N and 2H-decoupling probe including a z axis gradient coil, an automatic tuning-matching (ATM) and an automatic and refrigerate sample changer (SampleJet). A BTO 2000 thermocouple served for temperature stabilization at the level of approximately 0.1 K at the sample. Before measurement, samples were kept for at least 5 min inside the NMR probehead, for temperature equilibration at 310 K. For each serum water-soluble and lipid extract, a one-dimensional (1D) NMR spectrum was acquired with water peak suppression using a standard Nuclear Overhauser Effect Spectroscopy pulse sequence NOESY 1Dpresat (noesygppr1d.comp; Bruker BioSpin), as reported in literature (Lindon et al. 2007; Beckonert et al. 2007; Dona et al. 2014; Emwas et al. 2016) using 32 scans, 98,304 data points, a spectral width of 18,028 Hz, an acquisition time of 2.7 s, a relaxation delay of 4 s and a mixing time of 0.01 s.

2.3.3 Spectral processing

Free induction decays were multiplied by an exponential function equivalent to a 0.3 Hz line-broadening factor before applying Fourier transform. Transformed spectra were automatically corrected for phase and baseline distortions and calibrated (anomeric glucose doublet at 5.24 ppm for water-soluble extracts, and chloroform singlet at 7.25 ppm) using TopSpin 3.2 (Bruker Biospin). Each 1D spectrum of water-soluble extracts in the range between 0.2 and 10.00 ppm was segmented into 0.02 ppm chemical shift bins and the corresponding spectral areas were integrated using AMIX software (version 3.8.4, Bruker BioSpin). Binning is a means to reduce the number of total variables and to compensate for small shifts in the signals, making the analysis more robust and reproducible (Spraul et al. 1994; Holmes et al. 1994). Regions between 4.7 and 4.5 ppm containing residual H_2O signal were removed and the dimension of the system was reduced to 481 bins. The total spectral area was calculated on the remaining bins and total area normalization was carried out on the data prior to pattern recognition. Each 1D spectrum of lipid extracts in the range between 0.2 and 6.5 ppm was segmented into 0.02 ppm chemical shift bins, for a total of 315 bins, and the corresponding spectral areas were integrated using AMIX software (version 3.8.4, Bruker BioSpin). The total spectral area was calculated on the bins and total area normalization was applied on the data. To further validate the multivariate analysis, calculations with 0.002 ppm bins have been also performed.

2.4 Statistical analysis

All clinical and laboratory data were presented as the mean ± SD. The data were evaluated by independent *t*-test using the SPSS 13 program. Statistical significance was considered at P value < 0.05.

All metabolomic data analysis were performed using R, an open source software for the statistical analysis of data (Ihaka and Gentleman 1996). Multivariate data analysis was conducted on processed data and univariate statistical analysis was carried out on whole spectra by combining established methods.

Data reduction was carried out by means of projection into a Principal Component Analysis (PCA) subspace, only the first 20 components were retained in the model and the canonical analysis (CA) was applied to obtain the supervised separation of the analyzed groups. For the purpose of classification we used the K-nearest neighbors (k-NN) method ($k = 5$) applied on the PCA-CA scores (Cover and Hart 1967). Accuracy, sensitivity and specificity for the different classifications were assessed by means of 100 cycles of a Monte Carlo cross-validation scheme (MCCV, R script in-house developed). Briefly, 90 % of the data were randomly chosen at each iteration as a training set to build the model. Then the remaining 10 % was tested and sensitivity, specificity and accuracy for the classification were assessed. The procedure was repeated 100 times to

Table 1 Hematological parameters in the groups

Parameters	Healthy group (n = 10)	Diseased group (n = 50)	*P* values
[a]**pH**	**7.34 ± .018**	**7.39 ± 0.01**	**0.016**
[a]**PCO_2, mmHg**	**56.40 ± 1.66**	**50.24 ± 1.27**	**0.008**
pO2, mmHg	24.90 ± 1.62	24.84 ± .872	0.974
TCO_2, mmHg	31.9 ± .909	32.59 ± .924	0.515
[a]**HCO_3, mnol/L**	**30.17 ± .909**	**31.01 ± .896**	**0.008**
Base excess, mmol/L	3.98 ± .900	5.33 ± .907	0.300
[a]**WBC, $10^3/mm^3$**	**12.3 ± 1.35**	**17.0 ± 1.43**	**0.025**
RBC, $10^6/mm^3$	9.74 ± .327	9.76 ± .270	0.965
Platelets, $10^5/mm^3$	475 ± 32.7	397 ± 28.3	0.084
[a]**MCV, fL**	**29.9 ± .754**	**32.1 ± .499**	**0.026**
[a]**MCH, g/dL**	**10.4 ± .219**	**11.2 ± .154**	**0.009**
MCHC, g/dL	35.1 ± .414	35.2 ± .377	0.901
Hemoglobin, g/dL	10.2 ± .458	10.9 ± .270	0.255
Hematocrit, %	29.1 ± 1.47	31.0 ± .812	0.298

[a] Expressed as mean ± SD; probability for these numerical data can only be given a range. The parameters in bold are significantly different (*P* value < 0.05) in the comparison

Table 2 Biochemical parameters in the groups

Parameters	Healthy group (n = 10)	Diseased group (n = 50)	*P* values
[a]**Protein, g/dL**	**7.14 ± 0.11**	**6.40 ± 0.17**	**0.001**
[a]**Albumin, mg/dL**	**3.97 ± 0.06**	**3.42 ± 0.06**	**0.000**
[a]**BUN, mg/dL**	**9.200 ± 0.29**	**13.260 ± 1.62**	**0.017**
[a]**Creatinine, mg/dL**	**1.330 ± 0.06**	**1.014 ± 0.08**	**0.002**
[a]**Total bilirubin, mg/dL**	**0.90 ± 0.02**	**0.50 ± 0.04**	**0.000**
[a]**Glucose, mg/dL**	**60.70 ± 2.53**	**76.50 ± 3.73**	**0.001**
Lactate, mmol/L	2.46 ± .555	1.75 ± .220	0.259
[a]**Ca, mg/dL**	**10.3 ± 0.21**	**9.30 ± 0.21**	**0.003**
[a]**P, mg/dL**	**7.89 ± 0.21**	**6.89 ± 0.22**	**0.002**
Mg, mg/dL	1.32 ± 0.04	1.42 ± 0.04	0.084
Na, mEq/L	142.30 ± .651	140.88 ± .648	0.132
[a]**K, mEq/L**	**5.06 ± .190**	**3.94 ± .070**	**0.000**
SGOT, U/L	102 ± 12.4	100 ± 8.68	0.915
SGPT, U/L	25.9 ± 2.31	27.9 ± 4.19	0.671
[a]**ALP, U/L**	**553 ± 51.1**	**381 ± 34.5**	**0.012**
[a]GGT, U/L	28.1 ± 2.01	55.7 ± 12.4	0.033
CPK, U/L	315 ± 26.8	476 ± 78.5	0.058

[a] Expressed as mean ± SD; probability for these numerical data can only be given a range. The parameters in bold are significantly different (*P* value < 0.05) in the comparison

derived an average discrimination accuracy for each group of subjects.

The spectral regions related to the metabolites were assigned in the full resolution NMR profiles by using matching routines of AMIX 3.8.4 (Bruker BioSpin) in combination with the BBIOREFCODE (Bruker BioSpin) and published literature when available. These spectral regions were integrated to obtain the concentrations of metabolites in arbitrary units and the concentrations were analyzed to determine the discriminating metabolites among the groups of calves. Wilcoxon signed-rank test (Wilcoxon 1945) was chosen to infer differences among the groups on the biological assumption that metabolite concentrations are not normally distributed; false discovery rate correction was applied using the Benjamini–Hochberg method (Benjamini and Hochberg 1995). An adjusted P value < 0.05 was deemed significant.

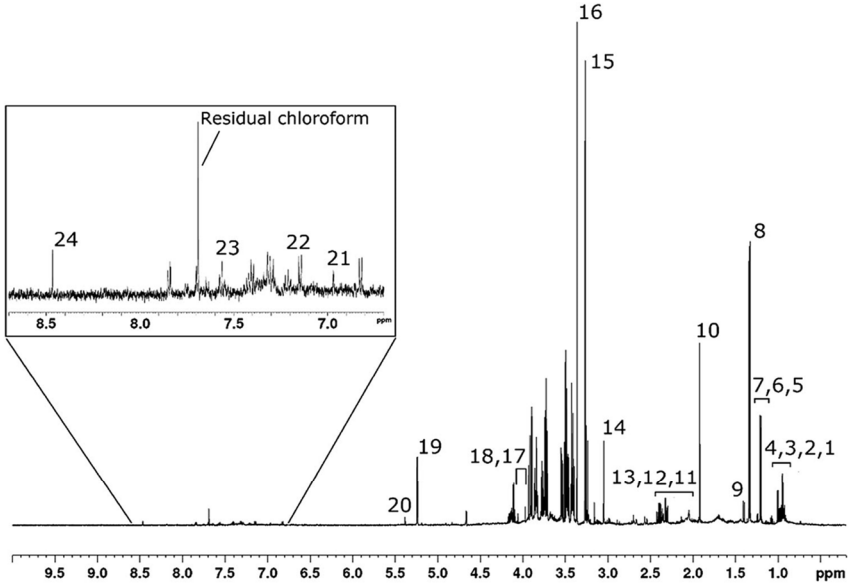

Fig. 1 A NOESY spectrum of a water soluble extract. The aromatic region in the *box* is magnified for clarity. The *numbers* represent the metabolites assigned in the spectrum: *1*, isoleucine; *2*, valine; *3*, propionate; *4*, 2-methylglutarate;*5*, ethanol; *6*, 3-hydroxybutyrate; *7*, fucose; *8*, lactate; *9*, alanine; *10*, acetate; *11*, NAG; *12*, methionine; *13*, pyruvate; *14*, unknown; *15*, choline; *16*, methanol; *17*, creatine; *18*, creatinine; *19*, glucose; *20*, allantoin; *21*, 3-methyl-histidine; *22*, tyrosine; *23*, phenylalanine; *24*, formate

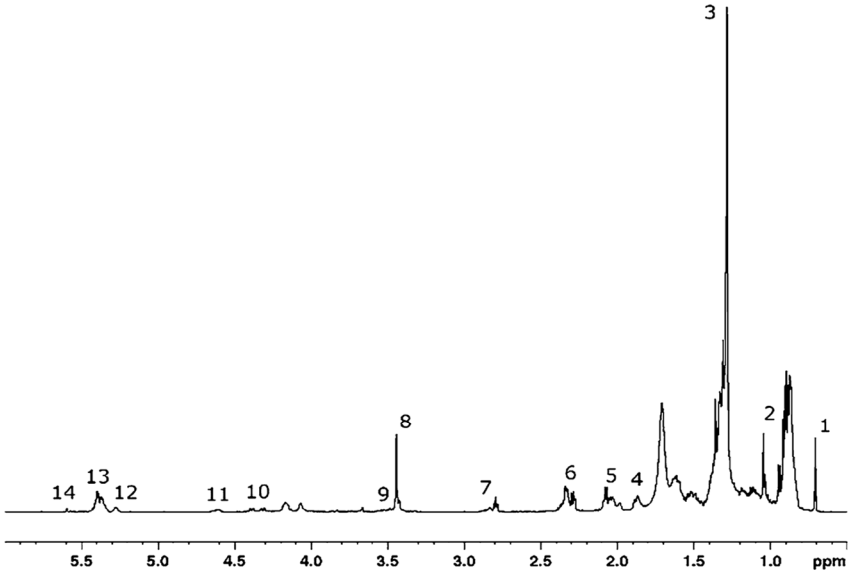

Fig. 2 A NOESY spectrum of a lipid extract. The *numbers* represent the lipid fractions assigned in the spectrum: *1*, cholesterol-C18; *2*, fatty acid $–CH_3$; *3*, fatty acid $(–CH_2–)_n$; *4*, total cholesterol; *5*, fatty acid $=CH–CH_2–CH_2–$; *6*, fatty acid $–CH_2–CO$; *7*, PUFA; *8*, phospholipids $–N(CH_3)_3$; *9*, free cholesterol –C(3)H; *10*, total lipids backbone; *11*, phosphatidylcholine $–PO–CH_2$; *12*, phosphoglycerides; *13*, UFA; *14*, Unassigned lipid fraction

3 Results

3.1 Clinical and laboratory data

All the ill calves had score three (repeated spontaneous coughs, copious bilateral mucopurulent discharge, heavy ocular discharge, head tilt or bilateral droop and watery, sifts through bedding). Fever, increased respiratory rate and depression were observed clinically. Abnormal lung sounds, mostly crackles (or rhonchi) and wheezes were present in thorax auscultation. There were no changes in hematological parameters except leukocytosis. Some biochemical parameters between diseased and healthy groups were within normal ranges despite of significant differences. Alterations in some membrane enzymes (ALP and GGT) were striking in diseased animals (Tables 1, 2).

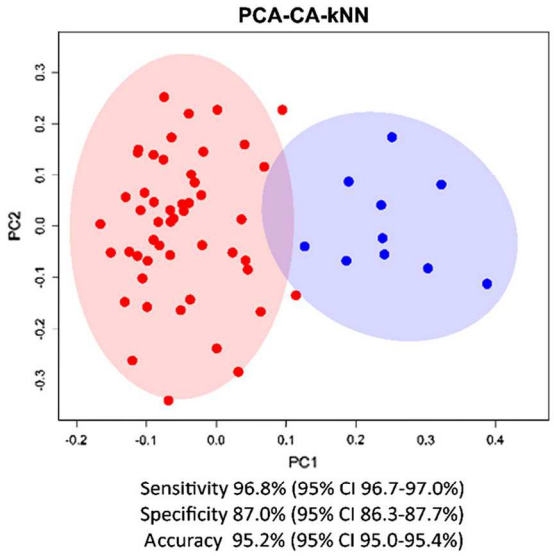

Fig. 3 PCA-CA-kNN *score* plot, discrimination between diseased calves (*red dots*, n = 50) and healthy calves (*blue dots*, n = 10), using the spectra of the water soluble extracts. Sensitivity, specificity and accuracy are also reported

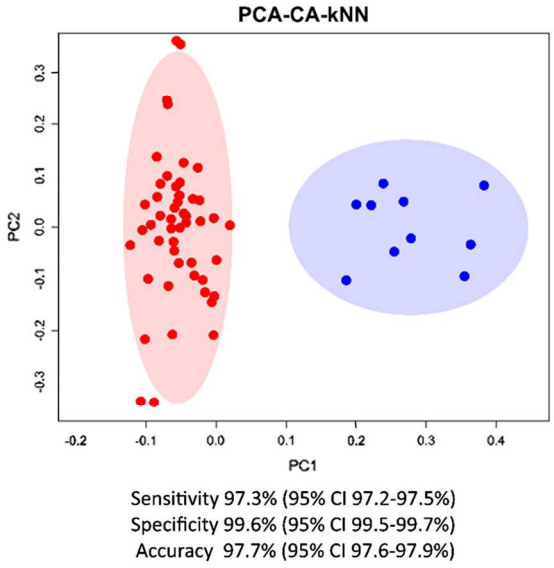

Fig. 4 PCA-CA-kNN *score* plot, discrimination between diseased calves (*red dots*, n = 50) and healthy calves (*blue dots*, n = 10), using the spectra of the lipid extracts. Sensitivity, specificity and accuracy are also reported

3.2 NMR-based metabolomic analysis

NMR spectra of the all samples (50 diseased + 10 healthy water soluble extracts, 50 diseased + 10 healthy lipid extracts) were acquired using a standard Nuclear Overhauser Effect Spectroscopy pulse sequence (Figs. 1, 2). The statistical models applied proved to be effective in discriminating between calves with bronchopneumonia and healthy calves using both kind of extracts.

NMR data from 10 control water soluble extracts and from 50 water soluble extracts of diseased calves were submitted to PCA-CA, and accuracy, sensitivity and specificity were obtained through a Monte Carlo cross-validation scheme using the k-NN classifier on the PCA-CA scores. The score plot of the first two components of PCA-CA-kNN, accuracy, sensitivity and specificity are reported in Fig. 3.

The statistical approach just described was applied also to the analysis of the 10 control lipid extracts and the 50 lipid extracts of diseased calves. The score plot of the first two components of PCA-CA-kNN, accuracy, sensitivity and specificity are reported in Fig. 4. To better explore the differences between the two groups of calves an integrated analysis merging the data from the lipophilic and hydrophilic phases were performed. The merged data-set was submitted to PCA-CA, and accuracy, sensitivity and specificity were obtained through a Monte Carlo cross-validation scheme using the k-NN classifier on the first 40 components of PCA-CA scores. The score plot of the first two components of PCA-CA-kNN, accuracy, sensitivity and specificity are reported in the supplementary materials (Supplemental Fig. 1). Finally, to assess the robustness of the results with respect to the binning size, the multivariate statistics was repeated using a 0.002 ppm buckets (Supplemental Figs. 2–3).

Over 30 metabolites were identified and quantified by ^{1}H-NMR from each data set (lipophilic and hydrophilic fractions) for each serum sample (Tables 3, 4; Figs. 5, 6). These data demonstrated that calves suffering from bronchopneumonia showed lower levels of propionate, ethanol, acetate, dimethylsulfone, allantoin, fraction C-18 of cholesterol, signals of $=CH–CH_2–CH_2–$ of fatty acids and the signals of –C(3)H of free cholesterol, and higher levels of 2-methylglutarate, phenylalanine, signals of $(–CH_2–)_n$ of fatty acids and signals of phosphatidylcholine $(–PO–CH_2)$.

4 Discussion

We evaluated NMR based metabolomics, for the first time, in calves with acute bronchopneumonia. Obtained data indicate that quantitative ^{1}H-NMR-spectroscopy metabolomics was a feasible tool for the identification of potential novel biomarkers of calf bronchopneumonia.

There is currently no gold standard method for the diagnosis of BRD complex in Holstein pre-weaned dairy calves (McGuirk and Peek 2014). The clinical diagnosis of

Table 3 Concentrations in arbitrary units (mean ± SD) of the metabolites assigned in the water soluble extracts

Number	Water soluble metabolites	Healthy group (n = 10)	Diseased group (n = 50)	*P* values
1	Isoleucine	0.00095 ± 0.00024	0.00091 ± 0.00033	7.22E − 01
2	Valine	0.00444 ± 0.00063	0.00506 ± 0.00177	5.93E − 01
3	**Propionate**	**0.0003 ± 0.00012**	**0.00009 ± 0.00006**	**9.58E − 05**
4	**2-methylglutarate**	**0.00023 ± 0.00008**	**0.00035 ± 0.00014**	**2.71E − 02**
5	**Ethanol**	**0.00321 ± 0.00186**	**0.00071 ± 0.00074**	**1.01E − 04**
6	3-hydroxybutyrate	0.0025 ± 0.00074	0.00192 ± 0.0015	1.33E − 01
7	Fucose	0.00117 ± 0.00038	0.001 ± 0.0005	3.680E − 01
8	Lactate	0.06873 ± 0.03407	0.07658 ± 0.04581	7.36E − 01
9	Alanine	0.00588 ± 0.00134	0.00551 ± 0.00245	8.11E − 01
10	**Acetate**	**0.00605 ± 0.00198**	**0.00304 ± 0.00208**	**1.77E − 03**
11	NAG	0.00285 ± 0.00087	0.0028 ± 0.00146	7.65E − 01
12	Methionine	0.00042 ± 0.00008	0.00039 ± 0.00023	2.88E − 01
13	Pyruvate	0.0008 ± 0.00025	0.00097 ± 0.00045	4.33E − 01
14	**Dimethyl-sulfone**	**0.0015 ± 0.00046**	**0.00051 ± 0.00048**	**1.40E − 04**
15	Choline	0.00061 ± 0.00014	0.00076 ± 0.0003	2.04E − 01
16	Methanol	0.07614 ± 0.0258	0.05971 ± 0.02851	1.65E − 01
17	Creatine	0.00303 ± 0.00045	0.00257 ± 0.00105	9.70E − 02
18	Creatinine	0.0007 ± 0.00011	0.00073 ± 0.00045	9.20E − 01
19	Glucose	0.00876 ± 0.00082	0.01093 ± 0.00399	6.25E − 02
20	**Allantoin**	**0.00041 ± 0.00004**	**0.00029 ± 0.00015**	**2.71E − 02**
21	3-methyl-histidine	0.00057 ± 0.00034	0.00059 ± 0.00032	9.29E − 01
22	Tyrosine	0.0007 ± 0.00019	0.00083 ± 0.00041	4.330E − 01
23	**Phenylalanine**	**0.00061 ± 0.00039**	**0.00108 ± 0.00058**	**4.27E − 02**
24	Formate	0.00024 ± 0.00008	0.00031 ± 0.00012	2.29E − 01

P values form the comparison healthy-diseased are also reported: the metabolites in bold are significantly different (*P* value < 0.05) in the comparison

Table 4 Concentrations in arbitrary units (mean ± SD) of the metabolites assigned in the lipid soluble extracts

Number	Lipid metabolites	Healthy group (n = 10)	Diseased group (n = 50)	*P* values
1	**Cholesterol-C18**	**0.01096 ± 0.00148**	**0.00854 ± 0.00306**	**4.976E − 02**
2	Fatty acid $–CH_3$	0.08914 ± 0.00637	0.10589 ± 0.03387	1.331E − 01
3	**Fatty acid $(–CH_2–)_n$**	**0.0708 ± 0.00451**	**0.08361 ± 0.01239**	**1.863E − 03**
4	Total Cholesterol	0.06619 ± 0.01317	0.08653 ± 0.053	5.472E − 01
5	**Fatty acid $=CH–CH_2–CH_2–$**	**0.0312 ± 0.0026**	**0.023 ± 0.00681**	**1.636E − 03**
6	Fatty acid $–CH_2–CO$	0.02635 ± 0.00284	0.02439 ± 0.00594	4.351E − 01
7	PUFA	0.00837 ± 0.0015	0.00756 ± 0.00258	4.845E − 01
8	Phospholipids $–N(CH_3)_3$	0.01651 ± 0.00179	0.01663 ± 0.00585	9.447E − 01
9	**Free cholesterol –C(3)H**	**0.00173 ± 0.00028**	**0.00059 ± 0.00058**	**1.292E − 04**
10	Total lipids backbone	0.00039 ± 0.00015	0.00035 ± 0.00025	3.894E − 01
11	**Phosphatidylcholine $–PO–CH_2$**	**0.00059 ± 0.0002**	**0.00121 ± 0.00097**	**4.976E − 02**
12	Phosphoglycerides	0.00193 ± 0.00027	0.00184 ± 0.0006	7.685E − 01
13	UFA	0.02232 ± 0.00285	0.01899 ± 0.00593	1.331E − 01
14	Unassigned lipid fraction	0.00029 ± 0.00005	0.00027 ± 0.00017	4.941E − 01

P values form the comparison healthy-diseased are also reported: the metabolites in bold are significantly different (*P* value < 0.05) in the comparison

BRD classically is based on clinical signs including lethargy, anorexia, abnormal breathing patterns (e.g., dyspnea, tachypnea), and increased rectal temperature. Some researchers advise to use ultrasonography for accurately detecting lung lesions. Wisconsin calf respiratory scoring chart is a simpler alternative, but with unknown accuracy (Buczinski et al. 2015; Ollivett et al. 2015). Clinical diagnosis of the disease in calves has been relatively facile using the scoring cart in the present study where routine clinical, hematological and biochemical data were in accordance with most references.

Metabolomics has considerable potential to improve diagnostics for childhood pneumonia. In severe childhood pneumonia, six identified metabolites (uric acid, L-histidine, hypoxanthine, glutamic acid, L-tryptophan, and ADP) related to the host response to infection through antioxidant, inflammatory, and antimicrobial pathways, as well as the energy metabolism, emerged as markers (Laiakis et al. 2010). In human patients with sepsis-induced pneumonia and acute lung injury, quantitative metabolomics data showed differences in the levels of some metabolites reflecting the complex pathology including oxidant stress, energy balance, apoptosis, endothelial barrier function, bile acid metabolism, protein catabolism, inflammation (Stringer et al. 2011; Seymour et al. 2013).

As mentioned in human medicine (Slupsky 2011; Cheng et al. 2013; Mussap et al. 2013; Fanos et al. 2014), NMR-based analysis of metabolites may provide new information for the diagnosis and etiology of pneumonia in calves with bronchopneumonia. In the present study, for the first time, over 30 metabolites were identified and quantified by ^{1}H-NMR from each data set (lipophilic and hydrophilic

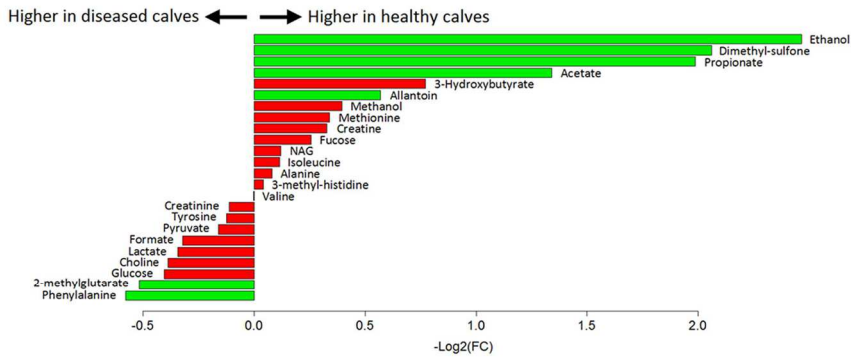

Fig. 5 Panel of water soluble metabolites assigned. Metabolites with –Log2 (FC) negative values had higher concentrations in diseased calves with respect to healthy calves. Metabolites with –Log2 (FC) positive values had higher concentration in healthy calves. *Green* bars represented metabolites whose concentration is significantly different (p value < 0.05) in the comparison, *red* bars represented metabolite values that were not statistically relevant

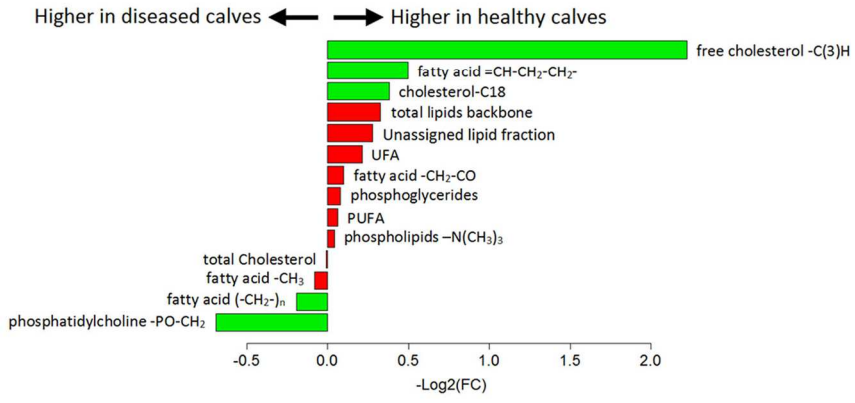

Fig. 6 Panel of lipid metabolites assigned. Metabolites with –Log2 (FC) negative values had higher concentrations in diseased calves with respect to healthy calves. Metabolites with –Log2 (FC) positive values had higher concentration in healthy calves. *Green* bars represented metabolites whose concentration is significantly different (p value < 0.05) in the comparison, *red* bars represented metabolite values that were not statistically relevant

fractions). The levels of 2-methylglutarate (energy metabolism), phenylalanine (neurology), phosphatidylcholine –PO–CH_2 (pulmonary surfactant), and fatty acid $(–CH_2–)_n$ were found to be high in the patients studied, while a reduction in levels of acetate, dimethyl-sulfone, propionate, ethanol and allantoin, free cholesterol –C(3)H, fatty acid =CH–CH_2–CH_2 and cholesterol-C18 was seen. 2-Methylglutaric acid is a metabolite of succinic acid, a citric acid cycle intermediate. Increasing phenylalanine is toxic for growing brain and causes disconnection of brain white matter pathways. Excessive phenylalanine inhibits the transport of other neutral amino acids across the blood–brain barrier (Aghasi et al. 2015; Crujeiras et al. 2015). Phosphatidylcholine is a major constituent of cell membranes and pulmonary surfactant and is an increasing evidence as a marker of oxidative diseases (Nakagawa et al. 2015), and may be crucial for breast cancer cell survival (Mori et al. 2015). Alterations to the pulmonary surfactant system have long been implicated in the course of inflammatory lung diseases such as pneumonia or aspiration (Schmidt et al. 2007). The relevance of these metabolites in identifying early calves with bronchopneumonia should be confirmed in future large prospective cohort studies.

5 Conclusion

This study showed that ^{1}HNMR-based quantitative metabolomics is a feasible approach for the identification of physiologically relevant metabolites associated with processes involved in the pathogenesis of acute bronchopneumonia (oxidant stress, energy deficit, and surfactant insufficiency). Although these metabolites may be meaningful for better understanding the pathogenic mechanisms, and for early diagnosis and prognosis of bronchopneumonia in calves, the extent of the predictive and prognostic value of this given set of metabolites (e.g., biomarker credentials) will be required for clinical trials.

Acknowledgments This work was financially supported by Selcuk University Scientific Research Projects Coordination Unit (Project No: 15401135). CERM/CIRMMP center of the ESFRI Instruct is gratefully acknowledged for the NMR access provision financially supported by the EC Contract iNEXT No 653706. This work was partially supported by Fondazione Veronesi that granted L.T through the Post-Doctoral Fellowship-2015.

Compliance with ethical standards

Conflict of interest We have no conflict of interest to declare.

Ethical approval The experimental design was approved by the Committee on Use of Animals in Research of the Selcuk University, Faculty of Veterinary Medicine (Protocol No. 33/2015).

References

Aghasi, P., Setoodeh, A., Sayarifard, A., Rashidiyan, M., Sayarifard, F., Rabbani, A., et al. (2015). Intellectual and developmental status in children with hyperphenylalaninemia and PKU who were screened in a national program. *Iranian journal of pediatrics, 25*(6), e3033.

Atzei, A., Atzori, L., Moretti, C., Barberini, L., Noto, A., Ottonello, G., et al. (2011). Metabolomics in pediatric respiratory diseases and bronchiolitis. *The Journal of Maternal-Fetal & Neonatal Medicine, 24*(Suppl 2), 59–62.

Beckonert, O., Keun, H. C., Ebbels, T. M. D., Bundy, J., Holmes, E., Lindon, J. C., et al. (2007). Metabolic profiling, metabolomic and metabonomic procedures for NMR spectroscopy of urine, plasma, serum and tissue extracts. *Nature Protocols, 2*(11), 2692–2703.

Benjamini, Y., & Hochberg, Y. (1995). Controlling the false discovery rate: a practical and powerful approach to multiple testing. Journal of the royal statistical society. Series B (Methodological), 289–300.

Buczinski, S., Ollivett, L. T., & Dendukuri, N. (2015). Bayesian estimation of the accuracy of the calf respiratory scoring chart and ultrasonography for the diagnosis of bovine respiratory disease in pre-weaned dairy calves. *Preventive veterinary medicine, 1*, 227–231.

Cheng, C. W., Chien, M. H., Su, S. C., & Yang, S. F. (2013). New markers in pneumonia. *Clinica Chimica Acta, 18*, 19–25.

Cohen, J. (1988). *Statistical power analysis for the behavioral sciences*. Mahwah: L. Erlbaum Associates.

Cover, T., & Hart, P. (1967). Nearest neighbor pattern classification. *IEEE Transactions on Information Theory, 13*, 21–27.

Crujeiras, V., Aldámiz-Echevarría, L., Dalmau, J., Vitoria, I., Andrade, F., Roca, I., et al. (2015). Vitamin and mineral status in patients with hyperphenylalaninemia. *Molecular Genetics and Metabolism, 115*(4), 145–150.

Dona, A. C., Jiménez, B., Schäfer, H., Humpfer, E., Spraul, M., Lewis, M. R., et al. (2014). Precision high-throughput proton NMR spectroscopy of human urine, serum, and plasma for large-scale metabolic phenotyping. *Analytical Chemistry, 86*(19), 9887–9894.

Emwas, A. H., Roy, R., McKay, R. T., Ryan, D., Brennan, L., Tenori, L., et al. (2016). Recommendations and standardization of biomarker quantification using NMR-based metabolomics with particular focus on urinary analysis. *Journal of Proteome Research, 15*(2), 360–373.

Fanos, V., Buonocore, G., & Mussap, M. (2014). Neonatomics and childomics: the right route to the future. *The Journal of Maternal-Fetal and Neonatal Medicine, 27*(Suppl 2), 1–3.

Friton, G. M., Cajal, C., & Ramirez-Romero, R. (2005). Long-term effects of meloxicam in the treatment of respiratory disease in fattening cattle. *Journal of the British Veterinary Association, 156*, 809.

Guterbock, W. M. (2014). The impact of BRD: the current dairy experience. *Animal Health Research Reviews, 15*, 130–134.

Holmes, E., Foxall, P. J., Nicholson, J. K., Neild, G. H., Brown, S. M., Beddell, C. R., et al. (1994). Automatic data reduction and pattern recognition methods for analysis of ^{1}H nuclear magnetic resonance spectra of human urine from normal and pathological states. *Analytical Biochemistry, 220*, 284–296.

Ihaka, R., & Gentleman, R. R. (1996). A Language for data analysis and graphics. *J Comput Stat Graph, 5*, 299–314.

Laiakis, E. C., Morris, G. A., Fornace, A. J., & Howie, S. R. (2010). Metabolomic analysis in severe childhood pneumonia in the Gambia, West Africa: findings from a pilot study. *PLoS One, 5*(9), e12655.

Lindon, C.J., Nicholson, J.K., & Holmes, E. (2007). The Handbook of Metabonomics and Metabolomics. Elsevier, 345–374.

McGuirk, S. M., & Peek, S. F. (2014). Timely diagnosis of dairy calf respiratory disease using a standardized scoring system. *Animal Health Research Reviews, 15*(2), 145–147.

Mori, N., Wildes, F., Kakkad, S., Jacob, D., Solaiyappan, M., Glunde, K., et al. (2015). Choline kinase-α protein and phosphatidylcholine but not phosphocholine are required for breast cancer cell survival. *NMR in Biomedicine, 28*(12), 1697–1706.

Mosier, D. (2014). Review of BRD pathogenesis: the old and the new. *Animal Health Research Reviews, 15*(2), 166–168.

Mussap, M., Noto, A., Cibecchini, F., & Fanos, V. (2013). The importance of biomarkers in neonatology. *Semin Fetal Neonatal Medicine, 18*, 56–64.

Nakagawa, K., Kato, S., & Miyazawa, T. (2015). Determination of phosphatidylcholine hydroperoxide (PCOOH) as a marker of membrane lipid peroxidation. *Journal of nutritional science and vitaminology, 61*(Suppl), S78–S80.

Ollivett, T. L., Caswell, J. L., Nydam, D. V., Duffield, T., Leslie, K. E., Hewson, J., et al. (2015). Thoracic ultrasonography and bronchoalveolar lavage fluid analysis in holstein calves with subclinical lung lesions. *Journal of Veterinary Internal Medicine, 29*, 1728–1734.

Schmidt, R., Markart, P., Ruppert, C., Wygrecka, M., Kuchenbuch, T., Walmrath, D., et al. (2007). Time-dependent changes in pulmonary surfactant function and composition in acute respiratory distress syndrome due to pneumonia or aspiration. *Respiratory Research, 27*(8), 55.

Seymour, C. W., Yende, S., Scott, M. J., Pribis, J., Mohney, R. P., Bell, L. N., et al. (2013). Metabolomics in pneumoniaand sepsis: an analysis of the GenIMS cohort study. *Intensive Care Medicine, 39*(8), 1423–1434.

Slupsky, C. M. (2011). Nuclear magnetic resonance-based analysis of urine for the rapid etiological diagnosis of pneumonia. *Expert Opinion on Medical Diagnostics, 5*(1), 63–73.

Smith, B. P. (2015). *Large Animal Internal Medicine* (5th ed.). St. Louis: Mosby Elsevier.

Spraul, M., Neidig, P., Klauck, U., Kessler, P., Holmes, E., Nicholson, J. K., et al. (1994). Automatic reduction of NMR spectroscopic data for statistical and pattern recognition classification of samples. *Journal of pharmaceutical and biomedical analysis, 12*, 1215–1225.

Stringer, K. A., McKay, R. T., Karnovsky, A., Quémerais, B., & Lacy, P. (2016). Metabolomics and its application to acute lung diseases. *Frontiers in Immunology, 29*(7), 44.

Stringer, K. A., Serkova, N. J., Karnovsky, A., Guire, K., Paine, R., & Standiford, T. J. (2011). Metabolic consequences of sepsis-induced acute lung injury revealed by plasma ^{1}H-nuclear magnetic resonance quantitative metabolomics and computational analysis. *American Journal of Physiology. Lung Cellular and Molecular Physiology, 300*, L4–L11.

Wheelock, C. E., Goss, V. M., Balgoma, D., Nicholas, B., Brandsma, J., Skipp, P. J., et al. (2013). Application of omics technologies to biomarker discovery in inflammatory lung diseases. *European Respiratory Journal, 42*, 802–825.

Wilcoxon, F. (1945). Individual Comparisons by Ranking Methods. *Biometrics bulletin, 1*, 80.

Supplementary materials:

Supplemental Table 1. Concentrations in arbitrary units (mean ± SD) of the metabolites assigned in the water soluble extracts. P-values form the comparison healthy-diseased are also reported: the metabolites in bold are significantly different (p-value<0.05) in the comparison (the lipid assignments have been done according to available literature Basoglu et al 2014).

Number	Water soluble metabolite	MSI level of identification	Database	Compound ID
1	Isoleucine	1	HMDB	HMDB00172
2	Valine	1	HMDB	HMDB00883
3	Propionate	1	HMDB	HMDB00237
4	2-methylglutarate	1	HMDB	HMDB00422
5	Ethanol	1	HMDB	HMDB00108
6	3-hydroxybutyrate	1	HMDB	HMDB00357
7	Fucose	1	HMDB	HMDB00174
8	Lactate	1	HMDB	HMDB00190
9	Alanine	1	HMDB	HMDB00161
10	Acetate	1	HMDB	HMDB00042
11	N-acetyl signals of glycoproteins	/	/	/
12	Methionine	1	HMDB	HMDB00696
13	Pyruvate	1	HMDB	HMDB00243
14	Dimethyl-sulfone	1	HMDB	HMDB04983
15	Choline	1	HMDB	HMDB00097
16	Methanol	1	HMDB	HMDB01875
17	Creatine	1	HMDB	HMDB00064
18	Creatinine	1	HMDB	HMDB00562
19	Glucose	1	HMDB	HMDB00122
20	Allantoin	1	HMDB	HMDB00462
21	3-methyl-histidine	1	HMDB	HMDB00479
22	Tyrosine	1	HMDB	HMDB00158
23	Phenylalanine	1	HMDB	HMDB00159
24	Formate	1	HMDB	HMDB00142

Supplemental Fig 1. PCA-CA-kNN score plot, discrimination between diseased calves (red dots, n = 50) and healthy calves (blue dots, n = 10), using a matrix were the lipophilic and hydrophilic data-sets are merged. Sensitivity, specificity and accuracy are also reported.

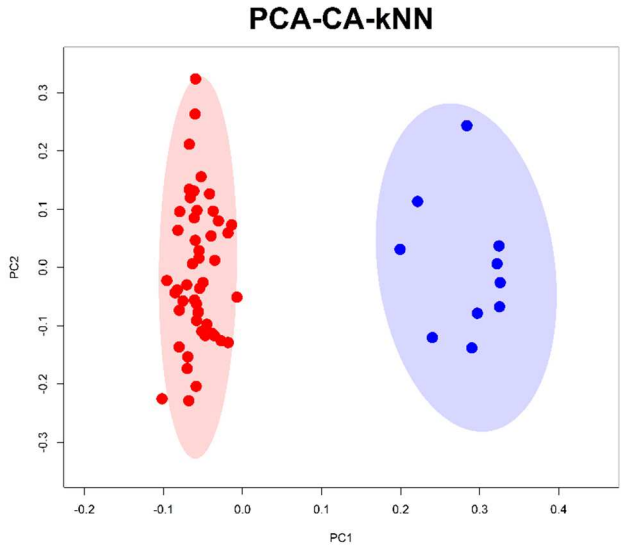

Sensitivity 98.1% (95% CI 98.0-98.3%)
Specificity 99.1% (95% CI 99.0-99.3%)
Accuracy 98.3% (95% CI 98.2-98.4%)

Supplemental Fig 2. PCA-CA-kNN score plot, discrimination between diseased calves (red dots, n = 50) and healthy calves (blue dots, n = 10), using the spectra of the water soluble extracts with the 0.002 binning size. Sensitivity, specificity and accuracy are also reported.

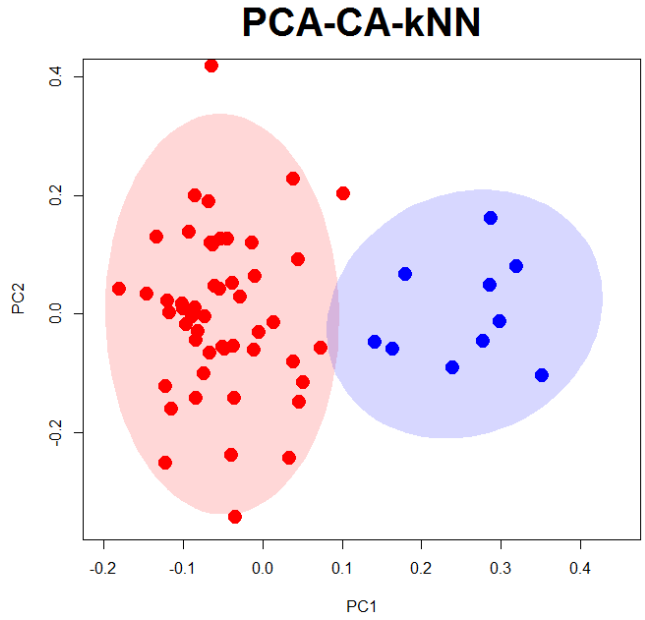

Sensitivity	92.9% (95% CI 92.3-93.5%)
Specificity	73.5% (95% CI 71.0-76.1%)
Accuracy	89.7% (95% CI 89.1-90.3%)

Supplemental Fig 3. PCA-CA-kNN score plot, discrimination between diseased calves (red dots, n = 50) and healthy calves (blue dots, n = 10), using the spectra of the lipid extracts with the 0.002 binning size. Sensitivity, specificity and accuracy are also reported.

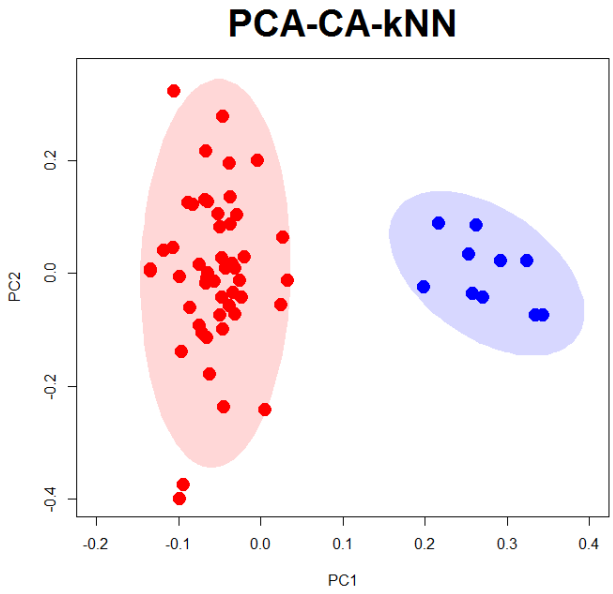

Sensitivity	99.5% (95% CI 99.2-99.9%)
Specificity	100.0% (95% CI 100.0%)
Accuracy	99.6% (95% CI 99.3-99.9%)

4.4.2 *Effects of boron supplementation on peripartum dairy cow's health*

A. Basoglu[1], N. Baspinar[2], L. Tenori[3], A. Vignoli[4], E. Gulersoy[1]

[1] Department of Internal Medicine, Faculty of Veterinary Medicine, Selcuk University, Aleaddin Keykubat Campus 42250 Selcuklu, Konya, Turkey
[2] Department of Biochemistry, Faculty of Veterinary Medicine, Selcuk University, Aleaddin Keykubat Campus 42250 Selcuklu, Konya, Turkey
[3] Consorzio Interuniversitario Risonanze Magnetiche di Metallo Proteine (CIRMMP), University of Flo-rence, Via Luigi Sacconi 6, 50019, Sesto Fiorentino (FI), Italy
[4] Magnetic Resonance Center (CERM), University of Florence, Via Luigi Sacconi 6, 50019, Sesto Fiorentino (FI), Italy

Published
Biol. Trace Elem. Res. 1–8 (2017). doi:10.1007/s12011-017-0971-9

Candidate's contributions: acquisition of NMR data, statistical analysis and interpretation of data, writing and review of the metabolomic section of the manuscript.

Biol Trace Elem Res
DOI 10.1007/s12011-017-0971-9

Effects of Boron Supplementation on Peripartum Dairy Cows' Health

Abdullah Basoglu[1] · Nuri Baspinar[2] · Leonardo Tenori[3] · Alessia Vignoli[4] · Erdem Gulersoy[1]

Received: 18 January 2017 / Accepted: 14 February 2017

Abstract Although many different dietary studies on the prevention of negative energy balance related diseases are often encountered, this is the first study investigating the effects of boron supplementation on peripartum dairy cows' health in the light of an omics approach. Twenty-eight healthy cows (1 control and 3 experimental groups) were enrolled from 2 months before predicted calving until 2 months after calving. Experimental groups were assigned to receive boron at increasing doses as an oral bolus. Production parameters, biochemical profile, Nuclear Magnetic Resonance based metabolomics profile, and mRNA abundance of gluconeogenic enzymes and lipid oxidation genes were determined. Pivotal knowledge was obtained on boron distribution in the body. Production parameters and mRNA abundance of the genes were not affected by the treatments. Postpartum nonesterified fatty acids, β-hydroxybutyrate, and triglyceride concentrations were significantly decreased in experimentals. The primary differences among groups were in lipid-soluble metabolites. There were significant differences in metabolites including postpartum valine, β-hydroxybutyrate, polyunsaturated fatty acid and citrate, propionate, isobutyrate, choline metabolites (betaine, phosphatidylcholine, and sphingomyelin), and some types of fatty acids and cholesterol in experimentals. Boron appears to be effective in minimizing negative energy balance and improving health of postpartum dairy cows.

Keywords Transition cow · Boron · Metabolomics · NMR · mRNA

Introduction

In dairy cows, transition from pregnancy to lactation is characterized by important metabolic adaptations aiming to counteract the negative energy balance (NEB) at the onset of lactation by a lipolysis from the adipose tissues. A glucose deficit together with excessive fatty acid mobilization and ketogenesis can lead to serious metabolic disorders and impairments of health and productivity of transition dairy cows [1–3]. Understandably, transition dairy cows have been the focus of considerable research, and general reviews are available. Over the past 40 years, use of blood sampling in the form of metabolic profiling has been applied to herd diagnostics with mixed impressions of diagnostic robustness [4, 5]. Omics sciences have found application in veterinary field for the characterization of the physiological and pathobiological mechanisms of cow diseases [6] but also in the framework of dairy cattle nutritional physiology, reproduction, and immunology [7]. Because major changes begin prepartum in the transition period, implementation of nutritional strategies at this time may have beneficial effects on hepatic metabolism. In the last decade, many peripartum dietary supplementations have been studied in dairy

Electronic supplementary material The online version of this article (doi:10.1007/s12011-017-0971-9) contains supplementary material, which is available to authorized users.

✉ Abdullah Basoglu
abbasoglu@selcuk.edu.tr

[1] Department of Internal Medicine, Faculty of Veterinary Medicine, Selcuk University, Aleaddin Keykubat Campus, 42250 Selcuklu, Konya, Turkey

[2] Department of Biochemistry, Faculty of Veterinary Medicine, Selcuk University, Aleaddin Keykubat Campus, 42250 Selcuklu, Konya, Turkey

[3] Consorzio Department of Experimental and Clinical Medicine, University of Florence, Largo Brambilla 3, 50134 Florence, Italy

[4] Magnetic Resonance Center (CERM), University of Florence, Via Luigi Sacconi 6, 50019 Sesto Fiorentino (FI), Italy

Published online: 22 February 2017

cows to understand the potential effects on liver metabolism and function. Trace mineral boron is a micronutrient with different and vitally important roles in metabolism that render it necessary for plant, animal, and human health, and, as recent research suggests, possibly for the evolution of life on Earth [8]. In our previous study [9], boron decreased the degree of fatty liver in dairy cows during early lactation; thus, in the light of the emergent omics approach, the present study was designed to evaluate the effects of boron supplementation on postpartum dairy cows' health.

Materials and Methods

Animals and Boron Supplementation

Twenty-eight healthy pregnant, multiparous, Holstein dairy cows with 3–3.5 body condition score (7 cows as control, and 3 experimental groups constituted by 8, 6, and 7 cows, respectively) were used; mean age was 3.5 years, mean 305-day milk production was 7.500 kg, and mean body weight was 650 kg at the start of the experiment.

The cows were offered drinking water (0.032 mg boron/L) and basal diets (0.55 mg boron/kg) (Table 1). Three experimental groups received 5, 10, and 15 g of borax (567, 1134, and 1701 mg of boron), respectively, as an oral bolus from 2 months before predicted calving until 2 months after calving. The bolus administration schedule was chosen to fit within the normal management activities of large dairies, and it required cows to be restrained in headlocks only once daily.

Blood and Liver Sampling

Blood samples were collected 1 month before expected calving, at calving, and 1 month after calving from the coccygeal vein into heparin and K-EDTA coated tubes. Serum and plasma samples harvested within an hour by centrifugation for 15 min at 3000 rpm were stored at −20 °C before analysis.

Table 1 Prepartum and postpartum ratios as fed

	Consumption (kg/d)	
Ingredient	Prepartum	Postpartum
Corn silage	10	12
Sugar beet pulp	–	10
Wheat straw	4	4.5
Hay	4	–
Concentrate[a]	2	8.5

[a] The concentrate consisted of 35% barley, 19.85% wheat, 15% wheat bran, 25% cotton seed meal, 3% limestone, 0.3% salt, and 0.35% vitamin-mineral mixture. It contained 21.5% crude protein and 2850 kcal/kg metabolizable energy

Liver biopsies were collected +1 week, 1 and 2 months relative to parturition, and were performed via the right, 11th to 12th intercostal space. Liver tissue was snap frozen in liquid nitrogen and stored at −80 °C until it was analyzed for mRNA isolation.

Serum Biochemistry

Serum samples were analyzed for biochemical profile including total protein, albumin, cholesterol, triglyceride (TG), glucose, β-hydroxybutyrate (BHB), blood urea nitrogen (BUN), alanine amino transaminase (ALT), aspartate amino transaminase (AST), lactate dehydrogenase (LDH), creatinine phosphokinase (CPK), gamma glutamyl transferase (GGT), Ca, Mg, P, lipid peroxidation (LPO) by routine spectrometric methods, and antioxidant potential (AOP) and nonesterified fatty acids (NEFA) by ELISA.

Boron concentrations were measured in blood, urine, milk, and feces samples by ICP-AES (VARIAN VISTA AX CCD) using Reference Material 8414 (National Institute of Standards and Technology).

Production variables including dry matter intake (DMI), energy intake, change of body condition score, and milk yields were determined.

Metabolomic Evaluation

Plasma samples extraction were performed at Selcuk University, Faculty of Veterinary Medicine, Konya/Turkey, and NMR measurements at CERM/CIRMMP center of the ESFRI Instruct, University of Florence, Florence/Italy. For the NMR metabolomics analysis, the dried water-soluble extracts were dissolved in 700 μL of $^{2}H2O$, centrifuged, and 600 μL were transferred into 5 mm NMR tubes for the analysis. Instead, the dried lipid extracts were dissolved in 800 μL of CDCl3, centrifuged, and 600 μL were transferred into 5 mm NMR tubes for the analysis.

One-dimensional NOESY ^{1}H NMR spectra for all samples (water- and lipid-soluble fractions) were acquired using a Bruker 600 MHz spectrometer operating at 600.13 MHz proton Larmor frequency. Each 1D spectrum of water-soluble extracts in the range between 0.2 and 10.00 ppm was segmented into 0.02-ppm chemical shift bins using AMIX software (version 3.9.15, Bruker BioSpin), regions between 4.8 and 4.5 ppm containing residual water signal were removed and the dimension of the system was reduced to 476 bins. The total spectral area was calculated on the remaining bins and total area normalization was carried out on the data prior to pattern recognition.

Each 1D spectrum of lipid extracts in the range between 0.2 and 6.5 ppm was segmented into 0.02-ppm chemical shift bins, for a total of 314 bins. Total area normalization was applied on the data prior to pattern recognition.

More information on analytical methods and spectral processing are detailed in our previous paper [6].

Hepatic mRNA Analysis

All RNA extraction and isolation were performed according to Kurar et al. [10]. Primers were either obtained from published sequences [11] or derived from cow sequences by using IDT PrimerQuest Tool program. The expression of GAPDH mRNA was employed as a reference gene selected as being the best-fit housekeeping gene in the experimental model in this study. Real time PCR reactions were performed on a LightCycler Nano Real Time PCR instrument (Roche Diagnostics, GERMANY) in 25 μL reaction volumes including 12.5 μL Maxima SYBR Green/ROX qPCR Master Mix (Thermo SCIENTIFIC, LITHUANIA), 10 pmol each primer and 2 μL isolated RNA sample (cDNA) as template.

Statistical Analyses

All data related to chemistry profile were presented as the mean ± SD. The data between groups were evaluated by one way ANOVA, and between periods Paired *t* test using SPSS 21.0 program. Statistical significance was considered at $p < 0.05$.

Before statistical analysis for gene analysis, the efficiencies of amplification of our target genes and internal control (GAPDH) were examined using qPCR amplification of serial dilutions of cDNA. On the basis of confirmation that the amplification efficiencies of the target and reference genes are nearly the same, data normalization process was performed according to Livak and Schmittengen [12] using $2^{-\Delta C}{}_{T}$ method, where $\Delta C'_T = C_{T,\ target} - C_{T,\ reference}$ (where $C_{T,\ target}$ and $C_{T,\ reference}$ are the threshold cycles for the target and reference genes amplifications, respectively).

All data analysis related with metabolomics was performed using R, an open source software for the statistical analysis of data [13]. Data reduction was carried out by means of projection into a principal component analysis (PCA) subspace, only the first 15 components were retained in the model and the canonical analysis (CA) was applied to obtain the supervised separation of the analyzed groups. For the comparisons of the lipid extracts among the different experimental groups at the same time (prepartum, partum, and postpartum), PCA alone showed a clear clusterization, so the PCA scores were directly used as input for the subsequent classification and validation.

Leave-one-out cross validation (LOOCV) was chosen as validation technique. That means that *N* separate times (with *N* the number of spectra in the dataset) the training set is built on all the data except for one spectrum, and a prediction is made for that spectrum. The average error across all *N* trials is computed and used to evaluate the model.

The spectral regions related to the metabolites were assigned in the NMR profiles by using matching routines of AMIX 3.9.15 (Bruker BioSpin) in combination with the BBIOREFCODE (Bruker BioSpin), public databases and published literature when available. These spectral regions were integrated to obtain the concentrations of metabolites in arbitrary units and the concentrations were analyzed to determine the discriminating metabolites among the groups of dairy cows. Kruskal-Wallis test [14] was chosen to infer differences among the groups on the biological assumption that metabolite concentrations are not normally distributed; false discovery rate correction was applied using the Benjamini-Hochberg method [15]. An adjusted p value <0.05 was deemed significant.

Results

Production Variables

In this study, all animals appeared healthy during the boron-diet treatment period, and there were no overt signs of toxicosis. Production results indicated that the DMI, energy intake, change of BCS, and milk yields were not affected by the treatments (>0.05) (Table 2).

Chemistry Profile

Increased boron ingestion increased serum, urine, milk, and feces boron concentrations. The percentage of boron in the body was increased with the 5, 10, and 15 g of borax as an oral bolus. Boron levels in body fluids (serum and milk, $p < 0.000$) were increasingly changed based on the dose (Table 3). Boron could not be completely absorbed from

Table 2 Production parameters

	Control	Exp 1	Exp 2	Exp 3
Milk (kg/day)	42.1	44.3	42.8	45.1
Fat (%)	3.5	3.4	3.1	3.5
Protein (%)	2.7	2.8	2.3	2.7
DMI (kg/day)				
Prepartum	13.4	13.7	13.9	14.3
Postpartum	17.2	19.0	18.5	18.8
Body weight				
Prepartum (kg)	3.5	3.4	3.1	3.7
Postpartum (kg)	3.8	3.0	2.9	3.0
Energy balance (Mcal/day)				
Prepartum	5.9	6.1	8.5	9.0
Postpartum	−4.3	−5.2	−4.0	−5.5

Table 3 Boron levels in the body

Boron	Periods	Control	Exp 1	Exp 2	Exp 3
Serum (mg/L)	Prepartum	0.030 ± 0.022	0.051 ± 0.031	0.062 ± 0.024	0.074 ± 0.037
	Partum	0.044 ± 0.028	0.114 ± 0.018^{Bb}	0.136 ± 0.063^{ABb}	0.225 ± 0.082^{Aa}
	Postpartum	0.048 ± 0.013	0.119 ± 0.009^{Bb}	0.145 ± 0.021^{ABb}	0.245 ± 0.012^{Aa}
Urine (mg/L)	Prepartum	0.537 ± 0.287	0.689 ± 0.270	0.893 ± 0.348	0.495 ± 0.226
	Partum	0.341 ± 1.044	2.683 ± 1.543^{Bb}	3.132 ± 1.839^{Bb}	3.724 ± 1.033^{Aa}
	Postpartum	0.355.013	2.721 ± 0.511^{Bb}	3.220 ± 0.921^{ABb}	3.942 ± 0.122^{Aa}
Milk (mg/L)	Prepartum	0.055 ± 0.151	0.085 ± 0.021	0.085 ± 0.021	0.095 ± 0.011
	Partum	0.068 ± 0.014	0.145 ± 0.050^{Bb}	0.155 ± 0.028^{Bb}	0.208 ± 0.018^{Ab}
	Postpartum	0.085 ± 0.011	0.155 ± 0.033^{Bb}	0.176 ± 0.015^{Bb}	0.225 ± 0.031^{Ab}
Feces (mg/kg)	Prepartum	0.085 ± 0.017	0.050 ± 0.013	0.039 ± 0.010	0.035 ± 0.022
	Partum	0,144 ± 0,049	0.121 ± 0.037^{Bb}	0.124 ± 0.020^{Bb}	0.129 ± 0.0237^{Bb}
	Postpartum	0.064 ± 0.034	0.123 ± 0.052^{Bb}	0.129 ± 0.018^{Bb}	0.139 ± 0.0205^{Bb}

P values for "capital letters" comparisons, i.e., for the comparison of the metabolites levels in the four treatment groups at the same sampling point. *P* values for "minuscules" comparisons, i.e., for the comparison of the metabolites levels in the three sampling points for the same treatment group

gastrointestinal tract. Urine was the most important excretion way of boron. Less boron was also eliminated by milk.

Compared with control group, the main differences in biochemical parameters of experimental groups included decreased AOP ($p < 0.001$), triglyceride ($p < 0.001$), NEFA ($p < 0.001$), and BHB ($p < 0.001$). Despite of significant changes in other biochemical parameters, they were within normal reference ranges (Supplemental Table 1).

Hepatic mRNA Abundance

Relative mRNA abundance of hepatic gluconeogenic enzymes such as cytosolic phosphoenolpyruvate carboxykinase (PEPCK) and pyruvate carboxylase (PC), also genes involved in fatty acid oxidation such as carnitine palmytoyltransferase-1 (CPT1) and peroxisome proliferator-activated receptor-α (PPAR-α) is presented in Table 4 and Supplemental Table 2. Dietary treatment had no significant effect on mRNA abundance for any of the genes analyzed.

NMR-Based Metabolomic Evaluation

For the multivariate analysis described in the following paragraphs, for both NMR data of water- and lipid-soluble extracts, PCA-CA or PCA were chosen as method to provide the clustering among the different experimental groups in the several comparisons reported and leave-one-out cross validation as validation technique to assess the prediction accuracies of the different models.

For each time point (prepartum, partum, and postpartum) the NMR data of the four experimental groups (control, exp 1, exp 2, and exp 3) were compared. The score plot of the first two components of PCA-CA, the confusion matrix, and the accuracy of each comparison are reported

Table 4 Postpartum gene expressions in liver samples

Genes	Postpartum	Control	Exp 1	Exp 2	Exp 3
CPT-1	1st week	3.116 ± 0.308	3.422 ± 0.316	3.108 ± 0.252	2.535 ± 0.168
	1st month	2.816 ± 0.145	3.339 ± 0.116	3.466 ± 0.210	2.013 ± 0.168
	2nd month	3.164 ± 0.394	3.558 ± 0.213	3.0150 ± 0.32	2.038 ± 0.676
PC	1st week	4.313 ± 0.413	3.768 ± 0.784	4.111 ± 0.816	2.952 ± 0.74
	1st month	5.225 ± 0.112	3.201 ± 0.784	3.926 ± 0.886	3.110 ± 0.25
	2nd month	3.350 ± 0.499	3.987 ± 0.313	4.094 ± 0.401	3.156 ± 0.98
PPARα	1st week	1.684 ± 0.435	1.697 ± 0.302	1.405 ± 0.195	1.412 ± 0.163
	1st month	1.775 ± 0.215	2.228 ± 0.302	1.531 ± 0.511	1.821 ± 0.116
	2nd month	1.428 ± 0.145	1.471 ± 0.139	1.234 ± 0.163	0.881 ± 0.376
PEPCK	1st week	36.723 ± 6.577	40.583 ± 3.333	33.343 ± 9.527	28.750 ± 9.344
	1st month	36.723 ± 6.617	41.624 ± 2.118	43.621 ± 2.421	32.151 ± 9.453
	2nd month	29.982 ± 3.669	37.565 ± 6.383	29.245 ± 4.773	27.691 ± 6.171

in Supplemental Fig. 1 for water-soluble extracts, and the score plot of the first two components of PCA, the confusion matrix, and the accuracy of each comparison are reported in Fig. 1 for lipid-soluble extracts. Likewise, for each experimental group (control, exp 1, exp 2, and exp 3), the NMR data were compared at the three different time points (prepartum, partum, and postpartum), and the results (PCA-CA score plots, confusion matrixes, and accuracies) were described in Supplemental Fig. 2 and Fig. 2 for water-soluble and lipid-soluble extracts, respectively. The results of the multivariate and the univariate analysis demonstrate that dairy cows fed with a diet containing boron show differences in the lipid metabolism especially postpartum. Instead, there are only weak differences in the water-soluble extracts profiles.

Over 30 metabolites were identified and quantified (arbitrary units) by ^{1}H–NMR using both kinds of data set (lipophilic and hydrophilic fractions) of each plasma sample (Supplemental Tables 3 and 4). This allowed us to identify differences in both water- and lipid-soluble metabolites; in particular, postpartum time point was characterized by lower plasma levels of valine, β-hydroxybutyrate, polyunsaturated fatty acid (PUFA), and citrate, and higher plasma levels of lactate, propionate, isobutyrate, and choline metabolites (betaine, phosphatidylcholine, and sphingomyelin). Moreover, many fatty acid fractions and cholesterol tended to be higher in postpartum period. Differences between groups were mainly observed in lipid-soluble metabolites.

Discussion

We evaluated the effects of supplementation with oral boron bolus on peripartum dairy cows' health in the light of an omics approach. The positive responses obtained in this experiment could be attributed to improvements in energy metabolism.

High-producing dairy cows enter a period of NEB during the first weeks of lactation. Different nutritional strategies have been used to restrict negative effects associated with the energy challenge in transition cows [16]. Trace minerals are an essential component of a feeding program for dairy herds [17]. The biochemical function of boron is still speculative. Lactating cows fed with approximately 620 mg of boron/100 kg of body weight per day have not showed toxic effects; instead, daily intakes of about 765 mg of boron/100 kg of body weight have deleterious effects [18, 19]. The signs of excessive boron ingestion are rather nonspecific [20]. In this current study, there were no overt signs of toxicosis. Boron levels were increased in body fluids based on the doses supplied; the greatest increase of boron was shown by urine samples, and the lowest by faces samples; serum and milk boron levels were similar. These evidences indicated that dietary boron could not be absorbed completely, and urine is its main elimination route.

The antioxidant and pro-oxidant properties of small-molecule sulfur and selenium compounds such as allicin, dimethylsulfone, methionine sulfoxide, and methylselenenic

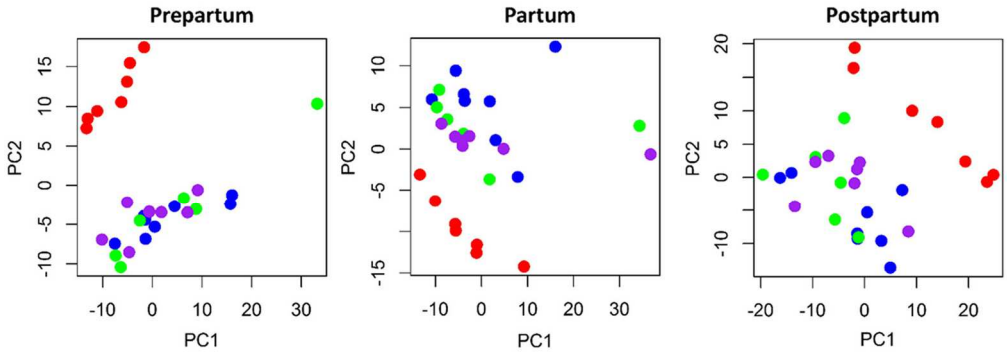

Fig. 1 PCA-CA score plots of lipid-soluble extracts, discrimination among control group (C) (*red dots*), experimental group 1 (Exp 1) fed with diet containing 60 ppm boron (*blue dots*), experimental group 2 (Exp 2) fed with diet containing 120 ppm boron (*green dots*), and experimental group 3 (Exp 3) fed with diet containing 180 ppm boron (*purple dots*) at three different times: prepartum, partum, and postpartum. The confusion matrix and the accuracy of each comparison are also reported

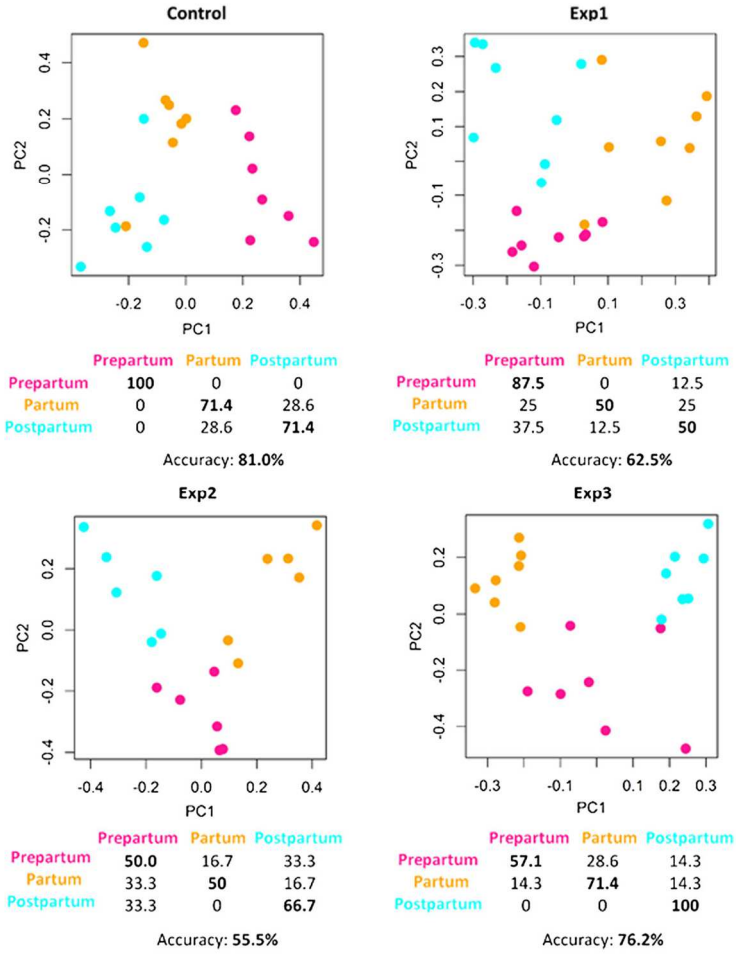

Fig. 2 PCA-CA score plots of lipid-soluble extracts, discrimination among prepartum (*pink dots*), partum (*orange dots*), and postpartum (*cyan dots*) times considering the same group: control, Exp 1, Exp 2, and Exp 3 groups. The confusion matrix and the accuracy of each comparison are also reported

acid are extremely complex and often greatly depend on experimental conditions. They are also effective in preventing oxidative damage to cellular components [21]. Regarding dimethylsulfone, AOP and LPO concentrations in the present study, boron appears not to have antioxidant effects.

To coordinate postpartum adaptations, liver metabolism is upregulated; mRNA abundance of gluconeogenic enzymes (PEPCK and PC) increase during early lactation [22]. Also, genes involved in fatty acid oxidation (CPT1 and PPAR-α) are altered and their mRNA abundance is positively correlated with circulating NEFA and BHB concentrations [7]. In the current study, no significant difference in expression of gluconeogenic enzymes and lipid oxidation genes was observed among treatments. This is convenient with decreases in gluconeogenesis and fat mobilization in the experimental cows around calving. Maybe boron is not a regulator of the genes' expression.

Generally, high milk production during lactation or inadequate energy intakes result in a NEB which induces ketosis and fatty liver [23]. Serum NEFA and BHB concentrations during week 1 are associated with the subsequent occurrence of clinical ketosis. Cows with BHB ≥1.2 mmol/L postpartum are considered to have subclinical ketosis [4, 24]. Additionally, elevated NEFA prepartum (>0.3 mmol/L) or postpartum (>0.6 mmol/L) can be used to assess postpartum disease risk for the herd [5]. In the present study, compared to the control group, the experimental groups had decreased postpartum triglyceride, NEFA, BHB, and PUFA, in spite of contradictory signals of fatty acids. Postpartum control and experimental 1 animals have been at risk for ketosis. These findings indicated that boron contributes to energy balance reducing lipolysis and ketogenesis in postpartum dairy cows.

Higher lactate concentrations in cows with high lipolysis might be due to either an increased anaerobe generation of lactate by peripheral tissues or lower utilization of lactate in the gluconeogenesis of these cows [25]. Propionate is the major glucogenic precursor taken up by the liver, with an estimated proportion of up to 32–73% of gluconeogenesis [26].

Members of the tricarboxylic acid cycle such as citrate decrease in association with increased ketone body formation [27]. According to Xu et al. [28], the primary differences in cows with fatty liver included increases in β-hydroxybutyrate, acetone, glycine, valine, trimethylamine-N-oxide, citrulline, and isobutyrate, and decreases in alanine, asparagine, glucose, γ-aminobutyric acid glycerol, and creatinine. Twenty-five NMR-based metabolites, including acetoacetate, acetone, lactate, glucose, choline, glutamic acid, and glutamine, were different among healthy, subclinical and clinical ketotic cows [23]. Li et al. [29] found 13 potential metabolic markers for plasma ketosis. In the current experiment, BHB levels measured routine spectroscopy were increased in postpartum control and experimental 1 animals; however, higher NMR-based isobutyrate and β-hydroxybutyrate levels were expected in at least postpartum control group. Also, postpartum lactate and propionate levels were higher and citrate lower than in control group. These glucogenic substrates could be attributed to differences in postpartum gluconeogenesis.

In a study using mass spectrometry, the concentration of triacylglycerides in plasma drops at the day of parturition whereas the plasma level of many phosphatidylcholines and two sphingomyelins increases steadily during early lactation. The abnormal decline of certain specific phosphatidylcholines and sphingomyelins could be regarded as a promising biomarker indicative of fatty liver disease [30, 31]. In the present experiment, postpartum betaine and sphingomyelin levels in the experimental groups (especially 3) were higher than in control group. In this respect, boron appears to have lipotropic effect. Our previous experiment [9] has shown that borax (100 mg/kg body weight dissolved in 1 L of warm water, by stomach tube, q 15 days, from a month before expected calving until a month after calving) decreases the degree of fatty liver in dairy cows during early lactation. In the current study, the results indicate that boron improves energy status and plasma ^{1}H NMR-based metabolomics could contribute to an understanding of boron mechanisms.

Conclusions

Supplemental boron was not completely absorbed from gastrointestinal tract inducing its high urinary excretion; instead, boron concentrations in serum and milk samples were found to be similar. Boron appears to be effective in minimizing NEB, preventing metabolic disorders and improving animal health. Especially lipid-soluble metabolites are affected due to boron dose. The results indicate that the omics, particularly ^{1}H NMR metabolomics combined with multivariate statistical analysis, can be used to access the changes and progression in peripartum period of dairy cows supplemented with boron.

Acknowledgements This work was financially supported by the Scientific and Technological Research Council of Turkey (TUBITAK, Project no: 213O181). CERM/CIRMMP center of the ESFRI Instruct is gratefully acknowledged for the NMR access provision financially supported by the EC Contract İNEXT No 653706.

Compliance with Ethical Standards

Ethical Approval The experimental design was approved by the Committee on Use of Animals in Research of the Selcuk University, Faculty of Veterinary Medicine (Protocol No. 45/2015).

References

1. Ingvartsen KL, Moyes K (2013) Nutrition, immune function and health of dairy cattle. Animal 7(Suppl 1):112–122
2. Suthar VS, Canelas-Raposo J, Deniz A, Heuwieser W (2013) Prevalence of subclinical ketosis and relationships with postpartum diseases in European dairy cows. J Dairy Sci 96:2925–2938
3. Sundrum A (2015) Metabolic disorders in the transition period ındicate that the dairy cows' ability to adapt is overstressed. Animals (Basel) 9:978–1020
4. Tatone EH, Gordon JL, Hubbs J, LeBlanc SJ, DeVries TJ, Duffield TF (2016) A systematic review and meta-analysis of the diagnostic accuracy of point-of-care tests for the detection of hyperketonemia in dairy cows. Prev Vet Med 130:18–32
5. Van Saun RJ (2016) Indicators of dairy cow transition risks: metabolic profiling revisited. Tierarztl Prax Ausg G Grosstiere Nutztiere 44:118–126
6. Basoglu A, Baspinar N, Tenori L, Vignoli A, Yildiz R (2016) Plasma metabolomics in calves with acute bronchopneumonia. Metabolomics 12:1–10
7. Loor JJ, Bionaz M, Drackley JK (2013) Systems physiology in dairy cattle: nutritional genomics and beyond. Annu Rev Anim Biosci 1:365–392
8. Pizzorno L (2015) Nothing boring about boron. Integr Med (Encinitas) 14:35–48
9. Basoglu A, Sevinc M, Birdane M, Boydak M (2002) Efficacy of borax in the prevention of fatty liver in dairy cows. J Vet Intern Med 16:732–735
10. Kurar E, Atli MO, Guzeloglu A, Ozsensoy Y, Semacan A (2010) Comparison of five different RNA isolation methods from equine endometrium for gene transcription analysis. Kafkas Univ Vet Fak Derg 16:851–855
11. Zou C, Qi H, Liu Z, Han L, Zhao C, Yang X (2013) Simvastatin activates the PPARγ-dependent pathway to prevent left ventricular hypertrophy associated with inhibition of rhoa signaling. Tex Heart Inst J 40:140–147
12. Livak KJ, Schmittgen TD (2001) Analysis of relative gene expression data using real-time quantitative PCR and the 2(−Delta Delta C(T)) method. Methods 25:402–408
13. Ihaka R, Gentleman RR (1996) A language for data analysis and graphics. J Comput Stat Graph 5:299–314
14. Kruskal WH, Wallis WA (1952) Use of ranks in one-criterion variance analysis. J Am Stat Assoc 47:583–621
15. Benjamini Y, Hochberg Y (1995) Controlling the false discovery rate: a practical and powerful approach to multiple testing. J R Stat Soc Ser B Methodol:289–300
16. Shahsavari A, D'Occhio MJ, Al Jassim R (2016) The role of rumen-protected choline in hepatic function and performance of transition dairy cows. Br J Nutr 116:35–44
17. Swecker WS Jr (2014) Trace mineral feeding and assessment. Vet Clin North Am Food Anim Pract 30:671–688

18. Owen EC (1944) The excretion of borate by the dairy cow. J Dairy Res 13:243–248
19. Green GH, Weeth HJ (1977) Responses of heifers ingesting boron in water. J Anim Sci 45:812–818
20. Brooke C, Boggs T (1951) Boric-acid poisoning; report of a case and review of the literature. Amer J Dis Child 32:465
21. Ramoutar RR, Brumaghim JL (2010) Antioxidant and anticancer properties and mechanisms of inorganic selenium, oxo-sulfur, and oxo-selenium compounds. Cell Biochem Biophys 58:1–23
22. Greenfield RB, Cecava MJ, Donkin SS (2000) Changes in mRNA expression for gluconeogenic enzymes in liver of dairy cattle during the transition to lactation. J Dairy Sci 83:1228–1236
23. Sun LW, Zhang HY, Wu L, Shu S, Xia C, Xu C (2014) ^{1}H-nuclear magnetic resonance-based plasma metabolic profiling of dairy cows with clinical and subclinical ketosis. J Dairy Sci 97:1552–1562
24. Kaufman EI, LeBlanc SJ, McBride BW, Duffield TF, DeVries TJ (2016) Short communication: association of lying behavior and subclinical ketosis in transition dairy cows. J Dairy Sci 99:7473–7480
25. Humer E, Khol-Parisini A, Gruber L, Wittek T, Aschenbach JR, Zebeli Q (2016) Metabolic adaptation and reticuloruminal pH in periparturient dairy cows experiencing different lipolysis early postpartum. Animal 10:1829–1838
26. Seal C, Reynolds C (1993) Nutritional implications of gastrointestinal and liver metabolism in ruminants. Nutr Res Rev 6:185–208
27. Baticz O, Tömösközi S, Vida L, Gaál T (2002) Relationship between concentration of citrate and ketone bodies in cow's milk. Acta Vet Hung 50:253–261
28. Xu C, Sun LW, Xia C, Zhang HY, Zheng JS, Wang JS (2016) ^{1}H-nuclear magnetic resonance-based plasma metabolic profiling of dairy cows with fatty liver. Asian-Australas J Anim Sci 29:219–229
29. Li Y, Xu C, Xia C, Zhang H, Sun L, Gao Y (2014) Plasma metabolic profiling of dairy cows affected with clinical ketosis using LC/MS technology. Vet Q 34:152–158
30. Artegoitia VM, Virginia M, Middleton JL, Harte FM, Campagna SR, de Veth MJ (2014) Choline and choline metabolite patterns and associations in blood and milk during lactation in dairy cows. PLoS One 26:e103412
31. Imhasly S, Bieli C, Naegeli H, Nyström L, Ruetten M, Gerspach C (2015) Blood plasma lipidome profile of dairy cows during the transition period. BMC Vet Res 11:252

Supplementary materials:

Supplemental Table 1 Biochemical parameters.

	Period	Control	Exp 1	Exp 2	Exp 3
AST, UI/L	Prepartum	74.571±3.308^{b}	84.125±3.388	82.166±3.477	88.714±10.432
	Partum	94.714±5.797^{a}	98.25±5.9	93.333±3.148	87±8.159
	Postpartum	94.857±5.629^{a}	81.75±4.647	95.5±5.038	96.142±5.654
ALT, UI/L	Prepartum	34.571±2.998^{AB}	27.5±3.105^{B}	38.666±1.054^{Aa}	32.1428±2.676^{AB}
	Partum	30.714±3.563	26.125±2.279	28±1.914^{b}	27±2.609
	Postpartum	26±3.429	26.875±2.868	33.5±2.348^{ab}	33.285±1.96
LDH, UI/L	Prepartum	2229.428±69.392^{AB}	2066.125±75.345^{B}	2293.333±26.889^{ABa}	2454±55.345^{Aa}
	Partum	2498.285±98.392^{A}	2162.875±69.412^{B}	2101.166±56.336^{Bb}	2194.857±54.686^{Bb}
	Postpartum	2457±158.931^{A}	2009.625±81.156^{B}	2157.666±44.66^{ABab}	2278.714±70.661^{ABab}
GGT, UI/L	Prepartum	23.285±1.972	21.25±1.013	23.666±2.485	24.857±1.932
	Partum	29.714±4.848	22.875±3.073	17.666±1.837	25.857±1.92
	Postpartum	32.142±4.245	22.75±1.46	23.5±1.024	24.571±1.888
CPK, UI/L	Prepartum	353.142±193.28	171.125±22.195	455±199.149	164.285±34.46
	Partum	207.428±22.238	232±22.477	248.666±44.364	159.285±20.549
	Postpartum	203.571±18.289^{AB}	173.25±16.409^{B}	281.166±36.016^{A}	240.285±22.059^{AB}
Ca, mg/dL	Prepartum	8.971±0.124^{A}	7.175±0.199^{B}	8.616±0.164^{Aa}	8.757±0.084^{Aa}
	Partum	8.614±0.196^{A}	7.45±0.233^{B}	7.7±0.204^{Bb}	7.728±0.217^{Bb}
	Postpartum	9.042±0.275^{A}	7.8±0.244^{B}	8.933±0.201^{Aa}	9.014±0.112^{Aa}
Mg, mg/dL	Prepartum	2.171±0.108	2.2±0.136	2.433±0.066	2.385±0.124
	Partum	2.428±0.168	2.45±0.11	2.65±0.071	2.528±0.161
	Postpartum	2.242±0.137	2.237±0.08	2.733±0.145	2.771±0.18
P, mg/dL	Prepartum	7.142±0.537	6.05±0.267	7.1±0.146^{a}	7.014±0.209
	Partum	6.114±0.427	6.05±0.268	5.633±0.412^{b}	5.957±0.347
	Postpartum	7.314±0.501	5.975±0.165	7.266±0.324^{a}	6.214±0.418
Glucose, g/dL	Prepartum	56.571±3.077^{Ab}	64.125±3.291^{Ab}	62.833±2.613^{Ab}	41.428±1.586^{Bb}
	Partum	78.571±0.841^{Aa}	75.25±2.373^{Aa}	76.5±2.86^{Aa}	59.142±1.818^{Ba}
	Postpartum	77±3.007^{Aa}	68.125±1.994^{Aab}	70.666±2.389^{Aab}	55.571±2.398^{Ba}
Protein, g/dL	Prepartum	8.214±0.204^{Aab}	6.937±0.387^{B}	8.166±0.172^{Aa}	8.528±0.194^{Aa}
	Partum	7.842±0.084^{Ab}	6.837±0.246^{B}	7±0.238^{ABb}	7.4±0.286^{ABb}
	Postpartum	8.642±0.224^{Aa}	7.625±0.188^{B}	8.316±0.164^{ABa}	8.428±0.149^{Aa}
Albumin, g/dL	Prepartum	3.7±0.053^{A}	3.125±0.116^{Bb}	3.866±0.055^{A}	3.714±0.059^{A}
	Partum	3.685±0.079	3.537±0.067^{a}	3.733±0.12	3.685±0.085
	Postpartum	3.385±0.214^{AB}	3.1±0.103^{Bb}	3.766±0.108^{A}	3.685±0.11^{A}
Cholesterol, mg/dL	Prepartum	143.428±8.055^{b}	183±27.969	154.333±21.004^{ab}	182.285±17.965^{ab}
	Partum	178.285±24.187^{Aab}	105.25±11.262^{B}	89.333±8.11^{Bb}	112.142±11.11^{Bb}
	Postpartum	222.857±26.607^{a}	190.125±28.277	232.333±37.505^{a}	223.142±33.455^{a}
TG, mg/dL	Prepartum	5.965±2.145^{C}	14.167±1.353^{ABa}	8.613±0.47^{BC}	17.105±1.835^{A}
	Partum	10.517±2.902	15.011±0.529^{a}	10.456±2.203	17.959±1.494
	Postpartum	3.296±0.651^{B}	4.910±0.832^{Bb}	5.528±0.818^{B}	14.450±1.33^{A}
BUN, mg/dL	Prepartum	8.714±0.521^{b}	9.125±0.953	8.5±0.223^{b}	7.285±0.285^{b}
	Partum	9.857±0.704^{ab}	11.75±0.901	10.5±0.806^{ab}	9.7143±0.644^{a}
	Postpartum	11.4286±0.528^{a}	11.375±0.679	11.8333±0.654^{a}	9.7143±0.473^{a}
AOP, mmol//L	Prepartum	0.386±0.015^{A}	0.369±0.014^{Aab}	0.344±0.015^{AB}	0.295±0.013^{Bab}
	Partum	0.368±0.017	0.404±0.013^{a}	0.408±0.022	0.373±0.021^{a}
	Postpartum	0.328±0.024	0.329±0.0101^{b}	0.337±0.033	0.292±0.028^{b}
LPO, μM/L	Prepartum	0.214±0.055	0.287±0.074	0.344±0.109	0.347±0.069

P-values for "capital letters" comparisons, i.e. for the comparison of the metabolites levels in the four treatment groups at the same sampling point. P-values for "minuscules" comparisons, i.e. for the comparison of the metabolites levels in the three sampling points for the same treatment group.

Supplemental Table 2 Gene primers.

Oligonucleotid ID	Nucleotid Sequence	PCR product (bp)	References
YWHAZ-F	5'- TGTAGGAGCCCGTAGGTCATCT -3'	102	NM_174814.2**
YWHAZ-R	5'- TTCTCTCTGTATTCTCGAGCCATCT-3'		
PEPCK-F	5'- AGGACAAATCCCAACGCCAT -3'	103	Castañeda-Gutiérrez et al. 2008*
PEPCK-R	5'- GCTGATCAATGCCTTCCCAGT -3'		
CPT1-F	5'- GCAGCGTTCTTCGTGACGTTA -3'	115	Castañeda-Gutiérrez et al. 2008*
CPT1-R	5'- ACCTGTCGAAACACCTGCCAT -3'		
PPARα-F	5'- GAAGGCTACTCCACGTTTCTT -3'	124	NM_001034036.1**
PPARα-R	5'- AGACCGCTGAACACCATTAC -3'		
PC-F	5'- CGGGAAGGTGATAGACATCAAG -3'	102	NM_177946.4**
PC-R	5'- GAGGTCACTACAGTCTCCATCT -3'		
GAPDH	GCTGAACGGGAAACTCACT CCTGCTTCACCACCTTCTT		

F: forward
R: reverse
*Castañeda-Gutiérrez E., Pelton S.H., Gilbert R.O., Butler W.R. (2009). "Effect of peripartum dietary energy supplementation of dairy cows on metabolites, liver function and reproductive variables", Anim Reprod Sci 112(3-4):301-315.
**without references, designed according to genebank mRNA access number.

Supplemental Table 3 Concentrations in arbitrary units (median ± mad) of the metabolites assigned in the water soluble extracts.

		Control	Exp 1	Exp 2	Exp 3	P-value*
Valine	**Prepartum**	0.001545 ± 0.000389	0.00166 ± 0.000238	0.002064 ± 0.000171	0.001332 ± 0.000076	> 0.05
	Partum	0.001345 ± 0.000325	0.001549 ± 0.000291	0.001594 ± 0.000227	0.001492 ± 0.000101	> 0.05
	Postpartum	0.001387 ± 0.000141	0.001313 ± 0.000288	0.001162 ± 0.000194	0.000972 ± 0.000169	> 0.05
	P-value**	> 0.05	> 0.05	> 0.05	**0.0150**	
Isobutyrate	**Prepartum**	0.00101 ± 0.00011	0.000926 ± 0.000043	0.000966 ± 0.00003	0.000828 ± 0.000048	> 0.05
	Partum	0.001077 ± 0.000061	0.000969 ± 0.000154	0.001131 ± 0.000096	0.001095 ± 0.000083	> 0.05
	Postpartum	0.00094 ± 0.000076	0.001216 ± 0.000038	0.001156 ± 0.000094	0.001194 ± 0.000049	> 0.05
	P-value**	> 0.05	**0.0295**	> 0.05	**0.0082**	
3-methyl-2-oxovalerate	**Prepartum**	0.001424 ± 0.000057	0.001267 ± 0.000118	0.001482 ± 0.000113	0.00114 ± 0.000054	> 0.05
	Partum	0.001408 ± 0.000088	0.001302 ± 0.000166	0.001364 ± 0.000172	0.00115 ± 0.000208	> 0.05

	Postpartum	0.001458 ± 0.000195	0.001528 ± 0.00017	0.001458 ± 0.000195	0.001358 ± 0.000072	> 0.05
	P-value**	> 0.05	> 0.05	> 0.05	> 0.05	
1,2-propanediol	**Prepartum**	0.002951 ± 0.000203	0.002436 ± 0.00022	0.003113 ± 0.000332	0.003199 ± 0.000407	> 0.05
	Partum	0.002598 ± 0.000113	0.002971 ± 0.00048	0.003277 ± 0.000556	0.002674 ± 0.000183	> 0.05
	Postpartum	0.003154 ± 0.000188	0.003778 ± 0.000696	0.004125 ± 0.000686	0.003053 ± 0.000237	> 0.05
	P-value**	> 0.05	**0.0295**	> 0.05	> 0.05	
Ethanol	**Prepartum**	0.002375 ± 0.000175	0.002347 ± 0.000131	0.002666 ± 0.000246	0.002521 ± 0.000276	> 0.05
	Partum	0.002565 ± 0.000167	0.002661 ± 0.000211	0.003069 ± 0.000281	0.002509 ± 0.000264	> 0.05
	Postpartum	0.002498 ± 0.000026	0.002497 ± 0.000184	0.002523 ± 0.000115	0.002186 ± 0.000127	> 0.05
	P-value**	> 0.05	> 0.05	> 0.05	> 0.05	
β-hydroxybutyrate	**Prepartum**	0.007957 ± 0.000667	0.008044 ± 0.001819	0.006963 ± 0.000427	0.007185 ± 0.000576	> 0.05
	Partum	0.013711 ± 0.001751	0.009615 ± 0.002023	0.011431 ± 0.001749	0.012456 ± 0.001708	> 0.05
	Postpartum	0.008206 ± 0.000754	0.011056 ± 0.001742	0.009405 ± 0.001929	0.010376 ± 0.000967	> 0.05
	P-value**	**0.0207**	> 0.05	> 0.05	**0.0082**	
Lactate	**Prepartum**	0.013407 ± 0.001244	0.013832 ± 0.003519	0.01391 ± 0.00345	0.018604 ± 0.001213	> 0.05
	Partum	0.015958 ± 0.001047	0.011206 ± 0.003186	0.011375 ± 0.00304	0.012167 ± 0.000424	> 0.05
	Postpartum	0.009858 ± 0.000173	0.015158 ± 0.00385	0.016261 ± 0.001923	0.019241 ± 0.005225	**0.0467**
	P-value**	**0.0094**	> 0.05	> 0.05	**0.0293**	
Arginine+lysine	**Prepartum**	0.005815 ± 0.000255	0.005535 ± 0.000592	0.006306 ± 0.000297	0.005613 ± 0.000203	> 0.05
	Partum	0.005827 ± 0.000389	0.005598 ± 0.000305	0.005157 ± 0.000911	0.005534 ± 0.000182	> 0.05
	Postpartum	0.005801 ± 0.000306	0.005548 ± 0.000732	0.005993 ± 0.000507	0.005884 ± 0.000323	> 0.05
	P-value**	> 0.05	> 0.05	> 0.05	> 0.05	
Acetate	**Prepartum**	0.026579 ± 0.003512	0.025619 ± 0.007022	0.023037 ± 0.00326	0.029494 ± 0.006499	> 0.05

	Partum	0.027055 ± 0.004448	0.027905 ± 0.004776	0.031321 ± 0.003363	0.033624 ± 0.002216	> 0.05
	Postpartum	0.025257 ± 0.002301	0.02744 ± 0.005711	0.026013 ± 0.005507	0.028738 ± 0.00273	> 0.05
	P-value**	> 0.05	> 0.05	> 0.05	> 0.05	
Propionate	**Prepartum**	0.000765 ± 0.000072	0.000675 ± 0.000086	0.00065 ± 0.000055	0.00067 ± 0.000052	> 0.05
	Partum	0.000784 ± 0.000018	0.000823 ± 0.000088	0.000892 ± 0.000064	0.00089 ± 0.000084	> 0.05
	Postpartum	0.000776 ± 0.000061	0.000884 ± 0.000118	0.000835 ± 0.000031	0.000786 ± 0.000062	> 0.05
	P-value**	> 0.05	> 0.05	> 0.05	**0.0293**	
Citrate	**Prepartum**	0.002904 ± 0.000298	0.003264 ± 0.000364	0.002936 ± 0.000252	0.00276 ± 0.000262	> 0.05
	Partum	0.003101 ± 0.000375	0.003024 ± 0.000439	0.003093 ± 0.000235	0.003238 ± 0.000198	> 0.05
	Postpartum	0.002744 ± 0.000399	0.001822 ± 0.000247	0.002818 ± 0.000246	0.001632 ± 0.000447	> 0.05
	P-value**	> 0.05	0.0295	> 0.05	**0.0239**	
Dimethylsulfone	**Prepartum**	0.001318 ± 0.000169	0.000967 ± 0.000277	0.000573 ± 0.0001	0.001142 ± 0.000291	> 0.05
	Partum	0.001351 ± 0.00032	0.001446 ± 0.000332	0.001375 ± 0.000356	0.001702 ± 0.000291	> 0.05
	Postpartum	0.001617 ± 0.000216	0.000676 ± 0.000177	0.000813 ± 0.000201	0.001138 ± 0.000176	**0.0497**
	P-value**	> 0.05	> 0.05	> 0.05	**0.0239**	
Betaine	**Prepartum**	0.011642 ± 0.002282	0.012563 ± 0.001815	0.013733 ± 0.001551	0.013899 ± 0.001714	> 0.05
	Partum	0.004601 ± 0.001345	0.003735 ± 0.000753	0.003339 ± 0.00042	0.004245 ± 0.000532	> 0.05
	Postpartum	0.004515 ± 0.000211	0.007997 ± 0.002121	0.008013 ± 0.001236	0.008271 ± 0.001732	> 0.05
	P-value**	**0.0094**	**0.0085**	> 0.05	**0.0082**	
Methanol	**Prepartum**	0.00364 ± 0.000194	0.00409 ± 0.00111	0.003855 ± 0.000576	0.003889 ± 0.000895	> 0.05
	Partum	0.004056 ± 0.000585	0.003755 ± 0.000874	0.002918 ± 0.000061	0.003666 ± 0.000356	> 0.05
	Postpartum	0.003159 ± 0.000178	0.002813 ± 0.000379	0.002989 ± 0.00049	0.003701 ± 0.000412	> 0.05

	P-value**	> 0.05	> 0.05	> 0.05	> 0.05	
Creatine	**Prepartum**	0.005219 ± 0.000196	0.004956 ± 0.00054	0.005527 ± 0.000404	0.005036 ± 0.000052	> 0.05
	Partum	0.004786 ± 0.000381	0.004673 ± 0.000303	0.004309 ± 0.000676	0.004431 ± 0.000142	> 0.05
	Postpartum	0.004545 ± 0.000461	0.005671 ± 0.0005	0.005912 ± 0.000444	0.005268 ± 0.000344	> 0.05
	P-value**	> 0.05	> 0.05	> 0.05	0.0181	
Creatinine	**Prepartum**	0.003151 ± 0.000057	0.002854 ± 0.000442	0.00266 ± 0.000095	0.002679 ± 0.000259	> 0.05
	Partum	0.002345 ± 0.000036	0.002376 ± 0.000108	0.002349 ± 0.000176	0.002218 ± 0.000102	> 0.05
	Postpartum	0.002303 ± 0.000093	0.002554 ± 0.00012	0.002706 ± 0.000075	0.002629 ± 0.00013	> 0.05
	P-value**	0.0094	> 0.05	> 0.05	> 0.05	
Glucose	**Prepartum**	0.002939 ± 0.000668	0.004677 ± 0.001304	0.004528 ± 0.000545	0.00361 ± 0.00036	> 0.05
	Partum	0.004657 ± 0.000728	0.004308 ± 0.000846	0.003425 ± 0.000648	0.004126 ± 0.000846	> 0.05
	Postpartum	0.003987 ± 0.000323	0.005548 ± 0.00039	0.004483 ± 0.000506	0.005754 ± 0.000468	> 0.05
	P-value**	> 0.05	> 0.05	> 0.05	0.0390	
Allantoin	**Prepartum**	0.000833 ± 0.000075	0.000832 ± 0.000062	0.000817 ± 0.000059	0.000702 ± 0.000164	> 0.05
	Partum	0.000922 ± 0.000105	0.001033 ± 0.000091	0.000945 ± 0.000079	0.000932 ± 0.000034	> 0.05
	Postpartum	0.000961 ± 0.000043	0.000787 ± 0.000068	0.000993 ± 0.000232	0.000931 ± 0.000143	> 0.05
	P-value**	> 0.05	> 0.05	> 0.05	> 0.05	
Tyrosine	**Prepartum**	0.00133 ± 0.000084	0.001445 ± 0.000225	0.001481 ± 0.000196	0.001196 ± 0.000163	> 0.05
	Partum	0.001355 ± 0.000204	0.001209 ± 0.000143	0.001452 ± 0.000074	0.001193 ± 0.000114	> 0.05
	Postpartum	0.001129 ± 0.000123	0.001019 ± 0.00018	0.00114 ± 0.000121	0.001261 ± 0.000163	> 0.05
	P-value**	> 0.05	> 0.05	> 0.05	> 0.05	
Hippurate	**Prepartum**	0.002712 ± 0.000371	0.002549 ± 0.000246	0.002499 ± 0.000229	0.002349 ± 0.000201	> 0.05
	Partum	0.002502 ± 0.000113	0.002397 ± 0.000228	0.002674 ± 0.000052	0.002237 ± 0.000132	> 0.05

	Postpartum	0.001961 ± 0.00029	0.002184 ± 0.000227	0.002654 ± 0.000098	0.002519 ± 0.000192	> 0.05
	P-value**	0.0442	> 0.05	> 0.05	> 0.05	
Formate	**Prepartum**	0.000313 ± 0.000025	0.000321 ± 0.000087	0.00024 ± 0.000022	0.000274 ± 0.000019	> 0.05
	Partum	0.000292 ± 0.000011	0.000313 ± 0.000032	0.000287 ± 0.00004	0.000288 ± 0.00005	> 0.05
	Postpartum	0.000329 ± 0.000044	0.000338 ± 0.000032	0.000344 ± 0.000027	0.00037 ± 0.00002	> 0.05
	P-value**	> 0.05	> 0.05	> 0.05	> 0.05	

The p-values of Kruskal test for every comparison are also reported: a p-value < 0.05 is deemed statistically relevant and reported in bold. *P-values for "horizontal" comparisons, i.e. for the comparison of the metabolites levels in the four treatment groups at the same sampling point. ** P-values for "vertical" comparisons, i.e. for the comparison of the metabolites levels in the three sampling points for the same treatment group.

Supplemental Table 4 Concentrations in arbitrary units (median ± mad) of the metabolites assigned in the lipid soluble extracts.

		Control	**Exp 1**	**Exp 2**	**Exp 3**	**P-value***
Cholesterol-C18	**Prepartum**	0.018879 ± 0.000551	0.013072 ± 0.001	0.012813 ± 0.00085	0.01321 ± 0.001138	**0.0028**
	Partum	0.02084 ± 0.00025	0.014482 ± 0.001821	0.016506 ± 0.000768	0.016969 ± 0.001165	**0.0036**
	Postpartum	0.021398 ± 0.001095	0.013847 ± 0.001393	0.009115 ± 0.001063	0.013077 ± 0.001705	**0.0032**
	P-value**	> 0.05	> 0.05	> 0.05	> 0.05	
Unknown lipid fraction	**Prepartum**	0.006395 ± 0.000294	0.080324 ± 0.004757	0.080689 ± 0.006389	0.072675 ± 0.006113	**0.0022**
	Partum	0.005415 ± 0.000339	0.0765 ± 0.003924	0.058733 ± 0.003619	0.058164 ± 0.00824	**0.0026**
	Postpartum	0.00586 ± 0.000154	0.104578 ± 0.00663	0.099285 ± 0.009836	0.092195 ± 0.002339	**0.0032**
	P-value**	> 0.05	0.0117	> 0.05	**0.0313**	
-CH_3 signals of fatty acids and cholesterol	**Prepartum**	0.140281 ± 0.00308	0.14921 ± 0.001499	0.14518 ± 0.001821	0.144731 ± 0.002957	**0.0311**
	Partum	0.149857 ± 0.001365	0.154581 ± 0.006414	0.151488 ± 0.003607	0.158237 ± 0.003001	> 0.05
	Postpartum	0.152827 ± 0.004265	0.159909 ± 0.00432	0.140916 ± 0.008381	0.152726 ± 0.004179	> 0.05
	P-value**	> 0.05	> 0.05	> 0.05	> 0.05	
-$(CH_2)_n$ signals of fatty acids	**Prepartum**	0.167777 ± 0.004883	0.18462 ± 0.000672	0.188863 ± 0.003086	0.187693 ± 0.004885	**0.0060**
	Partum	0.16086 ± 0.001865	0.173023 ± 0.00859	0.175282 ± 0.003704	0.164126 ± 0.002662	0.0127
	Postpartum	0.163449 ± 0.002581	0.173378 ± 0.007461	0.177668 ± 0.011752	0.174012 ± 0.013136	**0.0431**
	P-value**	> 0.05	> 0.05	> 0.05	**0.0404**	
-CH_2-CH_2-CO of fatty acids and	**Prepartum**	0.079475 ± 0.000838	0.088859 ± 0.000436	0.08785 ± 0.001689	0.087398 ± 0.000845	**0.0022**

total cholesterol	**Partum**	0.081965 ± 0.001132	0.090698 ± 0.001798	0.087328 ± 0.001955	0.091023 ± 0.00236	**0.0026**
	Postpartum	0.082647 ± 0.001722	0.095239 ± 0.002559	0.092957 ± 0.005108	0.093799 ± 0.003683	**0.0041**
	P-value**	> 0.05	**0.0379**	> 0.05	> 0.05	
-CH_2-CO signals of fatty acids	**Prepartum**	0.008488 ± 0.000446	0.005856 ± 0.000283	0.00571 ± 0.00019	0.006221 ± 0.000619	**0.0022**
	Partum	0.009471 ± 0.000336	0.006768 ± 0.000943	0.007731 ± 0.000274	0.008029 ± 0.000248	**0.0117**
	Postpartum	0.00978 ± 0.000572	0.006139 ± 0.000766	0.004794 ± 0.00034	0.006626 ± 0.001256	**0.0032**
	P-value**	**0.0186**	> 0.05	> 0.05	**0.0404**	
Polyunsaturated fatty acid	**Prepartum**	0.018882 ± 0.000141	0.016748 ± 0.000475	0.016292 ± 0.000154	0.015743 ± 0.000572	**0.0047**
	Partum	0.019163 ± 0.00042	0.01657 ± 0.000758	0.01773 ± 0.000509	0.017661 ± 0.000452	**0.0117**
	Postpartum	0.0181 ± 0.000606	0.01343 ± 0.000256	0.013405 ± 0.00076	0.013949 ± 0.000511	**0.0032**
	P-value**	> 0.05	**0.0117**	> 0.05	0.0313	
-$N(CH_3)_3$ signals of Phosphatidylcholine and sphingomyelin	**Prepartum**	0.037791 ± 0.000988	0.042644 ± 0.000845	0.042847 ± 0.001453	0.043019 ± 0.000846	**0.0063**
	Partum	0.039928 ± 0.001313	0.041994 ± 0.002578	0.04421 ± 0.001326	0.039473 ± 0.001364	> 0.05
	Postpartum	0.038806 ± 0.000527	0.034165 ± 0.001511	0.034377 ± 0.00458	0.034962 ± 0.005533	> 0.05
	P-value**	> 0.05	0.0117	> 0.05	**0.0404**	
Backbone signals of total plasma triglycerides	**Prepartum**	0.001118 ± 0.000163	0.000874 ± 0.000108	0.001023 ± 0.000111	0.000925 ± 0.000054	**0.0478**
	Partum	0.000636 ± 0.000155	0.000605 ± 0.000082	0.000525 ± 0.000021	0.000725 ± 0.00009	> 0.05
	Postpartum	0.000825 ± 0.000211	0.000964 ± 0.000066	0.001053 ± 0.000101	0.001008 ± 0.000135	> 0.05
	P-value**	**0.0186**	**0.0251**	> 0.05	**0.0313**	
Esterified cholesterol	**Prepartum**	0.000149 ± 0.000011	0.000937 ± 0.000063	0.000925 ± 0.000081	0.000833 ± 0.000079	**0.0022**
	Partum	0.000123 ± 0.000008	0.00083 ± 0.000045	0.000668 ± 0.000076	0.000685 ± 0.00009	**0.0026**
	Postpartum	0.000153 ± 0.000019	0.001255 ± 0.000084	0.001302 ± 0.000063	0.001112 ± 0.00007	**0.0032**
	P-value**	> 0.05	**0.0117**	> 0.05	**0.0313**	
Phosphoglycerides	**Prepartum**	0.003507 ± 0.00006	0.003859 ± 0.000101	0.003914 ± 0.000095	0.003909 ± 0.000054	**0.0077**
	Partum	0.003658 ± 0.000048	0.003899 ± 0.000203	0.003972 ± 0.000159	0.003533 ± 0.000094	> 0.05
	Postpartum	0.003516 ± 0.00016	0.003113 ± 0.000049	0.003242 ± 0.000391	0.003298 ± 0.000307	> 0.05
	P-value**	> 0.05	0.0163	> 0.05	> 0.05	
-CH=CH- signals of fatty acids	**Prepartum**	0.03941 ± 0.001208	0.033743 ± 0.00058	0.032929 ± 0.001094	0.032801 ± 0.002418	**0.0028**
	Partum	0.04171 ± 0.000703	0.034755 ± 0.000996	0.038011 ± 0.000785	0.037826 ± 0.001124	**0.0069**
	Postpartum	0.040628 ± 0.001306	0.028953 ± 0.000853	0.028882 ± 0.001304	0.030534 ± 0.002516	**0.0032**
	P-value**	> 0.05	**0.0117**	> 0.05	**0.0313**	

Sphingomyelin	**Prepartum**	0.00097 ± 0.000026	0.001047 ± 0.000063	0.00103 ± 0.000037	0.001052 ± 0.000076	> 0.05
	Partum	0.000923 ± 0.00005	0.000889 ± 0.000061	0.000888 ± 0.000009	0.000804 ± 0.00001	> 0.05
	Postpartum	0.000981 ± 0.000104	0.001098 ± 0.000077	0.00112 ± 0.000048	0.001091 ± 0.000154	> 0.05
	P-value**	> 0.05	**0.0200**	> 0.05	**0.0404**	

The p-values of Kruskal test for every comparison are also reported: a p-value < 0.05 is deemed statistically relevant and reported in bold. *P-values for "horizontal" comparisons, i.e. for the comparison of the metabolites levels in the four treatment groups at the same sampling point. ** P-values for "vertical" comparisons, i.e. for the comparison of the metabolites levels in the three sampling points for the same treatment group.

Supplemental Fig. 1 PCA-CA score plots of water-soluble extracts, discrimination among control group (C) (red dots), experimental group 1 (Exp 1) fed with diet containing 60 ppm boron (blue dots), experimental group 2 (Exp 2) fed with diet containing 120 ppm boron (green dots) and experimental group 3 (Exp 3) fed with diet containing 180 ppm boron (purple dots) at three different times: prepartum, partum and postpartum. The confusion matrix and the accuracy of each comparison are also reported.

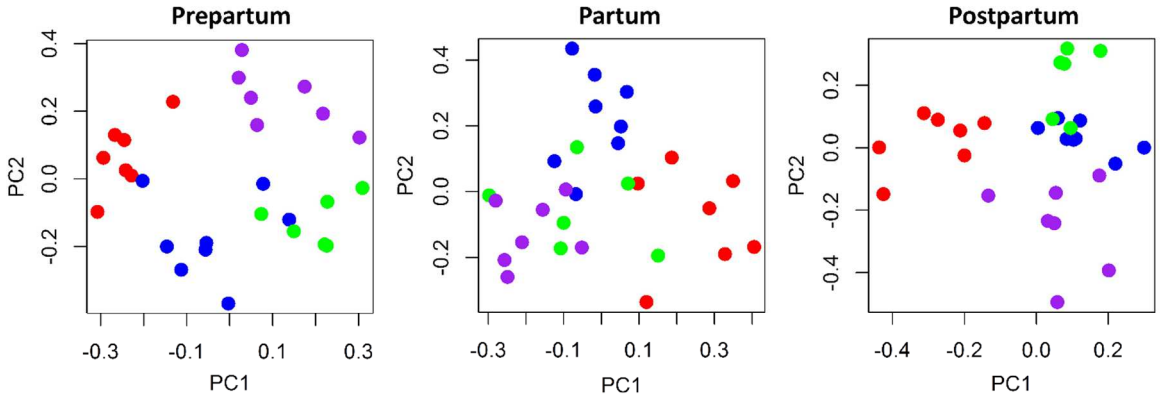

	Control	Exp1	Exp2	Exp3
Control	**42.9**	14.3	0	42.9
Exp1	37.5	**12.5**	37.5	12.5
Exp2	0	66.7	**16.7**	16.7
Exp3	0	57.1	0	**42.9**

Accuracy: **28.6%**

	Control	Exp1	Exp2	Exp3
Control	**0**	42.9	28.6	28.6
Exp1	25	**12.5**	12.5	50
Exp2	50	16.7	**0**	33.3
Exp3	0	28.6	28.6	**42.9**

Accuracy: **14.3%**

	Control	Exp1	Exp2	Exp3
Control	**71.4**	14.3	0	14.3
Exp1	12.5	**50**	25	12.5
Exp2	0	83.3	**16.7**	0
Exp3	14.3	28.6	0	**57.1**

Accuracy: **50.0%**

Supplemental Fig. 2 PCA-CA score plots of water-soluble extracts, discrimination among prepartum (pink dots), partum (orange dots) and postpartum (cyan dots) times considering the same group: control, Exp 1, Exp 2 and Exp 3 groups. The confusion matrix and the accuracy of each comparison are also reported.

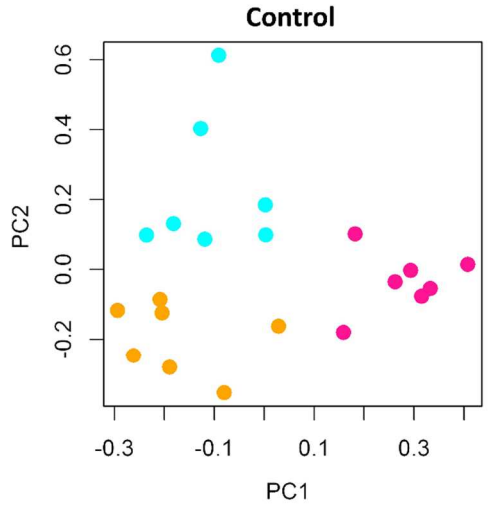

	Prepartum	Partum	Postpartum
Prepartum	**57.1**	28.6	14.3
Partum	0	**85.7**	14.3
Postpartum	0	14.3	**85.7**

Accuracy: **76.2%**

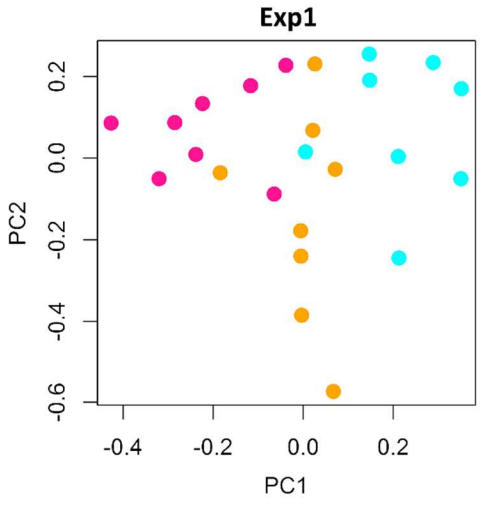

	Prepartum	Partum	Postpartum
Prepartum	**62.5**	37.5	14.3
Partum	12.5	**37.5**	50.0
Postpartum	12.5	62.5	**25**

Accuracy: **41.7%**

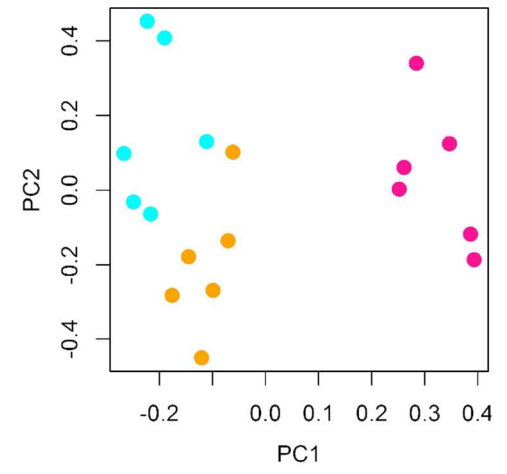

	Prepartum	Partum	Postpartum
Prepartum	**66.7**	16.7	16.7
Partum	33.3	**50.0**	16.7
Postpartum	33.3	50.0	**16.7**

Accuracy: **44.4%**

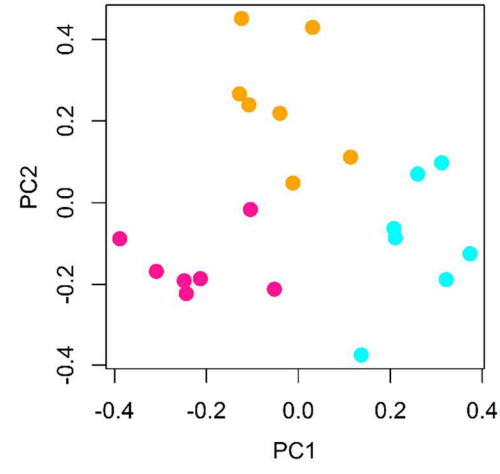

	Prepartum	Partum	Postpartum
Prepartum	**42.9**	28.6	28.6
Partum	0	**85.7**	14.3
Postpartum	0	0	**100**

Accuracy: **76.2%**

Chapter 5
Conclusions

The results achieved during these three years of research activity and reported in this thesis have allowed me to further illustrate the potential of NMR-based metabolomics in biomedicine. Metabolomics showed to be definitely a promising and powerful tool for better understanding biological systems, for deep comprehension of the effects of environment, lifestyle, and diet on the physiological status, for stratifying patients according to their own personal risk, and for monitoring efficacy or toxicity of drug treatments or life style interventions. The results obtained in each study here presented, by characterizing the molecular fingerprint of diseases or phenotypes through an untargeted approach, opened new significant perspectives. Therefore, it can be concluded that fingerprinting analysis by NMR has the potential not only to increase our knowledge on specific diseases, but also to be translated in clinical practice for diagnostic or prognostic purposes.

Despite this huge potential, metabolomics is still a relatively young discipline and many efforts need to be made to standardize procedures and to better characterize the metabolome. Metabolomics data could be greatly affected by various simple parameters, such as diet, microbiome, age, sex, and ethnicity; therefore, these aspects have to be further investigated to avoid misinterpretations of results. This thesis partially contributes to this aspect by characterizing the effects of sex and age on plasma metabolome of healthy volunteers.

Our results show how metabolomics can lead to design new non-invasive, rapid, economic, and sensitive diagnostic and prognostic tests. We have shown that serum NMR-metabolomics can be used for patient risk stratification both in early breast cancer patients with the aim at predicting the risk of recurrence, and in acute coronary syndrome patients, to evaluate the risk of death within two years after the

cardiovascular event. However, especially in the first case, a very large multicentre study (11 hospitals involved in South East of Asia and Africa, to the best of our knowledge, the broadest metabolomic breast cancer study), the major challenge was to overcome the problems related to the adoption of different protocols during sample collections and storage: since standardization of sample collection, handling and storage constitutes an essential condition to preserve sample stability and obtain reproducible results, the adoption of standard operating procedures for the preanalytical phase represents one of the turning points for the successful translation of metabolomics in very large multicenter studies and then into clinical practice.

The results obtained by our research activities demonstrate that alterations in metabolomic fingerprint can be associated to a pathophysiological state of an organism (e.g. Alzheimer's disease, chronic inflammatory rheumatic diseases, primary biliary cirrhosis). Moreover, the characterization of the metabolic fingerprint can be used to monitor patients during pharmacological treatments or life style interventions (e.g. the study on COPD treatment with ICS/LABA and the DAMA study). However, despite the importance of the collected data, the majority of these studies, as most metabolomic researches in the literature, are small scale studies, in which the number of samples ranges from tens to hundreds. Overcoming this limitation by much larger epidemiological studies, covering the analysis of tens of thousands of specimens, represents the next challenge for metabolomics and is expected to provide solid bases for the use of metabolomics for large population screening.

Another challenge of metabolomic research is its integration with classical clinical tools and other omics technologies (proteomics, transcriptomics, and genomics) providing a holistic perspective on complex interactions occurring in biological systems. Perfectly in line with this idea, we are working to improve our approach: 1) we are trying to integrate the metabolomic score able to predict the breast cancer risk of recurrence with the Oncotype DX score. This score is based on a genomic test that analyzes the activity of a group of genes that can affect how a cancer is likely to behave and respond to treatment. By combing these two different features we hope to improve our prediction accuracy and so to provide a tool that could be really implemented in the clinical practice, helping the clinicians to make a more informed decision about whether or not to recommend chemotherapy to treat early-stage, hormone-receptor-positive breast cancer. 2) Since our group has already defined the metabolic fingerprint of CD with good results (even in comparison with CBP), we are planning to integrate our knowledge with a comprehensive systems medicine approach involving both metabolomics of serum and urine and metagenomic analyses of the faecal gut microbiota, providing new insights into the complex mechanisms underpinning this disease and into how dysbiosis contributes to the pathogenesis. 3) we plan to integrate the data on NMR plasma metabolomic fingerprint with epigenetic and inflammatory markers to disentangle the mechanism of high breast density and cancer, and to deeply investigate the effects of life style treatments in these high-risk women.

In conclusion, these three years of research activity have contributed to the demonstration of the usefulness of metabolomics in biomedicine by a combination of biochemistry, analytical chemistry, bioinformatics and clinical data, and, moreover, it has shown that NMR-metabolomics can be really a valuable contributor to the development and implementation of precision medicine.

Bibliography

1. Alyass, A., Turcotte, M. & Meyre, D. From big data analysis to personalized medicine for all: challenges and opportunities. *BMC Med. Genomics* **8,** 33 (2015).
2. Deidda, M., Piras, C., Bassareo, P. P., Cadeddu Dessalvi, C. & Mercuro, G. Metabolomics, a promising approach to translational research in cardiology. *IJC Metab. Endocr.* **9,** 31–38 (2015).
3. Wishart, D. S. *et al.* HMDB: the Human Metabolome Database. *Nucleic Acids Res* **35,** D521–D526 (2007).
4. Claudino, W. M. *et al.* Metabolomics: available results, current research projects in breast cancer, and future applications. *J ClinOncol* **25,** 2840–2846 (2007).
5. Calabrò, A. *et al.* A Metabolomic Perspective on Coeliac Disease. *Autoimmune Dis.* **2014,** e756138 (2014).
6. Klupczyńska, A., Dereziński, P. & Kokot, Z. J. METABOLOMICS IN MEDICAL SCIENCES--TRENDS, CHALLENGES AND PERSPECTIVES. *Acta Pol. Pharm.* **72,** 629–641 (2015).
7. Wishart, D. S. Emerging applications of metabolomics in drug discovery and precision medicine. *Nat. Rev. Drug Discov.* **15,** 473–484 (2016).
8. Kosmides, A. K., Kamisoglu, K., Calvano, S. E., Corbett, S. A. & Androulakis, I. P. Metabolomic Fingerprinting: Challenges and Opportunities. *Crit. Rev. Biomed. Eng.* **41,** 205–221 (2013).
9. Psychogios, N. *et al.* The Human Serum Metabolome. *PLoS ONE* **6,** e16957 (2011).
10. Bertini, I., Luchinat, C. & Tenori, L. Metabolomics for the future of personalized medicine through information and communication technologies. *Pers. Med.* **9,** 133–136 (2012).

11. Ghini, V., Saccenti, E., Tenori, L., Assfalg, M. & Luchinat, C. Allostasis and Resilience of the Human Individual Metabolic Phenotype. *J. Proteome Res.* (2015). doi:10.1021/acs.jproteome.5b00275

12. Bouatra, S. *et al.* The Human Urine Metabolome. *PLoS ONE* **8,** e73076 (2013).

13. Wishart, D. S. *et al.* The human cerebrospinal fluid metabolome. *J. Chromatogr. B Analyt. Technol. Biomed. Life. Sci.* **871,** 164–173 (2008).

14. Wallner-Liebmann, S. *et al.* Individual Human Metabolic Phenotype Analyzed by 1H NMR of Saliva Samples. *J. Proteome Res.* **15,** 1787–1793 (2016).

15. Bezabeh, T., Somorjai, R. L. & Smith, I. C. P. MR metabolomics of fecal extracts: applications in the study of bowel diseases. *Magn. Reson. Chem. MRC* **47 Suppl 1,** S54-61 (2009).

16. Nicholson, J. K. & Lindon, J. C. Systems biology: Metabonomics. *Nature* **455,** 1054–1056 (2008).

17. Gallo, V. *et al.* Performance Assessment in Fingerprinting and Multi Component Quantitative NMR Analyses. *Anal. Chem.* **87,** 6709–6717 (2015).

18. Goodacre, R. *et al.* Proposed minimum reporting standards for data analysis in metabolomics. *Metabolomics* **3,** 231–241 (2007).

19. Xia, J., Sinelnikov, I. V., Han, B. & Wishart, D. S. MetaboAnalyst 3.0--making metabolomics more meaningful. *Nucleic Acids Res.* **43,** W251-257 (2015).

20. Hall, S. S. Revolution Postponed. *Sci. Am.* **303,** 60–67 (2010).

21. Maher, B. Personal genomes: The case of the missing heritability. *Nat. News* **456,** 18–21 (2008).

22. Cho, I. & Blaser, M. J. The Human Microbiome: at the interface of health and disease. *Nat. Rev. Genet.* **13,** 260–270 (2012).

23. Feil, R. & Fraga, M. F. Epigenetics and the environment: emerging patterns and implications. *Nat. Rev. Genet.* **13,** 97–109 (2012).

24. Spratlin, J. L., Serkova, N. J. & Eckhardt, S. G. Clinical Applications of Metabolomics in Oncology: A Review. *Clin. Cancer Res.* **15,** 431–440 (2009).

25. Dang, L. *et al.* Cancer-associated IDH1 mutations produce 2-hydroxyglutarate. *Nature* **462,** 739–744 (2009).

26. Tenori, L. *et al.* Metabolomic fingerprint of heart failure in humans: a nuclear magnetic resonance spectroscopy analysis. *Int. J. Cardiol.* **168,** e113-115 (2013).

27. Bain, J. R. *et al.* Metabolomics Applied to Diabetes Research. *Diabetes* **58,** 2429–2443 (2009).

28. Sas, K. M., Karnovsky, A., Michailidis, G. & Pennathur, S. Metabolomics and Diabetes: Analytical and Computational Approaches. *Diabetes* **64,** 718–732 (2015).

29. Blass, J. P. The mitochondrial spiral. An adequate cause of dementia in the Alzheimer's syndrome. *Ann. N. Y. Acad. Sci.* **924,** 170–183 (2000).

30. Bürklen, T. S. *et al.* The Creatine Kinase/Creatine Connection to Alzheimer's Disease: CK Inactivation, APP-CK Complexes, and Focal Creatine Deposits. *J. Biomed. Biotechnol.* **2006,** (2006).

31. Cunnane, S. *et al.* Brain fuel metabolism, aging, and Alzheimer's disease. *Nutrition* **27,** 3–20 (2011).

32. Strati, F. *et al.* New evidences on the altered gut microbiota in autism spectrum disorders. *Microbiome* **5,** 24 (2017).

33. Vander Heiden, M. G., Cantley, L. C. & Thompson, C. B. Understanding the Warburg Effect: The Metabolic Requirements of Cell Proliferation. *Science* **324,** 1029–1033 (2009).

34. Glunde, K., Jacobs, M. A. & Bhujwalla, Z. M. Choline metabolism in cancer: implications for diagnosis and therapy. *Expert Rev. Mol. Diagn.* **6,** 821–829 (2006).

35. Kirwan, J. Metabolomics for the practising vet. *In Pract.* **35,** 438–445 (2013).

36. Lindon, C. J., Nicholson, J. K. & Holmes, E. *The Handbook of Metabonomics and Metabolomics*. (Elsevier, 2007).

37. Carr, H. Y. & Purcell, E. M. Effects of Diffusion on Free Precession in Nuclear Magnetic Resonance Experiments. *Phys. Rev.* **94,** 630–638 (1954).

38. Fonville, J. M. *et al.* Evaluation of full-resolution J-resolved 1H NMR projections of biofluids for metabonomics information retrieval and biomarker identification. *Anal. Chem.* **82,** 1811–1821 (2010).

39. Beckonert, O. *et al.* Metabolic profiling, metabolomic and metabonomic procedures for NMR spectroscopy of urine, plasma, serum and tissue extracts. *Nat. Protoc.* **2,** 2692–2703 (2007).

40. Bertini, I., McGreevy, K. S. & Parigi, G. *NMR of Biomolecules: Towards Mechanistic Systems Biology*. (John Wiley & Sons, 2012).

41. Markley, J. L. *et al.* The future of NMR-based metabolomics. *Curr. Opin. Biotechnol.* **43,** 34–40 (2017).

42. Hu, J. Z. Magic Angle Spinning NMR Metabolomics. *Metabolomics Open Access* **6,** (2016).

43. Hochrein, J. *et al.* Data Normalization of 1H NMR Metabolite Fingerprinting Data Sets in the Presence of Unbalanced Metabolite Regulation. *J. Proteome Res.* **14,** 3217–3228 (2015).

44. Dieterle, F., Ross, A., Schlotterbeck, G. . & Senn, H. Probabilistic Quotient Normalization as Robust Method to Account for Dilution of Complex Biological Mixtures. Application in 1H NMR Metabonomics. *Anal. Chem.* **78,** 4281–4290 (2006).

45. Ren, S., Hinzman, A. A., Kang, E. L., Szczesniak, R. D. & Lu, L. J. Computational and statistical analysis of metabolomics data. *Metabolomics* **11,** 1492–1513 (2015).

46. Wold, S., Esbensen, K. & Geladi, P. Principal component analysis. *Chemom. Intell. Lab. Syst.* **2,** 37–52 (1987).

47. Wold, H. Estimation of principal components and related models by iterative least squares. (1966).

48. Stocchero, M. Analisi statistica multivariata di dati. in *Chemoinformatica* 37–69 (Springer Milan, 2012).

49. Bollard, M. E., Stanley, E. G., Lindon, J. C., Nicholson, J. K. & Holmes, E. NMR-based metabonomic approaches for evaluating physiological influences on biofluid composition. *NMR Biomed.* **18,** 143–162 (2005).

50. Westerhuis, J. A., van Velzen, E. J., Hoefsloot, H. C. & Smilde, A. K. Multivariate paired data analysis: multilevel PLSDA versus OPLSDA. *Metabolomics* **6,** 119–128 (2010).

51. Cover, T. & Hart, P. Nearest neighbor pattern classification. *Inf. Theory IEEE Trans. On* **13,** 21–27 (1967).

52. Cortes, C. & Vapnik, V. Support-Vector Networks. *J Mach Learn Rres* **20,** 273–297 (1995).

53. Breiman, L. Random Forests. *Mach. Learn.* **45,** 5–32 (2001).

54. Varmuza, K. & Filzmoser, P. *Introduction to Multivariate Statistical Analysis in Chemometrics*. (CRC Press, 2016).

55. Gromski, P. S., Xu, Y., Hollywood, K. A., Turner, M. L. & Goodacre, R. The influence of scaling metabolomics data on model classification accuracy. *Metabolomics* **11,** 684–695 (2015).

56. Wilcoxon, F. Individual Comparisons by Ranking Methods. *Biom. Bull.* **1,** 80 (1945).

57. Wilcoxon, F. Individual Comparisons by Ranking Methods. in *Breakthroughs in Statistics* (eds. Kotz, S. & Johnson, N. L.) 196–202 (Springer New York, 1992).

58. Kruskal, W. H. & Wallis, W. A. Use of Ranks in One-Criterion Variance Analysis. *J. Am. Stat. Assoc.* **47,** 583 (1952).

59. Bonferroni, C. E. Il calcolo delle assicurazioni su gruppi di teste. in *Studi in Onore del Professore Salvatore Ortu Carboni* 13–60 (1935).

60. Benjamini, Y. & Hochberg, Y. Controlling the False Discovery Rate: A Practical and Powerful Approach to Multiple Testing. *J. R. Stat. Soc. Ser. B Methodol.* **57,** 289–300 (1995).

61. Cliff, N. *Ordinal Methods for Behavioral Data Analysis*. (Psychology Press, 1996).

62. Bonadonna, G. *et al.* 30 years' follow up of randomised studies of adjuvant CMF in operable breast cancer: cohort study. *BMJ* **330,** 217 (2005).

63. Oakman, C. *et al.* Identification of a serum-detectable metabolomic fingerprint potentially correlated with the presence of micrometastatic disease in early breast cancer patients at varying risks of disease relapse by traditional prognostic methods. *Ann. Oncol.* **22,** 1295–1301 (2011).

64. Foley, S. F. *et al.* Multimodal Brain Imaging Reveals Structural Differences in Alzheimer's Disease Polygenic Risk Carriers: A Study in Healthy Young Adults. *Biol. Psychiatry* **81,** 154–161 (2017).

65. Paglia, G. *et al.* Unbiased Metabolomic Investigation of Alzheimer's Disease Brain Points to Dysregulation of Mitochondrial Aspartate Metabolism. *J. Proteome Res.* **15,** 608–618 (2016).

66. NASA - Myotendinous and Neuromuscular Adaptation to Long-term Spaceflight. Available at: https://www.nasa.gov/mission_pages/station/research/experiments/738.html#publications. (Accessed: 9th June 2017)

Acknowledgements

Numerous people have been interacting with me during these three of PhD. I would like to start expressing my thanks to my supervisor Professor Claudio Luchinat for his skillful guidance and his invaluable support to develop my research activity. I also dedicate my thanks to Professor Paola Turano for the knowledge and the advices provided to me.

Special thanks for the scientific and social moments shared together go to the metabolomic group – Gaia, Leonardo, Panteleimon, and Veronica - and to all the colleagues met during my time at CERM.

I would like also to thank all the people with whom I collaborated for their precious contributions to my research. In particular, I would like to give a special thank to Elena for her friendship.

I owe my thanks to my family and my closest friends for their invaluable support. Finally, the most important thank is dedicated to my parents, Mara e Loriano, for their endless love, patience, encouragements, and sustainment, for have always held my hand in their ones.